

VOLUME 76

MAY 25, 1972

NUMBER 11

JPCHAx

THE JOURNAL OF

PHYSICAL
CHEMISTRY

PUBLISHED BIWEEKLY BY THE AMERICAN CHEMICAL SOCIETY

THE JOURNAL OF PHYSICAL CHEMISTRY

BRYCE CRAWFORD, Jr., *Editor*

STEPHEN PRAGER, *Associate Editor*

ROBERT W. CARR, Jr., FREDERIC A. VAN-CATLEDGE, *Assistant Editors*

EDITORIAL BOARD: A. O. ALLEN (1970-1974), J. R. BOLTON (1971-1975),
F. S. DAINTON (1972-1976), M. FIXMAN (1970-1974),
H. S. FRANK (1970-1974), R. R. HENTZ (1972-1976), J. R. HUIZENGA (1969-1973),
W. J. KAUZMANN (1969-1973), R. L. KAY (1972-1976), W. R. KRIGBAUM (1969-1973),
R. A. MARCUS (1968-1972), W. J. MOORE (1969-1973), J. A. POPLER (1971-1975),
B. S. RABINOVITCH (1971-1975), H. REISS (1970-1974), S. A. RICE (1969-1975),
F. S. ROWLAND (1968-1972), R. L. SCOTT (1968-1972),
R. SEIFERT (1968-1972), W. A. ZISMAN (1972-1976)

CHARLES R. BERTSCH, *Manager, Editorial Production*

AMERICAN CHEMICAL SOCIETY, 1155 Sixteenth St., N.W., Washington, D. C. 20036

Books and Journals Division

JOHN K CRUM, *Director*

JOSEPH H. KUNEY, *Head, Business Operations Department*

RUTH REYNARD, *Assistant to the Director*

©Copyright, 1972, by the American Chemical Society. Published biweekly by the American Chemical Society at 20th and Northampton Sts., Easton, Pa. 18042. Second-class postage paid at Washington, D. C., and at additional mailing offices.

All manuscripts should be sent to *The Journal of Physical Chemistry*, Department of Chemistry, University of Minnesota, Minneapolis, Minn. 55455.

Additions and Corrections are published once yearly in the final issue. See Volume 75, Number 26 for the proper form.

Extensive or unusual alterations in an article after it has been set in type are made at the author's expense, and it is understood that by requesting such alterations the author agrees to defray the cost thereof.

The American Chemical Society and the Editor of *The Journal of Physical Chemistry* assume no responsibility for the statements and opinions advanced by contributors.

Correspondence regarding accepted copy, proofs, and reprints should be directed to Editorial Production Office, American Chemical Society, 20th and Northampton Sts., Easton, Pa. 18042. Manager: CHARLES R. BERTSCH. Assistant Editor: EDWARD A. BORGER.

Advertising Office: Century Communications Corporation, 142 East Avenue, Norwalk, Conn. 06851.

Business and Subscription Information

Remittances and orders for subscriptions and for single copies,

notices of changes of address and new professional connections, and claims for missing numbers should be sent to the Subscription Service Department, American Chemical Society, 1155 Sixteenth St., N.W., Washington, D. C. 20036. Allow 4 weeks for changes of address. Please include an old address label with the notification.

Claims for missing numbers will not be allowed (1) if received more than sixty days from date of issue, (2) if loss was due to failure of notice of change of address to be received before the date specified in the preceding paragraph, or (3) if the reason for the claim is "missing from files."

Subscription rates (1972): members of the American Chemical Society, \$20.00 for 1 year; to nonmembers, \$60.00 for 1 year. Those interested in becoming members should write to the Admissions Department, American Chemical Society, 1155 Sixteenth St., N.W., Washington, D. C. 20036. Postage to Canada and countries in the Pan-American Union, \$5.00; all other countries, \$6.00. Single copies for current year: \$3.00. Rates for back issues from Volume 56 to date are available from the Special Issues Sales Department, 1155 Sixteenth St., N.W., Washington, D. C. 20036.

This publication and the other ACS periodical publications are now available on microfilm. For information write to: MICROFILM, Special Issues Sales Department, 1155 Sixteenth St., N.W., Washington, D. C. 20036.

THE JOURNAL OF PHYSICAL CHEMISTRY

Volume 76, Number 11 May 25, 1972

JPCA 76(11) 1511-1668 (1972)

| | |
|--|------|
| Rates of Interaction of Vibrationally Excited Hydroxyl ($\nu = 9$) with Diatomic and Small Polyatomic Molecules S. D. Worley, R. N. Coltharp, and A. E. Potter, Jr.* | 1511 |
| Reaction of Ozone with Carbon Monoxide Louis M. Arin and Peter Warneck* | 1514 |
| Intermediates in the Reactions of Alkane and Cycloalkane Molecular Ions with Water Vapor J. J. DeCorpo, M. V. McDowell, and F. E. Saalfeld* | 1517 |
| Kinetics of the Cobalt-Catalyzed Autoxidation of Toluene in Acetic Acid. The Role of Cobalt E. J. Y. Scott* and A. W. Chester | 1520 |
| Temperature Effects in the Intersystem Crossing Process of Anthracene R. P. Widman and J. Robert Huber* | 1524 |
| Photoredox Chemistry of Bis(2,9-dimethyl-1,10-phenanthroline)copper(II) Complexes in Aqueous and Methanolic Media S. Sundararajan and E. L. Wehry* | 1528 |
| Pulse Radiolysis of Aqueous Thiocyanate Solutions. Nature of the Intermediate Transient Species D. Behar, P. L. T. Bevan, and G. Scholes* | 1537 |
| Radiolysis of Water by Tritium β Rays: Scavenging of Hydrogen Peroxide Precursors G. Lemaire, C. Ferradini, and J. Pucheault* | 1542 |
| An Electron Paramagnetic Resonance Study of the $\text{Cu}^+ - \text{NO}$ Complex in a Y-Type Zeolite C. C. Chao and J. H. Lunsford* | 1546 |
| Electronic Absorption Studies of the Radical Complex between Perylene and Tetracene Cations Tomoko Yamazaki and Katsumi Kimura* | 1549 |
| Torsional Frequencies and Enthalpies of Intramolecular Hydrogen Bonds of <i>o</i> -Halophenols G. L. Carlson, W. G. Fateley, A. S. Manocha, and F. F. Bentley* | 1553 |
| Vibrational Spectra and Structure of Organogermanes. XII. Normal Vibrations and Free Rotation in <i>p</i> -Chlorophenylgermane and <i>p</i> -Fluorophenylgermane J. R. Durig* and J. B. Turner | 1558 |
| Raman Spectra of Molten Alkali Metal Carbonates J. B. Bates, M. H. Brooker, A. S. Quist, and G. E. Boyd* | 1565 |
| Ultrasonic Absorption in Dioxane-Water Solutions of Magnesium Sulfate F. H. Fisher | 1571 |
| Relaxation Spectra of Molybdate Polymers in Aqueous Solution. Ultrasonic Attenuation Dan S. Honig and Kenneth Kustin* | 1575 |
| Magnetochemical Studies on Diphenyldialkoxysilanes R. D. Goyal, R. R. Gupta, and R. L. Mital* | 1579 |
| Predictions of the Rates of Hydrogen Abstraction by $\text{CH}_2(^3\text{B}_1)$ by the Bond-Energy Bond-Order Method Robert W. Carr, Jr. | 1581 |
| Steady-State Intermediate Concentrations and Rate Constants. Some HO_2 Results A. A. Westenberg* and N. deHaas | 1586 |
| Substituent Effects. IX. Correlation of Carbon-13, Proton-1, and Fluorine-19 Nuclear Magnetic Resonance Chemical Shifts of Some Aromatic Compounds by Pairwise Additivity Edmund R. Malinowski | 1593 |
| Action of Hemoglobin. Cooperative and Bohr Effects H. A. Saroff | 1597 |
| Relative Partial Molar Enthalpies and Heats of Dilution of Electrolytes in Water Lowell W. Bahe | 1608 |
| Significant Structure Liquid Theory of the Alkali Metals over the Normal Melting to Boiling Range Chen C. Hsu, Allen K. MacKnight, and Henry Eyring* | 1612 |

| | | |
|---|--|------|
| Thermochemistry of Fused Halide Systems. Enthalpies of Mixing of the Alkaline Earth Halides with the Alkali Halides | Terje Østvold | 1616 |
| Theory of Heats of Mixing of Certain Charge-Asymmetrical Molten Salts | H. Ted Davis | 1629 |
| Vapor-Phase Absorbance and Thermodynamic Properties of Cuprous Chloride and Cuprous Bromide | David L. Hilden and N. W. Gregory* | 1632 |
| Columns of Liquids Bearing a Constrained Chemical Activity Gradient | Robert C. Plumb* and Wilbur B. Bridgman | 1637 |
| Adsorption in Mordenite. I. Calculation of Adsorption Potentials of Nonpolar Molecules | Guillermo D. Mayorga and Donald L. Peterson* | 1641 |
| Adsorption in Mordenite. II. Gas Chromatographic Measurement of Limiting Heats of Adsorption of Nonpolar Molecules | Guillermo D. Mayorga and Donald L. Peterson* | 1647 |
| Correlations between the Electrochemical and Spectroscopic Behavior of Some Benzophenones and Thiobenzophenones | Rafik O. Loutfy* and Raouf O. Loutfy | 1650 |
| Electric Conduction of the Aluminum-Auramine-Stannic Oxide System | H. Shimoda, M. Sukigara, T. Sakata,* and K. Honda | 1655 |
| The Apparent Hydration Numbers of Alcohols in Aqueous Solution | Charles H. Spink* and John C. Wyckoff | 1660 |

COMMUNICATIONS TO THE EDITOR

| | | |
|--|---|------|
| Potential-Dependent Chronoamperometry: the EC Reaction | Lynn Marcoux* and T. J. P. O'Brien | 1666 |
|--|---|------|

AUTHOR INDEX

| | | | | |
|------------------------|----------------------|----------------------------|-----------------------------|-------------------------|
| Arin, L. M., 1514 | DeCorpo, J. J., 1517 | Huber, J. R., 1524 | Mital, R. L., 1579 | Scott, E. J. Y., 1520 |
| Bahe, L. W., 1608 | deHaas, N., 1586 | Kimura, K., 1549 | O'Brein, T. J. P., 1666 | Shimoda, H., 1655 |
| Bates, J. B., 1565 | Durig, J. R., 1558 | Kustin, K., 1575 | Østvold, T., 1616 | Spink, C. H., 1660 |
| Behar, D., 1537 | Eyring, H., 1612 | Lemaire, G., 1542 | Peterson, D. L., 1641, 1647 | Sukigara, M., 1655 |
| Bentley, F. F., 1553 | Fateley, W. G., 1553 | Loutfy, Rafik O., 1650 | Potter, A. E., Jr., 1511 | Sundararajan, S., 1528 |
| Bevan, P. L. T., 1537 | Ferradini, C., 1542 | Loutfy, Raouf O., 1650 | Puicheault, J., 1542 | Turner, J. B., 1558 |
| Boyd, G. E., 1565 | Fisher, F. H., 1571 | Lunsford, J. H., 1546 | Quist, A. S., 1565 | Warneck, P., 1514 |
| Bridgman, W. B., 1637 | Goyal, R. D., 1579 | MacKnight, A. K., 1612 | Saalfeld, F. E., 1517 | Wehry, E. L., 1528 |
| Brooker, M. H., 1565 | Gregory, N. W., 1632 | Malinowski, E. R., 1593 | Sakata, T., 1655 | Westenberg, A. A., 1586 |
| Carlson, G. L., 1553 | Gupta, R. R., 1579 | Manocha, A. S., 1553 | Saroff, H. A., 1597 | Widman, R. P., 1524 |
| Carr, R. W., Jr., 1581 | Hilden, D. L., 1632 | Marcoux, L., 1666 | Scholes, G., 1537 | Worley, S. D., 1511 |
| Chao, C. C., 1546 | Honda, K., 1655 | Mayorga, G. D., 1641, 1647 | | Wyckoff, J. C., 1660 |
| Chester, A. W., 1520 | Honig, D. S., 1575 | McDowell, M. V., 1517 | | Yamazaki, T., 1549 |
| Coltharp, R. N., 1511 | Hsu, C. C., 1612 | | | |
| Davis, H. T., 1629 | | | | |

In papers with more than one author the name of the author to whom inquiries about the paper should be addressed is marked with an asterisk in the by-line.

THE JOURNAL OF PHYSICAL CHEMISTRY

Registered in U. S. Patent Office © Copyright, 1972, by the American Chemical Society

VOLUME 76, NUMBER 11 MAY 25, 1972

Rates of Interaction of Vibrationally Excited Hydroxyl ($v = 9$) with Diatomic and Small Polyatomic Molecules

by S. D. Worley, R. N. Coltharp, and A. E. Potter, Jr.*

Earth Observations Division, NASA Manned Spacecraft Center, Houston, Texas 77058 (Received December 6, 1971)

Publication costs assisted by NASA

The present investigation follows the loss of OH^\dagger ($v = 9$) produced by the reaction of H and O_3 at the entrance of a fast-flow system in the presence of various diatomic and polyatomic molecules of aeronomic interest by observing the decay in intensity of the 9-7 emission band of OH^\dagger . Several loss processes for OH^\dagger have been found to be important. These are (1) radiative decay, (2) quenching by the walls of the flow-tube, (3) chemical reaction with ozone, and (4) interaction with other molecules present. In this study the first three loss processes were held essentially constant, while process 4 was varied, thus enabling the determination of the rate constants for quenching of OH^\dagger ($v = 9$) by the various molecules of interest. The rate constants ($k \times 10^{14}$ $\text{cm}^3 \text{ molecule}^{-1} \text{ sec}^{-1}$) measured were (k , M): 0.36, N_2 ; 15, NO; 4.8, N_2O ; 1.4, CH_4 ; 2.4, CO_2 ; 2.5, COS; 2.4, SO_2 ; 25, H_2S ; 20, H_2O .

Introduction

Very few reaction rate data have been reported for vibrationally excited molecules in their upper vibrational states. Until recently, experiments deriving vibrational deactivation parameters have been essentially limited to electronically excited states.¹ Work in these laboratories²⁻⁴ and in those of Hancock and Smith^{5,6} concerning reactions of vibrationally excited OH and CO, respectively, has begun basic kinetic studies of vibrationally excited species in their ground electronic states. Such studies should be continued, for upon refinement they should prove to be useful in testing current theoretical treatments of vibrational energy transfer.

Previous papers have reported the rate constants for the reaction of OH^\dagger ($v = 9$) with ozone² and with oxygen,⁴ the mean radiative lifetime of OH^\dagger ($v = 9$),² and the rates of reaction of OH^\dagger ($v = 2-9$) with ozone.³ The reason for concentrating on the $v = 9$ state of OH^\dagger in preference to the other vibrational states is that from the reaction between H and O_3 , OH^\dagger ($v = 9$) is the

highest level produced. Consequently, no complications in interpretation of the data arise from cascading from higher vibrational states, as would be the case if lower levels were studied.

Experimental Section

A complete description of the fast-flow reactor and the experimental techniques used in the current study has been given elsewhere,² and thus only the main points will be summarized here. The procedure followed was to monitor the intensity of the OH^\dagger decay at viewing ports spaced down a metal flow tube. The

(1) For example, see J. I. Steinfeld and W. Klemperer, *J. Chem. Phys.*, **42**, 3475 (1965).

(2) A. E. Potter, Jr., R. N. Coltharp, and S. D. Worley, *ibid.*, **54**, 992 (1971).

(3) R. N. Coltharp, S. D. Worley, and A. E. Potter, Jr., *Appl. Opt.*, **10**, 1786 (1971).

(4) S. D. Worley, R. N. Coltharp, and A. E. Potter, Jr., *J. Chem. Phys.*, **55**, 2608 (1971).

(5) G. Hancock and I. W. M. Smith, *Chem. Phys. Lett.*, **8**, 41 (1971).

(6) G. Hancock and I. W. M. Smith, *Appl. Opt.*, **10**, 1827 (1971).

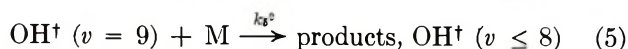
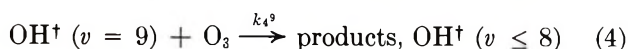
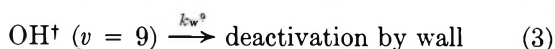
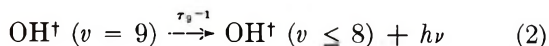
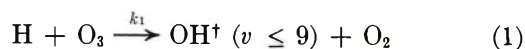
detector used in this study was a lead sulfide photoconductor cooled to 195°K. A 2.1–2.5- μ interference filter, which passed predominantly the 9–7 emission band of OH \dagger , completely covered the detector.⁷ A mechanical chopper was used to modulate the light intensity viewed by the detector, and the output signal was synchronously detected with a Princeton lock-in amplifier.

As in the earlier studies,^{2–4} the concentrations of H (ca. 4.5×10^{-9} mol l.⁻¹) and O₃ (ca. 1.7×10^{-8} mol l.⁻¹) and the flow rate (ca. 1.5×10^5 cm³ sec⁻¹) were adjusted to compress the initial H + O₃ reaction zone into the first few centimeters of the tube so that only loss processes for OH \dagger ($v = 9$) were followed at the viewing ports. A "blank" run, in which only H, 5% O₃/95% O₂, and argon were mixed in the tube, was made before each run in which a species of aeronomic interest, M, was added.

All gases used in this work were obtained from Matheson and were thought to be of sufficient purity to use directly from the cylinders. To obtain an adequate vapor pressure of H₂O in the flow tube, it was necessary to bubble high-purity argon through a porous fritted disk immersed in distilled water. The argon was then saturated with H₂O, and appropriate corrections were made in deriving the concentration of H₂O present in the tube. Since argon is a very poor quencher relative to the other species M in this study, its contribution to the reaction system can be neglected. Indeed, the earlier studies² showed that argon present in the flow tube merely acts to minimize wall deactivation.

Results

The reactions which have proved to be important^{2–4} in the current experiments in the flow tube are



Equation 1 represents the initial chemical reaction which produces OH \dagger ; the rate constant k_1 has been accurately measured by Phillips and Schiff⁸ to be $2.6 \pm 0.5 \times 10^{-11}$ cm³ molecule⁻¹ sec⁻¹. As stated previously, reaction 1 is essentially complete before the first viewing port in the flow tube, and thus its contribution may be neglected in the final rate equation. Equation 2 represents radiative decay, τ_9 being the mean radiative lifetime of OH \dagger ($v = 9$); a value of $6.4 \pm 1.4 \times 10^{-2}$ sec was found for τ_9 in one of the earlier works.² The third equation represents collisional deactivation by the walls of the flow tube. The k_w^9 used in this study, $6.2 \text{ sec}^{-1} \text{ Torr}/P$, where P is the

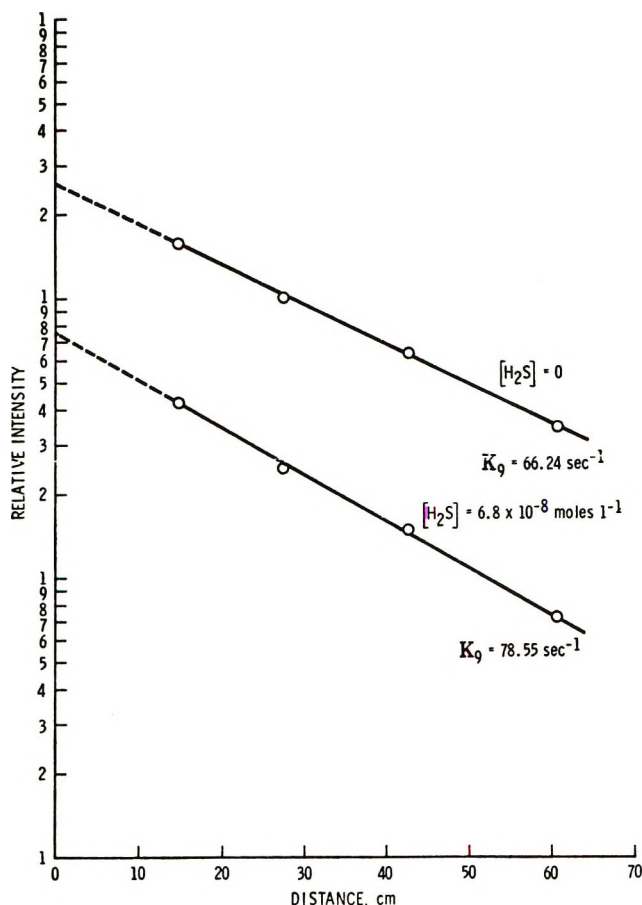


Figure 1. Decay of OH \dagger (9–7) radiation intensity with and without M present in the flow tube.

reaction tube pressure in Torr, was determined before.² Equation 4 represents the reaction of OH \dagger ($v = 9$) with ozone, the previously measured value of k_4^9 being $7.7 \pm 0.3 \times 10^{-12}$ cm³ molecule⁻¹ sec⁻¹; the contribution of this reaction was quite significant in the current experiments because ozone was always present in large excess relative to atomic hydrogen. The fifth equation illustrates the reaction of OH \dagger ($v = 9$) with various molecules, M; the rate constants k_5^9 are the parameters which were measured in this work. The rate equation for the loss processes described above (neglecting reaction 1) is

$$[d[\text{OH}^\dagger]/dt]_{v=9} = -\kappa_9[\text{OH}^\dagger]_9 \quad (6)$$

where

(7) The transmission of the interference filter employed in this study varied smoothly between 4 and 48% over the OH \dagger (9–7) emission band (2.10–2.27 μ) with a mean transmission of 22.6%, while the transmission over the OH \dagger (8–6) emission band (1.95–2.11 μ) was only 0 to 4.5% with a mean transmission of 1.4%. The transmission was 0.2% at the 8–6 band origin. The ratio of the mean spectral response of the cooled PbS detector in the range 2.10–2.27 μ to that in the range 1.95–2.11 μ was 1.11. From these data, the response of the detector-filter system to the 8–6 band was estimated to be $1/20$ of the response to the 9–7 band. It was considered that the rejection of the 8–6 band was sufficient that its contribution to the measured signal could be neglected.

(8) L. F. Phillips and H. I. Schiff, *J. Chem. Phys.*, **37**, 1233 (1962).

$$\kappa_9 = \tau_9^{-1} + k_w^9 + k_4^9[\text{O}_3] + k_5^9[\text{M}] \quad (7)$$

Expression 6 is a simple first-order rate equation, and since the intensity of the OH^\dagger 9-7 emission band is proportional to $[\text{OH}^\dagger]_9$, a semilog plot of the intensity I vs. time or distance of flow must be linear, as shown in Figure 1. Values of k_9 for a variety of M concentrations were determined from the linear plots in the manner described in the earlier work.² To minimize errors for k_5^9 arising from errors in the parameters τ_9 , k_w^9 , and k_4^9 , the "blank" runs (see Experimental Section) were compared directly with the runs in which M was introduced. Since the ozone concentration varied only slightly between the "blank run" and the typical runs with M present, the errors in these parameters essentially cancel, and the main source of error in k_5^9 is the measured value of the concentration of M. The error in [M] was estimated to be less than 5% for most of the M studied. Table I lists the molecules studied, the concentration ranges employed, and the average values of k_5^9 . The indicated errors in Table I represent the standard deviation from the mean of between 8 and 20 different experimental measurements, but the absolute error inherent in the measured values of k_5^9 is at least 5%, and more for some M (see Discussion section).

Table I: Rate Constants for Interactions of OH^\dagger ($v = 9$) with M

| M | [M] range $\times 10^6$, mol l. ⁻¹ | k_5^9 , cm ³ molecule ⁻¹ sec ⁻¹ |
|-------------------------------|--|--|
| O ₂ ^a | 0.1-1.9 | $7.7 \pm 0.3 \times 10^{-12}$ |
| O ₂ ^b | 67.0-332 | $1.0 \pm 0.1 \times 10^{-14}$ |
| N ₂ | 466-1078 | $3.6 \pm 0.5 \times 10^{-15}$ |
| NO | 2.8-6.8 | $1.5 \pm 0.3 \times 10^{-13}$ |
| N ₂ O | 9.3-47.5 | $4.8 \pm 2.2 \times 10^{-14}$ |
| CH ₄ | 34.5-104 | $1.4 \pm 0.2 \times 10^{-14}$ |
| CO ₂ | 19.2-43.5 | $2.4 \pm 1.0 \times 10^{-14}$ |
| COS | 12.4-49.2 | $2.5 \pm 1.5 \times 10^{-14}$ |
| SO ₂ ^c | 8.7-26.3 | $2.4 \pm 0.4 \times 10^{-14}$ |
| H ₂ S ^c | 1.1-6.8 | $2.5 \pm 0.9 \times 10^{-13}$ |
| H ₂ O ^c | 1.4-4.0 | $2.0 \pm 1.6 \times 10^{-13}$ |
| CO | 19.6-66.0 | |
| NH ₃ | 2.0-3.2 | |

^a Previously reported in ref 2. ^b Previously reported in ref 4.
^c Minimum rate constants. See text.

Discussion

The recent paper of Hancock and Smith⁶ reports the measurement of rates of de-excitation of CO^\dagger ($v = 4-13$) by a variety of small molecules, several of which have been included in this work. With the exception of N₂O, the ordering of the rate constants for M interacting with OH^\dagger ($v = 9$), *i.e.*, $\text{NO} > \text{N}_2\text{O} > \text{COS} \sim \text{CO}_2 > \text{O}_2$ (Table I) is qualitatively the same as that for

M interacting with CO^\dagger in its upper vibrational levels; *e.g.*,⁶ for CO^\dagger ($v = 13$), $\text{NO} > \text{COS} > \text{CO}_2 > \text{N}_2\text{O} > \text{O}_2$, for those M studied in the two works. Hancock and Smith⁶ assume only vibrational deactivation mechanisms (V-V and V-T energy transfer) in interpreting their data for CO^\dagger . However, such an interpretation is untenable for OH^\dagger ($v = 9$). Since the efficiency of V-T and V-V energy transfer processes depends on the reduced mass and vibrational frequencies of the collision partners,⁹ one would expect trends to appear in the data in Table I. For example, the vibrational frequency of N₂ (2331 cm⁻¹)¹⁰ is in nearer resonance with the 9-8 emission frequency (2236 cm⁻¹)¹¹ for OH^\dagger ($v = 9$) than is that (1555 cm⁻¹)¹⁰ for O₂ of similar reduced mass; yet O₂ interacts more efficiently with OH^\dagger ($v = 9$) than does N₂ (see Table I). It seems clear that chemical reaction must be considered in addition to vibrational deactivation as a mode of interaction for most of the M and OH^\dagger ($v = 9$). Thus, the values of k_5^9 in Table I represent a sum of vibrational deactivation processes and chemical reaction; this experiment could not distinguish between the various processes.

Methane is the only M for which reaction data involving OH has been studied previously.^{12,13} Our rate constant for OH^\dagger ($v = 9$) was 1.4×10^{-14} cm³ molecule⁻¹ sec⁻¹. The previous works^{12,13} reported values of 1.08×10^{-14} and 8.8×10^{-15} cm³ molecule⁻¹ sec⁻¹, respectively; these rate constants represent chemical reaction entirely because the OH generated in the experiments was in its ground vibrational state. Thus, the present reaction rate constant for CH₄ and OH^\dagger ($v = 9$) is reasonable, considering that vibrational excitation could increase chemical reaction rates. Earlier work³ in these laboratories has shown that k_4^9 for interaction of O₃ and OH^\dagger ($v = 2-9$) decreases as v becomes smaller; however, preliminary work¹⁴ seems to indicate that k_5^9 for O₂ increases, or remains constant, as v becomes smaller. Furthermore, the recent study⁶ of interactions of CO^\dagger ($v = 4-13$) has shown that when M = N₂, N₂O, CO, or COS, lower vibrational states of CO are deactivated more efficiently than upper ones, but the reverse is true when M = NO, He, and CO₂. It seems clear that many more kinetic studies are needed for reactions involving vibrationally excited reactants before one can begin to understand

(9) A. B. Callear, "Photochemistry and Reaction Kinetics," Cambridge University Press, New York, N. Y., 1967, Chapter 7.

(10) G. Herzberg, "Molecular Spectra and Molecular Structure I. Spectra of Diatomic Molecules," Van Nostrand-Reinhold, Princeton, N. J., 1950, p 62.

(11) J. W. Chamberlain, "Physics of the Aurora and Airglow," Academic Press, New York, N. Y., 1961.

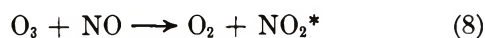
(12) W. E. Wilson and A. A. Westenberg, "11th International Symposium on Combustion," University of California, Berkeley, 1966.

(13) N. R. Greiner, *J. Chem. Phys.*, **46**, 2795 (1967).

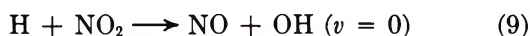
(14) A preliminary report of this work was presented at the 162nd National Meeting of the American Chemical Society under the title, "Quenching of Vibrationally Excited Hydroxyl by Oxygen," Washington, D. C., 1971.

the partitioning of the various deactivation and reaction processes.

The k_5^9 for the molecules denoted by footnote *c* in Table I may represent minimum rate constants. Small concentrations of M caused large decreases in intensity of the OH[†] 9-7 emission band, but the slope of the log *I* vs. distance plot did not change as markedly (see Figure 1). This probably indicates that M is reacting with one of the initial reactants, probably O₃ since it is always in excess relative to H. This would in effect cause the values of [M] and [O₃], which were used in deriving k_5^9 , to be too large, and the resulting k_5^9 to be too small. The k_5^9 reported in Table I for NO is questionable. There was *ca.* 0.7% NO₂ present in the NO as an impurity, and reaction 8 is of compar-

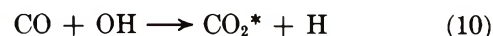


able rate ($2.1 \times 10^{-14} \text{ cm}^3 \text{ molecule}^{-1} \text{ sec}^{-1}$)¹⁵ to those reported in Table I. Small amounts of NO₂ cause large intensity decreases in the OH[†] 9-7 band because reaction 9 is very efficient ($4.8 \pm 0.5 \times 10^{-11} \text{ cm}^3 \text{ mole-}$



cule⁻¹ sec⁻¹)⁸ in competing with reaction 1. No k_5^9 have been reported in Table I for CO and NH₃. The reason for this omission is that the plots of log *I* vs. distance when M = CO or NH₃ had smaller slopes than

did the plots for the "blank" runs, and thus no value of k_5^9 could be determined. It is quite clear why CO is not suitable for study by this technique. The reaction of CO and OH (*v* = 0) as in eq 10 has been fol-



lowed by a fast-flow esr method at 300°K by Dixon-Lewis, *et al.*,¹⁶ their rate constant being $1.9 \times 10^{-13} \text{ cm}^3 \text{ molecule}^{-1} \text{ sec}^{-1}$. The H is thus being regenerated down the tube and can then further react with O₃ to produce additional OH[†] (*v* = 9), causing a lesser slope in the plot. The same process is probably occurring for NH₃, *i.e.*



It is concluded that the present technique can derive only minimum values for k_5^9 when M reacts significantly with O₃, and it cannot be used for studying those M which react with OH[†] to regenerate H. However, the method does seem to be worthwhile for studying reactions of M and OH[†] which do not suffer from these limitations.

(15) L. F. Phillips and H. I. Schiff, *J. Chem. Phys.*, **36**, 1509 (1962).

(16) G. Dixon-Lewis, W. E. Wilson, and A. A. Westenberg, *ibid.*, **44**, 2877 (1966).

Reaction of Ozone with Carbon Monoxide

by Louis M. Arin

Ionics, Inc., Watertown, Massachusetts 02172

and Peter Warneck*

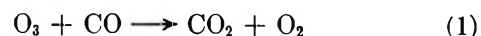
Max-Planck-Institut für Chemie (Otto-Hahn-Institut), 65 Mainz, West Germany (Received September 27, 1971)

Publication costs assisted by Max-Planck-Institut für Chemie

Ozone and carbon monoxide were found to react rapidly due to catalysis by a volatile impurity in the CO, but when the impurity was removed, the reaction was too slow for its rate to be measurable.

Recent observations by Seiler and Junge¹ have demonstrated that carbon monoxide, present in tropospheric air at a level of 10⁻⁷ parts per volume, is rapidly consumed in the stratosphere. The stratospheric oxidation of CO has been predicted theoretically^{2,3} on account of the reaction with OH radicals, but the observed decay of CO concentration with altitude above the tropopause¹ is much faster than the calculated photo-

chemical equilibrium concentrations of OH would allow. Hence, additional CO oxidation processes must be considered. One possibility is the reaction with ozone



(1) W. Seiler and C. Junge, *Tellus*, **21**, 447 (1969).

(2) J. Pressman and P. Warneck, *J. Atm. Sci.*, **27**, 155 (1970).

(3) E. Hestvedt, *Nature (London)*, **225**, 50 (1970).

The oxidation of CO by ozone had been studied previously by Harteck and Dondes⁴ in the temperature range 35–258°, where the reaction is most probably stimulated by the thermal decomposition of ozone. We have re-investigated this reaction at 23° to facilitate the direct observation of reaction 1. The results reported below show that the reaction is catalyzed by small amounts of impurities, but when these are removed, the rate of reaction 1 is very small.

The reaction was studied in a 12-l. thermostated Pyrex flask. Two Teflon-stoppered taps connected the flask to a mercury-free vacuum and gas-handling manifold on one side, and to an analytical train on the other. Samples taken for analysis were of about 3 cm³ volume. Ozone was determined by sweeping the sample with an inert carrier gas through an aqueous solution of 1% sodium diphenylamine sulfonate acidified with perchloric acid. This solution absorbs ozone completely.⁵ The resulting optical density of the solution is proportional to ozone concentration and was measured at the wavelength 590 mμ with a double-beam spectrophotometer. The concentrations of the other gases were determined by gas chromatography using a thermal conductivity detector and a molecular sieve 5A column. Ozone was generated from dry oxygen in a Siemens ozonizer, stored on silica gel in a trap subjected to Dry Ice temperature, freed from oxygen by pumping, and admitted to the flask through a line containing only Teflon-stoppered taps. Carbon monoxide was the best research grade available commercially (Matheson). The impurity content was given as H₂ < 5 ppm, O₂ < 10 ppm, A < 10 ppm, N₂ < 250 ppm, CO₂ < 10 ppm, total hydrocarbon content as methane < 2 ppm. An independent analysis indicated a methane impurity of about 1 ppm. The remaining gases used, hydrogen, oxygen, carbon dioxide and methane, were of research grade quality. Initial pressures of ozone were between 3 and 25 Torr, the range of CO partial pressures was similar.

The behavior of the reaction was unusual in that it occurred rapidly during the process of mixing the reactants, whereas thereafter the gas mixture was stable and the reaction was imperceptible except for the slow decay of ozone due to its thermal decomposition. Typical results are shown in Figure 1 for a run starting with the admixture of 15 Torr of CO to 22 Torr of ozone in the flask. Most experiments were performed in this manner, *i.e.*, by adding CO to ozone. The initial fast reaction was often accompanied by a bluish flash when mixing was rapid or by a luminous zone in the neck of the flask when the rate of mixing was kept slow. As expected, the reaction of ozone with carbon monoxide resulted in the production of carbon dioxide and oxygen. The ratio of CO₂ produced *vs.* CO consumed was, on the average, 0.98 ± 0.21 as determined from 22 runs. The oxygen product concentration could not be measured with sufficient

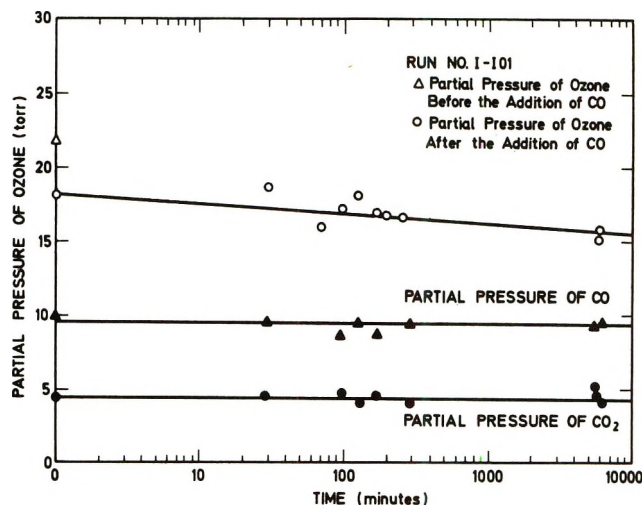


Figure 1. Change of reactant and product partial pressures with time after initial rapid reaction period.

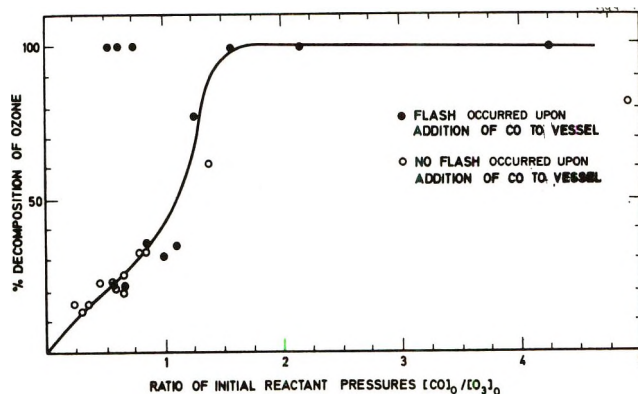


Figure 2. Percentage of ozone consumption *vs.* ratio of initial reactant pressures. Filled points indicate the observation of a flash upon mixing the reactants.

accuracy because it was falsified by the decomposition of ozone in the gas chromatograph inlet line. The consumption of ozone sometimes exceeded that of CO, namely, when the reactants were allowed to mix rapidly, and when the ratio of initial reactant concentrations, $(\text{CO})_0/(\text{O}_2)_0$, was greater than unity. Under these conditions the consumption of ozone was essentially complete, as Figure 2 indicates. This behavior may be due in part to the thermal decomposition of ozone induced by the release of heat from the reaction and/or to the dynamical heating effect upon gas entry discussed by Gray and coworkers.^{6,7} Disregarding those runs in which the consumption of ozone approaches 100%, one finds as the average of the ratio of ozone consumed to CO₂ produced: 1.01 ± 0.20 , as determined from 15

- (4) P. Harteck and S. Dondes, *J. Chem. Phys.*, **26**, 1734 (1957).
- (5) H. H. Bovee and L. J. Robinson, *Anal. Chem.*, **33**, 1115 (1961).
- (6) D. H. Fine, P. Gray, and R. Mackinven, 12th International Symposium on Combustion, Combustion Institute, Pittsburgh, Pa., 1969, p 545.
- (7) H. Goodman and P. Gray, *Trans. Faraday Soc.*, **66**, 2772 (1970).

runs. These results show that the stoichiometry of the reaction is essentially as written in reaction 1. However, the temporal behavior is inconsistent with that of a simple bimolecular rate law.

The unusual course of the reaction as demonstrated in Figure 1 may result from two mechanisms: (a) the products oxygen and/or carbon dioxide inhibit the reaction so that it is stopped after a certain amount of product is formed; or (b) the reaction is catalyzed by an impurity and ceases when the impurity is used up. A third possibility, the attainment of thermodynamic equilibrium, can be eliminated from the discussion, because the equilibrium values of reaction 1 lie far to the right and either ozone, or CO, or both should have been consumed completely. In most experiments, however, the reaction was incomplete.

To determine the effects of oxygen and CO₂ upon the reaction, mixtures of these gases with ozone were prepared and CO was added. No inhibition of the reaction was observed at partial pressures of oxygen up to 10 Torr and CO₂ up to 15 Torr. When carbon monoxide was added to the stable gas mixture resulting from the incomplete reaction of ozone with CO, the reaction proceeded further, consuming most of the remaining O₃. When more ozone was added to such a stable reaction mixture, no further reaction occurred. These results clearly indicate (a) that the reaction is not inhibited by O₂ or CO₂, (b) that it is caused by an impurity in the carbon monoxide, and (c) that conceivable impurities introduced with the ozone have no significant effect.

Since, as a precaution, carbon monoxide had always been introduced to the system *via* a liquid nitrogen-cooled spiral trap, iron carbonyl was not considered a likely impurity. This was verified when CO was taken from a glass container sealed by the manufacturer; the reaction proceeded as usual. Attempts to purify the carbon monoxide by low-temperature adsorption-desorption cycles using silica gel, charcoal, or molecular sieve as the sorbant were unsuccessful. However carbon monoxide subjected to the reaction with ozone so that ozone was consumed entirely could be freed from most of the product oxygen and CO₂ by adsorption on charcoal. Carbon monoxide purified in this manner, when admixed to ozone, produced *no* reaction. These observations therefore indicate that the impurity responsible for the reaction has a volatility similar to that of CO, precluding an effective separation by the applied trapping and sorption techniques; that the impurity present in the original CO is essentially consumed in the reaction; and that the CO thus purified is not again contaminated in the gas-handling manifold.

The volatile character of the impurity pointed to either hydrogen or methane. The effect of these gases was tested by adding them in amounts of about 1 Torr to the stable gas mixture produced by reacting incom-

pletely CO with ozone. Hydrogen was found to have no effect, but methane caused a slow further oxidation of CO. After 15 hr the consumption of ozone was essentially complete, but the amount of CO₂ formation from CO was only 15% of the ozone destroyed.

The results presented here show that the initial rapid reaction of ozone with CO is caused by an impurity in the carbon monoxide, that the impurity is consumed in the reaction, and that the carbon monoxide thus purified does not react noticeably with ozone. An upper limit for the rate of this uncatalyzed reaction 1 can be obtained from the decrease of ozone concentration in Figure 1 which being due mainly to the thermal O₃ decomposition is about twice the upper limit change of CO₂. The value of the rate coefficient thus derived is $k_1 \leq 4 \times 10^{-25}$ cm³/molecule sec. Clearly, this rate is so low that reaction 1 in its uncatalyzed mode can play no role in the oxidation of CO in the atmosphere. The catalyzed reaction, on the other hand, is so fast under the employed experimental conditions that a chain reaction is indicated.

Morris and Niki,⁸ in commenting on our results, have suggested iron carbonyl as the impurity responsible for the catalyzed reaction. However, this impurity is not expected to survive the low-temperature adsorption-desorption cycle to which CO was subjected without success of purification. The impurity implicated by the described experiments is methane. Since CO is generated commercially from methyl formate, with distillation at liquid nitrogen temperature being the final purification step, methane is an expected impurity. Both methane and carbonyl can, in principle, initiate a fast reaction chain by their interaction with ozone^{8,9} or atomic oxygen generated from the thermal decomposition of O₃. The present knowledge about the mechanisms of such reactions is largely speculative, and their detailed discussion is not warranted here. However, the present results do make apparent the importance of minor impurities in the reaction system under discussion. Quite possibly, also the experiments by Harteck and Dondes⁴ were affected in this way.

Acknowledgment. This work was carried out while the authors were with GCA Corporation, Bedford, Mass. It was supported jointly by the National Air Pollution Control Administration, Department of Health, Education and Welfare, and the Coordinating Research Council, Inc. We are grateful to Dr. J. Bufalini for supplying us with a hydrocarbon analysis of the employed carbon monoxide.

(8) E. D. Morris and H. Niki, *J. Amer. Chem. Soc.*, **92**, 5741 (1970).

(9) F. J. Dilleuth, D. R. Skidmore, and C. C. Schubert, *J. Phys. Chem.*, **64**, 1496 (1960), in investigating the methane-ozone reaction have observed severe explosions when ozone was in excess, thus demonstrating that chain reactions can be triggered in this system.

Intermediates in the Reactions of Alkane and Cycloalkane

Molecular Ions with Water Vapor

by J. J. DeCorpo,¹ M. V. McDowell, and F. E. Saalfeld*

Chemistry Division, Naval Research Laboratory, Washington, D. C. 20390 (Received October 6, 1971)

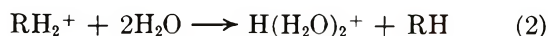
Publication costs assisted by the Naval Research Laboratory

Addition complexes have been detected in the reactions of certain molecular alkane ions with water vapor. These intermediates have relatively long lifetimes. A kinetic scheme has been proposed and the bimolecular rate coefficients for the formation of these addition complexes have been calculated.

In a recent paper, Sieck and Searles² have made a systematic study of the reactions of alkane and cycloalkane molecular ions with water vapor. Their results, in the case of ethane and propane, have been interpreted in terms of a bimolecular proton-transfer reaction, namely



where RH_2^+ is the molecular ion. However, according to the findings of Sieck and Searles, reactions in which RH_2^+ contains four or more carbon atoms appear to involve two water molecules, *viz.*



Moreover, their experiments were conducted at such pressures that the probability of a single three-body collision was negligible. Thus, reaction 2 must proceed *via* a bimolecular addition complex, $[\text{RH}_2 \cdot \text{H}_2\text{O}]^+$. The experiments of Sieck and Searles were conducted on a photoionization mass spectrometer which has a detection time of about 100 μsec . They were unable to detect this proposed ion-addition complex, although their data indicated that the complex should be long-lived.

This note reports the observation and bimolecular rate constants for the formation of the H_2O addition complex for several hydrocarbons. The results reported herein were obtained on a mass spectrometer with a detection time of approximately 1 μsec , which affords an advantage in observing the intermediate addition complex.

The addition complex may have a distribution of lifetimes, owing to some distribution of internal energies $N(E)$. Thus, the rate coefficient, k , determined herein represents a $k(E)$ averaged over the distribution of complexes which have an internal energy (E) with a corresponding lifetime of at least 1 μsec . An examination of the rate coefficients calculated from a simple ion-induced dipole treatment,³ shown in Table I, indicates that most of the addition complexes are detected.

That is, the complex has an average lifetime of 1 μsec or greater. This relatively long lifetime is consistent with the concept of a "sticky collision"⁴ between ions and molecules with a large number of internal degrees of freedom which can exchange energy.

The basic instrument utilized in this investigation was a Bendix Model 12-107 time-of-flight mass spectrometer, the design of which has been described previously.⁵ The instrument was operated in a pulsed mode and was modified by incorporation of a closed ion source and additional pumping to provide adequate pressure differential between the ion source and the source envelope. The ionization chamber was a closed $0.22 \times 0.31 \times 0.56$ in. stainless-steel box having entrance and exit orifices for the electron beam and an exit orifice for the ions, and a reaction path length of 0.11 in. The electron orifices as well as the ion exit orifice were 0.025-in. diameter holes.

A variable time-delay circuit was installed. This circuit allows a variable time delay from 0 to 10 μsec between the end of the pulsed electron beam and the onset of the drawout pulse, the reaction time being the sum of the time delay and the time necessary for the ion to be withdrawn from the reaction chamber. During this reaction time the ionization zone is field free; thus, the rates of an ion-molecule reaction can be considered thermal. The ion-source pressure was monitored directly with a Granville-Phillips capacitance manometer. The pressure in the ion source was maintained constant with a Granville-Phillips automatic pressure controller. The ion-source temperature was measured by means of a thermocouple and found to be 300°K.

In this study an electron-impact technique was employed; thus fragment ions as well as parent ions were

(1) NRC-NRL Resident Research Associate, 1970-1972.

(2) L. W. Sieck and S. K. Searles, *J. Chem. Phys.*, **53**, 2601 (1970).

(3) F. W. Lampe, S. L. Franklin, and F. H. Field, *Progr. React. Kinet.*, **1**, 79 (1961).

(4) M. Burton and S. L. Magee, *J. Phys. Chem.*, **56**, 842 (1952).

(5) C. W. Hand and H. Von Weyssenhoff, *Can. J. Chem.*, **42**, 195 (1964).

Table I

| Reactant ion | ΔH_f^a , kcal/mol | AP of complex (if obsd), eV | Exptl values, cm ³ /(molecule sec) | | Calcd values, cm ³ /(molecule sec) $k = 2\pi e(\alpha/\mu)^{1/2} d$ |
|---|---------------------------|-----------------------------|---|-------------------------|---|
| | | | k_1^b | k_1^c | |
| C ₂ H ₆ ⁺ | -17.9 | | | | |
| C ₃ H ₈ ⁺ | -20.0 | | | | |
| <i>n</i> -C ₄ H ₁₀ ⁺ | +4.3 | 11.4 ± 0.5 | 3.9 × 10 ⁻¹⁰ | 4.1 × 10 ⁻¹⁰ | 9.9 × 10 ⁻¹⁰ |
| <i>i</i> -C ₄ H ₁₀ ⁺ | +1.5 | 11.5 ± 0.5 | 3.0 × 10 ⁻¹⁰ | 4.4 × 10 ⁻¹⁰ | 9.9 × 10 ⁻¹⁰ |
| cyclo-C ₆ H ₁₀ ⁺ | 0.0 | 11.2 ± 0.5 | 9.5 × 10 ⁻¹¹ | 5.0 × 10 ⁻¹¹ | 9.7 × 10 ⁻¹⁰ |
| <i>n</i> -C ₅ H ₁₂ ⁺ | +1.0 | | | | |
| <i>n</i> -C ₆ H ₁₄ ⁺ | +10.0 | 11.0 ± 0.5 | 5.6 × 10 ⁻¹¹ | 1.5 × 10 ⁻¹¹ | 9.5 × 10 ⁻¹⁰ |
| cyclo-C ₆ H ₁₂ ⁺ | +16.0 | | | | |

^a ΔH for $\text{RH}_2^+ + \text{H}_2\text{O} \rightarrow \text{H}_3\text{O}^+ + \text{RH}$. Heats of formation were taken from ref 4 and 6 and M. A. Haney and J. L. Franklin, *J. Chem. Phys.*, **50**, 2028 (1969). ^b Ion ratio vs. $[\text{H}_2\text{O}]$. ^c Ion ratio vs. t . ^d $\alpha_{\text{H}_2\text{O}}$ = polarizability, μ = reduced mass.

available as reactants. Care was taken in choosing operating parameters, *i.e.*, pressure and electron energy, so that no additional ion-molecule reactions interfered in the mass region of interest.

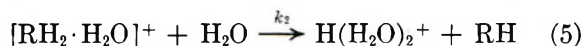
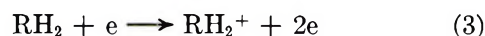
All mixtures used were at least 80 mol % H₂O. Since the ionizing energy of the electrons was above the ionization potential of H₂O (12.6 eV),⁶ H₂O⁺ was also present and a possible reactant. To aid in elucidation of whether RH₂⁺ or H₂O⁺ is reacting to form the addition complex, the appearance potentials (AP) of the product ion were measured. The product ion's AP was below the ionization potential of H₂O in all cases in which the complex was observed. Since the AP's of the hydrocarbon ions generally are a few electron volts below that of water, this supports our assumption that the hydrocarbon ion reacts with the neutral H₂O molecule. These results are listed in Table I; the large error limits are due to the low intensity of the intermediate ion current.

In addition, the ionization efficiency curves of the complexes showed linear behavior for several volts above their onset and well past the energy of onset for H₂O⁺. This type of behavior indicates that the complex is being formed from a single process, thus eliminating any interference to the complex formation from a reaction involving H₂O⁺. It is significant to our study that the complex is not formed from the reaction of H₂O⁺ and hydrocarbon, since the kinetic data were obtained at an electron energy above that of the ionization potential of H₂O.

Examination of the heats of reaction for the bimolecular proton-transfer process reveals that the ion-addition product, with the exception of *n*-hexane, is observed only in reactions that are slightly endothermic or virtually thermoneutral. This result is not surprising, since ion-molecule reactions that are quite exothermic probably form addition complexes that have high internal excitation energy, causing the intermediate complex to be short-lived. The heat of reaction reported in Table I for the *c*-C₅H₁₀⁺, H₂O reaction is

based on a value⁷ for the heat of formation of the C₅H₉ radical which is in doubt. It may well be that the reaction is exothermic or that the structure of the ion itself may no longer be cyclic, thus further complicating this particular system.

The kinetics of the formation process can be interpreted in light of the following scheme



where k_1 and k_2 are the specific rate constants for their respective processes.

If, at $t = 0$, $[\text{RH}_2^+] = [\text{RH}_2^+]_{t_0}$, where t_0 is the duration of the electron pulse, and if during the electron pulse no ions leave the ion source, then at some time t after the electron pulse, the situation is easily shown to be

$$[\text{RH}_2^+]_t = [\text{RH}_2^+]_{t_0} \exp(-k_1 t [\text{H}_2\text{O}]) \quad (6)$$

For the ion-addition complex formed with the rate constant k_1 and removed by k_2 of reaction 5, the differential equation describing its concentration is

$$\frac{d[\text{RH}_2 \cdot \text{H}_2\text{O}]^+}{dt} = k_1 [\text{RH}_2^+] [\text{H}_2\text{O}] - \sum k_2 [\text{RH}_2 \cdot \text{H}_2\text{O}]^+ [\text{H}_2\text{O}] \quad (7)$$

in which $\sum k_2$ is the sum of all processes leading to the removal of the addition product. Integration of (7) leads to the expression

$$[\text{RH}_2 \cdot \text{H}_2\text{O}]^+_t = \frac{k_1 [\text{RH}_2^+]_{t_0}}{\sum k_2 - k_1} [\exp(-k_1 t [\text{H}_2\text{O}]) - \exp(-\sum k_2 t [\text{H}_2\text{O}])] \quad (8)$$

(6) J. L. Franklin, J. G. Dillard, H. M. Rosenstock, J. T. Herron, K. Draxl, and F. H. Field, *Nat. Stand. Ref. Data Ser., Nat. Bur. Stand. (U. S.)*, No. 26 (1969).

(7) J. A. Kerr, *Chem. Rev.*, **66**, 465 (1966).

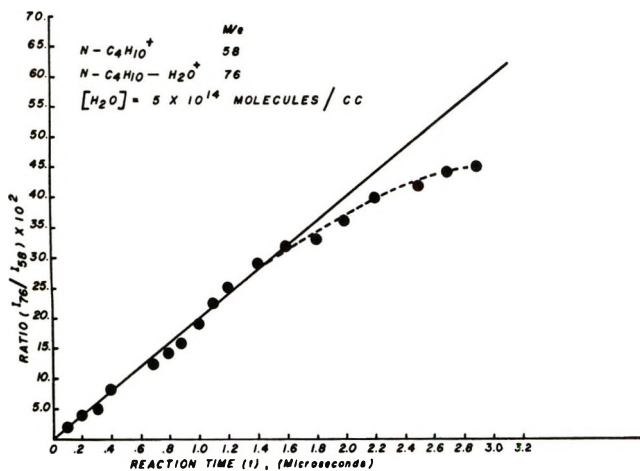


Figure 1. Intensity ratio of the ion-addition complex to that of the molecular ion vs. reaction time at constant pressure.

Then, following the example of Derwish, *et al.*,⁸ letting $\Sigma k_2 - k_1 = K$, it follows that

$$\frac{[\text{RH}_2 \cdot \text{H}_2\text{O}]^+_t}{[\text{RH}_2^+]_t} = \frac{k_1}{K} [1 - \exp(-Kt[\text{H}_2\text{O}])] \quad (9)$$

Differentiating with respect to the reaction time (t)

$$\frac{d \frac{[\text{RH}_2 \cdot \text{H}_2\text{O}]^+_t}{[\text{RH}_2^+]_t}}{d[t]} = k_1[\text{H}_2\text{O}] \exp(-Kt[\text{H}_2\text{O}]) \quad (10)$$

Thus, as $t \rightarrow 0$

$$\frac{d \frac{[\text{RH}_2 \cdot \text{H}_2\text{O}]^+_t}{[\text{RH}_2^+]_t}}{d[t]_{t=0}} = k_1[\text{H}_2\text{O}] \quad (11)$$

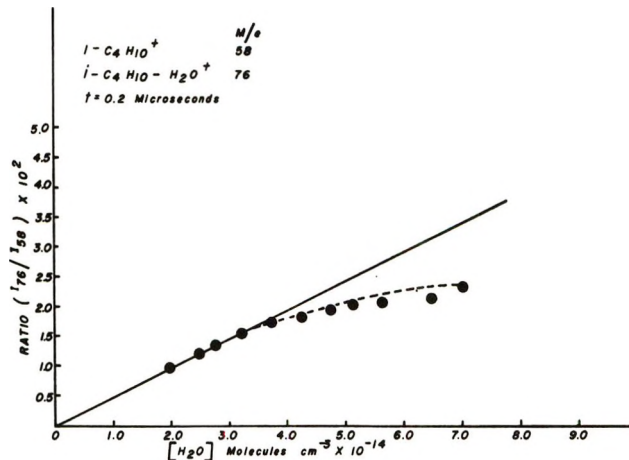


Figure 2. Intensity ratio of the ion-addition complex to that of the molecular ion vs. pressure at a constant reaction time.

Therefore, k_1 can be obtained from the initial slope of a plot of $[\text{RH}_2 \cdot \text{H}_2\text{O}]^+ / [\text{RH}_2^+]$ vs. t . Figure 1 illustrates this for the case of *n*-butane and H_2O . On the other hand, if eq 9 is differentiated with respect to pressure, as $[\text{H}_2\text{O}] \rightarrow 0$, eq 9 reduces to $k_1 t$. The specific rate constant is then obtained from the initial slope of the plot of $[\text{RH}_2 \cdot \text{H}_2\text{O}]^+ / [\text{RH}_2^+]$ vs. $[\text{H}_2\text{O}]$. This is illustrated in Figure 2 for the isobutane-water system. The rate constants obtained by both methods are shown in Table I. In all cases, the slopes fall off at higher pressures or reaction times. Consequently, under these conditions, from eq 9 the value of K must be positive, *i.e.*, $\Sigma k_2 > k_1$, indicating that the sum of the rate constants for the removal of the complex is greater than the one for its formation.

(8) G. A. W. Derwish, A. Galli, A. Giardini-Guidoni, and G. G. Volpi, *J. Chem. Phys.*, **39**, 1599 (1963).

Kinetics of the Cobalt-Catalyzed Autoxidation of Toluene in Acetic Acid.

The Role of Cobalt

by E. J. Y. Scott* and A. W. Chester

Mobil Research and Development Corporation, Central Research Division, Princeton, New Jersey 08540
(Received October 6, 1971)

Publication costs assisted by the Mobil Research and Development Corporation

The cobalt(III) acetate-catalyzed autoxidation of toluene in acetic acid was studied at 87° by determining hydrocarbon consumption and cobalt(III) concentration as a function of time. At steady-state concentrations of Co(III) and Co(II) acetates, the reaction is first order with respect to toluene concentration. A two-term rate law was found to hold

$$-\frac{d[\text{RH}]}{dt} = k_a \frac{[\text{Co(III)}]^{1/2}}{[\text{Co(II)}]} [\text{RH}] + k_b [\text{Co(III)}]^2 [\text{RH}]$$

where RH = toluene. At 87°, the values of the rate constants are $k_a = 1.0 \times 10^{-6} M^{1/2} \text{ sec}^{-1}$ and $k_b = 3.9 \times 10^{-3} M^{-2} \text{ sec}^{-1}$. The rate law is consistent with a two-path mechanism, derived from a Co(III) monomer-dimer equilibrium. The term half-order in Co(III) is consistent with oxidation of RH to its radical cation by the very active cobalt(III) monomer; the term second order in cobalt(III) arises from the oxidation of RH by the predominant cobalt(III) dimer.

The homogeneous catalytic autoxidation of hydrocarbons by transition metal salts has considerable theoretical and practical interest. For example, this area of chemistry is the basis for important industrial processes such as the manufacture of terephthalic acid from *p*-xylene.¹ Although the cobalt-catalyzed autoxidation of toluene to benzoic acid may be regarded as a prototype for the catalytic autoxidation of alkyl aromatics to aromatic carboxy acids, the kinetics of this system are not yet understood.

Morimoto and Ogata² observed the simple rate law (1) for the autoxidation of toluene catalyzed by Co(III) acetate in acetic acid at 90°.

$$-\frac{d[\text{RH}]}{dt} = k[\text{Co(III)}][\text{RH}] \quad (1)$$

Recent work done in this laboratory^{3,4} and reported in the literature^{5,6} led us to doubt this simple formulation. We therefore sought to find a more general rate law for the cobalt-catalyzed autoxidation of toluene.

Experimental Section

Toluene and cobalt acetate were Baker reagent grade, chlorobenzene was obtained from Matheson Coleman and Bell, and oxygen was obtained from Airco. Toluene, chlorobenzene, and stock solutions in glacial acetic acid were tested for peroxide iodometrically prior to use. No effect on reaction rate was noticed when toluene was first passed through a column of alumina and silica. Co(III) acetate was prepared by passing ozone through an acetic acid solution of Co(II) acetate tetrahydrate. The solution was evaporated at 35–40°

at a pressure of 4 mm on a rotary evaporator. The solid, obtained by further drying in a vacuum desiccator over P₂O₅, contained all its cobalt as cobalt(III).

The cobalt(III) acetate-catalyzed autoxidation of toluene in acetic acid was studied at 87° by determining hydrocarbon consumption and cobalt(III) concentration as a function of time. The reactor was a jacketed 100-ml round bottomed flask, fitted with condenser, stirrer, and thermometer. Trichloroethylene was refluxed in the outer jacket to maintain a temperature of 87°. Oxygen was admitted into the reactor through a sensitive pressure regulator set at 1.01 atm, a Wet Test meter, and a drying tower. Zero time was considered to be the time at which the temperature of the reactant solution attained 86°. During the heating period the thermal decomposition of cobaltic acetate decreased its concentration to almost half the initial value (see Figure 1). The initial volume of reactant solution was 80 ml and 1-ml samples were pipetted from the reactor at appropriate intervals. Toluene and chlorobenzene (internal standard) were analyzed on a 6-ft column of Polypak 2 at 200° using an F and M 810 chromatograph. Co(III) acetate was measured spectroscopically by absorption of a filtered

- (1) W. F. Brill, *Ind. Eng. Chem.*, **52**, 837 (1960).
- (2) T. Morimoto and Y. Ogata, *J. Chem. Soc. B*, **62**, 1353 (1967).
- (3) A. W. Chester, to be published.
- (4) E. J. Y. Scott, *J. Phys. Chem.*, **74**, 1174 (1970).
- (5) K. Sakota, Y. Kamiya, and N. Ohta, *Can. J. Chem.*, **47**, 387 (1969).
- (6) E. Koubeck and J. O. Edwards, *J. Inorg. Nucl. Chem.*, **25**, 1401 (1963).

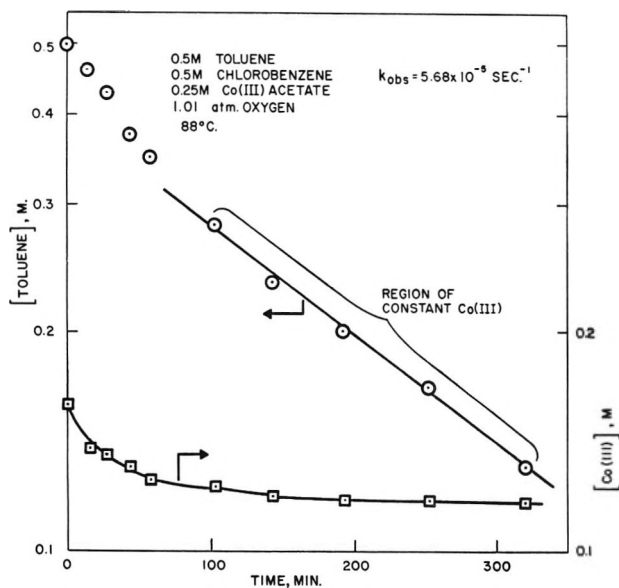


Figure 1. First-order plot for the Co(III) acetate-catalyzed autoxidation of toluene in acetic acid at 88°.

sample at 625 $m\mu$ on a Unicam SP800D spectrophotometer.

Results

The cobalt(III) acetate-catalyzed autoxidation of toluene in acetic acid was studied at 87° by determining hydrocarbon consumption and cobalt(III) concentration as a function of time. The change of \log [toluene] and \log [Co(III)] with time is shown in Figure 1. After the concentrations of Co(III) and Co(II) acetates reach steady-state values, the logarithm of the toluene concentration decreases linearly with time. The computed first-order rate constants (k_{obsd}) at 87° are shown in Table I. Comparison of the last two runs indicates that the reaction is approximately first order with respect to toluene concentration (see also Figure 4). These data may not be used directly to establish order with respect to Co(III) acetate until it is known to what extent Co(II) acetate affects the system.

The effect of 0.1 M Co(II) acetate tetrahydrate on the Co(III) acetate-catalyzed autoxidation of toluene

Table I: First-Order Rate Constants for the Cobalt-Catalyzed Autoxidation of Toluene in Acetic Acid at 87°^a

| [RH] ₀ | [Co(III)] _{ss} | [Co(II)] _{ss} | 10 ⁶ k_{obsd} , sec ⁻¹ |
|-------------------|-------------------------|------------------------|---|
| 0.5 | 0.0179 | 0.0446 | 0.455 |
| 0.5 | 0.053 | 0.0720 | 1.47 |
| 0.5 | 0.084 | 0.1035 | 2.93 |
| 0.5 | 0.1185 | 0.1315 | 5.68 |
| 1.0 | 0.112 | 0.138 | 4.74 |

^a [RH]₀ = initial molar concentration of toluene. [Co(III)]_{ss}, [Co(II)]_{ss} = steady-state molar concentration of Co(III) acetate and of Co(II) acetate. [Co]₀ = [Co(III)]_{ss} + [Co(II)]_{ss}.

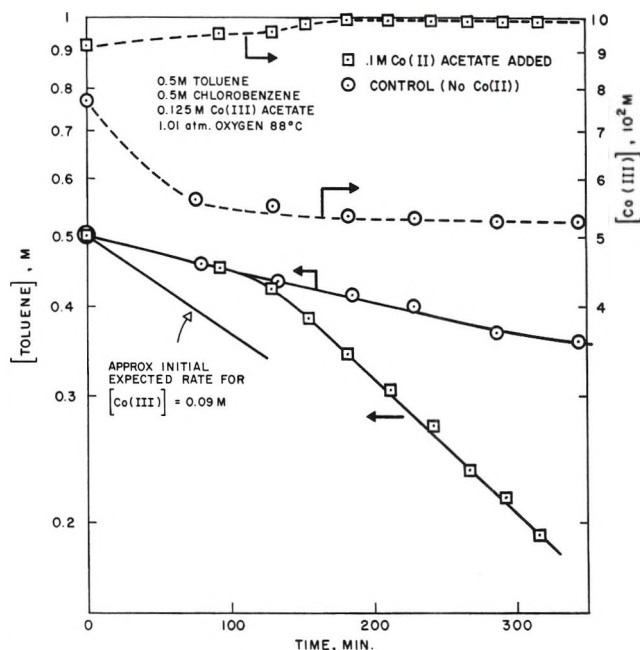


Figure 2. Inhibition effect of Co(II) acetate on Co(III) acetate-catalyzed autoxidation of toluene in acetic acid at 88°.

in acetic acid at 88° is shown in Figure 2. The Co(III) acetate concentration is higher in the presence of Co(II) acetate. However, no enhancement of rate is noticed for about 100 min. This "induction period" indicates that the reaction is retarded by Co(II) acetate. The effect of adding Co(II) acetate tetrahydrate after 100 min to the Co(III) acetate-catalyzed autoxidation of toluene is shown in Figure 3.⁷ The rate of autoxidation of toluene is sharply reduced and subsequently increases as Co(II) acetate is converted to Co(III) acetate. To determine whether the retarding effect could be ascribed to acetate ion or water, 0.1 M potassium acetate and 0.4 M water were added after 406 and 481 min, respectively. Water produced no change in rate while the retarding effect of potassium acetate was significant but small. The main retardation was therefore due to Co(II) acetate.

An initial attempt was made to relate the observed rate constants (k_{obsd}) to simple powers of the corresponding cobaltic acetate steady-state concentrations, *i.e.*, $1/2$, 1, and 2. Each of these orders had been proposed at various times by various workers for the reactions of cobaltic acetate with aromatic compounds in acetic acid solution.^{2,4,5,8} The observed rate constants in the present work were found to be nonlinearly dependent on $[Co(III)]^{1/2}$ and $[Co(III)]$ but linearly dependent on $[Co(III)]^2$. In view of the observed inhibition by Co(II) acetate the relations between k_{obsd} and $[Co(III)]^m [Co(II)]^{-1}$, where $m = 1/2, 1, \text{ or } 2$,

(7) This experiment was suggested by E. I. Heiba.

(8) E. I. Heiba, R. M. Dessau, and W. J. Koehl, Jr., *J. Amer. Chem. Soc.*, **91**, 6830 (1969).

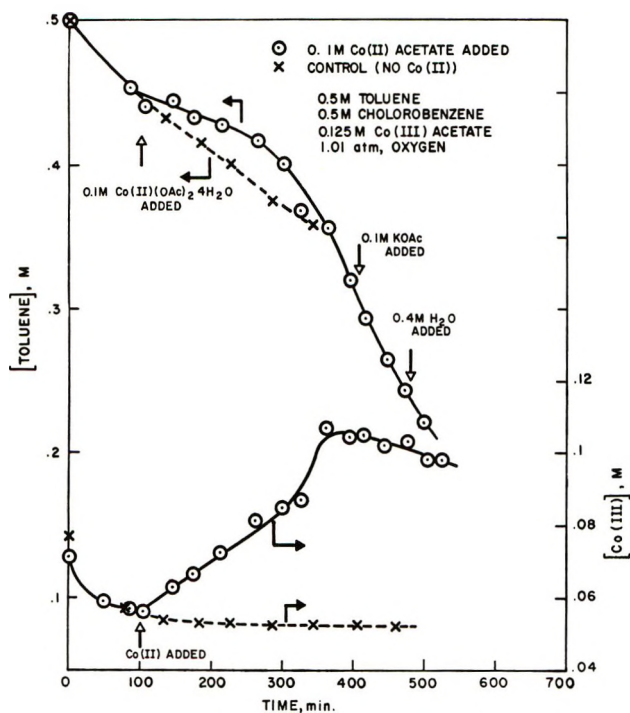


Figure 3. Addition of Co(II) acetate tetrahydrate to the Co(III) acetate-catalyzed autoxidation of toluene in acetic acid at 87°.

were also checked. Other negative orders of Co(II), such as $-1/2$ and -2 , seemed intrinsically unreasonable and had in fact not been previously proposed.

Except for simple second-order dependence, no linear relationship was found. In this instance the slope was computed to be $4.0 \times 10^{-3} M^{-2} \text{sec}^{-1}$ and the intercept $3.1 \times 10^{-6} \text{sec}^{-1}$. The positive intercept indicated that a second term in the rate expression was required to account for an increased reaction rate at low Co(III) acetate concentrations. Of the three plots of $\{k_{\text{obsd}} - 4.0 \times 10^{-3}[\text{Co(III)}]^2\}$ as functions of $[\text{Co(III)}]^m[\text{Co(II)}]^n$ where $m = 1/2, 1$, or 2 and $n = 0$ or -1 , only the case where $m = 1/2, n = -1$ gave an approximately linear plot with a positive slope. The rate expression⁹ most consistent with the data is therefore

$$-\frac{d[\text{RH}]}{dt} = \frac{k_a[\text{Co(III)}]^{1/2}[\text{RH}]}{[\text{Co(II)}]} + k_b[\text{Co(III)}]^2[\text{RH}] \quad (2)$$

The observed first-order rate constant with respect to RH is given by

$$k_{\text{obsd}} = k_a \frac{[\text{Co(III)}]^{1/2}}{[\text{Co(II)}]} + k_b[\text{Co(III)}]^2 \quad (2a)$$

which may be rearranged to

$$k_{\text{obsd}} \frac{[\text{Co(II)}]}{[\text{Co(III)}]^{1/2}} = k_a + k_b[\text{Co(II)}][\text{Co(III)}]^{1/2} \quad (3)$$

A plot according to (3) for $[\text{toluene}]_0 = 0.5 M$ is shown

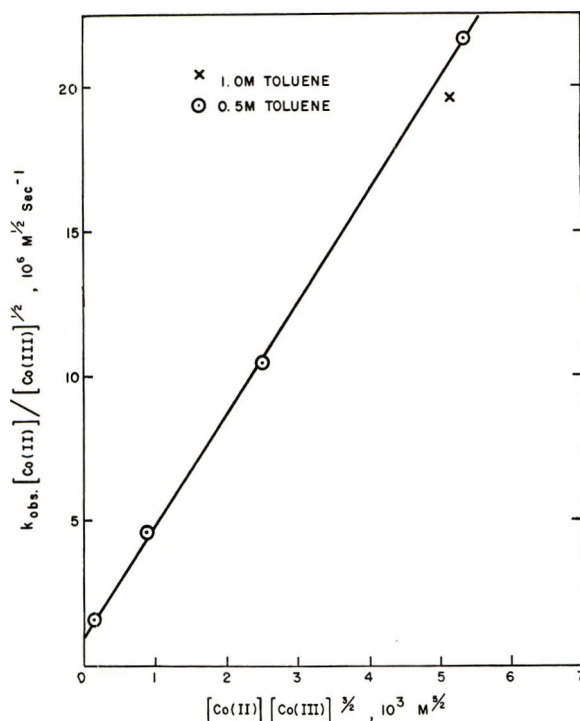


Figure 4. Test of rate expression $-d[\text{RH}]/dt = k_a[\text{Co(III)}]^{1/2}[\text{RH}]/[\text{Co(II)}] + k_b[\text{Co(III)}]^2[\text{RH}]$.

in Figure 4. The rate constants, obtained from the slope and intercept, are $k_a = 1 \times 10^{-6} M^{1/2} \text{sec}^{-1}$ and $k_b = 3.9 \times 10^{-3} M^{-2} \text{sec}^{-1}$ at 87°. Note that the point for $[\text{toluene}]_0 = 1.0 M$ in Figure 4 lies close to the line, confirming the first-order dependence on toluene. This rate expression is not necessarily the only one consistent with the data but is the one which is most consistent with the accumulated information of all research on this and closely related systems.

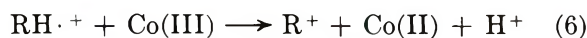
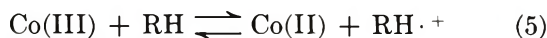
Discussion

The reaction of Co(III) acetate with alkyl aromatic hydrocarbons has been studied in the *absence* of oxygen. Heiba, Dessau, and Koehl⁸ and Sakota, Kamiya, and Ohta⁵ have independently postulated that the rate-determining step is an electron transfer from the aromatic hydrocarbon to Co(III). Heiba, *et al.*, studied the reaction with a competitive technique; in some related cases they were able to identify the epr spectrum of the intermediate radical cation.⁸ Sakota, *et al.*,⁵ studied the Co(III) oxidation of toluene and its derivatives kinetically and found the following rate law

$$-\frac{d[\text{Co(III)}]}{dt} = \frac{k[\text{RH}][\text{Co(III)}]^2}{[\text{Co(II)}]} \quad (4)$$

which is consistent with the following reaction scheme

(9) Co(III) concentration is the experimental total Co(III) concentration and comprises Co(III) in both monomeric and dimeric forms: $[\text{Co(III)}] = [\text{monomer}] + 2[\text{dimer}]$.



If the rate-limiting step is the same in the catalytic autoxidation of alkyl aromatics, a similar inverse dependence on Co(II) acetate concentration would be expected. Morimoto and Ogata² did not look for or observe such a dependence (Eq 1).

The present results also differ from those of Morimoto and Ogata in that no induction period was observed. Measurement of oxygen absorption and Co(III) acetate and toluene concentrations indicated that no induction period occurs when the reaction is initiated by Co(III) acetate. These results are consistent with those of other workers who did not observe an induction period when the autoxidation of *p*-xylene¹⁰ or *p*-toluic acid^{10,11} is similarly initiated. It is possible that Morimoto and Ogata's results were modified by the presence of a retarder. Morimoto and Ogata also observed that the steady-state Co(III) acetate concentration was 57% of the total cobalt present. In Table I, Co(III) acetate concentration varies from 29% [Co]₀ for [Co]₀ = 0.0625 M to 47% [Co]₀ for [Co]₀ = 0.25 M. This variation is consistent with an independent observation in the absence of oxygen that the rate of Co(III) acetate decomposition decreases with increasing Co(III) acetate concentration.³

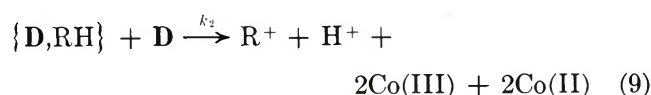
Mechanism

Rate law (2) is consistent with a two-path mechanism in which a cobalt(III) acetate dimer is the oxidant in one path and a cobalt(III) acetate monomer the oxidant in the other. It has previously been proposed that cobalt(III) acetate exists predominantly as a dimer in solution^{3,4,12} and a monomer-dimer equilibrium has been invoked to explain a variety of kinetic results.³⁻⁶ The monomer-dimer equilibrium may be written as



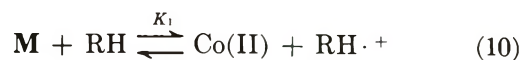
where **D** and **M** represent dimeric and monomeric Co(III) acetate.

The oxidation of RH by **D** probably involves the reversible formation of a complex {**D**,RH} followed by the irreversible, rate-determining reaction of the complex with a further **D** molecule.



The overall reaction is second order with respect to **D**; moreover, Co(II) acetate does not retard the reaction. The oxidation of RH by **M** involves a reversible electron transfer with formation of the radical cation RH·⁺,

followed by the irreversible, rate-determining loss of a proton to give the benzyl radical R·.



The involvement of Co(II) on the right side of equilibrium 10 results in a retardation of the monomer oxidation path by Co(II). The products, R⁺ and R· from (9) and (11) react further in non-rate-determining steps with the eventual formation of the aromatic acid. These steps have been adequately discussed by Morimoto and Ogata.²

Equations 9 and 11 predict that the addition of acetate ion should accelerate the reaction rate whereas the experimental data indicate a slight reduction in rate. However, the addition of acetate ion also was independently shown to accelerate the decomposition of cobaltic acetate,³ consistent with the reduction of cobaltic acetate concentration after the addition of potassium acetate (Figure 3). These compensating effects could not be separated.

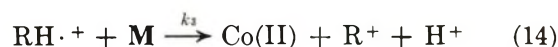
Combining (8), (9), (10), and (11) results in the rate law for the two paths

$$-\frac{d[\text{RH}]}{dt} = k_1 K_1 \frac{[\text{M}][\text{RH}]}{[\text{Co(II)}]} + k_2 K_2 [\text{D}]^2 [\text{RH}] \quad (12)$$

The incorporation of equilibrium 7 and the relationship derived from it results in rate law (2) with

$$k_a = \left(\frac{\sqrt{2}}{2}\right) k_1 K_1 K_D^{1/2}; \quad k_b = \frac{k_2 K_2}{4} \quad (13)$$

It is of interest, however, that the oxidation of RH by **D** is not retarded by Co(II). An alternate mechanism may be written in which only **M** is involved in oxidizing RH, *e.g.*, if equilibrium 10 is followed by reaction 11 and



in competition. Such a mechanism, however, results in a rate law in which Co(II) retardation occurs in both terms, a conclusion not in accord with the experimental results.

The nature of the electron transfer in the two paths bears some discussion. In the case of the monomer (**M**), the electron transfer undoubtedly occurs *via* an *outer-sphere* process. It is unlikely that alkyl aromatics would directly coordinate to Co(III) in acetic acid, a relatively polar solvent, prior to the electron transfer. The *outer-sphere* oxidation of alkyl aro-

(10) P. S. Landis, unpublished work.

(11) Y. Kamiya, M. Ohsu, and N. Ohta, *Kogyo Kagaku Zasshi*, **71**, 999 (1968).

(12) S. S. Lande and J. K. Kochi, *J. Amer. Chem. Soc.*, **90**, 5196 (1968); S. S. Lande, C. D. Falk, and J. K. Kochi, *J. Inorg. Nucl. Chem.*, **33**, 4101 (1971).

matics by a heteropolyion containing cobalt(III) has already been demonstrated.¹³ The oxidation by **M** can occur by conduction through the carboxyl group of a monodentate acetate ligand, with orbitals of the uncoordinated oxygen overlapping with aromatic π orbitals. A similar mechanism can be invoked where alkyl aromatics are more rapidly oxidized by cobalt(III) acetate in the presence of chloride,⁸ in which case the monomeric hexachlorocobaltate(III) ion is formed.¹⁴ The overlap of chloride orbitals with aromatic π orbitals undoubtedly facilitates electron transfer.

The oxidation by the dimer (**D**) is less easily explained, as is the nature of the intermediate "complex" $\{\mathbf{D}, \text{RH}\}$. Dimeric cobalt(III) acetate is thought to contain two bridging hydroxo groups and chelating acetate ligands^{3,5} although Lande and Kochi have proposed that bridging acetate is involved.¹² The electron transfer may occur *via* the bridging hydroxo groups; the need for *two* dimers during the electron transfer may be a requirement for more favorable energetics.

The proposed mechanism is consistent with the rate law derived from experiment and emphasizes the importance of the monomer-dimer equilibrium in solutions of cobalt(III) acetate. The mechanism

specifically accounts for the observed retardation by Co(II), a factor that was neither observed nor explained by Morimoto and Ogata.⁷ Both the monomer and dimer forms of cobalt(III) acetate are therefore active oxidants in the cobalt-catalyzed autoxidation of aromatics in acetic acid. Under the reaction conditions in this study, both terms contribute equally to the observed rate. However, the monomer is a much more reactive species since it is present to only a very small extent. The contribution of the monomer to the overall rate of oxidation would be increased by decreasing the Co(III) concentration. The contribution of the second term may be increased by increasing the Co(III) concentration since the second term is second order whereas the first term is half order with respect to Co(III).

Acknowledgment. The authors are indebted to Dr. P. S. Landis and Dr. E. I. Heiba for helpful discussions. The original oxidation apparatus was designed by Dr. P. S. Landis.

(13) A. W. Chester, *J. Org. Chem.*, **35**, 1797 (1970).

(14) A. W. Chester, E. I. Heiba, R. M. Dessau, and W. J. Koehl, *Inorg. Nucl. Chem. Letters*, **5**, 277 (1969).

Temperature Effects in the Intersystem Crossing Process of Anthracene

by R. P. Widman and J. Robert Huber*

Photochemistry and Spectroscopy Laboratory, Department of Chemistry, Northeastern University, Boston, Massachusetts 02115 (Received December 28, 1971)

Publication costs borne completely by The Journal of Physical Chemistry

The temperature effect in the intersystem crossing process (ISC) of anthracene in a polymethylmethacrylate matrix has been investigated between room temperature and 77°K. The temperature dependence of the ISC rate constant (k_T) can be expressed in terms of an Arrhenius-type function $k_T(T) = k_T^\circ + A \exp(-E/RT)$ with $E = 200 \pm 30 \text{ cm}^{-1}$ and $A = (3 \pm 0.6) \times 10^8 \text{ sec}^{-1}$. On the basis of recent theoretical results by Henry and Siebrand [*J. Chem. Phys.*, **54**, 1072 (1971)], ISC mechanisms consistent with this temperature behavior are discussed. The ISC route $S_1(^1B_{2u}) \rightsquigarrow T_3(^3B_{3u})$, with T_3 slightly above S_1 , involving a purely electronic spin-orbit coupling ($H_{nm}^{(1)}$) appears to be the most favorable mechanism.

The detailed mechanism of intersystem crossing (ISC) of planar polynuclear aromatic hydrocarbons continues to receive much attention from both the experimental and theoretical points of view.¹⁻³ Anthracene, whose intersystem crossing efficiency shows strong dependences on both solvent and temperature, represents a particularly interesting case. The variation of the ISC rate with temperature has been interpreted

in terms of temperature-dependent and temperature-independent processes. For this compound the second triplet state $T_2(^3B_{1g})$ lies energetically very close to the

(1) J. B. Birks, "Photophysics of Aromatic Molecules," Wiley-Interscience, New York, N. Y., 1970.

(2) W. S. Veeman and H. J. Van der Waals, *Mol. Phys.*, **18**, 63 (1970); R. Englman and J. Jortner, *ibid.*, **18**, 145 (1970).

(3) B. R. Henry and W. Siebrand, *J. Chem. Phys.*, **54**, 1072 (1971).

first excited singlet $S_1(^1B_{2u})$.⁴ The shift of the T_2 level relative to the S_1 level can be due to changes in the solvent cage with temperature, and can lead to temperature-independent or temperature-dependent ISC routes, depending on whether T_2 is shifted below or above S_1 .⁵ A recently proposed alternative explanation considers ISC in anthracene and its 9,10 derivatives to involve a temperature-independent process between S_1 and T_2 and a temperature-dependent process between S_1 and a higher lying $T_3(^3B_{3u})$ state.⁶ To provide further information about the still unresolved mechanistic possibilities for the ISC process in anthracene, we have carefully investigated the fluorescence quantum yield (ϕ_F) and the relative ISC quantum efficiency (ϕ_T) as a function of temperature in poly(methyl methacrylate) (PMM) matrices. The experimental findings are discussed on the basis of the recent theoretical results of Henry and Siebrand.³

Experimental Section

Solutions of anthracene (synthetic, zone refined; Eastman) in methyl methacrylate (Eastman) were degassed by the freeze-pump-thaw method and polymerized by standard procedures.⁷ The concentration of the solutions was $<10^{-4} M$. The emission measurements were performed with a spectrophotofluorimeter which is described elsewhere.⁸ The fluorescence quantum yields (ϕ_F) were determined relative to that of 9,10-diphenylanthracene in PMM ($\phi_F = 1.0$). Since changes in the density and in the refractive index of the PMM samples between room temperature and 77°K are very small ($<2\%$), no compensation was made for these effects.⁹ The measurements of ϕ_F in the range 298–77°K were repeated three times using two different excitation wave lengths. The relative quantum yields measured over a given temperature range are estimated to have better than 5% accuracy. Small changes in the absorption spectrum with temperature were taken into consideration. The relative intersystem crossing quantum efficiencies $\phi_T(T)$ were determined by the flash photolysis technique in terms of the initial optical density [$OD_0(\lambda)$] of the triplet-triplet absorption. The flash apparatus employed has been previously described.¹⁰ Cooling and temperature control of the sample were accomplished by the passage of liquid nitrogen through a copper block which held the PMM sample inside a Dewar vessel. An iron-constantan thermocouple attached directly to the sample served to measure the temperature.

Results and Discussion

The temperature dependence of the fluorescence quantum yield (ϕ_F) and of the relative ISC quantum efficiency ($OD_0 \propto \phi_T$) between room temperature and 77°K is shown in Figure 1. Over this range ϕ_F increases by a factor of 2 while ϕ_T decreases by about 45%. For anthracene it has been found that internal

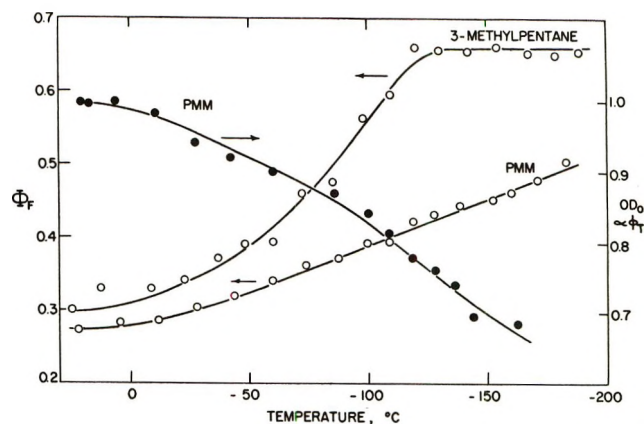


Figure 1. Temperature dependence of the fluorescence quantum yield ϕ_F and the relative intersystem crossing quantum efficiency $\phi_T (\propto OD_0)$ of anthracene in a PMM matrix and in 3-methylpentane (3MP) solution. In both solvents the $\phi_F(T)$ values have been determined relative to the room temperature value. Measurements in PMM were standardized against 9,10-diphenylanthracene in PMM ($\phi_F = 1.00$). Measurements in 3MP were standardized against quinine bisulfate in aqueous 0.1 *N* sulfuric acid ($\phi_F = 0.55$).

conversion ($S_1 \rightsquigarrow S_0$) is negligible¹¹ and that the radiative rate constant k_F is only slightly temperature dependent. Thus, the variation of ϕ_F with temperature is apparently related to changes in the ISC rate constant (k_T) with temperature. If k_T is expressed in terms of the Arrhenius-type function $k_T(T) = k_T^\circ + A \exp(-E/RT)$ (k_T° is the value of k_T at the limiting temperature of which no effect occurs, A is the frequency factor), the temperature dependence of $\phi_F = k_F/(k_F + k_T)$ can be written as

$$\ln(1/\phi_F - 1/\phi_F^\circ) = \ln A' - E/RT \quad (1)$$

where ϕ_F° is the limiting fluorescence quantum yield and $A' = A/k_F$. The value of $\phi_F^\circ = 0.60 \pm 0.05$ was determined by a polynomial regression analysis and extrapolation of the $\phi_F(T)$ data to 0°K. A plot of eq 1 is shown in Figure 2. Clearly, the proposed relationship does not reproduce the experimental findings over the entire temperature region. The plot, however, suggests that two temperature-dependent processes which can be described in the form of eq 1 with different activation energies E are operative. Between 298 and

- (4) R. E. Kellogg, *J. Chem. Phys.*, **44**, 411 (1966).
- (5) T. F. Hunter and R. F. Wyatt, *Chem. Phys. Lett.*, **6**, 221 (1970).
- (6) A. Kearvell and F. Wilkinson, *J. Chim. Phys.*, Special Edition, "Transitions Non Radiatives Dans Les Molecules," 125 (1970).
- (7) F. C. Unterleitner and E. I. Hormats, *J. Phys. Chem.*, **69**, 2516 (1965).
- (8) H. Pownall and J. R. Huber, *J. Amer. Chem. Soc.*, **93**, 6429 (1971).
- (9) D. J. Morantz and T. E. Martin, *Trans. Faraday Soc.*, **65**, 665 (1968).
- (10) J. R. Huber, R. P. Widman, and K. Weiss, *Rev. Sci. Instrum.*, **40**, 1103 (1969).
- (11) A. R. Horrocks and F. Wilkinson, *Proc. Roy. Soc., Ser. A*, **306**, 257 (1968).

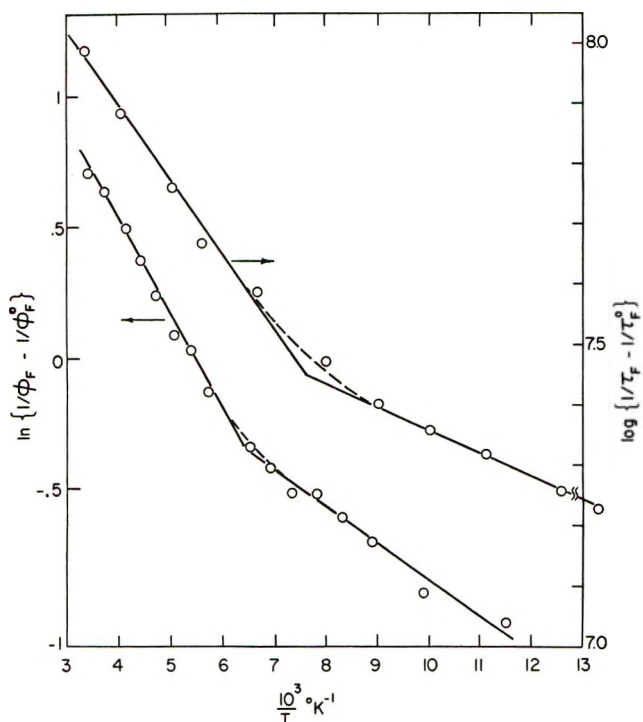


Figure 2. Temperature dependence of the fluorescence quantum yield ϕ_F and the fluorescence lifetime τ_F of anthracene in PMM according to eq 1 and 2, respectively. (The lifetime data have been taken from ref 12.)

ca. 150°K a good fit is obtained with $E_1 = 220 \text{ cm}^{-1}$, and below 150°K the data can be accommodated with $E_2 = 80 \text{ cm}^{-1}$. As expected, the variation of the triplet-triplet absorption $OD_0(T)$ with temperature (cf. Figure 1), when treated in an analogous manner shows parallel behavior to that of $\phi_F(T)$. In the temperature range 298–140°K the $OD_0(T)$ data provide an activation energy $E_1 = 170 \text{ cm}^{-1}$, and between 140–80°K an energy $E_2 = 80 \text{ cm}^{-1}$. To compare our findings with previously published data and to reveal the role played by the history of the matrix, the fluorescence decay data of Logan, *et al.*,¹² was treated by the procedure outlined above. The temperature dependence of the measured fluorescence lifetime $\tau_F(T)$ is then

$$\ln(1/\tau_F - 1/\tau_F^0) = \ln A - E/RT \quad (2)$$

where τ_F^0 is the lifetime at ca. 4°K. The plot of eq 2 (Figure 2) is seen to be essentially linear between 298 and 150°K with $E_1 = 190 \text{ cm}^{-1}$, and between 150 and 50°K with $E_2 = 60 \text{ cm}^{-1}$. The agreement of these apparent activation energies with those given above is good. It is noteworthy that ϕ_F for anthracene in 3-methylpentene (3MP) also increases by a factor of ca. 2 between 230 and 140°K (cf. Figure 1). Below 140°K, however, ϕ_F stays essentially constant. A similar result was recently reported for methyltetrahydrofuran (MTHF) solutions of anthracene.⁵ Our data suggest that two temperature-dependent processes are involved in ISC for anthracene. Above $\sim 140^\circ\text{K}$ a

process with $E_1 = 200 \pm 30 \text{ cm}^{-1}$ and $A_1 = (3 \pm 0.6) \times 10^8 \text{ sec}^{-1}$ appears to be dominant, while below this temperature there is a process with $E_2 = 80 \pm 20 \text{ cm}^{-1}$ and $A_2 = (7 \pm 2) \times 10^7 \text{ sec}^{-1}$. The low-temperature process, which will not be discussed in detail here, probably involves a specific interaction between the solute molecule and the PMM solvent cage. This explanation is suggested by the fact that in 3MP solution as well as in MTHF solution, no temperature effect is observed in this range (cf. Figure 1).

With respect to ISC mechanisms consistent with the first process, we may utilize the results of the theoretical study of ISC in planar aromatic hydrocarbons by Henry and Siebrand.³ These authors have partitioned the matrix element $H_{nm} = \langle {}^1\psi_n | T_N + H_{so} | {}^3\psi_m \rangle$ which governs the ISC process (T_N is the nuclear kinetic-energy operator, H_{so} the spin-orbit coupling operator) into the three components $H_{nm} = H_{nm}^{(1)} + H_{nm}^{(2)} + H_{nm}^{(3)}$, each of which represents a specific coupling mechanism. For this model $H_{nm}^{(1)}$ (a three-center integral) describes the purely electronic spin-orbit coupling between $\pi\pi$ states and $H_{nm}^{(2)}$ represents a vibronically induced Herzberg-Teller mechanism which can be expressed in terms of three-center spin-orbit integrals between $\pi\pi$ states and one-center vibronic integrals corresponding to C-C stretching modes. The third term $H_{nm}^{(3)}$, which represents the vibronically induced breakdown of the Born-Oppenheimer approximation is dominated by one-center spin-orbit integrals between $\pi\pi$ and $\pi\sigma$ states and by vibronic integrals corresponding to out-of-plane vibrations. The contribution of each of the three mechanisms in the ISC of anthracene (D_{2h} symmetry) between S_1 (26,470 cm^{-1}) and the two known triplets T_1 ($\sim 14,400 \text{ cm}^{-1}$) and T_2 ($\sim 26,000 \text{ cm}^{-1}$)⁴ may be analyzed in terms of symmetry restrictions and consistency with previous and present experimental findings. It is readily established that the term $H_{nm}^{(1)}$ between the $S_1({}^1B_{2u})$ and $T_1({}^3B_{2u})$ or $T_2({}^3B_{1g})$ states vanishes by symmetry. The term $H_{nm}^{(2)}$, which involves T_1 can be discounted since the corresponding mechanism would lead to in-plane polarization of the phosphorescence and the depopulation of T_1 via the τ_z spin level. This is in disagreement with the experimental results.^{13,14} On the other hand, the $H_{nm}^{(2)}$ process involving the T_2 state would require an ${}^1A_g \pi\pi$ state to be vibronically coupled to S_1 . The lowest 1A_g state is predicted to be 6.7 eV above the ground state, *i.e.*, 3.4 eV above S_1 , according to semiempirical calculations.¹⁵ Vibronic coupling over such a large energy gap is expected to be weak. Moreover, the observed temperature effect of ISC cannot be accounted for by this

(12) L. M. Logan, I. H. Munro, D. F. Williams, and F. R. Lipsett, "Molecular Luminescence," E. L. Lim, Ed., W. A. Benjamin, New York, N. Y., 1970, p 773.

(13) V. G. Krishna and L. Goodman, *J. Chem. Phys.*, **20**, 765 (1952).

(14) R. H. Clarke, *Chem. Phys. Lett.*, **6**, 413 (1970).

(15) R. Pariser, *J. Chem. Phys.*, **24**, 250 (1956).

$H_{nm}^{(2)}$ mechanism.³ The third mechanism, described by the element $H_{nm}^{(3)}$, involving the states S_1 and T_2 (T_1 to a much lesser degree) appears to be consistent with the experimental results. This mechanism is induced by low frequency out-of-plane bending modes, and it is therefore expected to show a significant temperature dependence.¹⁶ Hence, one might be tempted to attribute the observed temperature dependence of k_T to the change in the Boltzmann distribution of the active out-of-plane bending mode of anthracene. However, the lack of any temperature effect in 3MP and MTHF solutions below 140°K is incompatible with this mechanism and forces us to disregard it.

A reasonable explanation of the temperature dependence of k_T is possible if a third triplet level, slightly above S_1 , is taken into consideration. Such a state (T_3) with a ${}^3B_{3u}$ symmetry was predicted by Pariser.¹⁵ The transition $S_1({}^1B_{2u}) \rightsquigarrow T_3({}^3B_{3u})$ is orbitally allowed and should, therefore, be dominated by the first-order mechanism with $H_{nm}^{(1)} = \langle {}^3\phi_m({}^3B_{3u})/H_{so}^2(b_{1g})/{}^1\phi_n({}^1B_{2u}) \rangle$. Although the element $H_{nm}^{(1)}$ contains no explicitly temperature-dependent terms the population of a state T_3 which is energetically slightly above the S_1 state is expected to require an activation energy. This implies that the measured apparent activation energy $E_1 \approx 200 \text{ cm}^{-1}$ corresponds roughly to the energy gap between the S_1 and T_3 states. Then, if kT is smaller

than E_1 , the $S_1 \rightsquigarrow T_3$ route is no longer available and ISC might occur between S_1 and T_2 by the $H_{nm}^{(2)}$ mechanism and between S_1 and T_2 or T_1 by a $H_{nm}^{(3)}$ mechanism.

Finally, we recognize that a small temperature effect due to a level shift between the S_1 and T_2 or T_3 states cannot be unequivocally excluded from consideration. To estimate the possible extent of such level shifts we have measured the O-O bands of the absorption and emission of anthracene,¹⁷ phenanthrene, and naphthalene in PMM between 298 and 77°K. In general, all the O-O transitions are red shifted by $80 \pm 30 \text{ cm}^{-1}$. For a given compound, the relative shift among the O-O bands of absorption, fluorescence, and phosphorescence was always smaller than 60 cm^{-1} . Thus under our condition, the relative shifts between the energy levels are expected to be small, and they are not likely to play a dominant role in the ISC process.

Acknowledgment. This research was supported by the Air Force Cambridge Research Laboratories, Office of Aerospace Research, under Contract No. F19628-67-C-0118. Assistance through numerous discussions with Professor Karl Weiss is gratefully acknowledged.

(16) $k_T \propto \coth(h\nu_a/2kT)$ where ν_a is the frequency of the active out-of-plane vibration; see A. Albrecht, *J. Chem. Phys.*, **33**, 156 (1960).

(17) Only absorption and fluorescence for anthracene.

Photoredox Chemistry of Bis(2,9-dimethyl-1,10-phenanthroline)copper(II)

Complexes in Aqueous and Methanolic Media^{1a}

by S. Sundararajan and E. L. Wehry*^{1b}

Departments of Chemistry, University of Tennessee, Knoxville, Tennessee 37916, and Indiana University, Bloomington, Indiana 47401 (Received August 2, 1971)

Publication costs borne completely by The Journal of Physical Chemistry

Photolysis of bis(2,9-dimethyl-1,10-phenanthroline)copper(II) in aqueous or methanolic solution in the 27,000–40,000-cm⁻¹ frequency range produces the corresponding Cu(I) complex. The primary photoprocess is postulated to be homolytic cleavage of a Cu(II)–solvent coordinate bond; secondary reactions of oxidized solvent species with Cu(II) complexes and halide counterions affect product quantum yields. The Cu(I) product quantum yield is constant throughout the (π , π^*) and ligand \rightarrow metal charge-transfer spectral regions of Cu(dmp)₂²⁺, but the doublet (d, d) states are photochemically inert. A spin-allowed ligand \rightarrow metal charge-transfer excited state is concluded to be photoreactive; rates of radiationless relaxation thereto from higher lying excited states are concluded to be rapid. The analogous bis complex of Cu(II) with unsubstituted phenanthroline is photochemically unreactive; this observation is discussed in terms of structural differences in the two Cu(II) complexes.

Introduction

Although photochemical oxidation–reduction reactions of transition metal complexes are now receiving considerable study,² little attention has been devoted to the photoredox chemistry of copper complexes.³ Because the electronic spectra of complexes of Cu(I) and Cu(II) with 1,10-phenanthroline (phen) and 2,9-dimethyl-1,10-phenanthroline (dmp) have been treated in detail,⁴ these complexes represent suitable subjects for photochemical study. Complexes of dmp with Cu(II) are substantially stronger oxidizing agents than the corresponding complexes with the parent ligand, phen.⁵ While both Cu(phen)₂⁺ and Cu(dmp)₂⁺ are believed to be tetrahedral complexes,^{5a} Cu(phen)₂XY (X⁻ and Y⁻ = monodentate anions) exists in either a cis distorted-octahedral or trigonal-bipyramidal structure, depending upon the identity of X⁻ and Y⁻.⁶ Neither of these structures is energetically favorable for Cu(dmp)₂²⁺, owing to steric hindrance caused by the methyl substituents adjoining the chelating nitrogens in dmp. It is therefore probable^{5a} that the chelating nitrogens in Cu(dmp)₂²⁺ assume a flattened tetrahedral geometry. The energy required to convert this structure to the tetrahedral arrangement favored in the Cu(I) complexes is correspondingly smaller for Cu(dmp)₂²⁺ than for Cu(phen)₂²⁺, consistent with the greater ease of reduction of the former. Because the electronic spectra⁴ of Cu(dmp)₂²⁺ are similar, while their thermal redox properties⁵ and structures^{5,6} are significantly different, it was believed that a comparative investigation of the photochemistry of complexes of copper with dmp and phen would be informative with respect to correlations of both electronic spectra and structural features with photodecomposition modes.

Experimental Section

Materials. The compounds Cu(dmp)₂X₂, Cu(dmp)₂X, Cu(dmp)X₂, Cu(dmp)X,^{5a} Cu(phen)₂X₂, Cu(phen)₂X⁶ (X⁻ = Cl⁻, Br⁻, ClO₄⁻), and potassium ferrioxalate⁷ were prepared and purified by published procedures. Samples of dmp and phen were first purified by recrystallization from 25% aqueous ethanol followed by vacuum sublimation. Copper salts were recrystallized from dilute aqueous solutions of the appropriate mineral acid. Solid complexes were stored in the dark *in vacuo*. Sodium benzoate, methyl meth-

(1) (a) A preliminary account of this work has appeared: S. Sundararajan and E. L. Wehry, *J. Chem. Soc. D*, 267 (1970); (b) University of Tennessee.

(2) For recent reviews, see (a) V. Balzani and V. Carassiti, "Photochemistry of Coordination Compounds," Academic Press, London, 1970; (b) J. F. Endicott, *Israel J. Chem.*, 8, 209 (1970); (c) D. Valentine, Jr., *Annu. Surv. Photochem.*, 2, 341 (1970); 1, 457 (1969); (d) D. Phillips, "Photochemistry" (Chem. Soc. Specialist Periodical Report), 2, 243 (1971); 1, 124 (1970).

(3) Previous studies of Cu(II) complex photochemistry include (a) H. D. Gafney and R. L. Lintvedt, *J. Amer. Chem. Soc.*, 93, 1623 (1971); (b) G. A. Shagisultanova and L. A. Il'yukevich, *Russ. J. Inorg. Chem.*, 11, 510 (1966); (c) G. A. Shagisultanova, L. A. Il'yukevich, and L. I. Burdyko, *Russ. J. Phys. Chem.*, 39, 1458 (1965).

(4) (a) P. Day and N. Sanders, *J. Chem. Soc. A*, 1530, 1536 (1967); (b) R. J. P. Williams in "Biochemistry of Copper," J. Peisach, P. Aisen, and W. Blumberg, Ed., Academic Press, New York, N. Y., 1966, p 131; (c) A. S. Brill, R. B. Martin, and R. J. P. Williams in "Electronic Aspects of Biochemistry," B. Pullman, Ed., Academic Press, New York, N. Y., 1964, p 519.

(5) J. R. Hall, N. K. Marchant, and R. A. Plowman, *Aust. J. Chem.*, 15, 480 (1962); 16, 34 (1963); (b) B. R. James and R. J. P. Williams, *J. Chem. Soc.*, 2007 (1961); (c) R. Resnik, T. Cohen, and Q. Fernando, *J. Amer. Chem. Soc.*, 83, 3344 (1961).

(6) B. J. Hathaway, I. M. Proctor, R. C. Slade, and A. A. G. Tomlinson, *J. Chem. Soc. A*, 2219 (1969).

(7) C. G. Hatchard and C. A. Parker, *Proc. Roy. Soc., Ser. A*, 235, 518 (1953).

acrylate, and acrylonitrile were purified as previously described.⁸

Methanol was distilled over magnesium methoxide. The purified alcohol was stored in the dark over Molecular Sieves. Manipulations of methanolic solutions were performed in a drybox in an atmosphere of dry nitrogen. Methanol was checked for the presence of carbonyl impurities by fluorescence; any sample which yielded detectable luminescence when excited at $32,000\text{ cm}^{-1}$ ⁹ with a 150-W xenon lamp was discarded. Water was distilled in a borosilicate glass apparatus and stored in polyethylene containers.

Methods. Quantum yields were measured with a Hanovia 901C-1 150-W xenon lamp dispersed by a Bausch and Lomb 33-86-45 monochromator. Incident intensities were *ca.* 10^{14} photons sec^{-1} , and the incident bandwidth was 8 nm. Solutions were stirred with small magnetic stirring bars during photolyses. Ferrioxalate actinometry⁷ was employed. Samples were irradiated in 1-cm rectangular cells thermostated at $25.0 \pm 0.1^\circ$. In determination of product quantum yields, conversion of photolyte to products never exceeded 4%. Solutions of $\text{Cu}(\text{dmp})_2^{2+}$ in methanol and water exhibited no detectable change in visible absorption spectrum over 24-hr periods following preparation; the maximum duration of exposure in any quantum yield determination was 6 hr. When necessary, solutions were degassed by freeze-thaw cycles.⁹

Analyses for Cu(I) complexes proceeded by absorption spectrophotometry at 450 nm. Both $\text{Cu}(\text{dmp})_2^+$ and $\text{Cu}(\text{dmp})^+$ were generally detected as photoreduction products in both methanol and water. The following molar absorptivities were used to compute the concentrations of the various complexes: in methanol, for $\text{Cu}(\text{dmp})_2^+$, ϵ_{450} 7530; for $\text{Cu}(\text{dmp})^+$, ϵ_{450} 3750; in water, for $\text{Cu}(\text{dmp})_2^+$, ϵ_{450} 6160; for $\text{Cu}(\text{dmp})^+$, ϵ_{450} 3420. Concentrations of $\text{Cu}(\text{dmp})_2^{2+}$ remaining in solution were determined by absorption spectrophotometry at 740 nm (in water, ϵ_{740} 100; in methanol, ϵ_{740} 180). Other products formed upon photolysis of Cu(II) complexes in methanolic media (formaldehyde,^{10a} formic acid,^{10b} and ethylene glycol^{10c}) were determined by published procedures.¹⁰

Techniques employed in chemical scavenging experiments with vinyl monomers and benzoate have been described.⁸ A Hitachi RMU-6E mass spectrometer was used to examine solid reaction products obtained in the benzoate experiments.

Ion-exchange and conductance techniques were employed to determine whether $\text{Cu}(\text{dmp})_2\text{X}_2$ and $\text{Cu}(\text{dmp})_2\text{X}$ ($\text{X}^- = \text{Cl}^-, \text{Br}^-, \text{ClO}_4^-$) were dissociated in aqueous and methanolic solutions. Conductivities were measured with an Industrial Instruments RC 16B2 bridge and a cell with bright platinum electrodes. In cation-exchange experiments, a solution of the complex of interest was introduced into a column containing the Na^+ form (for water) or $(\text{C}_4\text{H}_9)_4\text{N}^+$ form (for

methanol) of Dowex 50W-X8 cation resin. Anions were eluted with pure solvent and determined by potentiometric silver titration. In anion-exchange experiments, a solution of the complex was stirred in a beaker with ion-exchange cellulose (DEAE Type 20; Schleicher and Schuell); after 1 hr of contact, the solution was decanted from the cellulose. The recovered cellulose was then washed with ten 100-ml portions of pure solvent; the washings were concentrated to a known volume and the anions determined by potentiometric silver titration.

A solvent-extraction procedure was used to determine the concentration of uncomplexed dmp present in aqueous solutions of $\text{Cu}(\text{dmp})_2^{2+}$. The solution was contacted in an equal volume of benzene-*n*-hexane (1:1); the mixture was agitated and the organic phase was removed. The process was repeated six times. The collected organic phases were then contacted with an aqueous solution containing CuCl_2 and hydroxylamine hydrochloride. The dmp was extracted back into the aqueous phase as $\text{Cu}(\text{dmp})^+$, the concentration of which was determined spectrophotometrically. Recovery of free dmp by this procedure was *ca.* 95% for standard aqueous dmp solutions.

Results

Dissociation of Counterions in $\text{Cu}(\text{dmp})_2\text{X}_2$. Because Cu(II)-dmp complexes are five-coordinate in the solid¹¹ and in nitromethane solution,^{5a} it was necessary to establish the extent of counterion dissociation in water and methanol. In water, cation and anion exchange indicated that dissociation of X^- ($= \text{Cl}^-, \text{Br}^-, \text{ClO}_4^-$) was essentially complete at the concentrations employed in photochemical runs. In cation-exchange experiments employing 100 ml of solutions $3.50 \times 10^{-3}\text{ M}$ in $\text{Cu}(\text{dmp})_2\text{X}_2$ (total moles of $\text{X}^- = 7.00 \times 10^{-4}$), the quantities of X^- recovered in the effluent (which contained no detectable quantity of copper complexes) were never less than 6.98×10^{-4} mol. Similarly, in anion-exchange experiments, at least 97% of the total possible quantity of anion was recovered in the washings from the cellulose exchanger (which were likewise free of copper complexes). Molar conductivities of $\text{Cu}(\text{dmp})_2\text{Cl}_2$ ($215\text{ ohm}^{-1}\text{ cm}^2\text{ mole}^{-1}$), $\text{Cu}(\text{dmp})_2\text{Br}_2$ ($209\text{ ohm}^{-1}\text{ cm}^2\text{ mole}^{-1}$), and $\text{Cu}(\text{dmp})_2(\text{ClO}_4)_2$ ($219\text{ ohm}^{-1}\text{ cm}^2\text{ mole}^{-1}$) were in the range expected for a 2:1 electrolyte¹² in aqueous media.

(8) (a) E. L. Wehry and R. A. Ward, *Inorg. Chem.*, **10**, 2660 (1971); (b) L. E. Cox, D. G. Peters, and E. L. Wehry, *J. Inorg. Nucl. Chem.*, **34**, 297 (1972).

(9) M. Goldman and E. L. Wehry, *Anal. Chem.*, **42**, 1178 (1970).

(10) (a) C. E. Bricker and H. R. Johnson, *Ind. Eng. Chem., Anal. Ed.*, **17**, 400 (1945); (b) S. U. Choi and N. N. Lichtin, *J. Amer. Chem. Soc.*, **86**, 3948 (1964); (c) N. N. Lichtin, *J. Phys. Chem.*, **63**, 1449 (1959).

(11) D. E. Billing, R. J. Dudley, B. J. Hathaway, and A. A. G. Tomlinson, *J. Chem. Soc. A*, 691 (1971).

(12) M. J. Jones, "Elementary Coordination Chemistry," Prentice-Hall, Englewood Cliffs, N. J., 1964, p 254.

Analogous results were obtained in *methanol*. In cation-exchange experiments, employing 100 ml of solutions $3.50 \times 10^{-3} M$ in $\text{Cu}(\text{dmp})_2\text{Cl}_2$ or $\text{Cu}(\text{dmp})_2\text{Br}_2$ (total quantity of halide = 7.00×10^{-4} mole), recoveries of Cl^- ($6.97 \pm 0.04 \times 10^{-4}$ moles, mean of five determinations) and Br^- ($6.96 \pm 0.04 \times 10^{-4}$ moles, mean of six determinations) in the effluents (which were free of copper complexes) indicated essentially complete counterion dissociation in the complexes. In anion-exchange experiments, employing 200 ml of solutions $3.00 \times 10^{-3} M$ in $\text{Cu}(\text{dmp})_2\text{X}_2$ (total quantity of halide = 1.20×10^{-3} mole), recoveries of Cl^- ($1.14 \pm 0.08 \times 10^{-3}$ moles, mean of four determinations) and Br^- ($1.15 \pm 0.06 \times 10^{-3}$ moles, mean of five determinations) in the washings indicated virtually complete counterion dissociation in methanol.

On the basis of these data, and the reported tendency of $\text{Cu}(\text{II})$ -dmp complexes to exhibit five-coordination,^{5a,11} we represent $\text{Cu}(\text{dmp})_2^{2+}$ as $\text{Cu}(\text{dmp})_2(\text{H}_2\text{O})^{2+}$ in aqueous media, and as $\text{Cu}(\text{dmp})_2(\text{CH}_3\text{OH})^{2+}$ in methanolic solution.

Thermal Dissociation of dmp from $\text{Cu}(\text{dmp})_2^{2+}$. Solvent extraction (see *Experimental*) of aqueous solutions $3.50 \times 10^{-3} F$ in $\text{Cu}(\text{dmp})_2(\text{ClO}_4)_2$ or $\text{Cu}(\text{dmp})_2\text{Cl}_2$ did not indicate the presence of detectable quantities of uncomplexed dmp. The sensitivity of the combined extraction-spectrophotometric procedure was such that a concentration of dmp equal to, or greater than, $4.50 \times 10^{-6} M$ would have been detected. Accordingly, the extent of dissociation of $\text{Cu}(\text{dmp})_2^{2+}$ to $\text{Cu}(\text{dmp})_2^+$ (or to the aquo ion) cannot have been greater than 0.08%.

In methanolic solution, 100-ml aliquots of solutions $3.50 \times 10^{-3} M$ in $\text{Cu}(\text{dmp})_2\text{Cl}_2$ were sorbed onto Dowex 50W-X8 cation resin; the effluent (which contained Cl^- ; *vide supra*) was tested for free dmp by addition of Cu^{2+} , followed by prolonged heating.^{5a} In no case was any detectable quantity of free dmp detected. Use of standard dmp solutions revealed that this analytical method was capable of detecting 4.00×10^{-6} mol of dmp, and we therefore conclude that the extent of dissociation of $\text{Cu}(\text{dmp})_2^{2+}$ to $\text{Cu}(\text{dmp})_2^+$ (or to the free ion) cannot have been greater than 0.06% in methanol.

Thermal Dissociation of dmp from $\text{Cu}(\text{dmp})_2^+$. Because spectrophotometric analyses were employed to establish product quantum yields, it was necessary to ascertain the stability of $\text{Cu}(\text{dmp})_2^+$ species in water and methanol. In water, solvent-extraction experiments established that dissociation of $\text{Cu}(\text{dmp})_2^+$, to $\text{Cu}(\text{dmp})^+$ and free dmp, was negligible. For the thermal reaction



the equilibrium constant at 25° in methanolic solution was determined spectrophotometrically to be $2.7 \times 10^{-6} M$. Therefore, for all product quantum yields in methanol, the measured absorbance at 450 nm and the

equilibrium constant for reaction 1 were used to compute quantum yields ($\Phi_{\text{Cu(I)}}$) for *total* Cu(I) species (*i.e.* $\text{Cu}(\text{dmp})_2^+ + \text{Cu}(\text{dmp})^+$), rather than for the individual complexes. Dissociation of $\text{Cu}(\text{dmp})^+$ to the solvated Cu(I) ion and free dmp was negligible, as demonstrated by spectrophotometric analysis of the effluent obtained from a cation-exchange column loaded with a methanolic solution $4.00 \times 10^{-3} M$ in $\text{Cu}(\text{dmp})\text{-Cl}$.

Photochemical Products and Stoichiometry. In water, solutions of $\text{Cu}(\text{dmp})_2^{2+}$ (pH 5.8, adjusted with concentrated HClO_4) underwent photoreduction, forming a mixture of $\text{Cu}(\text{dmp})_2^+$ and $\text{Cu}(\text{dmp})^+$. Solvent extraction showed that no appreciable quantity of "free" dmp was produced. No discernible quantities of metallic copper,^{3a} uncomplexed Cu(I), or uncomplexed Cu(II) were produced in the photoreduction. From spectrophotometry ($\lambda = 450 \text{ nm}$), it was concluded that the product distribution was *ca.* 70% $\text{Cu}(\text{dmp})_2^+$ and 30% $\text{Cu}(\text{dmp})^+$. In contrast, thermal reduction of $\text{Cu}(\text{dmp})_2^{2+}$, which proceeded at a measurable rate in water at 60°, produced >99% conversion of $\text{Cu}(\text{dmp})_2^{2+}$ to $\text{Cu}(\text{dmp})_2^+$. Ultraviolet spectral measurements ($\lambda 278 \text{ nm}$) showed that photoreduction of $\text{Cu}(\text{dmp})_2^{2+}$ caused partial conversion of dmp to non-absorbing products. The quantity of dmp destroyed was equal, within $\pm 2\%$, to the quantity of $\text{Cu}(\text{dmp})^+$ present at equilibrium. Because the quantity of $\text{Cu}(\text{dmp})_2^+$ plus $\text{Cu}(\text{dmp})^+$ formed was equal to that of $\text{Cu}(\text{dmp})_2^{2+}$ destroyed, all product quantum yields for aqueous systems refer to the sum of the two Cu(I) complexes ($\Phi_{\text{Cu(I)}}$) unless indicated otherwise.

Similar observations have been reported for photoreduction of $\text{Fe}(\text{phen})_3^{3+}$ in aqueous media, wherein it was concluded^{8a} that hydroxyl radical attack upon phen¹³ resulted in its destruction. Aqueous solutions $3.5 \times 10^{-2} M$ in H_2O_2 and $1.01 \times 10^{-5} M$ in dmp were irradiated at $37,800 \text{ cm}^{-1}$, at which frequency H_2O_2 photodecomposes to hydroxyl radicals.^{14,15} Ultraviolet spectral analyses of these solutions indicated rapid destruction of dmp to nonabsorbing products; in the absence of H_2O_2 , no detectable decomposition of dmp occurred. Similarly, OH radicals generated by photolysis of H_2O_2 rapidly attacked $\text{Cu}(\text{dmp})_2^+$, forming $\text{Cu}(\text{dmp})^+$; however, both $\text{Cu}(\text{dmp})_2^{2+}$ and $\text{Cu}(\text{dmp})^+$ decomposed much less rapidly under these conditions.

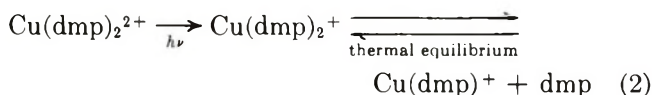
In *methanol*, photolysis of $\text{Cu}(\text{dmp})_2^{2+}$ produced a mixture of $\text{Cu}(\text{dmp})_2^+$ and $\text{Cu}(\text{dmp})^+$, the relative concentrations of which were equal, within $\pm 2\%$, to those

(13) A. A. Green, J. O. Edwards, and P. Jones, *Inorg. Chem.*, **5**, 1858 (1966).

(14) D. H. Volman and J. C. Chen, *J. Amer. Chem. Soc.*, **81**, 4141 (1959).

(15) In this experiment, the fractions of light absorbed by hydrogen peroxide and dmp were virtually equal (both species having absorbances, in 1-cm cells, of *ca.* 0.35 at $37,800 \text{ cm}^{-1}$ at the concentrations employed).

predicted from the equilibrium constant for thermal dmp release by $\text{Cu}(\text{dmp})_2^+$. No detectable quantity of dmp was destroyed, even upon extensive photolysis (>75% conversion of Cu(II) to Cu(I)), and no detectable amounts of $\text{Cu}(\text{dmp})_2^{2+}$, uncomplexed Cu(I), or uncomplexed Cu(II) were produced. Therefore, we represent the photoreduction in methanol as



An appreciable decrease in "pH" (measured with a glass electrode¹⁶) accompanied the photoreduction. Formaldehyde was detected as a product of photoreduction of $\text{Cu}(\text{dmp})_2^{2+}$ in methanol, but neither ethylene glycol nor formic acid was produced in detectable quantity.

Quantum Yields. In water, the quantum yield for formation of Cu(I) species ($\text{Cu}(\text{dmp})_2^+ + \text{Cu}(\text{dmp})^+$) was strongly frequency dependent (Figure 1). At frequencies less than $26,000 \text{ cm}^{-1}$, $\Phi_{\text{Cu(I)}}$ was less than 3×10^{-6} . A sharp increase in $\Phi_{\text{Cu(I)}}$ was observed in the $26,000\text{--}27,500\text{-cm}^{-1}$ region; above $27,500 \text{ cm}^{-1}$, $\Phi_{\text{Cu(I)}}$ was independent of further increases in frequency. Quantum yields were unaffected by changes in the counterion (Br^- , Cl^- , or ClO_4^-), or by addition of fivefold molar excesses of NaBr, NaCl, or NaClO_4 . All points in Figure 1 were determined using an incident intensity of $1.05 \pm 0.05 \times 10^{14}$ photons sec^{-1} .

Because $\Phi_{\text{Cu(I)}}$ in water was quite small (ca. 10^{-3}), it was important to establish that the measured $\Phi_{\text{Cu(I)}}$ did not in fact represent photolysis of a thermal decomposition product of $\text{Cu}(\text{dmp})_2^{2+}$ or of a trace impurity. We do not consider photolysis of thermal decomposition products ($\text{Cu}(\text{dmp})_2^+$ or the aquo Cu(II) ion) to be responsible for the observed photoreaction. As noted previously, thermal ligand release by $\text{Cu}(\text{dmp})_2^{2+}$ proceeds only to a very slight extent (less than 0.1%) in aqueous solution. Furthermore, photoreduction quantum yields for $\text{Cu}(\text{dmp})_2^{2+}$ in aqueous media were smaller, by a factor of 3, than those for $\text{Cu}(\text{dmp})_2^{2+}$, and aqueous solutions of $\text{Cu}(\text{ClO}_4)_2$ exhibited no detectable photochemistry whatsoever under our conditions of incident frequency and intensity.¹⁷ That the observed quantum yields may represent photolysis of a trace impurity cannot be rigorously excluded. However, the observed quantum yields were quite reproducible for different preparations involving different counterions. For $\bar{\nu} = 28,600 \text{ cm}^{-1}$ and $I_a = 1.05 \pm 0.05$ photons sec^{-1} , for $\text{Cu}(\text{dmp})_2\text{Cl}_2$, $\Phi_{\text{Cu(I)}} = 1.1 \pm 0.1 \times 10^{-3}$ (mean of 6 determinations); for $\text{Cu}(\text{dmp})_2\text{Br}_2$, $\Phi_{\text{Cu(I)}} = 1.1 \pm 0.1 \times 10^{-3}$ (mean of 6 determinations); and for $\text{Cu}(\text{dmp})_2(\text{ClO}_4)_2$, $\Phi_{\text{Cu(I)}} = 1.12 \pm 0.04 \times 10^{-3}$ (mean of 13 determinations). Different samples of dmp were used in preparation of each of these complexes, and the water used in each case was distilled in a different apparatus and stored in different (polyethylene) containers. This degree of reproduc-

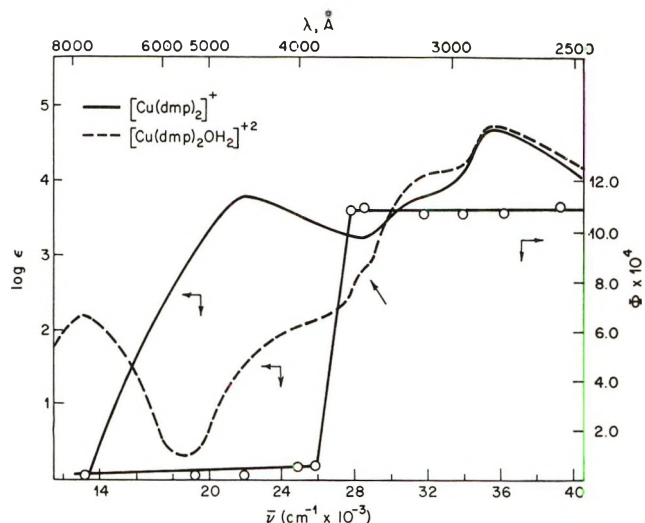


Figure 1. Electronic spectra of aqueous solutions of $\text{Cu}(\text{dmp})_2\text{OH}_2^{2+}$ and $\text{Cu}(\text{dmp})_2^{2+}$ (left ordinate); variation of Φ for appearance of total Cu(I) species with incident frequency (right ordinate). Charge-transfer band in $\text{Cu}(\text{dmp})_2\text{OH}_2^{2+}$ is indicated by arrow. In all Φ determinations, $I_a = 1.05 \pm 0.05 \times 10^{14}$ photons sec^{-1} .

ibility would not be anticipated if photolysis of a trace impurity were responsible for the measured product yields.

Product yields, $\Phi_{\text{Cu(I)}}$, in water decreased upon increases in either the incident intensity or initial concentration of $\text{Cu}(\text{dmp})_2^{2+}$ (Figure 2). At constant initial $[\text{Cu}(\text{dmp})_2^{2+}]$, the stoichiometry of conversion of $\text{Cu}(\text{dmp})_2^{2+}$ to $\text{Cu}(\text{dmp})_2^+$ decreased with increasing I_a ; e.g., when $[\text{Cu}(\text{dmp})_2^{2+}] = 3.50 \times 10^{-3} \text{ M}$ and $I_a = 2 \times 10^{13}$ photons sec^{-1} , the ratio of $\text{Cu}(\text{dmp})_2^+$ to $\text{Cu}(\text{dmp})^+$ in the final product mixture was >20, while, at the same initial $\text{Cu}(\text{dmp})_2^{2+}$ concentration but $I_a = 1.1 \times 10^{14}$ photons sec^{-1} , the $\text{Cu}(\text{dmp})_2^+/\text{Cu}(\text{dmp})^+$ product ratio was only 2.3.

In methanol, product quantum yields, $\Phi_{\text{Cu(I)}}$, were substantially larger than those observed in water. Quantum yields for formation of Cu(I) and formaldehyde were larger for the chloride salt of $\text{Cu}(\text{dmp})_2^{2+}$ than for the bromide, but the ratio of $\Phi_{\text{Cu(I)}}$ to $\Phi_{\text{CH}_2\text{O}}$ was not affected significantly by changing the counterion (Table I). The perchlorate salt of $\text{Cu}(\text{dmp})_2^{2+}$ was insufficiently soluble in methanol for quantum yields to be acquired. Product quantum yields in methanol varied with incident frequency in methanol in a manner very similar to that observed in water (compare Figures 1 and 3).

Product quantum yields decreased upon addition of LiCl or LiBr to methanolic solutions of $\text{Cu}(\text{dmp})_2\text{Cl}_2$ (Figure 4) or $\text{Cu}(\text{dmp})_2\text{Br}_2$. The value of $\Phi_{\text{Cu(I)}}$ attained a plateau in the presence of large excesses of

(16) R. G. Bates, M. Paabo, and R. A. Robinson, *J. Phys. Chem.*, **67**, 1833 (1963).

(17) S. Sundararajan, Ph.D. Dissertation, Indiana University, 1971.

Table I: Quantum Yields for Photoreduction of $\text{Cu}(\text{dmp})_2\text{X}_2$ in Methanol^a

| X ⁻ | $\Phi_{\text{Cu(I)}}^b$ | $\Phi_{\text{CH}_2\text{O}}$ | $\Phi_{\text{Cu(I)}}/\Phi_{\text{CH}_2\text{O}}$ |
|-----------------|-------------------------|------------------------------|--|
| Cl ⁻ | 0.110 ± 0.003^c | 0.050 ± 0.002 | 2.3 ± 0.1 |
| Br ⁻ | 0.087 ± 0.002 | 0.038 ± 0.001 | 2.3 ± 0.1 |

^a $\bar{\nu} = 28,600 \text{ cm}^{-1}$; $I_a = 1.1 \pm 0.1 \times 10^{14} \text{ photons sec}^{-1}$; $T = 25.0 \pm 0.1^\circ$; $[\text{Cu}(\text{dmp})_2\text{X}_2]_{t=0} = 2.80 \times 10^{-3} \text{ M}$. ^b $\text{Cu}(\text{dmp})_2^+ + \text{Cu}(\text{dmp})^+$. ^c Standard deviation.

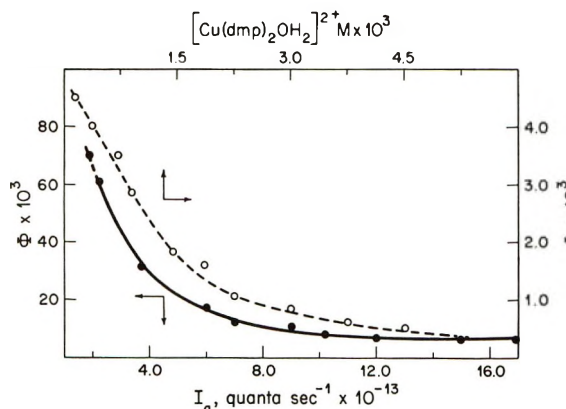


Figure 2. Variation of Φ for total Cu(I) species in aqueous solution with absorbed intensity (●, left ordinate, lower abscissa) and initial concentration of $\text{Cu}(\text{dmp})_2^{2+}$ (○, right ordinate, upper abscissa). In the I_a plot, $[\text{Cu}(\text{dmp})_2^{2+}] = 3.50 \times 10^{-3} \text{ M}$; in the concentration plot, $I_a = 1.1 \pm 0.1 \times 10^{14} \text{ quanta sec}^{-1}$.

LiCl or LiBr. Addition of NaClO_4 had no effect upon $\Phi_{\text{Cu(I)}}$ for either $\text{Cu}(\text{dmp})_2\text{Cl}_2$ or $\text{Cu}(\text{dmp})_2\text{Br}_2$ in methanol.

Chemical Scavenging Experiments. Use of benzoate as a scavenger for bulk hydroxyl radicals in aqueous systems is well established.¹⁸ When aqueous solutions $3.50 \times 10^{-3} \text{ M}$ in $\text{Cu}(\text{dmp})_2^{2+}$ were irradiated at 350 nm in the presence of $2 \times 10^{-2} \text{ F}$ sodium benzoate, the recovered solid reaction products^{8,18c} contained substantial quantities of salicylate, indicating production of bulk OH radicals accompanying the photoreduction. In "blank" solutions, treated identically but containing no $\text{Cu}(\text{dmp})_2^{2+}$, no detectable quantity of salicylate was produced.

Both the stoichiometry and quantum yield for photoreduction of $\text{Cu}(\text{dmp})_2^{2+}$ in water were affected by benzoate (Figure 5). At sufficiently high benzoate concentrations, the stoichiometry of conversion of $\text{Cu}(\text{dmp})_2^{2+}$ to $\text{Cu}(\text{dmp})_2^+$ was quantitative (no detectable quantity of dmp was destroyed), and Φ for appearance of $\text{Cu}(\text{dmp})_2^+$ attained a limiting value approximately twice $\Phi_{\text{Cu(I)}}$ observed in the absence of benzoate.

In methanol, vinyl monomers¹⁹ were employed to trap bulk radicals. Methanolic solutions $8.0 \times 10^{-5} \text{ M}$ in $\text{Cu}(\text{dmp})_2\text{Cl}_2$ or $\text{Cu}(\text{dmp})_2\text{Br}_2$ were photolyzed at $28,600 \text{ cm}^{-1}$ in the presence of varying concentrations

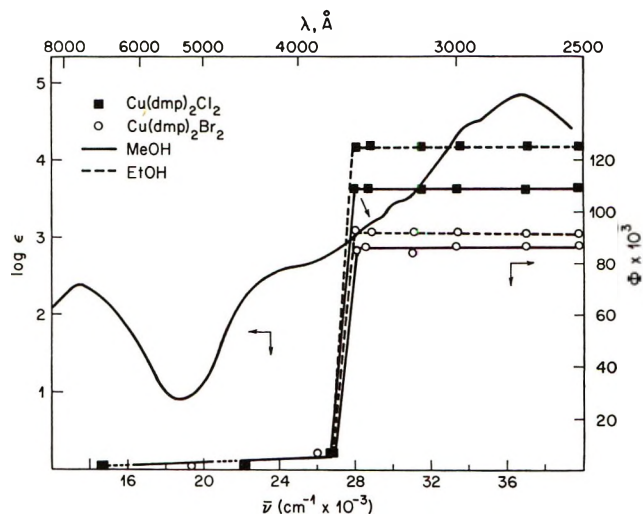


Figure 3. Electronic spectrum of $\text{Cu}(\text{dmp})_2^{2+}$ in methanol (left ordinate); variation of $\Phi_{\text{Cu(I)}}$ with incident frequency for $\text{Cu}(\text{dmp})_2\text{X}_2$ ($\text{X}^- = \text{Cl}^-, \text{Br}^-$) in methanol and ethanol (right ordinate). At all frequencies, $I_a = 1.05 \pm 0.05 \times 10^{14} \text{ quanta sec}^{-1}$.

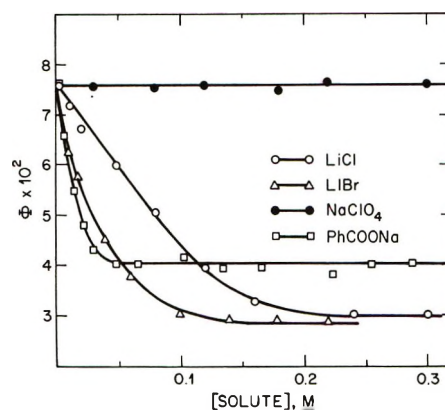


Figure 4. Influence of added solutes of Φ for photoreduction of $\text{Cu}(\text{dmp})_2^{2+}$ in methanol. Initial concentration of $\text{Cu}(\text{dmp})_2^{2+}$, $2.75 \times 10^{-3} \text{ M}$; $\bar{\nu} = 28,600 \text{ cm}^{-1}$; $I_a = 1.12 \pm 0.01 \times 10^{14} \text{ quanta sec}^{-1}$.

(0.003–0.25 M) of methyl methacrylate or acrylonitrile, effecting polymer formation. In the absence of Cu(II) complex, no detectable polymerization accompanied irradiation of methanolic solutions of either polymer at 350 nm. The purified polymer^{20a} was analyzed for $-\text{CH}_2\text{OH}^{20a}$ and halogen^{20b} end groups; both tests were strongly positive. Polymer obtained by photopolymerization of methyl methacrylate ($\bar{\nu} =$

(18) (a) M. Anbar, D. Meyerstein, and P. Neta, *J. Phys. Chem.*, **70**, 2660 (1966); (b) L. M. Dorfman, I. A. Tsaub, and D. A. Harter, *J. Chem. Phys.*, **41**, 2954 (1964); (c) H. G. C. Bates and N. Uri, *J. Amer. Chem. Soc.*, **75**, 2754 (1953).

(19) (a) G. Oster and N. Yang, *Chem. Rev.*, **68**, 125 (1968); (b) E. L. Wehry in "Analytical Photochemistry and Photochemical Analysis," J. M. Fitzgerald, Ed., Marcel Dekker, New York, N. Y., 1971, Chapter 6.

(20) (a) S. R. Palit and A. R. Mukherjee, *J. Polym. Sci.*, **58**, 1225 (1962); (b) M. K. Saha, P. Ghosh, and S. R. Palit, *J. Polym. Sci., Part A*, **2**, 1365 (1964).

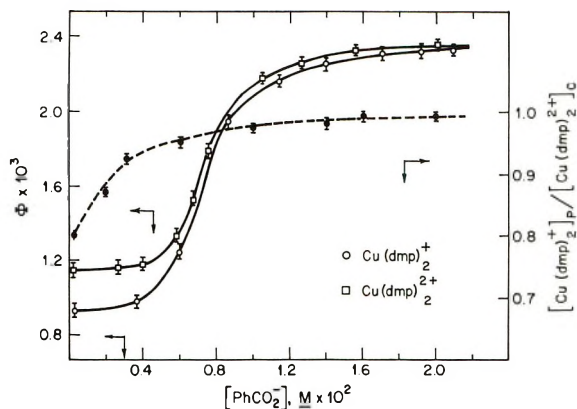


Figure 5. Effect of benzoate concentration upon Φ for appearance of Cu(dmp)_2^+ (O, left ordinate), Φ for consumption of Cu(dmp)_2^{2+} (□, left ordinate), and photoreduction stoichiometry (● right ordinate) in water. In all cases, $[\text{Cu(dmp)}_2^{2+}] = 3.50 \times 10^{-3} \text{ M}$ initially and $I_a = 1.1 \pm 0.1 \times 10^{14} \text{ quanta sec}^{-1}$.

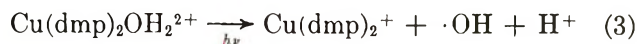
$38,500 \text{ cm}^{-1}$) in the presence of LiCl but in the absence of $\text{Cu(dmp)}_2\text{Cl}_2$ yielded negative tests for both $-\text{CH}_2\text{OH}$ and halogen end groups. As the concentration of monomer was increased (at constant initial concentration of $\text{Cu(dmp)}_2\text{X}_2$), the concentration of $-\text{CH}_2\text{OH}$ end groups in the polymer increased while that of halogen end groups declined. In an extreme case ($[\text{Cu(dmp)}_2\text{Cl}_2] = 8 \times 10^{-5} \text{ M}$; [methyl methacrylate] = 0.25 M), the $-\text{CH}_2\text{OH}$ test was extremely intense, while the halogen end group test was negative.

Methanolic solutions $8 \times 10^{-5} \text{ M}$ in $\text{Cu(dmp)}_2\text{X}_2$ were also photolyzed in the presence of varying concentrations ($0.004\text{--}0.03 \text{ M}$) of sodium benzoate. The residual solids⁸ were examined by mass spectrometry. Among species detected was one of empirical formula $\text{C}_8\text{H}_6\text{O}_3$, the empirical formula of the various isomers of methoxybenzoic acid or hydroxymethylbenzoic acid. Owing to the large number of substances present in the solid, no attempt was made to identify the compound(s) $\text{C}_8\text{H}_6\text{O}_3$ by fragmentation patterns. No evidence was noted for the presence of halobenzoic acids or salicylic acid in the solid scavenging product.

Photochemical Inertness of Cu(phen)_2^{2+} . In both aqueous and methanolic solutions, Cu(phen)_2^{2+} exhibited no detectable photochemistry in the $12,000\text{--}50,000\text{-cm}^{-1}$ region. We estimate that quantum yields for photodecomposition of Cu(phen)_2^{2+} do not exceed 1×10^{-6} in either solvent. Degassing of solutions had no effect upon the lack of observable photochemistry of Cu(phen)_2^{2+} in either solvent.

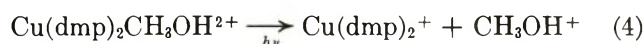
Discussion

The experimental results are consistent with the hypothesis that, in both water and methanol, the primary process in photoreduction of Cu(dmp)_2^{2+} is homolytic cleavage of a Cu(II) –solvent bond. In water, that process would be represented as

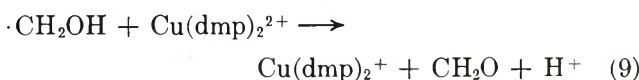
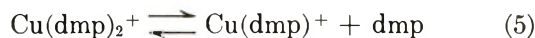


Benzoate scavenging clearly implicates formation of bulk $\cdot\text{OH}$ as a major process accompanying the photoreduction. The decomposition of dmp which normally accompanies photoreduction of Cu(dmp)_2^{2+} in water is suppressed by addition of a sufficient excess of benzoate. This observation indicates that attack of dmp by $\cdot\text{OH}$, a secondary thermal process, is the principal mode by which destruction of dmp occurs. That $\Phi_{\text{Cu(I)}}$ increases upon addition of benzoate, concomitant with a decrease in the extent of consumption of dmp (Figure 5), implies that homolytic cleavage of a Cu(II) –dmp bond, forming Cu(I) and $\text{dmp}\cdot^+$, is not an important pathway.

In methanol, we represent the primary photoprocess as



The primary process is followed by a number of thermal reactions, including reactions 5–11.



Scavenging experiments employing vinyl monomers clearly indicate production of $\cdot\text{CH}_2\text{OH}$ accompanying photoreduction of Cu(dmp)_2^{2+} in methanol. Benzoate scavenging experiments demonstrate formation of bulk $\cdot\text{CH}_2\text{OH}$ and/or $\text{CH}_3\text{O}\cdot$. That methanol is oxidized concomitant with photoreduction of Cu(dmp)_2^{2+} is indicated by production of formaldehyde. Other plausible primary processes (heterolytic Cu(II) – CH_3OH cleavage; homolytic Cu(II) –dmp cleavage followed by release of $\text{dmp}\cdot^+$) are inconsistent with the observed photoredox stoichiometry and the absence of detectable destruction of dmp.

An addition mechanism, plausible in view of the relatively low dielectric constant of methanol, is photoreduction of an ion pair



While scavenging experiments demonstrate formation of $\cdot\text{X}$ accompanying photoreduction of $\text{Cu(dmp)}_2\text{CH}_3\text{OH}^{2+}$, reaction 12 is unlikely to be the dominant process in this system, for four reasons. First, if $\cdot\text{X}$ were formed in the primary process, then, in a vinyl-monomer scavenging experiment, methanol and the

monomer would act as competitive scavengers of $\cdot X$ or X_2^- . Therefore, as the monomer concentration was increased, the relative concentrations of CH_2OH to X end groups in the polymer should decrease. Exactly the opposite effect was observed, strongly implying that X^- (reaction 10) and methyl methacrylate act as competitive scavengers for alcohol radicals,²¹ and that X is formed by secondary thermal reactions. Second, if an ion pair, $Cu(dmp)_2^{2+} \cdot X^-$, were the photoactive species, its concentration should increase as LiX is added to a methanolic solution of $Cu(dmp)_2X_2$; therefore, $\Phi_{Cu(I)}$ should be enhanced by addition of LiX . Exactly the opposite effect is observed (Figure 4). Third, $\Phi_{Cu(I)}$ for $Cu(dmp)_2Cl_2$ is substantially larger than that for $Cu(dmp)_2Br_2$ (Table I); if X^- were the electron donor in photoreduction of the $Cu(II)$ complex, this observation would be difficult to rationalize. Fourth, CH_3OH is an inefficient scavenger of Br or Br_2^- ;²² thus, it is difficult to rationalize efficient production of $CH_3O\cdot$ or $\cdot CH_2OH$ by methanol scavenging. Subsequent discussion therefore assumes the validity of reaction 4 as a description of the primary photoprocess in methanol.

While $Cu(dmp)_2^+$ is a stable species, the other product of reaction 4, CH_3OH^+ , is rapidly scavenged by CH_3OH , forming $CH_3O\cdot$ (reaction 6) or $\cdot CH_2OH$ (reaction 7). Though relative rates for reaction 6 and 7 are unknown, it appears established that both occur to a significant extent in liquid methanol.²³ In the absence of added scavengers, $CH_3O\cdot$ can be consumed by two thermal reactions, scavenging by methanol (reaction 8) or disproportionation

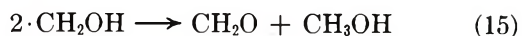


While reaction 13 exhibits a much higher second-order rate constant than reaction 8, the rate of production of $CH_3O\cdot$ in this system is probably insufficient for reaction 13 to be significant.²⁴ Therefore, virtually all $CH_3O\cdot$ radicals which escape scavenging by other solutes are probably converted to $\cdot CH_2OH$.

In methanolic solution, hydroxymethyl radicals can either dimerize



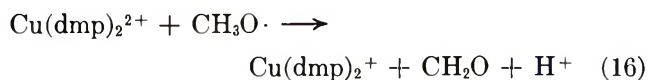
or disproportionate



In liquid methanol, $k_{13}/k_{14} = 10$.²³ Since ethylene glycol is not detected as a product in photolyzed solutions of $Cu(dmp)_2CH_3OH^{2+}$, neither reaction 14 nor 15 appears significant; formaldehyde, which is produced in significant yield, must therefore be formed by processes other than reaction 15.

Because $\cdot CH_2OH$ is a strongly reducing radical,²³ it is susceptible to scavenging by strong oxidizing agents. The strongest thermally stable oxidant in the system is $Cu(dmp)_2^{2+}$, which is a sufficiently powerful oxidant to

oxidize a dropping mercury electrode.^{5b} Therefore, a likely scavenging process is reaction 9, leading to formation of formaldehyde and $Cu(dmp)_2^+$. Indeed, Brackman,²⁵ in a study of thermal oxidation of methanol in the presence of metal chelates, including $Cu(phen)_2^{2+}$ (which is a less powerful oxidant than $Cu(dmp)_2^{2+}$), demonstrated the occurrence of reactions exactly analogous to reaction 9. It is also possible that significant scavenging of $CH_3O\cdot$ by $Cu(dmp)_2^{2+}$ may occur



Scavenging of $\cdot CH_2OH$ or $\cdot CH_3O$ by $Cu(dmp)_2^{2+}$ would affect values for $\Phi_{Cu(I)}$. We consider a limiting case. If all CH_3OH^+ escaping primary recombination is eventually converted to $\cdot CH_2OH$ by reactions 7 or 8, and if each $\cdot CH_2OH$ radical so formed undergoes reaction 9, $\Phi_{Cu(I)}$ should be exactly twice Φ_{CH_2O} .

The same prediction results from consideration of scavenging of $CH_3O\cdot$ by $Cu(dmp)_2^{2+}$, reaction 16. As noted in Table I, $\Phi_{Cu(I)}/\Phi_{CH_2O}$ is equal to 2.3 for both $Cu(dmp)_2Cl_2$ and $Cu(dmp)_2Br_2$. The agreement between prediction and experiment is rather good; the difference is attributed principally to scavenging of $CH_3O\cdot$ by X^- (*cf.* below).

From the discussion in the preceding paragraph, one predicts that $\Phi_{Cu(I)}$ will decrease in the presence of species which scavenge $CH_3O\cdot$ and/or $\cdot CH_2OH$; if the scavenger has no effect on the system other than scavenging these radicals, $\Phi_{Cu(I)}$ in the presence of a large excess of scavenger should be exactly half that observed in its absence. Additionally, Φ_{CH_2O} should decrease to virtually zero in the presence of a sufficient excess of scavenger. The influence of benzoate is in excellent agreement with these predictions. It is observed (Figure 4) that $\Phi_{Cu(I)}$ decreases in the presence of increasing benzoate concentrations, reaching a limiting value (at $[benzoate] \geq 0.05 F$) which is smaller than that observed in the absence of benzoate by a factor of 1.9. At benzoate concentrations greater than 0.020 F , the quantum yield for appearance of formaldehyde is undetectably small ($\Phi_{CH_2O} < 10^{-4}$). The products of benzoate scavenging experiments include species of empirical formula $C_8H_8O_3$, the formulas of methoxy-

(21) Attempts to observe growth and decay of Cl_2^- formed in flash photolysis of solutions of $Cu(dmp)_2Cl_2$ were unsuccessful due to the very strong absorption of $Cu(dmp)_2^+$ and $Cu(dmp)_2^{2+}$ in the spectral regions of interest.

(22) M. E. Langmuir and E. Hayon, *J. Phys. Chem.*, **71**, 3808 (1967).

(23) F. S. Dainton, G. A. Salmon, and P. Wardman, *Proc. Roy. Soc., Ser. A*, **313**, 1 (1969).

(24) P. Gray, R. Shaw, and J. C. J. Thynne, *Progr. React. Kinet.*, **4**, 63 (1967).

(25) W. Brackman, F. van de Craats, and P. J. Smit, *Recl. Trav. Chim. Pays Bas*, **83**, 1253 (1964); W. Brackman and C. J. Gaasbeek, *ibid.*, **85**, 221 (1966).

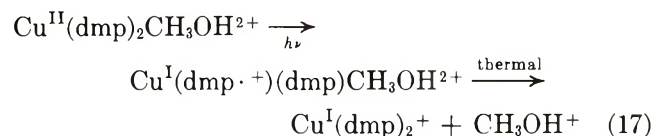
benzoic or hydroxymethylbenzoic acids which would result from scavenging of $\text{CH}_3\text{O}\cdot$ and $\cdot\text{CH}_2\text{OH}$, respectively.²⁶ The results of benzoate scavenging experiments thus agree well with predictions based on the assumption of efficient scavenging of $\cdot\text{CH}_2\text{OH}$ by $\text{Cu}(\text{dmp})_2^{2+}$.

The influence of added Br^- and Cl^- upon $\Phi_{\text{Cu(I)}}$ is more complex (Figure 4). Addition of excess LiBr or LiCl decreases $\Phi_{\text{Cu(I)}}$, with LiBr more effective. In the presence of large concentrations of either salt, $\Phi_{\text{Cu(I)}}$ reaches the same limiting value, which is smaller than that determined in the absence of excess LiX by a factor of 2.3. All methanolic solutions of $\text{Cu}(\text{dmp})_2 \cdot (\text{CH}_3\text{OH})_2^{2+}$ contained either Cl^- or Br^- ; scavengable $\text{X}\cdot$ was produced concomitant with photoreduction of the Cu(II) complex. Both I^- and NCS^- are known to scavenge $\text{CH}_3\text{O}\cdot$ radicals. The scavenging reaction 10 with I^- exhibits a second-order rate constant of $\geq 2 \times 10^6 \text{ M}^{-1} \text{ sec}^{-1}$ in liquid methanol.²⁷ Rate constants for the analogous reactions with Cl^- and Br^- have not been determined, but it appears safe to assume that, for reaction 10, $k_{\text{Br}^-} > k_{\text{Cl}^-}$. If halide ions intercept $\text{CH}_3\text{O}\cdot$, they decrease the rate of formation of $\cdot\text{CH}_2\text{OH}$ and therefore reduce the extent of secondary thermal reduction of $\text{Cu}(\text{dmp})_2^{2+}$ to $\text{Cu}(\text{dmp})_2^+$, reaction 9. Addition of halide should thus decrease the apparent value for $\Phi_{\text{Cu(I)}}$; furthermore, Br^- should more efficiently decrease $\Phi_{\text{Cu(I)}}$ than should Cl^- (see Figure 4). In the presence of sufficiently large excesses of either Cl^- or Br^- , $\Phi_{\text{Cu(I)}}$ should equal *ca.* 0.5 the value observed in the absence of excess halide, and $\Phi_{\text{CH}_3\text{O}}$ should equal $\Phi_{\text{Cu(I)}}$. Actually, $\Phi_{\text{Cu(I)}}$ on the plateau region of Figure 4 equals 0.40 $\Phi_{\text{Cu(I)}}$ observed in the absence of excess LiX , and, in the presence of excess halide, $\Phi_{\text{Cu(I)}/\Phi_{\text{CH}_3\text{O}}} = 1.2$.

Alternatively, it is possible that the data in Figure 4 are symptomatic of an external heavy-atom effect, which would promote nonradiative decay of the reactive excited state at the expense of photoreduction yields. The greater effect of Br^- than of Cl^- upon Φ is consistent with that hypothesis. There is presently virtually no impeccable evidence demonstrating the susceptibility of photoexcited states of transition-metal chelates to "external" heavy-atom quenching. The appearance of the quantum yield plots in Figure 4 (particularly the observed plateau and the fact that both Cl^- and Br^- produce the same limiting yield) is not easily understood in the context of a heavy-atom effect, nor is the lack of a similar counterion effect upon $\Phi_{\text{Cu(I)}}$ in water.

In both *water* and *methanol*, $\Phi_{\text{Cu(I)}}$ is essentially zero in the $d \rightarrow d$ region and becomes appreciable only at frequencies greater than $27,000 \text{ cm}^{-1}$ (Figures 1 and 3). The assigned frequency of $\pi \rightarrow d$ ("dmp to Cu(II) ") charge-transfer electronic absorption in $\text{Cu}(\text{dmp})_2^{2+}$ is $28,600 \text{ cm}^{-1}$.^{4b,c} Particularly in view of the fact that the frequency dependences of $\Phi_{\text{Cu(I)}}$ are so very similar

in the two solvents, it is tempting to conclude that the photochemically reactive state is the spin-allowed (doublet) (π, d) charge-transfer state. It is, however, bothersome that the photoreduction of $\text{Cu}(\text{dmp})_2^{2+}$ in both water and methanol involves oxidation of the solvent, rather than of coordinated dmp. One may rationalize this apparent discrepancy in at least two different ways. First, one may assert (with considerable justification) that simplified descriptions of electron-transfer excited states in mixed-ligand complexes of strongly π -bonding ligands, such as dmp, are too crude to enable accurate prediction of photodecomposition modes. In that view, any "ligand \rightarrow metal" charge-transfer transition would involve electron transfer from a molecular orbital extending over all ligands, including coordinated methanol or water. Alternatively, one may consider that, in either solvent, the actual primary process involves electron transfer from dmp to Cu(II) , followed by efficient thermal oxidation of either bulk or coordinated solvent (*e.g.*, in methanol)



There is no experimental evidence which vitiates a sequence of that type, though it is worthwhile to note that values of $\Phi_{\text{Cu(I)}}$ in both water and methanol are not detectably dependent upon pH. Such a dependence might be expected, and release of uncomplexed dmp or its oxidation products might become significant at low pH, if homolytic Cu(II) -dmp cleavage were an important primary process.

One must also consider the possible existence of solvent-to- Cu(II) charge-transfer excited states of accessible energy in the $\text{Cu}(\text{dmp})_2^{2+}$ species. In water, such a possibility appears remote, for charge-transfer absorption in aquocopper(II) species becomes significant only at frequencies greater than $48,000 \text{ cm}^{-1}$.²⁸ However, the ultraviolet spectrum of $\text{Cu}(\text{ClO}_4)_2$ in methanol exhibits a strong transition ($\log \epsilon = 3.34$) with $\bar{\nu}_{\text{max}} = 44,100 \text{ cm}^{-1}$, which may reasonably be considered a methanol \rightarrow copper(II) electron-transfer transition. This band is rather broad, with the onset of significant absorption being *ca.* $33,000 \text{ cm}^{-1}$. Clearly, one cannot exclude the possibility that states which may formally be described as "dmp-to- Cu(II) " and "methanol-to- Cu(II) " electron-transfer states may have comparable energies in $\text{Cu}(\text{dmp})_2\text{CH}_3\text{OH}^{2+}$.²⁹

(26) K. Schwetlick, R. Karl, and J. Jentzsch, *J. Prakt. Chem.*, **22**, 113, 125 (1963); K. Schwetlick, J. Jentzsch, R. Karl, and D. Walter, *ibid.*, **25**, 95 (1964).

(27) F. S. Dainton, I. V. Janovsky, and G. S. Salmon, *J. Chem. Soc. D*, 335 (1969).

(28) C. K. Jørgensen, "Absorption Spectra and Chemical Bonding in Complexes," Pergamon Press, London, 1962, p 286.

Irrespective of the detailed description of the photoactive excited state, it does appear justified to conclude that the photoreduction of $\text{Cu}(\text{dmp})_2^{2+}$ in both water and methanol proceeds through a spin-allowed doublet) ligand \rightarrow metal electron-transfer state. That the photoreduction quantum yield is constant throughout the 25,000–40,000- cm^{-1} region in both solvents implies that internal conversion from spin-allowed ligand-localized excited states to the active doublet charge-transfer state is rapid. Similar conclusions have previously been reported for other metal-phenanthroline complexes, on the basis of luminescence³⁰ and photochemical³¹ studies.

No spin-forbidden excited states of either ligand-field or ligand \rightarrow metal charge-transfer type can occur at accessible energies in $\text{Cu}(\text{dmp})_2^{2+}$, owing to the d^9 configuration of Cu(II); hence, no pathway exists for inter-system crossing from low-lying doublet charge-transfer states to the spin-forbidden (quartet) manifold. Therefore, the only process competing with internal conversion to the doublet ligand-field levels is photoreduction. Internal conversion from the doublet charge-transfer state(s) to lower lying doublet (d, d) states proceeds with substantially less than unit efficiency in methanol, as indicated by the frequency dependence of $\Phi_{\text{Cu(II)}}$ (Figure 3).

Finally we consider the observation that, while the two complexes exhibit similar electronic spectra,⁴ $\text{Cu}(\text{phen})_2^{2+}$ undergoes photoreduction less efficiently than $\text{Cu}(\text{dmp})_2^{2+}$, by a factor of at least 1000 in aqueous media and a factor of 10^5 in methanol. In both its ground and doublet charge-transfer excited states, $\text{Cu}(\text{dmp})_2^{2+}$ is a much stronger oxidizing agent than $\text{Cu}(\text{phen})_2^{2+}$. That $\text{Cu}(\text{dmp})_2^{2+}$ is significantly more

susceptible to thermal reduction than is $\text{Cu}(\text{phen})_2^{2+}$ has been attributed^{5a} to the fact that the distorted-tetrahedral coordination of dmp about Cu(II) requires only a relatively small energy to attain the tetrahedral geometry characteristic of $\text{Cu}(\text{dmp})_2^+$. The principal decay process competing with photochemistry in the low-lying doublet charge-transfer states of both $\text{Cu}(\text{dmp})_2^{2+}$ and $\text{Cu}(\text{phen})_2^{2+}$ must be internal conversion to lower lying doublets or to the ground state. There is no experimental or theoretical basis for estimating relative rates of nonradiative relaxation from the charge-transfer doublets in these species, since neither exhibits detectable luminescence in either aqueous or alcoholic media at either 298°K or liquid nitrogen temperature. That the energy barrier for structural rearrangement of $\text{Cu}(\text{dmp})_2^{2+}$ to $\text{Cu}(\text{dmp})_2^+$ is significantly smaller than that required for rearrangement of $\text{Cu}(\text{phen})_2^{2+}$ to $\text{Cu}(\text{phen})_2^+$ appears germane to the relative susceptibility of the Cu(II) complexes to photoreduction. In the absence of general information regarding radiationless processes in coordination compounds, more definitive statements regarding effects of structure upon photochemistry in these compounds cannot now be made.

Acknowledgment. This work was supported in part by Grant No. AM-11081 from the National Institutes of Health.

(29) In that regard, we emphasize that, while the frequency dependences of product quantum yields were very similar in the two solvents, absolute values of $\Phi_{\text{Cu(II)}}$ were larger (by a factor of 10^3) in methanol than in water.

(30) F. E. Lytle and D. M. Hercules, *J. Amer. Chem. Soc.*, **91**, 253 (1969); J. N. Demas and G. A. Crosby, *ibid.*, **93**, 2841 (1971).

(31) P. G. David, J. G. Richardson, and E. L. Wehry, *Inorg. Nucl. Chem. Lett.*, **7**, 251 (1971).

Pulse Radiolysis of Aqueous Thiocyanate Solutions. Nature of the Intermediate Transient Species

by D. Behar, P. L. T. Bevan, and G. Scholes*

Laboratory of Radiation Chemistry, School of Chemistry, University of Newcastle upon Tyne, NE1 7RU, England
(Received October 7, 1971)

Publication costs borne completely by The Journal of Physical Chemistry

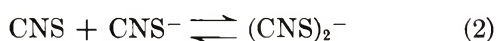
The pulse radiolysis of N₂O-saturated aqueous solutions of KCNS has been studied under both neutral and alkaline conditions, and the optical absorption spectra of the precursors of the (CNS)₂⁻ radical anion have been obtained. In neutral solution the precursor has λ_{max} 330 nm with ε₃₃₀ 900 M⁻¹ cm⁻¹, while in alkali it has a λ_{max} 390 nm and ε₃₉₀ 4600 M⁻¹ cm⁻¹. Kinetic considerations lead to their assignment as CNS and CNSOH⁻, respectively. The oxidation of CNS⁻ ions by OH radicals in these solutions is interpreted in terms of the reactions: OH + CNS⁻ → CNSOH⁻; CNSOH⁻ ⇌ CNS + OH⁻, K = 3.2 × 10⁻² M; and CNS + CNS⁻ ⇌ (CNS)₂⁻, K = 2 × 10⁵ M⁻¹. The rate constant for the dissociation of CNSOH⁻ has been found to be >5 × 10⁷ sec⁻¹. In alkaline solutions, oxidation of CNS⁻ by O⁻ also takes place, viz., O⁻ + CNS⁻ → CNSO²⁻, k = 3.7 × 10⁹ M⁻¹ sec⁻¹; CNSO²⁻ + H₂O ⇌ CNSOH⁻ + OH⁻. Under the conditions used (up to 0.8 M NaOH) the doubly charged adduct is converted completely to CNSOH⁻.

Introduction

The mechanism of the oxidation of CNS⁻ ions by OH radicals in aqueous systems was first investigated by Adams, *et al.*^{1,2} Pulse radiolysis studies showed the formation of a transient species which absorbed strongly in the visible (λ_{max} 480 nm), and this absorption was first assigned to the CNS radical, formed according to



It was pointed out,² however, that the experimental data would also be consistent with the transient species being (CNS)₂⁻, produced by the secondary equilibrium reaction



Subsequent detailed kinetic studies^{3,4} of the formation of the transient at low [CNS⁻] gave results which could be quantitatively explained if the absorption was entirely due to (CNS)₂⁻; it was reported that k₁ = 2.8 × 10¹⁰ M⁻¹ sec⁻¹ and K₂ = 2 × 10⁵ M⁻¹.

More recently,⁵ it has been shown that irradiation of frozen alkaline glasses (at 77°K) containing KCNS leads to the formation of an intermediate (λ_{max} 380 nm) which, on annealing, decays to produce (CNS)₂⁻; thus, in the glassy matrix, it was proposed that reaction of CNS⁻ with the radiation-produced holes (*e.g.*, O⁻) can produce a transient complex radical ion. In view of this observation, aspects of the pulse radiolysis of neutral and alkaline thiocyanate solutions have been reinvestigated, particularly with a view to the detection of OH(O⁻) adducts.

Experimental Section

The pulse radiolysis apparatus has been described.⁶ In the present work two linear accelerators were used,

of 5- and 10-MeV energy, respectively. Generally, pulses of 0.1 μsec in length were used, giving doses from 0.1 to 1.0 krad. Spectra were obtained using the kinetic spectroscopy method. The KCNS and NaOH used were of analytical reagent grade, and solutions were made up in triply distilled water.

Results and Discussion

Transient absorption spectra from 10⁻⁴ M KCNS solutions (saturated with N₂O to remove the radiation-produced solvated electrons, e_{aq}⁻ + N₂O → N₂ + OH + OH⁻) were recorded at various times after the electron pulse. Figures 1 and 2 show, respectively, the results obtained from solutions at natural pH (pH ≈ 5.6) and from solutions containing 0.1 M NaOH. The presence of a precursor of (CNS)₂⁻ is clearly indicated by the kinetic features, namely, that the formation of (CNS)₂⁻ at 480 nm is accompanied by a decay at lower wavelengths (see oscillograms). Moreover, the optical absorption spectrum of the precursor (the difference spectra in Figures 1 and 2) is different under the different pH conditions, viz., λ_{max}(neutral) 330 nm, λ_{max}(alkaline) 390 nm. In view of this evidence, it is concluded that the oxidation of CNS⁻ ions in these irradiated systems cannot be described simply in terms of reactions 1 and 2.

(1) G. E. Adams, J. W. Boag, and B. D. Michael, *Proc. Chem. Soc.*, 114 (1964).

(2) G. E. Adams, J. W. Boag, J. Carrant, and B. D. Michael, "Pulse Radiolysis," Academic Press, New York, N. Y., 1965, p 117.

(3) J. H. Baxendale and D. A. Stott, *Chem. Commun.*, 699 (1967).

(4) J. H. Baxendale, P. L. T. Bevan, and D. A. Stott, *Trans. Faraday Soc.*, 64, 2389 (1968).

(5) D. V. Bent, N. B. Nazhat, and G. Scholes, 4th International Congress of Radiation Research, Evian, Abstract 74, 1970.

(6) J. P. Keene, "Pulse Radiolysis," Academic Press, New York, N. Y., 1965, p 1.

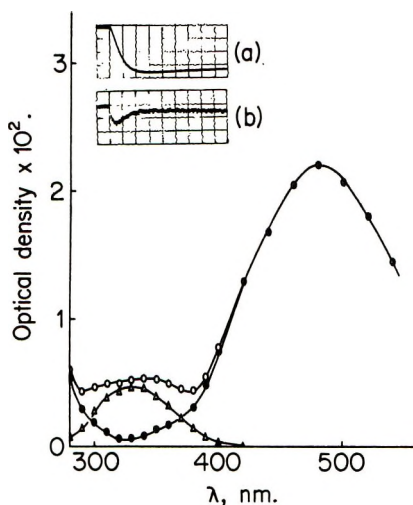


Figure 1. Transient absorption spectra in pulsed aqueous KCNS solutions ($10^{-4} M$) saturated with N_2O at natural pH: (O, ●) observed spectrum after $1 \mu\text{sec}$, (●, ●) contribution from $(CNS)_2^-$, (Δ) difference spectrum. Oscilloscope traces: (a) λ 480 nm, time scale $2 \mu\text{sec}$ per division, 3.5% absorption per division; (b) λ 330 nm, time scale $2 \mu\text{sec}$ per division, 0.9% absorption per division.

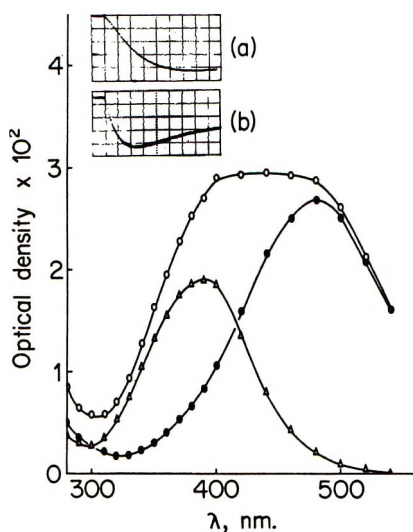
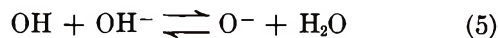


Figure 2. Transient absorption spectra in pulsed aqueous KCNS solutions ($10^{-4} M$) saturated with N_2O containing $10^{-1} M$ NaOH: (O) observed spectrum after $3.5 \mu\text{sec}$, (●) contribution from $(CNS)_2^-$, (Δ) difference spectrum. Oscilloscope traces: (a) λ 480 nm, time scale $2 \mu\text{sec}$ per division, 3.1% absorption per division; (b) λ 390 nm; time scale $2 \mu\text{sec}$ per division, 2.1% absorption per division.

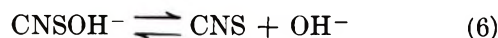
As an alternative mechanism, one may suppose, in the first instance, that the primary reaction with CNS^- ions leads to the formation of adducts, according to



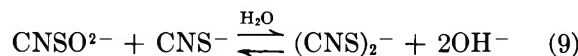
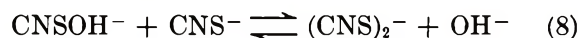
The relative extents of these two reactions will be governed by the dissociation process



for which $pK_a = 11.97$ and by the relative magnitude of the rate constants k_3 and k_4 . Given that the adducts may then enter into the pH-dependent equilibria



it then follows that $(CNS)_2^-$ can possibly arise from three equilibrium processes, *viz.*, reactions 2, 8, and 9.



On this basis, the observed precursors could be either the pair CNS - $CNSOH^-$ or the pair $CNSOH^-$ - $CNSO^{2-}$.

Representing D as the optical density due to $(CNS)_2^-$ at equilibrium, where $(CNS)_2^-$ and the precursors co-exist, and D_0 as the absorption if full conversion of $OH(O^-)$ radicals to $(CNS)_2^-$ were to be attained, then the variation of the ratio D_0/D with $[OH^-]$ can be predicted for various reaction schemes. Thus, assuming that the precursors are CNS and $CNSOH^-$ and that they enter the equilibria 2 and 6, it can be shown that

$$\frac{D_0}{D} = 1 + \frac{1}{K_2[CNS^-]} + \frac{[OH^-]}{K_6 K_2 [CNS^-]} \quad (I)$$

If the reaction of $CNSOH^-$ with CNS^- is also included in this scheme, an equation similar to I would then apply, since $K_6 K_2 = K_8$. On the other hand, for a reaction mechanism involving the pair $CNSOH^-$ - $CNSO^{2-}$, and the equilibria 7, 8, and 9, equation II

$$\frac{D_0}{D} = 1 + [OH^-] \left\{ \frac{1}{K_8 [CNS^-]} + \frac{[OH^-]}{K_9 [CNS^-]} \right\} \quad (II)$$

would apply. In order to distinguish between these reaction schemes, the effect of $[OH^-]$ on the equilibrium concentration of $(CNS)_2^-$ was studied. The solutions (N_2O saturated) contained a fixed amount of thiocyanate ($7.85 \times 10^{-5} M$), the $[OH^-]$ being varied from ~ 0.2 to $0.8 M$. Electron pulses of relatively small dose were used so that the equilibrium values of $(CNS)_2^-$ could be attained before appreciable decay of this species had taken place. It was found that the data could be expressed by eq I and *not* by eq II. Figure 3 shows the results plotted according to eq I, setting the intercept from the known values of $[CNS^-]$ and K_2 .⁴ We therefore conclude that the species absorbing at 330 and 390 nm correspond to CNS and $CNSOH^-$, respectively.

Although the absorption spectrum of the CNS radical in water is unknown, it has been determined in the gas

(7) J. Rabani and M. S. Matheson, *J. Amer. Chem. Soc.*, **86**, 3175 (1964).

phase⁸ and absorption bands are present in the range 330–440 nm. The molar extinction coefficient of CNS, $\epsilon_{\text{CNS}}^{330} 900 M^{-1} \text{ cm}^{-1}$, was obtained by kinetic treatment of the results (see below), using the reported value⁴ of $\epsilon_{(\text{CNS})_2^{-475}} 7600 M^{-1} \text{ cm}^{-1}$.

Support for the assignment of the 390-nm absorption to CNSOH⁻ arises from a comparison with the recently described^{9–11} physical properties of the transient thiocyanate-halide complexes, CNSX⁻ (Table I). The equilibrium constant of reaction 6 was determined from Figure 3; $K_2K_6 = 6.45 \times 10^3$, hence $K_6 = 3.2 \times 10^{-2} M$. Using these values and the equilibrium optical densities at differing pH values, the molar extinction coefficient for the CNSOH⁻ radical ion was assessed.

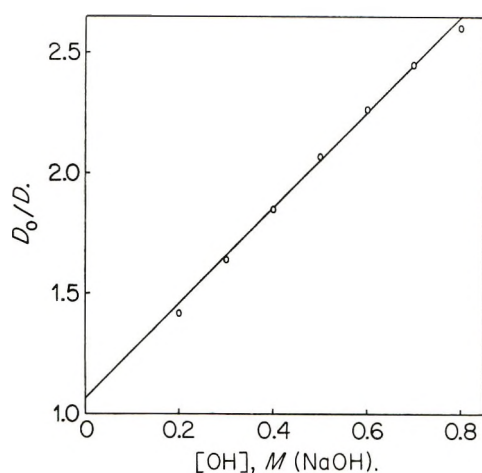


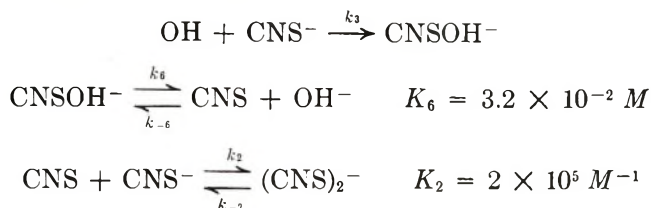
Figure 3. Variation of the equilibrium concentration of $(\text{CNS})_2^-$ with $[\text{OH}^-]$.

The ratio D_{390}/D_{475} at pH 13 and 14 was found to be 0.43 and 1.50, respectively. Given the relationships $D_{475} = (\epsilon_{(\text{CNS})_2^{-475}} [(\text{CNS})_2^-])$ and $D_{390} = (\epsilon_{(\text{CNS})_2^{-390}} [(\text{CNS})_2^-] + (\epsilon_{\text{CNSOH}^{-390}} [\text{CNSOH}^-])$, we calculate that $\epsilon_{\text{CNSOH}^{-390}} = 4600 M^{-1} \text{ cm}^{-1}$. It can be seen in Table I that these various properties of CNSOH⁻ fall very well into the general pattern for the thiocyanate complexes.

Questions arise about the relative kinetic significance of the equilibria 2 and 8 in the formation of $(\text{CNS})_2^-$, it being evident that eq 1 cannot distinguish between them. It follows from (8) that $[(\text{CNS})_2^-]/[\text{CNSOH}^-] = K_2K_6 [\text{CNS}^-]/[\text{OH}^-]$. For the solutions of natural pH (5.5), this leads to the relationship $[(\text{CNS})_2^-]/[\text{CNSOH}^-] = 2 \times 10^{12}[\text{CNS}^-]$, indicating that extremely low CNS⁻ concentrations ($\ll 10^{-6} M$) would be sufficient to allow full conversion of CNSOH⁻ to $(\text{CNS})_2^-$ by reaction 8; this is clearly not observed. Furthermore, since the forward reaction of equilibrium 8 is suppressed by alkali, we are of the view that this particular process does not contribute to $(\text{CNS})_2^-$ radical-ion formation under the conditions described here.

Kinetics in Neutral and Acid Solutions

The kinetics of formation of $(\text{CNS})_2^-$ from OH radicals are derived for the proposed mechanism



The concentrations of the transient species are proportional to their optical densities. For each transient, let D_t and D be the optical densities at time t and at equilibrium, and D_0 the optical density attained if all the OH radicals were converted to the relevant transient. At low $[\text{OH}^-]$ (neutral and acidic CNS⁻ solutions), we neglect the reverse reaction of equilibrium 6 (rate $\propto k_{-6}[\text{OH}^-]$). Under these conditions, the following equations express the buildup of the transients after the electron pulse.

for CNS

$$\frac{D_t - D}{D_0} = \frac{k_3'(k_6 - k_{-2})}{(k_6 - k_3')(k_6 - k_2' - k_{-2})} e^{-k_6 t} - \frac{k_6(k_3' - k_{-2})}{(k_6 - k_3')(k_3' - k_2' - k_{-2})} e^{-k_3' t} + \frac{k_2'k_3'k_6}{(k_2' + k_{-2})(k_3' - k_2' - k_{-2})(k_6 - k_2' - k_{-2})} \times e^{-(k_2' + k_{-2})t} \quad (\text{III})$$

for $(\text{CNS})_2^-$

$$\frac{D - D_t}{D_0} = \frac{k_2'k_3'}{(k_6 - k_3')(k_6 - k_2' - k_{-2})} e^{-k_6 t} - \frac{k_2'k_6}{(k_6 - k_3')(k_3' - k_2' - k_{-2})} e^{-k_3' t} + \frac{k_2'k_3'k_6}{(k_2' + k_{-2})(k_3' - k_2' - k_{-2})(k_6 - k_2' - k_{-2})} \times e^{-(k_2' + k_{-2})t} \quad (\text{IV})$$

where $k_2' = k_2[\text{CNS}^-]$ and $k_3' = k_3[\text{CNS}^-]$.

Baxendale, *et al.*,⁴ showed that at times $> 0.2 \mu\text{s}$ the kinetics of $(\text{CNS})_2^-$ formation in pulsed neutral and acidic solutions could be formally accounted for by a primary oxidation step (represented by the authors as $\text{CNS}^- + \text{OH} \rightarrow \text{CNS} + \text{OH}^-$ (1), but which is replaced here by (3)) followed by (2). It is thus concluded that $k_6 \gg k_3[\text{CNS}^-]$ and $(k_2[\text{CNS}^-])$

(8) R. N. Dixon and D. A. Ramsay, *Can. J. Phys.*, **46**, 2619 (1968).

(9) M. Schöneshöfer and A. Henglein, *Ber. Bunsenges. Phys. Chem.*, **73**, 289 (1969).

(10) M. Schöneshöfer, *Int. J. Radiat. Phys. Chem.*, **1**, 505 (1969).

(11) M. Schöneshöfer and A. Henglein, *Ber. Bunsenges. Phys. Chem.*, **74**, 393 (1970).

Table I: Comparison of Some Physical Properties of Thiocyanate Radical Ion Complexes (CNSX⁻)

| Species ^a | λ_{\max} , nm | ϵ_{\max} , $M^{-1} \text{ cm}^{-1}$ $\times 10^3$ | K_i , ^b M |
|----------------------|--------------------------|--|-----------------------------|
| CNSI ⁻ | 420 | 9.2 | 1.3×10^{-8} |
| CNSBr ⁻ | 400 | 7.3 | 6×10^{-4} |
| CNSOH ⁻ | 390 | 4.6 | 3.2×10^{-2} |
| CNSCl ⁻ | 390 | 4.7 | 1.5×10^{-1} |

^a Data for CNS⁻ halide complexes taken from ref 9-11.

^b Equilibrium constant for the reaction $\text{CNSX}^- \rightleftharpoons \text{CNS} + \text{X}^-$.

+ k_{-2}). Therefore, particularly at longer reaction times, the first exponential term of both eq III and IV can be neglected. Introduction of these conditions reduces eq III and IV to V and VI, respectively.

for CNS

$$\frac{D_t - D}{D_0} = -\frac{(k_3' - k_{-2})}{(k_3' - k_2' - k_{-2})} e^{-k_3' t} + \frac{k_2' k_3'}{(k_2' + k_{-2})(k_3' - k_2' - k_{-2})} e^{-(k_2' + k_{-2}) t} \quad (\text{V})$$

for (CNS)₂⁻

$$\frac{D - D_t}{D_0} = -\frac{k_2'}{(k_3' - k_2' - k_{-2})} e^{-k_3' t} + \frac{k_2' k_3'}{(k_2' + k_{-2})(k_3' - k_2' - k_{-2})} e^{-(k_2' + k_{-2}) t} \quad (\text{VI})$$

Equation VI is identical with that previously reported.⁴

Taking the values for $k_3 (=k_1)$, k_2 , and k_{-2} as $2.8 \times 10^{10} M^{-1} \text{ sec}^{-1}$, $6.8 \times 10^9 M^{-1} \text{ sec}^{-1}$, and $3.4 \times 10^4 \text{ sec}^{-1}$, respectively, concentration *vs.* time curves for CNS and (CNS)₂⁻ formation were constructed from eq III and IV, using various values for k_6 . Comparison with our data from neutral solutions, as well as those of Baxendale, *et al.*,⁴ indicates that $k_6 > 5 \times 10^7 \text{ sec}^{-1}$. At the reaction times studied ($>0.2 \mu\text{sec}$), the kinetics are thus accounted for by k_3 , k_2 , and k_{-2} .

The molar extinction coefficient of CNS at 330 nm was calculated from the difference traces at 330 nm. Equation III was used to find D_0^{330} from the known values of k_2' , k_{-2} , k_3' , k_6 , D_t^{330} , and t . From $D_0^{330} = \epsilon_{\text{CNS}}^{330} [\text{OH}]_0$ and $D_0^{475} = (\epsilon_{(\text{CNS})_2^-}^{475} [\text{OH}]_0)$, it follows that $\epsilon_{\text{CNS}}^{330} = (D_0^{330} \epsilon_{(\text{CNS})_2^-}^{475}) / D_0^{475}$. From the measured values of D_0^{475} , *viz.*, the optical density at 475 nm for complete conversion to (CNS)₂⁻ and $\epsilon_{(\text{CNS})_2^-}^{475} = 7600 M^{-1} \text{ cm}^{-1}$ (ref 4), we obtain $\epsilon_{\text{CNS}}^{330} = 900 M^{-1} \text{ cm}^{-1}$.

Kinetics in Alkaline Solutions

Under alkaline conditions, the reverse reaction of equilibrium 6 can no longer be neglected and the kinetics become rather more involved. The general solution for the formation of the transient absorption now has the form

$$D_t/D_0 = a_1 e^{-\lambda_1 t} + a_2 e^{-\lambda_2 t} + a_3 e^{-\lambda_3 t} \pm D/D_0 \quad (\text{VII})$$

where a_1 , a_2 , and a_3 are functions of k_3' , k_6 , k_{-6}' , k_2' , and k_{-2} , $\lambda_1 = k_3'$ and λ_2 and λ_3 are the roots of quadratic equation VIII. Given that $k_6 > 5 \times 10^7 \text{ sec}^{-1}$, and

$$k_6 k_2' + k_6 k_{-2} + k_{-6}' k_{-2} = 0 \quad (\text{VIII})$$

thus $k_{-6} > 1.5 \times 10^9 M^{-1} \text{ sec}^{-1}$, and using the values of k_2 and k_{-2} quoted above, it can be shown that, in solutions of $\text{pH} > 12$, $\lambda_2 (\approx k_6 + k_{-6}') \gg \lambda_3$; under these conditions, eq VII simplifies to

$$D_t/D_0 = a_1 e^{-\lambda_1 t} + a_3 e^{-\lambda_3 t} \pm D/D_0 \quad (\text{IX})$$

Equation IX is formally similar to eq V and VI, replacing λ_1 by k_3' and λ_3 by $(k_2' + k_{-2})$.

For the formation and decay of CNSOH⁻ (observed as the difference traces at 390 nm), the general equation now takes the form

$$\frac{D_t - D}{D_0} = a_1 e^{-\lambda_1 t} + a_3 e^{-\lambda_3 t} \quad (\text{X})$$

Thus, the rate of formation of CNSOH⁻ is governed by λ_1 , and the decay by λ_3 . Plots of $\log (D_t - D)$ *vs.* t are linear at longer reaction time (see Figure 4), indicating that the term containing λ_1 has become negligible and that the first-order constant is λ_3 . Values of λ_3 obtained in this way for solutions containing varying amounts of CNS⁻ and OH⁻ are shown in Table II. Also shown are values of λ_3 calculated from the above-stated rate constants. (Note that λ_3 is independent of the values of k_6 and k_{-6}' providing these are $>5 \times 10^7 \text{ sec}^{-1}$), and it can be seen that these agree quite well with the experimental values. Thus the decay of CNSOH⁻ is adequately described by equilibria 6 and 2.

Table II: Rates of Decay of CNSOH⁻ in Pulsed Alkaline Thiocyanate Solutions

| [CNS ⁻] $\times 10^4$, M | [OH ⁻], M | λ_3 (obsd) $\times 10^{-6}$, sec^{-1} | λ_3 (calcd) $\times 10^{-6}$, sec^{-1} |
|---|----------------------------|---|--|
| 1.0 | 0.1 | 2.1 | 2.00 |
| 1.13 | 0.1 | 2.3 | 2.21 |
| 0.4 | 0.02 | 1.9 | 2.02 |
| 2.0 | 0.3 | 1.8 | 1.66 |

The observed deviation from linearity at shorter reaction times (*cf.* Figure 4) represents the contribution from the term in λ_1 . From eq X it follows that a logarithmic plot of the deviation, expressed as optical density, should be linear with slope λ_1 and an example of this procedure is included in Figure 4. Values of λ_1 for solutions containing different amounts of CNS⁻ and OH⁻ are collected in Table III, and it can be seen that they conflict with the idea that the rate-determining

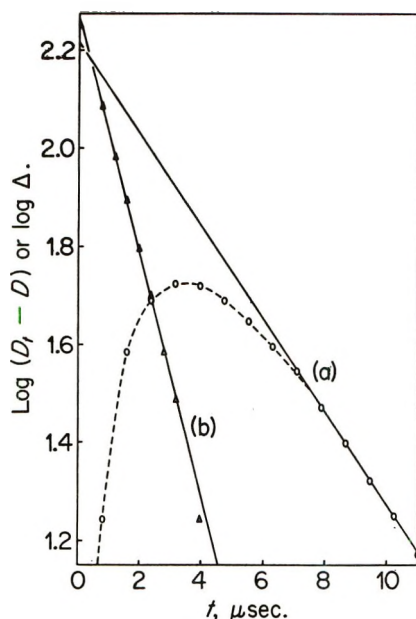


Figure 4. Kinetics of CNSOH^- in pulsed alkaline thiocyanate solutions, ($[\text{CNS}^-] = 10^{-4} M$, $[\text{OH}^-] = 10^{-1} M$): (a) logarithmic plot showing first-order decay at longer reaction times, (b) logarithmic plot of deviation of (a) from first-order kinetics at shorter reaction times (see text).

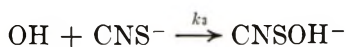
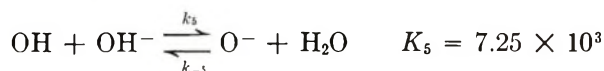
Table III: Rates of Formation of CNSOH^- in Pulsed Alkaline Thiocyanate Solutions

| $[\text{CNS}^-] \times 10^4, M$ | $[\text{OH}^-], M$ | $\lambda_1 \times 10^{-5}, \text{sec}^{-1}$ | $\lambda_1/[\text{CNS}^-] \times 10^{-9}, M^{-1} \text{sec}^{-1}$ | $k_4 \times 10^{-9}, M^{-1} \text{sec}^{-1}^a$ |
|---------------------------------|--------------------|---|---|--|
| 1.0 | 0.1 | 5.4 | 5.4 | 3.6 |
| 1.13 | 0.1 | 5.9 | 5.2 | 3.5 |
| 0.4 | 0.02 | 4.2 | 10.5 | 3.8 |
| 2.0 | 0.3 | 9.1 | 4.5 | 4.0 |

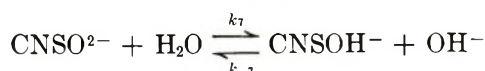
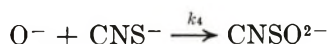
^a Mean $k_4 = 3.7 \pm 0.3 \times 10^9 M^{-1} \text{sec}^{-1}$.

constant is $k_3' (= k_3[\text{CNS}^-])$, where $k_3 = 2.8 \times 10^{10} M^{-1} \text{sec}^{-1}$.

Under alkaline conditions, we must thus consider oxidation of CNS^- by O^- (reaction 4). The rate of formation of CNSOH^- would then depend on the following reactions



$$k_3 = 2.8 \times 10^{10} M^{-1} \text{sec}^{-1}$$



An important consequence of the observed variation of $D_{(\text{CNS})_2^-}$ with $[\text{OH}^-]$ is that equilibrium 9 is excluded

and that $K_7 > 1$; therefore, for $[\text{OH}^-] < 1 M$ we can neglect $k_{-7}[\text{OH}^-]$. The formation of CNSOH^- will then be described by the equation

$$D_t/D_0 = 1 + a_1 e^{-k_7 t} + a_2 e^{-\lambda_4 t} + a_3 e^{-\lambda_5 t} \quad (\text{XI})$$

where a_1 , a_2 , and a_3 are functions of k_5' , k_{-5}' , k_3' , k_4' , and k_7 , and λ_4 and λ_5 are the roots of the quadratic equation

$$\lambda^2 = \lambda(k_5' + k_{-5}' + k_3' + k_4') +$$

$$k_5'k_4' + k_3'k_{-5}' + k_3'k_4' = 0 \quad (\text{XII})$$

Given the reported¹² values, $k_5 = 1.2 \times 10^{10} M^{-1} \text{sec}^{-1}$ and $k_{-5}' = 9.2 \times 10^7 \text{sec}^{-1}$, it follows that, in solutions above $\text{pH} \sim 12$, $\lambda_4 (\approx k_5' + k_{-5}') \gg \lambda_5$. If one now makes the assumption that $k_7 > k_6 > 5 \times 10^7 \text{sec}^{-1}$ (this assumption being not unreasonable, since one would expect the rate of hydrolysis of CNSO^{2-} to be greater than that of CNSOH^-), then $k_7 \gg \lambda_5$ at the concentrations of CNS^- and OH^- used. Equation XI then simplifies to

$$D_t/D = 1 + a_3 e^{-\lambda_5 t} \quad (\text{XIII})$$

and the rate of formation of CNSOH^- is determined solely by λ_5 . We can calculate λ_5 from eq XII using the known rate constants k_5 , k_{-5} , and k_3 , and various values of k_4 . The values of k_4 which correspond to λ_5 at the various CNS^- and OH^- concentrations used are given in Table III; a mean value of $k_4 = 3.7 \times 10^9 M^{-1} \text{sec}^{-1}$ is obtained. The formation of CNSOH^- in pulsed alkaline thiocyanate solutions can therefore be accounted for by reactions 5, 3, 4, and 7.

General Comments

The production of transient OH^- adducts of the type XOH^- should be a rather more general phenomenon, particularly from halides and pseudohalides. Indeed, the possibility of the formation of these in irradiated aqueous halide solutions has already been sporadically discussed in the literature.^{13,14} We have recently¹⁵ obtained optical evidence for a precursor of I_2^- in the pulse radiolysis of aqueous alkaline iodide solutions; this absorbs at $\sim 340 \text{nm}$ and, by analogy with the above observations, is probably attributable to IOH^- . Similar adducts are produced in irradiated aqueous alkaline glasses at low temperature, as noted above for systems containing CNS^- ions⁵ and also I^- ions.¹⁶ Symons and coworkers have recently identified XOH^- species (by esr spectroscopy) in certain solid systems irradiated at 77°K , e.g., ClOH^- from $\text{SrCl}_2 \cdot 6\text{H}_2\text{O}$

(12) G. V. Buxton, *Trans. Faraday Soc.*, **66**, 1656 (1970).

(13) M. Anbar and J. K. Thomas, *J. Phys. Chem.*, **68**, 3829 (1964).

(14) M. S. Matheson, W. A. Mulac, J. L. Weeks, and J. Rabani, *ibid.*, **70**, 2092 (1966).

(15) P. L. T. Bevan, M. Ebert, and G. Scholes, unpublished results.

(16) D. V. Bent, S. K. Ismail, and G. Scholes, unpublished results.

crystals¹⁷ and BrOH^- and IOH^- from frozen alkali halide solutions.¹⁸

Acknowledgment. The authors thank the staff of the Department of Physical Chemistry, Hebrew University of Jerusalem, Israel, and of the Paterson Labor-

atories, Christie Hospital and Holt Radium Institute, for providing facilities.

(17) R. C. Catton and M. C. R. Symons, *J. Chem. Soc. A*, 446 (1969).

(18) I. Marov and M. C. R. Symons, *ibid.*, 201 (1971).

Radiolysis of Water by Tritium β Rays: Scavenging of Hydrogen

Peroxide Precursors

by G. Lemaire, C. Ferradini, and J. Pucheault*

Centre nationale de la Recherche Scientifique, 94 Ivry, France (Received October 18, 1971)

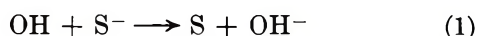
Publication costs borne completely by The Journal of Physical Chemistry

The influence of OH radical scavengers on the yield of H_2O_2 formation in 0.4 M H_2SO_4 solutions irradiated by tritium β rays was measured. Comparison with the results obtained with γ rays shows differences which can be explained by the increase in the number of "short tracks" (in the terminology of Mozumder and Magee).

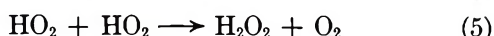
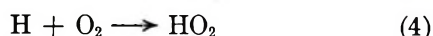
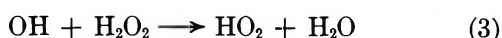
Introduction

In an earlier study,¹ we measured the initial yield of hydrogen peroxide formation in aerated 0.4 M H_2SO_4 solutions irradiated by tritium β rays. The value obtained, $G_0(\text{H}_2\text{O}_2) = 1.5 \pm 0.05$ molecules/100 eV, was in agreement with the molecular and radical yields determined by Collinson, Dainton, and Kroh,² that is: $G_{\text{H}} = 2.9$, $G_{\text{HO}_2} = 0$, $G_{\text{OH}} = 2.0$, $G_{\text{H}_2\text{O}_2} = 1.0$, and $G_{\text{H}_2} = 0.55$.

We felt it would be interesting to study the inhibition of molecular products by appropriate scavengers in order to see if this inhibition could be compared to that of γ rays. From this point of view, the use of bromide and chloride ions which inhibit the formation of H_2O_2 in the presence of air is particularly well suited. The mechanism of their action has been clearly established notably by Sworski³ as due to the occurrence of halide reactions,⁴ *i.e.*



in competition with those in the bulk of the solution



which do not change the formation yield of hydrogen peroxide since (1) + (2) is equivalent to (3)

$$G(\text{H}_2\text{O}_2) = G_{\text{H}_2\text{O}_2} + \frac{1}{2}(G_{\text{H}} - G_{\text{OH}})$$

Using the equation of material balance ($2G_{\text{H}_2\text{O}_2} + G_{\text{OH}} = 2G_{\text{H}_2} + G_{\text{H}}$), this yield can be expressed in terms of the molecular yields

$$G(\text{H}_2\text{O}_2) = 2G_{\text{H}_2\text{O}_2} - G_{\text{H}_2} \quad (I)$$

On the other hand, when S^- ions are present in high concentrations, it is recognized that the $G_{\text{H}_2\text{O}_2}$ molecular yield is diminished by $\Delta G_{\text{H}_2\text{O}_2}$ through the competition, in zones of high radical densities, of reaction 1 with the local formation of hydrogen peroxide



The fate of S, after diffusion, being identical with that described previously (reaction 2), it is as though supplementary OH radicals were recuperated by reaction 3, and the variation of the final yield can be reached by differentiating expression I, that is

$$\Delta G(\text{H}_2\text{O}_2) = 2\Delta G_{\text{H}_2\text{O}_2} \quad (II)$$

provided that the G_{H_2} yield is not modified by this heterogeneous process which can thus be expressed by

(1) G. Lemaire and C. Ferradini, *Radiochem. Radioanal. Lett.*, **5**, 175 (1970).

(2) E. Collinson, F. S. Dainton, and J. Kroh, *Proc. Roy. Soc.*, **265**, 422 (1962).

(3) T. J. Sworski, *J. Amer. Chem. Soc.*, **76**, 4687 (1954).

(4) E. J. Hart, *Radiat. Res.*, **1**, 53 (1954).

the corresponding decrease in the global yield of hydrogen peroxide.

We thus used Cl^- and Br^- scavengers in order to be able to compare these $G_{\text{H}_2\text{O}_2}$ inhibitions in the case of tritium β rays with those corresponding to other qualities of radiation. It is known that the hydrogen yield can be modified in high concentrations of halides and that in certain cases even the elemental halogen may appear.⁵⁻⁷ Thus we have limited our study to a region of concentration ($[\text{Cl}^-] < 1 M$, $[\text{Br}^-] < 10^{-2} M$), where these two phenomena do not interfere appreciably.⁸⁻¹⁰

Experimental Section

1. Irradiations by Tritium β Rays. Tritium is a pure β emitter with a half-life of 12.4 years. The maximum energy of the β rays is 18.6 keV while the median energy is 5.6 keV. We used tritiated water as "vector." The maximum path length of tritium β rays in water is 6μ and wall effects were thus avoided.

While there are no external irradiation problems, those of internal contamination are considerable since all the β rays emitted by a tritium source internal to the organism are totally absorbed by it. This consideration led us to perform all the manipulations in a ventilated glove box.

All the chemicals used were of Merck manufacture. The Pyrex containers were washed with boiling aqua regia. They were then rinsed in ordinary water, then in monodistilled water, and finally in triple-distilled water. When they had been dried they were put into an oven (600°) for 6 hr.

The tritiated water came from CEN (Saclay). Its activity was about 1 to 5 Ci cm^{-3} . Using a volume of tritiated water of about 1-2 cm^3 , the following operations were performed: after a first dilution to 20 cm^3 (with triple-distilled water), four distillations were carried out: the first in the presence of potassium permanganate, the second in the presence of barium hydroxide; the third and fourth were simple distillations performed in a Pyrex bidistillator. After this treatment, the average conductivity of the water was around 10^{-6} mho cm and its pH about 5.7, just after the end of the distillation. A second dilution with triple-distilled water whose conductivity was the same occurred when the active solutions were put in the Pyrex storage recipients.

The analyses were performed on samples of 1 cm^3 taken at regular intervals, taking into account the activity of the different solutions. The quantitative determination of H_2O_2 was done by cerimetry. The 0.4 M sulfuric solutions of ceric sulfate ($\sim 7 \times 10^{-4} M$) are slightly unstable and in order to take into account the eventual variations of Ce^{IV} during the day, analyses were made each morning in two ways: (1) by spectrophotometry at 320 nm with ϵ 5580 $M^{-1} \text{cm}^{-1}$, and

(2) by volumetry using a standard solution of ferrous ammonium sulfate.

Doses were determined by Fricke's method by adopting $G(\text{Fe}^{\text{III}}) = 12.7$ as the oxidation yield during radiolysis by tritium β rays, a value established by Hart.⁴ In order to do this, a tritiated $2 \times 10^{-3} M$ ferrous ammonium sulfate solution in 0.4 M H_2SO_4 was used. The quantities of ferric ions that had appeared were measured by cerimetry on 1- cm^3 samples of the solution taken at regular intervals. A constant rate of growth that leads to a dose rate of 5.68×10^{16} eV hr^{-1} was found in this particular case.

2. Irradiations by Cobalt-60 γ Rays. The same experiments were also carried out using ^{60}Co as a source of radiation (source of 300 Ci). The dosimetry was done using Fricke's method, taking $G(\text{Fe}^{\text{III}}) = 15.7$ and determining Fe^{III} concentrations by spectrophotometry.

Results

The experiments show that the formation of H_2O_2 in aerated 0.4 M H_2SO_4 solutions is linear with dose for the concentrations of chloride and bromide ions used and depends on these concentrations. Table I summarizes all the results.

Table I

| [KCl], M | Tritium β rays $G(\text{H}_2\text{O}_2)$ | ^{60}Co γ rays $G(\text{H}_2\text{O}_2)$ |
|--------------------|---|---|
| 0 | 1.5 | 1.20 |
| 10^{-4} | 1.39 | 1.13 |
| 10^{-3} | 1.16 | 1.08 |
| 10^{-2} | 1.03 | 0.94 |
| 5×10^{-2} | 0.82 | 0.87 |
| 10^{-1} | 0.7 | 0.70 |
| 5×10^{-1} | 0.13 | 0.53 |
| 1 | <0.1 | 0.18 |
| [KBr], M | $G(\text{H}_2\text{O}_2)$ | $G(\text{H}_2\text{O}_2)$ |
| 0 | 1.5 | 1.20 |
| 10^{-4} | 1.28 | 1.12 |
| 10^{-3} | 1.04 | 1.01 |
| 5×10^{-3} | 0.83 | |
| 10^{-2} | 0.58 | 0.81 |

One can see that, for irradiation by tritium β rays, $G(\text{H}_2\text{O}_2)$ is lowered from 1.5 to 0.13 molecules/100 eV when the concentration of chloride ions varies from 0 to $5 \times 10^{-1} M$. For a concentration of Cl^- equal to or greater than 1 M the inhibition is almost total.

(5) A. R. Anderson and B. Knight, *Proc. 2nd Int. Congr. Radiat. Res., Harrogate*, 57 (1962).

(6) S. A. Brusentseva and P. I. Dolin, *Proc. All-Union Conf. Radiat. Chem., 1st, Moscow*, 69 (1957).

(7) A. M. Kabakchi, *Russ. J. Phys. Chem.*, **30**, 1906 (1956).

(8) A. M. Koulkes-Pujo, *Ann. Chim.*, **5**, 707 (1960).

(9) J. Pucheault and C. Ferradini, *J. Chim. Phys.*, **58**, 606 (1961).

(10) A. Rafi and H. C. Sutton, *Trans. Faraday Soc.*, **61**, 509 (1965).

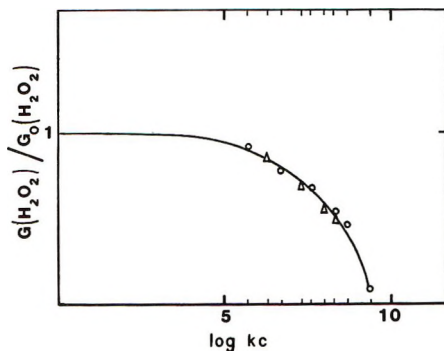


Figure 1. Influence of halide concentration on $G(\text{H}_2\text{O}_2)$: O, with $k_{\text{Cl}^-} = 4 \times 10^9 \text{ M}^{-1} \text{ sec}^{-1}$ for chloride; Δ , $k_{\text{Br}^-} = 1.6 \times 10^{10} \text{ M}^{-1} \text{ sec}^{-1}$ for bromide.

$G(\text{H}_2\text{O}_2)$ is lowered from 1.5 to 0.58 molecules/100 eV when the concentration of bromide ions increases from 0 to 10^{-2} M .

In the case of irradiation by ^{60}Co γ rays, $G(\text{H}_2\text{O}_2)$ is lowered from 1.2 to 0.18 when the concentration of chloride ions rises from 0 to 1 M and from 1.2 to 0.81 for bromide concentrations increasing from 0 to 10^{-2} M .

In conclusion, both in the case of γ rays and that of β rays, the identity of the mechanism for the two scavengers used is shown by the curve in Figure 1, which represents the ratio $G(\text{H}_2\text{O}_2)/G_0(\text{H}_2\text{O}_2)$ plotted against $\log kc$, where $G_0(\text{H}_2\text{O}_2)$ is the yield in absence of scavenger, C is the scavenger concentration at which the yield is $G(\text{H}_2\text{O}_2)$, and k is the rate constant of its reaction (1) with OH, that is, $4 \times 10^9 \text{ M}^{-1} \text{ sec}^{-1}$ for Cl^- and $1.6 \times 10^{10} \text{ M}^{-1} \text{ sec}^{-1}$ for Br^- .¹¹ It can be seen that, for each type of radiation, the points corresponding to the two halides, as we might expect, are on the same curve. Moreover the inhibition of the H_2O_2 yield for tritium β rays is greater than for γ rays (see experimental points in Figure 2). We will now discuss these results in relation to theoretical and other experimental work.

Discussion

Many mathematical analyses have been made to explain theoretically reactions which occur during the diffusion of radiolytic entities in the presence of solutes which scavenge these entities. These calculations have been treated notably by Magee¹² and by Kupperman,¹³ who suppose that initially the H and OH species are formed in sites that are microscopic in size and that during diffusion there occurs a combination between two identical radicals (reaction 6, for instance).

This sort of model, called the "one radical model," coupled with well chosen constants, gave results which are in reasonable agreement with experiments using γ rays. In this case, the sites where the radicals were produced—called "spurs"—were considered to consist on the average of isolated spherical zones which enclosed the tracks of secondary electrons of about 100 eV, thus having initial dimensions of about 10 \AA and

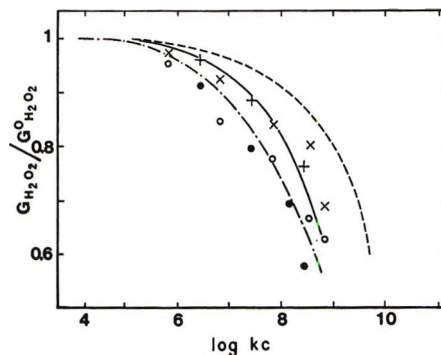


Figure 2. Inhibition of $G_{\text{H}_2\text{O}_2}$ by halides. Theoretical curves: —, isolated spurs; cylindrical tracks: - - -, 8.5×10^7 radicals/cm; - · - ·, 34×10^7 radicals/cm. Experimental points: tritium β rays: O, Cl^- ; ●, Br^- ; ^{60}Co γ rays: x, Cl^- ; +, Br^- .

containing about ten radicals. Schwarz, for instance,¹⁴ showed the validity of this model since, for many scavengers, the results could be plotted on curves similar to those in Figure 1, but calculated according to the preceding principles.

For many years, the subject of the influence of the nature and energy of the radiation was treated in terms of stopping power or LET (linear energy transfer, dE/dx). So defined, LET was considered to be the parameter which reflected this influence in a univocal way. The calculations were carried out following the model of the "string of beads" and of the "cylindrical tracks." For LET higher than that of electrons produced by ^{60}Co γ rays, the mean zones of heterogeneity are no longer considered to be isolated from one another along the track. As the LET increases, they draw closer together until there is an "overlapping;" this occurs when their average distance from one another is less than their diameter for an expansion where the radical-radical reactions became negligible (if, by diffusion, the radius grows ten times, the rate of the radical-radical reactions decreases by a factor of 10^6 , simply as a result of this expansion). However, according to this model, tritium β rays differ little from ^{60}Co γ rays: for a track of an electron of 5.6 keV (the average energy of the β spectrum), the average LET is about $10 \text{ keV}/\mu$, which corresponds to 10^7 radicals/cm and to a separation of spurs of 100 \AA that is about ten times their initial diameter. The radical and molecular yields should thus be little different from those for isolated "spurs" and, if one only takes into account these mean parameters, the model "string of beads" cannot explain differences that we have noted between the efficiencies with which halide ions decrease the molecular hydrogen peroxide yield for the two sorts of radiation.

(11) M. Burton and K. C. Kurien, *J. Phys. Chem.*, **63**, 899 (1959).

(12) J. L. Magee, *J. Chim. Phys.*, **52**, 52 (1955).

(13) A. Kupperman in "Actions Chimiques et Biologiques des Radiations," 5th Series, M. Haissinsky, Ed., Paris, 1961.

(14) H. A. Schwarz, *J. Amer. Chem. Soc.*, **77**, 4960 (1955).

In fact, it has been known for a long time that the zones of heterogeneity are of different sizes and that merely taking an average value for the corresponding parameters does not permit the interpretation of all radiolytic phenomena. There exists, in fact, a spectrum of secondary electron energies which correspond to cross sections of energy transfer which can be determined, for the lowest energies, according to the excitation function of the irradiated solvents and by using Born's approximation (Möller's formula, for example) for the highest. Thus Mozumder and Magee insisted particularly on the importance of this energy distribution of secondary electrons (classed in order of increasing energy as "spurs," "blobs," "short tracks," and "branch tracks") and elaborated a corresponding method of calculation.^{15,16} Burch,¹⁷ in a similar calculation, has already shown that by taking into consideration short tracks for tritium β rays, one calculates for the oxidation yield of Fe^{2+} in aerated sulfuric solution a value as low as 12.7. In the case of the inhibition of molecular products by scavengers, an application of this method is all the more necessary in that the results are determined by the characteristics of the zones in which the formation and inhibition of these products do actually take place; thus they cannot be determined with mean parameters which take into account zones in which these phenomena are not of primary importance.

For a certain number of these zones of heterogeneity (and above all short tracks which correspond to energy transfers of between 500 and 5000 eV), the mean density of the radicals formed along the secondary tracks thus defined is such that it is necessary to use the cylindrical model of diffusion in order to treat the problem of the scavengeability by various solutes. This treatment was carried out notably by Kupperman for high LET radiations and, comparing with the diffusion model for isolated spherical spurs, he came to the following different conclusions.

(a) Until about 100 keV/ μ , the density of radicals in cylindrical tracks is initially smaller than that in spurs as they were defined above as mean zones of heterogeneity for γ rays. The radical expansion by diffusion of the radiolytic species is certainly slower as is the corresponding lowering of concentrations, but this growth of importance of the time factor hardly favors at all the radical-radical reactions compared with the radical solute reactions. Theoretically it follows that, while the molecular yields are greater than for isolated spurs, the action of the scavengers should be more efficient in order to diminish these yields. This is the reverse of the prediction of Mozumder¹⁸ for the short tracks of tritium β rays.

(b) For higher LET, for example the mean LET along the track of the ^{210}Po α rays, the density of the radicals is, on the contrary, higher from the very beginning of the diffusion than in the case of isolated spurs.

The production of the molecular products must thus not only increase considerably but must also be inhibited by the scavengers with greater difficulty. This was remarked on by Burton and Kurien,¹¹ who irradiated halide solutions with external α ray sources using the same experimental principles as those described here.

In Figure 2 are drawn the inhibition curves for $G_{\text{H}_2\text{O}_2}$, curves which are calculated according to Kupperman theory (page 128 of ref 13) and concern the three types of diffusion examined qualitatively above: isolate spurs, cylindrical track with 8.5×10^7 radicals/cm, and high density tracks (34×10^7 radicals/cm). We have also plotted on this figure our experimental points for Cl^- and Br^- scavengers; the calculation of $G_{\text{H}_2\text{O}_2}$ from $G(\text{H}_2\text{O}_2)$ was done according to expression I taking for G_{H} the values of 0.45 for γ rays and 0.55 for tritium β rays.² On the one hand, we can see that the results for the γ rays correspond closely to the theoretical curve for isolated spurs; the values of the parameters of these mean spurs had furthermore been chosen to account for analogous phenomena. On the other hand, insofar as tritium β rays are concerned, the experimental points are even slightly to the left of the calculated curve for cylindrical tracks of low density which express an even greater scavengeability. It would seem that the major part of the hydrogen peroxide was thus formed (and eventually inhibited) in heterogeneous zones analogous to those of the "short tracks" of electrons from 500 to 5000 eV (50 to 10 keV/ μ ; 5.10^7 to 10^7 radicals/cm). The difference that was noted between the two sorts of radiation thus springs essentially from the difference in the distribution of the diverse heterogeneous zones; the proportion of energy spent in "short tracks" is much greater in the case of tritium β rays (primary electrons of low energy in the β spectrum, end of trajectories secondary electrons) while for ^{60}Co γ rays, the majority of the heterogeneous zones in which H_2O_2 is formed are smaller ("blobs" and "spurs") and have characteristics which are closer to those used for calculations of diffusion with spherical symmetry. From this point of view, the 50-keV X-rays used also by Burton and Kurien¹¹ are close to the ^{60}Co γ rays, and effectively, in Figure 2, their experimental points for the inhibition of $G(\text{H}_2\text{O}_2)$ by Cl^- ions can be placed between the two curves for the two sorts of radiation examined here.

Recently, Appleby and Gagnon¹⁹ published a study on the inhibition by Cu^{2+} of the molecular yield of hydrogen in solutions of tritiated water. These authors

(15) A. Mozumder and J. L. Magee, *Radiat. Res.*, **28**, 203 (1966).

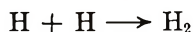
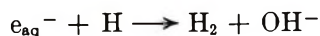
(16) A. Mozumder and J. L. Magee, *ibid.*, **28**, 215 (1966).

(17) P. R. J. Burch, *ibid.*, **11**, 481 (1959).

(18) A. Mozumder in "Advances in Radiation Chemistry," M. Burton and J. L. Magee, Ed., Interscience, New York, N. Y., 1969, p 71.

(19) A. Appleby and W. F. Gagnon, *J. Phys. Chem.*, **75**, 601 (1971).

noted that, in contradiction to our results for H_2O_2 , it is more difficult to inhibit the yield G_{H_2} than in the case of γ rays. Their interpretation is essentially based on the hypothesis that the differences in the spectrum of electrons for the two qualities of radiation brought about a variation in the relative importance of the reactions responsible for the formation of H_2 , that is



and no doubt a fourth process whose nature is still little understood. In each of the entities described by Mozumder and Magee (spurs, blobs, short tracks, and branch tracks) these processes would evolve differently and their inhibition by a scavenger would be different. This accounts for the differences of scavengability observed for H_2 produced by tritium β rays and by ^{60}Co γ rays, for which the distributions of the above entities are different.

Even though the origin of molecular H_2 is still a matter of controversy, it seems that this hypothesis is

very reasonable. The results of Appleby and Gagnon would thus not be in contradiction with our own interpretation on the formation of H_2O_2 . The latter comes from a process which seems to be less complex and is thus more appropriate for the study of heterogeneities during radiolysis.

We intend, in another paper, to present a method of analytical calculation which would permit the determination of the percentage of energy spent in "short tracks" for various qualities of radiation, calculations which can easily be applied in cases of complex spectrum like that of tritium β rays.²⁰ The present discussion, based on critical experimental work, underlines the inadequacy of the linear parameter $\text{LET} = -dE/dx$ and the need to take into consideration a LET that is doubly differentiated. A first approximation treats the secondary electrons which arise from energy transfer greater than 100 eV, for example, as independent; this leads to the concept of "LET spectra," advocated for a long time by many radiobiologists (see, for example, ref 21).

(20) J. Pucheault and G. Lemaire, to be published.

(21) P. Howard-Flanders, *Advan. Biol. Med. Phys.*, **6**, 553 (1958).

An Electron Paramagnetic Resonance Study of the Cu^+ -NO Complex in a Y-Type Zeolite

by C. C. Chao and J. H. Lunsford*

Department of Chemistry, Texas A&M University, College Station, Texas 77843 (Received December 28, 1971)

Publication costs assisted by The Robert A. Welch Foundation

The Cu^+ -NO complex in a Y-type zeolite was formed by the reaction of Cu^+ with adsorbed nitric oxide. The epr hyperfine structure reveals that the unpaired electron spends 20% of its time on the Cu^+ ion and is distributed about evenly between the $3d_{z^2}$ and $4s$ orbitals on the copper. The molecular axis of NO is essentially parallel to the axis of the $3d_{z^2}$ orbital.

It is known that Cu^{2+} in a Y-type zeolite can be reduced to Cu^+ with CO, and at low temperatures NO molecules can be adsorbed on the Cu^+ ions reversibly.¹ In this article we report on the results of epr studies on the Cu^+ -NO complex in Cu^+ -Y and the structural information deduced from this work.

The Cu^{2+} -Y samples were prepared by exchanging NaY in $\text{Cu}(\text{NO}_3)_2$ solutions three times. The extensively exchanged samples were degassed to 500° and reduced in an atmosphere of 500 Torr of CO at the

same temperature. The extent of reduction was monitored by observing the intensity change of the epr spectrum of the Cu^{2+} ion. Purified nitric oxide was admitted onto the samples at room temperature and usually at a pressure of 20 Torr. The epr measurements were carried out with an X-band spectrometer at 77°K and a Q-band spectrometer at about 120°K.

(1) C. M. Naccache and Y. Ben Taarit, *J. Catal.*, **22**, 171 (1971), and private communication.

Table I: *g* Values and Hyperfine Splitting (in G) for Cu⁺-NO, Cu²⁺, and Adsorbed NO

| Centers | <i>g</i> | <i>g</i> _⊥ | <i>A</i> | <i>A</i> _⊥ | Ref |
|---|------------------------|-----------------------|------------------------|-----------------------|-----------|
| Cu ⁺ -NO in Y-type zeolite | 1.89 | 2.009 | 240 | 190 (Cu) | This work |
| Cu ²⁺ in Y-type zeolite ^a | 2.39 | 2.06 | 120 | ~20 (Cu) | This work |
| ¹⁴ N on MgO | 1.89 | 1.996 | ... | 33 (N) | 2 |
| ¹⁴ N on ZnO | 1.94 | 1.979 | ... | 30 (N) | 3 |
| ¹⁴ N on NaY | 1.86 | 1.898 | ... | 28 (N) | 4 |
| ¹⁴ N on decationated Y | 1.95 | 1.996 | ... | 14 (Al) | 4 |

^a Partially reduced sample.

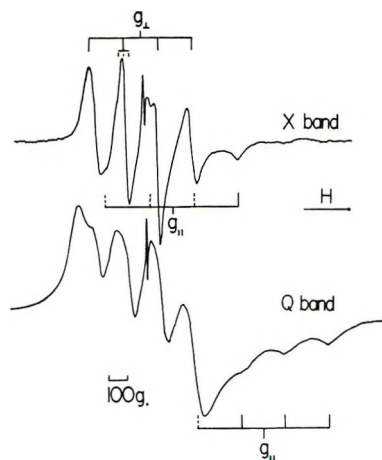


Figure 1. Epr spectra of the Cu⁺-NO complex. The small sharp peak is due to DPPH.

The spectra thus obtained are given in Figure 1. The intensity of lines decreased drastically as the temperatures rose above 120°K. No spectra could be obtained at a temperature above 150°K.

The X-band spectrum alone is rather ambiguous, but together with the Q-band spectrum they unmistakably show characteristics of randomly oriented paramagnetic centers which have an electron spin equal to 1/2 and *g*_⊥ > *g*_{||}. They also show that the electron spin is interacting with a nucleus of spin 3/2 which produces a large hyperfine splitting. The measured *g* values and hyperfine splitting constants are tabulated in Table I.²⁻⁴

The nuclear spin of ¹⁴N (99.6% natural abundance) is 1, whereas both ⁶³Cu (69.09%) and ⁶⁵Cu (30.91%) have a nuclear spin of 3/2. The observed hyperfine structure must come from the interaction of a paramagnetic electron with a Cu nucleus. If the paramagnetic electron completely resides in an orbital of nitric oxide, it can only interact with the copper nucleus by dipole-dipole interaction. The dipolar interaction of an electron in an adsorbed nitric oxide molecule with a copper nucleus is roughly given by $\mu_e \mu_I / r^3 = 0.2$ G which can account for only 0.1% of the hyperfine splitting observed. The possibility that the paramagnetic center is a free copper atom is also ruled out, since the epr spectrum of the matrix-isolated Cu atom is known to

have an isotropic hyperfine splitting of 6000 MHz (~2100 G).⁵ The species also cannot be Cu²⁺ ions since in order to produce Cu²⁺ the reaction Cu⁺ + NO → Cu²⁺NO⁻ must occur on the surface. The adsorption of NO on the transition metals has been extensively studied and the reaction M + NO → M⁺NO⁻ was not observed.⁶ It is unlikely that Cu⁺ more readily gives up an electron than a neutral metal to reduce the nitric oxide. Furthermore, the *g* values of this complex are quite different from the *g* values of normal Cu²⁺ ions in Y-type zeolites (Table I).

It appears most reasonable to postulate that the paramagnetic electron spends most of its time in the NO ligand and only a small fraction of its time in an empty orbital of Cu⁺. The contribution of the copper ion to the total wave function is a mixture of 3d and 4s atomic wave functions. The ground state of Cu⁺ is d¹⁰; however, the excited 3d⁹4s¹ states have their energy level very close to the ground state. Indeed, as Orgel⁷ has shown, the tendency of Cu⁺ to form linear structural salts can best be explained by 3d_{z²}-4s mixing. We assume in the zeolite that the first empty orbital of Cu⁺ is a mixture of 3d_{z²} and 4s orbitals which may be described by

$$\psi_{\text{Cu}^+} = \kappa d_{z^2} - \epsilon s \quad (1)$$

According to Abragam and Pryce,⁸ the nuclear hyperfine interaction of copper can be expressed in terms of the Hamiltonian

$$H = g_n \beta_n g_e \beta_e \left[\frac{8}{3} \pi \delta(r) \vec{S} \cdot \vec{I} + \frac{(\vec{L} - \vec{S}) \cdot \vec{I}}{r^3} + \frac{3(\vec{S} \cdot \vec{r})(\vec{r} \cdot \vec{I})}{r^5} \right] \quad (2)$$

Here *g*_n and *g*_e are *g* values of the nucleus and electron;

- (2) J. H. Lunsford, *J. Chem. Phys.*, **46**, 4347 (1967).
- (3) J. H. Lunsford, *J. Phys. Chem.*, **72**, 2141 (1968).
- (4) J. H. Lunsford, *ibid.*, **72**, 4163 (1968).
- (5) P. H. Kasai and D. McLeod, Jr., *J. Chem. Phys.*, **55**, 1566 (1971).
- (6) A. N. Terenin and L. M. Roev, *Actes Congr. Int. Catal.*, **2nd**, 2, 2183 (1961).
- (7) L. E. Orgel, *J. Chem. Soc.*, 4188 (1958).
- (8) A. Abragam and M. H. L. Pryce, *Proc. Roy. Soc., Ser. A*, **205**, 135 (1951).

β_n and β_e are the Bohr magneton of the nucleus and electron; $\delta(r)$ is the Dirac δ function; and \bar{L} , \bar{S} , and \bar{I} are the orbital, electron spin, and nuclear spin angular momentum operators, respectively. In the calculation of the hyperfine splitting constants several simplifications can be made. For $3d_{z^2}$ and $4s$ orbitals the \bar{L} component has vanishing matrix elements. Also, the S_x and S_y terms in eq 2 may be neglected since the electronic Zeeman energy term is much larger than the other terms in the spin Hamiltonian. Since the wave function has significant s character, the electron spin is approximately quantized along the external field. With such simplifications one arrives at the following expression for the hyperfine splitting

$$A = g_e \beta_e g_n \beta_n \left[\frac{8}{3} \pi |\psi_{\text{Cu}^+}(0)|^2 + \frac{\langle \cos^2 \alpha - 1 \rangle (3 \cos^2 \theta - 1)}{2 \langle r^3 \rangle} \right] \quad (3)$$

Here, α is the angle between r and the z axis of the hydrogenic wave function used; θ is the angle between H_0 and the z axis of the hydrogenic wave function. For the $3d_{z^2}$ orbital, $\langle 3 \cos^2 \alpha - 1 \rangle = 4/7$ and for the $4s$ orbital $\langle 3 \cos^2 \alpha - 1 \rangle = 0$. From the atomic beam measurements one has $g_e \beta_e g_n \beta_n \frac{8}{3} \pi |\psi_{4s}(0)|^2 = 5867$ MHz for $^{63}\text{Cu}^9$ and from the optical spectrum of the ^{63}Cu in the $3d^9 4s^2$ configuration one has $g_e \beta_e g_n \beta_n \langle r^{-3} \rangle_{3d} = 1080$ MHz.¹⁰

According to eq 3 the value of A will be largest when the static field is parallel to the axis of the $3d_{z^2}$ orbital and smallest when the static field is perpendicular to the z axis. This implies that if the z principal axis of the g tensor (*i.e.*, the molecular axis of NO) is parallel to the z axis of $3d_{z^2}$, one should observe that the g_{\parallel} is associated with the largest possible A value. If the molecular axis of NO is perpendicular to the z axis of $3d_{z^2}$, then the situation is just the reverse. Since the observed hyperfine splitting associated with g_{\parallel} is significantly larger than the one associated with g_{\perp} , the molecular axis of NO is essentially parallel to the axis of the $3d_{z^2}$ orbital. Assuming they are actually parallel to each other and using eq 1 and 3 along with

the measured values of A_{\parallel} or A_{\perp} , one obtains $\epsilon^2 = 0.098$ and $\kappa^2 = 0.107$. This means that the unpaired electron spends about 20% of its time on Cu^+ and is distributed about evenly between the $3d_{z^2}$ and $4s$ orbitals.

The ^{14}N hyperfine components in the perpendicular direction are poorly resolved; however, the breadth of the lines indicates that the splitting is on the order of 25 to 30 G. This is consistent with the splitting observed for NO on other surfaces (Table I).

The g values of this complex are similar to the g values of nitric oxide molecules adsorbed on MgO, ZnO, NaY, decationated-Y (Table I), etc., but there is one major difference; the Cu^+NO complex has $g_{\perp} > g_e$, whereas all the others have $g_e > g_{\perp}$. If the paramagnetic electron is completely localized in an orbital of NO, which has $2p\pi^*$ as its main component, the observed g values imply that the symmetry of the complex is lower than orthorhombic, and is probably triclinic. For this particular case g_{zx} and g_{yy} are expected to be very close to each other and they may be unresolved. The expressions of g values for O_2^- in orthorhombic and in triclinic symmetry were derived by Kanzig and Cohen¹¹ and by Miller and Haneman,¹² respectively. No such clear-cut conclusion concerning symmetry, however, can be made in the present case, since we know that 20% of the paramagnetic electron is in the Cu^+ . In CuF_2 , where the paramagnetic electron is also in a $3d_{z^2} 4s$ hybridized orbital, the value of g_{\perp} is 2.60.¹³ It is quite possible that g_{\perp} for Cu^+NO is 1% larger than g_e because of the delocalization of the electron into Cu^+ rather than because of triclinic symmetry.

Acknowledgments. The authors wish to acknowledge fruitful discussions with Drs. C. Naccache and Y. Ben Taarit. This work was supported by The Robert A. Welch Foundation under Grant No. A-257.

- (9) Y. Ting and H. Lew, *Phys. Rev.*, **105**, 581 (1957).
- (10) R. Ritschl, *Z. Phys.*, **79**, 1 (1932).
- (11) W. Kanzig and M. H. Cohen, *Phys. Rev. Lett.*, **3**, 509 (1959).
- (12) D. J. Miller and D. Haneman, *Phys. Rev. B*, **3**, 2918 (1971).
- (13) P. H. Kasai, E. B. Whipple, and W. Welter, Jr., *J. Chem. Phys.*, **44**, 2581 (1966).

Electronic Absorption Studies of the Radical Complex between Perylene and Tetracene Cations

by Tomoko Yamazaki and Katsumi Kimura*

*Physical Chemistry Laboratory, Institute of Applied Electricity, Hokkaido University, Sapporo, Japan
(Received November 29, 1971)*

Publication costs borne completely by The Journal of Physical Chemistry

Equilibrium constants and heat of formation of the 1:1 complex between the radical cations of perylene and tetracene have been obtained in a concentrated sulfuric acid solution by analyzing electronic absorption spectra. Absorption bands associated with interradical charge transfer were observed in the near-infrared region. Using the charge-transfer theory, the formation of the radical complex is interpreted in terms of a stabilization energy due to the interradical charge-transfer interactions, compared with the formation of the radical dimers. A possible geometry of this radical complex is suggested from the calculation of the charge-transfer stabilization energies carried out for various geometrical structures.

Introduction

Recently, the reversible dimerizations of the radical cations of *p*-phenylenediamine,¹ *p*-dialkoxybenzenes,² perylene, and tetracene³ in solution have been studied spectroscopically by Kimura, *et al.* Particularly in the perylene cation (perylene⁺) and the tetracene cation (tetracene⁺), equilibrium constants and heats of formation for the monomer-dimer equilibria have been determined in concentrated sulfuric acid.³ Furthermore, the present authors have recently reported in a short communication that a 1:1 radical complex can be formed between perylene⁺ and tetracene⁺ in concentrated sulfuric acid.⁴ This may be a typical example of a radical complex. So far, no examples have been reported for radical complexes except that consisting of two kinds of Würster's cations reported by Takemoto, *et al.*⁵ The formation of an ordinary charge-transfer (CT) complex is generally interpreted by Mulliken's theory,⁶ with which a number of studies have been carried out. It is of particular interest to apply the CT theory to the radical association.

Under these circumstances, we consider it important to investigate in more detail the formation of the perylene⁺-tetracene⁺ complex by means of the spectrophotometric technique. Comparison of thermodynamic data between the formation of the radical complex and the radical dimers will be of interest. In the present paper we report some thermodynamic data of complex formation, compared with those of the radical dimers, and discuss the formation of the radical complex by considering stabilization energy due to interradical charge transfer.

Experimental Section

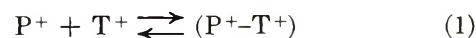
Spectrophotometers, absorption measurements at low temperatures, and method of purifying samples used here are the same as described before.³ Perylene and

tetracene are readily soluble in concentrated sulfuric acid, forming the stable radical cations. Electronic absorption spectra of the mixed solutions were measured at various concentrations of the component cations from 10⁻⁴ to 10⁻⁵ M and at various temperatures from -30 to 25°.

Experimental Results and Analysis

Upon mixing of the two cations, several new absorption bands are observed at 264, 310, 371, 480, and 722 nm in addition to the absorption bands of the cations themselves. Several isosbestic points exist, as shown in Figure 1. From the previous analysis of the absorption intensities, using the continuous-variation method, it has been revealed that the perylene⁺ and tetracene⁺ are in equilibrium with the 1:1 complex in solution.⁴

In order to determine the equilibrium constants and heat of formation of the perylene⁺-tetracene⁺ complex, electronic absorption spectra were analyzed as follows. In the mixed solution at low temperature, the following three equilibria may exist



where P⁺ and T⁺ represent perylene⁺ and tetracene⁺,

(1) K. Kimura, H. Yamada, and H. Tsubomura, *J. Chem. Phys.*, **48**, 440 (1968).

(2) H. Yamada and K. Kimura, *ibid.*, **51**, 5733 (1969).

(3) K. Kimura, T. Yamazaki, and S. Katsumata, *J. Phys. Chem.*, **75**, 1768 (1971).

(4) T. Yamazaki and K. Kimura, *Bull. Chem. Soc. Jap.*, **44**, 298 (1971).

(5) K. Takemoto, S. Nakayama, K. Suzuki, and Y. Ooshika, *ibid.*, **41**, 1974 (1968).

(6) R. S. Mulliken, *J. Amer. Chem. Soc.*, **74**, 811 (1952).

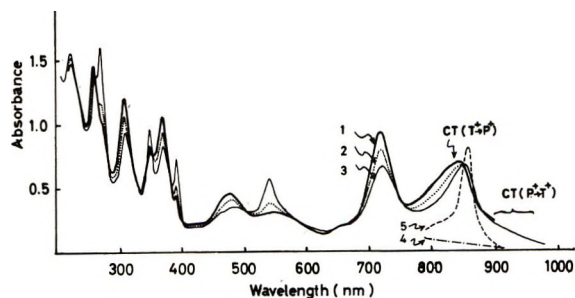


Figure 1. Temperature dependence of the absorption spectrum of the mixed solution of perylene⁺ ($2.38 \times 10^{-6} M$) and tetracene⁺ ($2.21 \times 10^{-6} M$): (1) 25°, (2) -10°; (3) -30°. Curves 4 and 5 are the longest wavelength absorptions of perylene⁺ and tetracene⁺, respectively, at room temperature.

respectively. Dimerization equilibria 2 and 3, appreciable at low temperatures, have already been studied in detail in our previous work,³ so that information about (1) can be derived in principle from the analysis of absorption intensities of the mixed solutions. However, in measuring absorption spectra, we found experimentally that dimerization equilibria 2 and 3 can almost be ignored, even at the low temperatures studied here, under the condition that the concentrations of perylene⁺ and tetracene⁺ are chosen close to each other. Therefore, in order to facilitate the analysis, in the present work the absorption measurements at the low temperatures were carried out with this condition. The resulting absorption data were able to be analyzed in terms of the following relationship associated with equilibrium 1⁷

$$y = Ax + B \quad (4)$$

where

$$x = c_a + c_b - (d - c_a\epsilon_a - c_b\epsilon_b)/(\epsilon_c - \epsilon_a - \epsilon_b) \quad (5)$$

$$y = c_a c_b / (d - c_a\epsilon_a - c_b\epsilon_b) \quad (6)$$

and coefficients A and B are expressed by

$$A = 1/(\epsilon_c - \epsilon_a - \epsilon_b) \quad (7)$$

$$B = A/K_c \quad (8)$$

Here, d is the optical density, c_a and c_b are the concentrations of P⁺ and T⁺, respectively, ϵ_a , ϵ_b , and ϵ_c are the molar extinction coefficients of P⁺, T⁺, and P⁺-T⁺, respectively, and K_c is the equilibrium constant of the complex formation.

Since two absorption bands peaking at 310 and 722 nm are relatively sharp, as seen from Figure 1, optical densities measured at these two wavelengths were employed in the present analysis. As seen from eq 4, plots of y against x should yield a line whose slope is related to ϵ_c and whose intercept is related to K_c . However, although ϵ_a and ϵ_b have already been known, ϵ_c itself is necessary in calculating x in order to plot and is unknown at the beginning of the analysis. The present

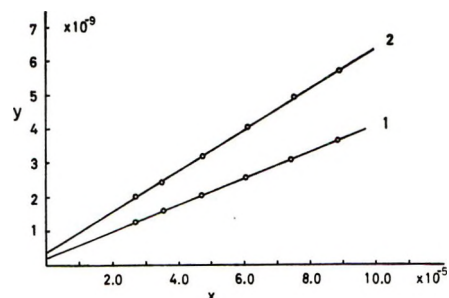


Figure 2. Examples of the plot of y against x calculated with the 25° absorption data obtained by changing c_b from 1.47×10^{-6} to $1.11 \times 10^{-4} M$ while keeping c_a constant ($2.27 \times 10^{-6} M$): (1) at 310 nm, (2) at 722 nm.

procedure of determining K_c was started with a trial value for ϵ_c . An improved ϵ_c value was obtained from the first plotted line, and was next used in the second calculation of x , producing a second improved ϵ_c value. This technique is continued until successive iteration gives a self-consistent ϵ_c value. The final plots are shown in Figure 2, from which it is seen that good straight lines are obtained at the two different wavelengths. Using a least-squares method, final ϵ_c values were determined to be, for instance, $\epsilon_c = 36,200$ at 310 nm and 28,400 at 722 nm at 25°. In Table I, equilibrium constant data thus obtained are shown, together with the corresponding entropy values. From the temperature dependence of K_c , the heat of formation has been determined to be $\Delta H = -7.7$ kcal/mol.

Table I: Thermodynamic Data of Complex Formation between Perylene⁺ and Tetracene⁺ in Concentrated Sulfuric Acid

| Temp, °C | 25 | 10 | -10 | -20 | -30 |
|----------------------------------|---------------|-------|-------|-------|-------|
| $K_c \times 10^{-5}$, l./mol | 1.78 | 3.92 | 12.3 | 19.9 | 33.1 |
| ΔS° , cal/(mol deg) | -1.82 | -1.64 | -1.40 | -1.60 | -1.84 |
| ΔH° | -7.7 kcal/mol | | | | |

Discussion

Thermodynamic Data of the Complex. As shown in Table II, it is interesting to note that the experimental value of the heat of formation of the radical complex lies between those of the radical dimers of perylene⁺ and tetracene⁺. The complex formation as well as the dimer formation of the radical cations may qualita-

Table II: Comparison of Heats of Formation (kcal/mol) for the Complex Formation and the Dimerization

| P ⁺ -T ⁺ | (P ⁺) ₂ | (T ⁺) ₂ |
|--------------------------------|--------------------------------|--------------------------------|
| -7.7 | -8.8 | -5.6 |

(7) R. P. Lang, *J. Amer. Chem. Soc.*, **84**, 1185 (1962).

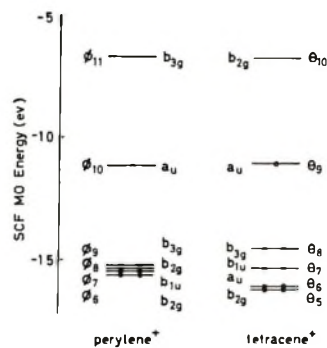


Figure 3. Energy levels of the SCF MO's of perylene⁺ and tetracene⁺.

tively be explained in terms of interradical charge transfer effects described later.

It is seen from Table I that the equilibrium constants of complex formation are much larger than those of the dimerizations obtained in our previous work.³ This fact reflects the smaller values of entropy in the complex formation. Unfortunately, there are no entropy data on other radical complex formations available for comparison.

Charge-Transfer Bands. In the absorption spectra of the mixed solutions, two new weak absorption bands probably due to charge transfer between the two cations are observed as seen in Figure 1, one of which is located at 900–1000 nm, the other at 830 nm. In the dimer spectra of perylene⁺ and tetracene⁺, the longest wavelength bands have previously been assigned to the transitions mainly characteristic of charge resonance (CR) between the two same cations.³ As shown in Figure 3, the half-occupied orbitals of perylene⁺ and tetracene⁺ are nearly equal to each other in energy level, so that absorption bands due to the interradical charge transfer may be expected to appear in the absorption spectrum of the complex.

We tried to explain these two new bands of the complex by taking the CT and back CT configurations in which an electron is transferred between perylene⁺ and tetracene⁺. The corresponding CT energies are approximately given by

$$E_{CT(P^+ \rightarrow T^+)} = I_{(P^+)} - A_{(T^+)} - C \quad (9)$$

$$E_{CT(T^+ \rightarrow P^+)} = I_{(T^+)} - A_{(P^+)} - C \quad (10)$$

where the I 's are the ionization energies, the A 's are the electron affinities, and C is the Coulomb energy. The electron affinities of perylene⁺ and tetracene⁺ were taken to be equal to the ionization energies of their parent molecules. Coulomb energies C were calculated on the basis of regular parallel configurations with an interplanar distance of 3.4 Å, by using a point-charge model in which the charges distributed over the carbon atoms are approximated by a point charge. The ionization energies of perylene⁺ and tetracene⁺ were estimated from the observed CR bands of their dimer spectra,

with the approximation of $I - A - C = E_{CR}$.⁸ From eq 9 and 10, we were able to obtain the CT energies, which are in fairly good agreement with those determined from the observed bands, as given in Table III. It may also be found that quite a good agreement is obtained between the theoretical and experimental splittings. It is thus concluded that the 900–1000-nm band is assigned to the CT($P^+ \rightarrow T^+$) and the 830 nm band to the CT($T^+ \rightarrow P^+$).

Table III: Charge-Transfer Energies (eV) of the Perylene⁺-Tetracene⁺ Complex

| | Calcd | Exptl |
|-------------------------------|-------|-----------|
| $E_{CT(P^+ \rightarrow T^+)}$ | 1.11 | 1.24–1.38 |
| $E_{CT(T^+ \rightarrow P^+)}$ | 1.40 | 1.49 |
| Splitting | 0.29 | 0.25–0.11 |

$$I_{(P^+)} = 11.05 \text{ eV}, I_{(T^+)} = 11.24 \text{ eV}, A_{(P^+)} = 7.10 \text{ eV},^a \\ A_{(T^+)} = 7.20 \text{ eV},^b C_{(P^+-T^+)} = 2.74 \text{ eV}$$

^a E. J. Calleges, *J. Phys. Chem.*, **72**, 3452 (1968). ^b F. T. Smith, *J. Chem. Phys.*, **34**, 793 (1961).

Stabilization Energy. In some of electronic absorption studies of ordinary molecular complexes, it has been pointed out that not only the lowest energy CT configuration but also some higher energy CT configurations including back CT's play an important role in the complex formations.^{9–12} We attempted to apply the CT theory to the radical complex under study. According to the second-order perturbation theory, the stabilization energy of the ground-state radical complex due to CT interactions can be expressed by

$$W = -\sum_i (\Phi_0 | H | \Phi_{CT_i})^2 / E_{CT_i} \quad (11)$$

where Φ_0 is the wave function of the ground electronic configuration with energy zero and Φ_{CT_i} is that of the i th CT configuration with energy E_{CT_i} .

In order to calculate the stabilization energy of the complex with eq 11, we took a total of eight configurations consisting of CT and back CT into account as follows

$$\Phi_{CT_i}: (\phi_9 \rightarrow \theta_9), (\phi_9 \rightarrow \theta_{10}), \\ (\phi_{10} \rightarrow \theta_9), (\phi_{10} \rightarrow \theta_{10}), (\theta_8 \rightarrow \phi_{10}), \\ (\theta_8 \rightarrow \phi_{11}), (\theta_9 \rightarrow \phi_{10}), (\theta_9 \rightarrow \phi_{11}) \quad (12)$$

(8) We used $C_{(P^+-P^+)} = 2.71 \text{ eV}$ and $C_{(T^+-T^+)} = 2.72 \text{ eV}$, calculated on the basis of the regular parallel dimer structure with an interplanar separation of 3.5 Å (see ref 3).

(9) J. N. Murrell, *J. Amer. Chem. Soc.*, **81**, 4389 (1959).

(10) R. S. Mulliken, *J. Chim. Phys. Physicochim. Biol.*, **61**, 20 (1963).

(11) S. Iwata, J. Tanaka, and S. Nagakura, *J. Amer. Chem. Soc.*, **88**, 894 (1966).

(12) H. Kuroda, T. Amano, I. Ikemoto, and H. Akamatu, *ibid.*, **89**, 6056 (1967).

Their CT energies were evaluated with

$$\begin{aligned} E_{CT(\phi_k \rightarrow \theta_i)} &= I_{(\phi_k)} - A_{(\theta_i)} - C \\ \bar{E}_{CT(\theta_m \rightarrow \phi_n)} &= I_{(\theta_m)} - A_{(\phi_n)} - C \end{aligned} \quad (13)$$

Here, $I_{(\phi_k)}$ and $I_{(\theta_m)}$ are the energies required to remove an electron from the ϕ_k and θ_m molecular orbitals, respectively, and $A_{(\theta_i)}$ and $A_{(\phi_n)}$ are the energies gained to attach an electron to the θ_i and ϕ_n molecular orbitals, respectively. In the present calculation, the ionization energy values of perylene⁺ and tetracene⁺ estimated in the preceding section were used as $I_{(\phi_{10})}$ and $I_{(\theta_8)}$, respectively, and $A_{(\phi_{10})}$ and $A_{(\theta_8)}$ were assumed equal to the ionization energies of their parent molecules (see the footnote in Table III). On the basis of these I and A values, other I 's and A 's were evaluated by taking the energy differences of the SCF MO's into account.

In eq 11, the matrix elements $(\Phi_0|H|\Phi_{CT_i})$ are reduced to terms involving $(\phi_k|H^{\text{core}}|\theta_i)$ and $(\theta_m|H^{\text{core}}|\phi_n)$, which can be approximated by KS ,¹³ where K is an empirical parameter and S is the overlap integral between the MO's under consideration. Therefore, we calculated W/K^2 with eq 11 by changing the geometry of the complex shown in Figure 4 in a systematic way as follows. Keeping a parallel structure with an interplanar separation of $Z = 3.4 \text{ \AA}$, the plane of tetracene⁺ was translated along the long (X) and the short (Y) axes of perylene⁺ in the regions of $X = 0\text{--}3.475 \text{ \AA}$ and $Y = 0\text{--}2.408 \text{ \AA}$, with intervals of $\Delta X = 0.695 \text{ \AA}$ and $\Delta Y = 0.602 \text{ \AA}$, respectively, as well as rotated around the Z axis in the region of $\alpha = 0\text{--}90^\circ$ with $\Delta\alpha = 15^\circ$. (These coordinates are defined in Figure 4.) From such calculations it was found that each of the calculated W/K^2 curves shows a minimum position at the regular geometry ($X = Y = 0$ and $\alpha = 0^\circ$). In Figure 5, several examples of angular dependence of the stabilization energies, which were computed with a K value of 19.3 eV estimated as described below, are demonstrated. We therefore conclude that the maximum stabilization is obtained at the regular position.

Applying the same theoretical treatment to the stabilization energy of the perylene⁺ dimer, and selecting the stabilization energy so as to reproduce the experimentally determined heat of formation, it was found that K assumes 19.3 eV when we adopt the reasonable regular parallel structure with an interplanar separation of $Z = 3.50 \text{ \AA}$. In Figure 6, variations of the stabilization energies with the interplanar separation are shown for the perylene⁺ and tetracene⁺ dimers as well as the complex. From curve 3 shown in Figure 6, this K value was found to reproduce the experimental heat of formation of the tetracene⁺ dimer at $Z = 3.57 \text{ \AA}$. Furthermore, for the perylene⁺-tetracene⁺ complex, $Z = 3.43 \text{ \AA}$ is obtained from the curve shown in Figure 6. The K value of 19.3 eV mentioned above seems reasonable, since a value of 22 eV has been employed by

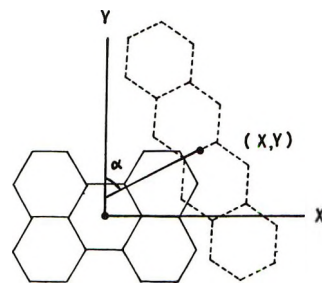


Figure 4. Coordinates of tetracene⁺ relative to perylene⁺.

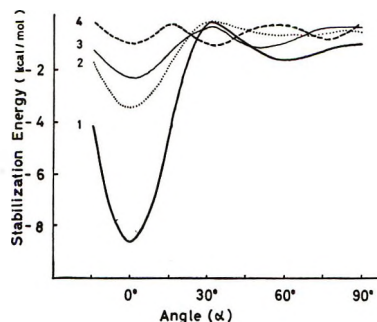


Figure 5. Rotational angle dependence of calculated CT stabilization energies of the perylene⁺-tetracene⁺ complex for several different geometries, with $Z = 3.4 \text{ \AA}$: (1) $X = Y = 0$; (2) $X = 2.085 \text{ \AA}$, $Y = 0$; (3) $X = 0$, $Y = 1.204 \text{ \AA}$; (4) $X = 2.085 \text{ \AA}$, $Y = 1.204 \text{ \AA}$.

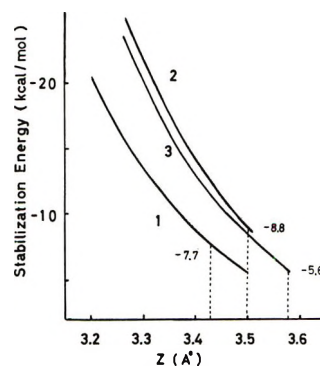


Figure 6. Variations of the calculated CT stabilization energies with interplanar separation: (1) the perylene⁺-tetracene⁺ complex, (2) the perylene⁺ dimer, (3) the tetracene⁺ dimer.

Kuroda, *et al.*,¹² in order to interpret the CT stabilization energies of the tetracyanoethylene complexes with naphthalene and pyrene.

Although the eight CT configurations were taken into account in our calculations, it should be mentioned that in the regular parallel structure the stabilization energy is contributed mainly from the two CT configu-

(13) $KS(\phi_0\theta_0)$, $2^{-1/2}KS(\phi_0\theta_{10})$, $-2^{1/2}KS(\phi_{10}\theta_0)$, $-KS(\phi_{10}\theta_{10})$, $KS(\theta_0\phi_{10})$, $2^{-1/2}KS(\theta_0\phi_{11})$, $-2^{1/2}KS(\theta_0\phi_{10})$, $-KS(\theta_0\phi_{11})$ in the order of eq 12, using wave functions of $\Phi_0 = 2^{-1/2}(|\phi_{10}\theta_0\rangle + |\theta_0\phi_{10}\rangle)$, $\Phi_{CT1} = 2^{-1/2}(|\phi_{10}\theta_0\rangle + |\phi_0\theta_{10}\rangle)$, $\Phi_{CT2} = 1/2(|\phi_0\theta_{10}\theta_{10}\rangle + |\theta_0\phi_{10}\theta_0\rangle - |\phi_0\theta_{10}\theta_{10}\rangle - |\theta_0\phi_{10}\theta_0\rangle)$, $\Phi_{CT3} = |\phi_0\theta_0\theta_0\rangle$, etc.

Table IV: Stabilization Energies and CT Contributions for Several Typical Geometries of the Perylene⁺-Tetracene⁺ Complex

| X, Å | Y, Å | α , deg | -W, kcal/ mol | Contribution, % | | | | | | | |
|-------|-------|-------------------|---------------------|-----------------|--------|--------|---------|--------|--------|--------|--------|
| | | | | 9 → 9 | 10 → 9 | 9 → 10 | 10 → 10 | 10 ← 8 | 11 ← 8 | 10 ← 9 | 11 ← 9 |
| 0 | 0 | 0 | 8.65 | 0 | 55.6 | 0 | 0 | 0 | 0.4 | 44.0 | 0 |
| 0 | 0 | 30 | 0.16 | 0 | 27.6 | 20.3 | 0 | 0 | 30.2 | 21.9 | 0 |
| 0 | 1.204 | 75 | 0.26 | 66.4 | 1.0 | 4.3 | 3.3 | 17.3 | 0 | 0.7 | 7.0 |
| 0.695 | 0 | 30 | 0.33 | 14.5 | 7.2 | 3.4 | 46.5 | 4.4 | 10.9 | 5.9 | 7.2 |
| 2.085 | 1.806 | 45 | 0.40 | 8.4 | 22.9 | 6.6 | 8.1 | 14.1 | 2.4 | 18.6 | 18.8 |

rations of ($\phi_{10} \rightarrow \theta_9$) and ($\theta_9 \rightarrow \phi_{10}$), with minor contributions from the other higher energy CT's. In Table IV, the results of CT contributions are given for several typical geometries, and it is interesting to note that all

the geometries other than the regular structure yield considerably smaller amounts of stabilization energy, which are contributed by the higher energy CT terms appreciably (see Table IV).

Torsional Frequencies and Enthalpies of Intramolecular Hydrogen Bonds of *o*-Halophenols

by G. L. Carlson,^{1a} W. G. Fateley,^{1a} A. S. Manocha,^{1a,b} and F. F. Bentley*^{1c}

Mellon Institute of Science, Carnegie-Mellon University, Pittsburgh, Pennsylvania 15213,
and Air Force Materials Laboratory (LPA), Air Force Systems Command,
Wright-Patterson Air Force Base, Ohio 45433 (Received November 22, 1971)

Publication costs assisted by Mellon Institute of Science, Carnegie-Mellon University

Torsional frequencies for the cis and trans forms of the *o*-halophenols have been observed, both in the vapor phase and as solutions in cyclohexane. These frequencies have been used to calculate the parameter V_1 of the potential function for internal rotation, which is the energy difference between the cis and trans isomers. The energy differences obtained show that the strength of the intramolecular hydrogen bond in the *o*-halophenols decreases in the order F = Cl > Br > I for the vapor phase, while the order for solutions in cyclohexane is Cl > Br > I ≥ F. The present data also give unequivocal evidence for the existence of cis and trans forms of *o*-fluorophenol.

Introduction

It is well established that the *o*-halophenols exist as mixtures of two isomers—a trans form with the hydroxyl hydrogen pointed away from the halogen and a cis form which is intramolecularly hydrogen bonded.² The presence of these two forms is evidenced by two bands in the O-H stretching region of the infrared spectrum for the *o*-chloro-, -bromo-, and -iodophenol, but only a single band in the case of the *o*-fluoro derivative, both in solution³⁻⁸ and in the vapor phase.⁹

The enthalpy differences between the cis and trans forms have also been extensively investigated, with considerable disagreement between various authors as to the relative order of the intramolecular hydrogen bond strengths with the different halogens, particularly

fluorine. These enthalpy determinations involved temperature-dependence measurements on the two

(1) (a) Mellon Institute of Science; (b) work done by Mr. Manocha is in partial fulfillment of the requirements for the Doctor of Philosophy degree at Carnegie-Mellon University; (c) Chief, Analytical Branch, Air Force Materials Laboratory.

(2) (a) O. R. Wulf and U. Liddel, *J. Amer. Chem. Soc.*, **57**, 1464 (1935); (b) L. Pauling, *ibid.*, **58**, 94 (1936).

(3) A. W. Baker and W. W. Kaeding, *ibid.*, **81**, 5904 (1959).

(4) A. W. Baker and A. T. Shulgin, *Spectrochim. Acta*, **22**, 95 (1966).

(5) A. W. Baker and A. T. Shulgin, *J. Amer. Chem. Soc.*, **80**, 5358 (1958).

(6) A. W. Baker and A. T. Shulgin, *Can. J. Chem.*, **43**, 650 (1965).

(7) A. W. Baker, *J. Amer. Chem. Soc.*, **80**, 3598 (1958).

(8) D. A. K. Jones and J. G. Wilkinson, *Chem. Ind. (London)*, 661 (1960).

(9) Tien-sung Lin and E. Fishman, *Spectrochim. Acta, Ser. A*, **23**, 491 (1967).

O-H stretching bands,³⁻⁹ nuclear magnetic resonance studies,¹⁰ competitive hydrogen bonding,¹¹ and dipole moment measurements.¹² *o*-Fluorophenol was particularly difficult to study because it exhibits only one O-H stretching band, and the nmr results indicated that the amount of cis isomer present must be very small.

We have recently been engaged in a study of the OH torsional vibrations in substituted phenols and have observed the torsional frequencies for both the cis and trans isomers of the *o*-halophenols in cyclohexane solutions and in the vapor phase. Knowing the torsional frequencies for both isomeric forms, the parameters V_1 and V_2 in the potential function for internal rotation can be evaluated. The parameter V_1 gives directly the ΔH value for the energy difference between the cis and trans isomers and is not subject to the errors associated with the temperature-dependent intensity measurements used in previous determinations of ΔH values for the *o*-halophenols. Furthermore, the observation of two torsional frequencies for *o*-fluorophenol is direct and unequivocal evidence that this molecule also exists in both isomeric forms.

Experimental Section

Samples of *o*-fluoro-, -chloro-, -bromo-, and iodo-phenol were all commercially available in high purity. Authenticity of the samples was checked by comparison of their mid-infrared spectra with published reference spectra. Previous authors⁹ have noted that purity of the samples is extremely important in equilibrium studies involving temperature-dependent measurement of intensities. An advantage of the present method of ΔH evaluation is that small amounts of impurities should have negligible effects because we are concerned with frequency measurements which are much less subject to impurity effects than are intensity measurements.

Far-infrared spectra were obtained with a Digilab FTS-14 Fourier transform spectrometer operating in its far-infrared mode. A 3- μ Mylar beam splitter was used to cover the 600-100-cm⁻¹ region. Solution spectra were obtained at a resolution of 8 cm⁻¹, gas-phase spectra at 4-cm⁻¹ resolution.

Cyclohexane solution spectra were obtained with a 5-mm thick cell equipped with polyethylene windows. Sample concentrations were in the range 0.01-0.02 *M*. Gas-phase spectra were obtained using a Model GH-9N Beckman RIIC 9-cm heated gas cell equipped with CsI windows.

Solution spectra of the phenol-*O-d* analogs were obtained by deuteration of the samples directly in cyclohexane solution by a technique which has been described previously.¹³ The gas-phase spectrum of *o*-fluorophenol-*O-d* was also obtained employing the heated gas cell and a sample which had been shaken

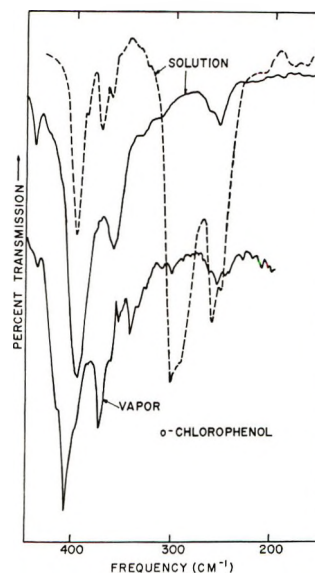


Figure 1. Far-infrared spectra of *o*-chlorophenol: solution spectra (—) *o*-chlorophenol, 0.01 *M* in cyclohexane, 5-mm cell; (---) *o*-chlorophenol-*O-d*, ~ 0.02 *M* in cyclohexane, 5-mm cell; vapor spectrum, vapor pressure at $\sim 70^\circ$ in heated 9-cm gas cell.

with D₂O followed by distillation and drying over molecular sieves.

Results

The solution and gas-phase far-infrared spectra of *o*-chlorophenol are shown in Figure 1 and are typical of the results obtained for the chloro, bromo, and iodo derivatives. The two prominent bands in the 340-410-cm⁻¹ region, both of which show a shift on deuteration of ~ 1.35 , are attributed to the torsional frequencies of the cis (bonded) and trans (free) isomers. The far-infrared spectra of *o*-fluorophenol and *o*-fluorophenol-*O-d*, both in solution and vapor phases, are shown in Figure 2. Again, the two bands in the 340-410-cm⁻¹ region are present; however, in the *O-d* analog, only one unusually broad band is observed in the O-D torsional region (250-300 cm⁻¹). Possibly another vibration, presumably one of the C-F bends,¹⁴ is interfering with the OD torsions, resulting in a broad band which makes it impossible to confirm the presence of two isomers of *o*-fluorophenol on the basis of the deuteration shifts. However, there is no doubt that both the 342- and 379-cm⁻¹ bands in the vapor spectra and the 332- and 366-cm⁻¹ bands in the solution spectra decrease in intensity on deuteration, and by analogy with

(10) E. A. Allan and L. W. Reeves, *J. Phys. Chem.*, **66**, 613 (1962); **67**, 591 (1963).

(11) H. Bourassa-Bataille, P. Sauvageau, and C. Sandorfy, *Can. J. Chem.*, **41**, 2240 (1963).

(12) J. H. Richards and S. Walker, *Trans. Faraday Soc.*, **57**, 412 (1961).

(13) G. L. Carlson, W. G. Fateley, and F. F. Bentley, *Spectrochim. Acta*, in press.

(14) J. H. S. Green, *Spectrochim. Acta, Ser. A*, **26**, 1913 (1970).

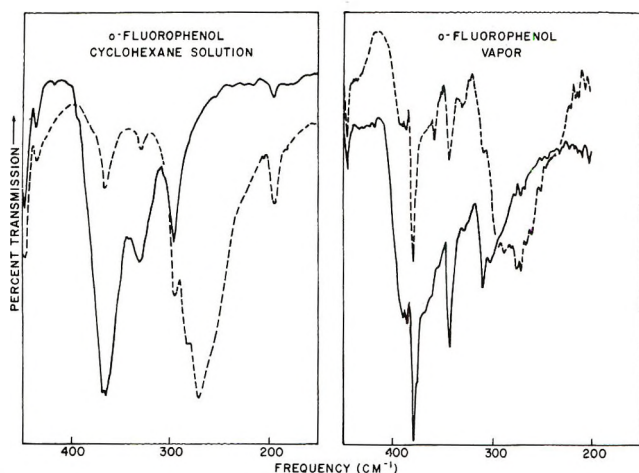


Figure 2. Far-infrared spectra of *o*-fluorophenol: cyclohexane solution spectra (—) *o*-fluorophenol, 0.01 *M*, 5-mm cell; (---) *o*-fluorophenol-*O*-*d*, ~0.02 *M*, 5-mm cell; vapor spectra (obtained with heated 9-cm gas cell at ~70°) (—) *o*-fluorophenol; (---) *o*-fluorophenol-*O*-*d*.

the chloro, bromo, and iodo derivatives, their assignment as the *cis* and *trans* isomer torsions is straightforward.

The torsional frequencies observed for the *o*-halophenols are given in Table I. The frequency accuracy of the Digilab FTS-14 is much better than 1 cm^{-1} ; therefore, for the vapor phase where the bands are sharp, the accuracy should be better than $\pm 1 \text{ cm}^{-1}$. However, in solution, the bands are broader and the uncertainty in choosing the band center may be greater than ± 1 .

Table I: Far-Infrared Torsional Frequencies (cm^{-1}) for *o*-Halophenols

| Compound, isomer | Vapor $\nu_{\tau\text{OH}}$ | ---Cyclohexane solution--- | | |
|--------------------------------------|--------------------------------|----------------------------|-----------------------|---|
| | | $\nu_{\tau\text{OH}}$ | $\nu_{\tau\text{OD}}$ | $\nu_{\tau\text{OH}}/\nu_{\tau\text{OD}}$ |
| <i>o</i> -Fluorophenol, <i>cis</i> | 379 | 366 | 269 | 1.36 |
| <i>o</i> -Fluorophenol, <i>trans</i> | 342 | 332 | <i>a</i> | <i>a</i> |
| <i>o</i> -Chlorophenol, <i>cis</i> | 407 | 396 | 300 | 1.32 |
| <i>o</i> -Chlorophenol, <i>trans</i> | 373 | 361 | 261 | 1.38 |
| <i>o</i> -Bromophenol, <i>cis</i> | 404 | 395 | 298 | 1.325 |
| <i>o</i> -Bromophenol, <i>trans</i> | 372 | 361 | 252 | 1.43 |
| <i>o</i> -Iodophenol, <i>cis</i> | 386 | 378 | 285 | 1.325 |
| <i>o</i> -Iodophenol, <i>trans</i> | 357 | 345 | 246 | 1.40 |

^a Not observed because of unusual width of 269- cm^{-1} band (see text).

Discussion

Assignment of Torsional Frequencies. It is well established that the only O-H vibration in monomeric phenol which falls below 500 cm^{-1} is the torsion.¹⁵ This is also the case for halo-substituted phenols.^{16,17} (Of course there are other vibrations of the aromatic ring below 500 cm^{-1} ; however, these vibrations are not

affected by deuteration. Thus, they are easily recognizable and are not considered in this study.) Since phenol is known to be monomeric in the vapor phase, and we feel this is also the case for dilute cyclohexane solutions,¹³ the assignment of bands which show the appropriate deuterium shifts as the torsions is straightforward. Furthermore, since for each *o*-halophenol there are two bands which shift on deuteration, it seems reasonable that these are the torsional frequencies for the *cis* and *trans* forms.

The intramolecular hydrogen bonding which occurs for the *cis* isomer would be expected to increase the barrier hindering internal rotation. Therefore, the frequency which gives the higher barrier is assigned to the *cis* form; in each case, this is found to be the higher frequency. The assignments of the *cis*-2-halophenol frequencies given in Table I are in good agreement with the earlier work of Nyquist, who also gives additional justification for these assignments.¹⁷ The assignment of the higher frequency to the *cis* isomer and the lower frequency to the *trans* form also correlates with the observed intensities, for the energy of the hydrogen bond should favor the *cis* configuration by about a factor of 10.³

Calculation of Barrier Heights. The potential associated with internal rotation of the phenolic OH group is adequately represented by the Fourier cosine series $V(\alpha) = \frac{1}{2} \sum_N V_n (1 - \cos n\alpha)$, and for the *o*-halophenols the series can be truncated at $n = 2$. (It has been shown by an approximate calculation that higher (V_4) terms are negligibly small.¹⁶ More refined calculations demonstrating this point will be published at a later date.¹⁸) The wave equation for the internal rotation problem is a Mathieu-type equation in one dimension

$$[P_\alpha F(\alpha) P_\alpha + V(\alpha)] M(\alpha) = E M(\alpha)$$

where $F(\alpha)$ is the reduced moment of inertia, P_α is the momentum conjugate to α , E is the energy eigenvalue corresponding to the eigenfunction $M(\alpha)$ of the above equation, and $M(\alpha)$ is a function expressed as an expansion in some chosen basis set.

For the *o*-halophenols, the value of $F(\alpha)$ was calculated to be 22.47 cm^{-1} , where the geometry and dimensions of the phenol framework were taken from recent microwave data.¹⁹ Because the center of mass of the O-H rotor lies on the internal rotation axis, F is the same for the *cis* and *trans* isomers and virtually independent of the mass of the halogen substituent.

The eigenfunctions for this problem can be expanded

- (15) J. C. Evans, *Spectrochim. Acta*, **16**, 1383 (1960).
- (16) W. G. Fateley, F. A. Miller, and R. E. Witkowski, Technical Documentary Report No. AFML-TR-66-408, Jan 1967.
- (17) R. A. Nyquist, *Spectrochim. Acta*, **19**, 1655 (1963).
- (18) A. S. Manocha, manuscript in preparation.
- (19) T. Pederson, N. W. Larsen, and L. Nygaard, *J. Mol. Struct.*, **4**, 59 (1969).

Table II: V_1 and V_2 Values (kcal/mol) for *o*-Halophenols

| Phenol | Vapor | | Cyclohexane solution | |
|------------------|-------------|-------------|----------------------|-------------|
| | V_1 | V_2 | V_1 | V_2 |
| <i>o</i> -Fluoro | 1.63 ± 0.06 | 4.72 ± 0.03 | 1.44 ± 0.12 | 4.44 ± 0.06 |
| <i>o</i> -Chloro | 1.63 ± 0.06 | 5.46 ± 0.03 | 1.62 ± 0.12 | 5.16 ± 0.06 |
| <i>o</i> -Bromo | 1.53 ± 0.06 | 5.40 ± 0.03 | 1.57 ± 0.12 | 5.15 ± 0.06 |
| <i>o</i> -Iodo | 1.32 ± 0.06 | 4.97 ± 0.03 | 1.45 ± 0.12 | 4.74 ± 0.06 |

in terms of an orthonormal set of free-rotor basis functions

$$M_n(\alpha) = \sum_m a_{nm} e^{im\alpha}$$

where $m = 0, \pm 1, \pm 2, \dots$. These exponential basis functions lead to the following matrix elements

$$H_{mm} = m^2 F + (1/2) \sum_N V_N$$

$$H_{mm'} = -\frac{V_N}{4} \delta_{mm'}$$

The value of $\delta_{mm'}$ is one when $m' = m \pm N$ and zero in all other cases.

Torsional energies were computed by diagonalizing the matrix using an appropriate number of basis functions (the size of the basis set chosen was sufficient to give convergence of the eigenvalues of interest) and an initial set of potential constants. From the torsional energies so obtained, the torsional frequencies were calculated for the cis and trans forms and compared with the observed frequencies. The values of V_n were then refined to give the best fit to the observed data through an iterative numerical procedure.

The calculated values of V_1 and V_2 for each halophenol, both in cyclohexane solution and in the vapor phase, are summarized in Table II. The errors cited are based on an accuracy of $\pm 1 \text{ cm}^{-1}$ for the vapor frequencies and $\pm 2 \text{ cm}^{-1}$ for the solution frequencies.

The magnitude of V_1 will be almost entirely determined by the strength of the intramolecular hydrogen bond, while V_2 , the twofold barrier, will arise mainly from the overlap between the π orbitals of the oxygen and the aromatic ring.

Enthalpies of Intramolecular Bridge Bonds in o-Halophenols. The values of V_1 obtained in the previous section for each of the *o*-halophenols are very nearly equal to the energy difference or ΔH between the cis and trans isomers. Our values are compared with previously reported enthalpy values in Table III.

The ΔH values are a measure of the strength of the bridge bonds in the *o*-halophenols, and there has been considerable discussion as to the order of these bond strengths for the fluoro, chloro, bromo, and iodo derivatives.^{6,9,11} The orders proposed by various authors are summarized in Table IV and compared with the order of bond strengths derived from the ΔH values obtained in this work.

Table III: Enthalpies of *o*-Halophenols, $-\Delta H$ (kcal/mol)

| Compound | Vapor | | Solution | | | |
|------------------------|-----------|-------|------------------------|-------------------------|-------|-------------------------|
| | This work | Ref 9 | This work, cyclohexane | Ref 6, CCl ₄ | Ref 8 | Ref 10, CS ₂ |
| <i>o</i> -Fluorophenol | 1.63 | | 1.44 | | | |
| <i>o</i> -Chlorophenol | 1.63 | 3.41 | 1.62 | 1.44 | 1.27 | 2.3 |
| <i>o</i> -Bromophenol | 1.53 | 3.13 | 1.57 | 1.21 | 1.86 | 2.0 |
| <i>o</i> -Iodophenol | 1.32 | 2.75 | 1.45 | 1.08 | 1.00 | 1.5 |

Table IV: Order of Bridge-Bond Strengths in *o*-Halophenols

| Ref | Order of bridge-bond strength | Phase, solvent |
|------------------------|-------------------------------|--|
| This work ^a | F = Cl > Br > I | Vapor |
| 9 ^b | Cl > Br > I | Vapor |
| This work ^a | Cl > Br > I ≥ F | Cyclohexane solution |
| 6 ^b | Cl > Br > F > I | CCl ₄ solution |
| 10 ^c | Cl > Br > I > F | CS ₂ solution |
| 12 ^d | Cl = Br > F > I | CCl ₄ and cyclohexane ^f solution |
| 11 ^e | Cl > Br > I > F | CCl ₄ solution |

^a Infrared-torsion. ^b Infrared-temperature dependence.

^c Nmr. ^d Dipole moments. ^e Competitive hydrogen bonding.

^f Different order obtained with benzene and dioxane solvents.

It is seen in Table III that although there is reasonable agreement between the order of ΔH values for the chloro, bromo, and iodo derivatives obtained by various workers, there is considerable disagreement between the magnitudes of these values, both in the vapor and solution phases. The data obtained by the method of temperature-dependent measurements on infrared intensities⁶⁻⁹ are subject to several assumptions and inaccuracies: (a) it must be assumed that the intrinsic intensity of the trans and cis bands remains the same for all of the *o*-halophenols; (b) the assumption that the absorption coefficients of the bands are temperature independent was not tested;²⁰ and (c) the intensity measurements had to be made on two bands of very different intensities. These factors probably all combine to produce error of unknown magnitude in the ΔH values. The values given by Allan and Reeves from nmr mea-

(20) K. O. Hartman, G. L. Carlson, R. E. Witkowski, and W. G. Fateley, *Spectrochim. Acta, Ser. A*, **24**, 157 (1968).

surements¹⁰ do not suffer from these same drawbacks, but the difficulty encountered with *o*-fluorophenol indicates some shortcoming in the method.

The ΔH values obtained in the present study should be subject to only three sources of error and do not depend at all on difficult intensity measurements. As shown previously, the calculated barriers depend only on an accurate torsional frequency, a parameter, F , determined from the geometry of the molecule, and the form of the potential function employed. We feel that our frequency accuracy, at least for the gas phase where the bands are sharp, is better than $\pm 1 \text{ cm}^{-1}$, and we have found that the parameter F is insensitive to small errors in the molecular geometry. Furthermore, the potential function used has been tested in a large number of examples and is felt to be quite good where it is established that both the *cis* and *trans* isomers are planar.

It can be seen from Table IV that for the gaseous *o*-halophenols there is agreement as to the order of hydrogen-bond strengths between the present study and that of Lin and Fishman, except that the latter authors could not determine a ΔH value for the fluoro compound by their method. The bond strength order for the vapor state is then $F = \text{Cl} > \text{Br} > \text{I}$, which means that there is the least amount of *trans* isomer present in the chloro and fluoro derivatives and most in the iodo compound.

There is less agreement between the various studies for the *o*-halophenols in solution. The inaccuracies inherent in each of the older studies have been evaluated by Bourassa-Bataille, *et al.*,¹¹ and these authors concluded that the most reliable order is $\text{Cl} > \text{Br} > \text{I} > \text{F}$. Our results are in agreement with this order, except that we find the bridge-bond strengths for the iodo and fluoro compounds to be essentially the same. It might be argued that our results are for cyclohexane solutions, while CCl_4 was used as a solvent in most of the other studies. However, the dipole moment work of Richards and Walker,¹² although giving a different order, does show that the behavior in cyclohexane is the same as in CCl_4 .

Conclusions

It is then concluded that the intramolecular hydrogen-bond strength in *o*-halophenols decreases in the following orders: vapor phase, $F = \text{Cl} > \text{Br} > \text{I}$; solution (cyclohexane or CCl_4), $\text{Cl} > \text{Br} > \text{I} \geq \text{F}$. The most interesting aspect of these results is the behavior

of fluorine, which forms nearly the strongest bridge hydrogen bond in the vapor and the weakest in solution. The other three halogens maintain the order $\text{Cl} > \text{Br} > \text{I}$ whether in solution in an inert solvent or in the vapor phase.

Although theories involving competitive resonance interactions and interorbital repulsions have been advanced to explain the order of intramolecular hydrogen bond strengths derived from previous studies,³ the orders obtained in the present work can apparently be explained on a much simpler basis. In the gas phase, the order $F = \text{Cl} > \text{Br} > \text{I}$ does not appear to contradict the order which would be expected from a consideration of the size and electronegativity characteristics of the halogen. On the basis of electronegativity alone, the order would be $F > \text{Cl} > \text{Br} > \text{I}$; however, the small size of fluorine reduces its hydrogen bond strength because the O-H group cannot get close enough for optimum bonding.

In inert solvent solutions, the intramolecular bond strength order for the three heaviest halogens is the same as in the vapor, and, in fact, there is very little change in their ΔH values on going from vapor to solution. *o*-Fluorophenol, however, shows the smallest ΔH value in solution which means the largest *trans/cis* ratio and, correspondingly the weakest bridge hydrogen bond. Apparently, in the case of the fluoro compound, the *trans* isomer is being stabilized. Since hydrogen bonding with the solvent, cyclohexane, is unlikely, the most reasonable explanation seems to be some intermolecular association involving *trans-o*-fluorophenol. Allan and Reeves have discussed intermolecular hydrogen bonding in *o*-halophenols and have found that *cis-trans* dimers may occur in the chloro, bromo, and iodo compounds at concentrations of 2 mol % in inert solvents, but they presented no data for the fluoro compound.⁸ Jaffe²¹ has also discussed the factors governing the strengths of intra- and intermolecular bonds in these compounds. Our data indicate that this type of dimerization must be very small in the case of the *o*-chloro-, bromo-, and -iodophenol but becomes significant for *o*-fluorophenol.

Acknowledgment. Partial support was obtained from the United States Air Force, Wright-Patterson Air Force Base, Contract No. F 33-615-71-C-1157 and Carnegie-Mellon University.

(21) H. H. Jaffe, *J. Amer. Chem. Soc.*, **79**, 2373 (1957).

Vibrational Spectra and Structure of Organogermanes. XII. Normal Vibrations and Free Rotation in *p*-Chlorophenylgermane and *p*-Fluorophenylgermane

by J. R. Durig* and J. B. Turner^{1b}

Department of Chemistry, University of South Carolina, Columbia, South Carolina 29208 (Received July 12, 1971)

Publication costs borne completely by The Journal of Physical Chemistry

The infrared spectra of liquid and gaseous *p*-chlorophenylgermane and *p*-fluorophenylgermane have been recorded from 4000 to 200 cm^{-1} . The Raman spectra of the liquids have also been recorded, and depolarization values have been measured. The vapor-phase spectra show that the germyl group is freely rotating for these molecules. Thus, the local symmetry of the phenyl ring can be considered as C_{2v} and the phenyl vibrations have been assigned according to this symmetry. The effective symmetry of the GeH_3 group is essentially C_{3v} . All spectra have been interpreted in detail, and the fundamental vibrations have been assigned based on previous assignments of disubstituted benzene and its isotopic derivatives, depolarization ratios, and vapor-phase infrared band contours. The free rotation of the germyl group shows that the sixfold barrier to internal rotation around the C-Ge bond is negligibly small.

Introduction

Recently we have investigated² the spectra of phenylgermane and its deuterated analogs, in which free rotation of the germyl group was observed. In continuing our investigations of organogermanium compounds, we have recorded the infrared, far-infrared, and Raman spectra of *p*-fluorophenylgermane and *p*-chlorophenylgermane. No vibrational data have been previously reported for either of these molecules. The present study was undertaken to examine the effect of a halogen in the para position upon the vibrational-rotational fine structure for the "degenerate" GeH_3 fundamentals. Therefore, we have analyzed the vibrational spectra for these two molecules in detail, and discuss the proposed assignment with its ramifications.

Experimental Section

The preparation of *p*-chlorophenylgermane was carried out in the following way. A 250-ml three-necked flask, containing 2.5 g of Grignard grade magnesium and a magnetic stir bar, was fitted with a water-cooled condenser, a 100-ml dropping funnel, and a thermometer. Approximately 20 g of 1-bromo-4-chlorobenzene was dissolved in 100 ml of anhydrous diethyl ether and added slowly to the flask containing the magnesium. Reaction was not spontaneous but could be initiated by heating. Following complete addition at reduced temperature, the mixture was refluxed for 1 hr and then cooled. Excess magnesium was removed and the mixture placed in a dropping funnel. This funnel was connected to a three-necked 500-ml flask equipped with a magnetic stirrer, heating mantle, condenser, and thermometer. Into this flask, 150 ml of anhydrous ether containing 25 ml (approximately 46 g) of GeCl_4 was transferred. Proper care was exercised to preclude any contact of either reactant with moisture. The quantity

of GeCl_4 was chosen to be appreciably in excess and ether was used to maintain a low reflux temperature to favor monosubstitution on the GeCl_4 . The *p*-chlorophenylmagnesium bromide in ether was added dropwise to the GeCl_4 at 0° with constant stirring, and a dense white precipitate formed; it was necessary to stir vigorously. The dropwise addition of *p*-chlorophenylmagnesium bromide solution was complicated by the settling of the relatively insoluble Grignard. After the addition was complete, the reaction was refluxed for 70 hr. Solid material was removed by filtering through a medium-porosity sintered-glass filtering funnel and the residue washed well with ether. The filtrate was placed in a 250-ml flask and the ether was distilled from the reaction mixture. When the temperature of the distilling flask began to rise above 35° , the flask was cooled, the pressure was lowered, and all materials which were volatile at 10 Torr and up to 40° were removed. The remaining material was a slightly yellow solid which hydrolyzed readily upon exposure to air. This solid was immediately dissolved in anhydrous ether and placed in a 25-ml dropping funnel. No problems of solubility were incurred if proper precautions had been taken to prevent hydrolyses. For complete reduction of the amount of *p*-chlorophenylgermanium trichloride produced by 100% yield, 2.7 g of LiAlH_4 would be needed. Since in all probability a mixture of RGeCl_3 , R_2GeCl_2 , and R_3GeCl was present, 2.5 g was used and expected to be a considerable excess, which was found to be the case. The reduction was carried out in a

(1) (a) For part XI, see *Spectrochim. Acta, Part A*, **27**, 1623 (1971); (b) taken from a thesis submitted by J. B. T. in partial fulfillment of the requirements for the Ph.D. degree, University of South Carolina, Jan 1970.

(2) J. R. Durig, C. W. Sink, and J. B. Turner, *J. Chem. Phys.*, **49**, 3422 (1968).

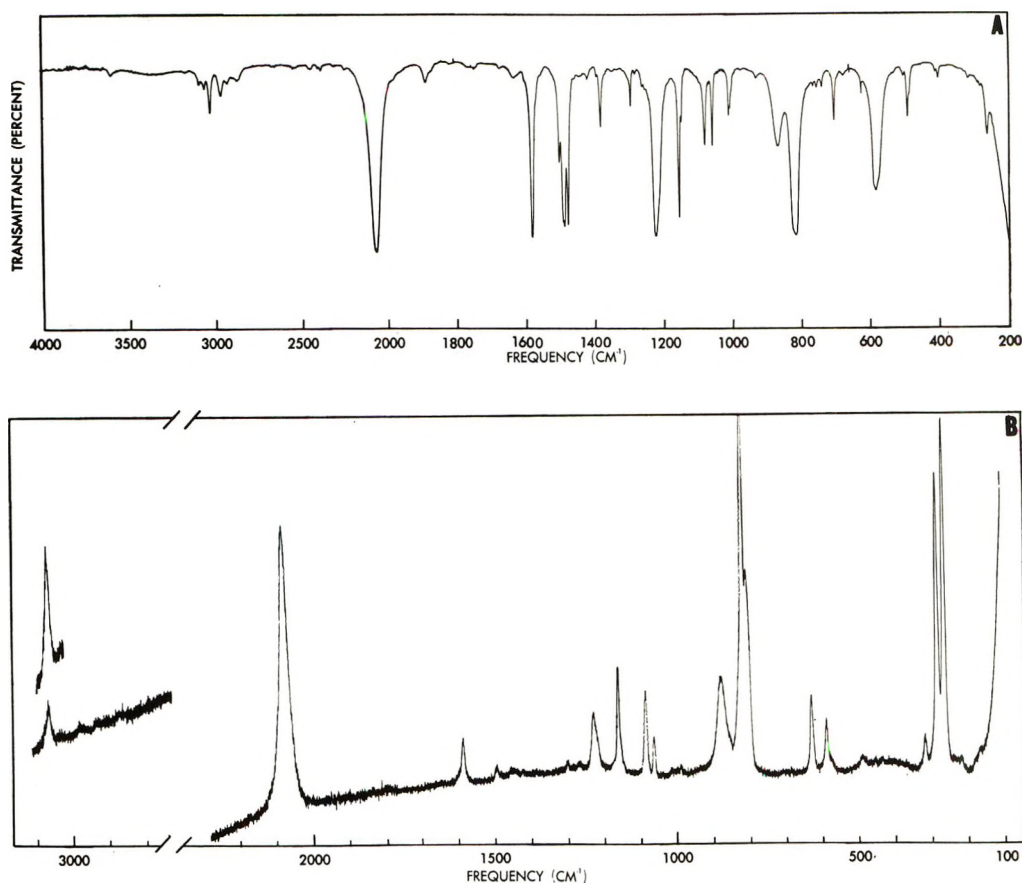


Figure 1. (A) Mid-infrared spectrum of *p*-fluorophenylgermane. (B) Raman spectrum of *p*-fluorophenylgermane.

manner analogous to the $(C_6H_5)_2GeH_2$ preparation.³ The sample of *p*-chlorophenylgermane was collected at 8 Torr and 60° . Any attempt to collect the other substituted germanes was futile. The reaction mixture turned yellow, then red as thermal decomposition and polymerization occurred. The yield was extremely low, approximately 1 ml. The sample of *p*-fluorophenylgermane was prepared in a similar manner. The Grignard reaction was easier to initiate with *p*-bromofluorobenzene than with *p*-bromochlorobenzene, and the final product (*p*-fluorophenylgermane) was collected at 6 Torr and 50° . These compounds have fairly high boiling points and degraded on those gas chromatographic columns tried; *i.e.*, Carbowax, UCON, diisodecyl phthalate. When the infrared spectra were taken, it was apparent that only the GeH_3 substituent was present, with no spectroscopically observed GeH_2 or GeH moiety. The samples showed a very weak Raman line at 998 cm^{-1} which is the most intense band other than the GeH stretch in the Raman of monosubstituted phenylgermanes. From the intensity of this line it can be assumed with confidence that the trace of phenylgermane would not contribute any other observable lines, and these two compounds were thus examined as prepared.

The infrared spectra between 4000 and 200 cm^{-1} were recorded with a Perkin-Elmer Model 621 spectro-

photometer and between 500 and 33 cm^{-1} with a Beckman IR-11 spectrophotometer. Both instruments were purged with dry air and calibrated with standard gases.⁴ For studies of the vapor phase, 20-cm cells with cesium iodide windows were used in the mid-infrared, whereas a Beckman 10-m variable-path cell with polyethylene windows was used for recording the far-infrared spectra. The infrared spectra of the liquids were obtained as a capillary film between cesium iodide plates. The infrared spectrum of liquid *p*-fluorophenylgermane is shown in Figure 1A and portions of the vapor spectrum are shown in Figure 2. The corresponding infrared spectra of liquid and gaseous *p*-chlorophenylgermane are shown in Figures 3A and 4, respectively. The observed frequencies are listed⁵ in Tables I and II.

(3) J. R. Durig, J. B. Turner, B. M. Gibson, and C. W. Sink, *J. Mol. Struct.*, **4**, 79 (1969).

(4) (a) "IUPAC, Tables of Wavenumbers for the Calibration of Infrared Spectrometers," Butterworths, Washington, D. C., 1961; (b) R. T. Hall and J. M. Dowling, *J. Chem. Phys.*, **47**, 2454 (1967); **52**, 1161 (1970).

(5) Listings of all of the observed bands, along with the frequencies for the individual branches, will appear immediately following this article in the microfilm edition of this volume of the journal. Single copies may be obtained from the Business Operations Office, Books and Journals Division, American Chemical Society, 1155 Sixteenth Street, N.W., Washington, D. C. 20036, by referring to code number JPC-72-1558. Remit check or money order for \$3.00 for photocopy or \$2.00 for microfiche.

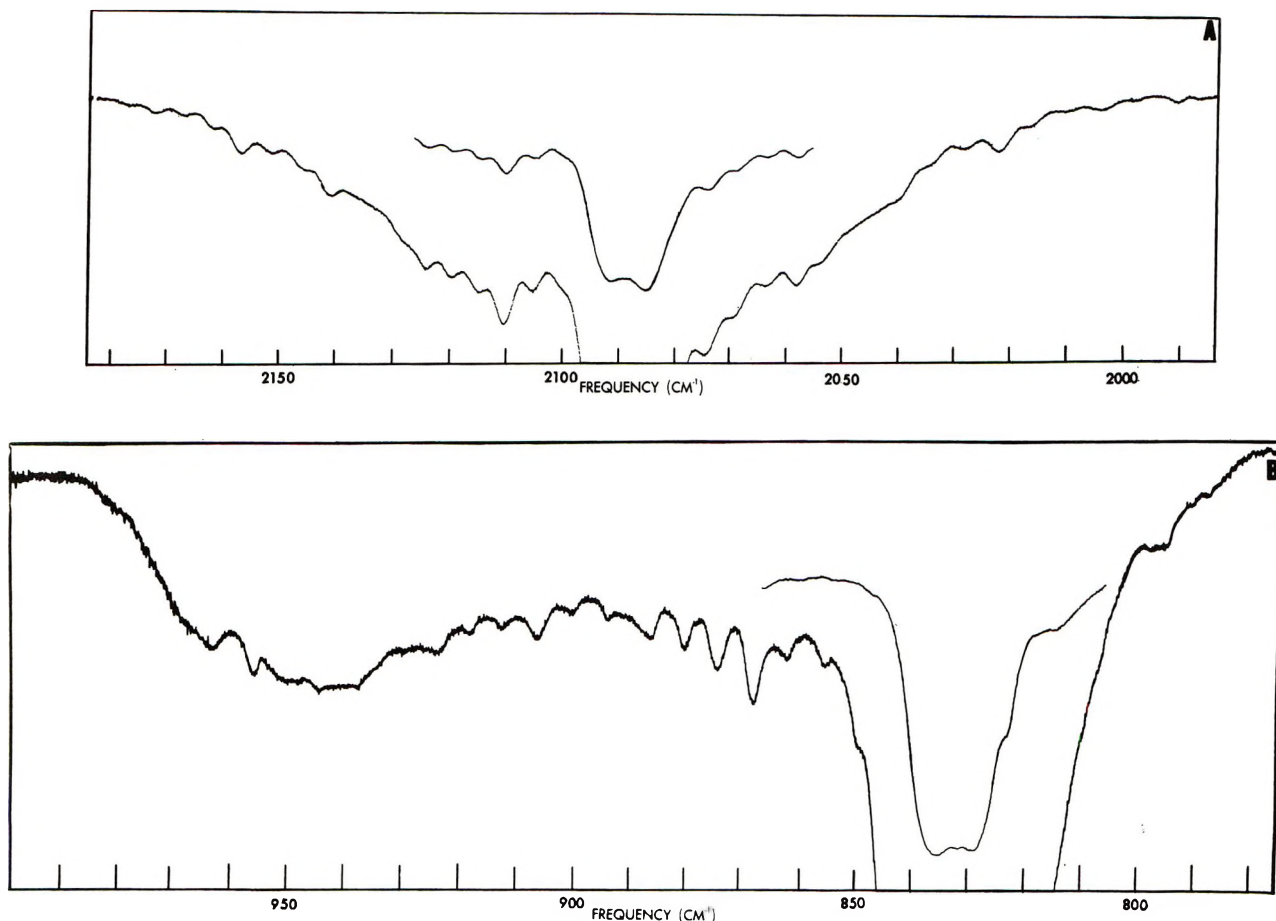


Figure 2. (A) Gas-phase infrared spectrum showing the GeH₃ stretching region of *p*-fluorophenylgermane. (B) Gas-phase infrared spectrum showing the GeH₃ deformation region of *p*-fluorophenylgermane.

The Raman spectra of the liquid samples sealed in glass capillaries were recorded with a Cary Model 81 spectrophotometer equipped with a SpectraPhysics Model 125 helium-neon laser. The instrument was calibrated with emission lines from a neon lamp over the spectral range 0–4000 cm⁻¹. Qualitative depolarization values were obtained in the manner described by Hawes, *et al.*⁶ The frequencies of the observed lines are listed⁵ in Tables I and II, and the spectra are shown in Figures 1B and 3B. All listed frequencies are believed to be accurate to ± 1 cm⁻¹ for all sharp bands.

Vibrational Assignment

Phenyl Modes. The vapor-phase spectra of *p*-fluorophenylgermane and *p*-chlorophenylgermane exhibit fine structure on those bands known to be characteristic of the germyl group. This feature in the spectra is indicative of free or nearly free internal rotation about the Ge–C bond, as explained in the final section of this paper. The effective symmetry of the phenyl group is then *C*_{2v}, with the 30 fundamental vibrations of the substituted benzene ring factoring into 11a₁, 3a₂, 10b₁, and 6b₂ symmetry. These fundamentals are described by an adaptation of Whiffen's⁷ notation for para disubstituted benzenes renumbered to correspond to Herz-

berg's notation.⁸ A pictorial representation of the motions of the phenyl ring has been presented by Scherer⁹ for the complete series of chlorinated benzenes, and approximate descriptions of these motions are listed in Table III. This table includes the numbering system employed in this paper and corresponding numbers used in the *p*-dihalobenzene papers.^{7,10,11}

The assignment of fundamental frequencies is facilitated by comparison with the assignments for phenylgermane² and reference to the spectral data for the symmetrical and unsymmetrical dihalogenobenzenes,^{7,9,11} with particular reference to those unsymmetrical dihalogenobenzenes, *p*-bromofluorobenzene and *p*-bromochlorobenzene. These two, from the standpoint of

(6) R. C. Hawes, K. P. George, D. C. Nelson, and R. Beckwith, *Anal. Chem.*, **38**, 1842 (1966).

(7) A. Stojiljkovic and D. H. Whiffen, *Spectrochim. Acta*, **12**, 47 (1958).

(8) G. Herzberg, "Infrared and Raman Spectra of Polyatomic Molecules," Van Nostrand, Princeton, N. J., 1945, p 271.

(9) J. R. Scherer, *Spectrochim. Acta*, **19**, 601 (1963); **21**, 321 (1965); *Spectrochim. Acta, Part A*, **24**, 747 (1968).

(10) A. Stojiljkovic and D. H. Whiffen, *Spectrochim. Acta*, **12**, 57 (1958).

(11) P. N. Gates, K. Radcliffe, and D. Steele, *Spectrochim. Acta, Part A*, **25**, 507 (1968).

Table III: Vibrational Fundamentals for *p*-Fluorophenylgermane and *p*-Chlorophenylgermane^a

| F-C ₆ H ₄ -GeH ₃ | | Cl-C ₆ H ₄ -GeH ₃ | | Assign no. | Assign ^b no. | Description ^c |
|---|--------------|--|--------------|------------|-------------------------|---|
| Raman | Infrared | Raman | Infrared | | | |
| Species A ₁ | | | | | | |
| 3065 | 3065 (w) | 3085 (ms, p) | 3082 (w) | 1 | 1 | C-H stretch |
| 3065 | 3065 (w) | 3056 (s, p) | | 2 | 18 | C-H stretch |
| 1590 (ms, dp) | 1595 (s) | 1588 (m, dp) | 1593 (m) | 3 | 2 | C-C stretch |
| 1498 (s, p) | 1498 (s, A) | 1480 (w) | 1493 (s, A) | 4 | 19 | C-H bend (60%), C-C stretch (40%) |
| 1230 (vs, p) | 1239 (s, A) | 1181 (w, p) | 1180 (w) | 5 | 3 | C-H bend (in plane) |
| 1162 (ms, p) | 1163 (m, A) | 1101 (w, p) | 1098 (m) | 6 | 20 | Ring (70%), C-X stretch (30%) |
| 1086 (ms, p) | 1089 (m) | 1079 (s, p) | 1083 (m, A) | 7 | 4 | Ring (50%), C-X stretch (30%), C-H bend (20%) |
| | 1015 (w) | | 1015 (w, A) | 8 | 21 | Ring (60%), C-H bend (25%) |
| 807 (w, p) | 817 | 730 (vs, p) | 731 (m, A) | 9 | 5 | C-C-C (55%), C-X stretch (45%) |
| 592 (w) | 593 (m) | 492 (vw) | 492 (vw) | 10 | 22 | C-X stretch (70%), ring |
| 268 (mw, p) | 267 (m) | 246 (s, p) | 246 (m) | 11 | 6 | Ring, C-X stretch (30%) |
| Species A ₂ | | | | | | |
| | 947 (m) | | 960 (vvw) | 12 | 16 | C-H (out of plane) |
| (813) ^d | | (813) ^d | | 13 | 7 | (C-H (out of plane)) |
| | 398 (w) | (410) ^d | | 14 | 17 | Ring deformation |
| Species B ₁ | | | | | | |
| | 3106 (w) | | 3098 (w) | 15 | 11 | C-H stretch |
| 3072 (mw, dp) | 3079 (w) | 3044 (w, dp) | 3040 (m) | 16 | 23 | C-H stretch |
| 1590 (ms, dp) | 1595 (s, B) | 1588 (m, dp) | 1593 (m) | 17 | 12 | C-C stretch |
| | 1388 (m) | | 1381 (ms) | 18 | 24 | C-C stretch (50%), C-H bend (50%) |
| 1305 (w) | 1306 (w) | 1301 (w, dp) | 1300 (m) | 19 | 13 | C-H (in plane) |
| 1270 (vw) | 1259 (w) | | 1240 (w) | 20 | 25 | Ring |
| 1065 (m) | 1068 (m) | (1079) ^d | | 21 | 26 | C-H bend (50%), ring (36%) |
| 632 (ms, dp) | 632 (w) | 628 (m, dp) | 630 (vw) | 22 | 14 | C-C-C (in plane) |
| | 420 (w) | (418) ^d | | 23 | 15 | C-X (in plane) |
| 287 (ms, dp) | 289 (m) | 249 (vw) | | 24 | 27 | C-X (in plane) |
| Species B ₂ | | | | | | |
| | 936 (m) | | 926 (vw) | 25 | 8 | C-H (out of plane) |
| (812) ^d | | (812) ^d | | 26 | 28 | C-H (out of plane) |
| | 672 (w) | | 708 (m) | 27 | 9 | Ring deformation |
| 493 (vw) | 485 (vw) | | 465 (m) | 28 | 29 | Ring deformation |
| 323 (vw, dp) | 315 (m, C) | 312 (vw) | 316 (m) | 29 | 10 | Ring |
| 228 (w) | 227 (w) | 198 (vw) | | 30 | 30 | C-X bend |
| GeH ₃ Vibrations | | | | | | |
| | 580 (m, b) | 584 (vw) | 580 (ms, B) | | | In-plane GeH ₃ rock |
| | 594 (m) | | 594 (s) | | | Out-of-plane GeH ₃ rock |
| 821 (s, p) | 834 (vs, A) | 822 (ms, p) | 834 (vs, A) | | | Sym GeH ₃ deformation |
| 879 (s, dp) | 874 (vs) | 880 (vs, dp) | 878 (vs) | | | Antisym GeH ₃ |
| | 2073 (vs) | | 2074 (vs) | | | Antisym GeH ₃ stretch |
| 2078 (vs, p) | 2085 (vs, A) | 2077 (vs, p) | 2088 (vs, A) | | | Symmetric GeH ₃ stretch |

^a Abbreviations used: m, medium; s, strong; w, weak; v, very; A, B, and C, individual band type; p and dp, polarized and depolarized. ^b Used in *p*-dihalobenzenes. ^c The approximate descriptions were taken from ref. 8. ^d Estimated, not observed.

mass, should have motions very similar to the phenyl motions of *p*-fluorophenylgermane and *p*-chlorophenylgermane, respectively. Band contours obtained from vapor-phase infrared spectra considered with polarization data from the Raman spectra further simplify assignments. All species are Raman active, and all except the a₂ modes are infrared active. The a₁ species give rise to polarized Raman lines with A-type infrared vapor-phase contours. The b₁ and b₂ modes should give rise to B- and C-type infrared bands, respectively.

The majority of the fundamentals are readily assigned. Only those requiring some explanation will be discussed, such as ν_1 , ν_2 , ν_{15} , and ν_{16} , the symmetric and antisymmetric C-H stretching modes. In *p*-bromofluorobenzene, the two symmetric stretching motions are assigned at 3007 and 3066, whereas the antisymmetric stretching C-H motions are located at 3115 and 3007 cm⁻¹. In *p*-fluorophenylgermane, the Raman line at 3065 cm⁻¹ can be shown by polarization measurements to contain both a polarized and a depolarized

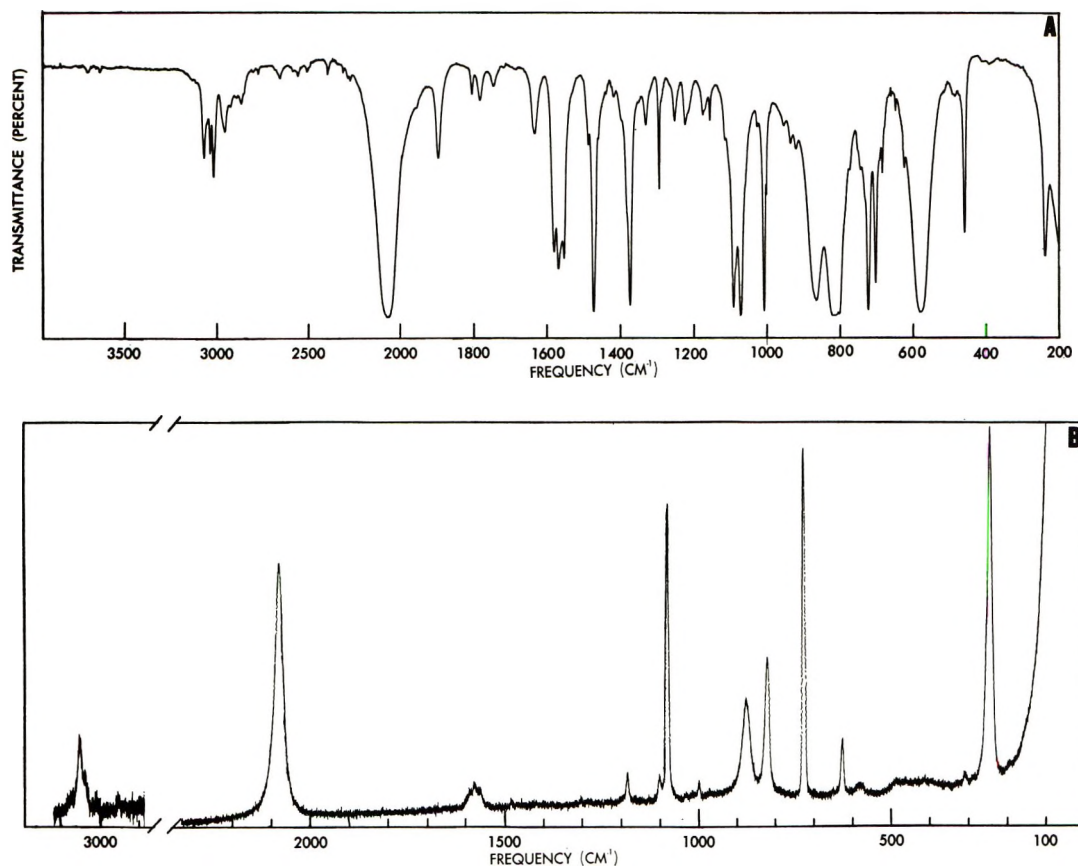


Figure 3. (A) Liquid-phase mid-infrared spectrum of *p*-chlorophenylgermane. (B) Raman spectrum of *p*-chlorophenylgermane.

component, which are centered at 3065 and 3072 cm^{-1} , respectively. Since no other polarized line or A-type infrared band occurs in this region, ν_1 and ν_2 are assumed to be coincident and fall at 3065 cm^{-1} . The two b_1 modes, ν_{15} and ν_{16} , are assigned to the infrared gas-phase band at 3106 cm^{-1} and the depolarized Raman line at 3072 cm^{-1} . In *p*-chlorophenylgermane, the infrared band at 3098 cm^{-1} is assigned to b_1 mode ν_{15} . The intense Raman line at 3056 cm^{-1} has shoulders centered at 3085 and 3045 cm^{-1} . The shoulder at 3085 cm^{-1} proves to be polarized, whereas the 3045- cm^{-1} band becomes much more distinct and is obviously depolarized. The a_1 modes, ν_1 and ν_2 , are assigned to bands at 3085 and 3056 cm^{-1} , whereas the b_1 mode, ν_{16} , is assigned to the 3044- cm^{-1} band.

The C-C stretching motions of a_1 and b_1 symmetry, ν_3 and ν_{17} , are, in the present case as in the almost isobaric dihalogenobenzene analogs, coincident at 1588 cm^{-1} in *p*-chlorophenylgermane and 1587 cm^{-1} in *p*-fluorophenylgermane. These Raman lines are depolarized. The remaining C-C stretching modes are strongly coupled with the C-H bending modes. They are derived from the degenerate 1485- and 1035- cm^{-1} bands in benzene, and one component of the higher frequency band, ν_4 , does not appreciably change frequency with substitution. This falls at 1498 cm^{-1} in *p*-fluorophenylgermane and 1480 cm^{-1} in *p*-chlorophenyl-

germane and is made up of approximately 40% C-C stretch and 60% C-H bend. The other component, ν_{18} , is lowered because the substitution has reduced the percentage of the C-H bending participation (50%) in the normal coordinate. In *p*-fluorophenylgermane the b_1 mode, ν_{18} , is assigned to the 1390- cm^{-1} infrared band and in *p*-chlorophenylgermane to the band at 1379 cm^{-1} ; neither band is observed in the Raman spectrum.

The assignments for ν_8 and ν_{21} are made and correspond with those for similar molecules. The spectra in the spectral region expected for these fundamentals require close attention. The a_1 mode, ν_8 , characteristically occurs near 1000 and is frequently not seen in the Raman spectrum; such is the present case. In the spectrum of *p*-fluorophenylgermane, the infrared band at 1016 cm^{-1} , like the corresponding band at 1015 cm^{-1} in the spectrum of *p*-chlorophenylgermane, has no Raman counterpart. These are therefore assigned to ν_8 . The b_1 mode, ν_{21} , generally occurs near 1100 cm^{-1} and also is not usually observed in the Raman effect. In *p*-fluorophenylgermane, there is a band at 1088 cm^{-1} , but it has a counterpart in the Raman spectrum which is polarized. It is moderately strong and more satisfactorily assigned to the a_1 mode, ν_7 . The b_1 mode, ν_{21} , is therefore unobserved. Similarly, ν_8 is assigned to the infrared band at 1015 cm^{-1} for *p*-chlorophenylgermane. Also, for *p*-chlorophenylgermane the 1098-

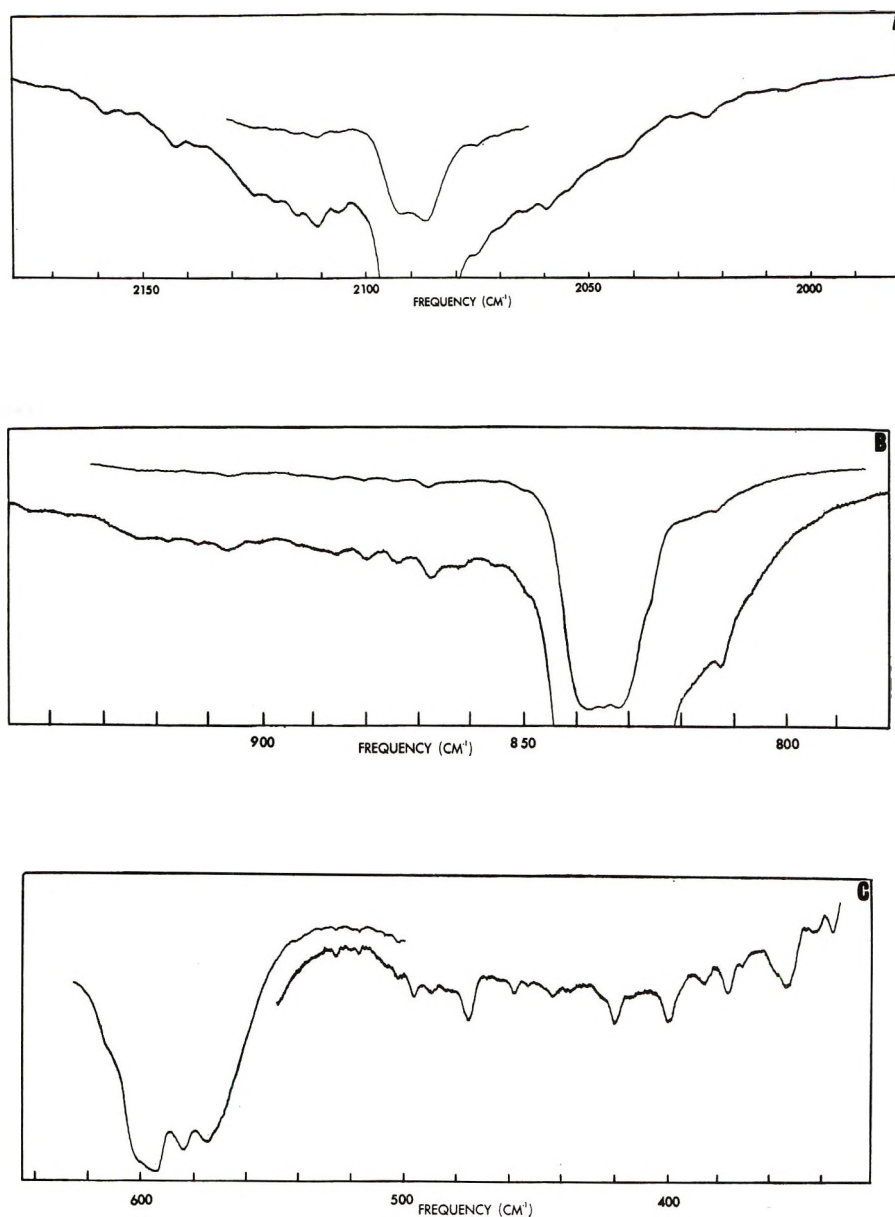


Figure 4. (A) Gas-phase infrared spectrum showing the GeH_3 stretching region of *p*-chlorophenylgermane. (B) Gas-phase infrared spectrum showing the GeH_3 deformation of *p*-chlorophenylgermane. (C) Gas-phase infrared spectrum showing the GeH_3 rocking region of *p*-chlorophenylgermane.

cm^{-1} infrared band has a polarized Raman counterpart and is assigned as the a_1 mode, ν_6 . The b_1 mode, ν_{21} , again is unobserved.

The a_2 modes, ν_{13} and ν_{14} , usually are weak or unobserved, and these molecules present no exceptions. Only ν_{14} in *p*-fluorophenylgermane is observed at 410 cm^{-1} . The a_2 mode, ν_{12} , is easily assigned to the 947-cm^{-1} band in *p*-fluorophenylgermane and the 960-cm^{-1} band in *p*-chlorophenylgermane.

The vibrational modes, ν_{10} and ν_{11} , in *p*-chlorophenylgermane are assigned to bands at 492 and 246 cm^{-1} , respectively. In the *p*-dihalophenylgermanes, ν_{10} plus ν_7 produces moderately intense infrared bands. This combination is observed in the spectrum of *p*-chlorophenylgermane at 1575 cm^{-1} , leading to further con-

fidence in the assignment. In *p*-fluorophenylgermane, ν_{10} and ν_{11} are assigned to bands at 592 and 268 cm^{-1} , respectively. The combination of ν_{10} plus ν_7 is found at 1678 cm^{-1} for *p*-fluorophenylgermane.

The C-H out-of-plane deformations, ν_{25} and ν_{12} , can be readily assigned as 936 and 926 cm^{-1} for ν_{25} and 960 and 947 cm^{-1} for ν_{12} for *p*-chlorophenylgermane and *p*-fluorophenylgermane, respectively. Both ν_{13} and ν_{26} fall in the region of the spectrum where the strong GeH_3 deformation occurs. Thus, one can only assume that they fall near 812 cm^{-1} and are obscured by the GeH_3 motion.

The out-of-plane ring motion, ν_{29} , and the C-X bend, ν_{30} , for *p*-chlorophenylgermane should lie near 300 and 100 cm^{-1} , respectively. The infrared band at 316 cm^{-1}

is assigned to ν_{29} . There is not a band around 100 cm^{-1} , but there is a weak band at 198 cm^{-1} which is tentatively assigned as ν_{30} . In *p*-fluorophenylgermane, ν_{29} is assigned to the band at 323 cm^{-1} , and again there is a weak band at 228 cm^{-1} which is tentatively assigned as ν_{30} .

GeH₃ Motions. Since the GeH₃ group is freely rotating, its symmetry is essentially C_{3v} . The eight vibrations are divided into three degenerate vibrations of species e and two nondegenerate vibrations of species a. The symmetric GeH₃ stretching vibration is readily assigned to the polarized Raman line at 2078 cm^{-1} in *p*-fluorophenylgermane, which corresponds to a liquid-phase infrared band centered at 2077 cm^{-1} . In *p*-chlorophenylgermane, the Raman line is centered at 2078 cm^{-1} . These Raman lines are symmetrical, with no shoulder apparent on the high wave number side. Thus, the doubly degenerate antisymmetric GeH₃ stretching motion appears to be degenerate with the symmetric mode.

The symmetric deformation is readily assigned to the polarized Raman line at 822 cm^{-1} in *p*-chlorophenylgermane and also occurs at 822 cm^{-1} in the infrared spectrum of the liquid. This vibration is observed at 821 cm^{-1} in the Raman effect (826 cm^{-1} in the infrared) for *p*-fluorophenylgermane. These values agree very well with the assignment for the corresponding motions for the phenylgermane molecule.

The in-plane rocking mode is assigned to the weak Raman line at 584 cm^{-1} in *p*-chlorophenylgermane, whereas the out-of-plane rocking motion is assigned to the strong liquid phase infrared band at 591 cm^{-1} . In *p*-fluorophenylgermane neither band appears in the Raman spectrum, but two bands are found in the infrared spectrum. The in-plane rocking mode occurs at 587.5 cm^{-1} and the out-of-plane rock at 593 cm^{-1} . The analysis of the gas-phase spectra for this region for both molecules is not clear. There appears to be a B-type band with other bands overlapping it on the high wave number side. In *p*-chlorophenylgermane, the B band center of 580.7 cm^{-1} in the infrared spectrum is in good agreement with the 584-cm^{-1} Raman line. The stronger Raman line at 594 cm^{-1} corresponds to the infrared frequency at 591 cm^{-1} . In *p*-fluorophenylgermane, there is a further complication in that ν_{10} occurs at 592 cm^{-1} in the Raman effect and is probably contributing to the complexity of the gas-phase spectrum in this region. The center of the B-type band at 580 cm^{-1} is assigned to the in-plane rocking mode. The out-of-plane rocking mode is then assigned to the 594-cm^{-1} gas-phase infrared band, which is strongly overlapped by ν_{10} .

The approximate rotational constants for *p*-chlorophenylgermane and *p*-fluorophenylgermane have been calculated using microwave results of compounds containing Ge-H bonds,¹² Ge-C¹³ bonds,¹³ and other bond lengths from Keidel and Bauer.¹⁴ The valence angles

about the germanium atom were taken as tetrahedral and all other angles as 120° . The values obtained for *p*-fluorophenylgermane were $A = 0.178\text{ cm}^{-1}$, $B = 0.0203\text{ cm}^{-1}$, $C = 0.183\text{ cm}^{-1}$; for *p*-chlorophenylgermane $A = 0.178\text{ cm}^{-1}$, $B = 0.0146\text{ cm}^{-1}$, $C = 0.0150\text{ cm}^{-1}$. These are so small that no fine structure from molecular rotation can be expected in the vapor-phase infrared spectra.

All the infrared bands attributed to the antisymmetric modes of the germyl group exhibit clearly resolved fine structure. The subbands of the antisymmetric stretching and deformational bands show an alternation of intensity strong, weak, weak, which is characteristic of perpendicular vibrations of molecules having a threefold symmetry axis. The rocking mode for *p*-chlorophenylgermane also shows erratic fine structure, which was not observed in the original vibrational study of phenylgermane.² However, in a more recent infrared study¹⁵ of phenylsilane and phenylgermane, some fine structure was observed on the rocking modes also. A similar erratic pattern was observed. Fleming and Banwell¹⁶ showed that as the energy difference of the two interacting modes increases, the net effect upon the fine structure increases until band contours for non-interacting vibrational species should be observed. Thus, the erratic fine structure for the rocking modes of *p*-chloro- and *p*-fluorophenylgermanes results presumably because the in-plane and out-of-plane motions, though not coincident, overlap sufficiently to thereby give the rotational fine structure of the region. The deviation from the strong-weak-weak alternation is most pronounced on the rocking motions which are split by approximately 14 cm^{-1} . Thus, the rotational fine structure for the perpendicular vibrations of the germyl moiety must be due to the nearly free rotation of the GeH₃ group about the Ge-C axis, since the spacing between successive subbands is more than an order of magnitude greater than that required for rotation of the entire molecule. The fine structure is consistent with a barrier of a few calories and is probably in the range of 10–20 cal.

The frequencies of the Q branches of the stretching modes are listed⁵ in Tables IV and V, with assignments based on the pattern of relative intensities. The $K = 0$ subband and the subbands corresponding to multiples of three are relatively strong. Also, the member of a pair of weak bands nearer the band center should be stronger than the adjacent one.¹⁷ The rotational

(12) G. R. Wilkinson and M. K. Wilson, *J. Chem. Phys.*, **44**, 3867 (1966).

(13) V. W. Laurie, *J. Chem. Phys.*, **30**, 1210 (1959).

(14) F. A. Keidel and S. H. Bauer, *J. Chem. Phys.*, **25**, 1218 (1957).

(15) J. R. Durig, C. W. Sink, and J. B. Turner, *Spectrochim. Acta, Part A*, **25**, 629 (1969).

(16) J. W. Fleming and C. N. Banwell, *J. Mol. Spectrosc.*, **31**, 318 (1969).

(17) G. Herzberg, ref 8, p 425.

structure on the deformation and rocking modes is so perturbed as to preclude any attempt to analyze it other than to reiterate that this is evidence for free rotation of the germyl group. An average of the distance between unperturbed subbands was taken in order to calculate the Coriolis coupling ζ for the antisymmetric deformation. The average spacing proved to be 6.3 cm^{-1} in both molecules.

Since the average spacing of the Q branches of each of these bands is equal to $[2A'(1 - \zeta) - (B' + C')]$,^{18,19} the Coriolis coupling constant (ζ) for the antisymmetric modes can be calculated. For the antisymmetric stretching mode, it is -0.019 for *p*-fluorophenylgermane and -0.014 for *p*-chlorophenylgermane. For the antisymmetric deformation modes, ζ is -0.168 for *p*-fluorophenylgermane and -0.171 for *p*-chlorophenylgermane.

The frequencies of the Q branches of the degenerate GeH stretching fundamental were found to fit by a least squares the following equations

$$\nu_{\text{sub}} = 2075.9 \pm 5.69K - 0.02K^2$$

$$\nu_{\text{sub}} = 2076.11 \pm 5.65K - 0.01K^2$$

for *p*-fluorophenylgermane and *p*-chlorophenylgermane, respectively. The band centers were calculated to be 2073.2 and 2074.4 cm^{-1} , respectively. The symmetric stretching frequencies taken from the gas-phase spectra were 2085.2 and 2088.5 cm^{-1} , respectively; thus the degenerate antisymmetric and symmetric stretching modes are very nearly degenerate.

In conclusion, the molecules *p*-chlorophenylgermane and *p*-fluorophenylgermane can be said to possess an extremely small barrier to internal rotation and, therefore, there is essentially "free rotation" about the Ge-C bond at room temperature.

Acknowledgment. The authors gratefully acknowledge the financial support given this work by the National Science Foundation under Grant No. GP-20723.

(18) C. V. Stephenson, W. C. Coburn, Jr., and W. S. Wilcox, *Spectrochim. Acta*, **17**, 933 (1961).

(19) D. H. Whiffen, *J. Chem. Soc.*, 1350 (1956).

Raman Spectra of Molten Alkali Metal Carbonates¹

by J. B. Bates, M. H. Brooker, A. S. Quist, and G. E. Boyd*

Oak Ridge National Laboratory, Oak Ridge, Tennessee 37830 (Received December 23, 1971)

Publication costs assisted by the Oak Ridge National Laboratory

Raman spectra of molten Li_2CO_3 and $\text{Li}_2\text{CO}_3\text{-LiCl}$, $\text{Li}_2\text{CO}_3\text{-CaCO}_3$, $\text{Na}_2\text{CO}_3\text{-NaCl}$, and $\text{K}_2\text{CO}_3\text{-KCl}$ eutectic mixtures were measured over the frequency interval from 150 to 2000 cm^{-1} . Raman and infrared spectra at 25° of saturated aqueous solutions of Na_2CO_3 and K_2CO_3 were recorded, and Raman spectra of the crystalline Li_2CO_3 , Na_2CO_3 , and K_2CO_3 were obtained from 25 to 692° . The Raman forbidden $D_{3h} \nu_2(A_2'')$ mode of carbonate ion was observed at *ca.* 880 cm^{-1} , and the $\nu_3(E')$ mode was split in the molten salt spectra. The ν_3 mode also exhibited two components in the aqueous solution spectra, and the frequencies of the Raman components were noncoincident with those in the infrared.

Introduction

The relatively high melting points and thermal instability of the alkali metal and alkaline earth carbonates account for the fact that a single, recent paper by Maroni and Cairns^{2a} is the only published report of the Raman spectra of CO_3^{2-} ion in carbonate melts.^{2b} Techniques developed in this laboratory³⁻⁵ for measuring Raman spectra of corrosive fluoride containing melts at temperatures to 800° have permitted us to undertake an extensive investigation of molten carbonates.

A more complete characterization of the physical properties of molten carbonates is of practical impor-

tance in view of the potential use of these materials for removing sulfur dioxide pollutants from stack emis-

(1) Research sponsored by the U. S. Atomic Energy Commission under contract with the Union Carbide Corporation.

(2) (a) V. A. Maroni and E. J. Cairns, *J. Chem. Phys.*, **52**, 4915 (1970). (b) The Raman spectrum of carbonate ion dissolved in molten LiF-NaF-KF has been reported: F. L. Whiting, G. Maman-tov, G. M. Begun, and J. P. Young, *Inorg. Chim. Acta*, **5**, 260 (1971).

(3) (a) A. S. Quist, *Appl. Spectrosc.*, **25**, 80 (1971); (b) A. S. Quist, *ibid.*, **25**, 82 (1971).

(4) A. S. Quist, J. B. Bates, and G. E. Boyd, *J. Chem. Phys.*, **54**, 4896 (1971).

(5) A. S. Quist, J. B. Bates, and G. E. Boyd, *J. Phys. Chem.*, **76**, 78 (1972).

sions.⁶ Raman spectra of the CO_3^{2-} ion in ionic melts are also basically interesting from the standpoint of determining the relative magnitudes and causes of spectral perturbations for this and other small polyatomic anions in the molten state. Numerous studies of the vibrational spectra of alkali metal nitrates from dilute solutions to the molten salt (*cf.*, for example, ref 7-9) have shown that there is an apparent breakdown in the "free" ion, D_{3h} , selection rules for NO_3^- ion: the $\nu_1(A_1')$ mode becomes infrared active, the $\nu_2(A_2')$ mode becomes Raman active, the $\nu_3(E')$ mode is split, and two bands have been observed in the $\nu_4(E')$ region for the LiNO_3 and NaNO_3 melts. Similar effects are expected with CO_3^{2-} ion in aqueous solution and molten salts.

This paper will present measurements of the Raman spectra of molten Li_2CO_3 - LiCl , Li_2CO_3 - CaCO_3 , Na_2CO_3 - NaCl , and K_2CO_3 - KCl eutectic mixtures. Raman spectra of molten Li_2CO_3 and saturated aqueous solutions of Na_2CO_3 and K_2CO_3 also were obtained, and the spectra of the crystalline alkali metal carbonates from 25 to 692°C were observed. Vibrational spectra of crystalline lithium and sodium carbonates from 77°K to 25°C have been reported in a recent publication¹⁰ from this laboratory, and the spectra of crystalline K_2CO_3 in this temperature range are currently being investigated. Effects caused by disordering of CO_3^{2-} in Na_2CO_3 were apparent in the vibrational spectra discussed in ref 10, and it now appears that K_2CO_3 exhibits a disorder similar to that reported from X-ray diffraction studies with Na_2CO_3 .¹¹ Crystalline Li_2CO_3 exhibits an ordered structure at room temperature; hence, it was of interest to intercompare the spectra of solid Li_2CO_3 , Na_2CO_3 , and K_2CO_3 at increasing temperature intervals above 25°C.

Experimental Section

The relatively high melting points¹² of K_2CO_3 (mp 898°) and Na_2CO_3 (mp 858°) precluded the possibility of measuring the Raman spectra of their melts because the temperature limit of the presently available furnace is 800°. Therefore, the alkali metal chloride eutectics of these salts were studied. Lithium carbonate melts at 726°¹² and thus the pure melt as well as the LiCl eutectic was investigated.

The eutectic mixtures¹³ of Li_2CO_3 - LiCl (60 mol % LiCl), Li_2CO_3 - CaCO_3 (33 mol % CaCO_3), Na_2CO_3 - NaCl (57 mol % NaCl), and K_2CO_3 - KCl (65 mol % KCl) were prepared from accurately weighed quantities of the anhydrous salts. With the exception of CaCO_3 , which was used "as received," the reagent grade chemicals were dissolved in water, mixed with Norit A decolorizing carbon, filtered through a fine glass frit, and recrystallized. Each salt was dried for at least 24 hr at 180° and cooled in a drybox. The eutectic mixtures were weighed, thoroughly ground in a drybox, loaded into the Pt-Ir windowless cell,^{3a} and

placed in a quartz tube which had an optical flat sealed to one end. The samples were further dried at about 300° under vacuum for about 2 hr. Approximately 2 atm of dry CO_2 was introduced into the quartz tube and condensed by inserting the tube into a liquid nitrogen trap. The quartz tube containing the Pt-Ir windowless cell was sealed off, warmed to room temperature, and placed in the high-temperature furnace.^{3b} Detailed sampling procedures for use with the windowless cells have been described elsewhere.³⁻⁵ It was estimated that at the temperatures prevailing in the melts the CO_2 over-pressure was about 5 atm.

Powdered crystalline samples of the carbonates to be studied from 25 to 692° were sealed in 1-mm o.d. Pyrex capillary tubes under vacuum. The samples were heated by placing the capillaries into a horizontal slot in an aluminum block^{3b} and inserting the block into the Raman furnace. Spectra of Li_2CO_3 above 500° were obtained by placing the sample in a quartz tube and tamping the surface to a 45° angle prior to illumination with the laser beam.

Raman spectra of the solid and molten carbonates were measured with a Jarrell-Ash Model 25-300 spectrophotometer. The 4880-Å line of a Coherent Radiation 52B-A argon ion laser operating at about 1.2 W was the exciting source. A narrow band pass interference filter was employed to remove Ar^+ emission lines when required. Raman and infrared spectra of saturated aqueous solutions of Na_2CO_3 and K_2CO_3 also were recorded. Infrared spectra of the K_2CO_3 solutions were measured by multiple internal reflectance with a Wilks Model 9 MIR reflectance assembly and a 60° AgCl prism. Sodium carbonate is about 70% less soluble than K_2CO_3 ; therefore, it was necessary to measure the infrared spectrum of aqueous Na_2CO_3 solution by transmission through a droplet squeezed between two AgBr plates. The infrared spectrophotometer was a Perkin-Elmer Model 621.

Frequency calibrations for the Raman spectra were based on the argon ion laser emission lines. Polystyrene films served for the infrared wave number calibration. The estimated frequency accuracy is presented as a footnote to Table I.

(6) R. D. Oldenkamp and E. D. Margolin, *Chem. Eng. Progr.*, **65**, 73 (1969).

(7) D. W. James and W. H. Leong, *J. Chem. Phys.*, **51**, 640 (1969).

(8) M. H. Brooker, A. S. Quist, and G. E. Boyd, *Chem. Phys. Lett.*, **5**, 357 (1970); **9**, 242 (1971).

(9) D. E. Irish, D. L. Nelson, and M. H. Brooker, *J. Chem. Phys.*, **54**, 654 (1971).

(10) M. H. Brooker and J. B. Bates, *ibid.*, **54**, 4788 (1971).

(11) G. C. Dubbeldam and P. M. DeWolf, *Acta Crystallogr., Sect. B*, **25**, 2665 (1969).

(12) G. J. Janz, E. Neuenschwander, and F. J. Kelley, *Trans. Faraday Soc.*, **59**, 841 (1963).

(13) E. M. Levin, C. R. Robbins, and H. F. McMurdie, "Phase Diagrams for Ceramists," American Ceramic Society, Columbus, Ohio, 1964, pp 323, 501-532.

Table I: Bands Observed in the Raman Spectra of Molten and Aqueous Carbonates

| Assignment | Frequency, cm^{-1} ^{a, b} | | | | | | | |
|-----------------------|---|--------------------------|--------------------------|--------------------------|----------------------------------|-------------------------|----------------------------|--|
| | Pure (765°) | Li_2CO_3 | | Na_2CO_3 | | K_2CO_3 | | |
| | | LiCl^c (625°) | CaCO_3^c (775°) | NaCl^c (745°) | Aq soln (25°) | KCl^c (670°) | Aq soln (25°) | |
| $\nu_1(\text{A}_1')$ | 1072 s, p | 1074 s, p | 1072 s, p | 1050 s, p | 1067 s, p [1063] ^d | 1040 s, p | 1064 s, p [1060] | |
| $\nu_2(\text{A}_2'')$ | 878 vw | 872 vw | 874 vw | 880 vw | [880] | n.o. | [882] | |
| $\nu_3(\text{E}')$ | 1496 m 1418 m | 1496 m 1422 m | 1510 m 1418 m | 1440 m 1400 m | 1412 m [1405] 1380 m [1360] | 1407 m 1380 m | 1432 [1410] 1389 [1355] | |
| $\nu_4(\text{E}')$ | 702 w | 704 w | 712 w | 695 w | 681 w | 687 w | 686 w | |
| $2\nu_2$ | 1752 w | 1748 w | 1742 w | 1758 w | n.o. | 1764 w | n.o. | |

^a Frequency accuracy: $\nu_1 (\pm 2)$, $\nu_2 (\pm 5)$, $\nu_3 (\pm 10)$, $\nu_4 (\pm 5)$, $2\nu_2 (\pm 5)$. ^b s = strong; m = medium; w = weak; v = very; p = polarized; n.o. = band not observed. ^c Eutectic compositions: Li_2CO_3 -LiCl (60 mol % LiCl, mp 506°); Li_2CO_3 - CaCO_3 (33 mol % CaCO_3 , mp 662°); Na_2CO_3 -NaCl (57 mol % NaCl, mp 640°); K_2CO_3 -KCl (65 mol % KCl, mp 630°). ^d [] indicates an infrared value.

Results

Raman spectra of molten lithium carbonate and the Li_2CO_3 -LiCl and Na_2CO_3 -NaCl eutectics are shown in Figures 1 and 2, respectively. Infrared and Raman spectra of aqueous K_2CO_3 and the Raman spectrum of molten K_2CO_3 -KCl at 670° in the region from 1250 to 1800 cm^{-1} are presented in Figure 3. The frequencies and assignments of the bands observed in the molten salt and aqueous solution spectra are collected in Table I.

The vibrational spectra of the molten salts and aqueous solutions (Figures 1-3 and Table I) indicate an apparent breakdown in the D_{3h} selection rules of the CO_3^{2-} ion in these media. Contrary to strict selection rules, the $\nu_1(\text{A}_1')$ symmetric stretching mode appeared in the infrared spectra of the saturated Na_2CO_3 and K_2CO_3 solutions, the $\nu_2(\text{A}_2'')$ bending mode was observed in the 870-880- cm^{-1} region in the Raman spectrum of the Li_2CO_3 and Na_2CO_3 melts, and the $\nu_3(\text{E}')$ antisymmetric stretching mode was split in spectra of the aqueous solutions as well as in the melt. The ν_3 splitting decreased from a maximum value of ca. 92 cm^{-1} in the CaCO_3 - Li_2CO_3 eutectic to a minimum value of ca. 27 cm^{-1} in the KCl- K_2CO_3 eutectic melt (Table I). The frequencies of the ν_3 components in infrared spectra of aqueous Na_2CO_3 and K_2CO_3 did not appear to be coincident with those in the Raman spectra of the same solutions. It is also interesting to note in Table I that while the Raman components of ν_3 in aqueous Na_2CO_3 have lower frequencies than the Raman components observed in molten Na_2CO_3 -NaCl (i.e., 1380 and 1412 cm^{-1} vs. 1400 and 1440, respectively), the reverse is true for the ν_3 frequencies observed from Raman spectra of aqueous K_2CO_3 and molten K_2CO_3 -KCl (i.e., 1389 and 1432 vs. 1380 and 1407, respectively). Only one band was observed in the $\nu_4(\text{E}')$ antisymmetric stretching region for each of the melts.

The overlap of the two bands in the ν_3 region of the melt and aqueous solution spectra introduced a large

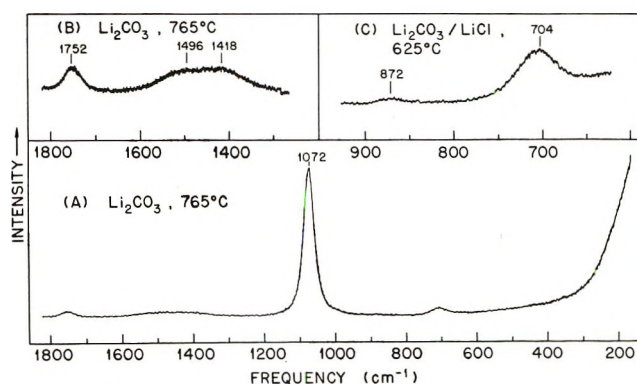


Figure 1. Raman spectra of molten Li_2CO_3 at 765° and molten Li_2CO_3 -LiCl eutectic mixture (60 mol % LiCl) at 625°.

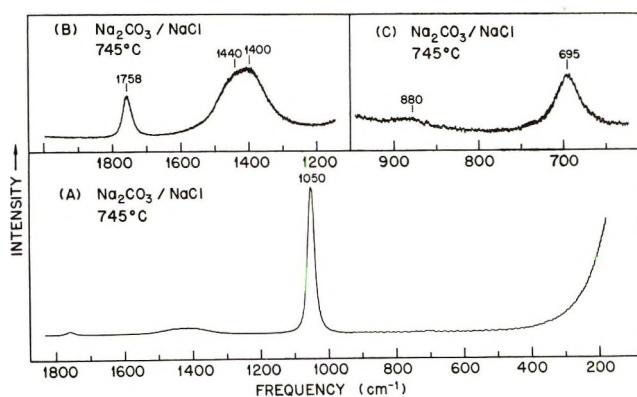


Figure 2. Raman spectra of molten Na_2CO_3 -NaCl eutectic mixture (57 mol % NaCl) at 745°.

uncertainty in the visual location of peak frequencies ($\pm 10 \text{ cm}^{-1}$). To provide additional evidence bearing on the apparent noncoincidence between the infrared and Raman band frequencies in the ν_3 region of aqueous Na_2CO_3 and K_2CO_3 , each ν_3 spectrum was resolved into two components with nonlinear least-squares computer techniques assuming each component to have a Gaussian shape.¹⁴ Data points (intensity vs. frequency)

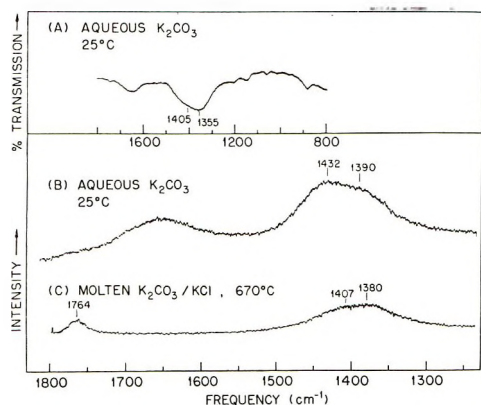


Figure 3. Vibrational spectra of the $\nu_3(E')$ and $2\nu_2$ regions of CO_3^{2-} : (A) infrared spectrum of aqueous K_2CO_3 (saturated) at 25° ; (B) Raman spectrum of aqueous K_2CO_3 (saturated) at 25° ; (C) Raman spectrum of molten K_2CO_3 -KCl eutectic mixture (65 mol % KCl).

were measured at 5-cm^{-1} intervals from recorded spectra.¹⁵ The results from these computer resolutions are given in Table II. Standard deviations between the observed and computed intensities of the total band envelopes also are included as these provide a statistical test of the model chosen for the ν_3 envelopes (*i.e.*, two

Table II: Computer Resolution of the ν_3 Region of the Raman and Infrared Spectra of Aqueous Na_2CO_3 and K_2CO_3

| | | Fre- quency ^a | Width ^b | Intensity ^c | Std. dev. ^d |
|------------------------------|---------|-----------------------------|--------------------|------------------------|---------------------------|
| (A) Na_2CO_3 | | | | | |
| Raman | Band I | 1430 | 58 | 29 | 0.003 |
| | Band II | 1381 | 79 | 69 | |
| Infrared | Band I | 1397 | 109 | 44 | 0.01 |
| | Band II | 1356 | 61 | 14 | |
| (B) K_2CO_3 | | | | | |
| Raman | Band I | 1449 | 52 | 13 | 0.007 |
| | Band II | 1400 | 115 | 36 | |
| Infrared | Band I | 1429 | 78 | 89 | 0.004 |
| | Band II | 1351 | 92 | 171 | |

^a Frequency in cm^{-1} . ^b Full width at half band height in cm^{-1} . ^c Band area in arbitrary units. ^d Standard deviation of calculated intensities *vs.* observed intensities for ν_3 band envelope.

Gaussians). Examples of the computed band envelopes and Gaussian components for the Raman and infrared spectra of aqueous K_2CO_3 are presented in Figure 4. The points shown are the observed data.

Raman spectra in the lattice mode regions of crystalline Li_2CO_3 , Na_2CO_3 , and K_2CO_3 observed from 80°K to *ca.* 500°C are shown in Figure 5. In addition, spectra were obtained for solid Li_2CO_3 just below the melting point (726°) which differed negligibly from those obtained at 507° . Frequencies and assignments of the

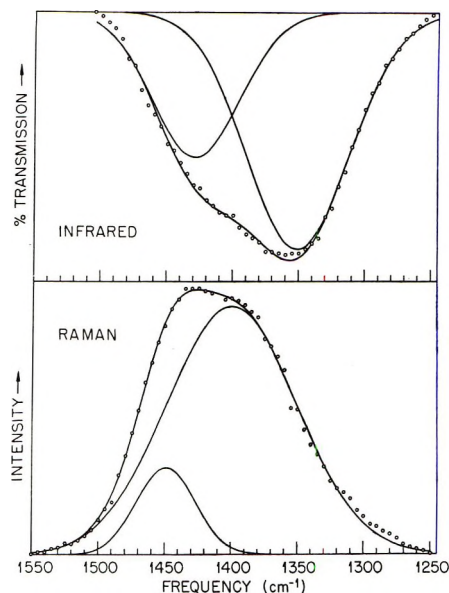


Figure 4. Resolution of ν_3 band envelope observed from Raman and infrared spectra of aqueous K_2CO_3 using nonlinear least-squares computer techniques.

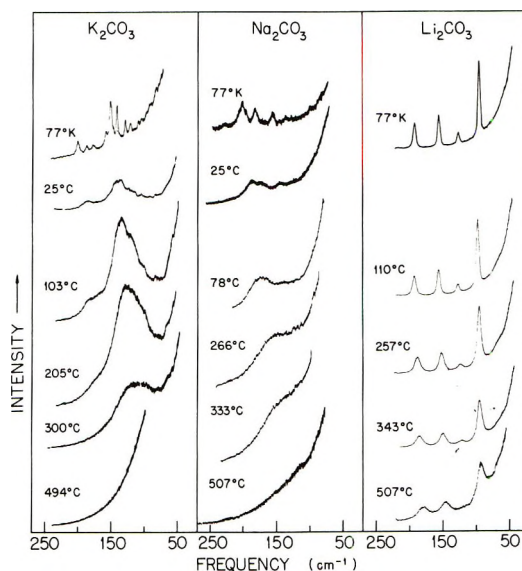


Figure 5. Raman spectra of the lattice mode regions of crystalline lithium, sodium, and potassium carbonates.

bands observed in the internal and external mode regions at selected temperatures are collected in Table III. The spectra of Figure 5 reveal a striking difference between the behavior of solid Li_2CO_3 on one hand and solid Na_2CO_3 and K_2CO_3 on the other. Whereas the four sharp lattice bands observed in Li_2CO_3 at 77°K were still apparent at 507° and three bands were observed at 692° (34° below the melting point), distinct features in

(14) R. E. Biggers, J. T. Bell, E. C. Long, and O. W. Russ, "Mathematical Resolution of Complex Overlapping Spectra with Nonlinear Least-Squares Computer Techniques," ORNL-3834, 1971.

(15) Sampling density corresponds to *ca.* 2 points over each interval of a 10-cm^{-1} spectral slit width.

Table III: Bands Observed in Raman Spectra of Crystalline Li_2CO_3 , Na_2CO_3 , and K_2CO_3 at Selected Temperatures from 25 to 692°

| Li ₂ CO ₃ (mp 726°) | | | | Frequency, cm ⁻¹ ^a | | | K ₂ CO ₃ (mp 898°) | | | Assign- ment ^a |
|---|------|------|------|--|------|---------|--|---------|------|------------------------------|
| 25° | 257° | 507° | 692° | 25° | 266° | 507° | 25° | 300° | 495° | |
| 95 | 95 | 93 | 90 | 146 | | | 48 | | | |
| 126 | 123 | 121 | ... | 172 | 148 | n.o. | 137 | 110 | n.o. | ν_{L} |
| 156 | 152 | 145 | 140 | 185 | | | 143 | | | |
| 192 | 188 | 179 | 171 | 220 | | | 186 | | | |
| 711 | | 710 | 711 | 702 | 700 | 700 | 686 | | | |
| 748 | | 738 | 728 | | | | 689 | 689 | 690 | $\nu_4(\text{E}')$ |
| | | | | | | | 694 | | | |
| | | | | | | | 696 | | | |
| 1091 | 1090 | 1086 | 1081 | 1079 | 1077 | 1072 | 1063 | 1059 | 1057 | $\nu_1(\text{A}_1')$ |
| | | | | 1083 | | | | | | |
| 1459 | 1451 | 1430 | 1420 | 1422 | 1418 | 1396(?) | 1400 | 1386(?) | 1388 | $\nu_3(\text{E}')$ |
| | | | | 1431 | | | 1408 | 1390 | | |
| | | | | | | | 1418 | | | |

^a ν_{L} denotes lattice modes; n.o. = band not observed; (?) uncertain band.

the low-frequency regions of Na_2CO_3 and K_2CO_3 gradually disappeared until at *ca.* 300° only a single, broad band was observed. At temperatures near 500°, only a broadened Rayleigh wing background was detected in the 50–250-cm⁻¹ region of Na_2CO_3 and K_2CO_3 . As shown in Table III, the two components of ν_4 in the Raman spectrum of Li_2CO_3 at 25° also were observed at 692° (only one band was present after fusion), while the splitting observed for ν_1 and ν_3 in Na_2CO_3 and for ν_4 in K_2CO_3 was no longer apparent above *ca.* 250°. While the ν_3 split in K_2CO_3 was discernible at 300°, it disappeared above *ca.* 350°.

Discussion

The apparent breakdown in D_{3h} selection rules of the CO_3^{2-} ion in the molten salts and aqueous solutions studied in this work (*i.e.*, the appearance of ν_2 ¹⁶ and the splitting of ν_3) is believed to be caused by mechanisms which produce similar effects observed with NO_3^- ion from spectra of molten and aqueous nitrates.^{7–9,17–20} The splitting of ν_3 in nitrate melts and aqueous solutions has been variously ascribed to (a) lowering of the D_{3h} “free” ion symmetry by forming cation–anion contact ion pairs,¹⁷ (b) dynamic coupling of correlated motions of nitrate ions in the unit cell of a quasicrystalline structure,¹⁸ (c) longitudinal optical (LO)–transverse optical (TO) mode effects,¹⁹ which also require a lattice model of molten salts, (d) local field anisotropy,²⁰ and (e) vibrational–rotational coupling interactions.²¹ In view of the similarities observed between nitrate and carbonate melt spectra, an interpretation of the latter in the light of the theories of molten nitrates will be considered first.

The assignment of the two bands in the ν_3 region of the CO_3^{2-} ion in molten carbonates (Figures 1–3 and Table I) to an LO–TO pair does not seem reasonable because the molten carbonate or carbonate–chloride

eutectic mixture must then possess sufficient long-range order to allow for the existence of polarized phonon states. X-Ray diffraction measurements on molten Li_2CO_3 , Na_2CO_3 , and K_2CO_3 reported by Zarzycki²² gave no indication of long-range order in these melts. Studies with melts of the alkali metal nitrates²³ and with melts of the alkali metal halides²⁴ also gave no indication of long-range order in these ionic liquids. The diffraction experiments instead indicate that molten carbonates as well as nitrates and the alkali metal halides exhibit a large degree of inhomogeneity with respect to interionic distances and average (anion–cation) coordination numbers. In particular, Levy, *et al.*,²⁴ contend that their results with alkali metal halide melts argue against a “pseudocrystalline” model for molten salts.

The fact that two components of ν_3 were found with aqueous solutions of Na_2CO_3 and K_2CO_3 (Tables I and II and Figures 3 and 4) appears to support the view that the splitting observed for this mode in melt spectra cannot be caused by an LO–TO effect or by dynamic coupling. This argument would be supported if it can be established that the splitting of ν_3 is produced by the same mechanism in molten salts and in aqueous systems, because in the latter no ordering of CO_3^{2-} ions is expected.

(16) Although a component of ν_2 is predicted to be Raman active in crystalline Li_2CO_3 (ref 10), it has not yet been observed.

(17) S. C. Wait, Jr., A. T. Ward, and G. J. Janz, *J. Chem. Phys.*, **45**, 133 (1966).

(18) J. P. Devlin, P. C. Li, and G. Pollard, *ibid.*, **52**, 2267 (1970).

(19) J. P. Devlin, D. W. James, and R. Frech, *ibid.*, **53**, 4349 (1970).

(20) D. E. Irish and A. R. Davis, *Can. J. Chem.*, **46**, 943 (1968).

(21) M. H. Brooker, G. Chang, A. R. Davis, and D. E. Irish, unpublished data.

(22) J. Zarzycki, *Discuss. Faraday Soc.*, **32**, 38 (1961).

(23) K. Furukawa, *ibid.*, **32**, 53 (1961).

(24) H. A. Levy, P. A. Agron, M. A. Bredig, and M. D. Danford, *Ann. N. Y. Acad. Sci.*, **79**, 762 (1960).

Similarities observed between melt spectra and spectra of the disordered solid phase of the crystalline material near its melting point have been cited as supporting evidence for the quasicrystalline model for molten nitrates.²⁵ The effect of increasing temperature on the Raman spectrum of solid Li_2CO_3 is quite different from that observed for solid Na_2CO_3 and K_2CO_3 (Table III), but the melt spectra of all these compounds exhibit identical features (*i.e.*, splitting of ν_3 and the appearance of ν_2). The Raman spectra of crystalline K_2CO_3 and Na_2CO_3 (Figure 5) indicate that these solids are highly disordered above 300° while Li_2CO_3 appears to retain an ordered lattice at temperatures up to the melting point (Table III and Figure 5). If the behavior of the alkali metal carbonate melts is to be compared with that of a disordered solid, then the sodium and potassium melt spectra should resemble the spectra of the corresponding solids at *ca.* 500° . However, as shown in Tables I and III, the melt and solid state spectra were quite different with respect to the appearance of ν_2 and the splitting of ν_3 . From these considerations, it may be inferred that a comparative study of the Raman spectra of molten and solid alkali metal carbonates at high temperatures does not support a quasicrystalline model for these melts.

The "contact ion" model which has been used to interpret vibrational spectra of molten nitrates¹⁷ assumes that a lowering of the D_{3h} symmetry is brought about by formation of a bond between a cation and an oxygen atom on the nitrate ion. Normal coordinate calculations based on a Urey-Bradley potential field for the $(\text{M}^+)(\text{NO}_3^-)$ complex were employed to obtain estimates of the M-O bond strength. The contact ion model can account for the apparent breakdown in D_{3h} selection rules, and it does not require the untenable assumptions implicit in the quasicrystalline model. However, this model may be too specific for molten salts in view of the X-ray diffraction experiments mentioned above.²²⁻²⁴ The interpretation of the molten carbonate²² and nitrate²³ diffraction data requires the placement of several cations in the first (nearest-neighbor) coordination sphere of the anion. Similarly, the coordination numbers of nearest neighbors in molten alkali halides were found to vary from 3.5 to 5.6.²⁴ Thus, the assumption that only ion pairs or triplets such as $(\text{M}^+)(\text{CO}_3^{2-})$ or $(\text{M}^+)_2(\text{CO}_3^{2-})$ will exist as dominant stable species (with respect to the time of measurement) in molten carbonates is not supported by the diffraction data.

The splitting of the ν_3 mode and the appearance of the Raman forbidden ν_2 mode in spectra of the CO_3^{2-} ion in molten carbonates may be accounted for by assuming that the time averaged environment about CO_3^{2-} ions in these melts is anisotropic. A "snapshot" of the melt might show that the potential energy surface determined by the interionic interactions of a given CO_3^{2-} anion with neighboring ions is highly asym-

metric (anisotropic). The anisotropy of the potential field causes a splitting of the degenerate ν_3 mode and the Raman activity of ν_2 . This field, or potential surface, primarily arises from coulomb (charge-charge) interactions, but other effects such as charge-induced dipole terms may be important. The field about the anions is averaged because of the ionic movement in the melt.

Another effect which may be important in understanding the spectra of molten carbonates is that caused by the librational motion of CO_3^{2-} ions. Broad, low-frequency Raman bands ($<200\text{ cm}^{-1}$) assigned to anion libration have been observed in the Raman spectra of molten nitrates.^{8,18} Similar bands were not found in the molten carbonate spectra because the high temperatures required in these measurements resulted in a very broad (Rayleigh) background extending well beyond 300 cm^{-1} (Figure 1). The (excited) ($n > 0$) librational levels of CO_3^{2-} ions in carbonate melts are highly populated²⁶ and exhibit large mean amplitudes. Thus a strong Coriolis-like interaction between the CO_3^{2-} vibrational modes and the large amplitude anion librations in the molten salts may occur, and these interactions may account for the splitting of ν_3 and the Raman activity of ν_2 .

One marked difference between the Raman spectra of the carbonates and those of the nitrates was the observation of only a single band in the ν_4 region of each of the aqueous and molten carbonate systems. It was previously reported^{7,8} that two bands were present in the ν_4 region of the Raman spectra of molten LiNO_3 and molten NaNO_3 . The apparent lack of splitting of ν_4 in molten carbonates perhaps may be due to a considerable reduction in magnitude of the perturbation on ν_4 as compared to ν_3 . Alternatively, it has been proposed that the ν_4 splitting of NO_3^- ion in molten and aqueous nitrates is caused by two types of nitrate environments. If this explanation is valid, it suggests that there is effectively a single environment about the CO_3^{2-} ions in the molten and aqueous carbonate systems studied in this work.

The similarities noted between the vibrational spectra of aqueous and molten nitrates and the spectra of aqueous and molten carbonates suggest that there are certain common properties of the liquid and dissolved states of molecular anions which give rise to spectral perturbations. The qualitative interpretation of the molten carbonate Raman spectra presented above represents an alternative approach to understanding ionic melts in which no assumptions of lattice-like ordering or of the formation of specific cation-anion complexes are required. Existing interpretations of the aqueous solution spectra, however, are inadequate

(25) J. P. Devlin and D. W. James, *Chem. Phys. Lett.*, **7**, 237 (1970).

(26) For example, the Boltzmann factor, N_n/N_0 , for $n = 5$, $\nu = 150\text{ cm}^{-1}$, and $T = 700^\circ$, is 0.33.

because they do not account for the lack of coincidence observed between the infrared and Raman active components of ν_3 in spectra of CO_3^{2-} ion (Table II). For the most part, the nature of these effects has not yet

been elucidated or interpreted with a unified theory in spite of the large experimental effort that has been devoted to the study of ionic melts and aqueous solutions.

Ultrasonic Absorption in Dioxane-Water Solutions of Magnesium Sulfate

by F. H. Fisher

University of California, San Diego, Marine Physical Laboratory of the Scripps Institution of Oceanography, San Diego, California 92152 (Received November 12, 1971)

Publication costs assisted by the Office of Naval Research and the National Science Foundation

Ultrasonic absorption in the primary relaxation frequency region has been measured in a 0.02 M solution of MgSO_4 in a solvent of 37% by weight dioxane-water; measurements were made at 24° over a frequency range from 40 to 325 kHz. The maximum value of absorption per wavelength is 6.3×10^{-5} and the relaxation frequency is 109 kHz. Contrary to earlier results at low concentrations, in which $(\alpha\lambda)_{\text{III}m}$ increased with added dioxane in 13 and 25% by wt dioxane-water solvents, $(\alpha\lambda)_{\text{III}m}$ is less than the value in aqueous solution. The decrease in absorption is discussed in terms of the relaxation theory of multistep dissociation.

Introduction

High ultrasonic absorption in the ocean, about 30 times greater than water at frequencies below 100 kHz, is due to the relatively small amount of MgSO_4 present.¹⁻⁴ Measurements of ultrasonic absorption over a wide range of frequencies and concentrations in aqueous solutions of MgSO_4 were explained quantitatively by Eigen and Tamm⁵ in terms of coupled, pressure-dependent chemical reactions. A three-step multistate dissociation process was selected to account for the observed relaxation absorption peaks. Eigen and Tamm also explained the absorption and relaxation frequencies observed in MgSO_4 solutions in mixed solvents consisting of water with varying amounts of ethanol, methanol, and dioxane. A review of ultrasonic propagation in electrolytic solutions by Stuehr and Yeager⁶ includes an extensive summary of ultrasonic absorption in mixed solvents as well as a brief presentation of the work of Eigen and Tamm. Stuehr and Yeager concluded that differences in the primary relaxation frequency of MgSO_4 solutions in methanol-water and dioxane-water solvents was evidence of specific solvent interactions with the relaxation process and that the static dielectric constant, D , cannot be used alone to describe the contribution of the solvent to the observed relaxation effect. Measurements of ultrasonic absorption by Atkinson and Kor⁷ in MnSO_4 solutions have given further evidence of the importance of specific solvent effects in ultrasonic relaxation processes.

In dioxane-water solvents, Bies observed increased absorption as the solvent was varied by adding dioxane, a nonpolar liquid. For a 13% by wt dioxane-water mixture ($D = 67.0$), maximum absorption per wavelength increased by nearly a factor of 2 over that in aqueous solution for a concentration of 0.005 M MgSO_4 ; however, at higher concentrations, 0.027⁸ and 0.5 M ,⁹ the increase was only a factor of ~ 1.25 . For 0.5 M MgSO_4 in a 25% dioxane-water solvent ($D = 56.5$), the maximum absorption per wavelength decreased to the value in aqueous solution, a reversal of the dependence

(1) R. W. Leonard, Technical Report No. 1 (Contract N6onr 27507), Department of Physics, University of California, Los Angeles, Calif., June 1953.

(2) O. B. Wilson and R. W. Leonard, *J. Acoust. Soc. Amer.*, **26**, 223 (1954).

(3) O. B. Wilson, Jr., Technical Report No. IV (Contract N6onr 27507), Department of Physics, University of California, Los Angeles, Calif., June 1951.

(4) G. Kurtze and K. Tamm, *Acustica*, **3**, 33 (1953).

(5) (a) M. Eigen and K. Tamm, *Ber. Bunsenges. Phys. Chem.*, **66**, 93 (1962); (b) M. Eigen and K. Tamm, *ibid.*, **66**, 107 (1962); (c) K. Tamm, "Handbuch der Physik," Vol. 11/1, S. Flügge, Ed., Springer-Verlag, Berlin, 1961, p 202 ff. Note: Translations of 5a and b arranged for by F. H. Fisher and G. Atkinson with an introduction by K. Tamm are available as Reference 68-41, Scripps Institution of Oceanography, Oct 1, 1968.

(6) J. Stuehr and E. Yeager, "Physical Acoustics," Vol. II, Part A, W. P. Mason, Ed., Academic Press, New York, N. Y., 1965, pp 373-452.

(7) G. Atkinson and S. K. Kor, *J. Phys. Chem.*, **69**, 128 (1965).

(8) D. A. Bies, *J. Chem. Phys.*, **23**, 428 (1955).

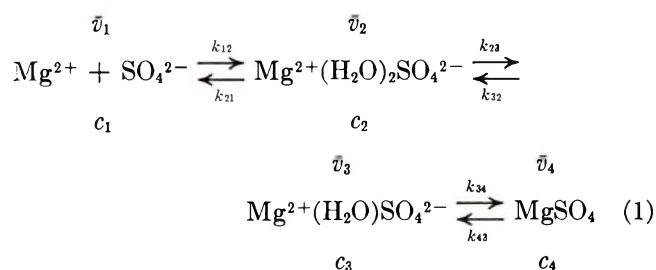
(9) F. H. Fisher, *J. Acoust. Soc. Amer.*, **38**, 805 (1965).

of absorption at low concentrations³ on the amount of dioxane in the solvent. Since the increase in absorption for 0.02 and 0.5 *M* solutions is the same in going from water to a 13% dioxane–water solvent, the reversal observed at high concentration suggests that a similar effect may be found at lower concentration.

In this work ultrasonic absorption was measured near 25° in a 0.02 *M* solution of MgSO₄ in 37% dioxane–water solvent (*D* = 45.5) over a frequency range of 40 to 325 kHz. The maximum absorption per wavelength decreased to a value below that observed in aqueous solution for the same concentration.

The results of this work are discussed on the basis of the multistate dissociation theory using the multistate parameters reported by Eigen and Tamm⁵ (ET) and the more recent ones reported by Bechtler, Breitschwerdt, and Tamm¹⁰ (BBT) which differ drastically from each other.

The reaction proposed by ET to explain absorption in aqueous solutions of MgSO₄ is a multistep association and dissociation process represented by



where the k_{ij} are the rate constants, c_i , the concentration, and \bar{v}_i the partial molal volumes. Stepwise removal of water molecules leads to state 4 in which the ions are in direct contact. The contribution of each step to the absorption can be expressed in terms of absorption per wavelength as follows

$$\alpha\lambda = \sum_i (\alpha\lambda)_i = \sum_i \frac{\pi\beta_i}{\beta_0} \frac{\omega\kappa_i}{(\omega^2 + \kappa_i^2)} \quad (2)$$

where α is the amplitude absorption coefficient, β_i the chemical compressibility associated with step i , β_0 the isothermal compressibility, ω the angular sound frequency, and κ_i the relaxation frequency.

This paper discusses only the absorption at the lowest, or primary, relaxation frequency ($\kappa_i = \kappa_{\text{III}}$) attributed to step 3 due to transitions between states 3 and 4. Since all the reactions in eq 1 are coupled to each other, the relaxation frequency and absorption associated with each step are expressed in terms involving all the reactions. The absorption associated with the relaxation frequency κ_{III} is

$$(\alpha\lambda)_{\text{III}} = \frac{\pi\beta_{\text{III}}}{\beta_0} \frac{\omega\kappa_{\text{III}}}{(\omega^2 + \kappa_{\text{III}}^2)} \quad (3)$$

In eq 3, the maximum value of $(\alpha\lambda)_{\text{III}}$ occurs when $\omega = \kappa_{\text{III}}$, that is

$$(\alpha\lambda)_{\text{IIIIm}} = \frac{\pi\beta_{\text{III}}}{2\beta_0} \quad (4)$$

Equation 4 will be evaluated after the presentation of the experimental results.

Experimental Results

At low frequencies the spherical resonator technique has been utilized^{1–4,6} for making ultrasonic absorption measurements. The resonator, containing the solution of interest, is excited to resonant modes with the solution of interest. Measurement of the decay rates of these modes, with a sound level recorder, yields a value for ultrasonic absorption of the solution and the resonator. By replacing the solution of interest with a solution having the same velocity (made up of the same solvent and a salt that has no absorption), it is possible to make accurate mode corrections for the absorption of the solvent and resonator. The addition of a thermistor to the neck of the resonator ensures that the series of measurements are made at the same temperature and allows for more precise corrections. Intermittent monitoring of an easily identified resonant mode assures the rapid identification of other modes once the mode structure of the resonator has been determined. The resonator was suspended from thin piano wires within a bell jar, and measurements were made with the outside of the sphere exposed to a vacuum to reduce acoustic radiation losses. Measurements of sound velocity were made with an interferometer. The sound velocity for both the MgSO₄ and correction solution was 1583 m/sec.

A solution of 0.02 *m* MgSO₄ in 37% by wt dioxane–water was prepared and placed in a 12-l. resonator. To prevent errors due to bubbles, ultrasonic degassing was conducted, under vacuum, for about 1 hr.

The results of the absorption measurements are shown in Table I, and a least-squares fit of eq 3 to the data yielded the results shown in Figure 1.

To compare the results obtained for MgSO₄ in water and mixtures of water and dioxane, a summary of the

Table I: Sound Absorption, α , and Absorption per Wavelength, $\alpha\lambda$, as a Function of Frequency in 0.02 *M* MgSO₄ in 37% Dioxane–Water Solvent at 23.75°

| <i>f</i> , kHz | α_{soln} , db/sec | α_{cor} , db/sec ^a | α , db/sec | λ , cm | $\alpha \times 10^5$, cm ⁻¹ | $\alpha\lambda \times 10^5$ |
|----------------|---------------------------------|---|-------------------|----------------|---|-----------------------------|
| 39.441 | 25.3 | 10.4 | 14.9 | 4.014 | 1.08 | 4.35 |
| 75.659 | 58.2 | 19.2 | 39.1 | 2.093 | 2.84 | 5.94 |
| 113.704 | 87.7 | 29.7 | 58.0 | 1.392 | 4.22 | 5.87 |
| 189.297 | 159.0 | 67.0 | 92.0 | 0.8363 | 6.69 | 5.59 |
| 325.535 | 217.0 | 103.0 | 114.0 | 0.4863 | 8.29 | 4.03 |

^a The correction α_{cor} obtained without MgSO₄ is subtracted from α_{soln} with MgSO₄ to obtain α .

(10) A. Bechtler, K. G. Breitschwerdt, and K. Tamm, *J. Chem. Phys.*, **52**, 2975 (1970).

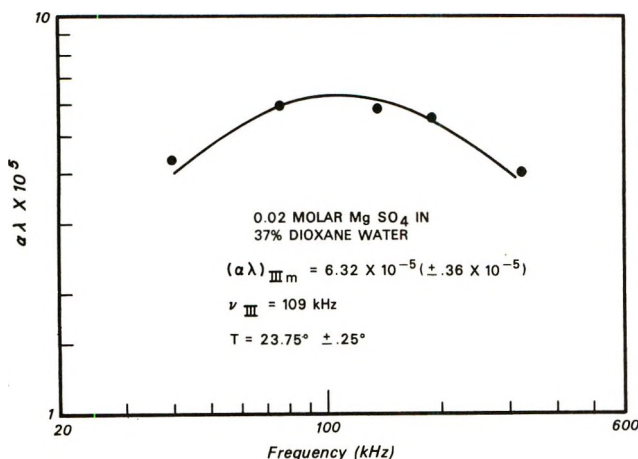


Figure 1. Sound absorption amplitude coefficient per wavelength $(\alpha\lambda)_{III}$ vs. frequency.

earlier work is shown in Table II. It is seen that there is a decrease in the absorption at 0.02 *M* similar to the reversal at 0.5 *M* as the dielectric constant is lowered. In fact, for 0.02 *M*, the absorption is less than in the aqueous solution.

Table II: Maximum Absorption per Wavelength, $(\alpha\lambda)_{III m}$, and Relaxation Frequency, $\nu_{III} = \kappa_{III}/2\pi$, as a Function of Solvent Dielectric Constant *D* and Concentration *c* (moles/liter) for MgSO₄ Solution at ~25°

| | <i>c</i> , mol/l. | <i>D</i> (solvent) | | | |
|---------------------------------------|----------------------|--------------------|------------------|------------------|------------------|
| | | 78.5 | 67.0 | 56.5 | 45.5 |
| $(\alpha\lambda)_{III m} \times 10^5$ | 0.005 | 1.5 ^a | 2.7 ^b | 3.4 ^b | |
| | 0.02 | 8.0 ^a | 10 ^b | | 6.3 ^d |
| | 0.5 | 175 ^c | 215 ^c | 177 ^c | |
| ν_{III} , kHz | 0.005 | 140 ^a | 200 ^b | 155 ^b | |
| | 0.02 | 150 ^a | 230 ^b | | 109 ^d |
| | 0.5 | 195 ^c | 159 ^c | 197 ^c | |

^a Wilson and Leonard.² ^b Bies.⁸ ^c Fisher.⁹ ^d This work.

Discussion of Results

In eq 4 the maximum value of absorption per wavelength, $(\alpha\lambda)_{III m}$, depends only on the chemical compressibility, β_{III} , and the isothermal compressibility, β_0 . For the dioxane-water solvent, β_0 decreases slightly in the range of mixture discussed here which means $(\alpha\lambda)_{III m}$ increases slightly even if β_{III} remains fixed. The measured decrease in $(\alpha\lambda)_{III m}$, therefore, means that β_{III} must decrease. For β_{III} , Eigen and Tamm derive the following equation

$$\beta_{III} = \left[\frac{(c_1' + c_2 + c_3)c_4}{c_1' + c_2 + c_3 + c_4} \right] \frac{(\Delta V_{III})^2}{1000RT} = \frac{c\Gamma^*}{1000} \frac{(\Delta V_{III})^2}{RT} \quad (5)$$

where

$$\Delta V_{III} = \bar{v}_4 - \bar{v}_3 + \frac{k_{32}}{k_{23}' + k_{32}} \Delta V_{II} \quad (6)$$

$$\Delta V_{II} = \bar{v}_3 - \bar{v}_2 + \frac{k_{21}}{k_{12}' + k_{21}} (\bar{v}_2 - \bar{v}_1) \quad (7)$$

$$c_1' = c_1 / (2 + \partial \ln \pi^f / \partial \ln \sigma) \quad (8)$$

$$k_{12}' = k_{12} \sigma c (2 + \partial \ln \pi^f / \partial \ln \sigma) \quad (9)$$

$$c_1 = \sigma c \quad (10)$$

and the conventional equilibrium constant

$$K = \frac{c\sigma^2\pi^f}{1 - \sigma} \quad (11)$$

where π^f is the activity coefficient product, and concentration is in moles/liter.

The conventional equilibrium constant, *K*, is related to the partial equilibrium constants *K*_{*ij*} as follows

$$K = \frac{K_{12}K_{23}K_{34}}{1 + K_{34}(1 + K_{23})} \quad (12)$$

where

$$K_{12}/\pi^f = k_{21}/k_{12} = c_1^2/c_2 \quad (13)$$

$$K_{23} = k_{32}/k_{23} = c_2/c_3 \quad (14)$$

$$K_{34} = k_{43}/k_{34} = c_3/c_4 \quad (15)$$

For the relaxation frequency

$$\kappa_{III} = k_{43} + k_{34}' \quad (16)$$

where

$$k_{34}' = k_{34} [k_{23}' / (k_{23}' + k_{32})] \quad (17)$$

and

$$k_{23}' = k_{23} [k_{12}' / (k_{12}' + k_{21})] \quad (18)$$

For the reactions shown in eq 1 ET point out that lowering the solvent dielectric constant means that k_{43}/k_{34} , k_{32}/k_{23} , and k_{21}/k_{12} will decrease. Therefore, all the equilibria in eq 1 are shifted to the right, resulting in an increase in *c*₄. To evaluate *c*Γ* in eq 4, $(\partial \ln \pi^f / \partial \ln \sigma)$ must be known. On the basis of electrical conductance data¹¹ in aqueous and dioxane-water solutions, $(\partial \ln \pi^f / \partial \ln \sigma) \cong -0.1$, for both 0.005 and 0.02 *M* solutions of MgSO₄ in the solvents considered here; therefore, $c_1' = c_1/1.9$, independent of concentration and solvent. This agrees with Stuehr and Yeager⁶ for aqueous solutions but not with the value $(\partial \ln \pi^f / \partial \ln \sigma) = -1$ obtained by BBT.¹⁰ The equation for π^f used in these calculations is the same one used in earlier conductance work.¹²

From conductance data¹¹ values of $1 - \sigma = (c_2 + c_3 + c_4)/c$ are shown in Table III as a function of dielectric constant. Since $c_1' = c/1.9$, values of *c*Γ* can

(11) F. H. Fisher and A. P. Fox, to be submitted to *J. Phys. Chem.*

(12) F. H. Fisher, *ibid.*, **66**, 1607 (1962).

Table III: Values of $1 - \sigma = (c_2 + c_3 + c_4)/c$ for MgSO_4 Solutions in Dioxane-Water Solvents at 25° as a Function of Dielectric Constant D and Concentration c (moles/liter)

| D | $c = 0.005$ | $c = 0.02$ |
|------|--------------|--------------|
| | $1 - \sigma$ | $1 - \sigma$ |
| 78.5 | 0.24 | 0.39 |
| 67.0 | 0.36 | 0.46 |
| 56.5 | 0.52 | 0.66 |
| 45.5 | 0.72 | 0.80 |

Table IV: $c\Gamma^* = (c_1' + c_2 + c_3)c_4/(c_1' + c_2 + c_3 + c_4)$ vs. c_4 for 0.02 M MgSO_4 in 37% Dioxane-Water Solvent at 25°

| c_4 mol/l. | $c\Gamma^*$ mol/l. |
|-----------------|-----------------------|
| 0.0016 | 0.00146 |
| 0.0048 | 0.00353 |
| 0.0088 | 0.00452 |
| 0.0128 | 0.00375 |
| 0.0160 | 0.00186 |

be calculated as a function of c_4 for $c = 0.02$ and $D = 45.5$; these are shown in Table IV.

It is seen that $c\Gamma^*$ goes through a maximum before it decreases. The value of c_4 for 0.02 M MgSO_4 in the $D = 45.5$ solvent is unknown; it is at least twice the initial value it has in aqueous solution since $(1 - \sigma)$ doubles in going from $D = 78.5$ to $D = 45.5$. Because $c\Gamma^*$ does go through a maximum as c_4 increases, one might explain the decrease in absorption in this fashion. However, the maximum value c_4 can have is 0.016 mol/l., since $c_1 = \sigma c = 0.004$ mol/l.; for this value of c_4 , $c\Gamma^* = 0.00186$.

For the 0.02 M aqueous MgSO_4 solution $c\Gamma^*$ varies according to what set of multistate parameters shown in Table V are used. For the BBT parameters, $c\Gamma^* = 0.0016$; for the ET parameters selected by Fisher⁹ to describe pressure effects on electrical conductance¹² and absorption,⁹ $c\Gamma^* = 0.00040$. In both cases, the aqueous values of $c\Gamma^*$ are less than the lowest value $c\Gamma^*$ can have for $D = 45.5$ after $c\Gamma^*$ has gone through its maximum. Therefore, any decrease in $(\alpha\lambda)_{\text{III}m}$ must be due to a decrease in ΔV_{III} .

Table V: Multistate Parameters for Aqueous MgSO_4 ^a

| | BBT | ET |
|-----------------------------|-------|------|
| K_{12} | 0.025 | 0.04 |
| K_{23} | 0.31 | 1 |
| K_{34} | 2.5 | 9 |
| $\Delta V_{12} = v_1 - v_2$ | -14 | ~0 |
| $\Delta V_{23} = v_2 - v_3$ | +13 | -18 |
| $\Delta V_{34} = v_3 - v_4$ | -5 | -3 |

^a Solutions: Bechtler, Breitschwerdt, and Tamm (BBT) and Eigen and Tamm (ET).

Changes in ΔV_{III} can occur due to changes in the partial molal volumes and changes in the reaction rates as the solvent dielectric constant is lowered.

If the ΔV_{ij} in Table V do not change significantly as the solvent dielectric constant is lowered, then it may be possible to use the data presented here to discriminate between the two sets of parameters, ET and BBT. Since the effect of pressure on sound absorption⁹ and the dissociation constant, K ,¹¹ for MgSO_4 solutions is very nearly the same in dioxane-water solvents as in water, it may be reasonable to assume the ΔV_{ij} do not change significantly from those derived for aqueous solutions.

For the ET parameters, $\Delta V_{\text{III}} = \bar{v}_3 - \bar{v}_2$. Since the sign of ΔV_{III} is the same as for $\bar{v}_4 - \bar{v}_3$, and since k_{32}/k_{23} decreases with decreasing dielectric constant, ΔV_{III} will decrease as the dielectric decreases. Since ΔV_{III} is large compared to $\bar{v}_4 - \bar{v}_3$, shifts in k_{32}/k_{23} can produce substantial changes in ΔV_{III} . For the BBT parameters in aqueous solution (eq 6 and 7)

$$\Delta V_{\text{III}} = 5 + 0.67[-13 + 0.85(+14)] =$$

$$4.33 \text{ cm}^3/\text{mol}$$

making use of BBT values of $k_{12}' = 1.7 \times 10^8 \text{ sec}^{-1}$ and $k_{21} = 10^9 \text{ sec}$. A decrease in k_{32}/k_{23} will produce an increase in ΔV_{III} , in this case. Therefore, under the assumption that the ΔV_{ij} are nearly the same as in aqueous solution, the parameters selected by BBT cannot be used to explain the measurements reported here. The ET parameters, at least, offer a possible explanation of the decrease in $(\alpha\lambda)_{\text{III}m}$ to below the aqueous solution value.

A quantitative explanation of the measurements reported here will require for each solvent the same extensive ultrasonic absorption measurements as a function of frequency and concentration that have been made in aqueous solutions.

The results for relaxation frequency at the low concentration are in agreement with the explanation that Eigen and Tamm⁵ gave for Bies' results, a slight initial increase followed by a decrease in κ_{III} . As yet, there is no explanation for the unusual behavior of κ_{III} in 0.5 M MgSO_4 solutions in dioxane-water solvents. Stuehr and Yeager⁶ have questioned the 0.5 M results. If the BBT parameters (which include a third relaxation as opposed to only two relaxations in the ET paper) are correct, failure to account for this might explain the results for κ_{III} at 0.5 M concentration.

Summary

For 0.02 M MgSO_4 solutions in dioxane-water solvents, both $(\alpha\lambda)_{\text{III}m}$ and κ_{III} go through a maximum with increasing dioxane. These results are further evidence of the importance of specific solvent effects in the processes discussed here. It is pointed out how these measurements can be used to discriminate between conflicting sets of multistate parameters used to explain ultrasonic absorption in aqueous solutions. A

quantitative explanation of the results reported here will require extensive ultrasonic absorption measurements as a function of frequency and concentration in the various solvents.

Acknowledgment. I wish to acknowledge Professor E. Yeager's kindness in making it possible for me to perform this experiment at the Department of Chemistry, Case-Western Reserve University. In addition I wish to thank Mr. A. Barksdale of Case-Western

University for his assistance with the experiment and Mr. O. E. Dial, Jr., of this laboratory for his assistance with the curve fitting. I wish to thank Professors Yeager and Stuehr of Case-Western Reserve University, and Dr. F. V. Hunt and Dr. H. Bezdek of this laboratory for their helpful comments on the manuscript. This paper represents results in research sponsored under the Office of Naval Research and the National Science Foundation.

Relaxation Spectra of Molybdate Polymers in Aqueous Solution.

Ultrasonic Attenuation

by Dan S. Honig and Kenneth Kustin*

Department of Chemistry, Brandeis University, Waltham, Massachusetts 02154 (Received April 16, 1971)

Publication costs assisted by the National Institutes of Health

Ultrasonic attenuation studies (7–214 MHz) were carried out on acidified solutions of sodium molybdate at an ionic strength of 1.0 *M*. The Na_2MoO_4 concentration varied between 0.05 and 0.20 *M*, and the hydrogen ion concentration extended from 5×10^{-7} to 3×10^{-6} *M*. A single relaxation time ($7.1\text{--}9.10 \times 10^{-10}$ sec) was observed. This effect was assigned to a two-step mechanism consisting of protonations of MoO_4^{2-} and $\text{Mo}_7\text{O}_{24}^{6-}$. The following rate constants were thus determined: $\text{H}^+ + \text{MoO}_4^{2-}$, $k = 5 \times 10^9 \text{ M}^{-1} \text{ sec}^{-1}$; $\text{H}^+ + \text{Mo}_7\text{O}_{24}^{6-}$, $k = 7 \times 10^{10} \text{ M}^{-1} \text{ sec}^{-1}$. The relatively low value obtained for reaction of H^+ with MoO_4^{2-} was interpreted as indicating that addition of a proton to tetrahedral MoO_4^{2-} ion is not simply a direct proton attachment process, but also involves conversion of MoO_4^{2-} to an octahedral configuration.

The kinetics of molybdenum(VI) isopolyanion formation has been studied by several investigators.^{1–4} Rapid-mixing experiments demonstrated that both protonation and condensation were quite rapid, protonation being more so.¹ The kinetics of polymerization have also been investigated with the temperature-jump method,⁴ but only the overall monomer \rightleftharpoons heptamer \rightleftharpoons octamer steps could be characterized. Relaxation times for these processes were all longer than 100 μsec under the experimental conditions (pH 6.50–5.50, total $[\text{Na}_2\text{MoO}_4]$ 0.01–0.25 *M*, ionic strength (NaNO_3) 1.0 *M*, and 25°).⁴

Ultrasonic absorption experiments were undertaken in an attempt to observe (a) intermediate aggregation steps, (b) counterion binding of the polymers with sodium ion,⁵ or (c) the kinetics of any protolytic steps. The detection of intermediate steps was, from the outset, doubtful, as the most comprehensive equilibrium studies report no detectable polymers in Na^+ media below heptamer.^{5,6} Effects due to intermediates

would therefore be too small to observe.^{7,8} On the other hand, protolytic and/or complexation equilibria should be observable.^{7,9}

Results and Treatment of Data

Acidified solutions of sodium molybdate, ionic strength, μ , 1.0 *M*, were prepared as described previously,⁴ without degassing. Ultrasonic absorption measurements were carried out from 7 to 214 MHz

(1) G. Schwarzenbach and J. Meier, *J. Inorg. Nucl. Chem.*, **8**, 302 (1958).

(2) J. Asay and E. M. Eyring, unpublished results.

(3) O. Glemser and W. Höltje, *Angew. Chem., Int. Ed. Engl.*, **5**, 736 (1966).

(4) D. S. Honig and K. Kustin, *Inorg. Chem.*, **11**, 65 (1972).

(5) J. Aveston, E. W. Anacker, and J. S. Johnson, *ibid.*, **3**, 735 (1964).

(6) Y. Sasaki and L. G. Sillén, *Ark. Kemi.*, **29**, 253 (1967).

(7) M. Eigen and L. De Maeyer, *Tech. Org. Chem.*, **8**, 895 (1963).

(8) J. Stuehr and E. Yeager in "Physical Acoustics," Vol. 2A, W. P. Mason, Ed., Academic Press, New York, N. Y., 1965, p 376.

(9) Reference 8, p 398.

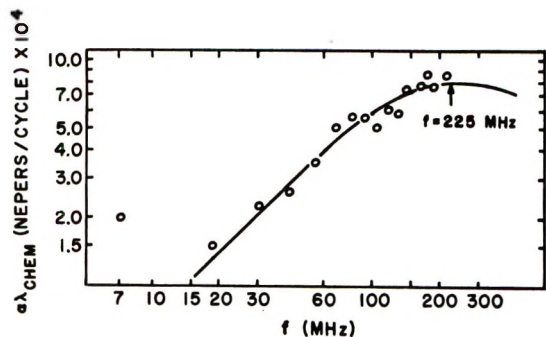


Figure 1. Ultrasonic absorption of 0.20 M Na_2MoO_4 at $[\text{H}^+] = 1.0 \times 10^{-6} \text{ M}$, $\mu = 1.0 \text{ M}$, and 25° . Curve fitting with the use of a clear plastic template of the curve given by (1). The $\alpha\lambda$ value at 7 MHz is approximate.

(lower accuracy is to be associated with the measurements at 7 MHz) using the pulse technique. The particular apparatus has been described fully elsewhere, both in theoretical and practical aspects.^{10,11}

Equation 1 can be used to obtain relaxation times.¹⁰

$$(\alpha\lambda)_{\text{chem}} = \frac{\omega\tau}{1 + \omega^2\tau^2}(\text{constant}) \quad (1)$$

In (1), $(\alpha\lambda)_{\text{chem}} = (\alpha\lambda)_{\text{soln}} - (\alpha\lambda)_{\text{water}}$ (the value of $(\alpha\lambda)_{\text{water}}$ is $(3.24 \times 10^{-11})f$);¹⁰ $\alpha\lambda$ is the attenuation coefficient per wavelength λ , $\omega = 2\pi f$ (radians per second), $f =$ frequency (Hz), and τ is the relaxation time (seconds). A log-log plot of $(\alpha\lambda)_{\text{chem}}$ vs. ω (or f) is made, and the data points are evaluated graphically by the template method.¹⁰ Within experimental error, a maximum in $(\alpha\lambda)_{\text{chem}}$ will be observed when $\omega\tau = 1$.^{7,8,10} Multiple relaxation spectra would necessitate further analysis, for example, with the use of a computer, for separation of individual curves. A representative plot of eq 1 is shown in Figure 1. Within experimental error, only one relaxation process is observed.

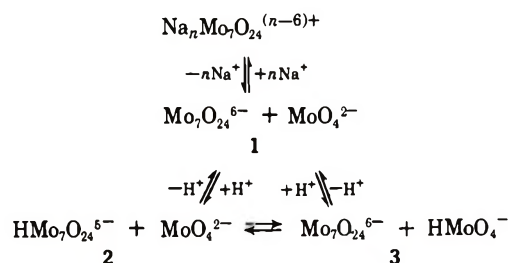
The results of the ultrasonic experiments are given in Table I. The lack of any significant difference or trend in $(\alpha\lambda)_{\text{soln}} - (\alpha\lambda)_{\text{water}}$ over the frequency range for solution 8 (and also solution 7) allows the use of $(\alpha\lambda)_{\text{water}}$ in eq 1. The fact that $(\alpha\lambda)_{\text{chem}}$ is a maximum at the upper end of the frequency range, and is of relatively small amplitude (so that the scatter can be significant), makes the determination of τ somewhat uncertain. For solutions 1–4, the peak frequency can be determined to better than $\pm 10\%$. For solutions 5 and 6, the relative error in the peak frequency exceeds 10% , and may be as high as $\pm 20\%$. In addition, the possibility of multiple relaxation times cannot be categorically ruled out for these two solutions. For some of the runs, $(\alpha\lambda)_{\text{chem}}$ at 7 MHz was definitely greater than at 18 MHz, suggesting relaxation processes $\leq \sim 1$ MHz (see Figure 1).

As can be seen, peak frequency and amplitude are most sensitive to $\text{Mo}_7\text{O}_{24}^{6-}$ concentration, though com-

parison of solutions 6 and 7 indicates that processes involving MoO_4^{2-} also contribute. No obvious indication of intermediate polymerization steps (e.g., dimerization, etc.) is observed. The possibility of $(\alpha\lambda)_{\text{chem}}$ being due to complexation of Na^+ with MoO_4^{2-} can be ruled out (solution 8), as would be expected.¹²

The full reaction scheme describing the kinetic behavior of molybdate monomer and heptamer at frequencies from 7 to 220 MHz can be simplified.¹³ That is, at these pH's (< 7) reaction with OH^- can be omitted from consideration. At the same time, contributions to the relaxation process from sodium ion-polymer complex formation may have to be included eventually, and are shown in Scheme I to be considered initially.

Scheme I



A further *a posteriori* examination of the data permits additional reductions in the number of steps that need be considered to assign the observed relaxation processes. Contributions from the proton exchange process, $2 \rightleftharpoons 3$, are not likely to be significant; first because the fit was poor and second because the rate constants have to be $\geq 5 \times 10^{10} \text{ M}^{-1} \text{ sec}^{-1}$, which is unlikely.^{13,14} The results also do not seem to point to complexation of Na^+ by $\text{Mo}_7\text{O}_{24}^{6-}$ as being a primary contributor to $(\alpha\lambda)_{\text{chem}}$ as either (a) τ would be expected to remain the same,¹⁵ or (b) τ should decrease as $[\text{Na}^+]$ increased from solutions 1 to 6; however, τ generally increased. While the observed effect does not seem to be entirely or appreciably due to this complexation, the small range in peak frequency prevents a categorical dismissal of this process, and it is possible that it contributes to some extent to $(\alpha\lambda)_{\text{chem}}$. However, as the results point away from this effect, and as there is considerable uncertainty regarding the existence of this complexation,⁵ it is reasonable to treat the data according to a protolytic mechanism, as a first approximation. Therefore, the most likely causes for $(\alpha\lambda)_{\text{chem}}$ are hydrogen ion processes involving both heptamer and monomer.

(10) R. S. Brundage, Ph.D. Thesis, Brandeis University, 1969.

(11) R. S. Brundage and K. Kustin, *J. Phys. Chem.*, **74**, 672 (1970).

(12) Reference 8, p 401.

(13) M. Eigen, *Angew. Chem., Int. Ed. Engl.*, **3**, 1 (1964).

(14) M. Eigen, W. Kruse, G. Maass, and L. DeMaeyer, *Progr. React. Kinet.*, **2**, 287 (1964).

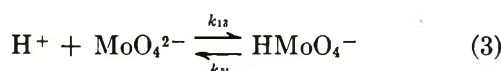
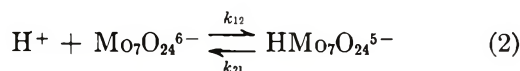
(15) Reference 8, p 452.

Table I: Results of Ultrasonic Attenuation Experiments at 1.0 M Ionic Strength and 25°^a

| Soln | [Mo(VI)] _{tot} | [H ⁺] × 10 ⁸ | [MoO ₄ ²⁻] ^b × 10 ² | [Mo ₇ O ₂₄ ⁶⁻] ^b × 10 ² | f, ^c MHz | αλ _{chem} ^d × 10 ⁴ | τ, sec × 10 ¹⁰ |
|------|-------------------------|--|---|--|------------------------|--|------------------------------|
| 1 | 0.20 | 1.78 | 6.09 (6.03) | 1.97 (1.85) | 220 | 11.6 | 7.24 |
| 2 | 0.15 | 3.16 | 3.09 (3.04) | 1.67 (1.50) | 215 | 10.7 | 7.41 |
| 3 | 0.15 | 1.78 | 5.74 (5.69) | 1.31 (1.23) | 200 | 7 | 7.96 |
| 4 | 0.20 | 1.00 | 11.0 (11.0) | 1.27 (1.23) | 225 | 8 | 7.08 |
| 5 | 0.10 | 3.16 | 2.87 (2.83) | 1.00 (0.90) | 175 | 5 ^e | 9.10 |
| 6 | 0.20 | 0.56 | 17.6 (17.6) | 0.33 (0.33) | 175 | 4.5 ^f | 9.10 |
| 7 | 0.05 | 3.16 | 2.47 (2.44) | 0.35 (0.32) | No effect | | |
| 8 | 0.20 | 1.0 × 10 ⁻⁴ ^g | 20.0 | | No effect ^h | | |

^a Concentration units are molar: ionic strength of solution 1 is 0.85 M. ^b Calculated from modified stability constants of ref 4; numbers in parentheses underneath are calculated from unmodified stability constants of Aveston, *et al.*⁵ ^c Frequency at peak; τ = (2πf)⁻¹. ^d Excess absorption at peak in nepers/cycle. ^e Scatter appreciable. ^f Effect small, and scatter considerable. ^g No acid added. ^h Error in (αλ)_{soln} of up to ±~5%; (αλ)_{soln} - (αλ)_{water} was (1-1.5) × 10⁻⁴ neper/cycle for some points, but this was random and indicates degree of scatter; see Figure 1.

The reactions are



with

$$K_2 = [\text{HMo}_7\text{O}_{24}^{5-}]/[\text{H}^+][\text{Mo}_7\text{O}_{24}^{6-}] = k_{12}/k_{21}$$

$$K_3 = [\text{HMoO}_4^-]/[\text{H}^+][\text{MoO}_4^{2-}] = k_{13}/k_{31}$$

The values of K_2 and K_3 are known,⁶ although there is some uncertainty in K_2 .⁴ Aveston, *et al.*, give log $K_2 = 4.62$.⁵ The results of our temperature-jump study indicate their equilibrium scheme is valid, but that log $K_2 = 3.62$.⁴ We have treated our results using both values. Agreement is somewhat better with log $K_2 = 3.62$, but both fit within experimental error.

The relaxation times for coupled reactions such as eq 2 and 3 have been derived.⁷ The result is

$$1/\tau_{+,-} = (1/2)[(a_{11} + a_{22}) \pm \sqrt{(a_{11} + a_{22})^2 - 4(a_{11}a_{22} - a_{12}a_{21})}] \quad (4)$$

where

$$a_{11} = k_{12}(\overline{[\text{H}^+]} + \overline{[\text{Mo}_7\text{O}_{24}^{6-}]} + 1/K_2)$$

$$a_{12} = k_{12}\overline{[\text{Mo}_7\text{O}_{24}^{6-}]}$$

$$a_{21} = k_{13}\overline{[\text{MoO}_4^{2-}]}$$

$$a_{22} = k_{13}(\overline{[\text{H}^+]} + \overline{[\text{MoO}_4^{2-}]} + 1/K_3)$$

The bar over the concentrations refers to equilibrium conditions. A nonlinear least-squares routine,¹⁶ em-

Table II: Comparison of Observed and Calculated Relaxation Frequency^{a,b}

| Soln | f _{obsd} | f _{+,calcd} ^c | f _{-,calcd} ^c |
|------|-------------------|-----------------------------------|-----------------------------------|
| 1 | 220 | 267 (259) | 0.65 (0.24) |
| 2 | 215 | 211 (195) | 0.50 (0.24) |
| 3 | 200 | 191 (185) | 0.79 (0.24) |
| 4 | 225 | 227 (226) | 1.1 (0.25) |
| 5 | 175 | 135 (125) | 0.63 (0.24) |
| 6 | 175 | 172 (173) | 2.1 (0.27) |

^a Frequency in megahertz; τ = (2πf)⁻¹. ^b Numbers in parentheses were calculated using the value of Aveston, *et al.*,⁵ for K_2 (log $K_2 = 4.62$). The numbers directly above were calculated using the value determined from our temperature-jump study,⁴ with log $K_2 = 3.62$. ^c τ_{+,calcd} = (2πf₊)⁻¹, τ_{-,calcd} = (2πf₋)⁻¹.

ploying an IBM 1130 computer, was used to calculate k_{12} and k_{13} ; with these values, τ₊ and τ₋ were calculated. The rate constants thus obtained are

$$\log K_2 = 3.62$$

$$k_{12} = (6.9 \pm 0.7) \times 10^{10} \text{ M}^{-1} \text{ sec}^{-1} \quad (\text{I})$$

$$k_{13} = (4.8 \pm 1.2) \times 10^9 \text{ M}^{-1} \text{ sec}^{-1}$$

$$\log K_2 = 4.62$$

(16) We wish to thank Dr. A. Gottlieb for adapting the nonlinear least-squares program (AGNLS) for use on the IBM 1130.

$$k_{12} = (7.2 \pm 0.9) \times 10^{10} M^{-1} \text{sec}^{-1} \quad (\text{II})$$

$$k_{13} = (4.8 \pm 1.2) \times 10^9 M^{-1} \text{sec}^{-1}$$

A comparison of calculated and observed peak frequencies is afforded by Table II. The slower relaxation time lies outside the range of our apparatus. The already mentioned increase in $(\alpha\lambda)_{\text{chem}}$ from 18 to 7 MHz is consistent with calculated values of τ_{-} .

Upper limits for the volume changes involved were also calculated.¹⁰ For eq 3, $\Delta V \lesssim \pm 20 \text{ cm}^3 \text{ mol}^{-1}$. The value of ΔV for eq 2 depends on the value of K_2 chosen. With $\log K_2 = 4.62$, $\Delta V \lesssim \pm 20 \text{ cm}^3 \text{ mol}^{-1}$; with $\log K_2 = 3.62$, $\Delta V \lesssim \pm 30\text{--}35 \text{ cm}^3 \text{ mol}^{-1}$.

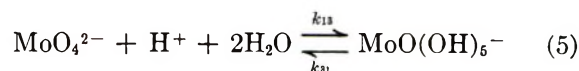
The volume changes are comparable to those determined for other protolytic reactions.⁹ The only conclusion to be drawn is that $\log K_2$ should not be much less than 3.62, as ΔV would become unreasonably large.

Discussion

The values obtained for k_{12} and k_{13} can be compared with other values obtained for the recombination of H^+ with bases, even though most of the other studies were done at a lower ionic strength.^{14,15,17} Recombination of H^+ with $\text{Mo}_7\text{O}_{24}^{6-}$ ($k_{12} \sim 7 \times 10^{10} M^{-1} \text{sec}^{-1}$) is most likely diffusion controlled; k_{12} is similar to that for other inorganic acids.^{14,15,17} Recombination of H^+ with MoO_4^{2-} ($k_{13} \sim 5 \times 10^9 M^{-1} \text{sec}^{-1}$), however, seems to be slower than would be expected for a diffusion-controlled reaction, regardless of being compared with

other inorganic oxy acids,^{14,15,17} or with k_{12} . That is, the formal charge difference between $\text{Mo}_7\text{O}_{24}^{6-}$ and MoO_4^{2-} would not be expected to cause the observed difference.^{14,15,17}

Molybdenum(VI) has tetrahedral coordination in MoO_4^{2-} (with closely associated water molecules),¹⁸ but the coordination is octahedral in the isopolyanions.¹⁹ The results of equilibrium and rapid-mixing studies of protonation of MoO_4^{2-} were interpreted as indicating expansion of coordination upon protonation.^{1,20,21} Equation 3 can be rewritten as



This expansion of coordination could account for the relatively low value of k_{13} .

Acknowledgment. The authors gratefully acknowledge partial support from Public Health Service Grant No. GM-08893-09 from the National Institute of General Medical Sciences.

(17) Reference 7, p 1031.

(18) R. H. Busey and O. L. Keller, Jr., *J. Chem. Phys.*, **41**, 215 (1964).

(19) (a) I. Lindquist, *Ark. Kemi*, **2**, 325, 349 (1949); (b) H. T. Evans, Jr., *J. Amer. Chem. Soc.*, **90**, 3275 (1968); (c) E. Shimao, *Nature (London)*, **214**, 170 (1967).

(20) E. F. C. H. Rohwer and J. J. Cruywagon, *J. S. Afr. Chem. Inst.*, **16**, 26 (1963); **17**, 145 (1964); **22**, 198 (1969).

(21) D. V. S. Jain, *Ind. J. Chem.*, **8**, 945 (1970).

Magnetochemical Studies on Diphenyldialkoxysilanes

by R. D. Goyal, R. R. Gupta, and R. L. Mital*

Chemistry Department, Rajasthan University, Jaipur-4, India (Received September 21, 1971)

Publication costs borne completely by The Journal of Physical Chemistry

Diamagnetic susceptibilities of some diphenyldialkoxysilanes, $(C_6H_5)_2Si[O(CH_2)_n-H]_2$, are reported. χ_{Si} for these compounds was obtained from the intercept of χ_M vs. n . π orbitals of the benzene ring are not conjugated with the silicon atom directly bound to the ring and no back-donation occurs in aromatic silicon systems. χ_M of these compounds also has been calculated theoretically from different wave-mechanical approximations. A poor agreement has been obtained between the observed χ_M values and the corresponding values calculated according to the method of Baudet, *et al.* This poor agreement has been analyzed in the light of different environmental conditions present in these molecules. Excellent agreement is obtained between experimental and calculated values using Hamerka's method, which is attributed to the fact that in this approximation, the various structural factors, that contribute the molecular diamagnetism, have been taken into account.

Introduction

It has been recently established¹⁻⁵ that molecular diamagnetism is of much importance, usefulness, and interest in structural silicon chemistry. The results of such studies have been used to explain abnormal behavior¹⁻⁵ of silicon compounds containing Si-O bonds in comparison to analogous carbon compounds containing C-O bonds. Although much controversy⁶ regarding the nature of $(C_6H_5)_2Si$ bonds exists, no study appears to have been made on diphenyldialkoxysilanes with regard to molecular diamagnetism. The present investigation was undertaken with a view to extend experimental and theoretical studies of diamagnetism and to analyze the results in the light of structural factors. These studies provide information concerning bonding between the benzene ring and the silicon atom.

Experimental Section

Six diphenyldialkoxysilanes $(C_6H_5)_2Si-(OR)_2$ have been synthesized and characterized.⁷ Their susceptibilities⁸ have been measured with a sensitive Gouy balance calibrated with a number of standard substances and tried for more than 3 years in our laboratory. Reproducibility of the results was quite satisfactory. The Gouy force is of the order of ± 0.05 mg. The Gouy tube was hung in such a manner that its one end remained in the field, while the other end was outside the field, so that susceptibility could be calculated by a well-established method.^{1,9} These susceptibility values are summarized in Table I.

Results and Discussion

A plot of χ_M against n for diphenyldi- n -alkoxysilanes represented by $(C_6H_5)_2Si-[O(CH_2)_n-H]_2$ has been made. A linear plot is obtained and the ordinate intercept of this plot is 135.2 which represents the mean susceptibility contribution of $(C_6H_5)_2Si-[O(CH_2)_n-H]_2$ when $n = 0$. Taking $\chi_{C_6H_5} = 51.6$,¹⁰ $\chi_O = 5.4$,¹¹

$\chi_H = 2.0$,¹¹ and using the additivity rule in the form $\chi_{(C_6H_5)_2Si-[O(CH_2)_n-H]_2} = 2\chi_{C_6H_5} + 2\chi_H + 2\chi_O + \chi_{Si} = 135.2$ the mean χ_{Si} in the series has been calculated to be 17.2 units. $\chi_M = 168.4$ (for $n = 3/2$) and $\chi_M = 212.8$ (for $n = 7/2$) gives $\chi_{CH_2} = 44.4/(2 \times 2) = 11.10$ in this series.

It has been reported that χ_{Si} is $(20.6-21.0)$ ⁵ in silicon compounds containing four C-Si bonds. It has been further reported¹ that the value of χ_{Si} in silicon compounds depends on the number of Si-O bonds present in a particular molecule. $\chi_{Si} = 17.0$,¹ $\chi_{Si} = 18.42$,¹ and $\chi_{Si} = 14.33$ ¹ have been reported in compounds containing two, one, and four Si-O bonds, respectively. These values refer to compounds which contain only one silicon atom. This variation in Si has been attributed to the back-bonding ($p_\pi-d_\pi$) between oxygen and silicon atoms. $\chi_{Si} = 17.2$ and $\chi_{CH_2} = 11.10$ in this series of diphenyldi- n -alkoxysilanes are comparable with $\chi_{Si} = 17.00$ and $\chi_{CH_2} = 11.17$ in dimethyldi- n -alkoxysilanes. This observation shows that χ_{Si} in both the series is almost the same. It can be noticed

(1) R. R. Gupta, Ph.D. Thesis, Rajasthan University, Jaipur, India, 1968.

(2) R. L. Mital and R. R. Gupta, *Inorg. Chim. Acta Rev.*, **4**, 97 (1970).

(3) R. L. Mital, *J. Phys. Chem.*, **68**, 1613 (1964).

(4) R. L. Mital and R. R. Gupta, *J. Amer. Chem. Soc.*, **91**, 4664 (1969).

(5) E. W. Abel, R. P. Bush, C. R. Jenkins, and T. Zobel, *Trans. Faraday Soc.*, **60**, 1214 (1964).

(6) E. A. V. Ebsworth, "Volatile Silicon Compounds," Pergamon Press, Oxford, 1963, p 80.

(7) B. C. Pant, Ph.D. Thesis, Rajasthan University, Jaipur, India, 1963.

(8) All the susceptibility values are in -10^{-6} cgs units throughout the paper.

(9) B. N. Figgis and R. S. Nyholm, *J. Chem. Soc.*, 4190 (1958).

(10) W. Haberditzl, *Sitzben., Deut. Akad. Wiss. Berlin, Kl. Chem. Geol., Biol.*, No. 2 (1964); *Angew. Chem., Int. Ed. Engl.*, **5**, 288 (1966).

(11) W. Haberditzl, *Z. Chem.*, **1**, 255 (1961).

Table I: Diamagnetic Susceptibility Data on Diphenyldialkoxysilanes of the General Formula $[(C_6H_5)_2Si-(OR)_2]$

| R | χ_M (exptl) | χ_{Si} | χ_M (calcd) | |
|---|------------------|-------------------|---|-------------------------------------|
| | | | From Baudet's wave-mechanical method ^b | From Hamaka's equation ^c |
| CH ₃ | 156.80 | 17.2 ^a | 163.90 | 156.82 |
| C ₂ H ₅ | 179.25 | 17.2 ^a | 186.60 | 179.02 |
| CH ₃ -(CH ₂) ₂ | 201.58 | 17.2 ^a | 209.30 | 201.22 |
| (CH ₃) ₂ -CH | 202.46 | ... | 209.30 | ... |
| CH ₃ -(CH ₂) ₃ | 223.62 | 17.2 ^a | 232.00 | 223.42 |
| (CH ₃) ₂ -CH C ₂ H ₅ | 224.46 | ... | 232.00 | ... |

^a Average value of χ_{Si} , determined from the plot of χ_M against n in the series $(C_6H_5)_2Si-[O(CH_2)_n-H]_2$. ^b References 13 and 14. ^c Reference 16.

that the replacement of two C₆H₅ groups by two CH₃ groups does not affect χ_{Si} or in other words the behavior of a CH₃ group is similar to that of a C₆H₅ group towards χ_{Si} . It can be concluded that the π orbitals of a benzene ring cannot become conjugated with the d orbitals of a silicon atom directly bound to the ring otherwise χ_{Si} should be affected by replacement of a methyl group by a phenyl group. These studies support ultraviolet studies⁶ by showing that no back-donation occurs in aromatic silicon systems.

The iso isomers have larger diamagnetic susceptibilities than the normal isomers and are analogous to related series of carbon compounds.^{1,12} The larger diamagnetism of the iso isomer relative to that of the normal isomer is explicable in terms of the argument of Angus.¹³

Calculation of Diamagnetic Susceptibility

χ_M values of these compounds have been calculated theoretically by Baudet's wave-mechanical method.¹⁴⁻¹⁶ In this method for calculation of χ_M , the contributions to the molecular susceptibility from the following sources are taken into account: (a) from the inner shells of electrons of each atom present (ISE), (b) from the bonding electrons in each bond (BE), (c) from the non-bonding lone-pair electrons in the outer shells (NBE), and (d) from the π electrons present in each bond. χ_M is expressed in the form $\chi_M(\text{theoret}) = \Sigma\chi_{ISE} + \Sigma\chi_{BE} + \Sigma\chi_{NBE} + \Sigma\pi$ electrons. Using the values of χ_{ISE} , χ_{BE} , χ_{NBE} , π electrons, and $\chi_{C_6H_5} = 51.6$, the χ_M values of these silicon compounds have been calculated and summarized in the Table I. A critical comparison of the calculated and experimental values shows a poor agreement between them (the percentage deviation is 3.5-5%). Although all the above contributions to the molecular susceptibility have been considered, structural factors (such as p_π - d_π bonding between silicon and oxygen

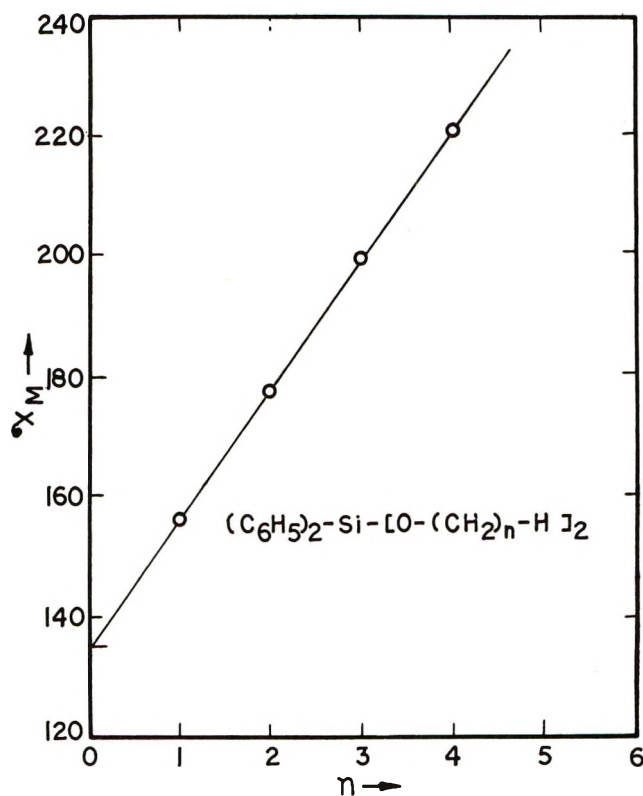


Figure 1. A plot of χ_M against n for the series $[(C_6H_5)_2Si-(OC_nH_{2n+1})_2]$.

atoms), which cannot be neglected, have not been taken into consideration in calculating wave-mechanically the magnetic susceptibility data, and this may be a probable reason for the poor agreement between calculated and observed χ_M values. Moreover, this method fails to give different χ_M values for positional isomers and contradicts experimental results.

An attempt has been also made to calculate χ_M of these compounds from Hamaka's wave-mechanical equation¹⁷ in which the molecular susceptibility of a compound is considered to be made up from (1) each atom, (2) each bond, and (3) each interaction between any two bonds starting from the same atom. Mathematically this equation can be represented by $\chi_M = \chi_{atoms} + \chi_{bonds} + \chi_{bond\ interactions}$. The sizes of the terms in this equation depend on the atoms involved. Hamaka's equation for a compound $(C_6H_5)_aSi-(OC_nH_{2n+1})_b$ can be expressed as

$$M = aA + bB + abC \quad (\text{where } a + b = 4)$$

(12) P. W. Selwood, "Magneto-chemistry," Interscience, New York, N. Y., 2nd ed, 1955, p 95.

(13) W. R. Angus and W. K. Hill, *Trans. Faraday Soc.*, **39**, 197 (1943).

(14) J. Baudet, *J. Chim. Phys.*, **58**, 288 (1961).

(15) A. Pacault, J. Hoarau, and A. Marchand, "Advances in Chemical Physics," Vol. 3, I. Prigogine, Ed., Interscience, New York, N. Y., 1961, p 171.

(16) J. Baudet, J. Tillieu, and J. Guy, *C. R. Acad. Sci., Paris*, **244**, 2920 (1957).

(17) H. F. Hamaka, *J. Chem. Phys.*, **34**, 1996 (1961).

where A , B , and C are the parameters related to Hamerka's various terms as explained below.

$$A = 0.25\chi_{\text{Si}} + \chi_{\text{C}_6\text{H}_6} + \chi_{\text{Si}-\text{C}_6\text{H}_5} + 1.5\chi_{\text{Si}-(\text{C}_6\text{H}_5)_2}$$

where $\chi_{\text{Si}-(\text{C}_6\text{H}_5)_2}$ is the term due to the interactions of two Si-C₆H₅ bonds to the same silicon atom. Similarly for other terms

$$B = 0.25\chi_{\text{Si}} + \chi_{\text{OC}_n\text{H}_{2n+1}} +$$

$$\chi_{\text{Si}-\text{OC}_n\text{H}_{2n+1}} + 1.5\chi_{\text{Si}-(\text{OC}_n\text{H}_{2n+1})_2}$$

$$C = \chi_{\text{Si} < \text{C}_6\text{H}_5 / \text{OC}_n\text{H}_{2n+1}} - 0.5\chi_{\text{Si}-(\text{C}_6\text{H}_5)_2} - 0.5\chi_{\text{Si}(\text{OC}_n\text{H}_{2n+1})_2}$$

As regards the difference between methyl and ethyl compounds, the same treatment leads to the conclusion that there will be a certain increment in susceptibility on replacing a methyl group by an ethyl group, but no

other parameter will be changed. χ_M for Si-(C₆H₅)₄ = 212.20¹ gives $A = 53.05$ units and χ_M for Si-(OCH₃)₄ = 89.98¹ gives $B = 22.5$ units. χ_M for (C₆H₅)₂-Si-(OCH₃)₂ = 156.80¹ gives $C = 1.43$. Using these values of A , B , and C and $\chi_{\text{CH}_2} = 11.10$ in the present homologous series, χ_M values of these compounds have been calculated and summarized in Table I. An excellent agreement is obtained between observed and calculated χ_M values. In calculating χ_M by Hamerka's equation all the structural factors (including p_π-d_π bonding between silicon and oxygen), which do affect diamagnetism, have been considered, and this no doubt accounts for the excellent agreement between the calculated and experimental values.

Acknowledgment. Thanks are due to Professor R. C. Mehrotra, Head of the Chemistry Department, for providing facilities in the department.

Predictions of the Rates of Hydrogen Abstraction by CH₂(³B₁)

by the Bond-Energy Bond-Order Method¹

by Robert W. Carr, Jr.

Department of Chemical Engineering and Materials Science, University of Minnesota, Minneapolis, Minnesota 55455
(Received January 5, 1972)

Publication costs borne completely by The Journal of Physical Chemistry

Activation energies for 25 hydrogen atom transfer reactions to CH₂(³B₁) were calculated by the bond-energy bond-order method. The computed activation energies cover the range 7.9 kcal mol⁻¹ to 44.2 kcal mol⁻¹. Rate constants were calculated by using the empirical activation energies in conjunction with transition state theory over the temperature range 300 to 650°K. The computational results indicate that the low reactivity of CH₂(³B₁) toward CH bonds is due to high activation energies.

Introduction

The presence of free radicals in reactions of methylene with hydrocarbons is well established.² Their source has been attributed to abstraction of hydrogen from C-H bonds by methylene with the formation of methyl radicals and the corresponding radical cofragments. Recent work indicates that the free-radical precursor is the ubiquitous triplet ground state of methylene, CH₂(³B₁).³ Furthermore, the work with alkane substrates clearly indicates the importance of a hydrogen abstraction reaction of triplet methylene,⁴ although other reactions can contribute to the free radical component of the reaction.⁵

The rate of hydrogen abstraction by triplet methylene is only qualitatively known. Triplet methylene is

sufficiently unreactive at 300°K that Braun, Bass, and Pilling⁵ were unable to observe any reaction with either hydrogen or methane in their flash photolysis

(1) Supported by the U. S. Atomic Energy Commission under contract No. AT(11-1) 2026. This is AEC document COO-2026-7.

(2) H. M. Frey and G. B. Kistiakowsky, *J. Amer. Chem. Soc.*, **79**, 6373 (1957); H. M. Frey, *Proc. Chem. Soc.*, 318 (1959); W. E. Doering and H. Prinzbach, *Tetrahedron*, **6**, 24 (1959).

(3) J. W. Simons and B. S. Rabinovitch, *J. Phys. Chem.*, **68**, 1322 (1964); R. W. Carr, Jr., and G. B. Kistiakowsky, *ibid.*, **70**, 119 (1966); S. Y. Ho and W. A. Noyes, Jr., *J. Amer. Chem. Soc.*, **89**, 5091 (1967).

(4) G. Z. Whitten and B. S. Rabinovitch, *J. Phys. Chem.*, **69**, 4348 (1965); R. W. Carr, Jr., *ibid.*, **70**, 1970 (1966); R. W. Carr, Jr., and B. M. Herzog, *ibid.*, **71**, 2688 (1967); M. L. Halberstadt and J. R. McNesby, *J. Amer. Chem. Soc.*, **89**, 3417 (1967).

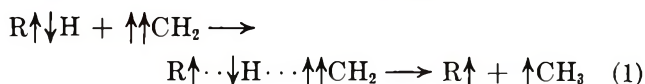
(5) W. Braun, A. M. Bass, and M. Pilling, *J. Chem. Phys.*, **52**, 5131 (1970).

experiments. They estimated an upper limit of $5 \times 10^{-14} \text{ cm}^3 \text{ molecule}^{-1} \text{ sec}^{-1}$ for the rate constant of both reactions. In earlier work, Rowland, McKnight, and Lee⁶ found that the triplet methylene-butene-2 reaction occurs with a collision yield of less than 10^{-4} . More recently Lee, Russell, and Rowland⁷ presented evidence that the collision efficiency of the triplet methylene reaction with methane- d_4 is $<10^{-9}$, while Walsh and Frey⁸ also concluded that triplet methylene has a very low reactivity toward C-H bonds. The latter authors questioned whether any H abstraction from neopentane occurred in their experiments. In both the methane- d_4 and neopentane⁸ systems products arising through the agency of triplet methylene were explicable with mechanisms excluding hydrogen abstraction by triplet methylene.

Whether the experiments yielding evidence for hydrogen abstraction are in conflict with those where abstraction did not occur cannot be unambiguously settled by the data currently available. It is certainly true that failure to observe abstraction has only occurred with substrates having higher C-H bond energies, but rate data for an independent assessment of the mechanisms derived from "steady-state" experiments are not yet available. In the absence of such data, it seemed reasonable to attempt some empirical calculations. Activation energies calculated by the bond-energy bond-order method^{9,10} and rate constants calculated from transition state theory are presented here for abstraction of hydrogen from 18 compounds. They were selected to cover a range of bond energies, bond lengths, and atoms to which the hydrogen is bonded, as well as to include substrates with which triplet methylene reactions have been previously investigated. By using the computed rate data, the experimental observations noted above on the reactivity of triplet methylene toward C-H bonds were found to be mutually compatible.

Computations and Computational Results

The conventional bond-energy bond-order method was used for these computations.^{9,10} Transfer of hydrogen from the donor molecule, RH, to triplet methylene $^3\text{CH}_2$, was assumed to occur *via* a linear transition state with conservation of bond order



$$n_1 + n_2 = 1 \quad (2)$$

where n_1 and n_2 are the bond orders of the breaking and forming bonds, respectively, and the arrows in eq 1 represent electron spin orientation.

The potential energy along the reaction coordinate was calculated in the orthodox manner by summing the contributions of the three binary interactions, R-H, H-CH₂, and R-CH₂. Using the single progress

variable, n , where $n_1 = n$, $n_2 = 1 - n$, leads to the equation

$$V = D_{\text{RH}}[1 - n^p] - D_{\text{H-CH}_2}[1 - n]^q + V_{\text{R-CH}_2} \quad (3)$$

In (3), p and q are empirically determined from bond-energy bond-length correlations¹¹ with the inclusion of noble gas diatomic pairs for the zero-order bond energy.^{9,10} $D_{\text{R-H}}$ and $D_{\text{H-CH}_2}$ are single bond dissociation energies, D_e , measured from the minimum of potential energy, and $V_{\text{R-CH}_2}$ is the repulsion energy between the end groups owing to their equivalent electron spin orientations. In cases where the hydrogen-abstracting species is an electronic doublet Johnston and coworkers successfully used either 0.5⁹ or 0.65¹² of Sato's anti-Morse function for $V_{\text{R-CH}_2}$. For abstractions by O(³P) Mayer and Schieler¹³ obtained good agreement with experiment by using the unmodified Sato function to account for the increased repulsion in the transition state when the abstracting species is initially in a triplet state. In these calculations on H abstractions by the isoelectronic $^3\text{CH}_2$, the unmodified Sato function, eq 4, was also used. In (4), R_3 is the dis-

$$V_{\text{R-CH}_2} = D_{\text{R-CH}_2}[\exp(-\beta R_3)] \times [1 + 1/2 \exp(-\beta R_3)] \quad (4)$$

placement of R-CH₂ from its single bond equilibrium distance, and β is the Morse parameter. By substitution of (4) into (3), and expressing R_3 in terms of n , eq 5 re-

$$V = D_{\text{R-H}}[1 - n^p] - D_{\text{H-CH}_2}[1 - n]^q + 2D_{\text{R-CH}_2}B(n - n^2)^\gamma [1 + B(n - n^2)^\gamma] \quad (5)$$

sults, where $B = 1/2 \exp(-\beta \Delta r_s)$, $\Delta r_s = r_{\text{R-H}} + r_{\text{R-CH}_2} - r_{\text{R-CH}_2}$, $\gamma = 0.26\beta$, and r is equilibrium bond length. To compute the potential energy of activation, V^* , the value of $n = n^*$ at the maximum of V was evaluated by an iterative procedure on the University of Minnesota CDC 6600 digital computer from eq 6.

$$\left(\frac{dV}{dn}\right) = 0 = -D_{\text{RH}}p(1 - n^p) + D_{\text{RCH}_2}(1 - n)^{q-1} + 2\gamma D_{\text{RCH}_2}B(1 - 2n) \times (n - n^2)^{\gamma-1} [1 + 2B(n - n^2)^\gamma] \quad (6)$$

The value of n^* was substituted into eq 5, yielding V^* .

(6) F. S. Rowland, C. McKnight, and E. K. C. Lee, *Ber. Bunsenges. Phys. Chem.*, **72**, 236 (1968).

(7) P. S. T. Lee, R. L. Russell, and F. S. Rowland, *J. Chem. Soc. D*, **18** (1970).

(8) H. M. Frey and R. Walsh, *J. Chem. Soc. A*, 2115 (1970).

(9) H. S. Johnston and C. Parr, *J. Amer. Chem. Soc.*, **85**, 2544 (1963).

(10) H. S. Johnston, "Gas Phase Reaction Rate Theory," Ronald Press, New York, N. Y., 1966.

(11) L. Pauling, *J. Amer. Chem. Soc.*, **69**, 542 (1947).

(12) S. W. Mayer, L. Schieler, and H. S. Johnston, Eleventh Symposium (International) on Combustion, Proceedings, 1967, p 837.

(13) S. W. Mayer and L. Schieler, *J. Phys. Chem.*, **72**, 2628 (1968).

Specific rate constants were calculated on the CDC 6600 by transition state theory¹⁴

$$k(T) = \kappa\omega^*K^* \quad (7)$$

where κ is the transmission coefficient, ω^* is the average rate of crossing the barrier, and the equilibrium constant for the equilibrium between reactants and transition states, K^* , is

$$K^* = \frac{Q^\ddagger}{Q_A Q_B} \exp(-V^*/RT) \quad (8)$$

In eq 8, the partition functions, Q , were evaluated by the local properties formulation.¹⁵ For these computations, κ was made equal to unity, and tunneling corrections were not done, since the one-dimensional treatment, which would be dictated by the fact that the BEBO method yields only a trace of $V(r)$ along the reaction path for collinear reactant configurations, is incorrect.¹⁶ The rate constants reported here are therefore deliberately smaller than those that would be obtained were tunneling corrections made, but the uncertainties in computed values of V^* are undoubtedly sufficient to cause uncertainties in $k(T)$ comparable to or even greater than errors introduced by ignoring tunneling. Other uncertainties in the rate constants arise from the molecular models used for the partition function calculations. In this paper, R and CH₂ were treated as point masses, which assumes that the important molecular changes during reaction occur only in the reaction coordinate. This treatment, which simplifies the calculations enormously, has been tested for hydrogen transfer to methyl from molecular hydrogen.¹⁷ The point mass assumption gave rate constants which were 6.2 times greater than those obtained from a model where the motions of each atom of the activated complex were treated separately. Some support for the use of the point mass model is contained in the work of Mayer and Schieler,¹³ who used it on hydrogen transfer to O(³P) from molecules as large as *n*-butane and obtained good agreement with experimental data.

Arrhenius pre-exponential factors were computed from the equation

$$A = B(T) \exp(\theta) \quad (9)$$

where $\theta = d \ln B(T)/d \ln T$, and $B(T)$ was calculated from

$$B(T) = 1.81 \times 10^{10} \kappa\omega^*K^* \times \exp(V^*/RT) \text{ cm}^3 \text{ mol}^{-1} \text{ sec}^{-1} \quad (10)$$

Activation energies were obtained by making Arrhenius plots of $k(T)$ computed at 300, 350, 450, 550, and 650°K. The Arrhenius plots were very nearly linear over this temperature range.

The input data for these calculations are contained in Table I. The equilibrium bond lengths were taken

from the 51st edition of the "Handbook of Chemistry and Physics," except where other literature citations are given. Single bond stretching frequencies were either selected from various literature sources, as noted, or were assumed to have commonly accepted approximate values, such as either 2900 or 3000 cm⁻¹ for C-H stretching, and 950 cm⁻¹ for C-C stretching. Other values appearing in the table without citation are estimates. Single bond dissociation energies were either taken from the specific literature citations listed, or where no citation is given, were calculated from thermochemical data.¹⁸ The value of $\Delta H_f^\circ_{298}$ (³CH₂) = 93.7 kcal mol⁻¹ (*Nat. Bur. Stand. (U. S.), Tech. Note, 270-3*) was adopted for these calculations. The results are listed in Table II.

Discussion

The bond-energy bond-order method predicts appreciable activation energies for all of the reactions included in this work. Owing to the absence of experimentally determined activation energies their accuracy cannot be precisely established. Nevertheless, on the basis of previous work with the BEBO method, the accuracy may reasonably be expected to be in the vicinity of 1–2 kcal mol⁻¹ found by Johnston and Parr⁹ for a large number of hydrogen transfers to atoms and radicals of doublet multiplicity, or perhaps even in the range of 0.8 kcal mol⁻¹ reported by Mayer and Schieler¹³ for the mean deviation of computed activation energies from experimental values for reactions of O(³P). For the purposes of the following discussion, activation energies will be assumed to be accurate to 1–2 kcal mol⁻¹, and rate constants will be considered accurate to at least an order of magnitude.^{9–11,13}

The data contained in Table II show the expected general trend of increasing activation energy with increasing dissociation energy of the bond which is broken during reaction. This trend is confirmed by the usual Polanyi-Semenov plots of activation energy *vs.* dissociation energy or the alternative reduced plots suggested¹⁹ for comparison of experimental data with BEBO predictions. While these graphs are not included here, they may be rapidly made from the data of Tables I and II and used for the prediction of activa-

(14) S. Glasstone, K. J. Laidler, and H. Eyring, "Theory of Rate Processes," McGraw-Hill, New York, N. Y., 1941.

(15) D. R. Herschbach, H. S. Johnston, and D. Rapp, *J. Chem. Phys.*, **31**, 1652 (1959); T. E. Sharp and H. S. Johnston, *ibid.*, **37**, 1541 (1962).

(16) Reference 10, p 47.

(17) H. S. Johnston, *Advan. Chem. Phys.*, **3**, 131 (1960).

(18) The sources of thermochemical data for the stable reactant molecules were taken either from the JANAF tables or *Nat. Bur. Stand. (U. S.), Circ.*, No. 500 (1952), while for atoms and free radicals the sources were *Nat. Bur. Stand. (U. S.), Tech. Note*, 270-1 and 270-3; "Handbook of Chemistry and Physics," 51st ed, Chemical Rubber Publishing Co., Cleveland, Ohio, 1971; or D. M. Golden and S. W. Benson, *Chem. Rev.*, **69**, 125 (1969).

(19) Reference 10, p 208.

Table I: Single Bond Properties of Bonds Involved in Hydrogen Atom Transfer to $\text{CH}_2(^3\text{B}_1)$

| Bond broken | Properties of bond which breaks | | | "End-group" (Y-CH ₂) properties | | |
|---------------------------------------|---------------------------------|-----------------------------|--|---|-----------------------------|--|
| | r , Å | ν , cm ⁻¹ | D_0 , ⁱ kcal mol ⁻¹ | r , Å | ν , cm ⁻¹ | D_0 , ⁱ kcal mol ⁻¹ |
| H-H | 0.7416 ^a | 4405 ^a | 109.5 ^a | 1.079 ^b | 2740 ^b | 114.0 ^c |
| CH ₃ -H | 1.094 ^d | 2916 ^d | 107.5 ^e | 1.536 ^d | 945 ^d | 102.6 |
| C ₂ H ₅ -H | 1.107 | 2953 ^d | 102.2 ^f | 1.54 | 950 | 99.7 |
| C ₃ H ₇ -H | 1.101 | 2900 | 102 | 1.54 | 950 | 100.2 |
| sec-C ₃ H ₇ -H | 1.073 | 2900 | 98.7 | 1.54 | 950 | 98.8 |
| C ₄ H ₉ -H | 1.101 | 2900 | 102 | 1.54 | 950 | 99.9 |
| sec-C ₄ H ₉ -H | 1.073 | 2900 | 98.8 | 1.54 | 950 | 98.4 |
| (CH ₃) ₃ C-H | 1.07 | 2900 | 95.1 | 1.54 | 950 | 94.2 |
| HO-H | 0.958 | 3756 ^d | 123.4 ^d | 1.427 | 1050 | 112.9 |
| H ₂ C=CH-H | 1.086 ^d | 3026 ^d | 112 ^g | 1.44 | 1400 | 121.5 |
| H ₂ C=CHCH ₂ -H | 1.101 | 2900 | 92.9 | 1.54 | 950 | 87.8 |
| H ₂ C=C(-H)CH ₃ | 1.07 | 3000 | 104.2 | 1.54 | 950 | 106 |
| CH ₃ CH=CH-H | 1.07 | 3000 | 108 | 1.54 | 950 | 120 |
| F-H | 0.917 ^a | 4138.5 ^a | 140.7 ^c | 1.38 | 1200 | 118 |
| Cl ₃ C-H | 1.073 | 2900 | 100 | 1.54 | 900 | 101 |
| HCl ₂ C-H | 1.068 | 2900 | 102.5 | 1.54 | 900 | 103.7 |
| H ₂ ClC-H | 1.11 | 2900 | 105 | 1.54 | 950 | 104.1 |
| F ₃ C-H | 1.098 | 2900 | 110.4 | 1.54 | 950 | 116.3 |
| NH ₂ -H | 1.008 | 3337 ^d | 107.8 | 1.474 | 1100 | 94.7 |
| CHO-H | 1.06 | 2760 ^d | 90.9 | 1.516 | 900 | 95.9 |
| HO ₂ -H | 0.96 | 3500 | 94 ^g | 1.43 | 800 | 95 |
| NC-H | 1.064 ^d | 3311 ^d | 130 ^h | 1.46 | 900 | 132 |

^a G. Herzberg, "Spectra of Diatomic Molecules," Van Nostrand, Princeton, N. J., 1950. ^b G. Herzberg, *Proc. Roy. Soc., Ser. A*, **262**, 291 (1961). ^c Computed with thermochemical data from D. D. Wagman, W. H. Evans, I. Halow, V. B. Parker, S. M. Bailey, and R. H. Schumm, *Nat. Bur. Stand. (U. S.), Tech. Note*, 270-1 (1965); *ibid.*, 270-3 (1968). ^d G. Herzberg, "Electronic Spectra of Polyatomic Molecules," Van Nostrand, Princeton, N. J., 1967. ^e W. A. Chupka, *J. Chem. Phys.*, **48**, 2337 (1968). ^f S. W. Benson, *J. Chem. Educ.*, **42**, 502 (1965). ^g D. M. Golden and S. W. Benson, *Chem. Rev.*, **69**, 125 (1969). ^h Computed using $\Delta H_{1^\circ}(\text{CN}) = 105.5 \text{ kcal mol}^{-1}$ (J. A. Berkowitz, W. A. Chupka, and T. A. Walter, *J. Chem. Phys.*, **50**, 1497 (1969)). ⁱ The values of D_0 were calculated from D_e by addition of zero point energy.

tion energies of other hydrogen atom transfer reactions to triplet methylene.

The range of predicted activation energies runs from 7.9 kcal mol⁻¹ for abstraction at the allyl position in propylene, to 44.2 kcal mol⁻¹ for hydrogen cyanide. The range and magnitude of these activation energies are larger than those of hydrogen transfers to atoms or monoradicals for which the reaction exothermicity is similar in magnitude to those of the methylene reactions. For example, in the reaction $^3\text{CH}_2 + \text{C}_2\text{H}_6 \rightarrow \text{CH}_3 + \text{C}_2\text{H}_5$, $\Delta H_{298}^\circ = -15 \text{ kcal mol}^{-1}$, the computed activation energy of 15.7 kcal mol⁻¹ is larger than the activation energy of 10 kcal mol⁻¹, also computed by the BEBO method,⁹ for $\text{CH}_3 + \text{C}_2\text{H}_6 = \text{CH}_4 + \text{C}_2\text{H}_5$, $\Delta H_{298}^\circ = -5 \text{ kcal mol}^{-1}$. When similar comparisons were made between other reaction pairs, the more exothermic abstraction by triplet methylene always had the higher activation energy. The source of the "high" activation energies of the triplet methylene reactions lies in the use of the "doubled triplet repulsion energy." Trial calculations in which the unmodified BEBO method of using one-half of eq 4 to estimate end-group repulsion were done resulted in activation energies which were approximately one-half of those listed in Table II. The use of a doubled

triplet repulsion energy in these calculations is justified by its success in the hydrogen abstraction reactions of O(³P), and by the failure of rate constants obtained with undoubled triplet repulsion to agree with many of the experimental observations on triplet methylene reactivity discussed below.

The calculational results would ascribe the low reactivity of triplet methylene toward carbon-hydrogen bonds to the magnitude of the activation energies necessary for abstraction. The calculated Arrhenius pre-exponential factors had "normal" values for all cases examined, as expected, owing to the adiabaticity of transition state theory. It was not necessary to invoke small transmission coefficients to obtain agreement with such experimental data as are presently available. Thus the BEBO method, at least in those few cases where limited tests are possible, predicts that H abstraction by triplet methylene occurs as a spin-allowed process, the interaction of a triplet with a singlet to form two doublets. Moreover, the simple valence-bond picture of eq 1 implies that the activated complex may be a triplet state, and therefore presumably of very short lifetime, as only single σ bonds are involved. It is interesting to speculate that the reaction may proceed by a direct mechanism on a repulsive surface,

Table II: Potential Energies of Activation, Arrhenius Parameters, and 300°K Rate Constants Computed for H-Atom Transfer to CH₂(³B₁)

| Reactant | V^* , kcal mol ⁻¹ | $A \times 10^{-13}$, cm ³ mol ⁻¹ sec ⁻¹ | E_a , kcal mol ⁻¹ | log k at 300°K, cm ³ mol ⁻¹ sec ⁻¹ |
|---|-----------------------------------|---|-----------------------------------|--|
| H ₂ | 21.3 | 5.92 | 19.7 | -0.27 |
| CH ₄ | 27.0 | 24.9 | 25.6 | -4.07 |
| C ₂ H ₆ | 17.0 | 12.2 | 15.7 | 3.04 |
| C ₃ H ₈ ^a | 15.4 | 4.08 | 14.2 | 3.70 |
| C ₃ H ₈ ^b | 14.0 | 3.86 | 12.9 | 4.63 |
| <i>n</i> -C ₄ H ₁₀ ^a | 14.4 | 2.06 | 13.1 | 4.15 |
| <i>n</i> -C ₄ H ₁₀ ^b | 13.0 | 1.93 | 11.7 | 5.07 |
| <i>i</i> -C ₄ H ₁₀ ^c | 10.6 | 1.87 | 9.52 | 6.65 |
| <i>i</i> -C ₅ H ₁₂ ^a | 13.9 | 2.06 | 12.6 | 4.55 |
| <i>i</i> -C ₅ H ₁₂ ^b | 12.4 | 1.94 | 11.1 | 3.23 |
| <i>i</i> -C ₅ H ₁₂ ^c | 9.9 | 1.86 | 8.8 | 7.08 |
| H ₂ O | 31.3 | 2.08 | 29.3 | -7.52 |
| C ₂ H ₄ | 14.0 | 10.9 | 12.4 | 5.37 |
| C ₂ H ₆ ^d | 8.8 | 2.05 | 7.9 | 7.80 |
| C ₃ H ₆ ^e | 18.8 | 1.93 | 17.4 | 0.91 |
| C ₃ H ₆ ^f | 25.7 | 1.79 | 24.4 | -4.17 |
| H-F | 38.4 | 1.19 | 36.3 | -9.30 |
| CHCl ₃ | 14.3 | 5.67 | 12.9 | 4.66 |
| CH ₂ Cl ₂ | 16.9 | 3.84 | 15.7 | 2.59 |
| CH ₃ Cl | 17.3 | 7.79 | 16.3 | 2.51 |
| CHF ₃ | 22.8 | 5.74 | 21.4 | -1.58 |
| NH ₃ | 16.5 | 7.0 | 14.5 | 3.51 |
| H ₂ CO | 12.7 | 3.76 | 12.1 | 5.16 |
| H ₂ O ₂ | 16.2 | 1.79 | 14.8 | 2.77 |
| HCN | 45.8 | 8.51 | 44.2 | -18.9 |

^a Reaction at primary position. ^b Reaction at secondary position. ^c Reaction at tertiary position. ^d Reaction at allyl position. ^e Reaction at secondary vinyl position. ^f Reaction at primary vinyl position.

in which case the free-radical products of the abstraction could be initially formed with a nonequilibrium distribution of translational energy. It might be instructive to search for "hot" methyl radicals in a triplet methylene abstraction reaction.

Much of the data on hydrogen abstraction by triplet methylene is in the form of rate constant ratios. Ratios of various rate constants, made from the 300°K rate constants listed in Table II, compare favorably with their experimentally determined counterparts. The "per-bond" ratio of abstraction of hydrogen from the secondary position of propane to abstraction from the primary position has been reported as 9 by Whitten and Rabinovitch,⁴ 14 by Ho and Noyes,³ and 9-10 by Mitschele.²⁰

Ring and Rabinovitch²¹ listed average values of 14 and 150 for secondary to primary and tertiary to primary ratios, respectively, for propane, *n*-butane, and isopentane. The BEBO calculations give primary to secondary ratios of 8.4, 8.3, and 9 for propane, *n*-butane, and isopentane, respectively, and primary to tertiary ratios of 314 and 337 for isobutane and isopentane, respectively. Thus the BEBO method yields rate con-

stants which predict the experimentally observed order of selectivity of triplet methylene with primary, secondary, and tertiary C-H bonds. The good agreement between experiment and calculation for the secondary to primary ratio is perhaps better than could be expected, and the factor of 2 difference for the tertiary to primary ratio is probably not serious in view of the limited accuracy of the computational method.

The rate constants listed in Table II are also in accord with other rate data currently available. The 300°K values of 0.5 and 8.5×10^{-5} cm³ mol⁻¹ sec⁻¹ for the reaction with hydrogen and methane, respectively, are certainly well below the upper limit of 3×10^{10} cm³ mol⁻¹ sec⁻¹ set on both of these reactions by the experiments of Braun, Bass, and Pilling.⁵ Lee, Russell, and Rowland⁷ demonstrated that triplet methylene is so unreactive toward methane-*d*₄ that it reacts solely with itself or other radicals present, to the exclusion of any abstraction from methane-*d*₄. They estimated that the reactive collision yield had to be $<10^{-9}$ in order to explain their results. This can be compared with the collision yield of about 10^{-18} for abstraction of hydrogen from light methane which is given by the present calculations. Finally, Frey and Walsh⁸ expressed doubt whether triplet methylene abstracted hydrogen from neopentane in their experiments. If abstraction occurred, it must have been a minor part of the reaction. Although neopentane was not included in these BEBO calculations, the rate constant may be quite similar to that for the primary C-H bonds of isopentane, 3.6×10^4 cm³ mol⁻¹ sec⁻¹, for which a collision yield of 1.4×10^{-10} may be obtained. Admittedly, when methylene is generated by steady illumination, the value of the abstraction rate constant below which triplet methylene will react predominantly by self-association or other radical-methylene reactions, and above which abstraction is experimentally detectable, depends on the incident light intensity and the stable molecule reactant concentrations. However, the apparatus and experimental conditions commonly used for various steady illumination investigations of methylene reactivity are sufficiently similar that a rate constant of about 10^4 cm³ mol⁻¹ sec⁻¹²² is probably an adequate, although admittedly imprecise, average value for the threshold above which abstraction will be important in these systems, and below which it will be kinetically unimportant. Assuming such a rate constant as a figure of merit in order

(20) C. J. Mitschele, Ph.D. Thesis, University of California, Riverside, 1968.

(21) D. F. Ring and B. S. Rabinovitch, *Can. J. Chem.*, **46**, 2435 (1968).

(22) $k(T) = 10^4$ cm³ mol⁻¹ sec⁻¹ corresponds to collision yields in the range 10^{-9} , which were previously mentioned in ref 7. These figures can be arrived at with a simple steady-state kinetic model, using the data of ref 5 for the rate of the CH₂ + CH₂ association reaction, and reasonable values of typical experimental conditions. They are, of course, subject to considerable variation depending upon experimental conditions.

to give a common basis for discussion, the qualitative observations that triplet methylene does not abstract deuterium from methane- d_4 ⁷ and most probably does not abstract hydrogen from neopentane⁸ are corroborated by the BEBO calculations.

The observations that triplet methylene abstracts hydrogen predominantly from the secondary or tertiary positions in alkanes and abstracts from the allyl position in butene-2, very nearly to the exclusion of abstraction from the vinyl position,²³ may be understood in terms of competition between abstraction and self-association of triplet methylene or its reactions with other radicals. Using the "threshold" rate constant criterion of 10^4 cm³ mol⁻¹ sec⁻¹, the preceding observations are predicted by these BEBO calculations. While the above considerations are necessarily qualitative because the

calculated rate constants are only approximate, they are capable of rationalizing the results of recent work on the reactivity of triplet methylene and thus (hopefully) the empiricism of the present calculations can be justified in the light of whatever insight into triplet methylene reactivity they have provided. A more detailed understanding of triplet methylene reactivity, as well as an adequate test of the applicability of the BEBO method to hydrogen transfer to triplet methylene, must await experimental values of rate constants and Arrhenius parameters.

Acknowledgment. The author thanks Mrs. Marianne Litzinger for writing the computer program, and Mr. William Chin for assistance with the computations.

(23) T. W. Eder, Ph.D. Thesis, University of Minnesota, 1969.

Steady-State Intermediate Concentrations and Rate Constants. Some HO₂ Results

by A. A. Westenberg* and N. deHaas

Applied Physics Laboratory, The Johns Hopkins University, Silver Spring, Maryland 20910 (Received December 21, 1971)

Publication costs assisted by the Applied Physics Laboratory

The equations governing the decay of H atoms in the H-O₂-M system are derived, using the steady-state approximation for the concentration of the intermediates HO₂, O, and OH. The validity of this approximation is demonstrated experimentally for a room temperature fast flow system containing a trace of H in an inert carrier (Ar or He) with an excess of O₂ added through a movable injector. Measurement of the absolute concentrations of H and of steady-state OH and O (by esr spectroscopy) allows the relative rates of reaction by the three paths $H + HO_2 \xrightarrow{k_2} H_2 + O_2$, $H + HO_2 \xrightarrow{k_3} OH + OH$, and $H + HO_2 \xrightarrow{k_4} H_2O + O$ to be determined. The rate constants $k_2/k_3/k_4$ have the respective fractional values 0.62:0.27:0.11. From the H decay rates the rate constant k_1 for $H + O_2 + M \rightarrow HO_2 + M$ is then determined to be $6.8 \pm 1.0 \times 10^{15}$ cm⁶ mol⁻² sec⁻¹ for M = Ar or He, in excellent agreement with two previous literature values. The analysis is then extended to include the case where an excess of CO (compared to H) is also added to the H-O₂-M system in order to evaluate the possible significance of the reaction $CO + HO_2 \xrightarrow{k_7} CO_2 + OH$. It is shown that the ratio k_7/k_3 may be evaluated by two methods. In method I only (HO₂) is assumed to be in steady state (a reasonable assumption), and a number of runs give an average value $k_7/k_3 = 0.06 \pm 0.02$. Method II assumes (OH) and (O) to be at their steady-state values also (possibly less reasonable), which yields a considerably higher k_7/k_3 . In either case, the appreciable contribution of k_7 is incompatible with a large activation energy for this reaction, a result which (it is argued) is not surprising.

I. Introduction

The ubiquitous radical HO₂ is one of those whose reaction rates with other species are usually "estimated," there being practically no reliable measurements available. A direct mass spectrometer monitoring of the second-order decay of HO₂ in a linear flow system permitted Foner and Hudson¹ to evaluate the rate constant for $HO_2 + HO_2 \rightarrow H_2O_2 + O_2$, although there was apparently a complicating wall reaction as well. This is the only direct measurement of an HO₂ reaction of

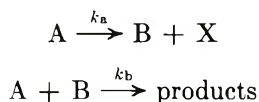
which we are aware. Other data which have been reported involve indirect experiments of various kinds, usually of rates of HO₂ reactions relative to others. Some of these have been reviewed.^{2,3}

(1) S. N. Foner and R. L. Hudson, *Advan. Chem. Ser.*, **No. 36**, 34 (1962).

(2) F. Kaufman, *Ann. Geophys.*, **20**, 106 (1964).

(3) D. L. Baulch, D. D. Drysdale, and A. C. Lloyd, High Temperature Reaction Rate Data Report No. 3, Leeds University (1969).

The HO₂ situation is typical of reactive intermediates which are difficult to prepare in a controlled fashion, and even more difficult to measure. The relatively recent advent of esr spectroscopy as a quantitative detector of a number of gas phase free radicals offers the potential, at least, of an approach to such rate measurements which has received relatively little attention, although the principle has been used.² As the simplest possible example, consider the consecutive competitive pair of reactions



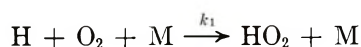
where B is a free-radical intermediate. If conditions are such that the steady-state approximation is applicable to B, *i.e.*, $k_b(A)_0 \gg k_a$ and the reaction time is longer than the induction time, then the radical concentration is given by the well-known relation $(B) = k_a/k_b$. The degree to which this approximation is approached in various cases has been discussed analytically by Giddings and Shin.⁴ Thus if the steady-state (B) can be measured and k_a is known, the rate constant k_b can be determined. Measurement of (B) allows the evaluation of the relative rate k_a/k_b at least.

In the case of HO₂, esr detection in the gas phase has not yet been feasible (nor is it likely to become so). Nevertheless, by measuring certain other steady-state species it is possible to make relative measurements of some important HO₂ rates, as is shown in the present paper.

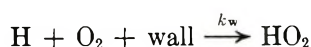
All numerical rate constants quoted are in cm³-mole-sec units.

II. Steady-State Analysis

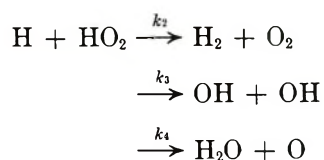
For present purposes, a clean method of generating HO₂ at room temperature is the reaction



There may also be a heterogeneous contribution



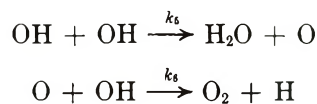
which was suggested in the work of Clyne and Thrush⁵ and confirmed here. The HO₂ concentration available in this way is kept low⁶ by the subsequent steps



In the presence of relatively large (H) these reactions will predominate in consuming HO₂, so that reaction of HO₂ with either O or OH, or with itself, will be negligible. This has been discussed in detail previously.⁵ Wall loss of HO₂ is also reported⁷ to be

negligible on a boric acid treated surface such as used in the experiments to be described.

The OH and O formed will undergo the reactions



which complete the mechanism if no further substances are added.

Let us consider the case where O₂ is in large excess compared to all other reactive species so that both (O₂) and (M) may be taken to be constant (in a reactor at constant temperature and pressure). We now apply the steady-state approximation to each of the intermediates HO₂, O, and OH in turn. Whether or not this is justified in each case is discussed later. Certainly a steady-state (HO)₂ should be attained first, since the slow initiating reactions are followed by reactions 2, 3, and 4 which ought to be very fast, and the required condition $k(H)_0 \gg [k_1(M) + k_w](O_2)$ should obtain after a very short time ($k = k_2 + k_3 + k_4$). The steady-state condition gives

$$(HO_2)_s = [k_1(M) + k_w](O_2)/k \quad (1)$$

$$(OH)_s = \left\{ \frac{[k_1(M) + k_w](2 - k_4/k_3)(H)(O_2)}{3k_5(1 + k_4/k_3)(1 + x)} \right\}^{1/2} \quad (2)$$

$$(O)_s = \frac{1}{k_6} \left\{ \frac{4k_5[k_1(M) + k_w](1 + k_4/k_3)(H)(O_2)}{3(2 - k_4/k_3)(1 + x)} \right\}^{1/2} \quad (3)$$

where the definition $x = k_2/(k_3 + k_4)$ has been used, following Clyne and Thrush.⁵ The expression for H decay normalized to some reference value (H)₀ then becomes

$$\frac{d \ln [(H)_0/(H)]}{dt} = 2(O_2)[k_1(M) + k_w] \left[\frac{3x + 2}{3x + 3} \right] \quad (4)$$

These relations may be combined in several ways which will be useful. Dividing (2) by (3) yields

$$\frac{(OH)_s}{(O)_s} = \frac{k_6 \left[\frac{2 - k_4/k_3}{1 + k_4/k_3} \right]}{2k_5} \quad (5)$$

which permits k_4/k_3 to be determined from a measurement of the steady-state ratio (OH)_s/(O)_s and knowledge of k_6/k_5 . Then the product

$$(OH)_s(O)_s = \frac{2[k_1(M) + k_w](H)(O_2)}{3k_6(1 + x)} \quad (6)$$

and the quantity defined from eq 4

(4) J. C. Giddings and H. K. Shin, *Trans. Faraday Soc.*, **57**, 468 (1961).

(5) M. A. A. Clyne and B. A. Thrush, *Proc. Roy. Soc., Ser. A*, **275**, 559 (1963).

(6) S. N. Foner and R. L. Hudson, *J. Chem. Phys.*, **36**, 2681 (1962).

(7) I. A. Vardanyan, G. A. Gachyan, and A. B. Nalbandyan, *Dokl. Akad. Nauk SSSR*, **193**, 123 (1970); *Engl. Trans.*, **193**, 498 (1970).

$$B_M = \frac{1}{(O_2)} \frac{d \ln [(H)_0/(H)]}{dt} = 2[k_1(M) + k_w] \left[\frac{3x+2}{3x+3} \right] \quad (7)$$

may be combined to give

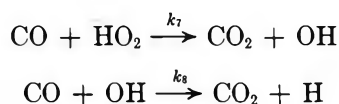
$$k_6(3x+2) = B_M \left\{ \frac{[(H)/(O_2)]}{[(OH)_s/(O_2)][(O)_s/(O_2)]} \right\} \quad (8)$$

where B_M denotes the experimental H decay slope at a given value of (M) and (O_2) . x may thus be evaluated from a measured B_M , the bracketed quantity in eq 8, and knowledge of k_6 . Finally, the slope of a plot of B_M vs. (M) gives

$$\frac{dB_M}{d(M)} = 2k_1 \left[\frac{3x+2}{3x+3} \right] \quad (9)$$

which allows k_1 to be found once x is known, and then the wall constant k_w from eq 7.

Now consider what happens when another reactant, say CO, is added to the reacting mixture in amounts large enough compared to (H) so that its concentration may also be taken constant, along with (O_2) and (M). The termolecular reaction $H + CO + M \rightarrow HCO + M$ will not occur appreciably in competition with reaction 1 if (O_2) and (CO) are roughly comparable, since it has a rate constant more than two orders of magnitude less⁸ than k_1 . The only other possible additional reactions are



Reaction 8 is sure to be important, since it is known^{9,10} to be reasonably fast ($k_8 \simeq 10^{11}$) at room temperature. Reaction 7 is of greatest present interest, and the assessment of its possible importance was one of the main reasons for undertaking this work.

Proceeding with a steady-state analysis as before, if HO_2 is in a steady state

$$(HO_2)_s = \frac{[k_1(M) + k_w](O_2)(H)}{k(H) + k_7(CO)} \quad (10)$$

which may be used in the sum of the (H) and (OH) rates to give

$$\begin{aligned} \frac{d(H)}{dt} + \frac{d(OH)}{dt} = & -2[k_1(M) + k_w](H)(O_2) \times \\ & \left[\frac{k_2 + k_4}{k + k_7(CO)/(H)} \right] - 2k_5(OH)^2 \end{aligned}$$

or in integrated form between times t_i and t_j

$$\begin{aligned} \frac{(H)_i}{(O_2)} - \frac{(H)_j}{(O_2)} + \frac{(OH)_i}{(O_2)} - \frac{(OH)_j}{(O_2)} = & \\ & 2[k_1(M) + k_w] \left[\frac{k}{k_3} - 1 \right] \times \\ & (O_2) \int_{t_i}^{t_j} \frac{[(H)/(O_2)] dt}{k/k_3 + k_7(CO)/k_3(H)} + \\ & 2k_5(O_2) \int_{t_i}^{t_j} [(OH)/(O_2)]^2 dt \quad (11) \end{aligned}$$

This expression will be useful later.

If both OH and O are in steady state *in addition* to HO_2 , setting their rates equal to zero and using (10) leads to

$$\frac{k_7}{k_3} = \frac{(1 + k_4/k_3)(1 + x)G - (2 - k_4/k_3)}{(1 - G)(CO)/(H)} \quad (12)$$

where the quantity G is defined by

$$G = \frac{(OH)_s/(O_2)}{k_1(M) + k_w} \left[3k_5 \frac{(OH)_s}{(H)} + k_8 \frac{(CO)}{(H)} \right] \quad (13)$$

Use of eq 12 to determine k_7/k_3 involves a higher level of assumption than eq 11, and results by both methods will be compared.

III. Experimental Section

A fixed cavity-movable injector discharge flow apparatus essentially as described previously¹¹ was employed. All sections of the reactor downstream of the discharge were coated with H_3BO_3 to reduce wall losses. H atoms were furnished from a trace of H_2 added to the argon or helium carrier upstream of the discharge, which dissociated the H_2 nearly completely. O_2 was metered into the movable injector in large excess compared to H for generation of HO_2 , and CO was metered and mixed with the O_2 before entering the injector for the runs where it was desired. Procedures for metering flows, measuring pressure, etc., have all been described. All runs were performed at room temperature.

Two significant departures from our previous technique deserve special comment. The first concerns the method of measuring absolute OH concentrations. The basic principle as described¹² is to compare the integrated OH signal with that of a known pressure of NO, the latter being usually accomplished by a separate filling of the reactor with pure NO. In the present

(8) T. Hikida, J. A. Eyre, and L. M. Dorfman, *J. Chem. Phys.*, **54**, 3422 (1971).

(9) G. Dixon-Lewis, W. E. Wilson, and A. A. Westenberg, *ibid.*, **44**, 2877 (1966).

(10) N. R. Greiner, *ibid.*, **46**, 2795 (1967).

(11) A. A. Westenberg and N. deHaas, *ibid.*, **47**, 1393 (1967).

(12) A. A. Westenberg, *ibid.*, **43**, 1544 (1965). It should be noted that an error of a factor of 2 in deriving the NO and OH matrix elements in this paper has been pointed out by W. H. Breckenridge and T. A. Miller, *ibid.*, **56**, 475 (1972). The error cancels out when the OH/NO calibration relations are computed, so that the Q_{OH} values in Table III of this reference are correct. The factor Q_0 for electron concentrations should be divided by 2, however.

case, since an appreciable concentration of O_2 always existed in the reactor anyway, it was much more convenient (and probably more reliable) to measure the OH intensity relative to that of the O_2 signal, and then use an empirical cavity factor to convert from the magnetic dipole O_2 case to the electric dipole NO and OH transitions. This empirical factor was determined by measuring the first moment¹³ I_{NO} (using line a of the NO spectrum in our nomenclature¹²) with a pressure P_{NO} of pure NO in the reactor tube passing through the cavity and a given set of instrumental variables, and I_{O_2} at P_{O_2} (using line E of the O_2 spectrum¹³) with pure O_2 at the same instrumental settings. The desired factor was then given by $(I_{NO}/I_{O_2})(P_{O_2}/P_{NO})$, which was, of course, specific to our cavity¹⁴ (TE_{011}) and flow tube. In this way the desired ratios $(OH)/(O_2)$, as well as $(H)/(O_2)$, could both be found from the same calibration measurement on the known O_2 concentration present during a kinetic run. The $(H)/(O_2)$ did not, of course, require the empirical factor since H exhibits magnetic dipole transitions and thus responds to the same geometry of microwave field vector as O_2 .

The other detail of technique worth noting was that some of the steady-state O concentrations to be measured were so low as to make integrated intensities difficult to obtain reliably. In these cases, a separate O signal was obtained with a larger concentration furnished by admitting some O_2 to the carrier flow upstream of the discharge (which did not otherwise perturb the pressure or overall mixture in the cavity appreciably), and the desired low (O) was evaluated from the moment of this larger (O) and the ratio of signal peak heights, the latter being much easier to measure at very low signal/noise. Since the line widths were identical in the two cases, this scaling procedure was perfectly valid. The same technique was used for low (OH) in some of the runs with CO present, a larger OH signal for integration being obtained with the CO turned off.

IV. Results and Discussion

The H- O_2 -M system with no other added species is considered first. The analysis leading to eq 1-9 was based on the steady-state approximation applying to all three species HO_2 , OH, and O. Equation 4 then predicts a straightforward, pseudo-first-order, logarithmic decay of (H) at any fixed pressure, *i.e.*, (M), and eq 2 predicts that $(OH)_s^2 \propto (H)$. The latter is a much more sensitive test of the steady-state condition, since reactions 1-4 dominate the (H) decay process and a steady state for (HO_2) alone gives essentially a linear logarithmic (H) decay behavior. By proper choice of flows and total pressure it was possible to attain reasonably well the desired conditions where $(OH)_s^2 \propto (H)$ and examples are given in Figure 1. By increasing the linear flow velocity it was always possible to reach a regime where the available reaction

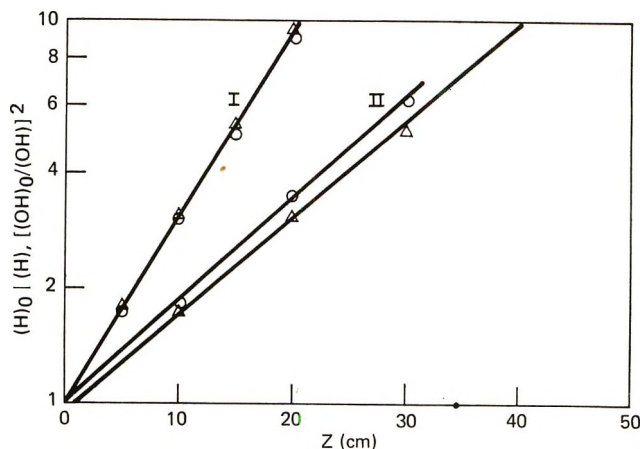


Figure 1. Examples of (H) and (OH)² decay down flow tube, showing that $(OH)^2 \propto (H)$: \circ , $(H)_0/(H)$; Δ , $[(OH)_0/(OH)]^2$. Run I: $P = 2.73$ Torr, $v = 270$ cm/sec, $(O_2) = 1.69 \times 10^{-8}$ mol/cm³. Run II: $P = 1.60$ Torr, $v = 425$ cm/sec, $(O_2) = 2.34 \times 10^{-8}$ mol/cm³. $z = 0$ was 16 cm from the cavity center.

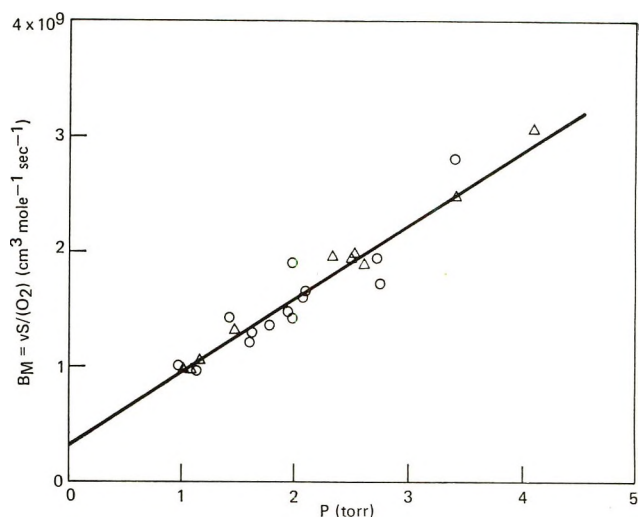


Figure 2. Plot of $vS/(O_2)$ against total pressure in reactor: $S = d \ln [(H)_0/(H)]/dz$; \circ , M = argon; Δ , M = helium.

time was insufficient for attainment of $(OH)_s$, and the (OH) could even be observed to increase while (H) was decreasing. Absolute values of (H), (OH), and (O) were only measured when the condition $(OH)_s^2 \propto (H)$ was shown to exist.

Letting the H decay slope $S = d \ln [(H)_0/(H)]/dz$, eq 7 requires that a plot of $BM = vS/(O_2)$ against (M) be linear, where v is the linear flow velocity. The results of a large number of such runs are plotted in Figure 2. The experimental slope S_e in each case was corrected for longitudinal diffusion¹¹ by the relation $S = S_e(1 + S_e D_H/v)$, where D_H is the diffusion coefficient of H in the carrier gas (Ar or He) at the pressure of the experiment. The corrections in Ar and He

(13) A. A. Westenberg and N. deHaas, *J. Chem. Phys.*, **40**, 3087 (1964).

(14) A. A. Westenberg and N. deHaas, *ibid.*, **43**, 1550 (1965).

Table I: H Decay Slopes (S) and Steady State $(\text{OH})_s$ and $(\text{O})_s$ Data (at $z = 0$) Combined According to Eq 7 and 8

| P_i Torr | v_i cm/sec | S_i cm ⁻¹ | B_M , cm ³ mol ⁻¹ sec ⁻¹ × 10 ⁸ | $\frac{(\text{H})}{(\text{O}_2)}$ × 10 ⁻⁴ | $\frac{(\text{OH})_s}{(\text{O}_2)}$ × 10 ⁻⁴ | $\frac{(\text{O})_s}{(\text{O}_2)}$ × 10 ⁻⁴ | $\frac{(\text{OH})_s}{(\text{O})_s}$ | $\frac{B_M[(\text{H})/(\text{O}_2)]}{[(\text{OH})_s/(\text{O}_2)][(\text{O})_s/(\text{O}_2)]}$ × 10 ¹⁴ |
|-------------------|-----------------|---------------------------|---|---|--|---|--------------------------------------|--|
| 2.50 ^a | 320 | 0.145 | 19.2 | 107 | 10.3 | 1.29 | 7.98 | 1.55 |
| 2.62 ^a | 300 | 0.161 | 18.9 | 68 | 8.9 | 1.40 | 6.38 | 1.03 |
| 2.33 ^a | 330 | 0.136 | 19.6 | 163 | 13.8 | 1.67 | 8.26 | 1.39 |
| 2.07 ^b | 275 | 0.103 | 16.1 | 266 | 14.8 | 2.36 | 6.27 | 1.23 |
| 2.73 ^b | 270 | 0.122 | 19.4 | 241 | 16.6 | 2.49 | 6.67 | 1.13 |
| 1.60 ^b | 425 | 0.067 | 12.1 | 210 | 11.7 | 1.89 | 6.19 | 1.15 |
| 2.11 ^b | 340 | 0.078 | 16.6 | 375 | 17.1 | 2.39 | 7.15 | 1.52 |
| | | | | | | | Av 7.0 ± 0.8 | 1.3 ± 0.2 |

^a Helium carrier. ^b Argon carrier; $B_M = vS(\text{O}_2)$.

never exceed 12 and 24%, respectively. As Figure 2 demonstrates, there is no distinction between the data with $M = \text{Ar}$ or $M = \text{He}$, a conclusion previously noted by Clyne and Thrush⁵ and in some earlier results from this laboratory.¹⁵ (The latter work over a smaller pressure range did not show the finite intercept indicating a second-order wall term clearly apparent in Figure 2.)

The slope in Figure 2 gives a value

$$2k_1(3x + 2)/(3x + 3) = 1.20 \pm 0.05 \times 10^{16} \text{ cm}^6 \text{ mol}^{-2} \text{ sec}^{-1}$$

and the intercept is

$$2k_w(3x + 2)/(3x + 3) = 3.2 \times 10^8 \text{ cm}^3 \text{ mol}^{-1} \text{ sec}^{-1}$$

Equations 5 and 8 were then applied to a number of runs in which integrated intensities were measured to determine $(\text{H})/(\text{O}_2)$, $(\text{OH})_s/(\text{O}_2)$, and $(\text{O})_s/(\text{O}_2)$ at a given injector position ($z = 0$). The results are summarized in Table I. It is seen that the quantities in the final two columns are reasonably constant as predicted, and we get

$$\frac{k_6 \left[\frac{2 - k_4/k_3}{1 + k_4/k_3} \right]}{2k_5} = 7.0 \pm 0.8$$

$$k_6(3x + 2) = 1.3 \pm 0.2 \times 10^{14} \text{ cm}^3 \text{ mol}^{-1} \text{ sec}^{-1}$$

To proceed further with these basic experimental data, we need first a value for k_6 . For this we prefer the recent work from this laboratory¹⁶ which gave $k_6 = 1.9 \pm 0.2 \times 10^{13} \text{ cm}^3 \text{ mol}^{-1} \text{ sec}^{-1}$ at room temperature. (Other literature values^{2,5,17} are in the range $3 \pm 1 \times 10^{13}$.) With the mean deviation shown, the above value for $k_6(3x + 2)$ yields $x = 1.6 \pm 0.3$. With x thus determined, the basic data then give $k_1 = 6.8 \pm 1.0 \times 10^{15} \text{ cm}^6 \text{ mol}^{-2} \text{ sec}^{-1}$ (for $M = \text{Ar}, \text{He}$), and also $k_w = 1.8 \times 10^8 \text{ cm}^3 \text{ mol}^{-1} \text{ sec}^{-1}$. The latter is, as noted earlier, specific to the present apparatus and of no particular significance, except that it is needed in analyzing the data obtained later.

The remaining data require the ratio k_6/k_5 to extract a value for k_4/k_3 . Since there are no direct data on the

ratio k_6/k_5 we must use the individual k_6 and k_5 , with the source of the former noted above. For k_5 the situation is not as well defined. There are three values in the literature obtained from careful fast flow experiments, *i.e.*, $k_5 = 0.5, 0.8$, and 1.5×10^{12} (from ref 17, 2, and 9). The first value was obtained after quite a sizable correction for a first-order wall loss of OH which was not observed in the other two experiments. In any case, k_5 seems uncertain by at least a factor of 2 (and perhaps 3). Exercising the privilege of personal bias and using the value $k_5 = 1.5 \times 10^{12}$, the present basic data give $k_4/k_3 = 0.39 \pm 0.06$, where the indicated error represents simply the mean deviation of the experimental $(\text{OH})_s/(\text{O})_s$ from which k_4/k_3 was derived *via* eq 5. The experimental data and the results derived from them are summarized in Table II.

In comparing these results with others available in the literature we note first that our value of 1.20×10^{16} for $2k_1(3x + 2)/(3x + 3)$ is in near-perfect agreement with the 1.26×10^{16} reported by Clyne and Thrush,⁵ which should be the case since this quantity reflects simply the basic H decay slope as a function of (M) . They also derived a value of $x = 0.5 \pm 0.2$ by an entirely different method than ours, namely, by measuring the ratio of H_2O formed to H consumed, which can be shown to equal $(3x + 2)^{-1}$ if HO_2 , OH, and O are in steady state. Since their value of x was based on only three estimates of this quantity, requiring a difficult H_2O measurement, the fact that it is in poor agreement with our $x = 1.6$ is not too disturbing. The latter value would appear more reliable. Bennett and Blackmore¹⁸ have estimated x to be 0.5–1.0, again with considerable uncertainty.

The k_1 extracted is not very sensitive to the x value, and our $k_1 = 6.8 \pm 1.0 \times 10^{15}$ agrees well with Clyne

(15) A. A. Westenberg, J. M. Roscoe, and N. deHaas, *Chem. Phys. Lett.*, **7**, 597 (1970).

(16) A. A. Westenberg, N. deHaas, and J. M. Roscoe, *J. Phys. Chem.*, **74**, 3431 (1970).

(17) J. E. Breen and G. P. Glass, *J. Chem. Phys.*, **52**, 1082 (1970).

(18) J. E. Bennett and D. R. Blackmore, "Thirteenth Symposium on Combustion," The Combustion Institute, Pittsburgh, Pa., 1971, p 51.

Table II: Results Derived from Steady-State Analysis of H-O₂-M System (M = Ar, He)

| Quantity | Value | Remarks |
|--|--|--|
| Basic Data | | |
| $k_6(3x + 2)$ | $1.3 \pm 0.2 \times 10^{14}$ (cm ³ mol ⁻¹ sec ⁻¹) | From data of Table I and eq 8 |
| $2k_1(3x + 2)/(3x + 3)$ | $1.20 \pm 0.05 \times 10^{16}$ (cm ⁶ mol ⁻² sec ⁻¹) | From data of Figure 2 and eq 9 |
| $\frac{k_6(2 - k_4/k_3)}{2k_5(1 + k_4/k_3)}$ | 7.0 ± 0.8 | From data of Table I and eq 5 |
| Derived Data | | |
| $x = k_2/(k_3 + k_4)$ | 1.6 ± 0.3^a 0.8 | Uses $k_6 = 1.9 \pm 0.2 \times 10^{13}$ Uses $k_6 = 3 \times 10^{13}$ |
| k_1 | $6.8 \pm 1.0 \times 10^{16}^a$ 7.3×10^{16} (cm ⁶ mol ⁻² sec ⁻¹) | Uses $x = 1.6 \pm 0.3$ Uses $x = 0.8$ |
| k_4/k_3 | 0.39 ± 0.06^a 0.76 0.89 1.18 | Uses $k_6/k_5 = 19/1.5 = 12$ Uses $k_6/k_5 = 30/1.5 = 20$ Uses $k_6/k_5 = 19/0.8 = 24$ Uses $k_6/k_5 = 30/0.8 = 37$ |
| $k_2/k, k_3/k, k_4/k$ | 0.62, 0.27, 0.11 ^a 0.44, 0.32, 0.24 0.62, 0.20, 0.18 0.44, 0.26, 0.30 | Uses $x = 1.6, k_4/k_3 = 0.39$ Uses $x = 0.8, k_4/k_3 = 0.76$ Uses $x = 1.6, k_4/k_3 = 0.89$ Uses $x = 0.8, k_4/k_3 = 1.18$ |

^a Preferred result.

and Thrush's 7.9×10^{15} . The pulse radiolysis value of Hikida, *et al.*,⁸ is $5.9 \pm 0.3 \times 10^{15}$, which is also in agreement with our own within experimental error.

The distribution of the rates between the three possible paths k_2, k_3, k_4 is given at the bottom of Table II. It is in rather poor agreement with the distribution 0.43, 0.05, 0.52 reported by Dodonov, *et al.*,¹⁹ although their method seems considerably less direct than our own. The main disagreement is in the relative importance of k_3 and k_4 . We believe our distribution may be reasonable, however. The respective exothermicities of the three paths are 57, 38, and 55 kcal/mol. Since reactions 2 and 3 both involve the simple abstraction of H or O from either end of the H-O-O radical, it would be expected that $k_2 > k_3$, since the H-O bond in HO₂ is considerably weaker than the O-O bond. Reaction 4 is the slowest of the trio, which is also not surprising. Even though the exothermicity is about the same as reaction 2 it is a reaction where the colliding H must take the place of the end O atom in H-O-O, a relatively unlikely process. These conclusions about the relative importance of reactions 2, 3, and 4 are not significantly affected by the uncertainty in k_5 noted earlier. The value assumed for k_6 also affects the distribution, and the various possibilities are given in Table II. We prefer the combination $k_6 = 1.9 \times 10^{13}$, $k_5 = 1.5 \times 10^{12}$.

We are now in a position to consider the results of adding CO to the H-O₂-M reacting mixture. Unlike the case without CO, there is now no simple proportionality between (OH) and (H) to test the attainment

of a steady-state condition. The time required for attaining a steady state (HO₂) is not lengthened by adding (CO), and under similar conditions this should still be very short (of the order of a millisecond, which is similar to the mixing time itself). Thus, let us assume first that *only* (HO₂) is in steady state. As shown earlier, this leads to eq 10 for (HO₂)_s and the integral relation given as eq 11. Knowing all the rate constants (or ratios) which appear in this equation (from the results without CO, and elsewhere) a measurement of (H)/(O₂) and (OH)/(O₂) between two positions of the movable injector allows k_7/k_3 to be determined by iteration. Let us call this method I.

Numerical values required in eq 11 were those derived from this work as given in Table II, in addition to $k_5 = 1.5 \times 10^{12}$ as discussed earlier, and $k_8 = 1.0 \times 10^{11}$ (the average of values from ref 9 and 10). Actually, the second term on the right side of eq 11 contributes very little, so that the precise value assumed for k_5 is not very important. The integrals were evaluated numerically using various assumed values of k_7/k_3 , the measurements (taken at 5-cm intervals) extending over a distance of 20 or 30 cm in the reactor (≈ 60 - 90 msec). The k_7/k_3 values giving the best fit to the measured changes in H and OH on the left side of eq 11 are summarized in Table III as method I.

The second method of data analysis in the presence of CO is to assume both OH and O are in steady state

(19) A. F. Dodonov, G. K. Lavrovskaya, and V. L. Tal'roze, *Kinet. Katal.*, **10**, 701 (1969).

Table III: Summary of Results for $k_7/k_3^{a,b}$

| P. Torr | (O ₂) × 10 ⁸ , mol/cm ³ | (CO) × 10 ⁸ , mol/cm ³ | (CO)/(H) (at z = 0) | (OH)/(H) | k_7/k_3 | |
|------------|--|---|------------------------|----------|-----------|-----------|
| | | | | | Method I | Method II |
| 2.08 | 2.54 | 0.92 | 19.2 | 0.025 | 0.045 | Neg. |
| 1.95 | 2.14 | 0.95 | 21.4 | 0.018 | 0.032 | 1.82 |
| 3.27 | 3.29 | 1.02 | 26.6 | 0.035 | 0.077 | 0.34 |
| 3.86 | 3.43 | 1.45 | 59.7 | 0.033 | 0.043 | 0.28 |
| 3.78 | 3.34 | 0.81 | 33.3 | 0.053 | 0.075 | 0.29 |
| 5.25 | 3.15 | 0.80 | 28.6 | 0.062 | 0.10 | 0.28 |
| 3.47 | 2.93 | 0.84 | 25.9 | 0.038 | 0.055 | 0.28 |
| 3.48 | 2.94 | 0.82 | 25.0 | 0.042 | ... | 0.49 |
| 2.77 | 2.34 | 0.65 | 12.7 | 0.026 | ... | 0.21 |
| 3.52 | 2.99 | 0.86 | 28.5 | 0.041 | ... | 0.36 |

Av 0.06 ± 0.02

^a Method I: (HO₂) assumed in steady state, iteration in eq 11. Method II: (HO₂), (OH), and (O) assumed in steady state, eq 12 and 13. ^b Constants used: $k_1 = 6.8 \pm 1.0 \times 10^{16}$, $k_w = 1.8 \times 10^8$, $k/k_3 = 3.70$, $k_4/k_3 = 0.39 \pm 0.06$, $x = 1.6 \pm 0.3$, $k_5 = 1.5 \times 10^{12}$, $k_8 = 1.0 \times 10^{11}$.

(in addition to HO₂) and use eq 12 and 13. This is a simpler procedure of course, since the solution for k_7/k_3 is in closed form. A summary of results with this method is given in the final column of Table III, using the same required constants as with method I and the measured (OH) and (H) at the $z = 0$ position. The difference in the results by the two methods is apparent. Except for the first two runs which seem clearly anomalous, the k_7/k_3 values by method II show somewhat less scatter than those by I and are consistently higher. In view of the additional assumptions involved in II, however, and the lack of a good way to check that (OH) and (O) really attain a steady-state condition as assumed, we are inclined to favor the results of method I. It seems most unlikely that the addition of CO to the H-O₂-M system, which was shown earlier to give the behavior expected of a steady-state (HO₂) condition, would cause this assumption to be invalidated, since all the CO does to HO₂ is to add to its consumption rate. This could only tend to make the steady-state (HO₂) assumption *more* valid, and it is the only assumption involved in method I. On the other hand, it is conceivable that the addition of an appreciable OH generating reaction such as reaction 7 might upset the (OH) steady-state condition and invalidate method II. This point remains moot.

The value for k_7/k_3 measured (about 0.06 by method I) seems somewhat unexpected at first sight, since it implies that reaction 7 must be moderately fast if reaction 3 is very fast, as is likely. For example, if $k_3 \simeq 10^{13}$ (the analogous reaction $H + NO_2 \rightarrow NO + OH$ has a rate constant²⁰ of 3×10^{13}), then we would have $k_7 \simeq 6 \times 10^{11}$. The only previous estimate of k_7 in the literature (based on anything more than conjecture) of which we are aware is that of Baldwin and coworkers²¹ from the CO-sensitized decomposition of H₂O₂ at 440°, who infer that the activation energy E_7 is at least 23 kcal/mol. Based on their estimated pre-exponential factor of 6×10^{13} (which is "normal"),

this would give a completely negligible k_7 at room temperature, which is at variance with the conclusion of the present work.

On closer examination it seems to us that there is no reason why k_7 should not be reasonably large—comparable to k_8 , or even larger. Reaction 7 is considerably more exothermic than reaction 8 (64 kcal/mol compared to 25). Both reactions represent the abstraction of an O atom by CO, and the O-O bond broken in HO₂ is much weaker than the O-H bond in OH, as reflected by the difference in exothermicity. Thus on an energetic basis it might be expected that $k_7 \geq k_8$. Nor are there any spin conservation problems with reaction 7, which is analogous to reaction 8 in this respect. We conclude, therefore, that our result for k_7 is reasonable and that a very high activation energy for this reaction would be surprising.

Appendix

To communicate a feeling for the sensitivity of the derived k_7/k_3 to the basic experimental measurements, the iteration for the first run in Table III will be outlined as a typical example. Over a 20-cm range in the reactor, the ratio (H)/(O₂) decreased from 189×10^{-4} to 50×10^{-4} , while (OH)/(O₂) decreased from 4.8×10^{-4} to 1.8×10^{-4} . Thus the left side of eq 11 had an experimental value $\Delta = 142 \pm 19 \times 10^{-4}$, where the assigned error limit represents the pessimistic estimated error¹³ of about ±10% in measuring the esr integrated intensities. The dominance of the (H) measurement in determining Δ is apparent. We now use the rate constant values indicated above and iterate the right side of eq 11 with k_7/k_3 (numerically integrating at 5-cm intervals corresponding to the measured decays of H and OH). Denote the first

(20) L. F. Phillips and H. I. Schiff, *J. Chem. Phys.*, **37**, 1233 (1962).

(21) R. R. Baldwin, R. W. Walker, and S. J. Webster, *Combust. Flame*, **15**, 167 (1970).

Table IV

| I_2 | Assumed k_7/k_3 | I_1 | $I_1 + I_2$ |
|----------------------|----------------------|----------------------|----------------------|
| 4.5×10^{-4} | 0 | 192×10^{-4} | 196×10^{-4} |
| | 0.01 | 176 | 180 |
| | 0.02 | 162 | 166 |
| | 0.03 | 152 | 156 |
| | 0.04 | 142 | 146 |
| | 0.05 | 133 | 137 |

term on the right side of eq 11 by I_1 and the second by I_2 , the value of k_7/k_3 affecting only I_1 . The iteration

in Table IV was then obtained. Interpolation between the last two iterations yields the $k_7/k_3 = 0.045$ given in Table III. From the error estimated for Δ one would infer an error of about ± 0.02 in k_7/k_3 . The result is more sensitive to the value used for k/k_3 . If a k/k_3 larger than the 3.70 (a lower limit according to the possibilities of Table II) measured in the present work (with no CO) is used, the values of k_7/k_3 derived from the data would be larger than those quoted in Table III. For example, use of $k/k_3 = 5$ gives an iteration value $k_7/k_3 = 0.08$ instead of 0.045 for the first run in Table III.

Substituent Effects. IX. Correlation of Carbon-13, Proton-1, and Fluorine-19 Nuclear Magnetic Resonance Chemical Shifts of Some Aromatic Compounds by Pairwise Additivity

by Edmund R. Malinowski

Department of Chemistry and Chemical Engineering, Stevens Institute of Technology, Hoboken, New Jersey 07030
(Received January 6, 1972)

Publication costs borne completely by The Journal of Physical Chemistry

Carbon-13 shifts of heterocyclic nitrogen-containing aromatic compounds are found to be pairwise additive. Proton shifts of chloro- and hydroxy-substituted benzenes also obey pairwise additivity. Similarly, the fluorine shifts of chlorinated perfluorobenzenes are pairwise additive. The additivity scheme is expressed in terms of pairwise corrections to direct additivity. The pairwise corrections are believed to be the result of interactions between pairs of substituents within the molecule, in accord with the theoretical work of Vladimiroff and Malinowski.

Introduction

Empirical correlations of nmr chemical shifts are extremely useful for assigning shifts and, hence, for deducing the structures of molecules. Such schemes are usually based upon the observation of shifts of a series of molecules which differ in structure in some systematic manner, such as the introduction of substituent groups into parent molecules. An ideal correlation involves a minimum number of empirical parameters while yielding a maximum degree of accuracy. Furthermore, empirical correlations provide valuable clues for deciphering the theoretical nature of nmr phenomena.

The pairwise additivity rule is a general scheme which has been shown¹ to be obeyed by a large variety of nuclei and a large variety of molecular systems. Spin-spin couplings as well as chemical shifts have been correlated

with the pairwise rule. For example, the shifts of carbon-13,² fluorine-19,¹ boron-11,¹ aluminum-27,³ and proton-1¹ and couplings such as C-H,⁴⁻⁶ C-F,⁷ Si-H,⁷ and Sn-H⁸ follow pairwise additivity. Using McWeeny group functions, Vladimiroff and Malinowski¹ were able

(1) T. Vladimiroff and E. R. Malinowski, *J. Chem. Phys.*, **46**, 1830 (1967).

(2) E. R. Malinowski, T. Vladimiroff, and R. F. Tavares, *J. Phys. Chem.*, **70**, 2046 (1966).

(3) E. R. Malinowski, *J. Amer. Chem. Soc.*, **91**, 4701 (1969).

(4) E. R. Malinowski, L. Z. Pollara, and J. P. Larmann, *ibid.*, **84**, 2649 (1962).

(5) E. R. Malinowski, *ibid.*, **83**, 4479 (1961).

(6) A. W. Douglas, *J. Chem. Phys.*, **40**, 2413 (1964).

(7) T. Vladimiroff and E. R. Malinowski, *J. Amer. Chem. Soc.*, **86**, 3575 (1964).

(8) T. Vladimiroff and E. R. Malinowski, *J. Chem. Phys.*, **42**, 440 (1965).

to theoretically account for pairwise additivity in nmr in a general fashion. They showed that the pairwise contributions arise when the wave function of each substituent group suffers a linear correction due to the presence of each neighboring group.

The present investigation is a continuation of the study of pairwise additivity. In particular we wish to draw attention to the fact that carbon-13, proton-1, and fluorine-19 shifts of aromatic compounds obey pairwise additivity.

¹³C Shifts of Heterocyclic Nitrogen-Containing Aromatic Compounds

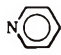
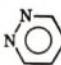
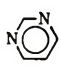

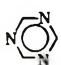
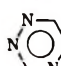
We focused attention on the carbon-13 shifts of six-membered nitrogen heterocycles to see the effect on the shift when a C-H group of benzene was replaced by a nitrogen atom. Using the data of Lauterbur,⁹ we first investigated direct additivity. The direct additive terms are readily obtainable by referencing the ¹³C shifts of pyridine with respect to benzene. For carbon nuclei located at positions α , β , and γ to the nitrogen, the direct additive contributions are -21.9 , $+4.2$, and -7.7 ppm, respectively. Table I shows a comparison between the experimental shifts and those calculated by direct additivity when applied to aromatic compounds containing two or more nitrogens. The difference between the observed and calculated shifts is as large as 13.3 ppm, far in excess of experimental error, which is estimated to be approximately ± 0.2 ppm.

For the heterocyclic aromatic compounds containing two nitrogen atoms, these differences are caused by nitrogen-nitrogen interactions and can be viewed as a nitrogen-nitrogen pairwise term. Each term varies according to the exact location of the nitrogen atoms in the molecule. Symbols o, m, and p, as shown in Table I, are used to designate the positions of the nitrogens relative to one another, *i.e.*, ortho, meta, and para. For example, $(\alpha \gamma)_m$ symbolizes the pairwise correction when one nitrogen is α and the other γ to the carbon-13 in question, and the nitrogens are meta to each other. Throughout the entire correlation, it is essential that all shifts be referenced with respect to benzene in the same solvent, although the experimental measurements may be carried out relative to some other standard.

For *s*-triazine, direct additivity yields a shift of -51.5 ppm, which is in poor agreement with the experimental value, -39.0 ppm (see Table I). The inclusion of pairwise terms gives $\delta = 2\alpha + \gamma + (\alpha \alpha)_m + 2(\alpha \gamma)_m = -36.8 \pm 2.4$ ppm, which agrees favorably with the experimental value.

For *s*-tetrazine, direct additivity yields $\delta = 2\alpha + 2\beta = -35.4$ ppm, whereas pairwise additivity yields $\delta = 2\alpha + 2\beta + (\alpha \alpha)_m + 2(\alpha \beta)_o + 2(\alpha \beta)_p + (\beta \beta)_m = -36.2 \pm 4.8$ ppm. Both of these predictions agree with the observed value -33.4 ppm. However, the agreement with direct additivity, in this case, is

Table I: Comparison between Observed ¹³C Shift and That Calculated by Direct Additivity. Direct and Pairwise Parameters

| Compound | Obsd ^a ¹³ C shifts, ppm | Calcd by direct additivity, ppm | Dif- ference, ^b ppm | Pair- wise param- eter, NN |
|---|--|---|---|--|
|  | -21.9 $+4.2$ -7.7 | α β γ | | |
|  | -23.9 $+1.0$ | $\alpha + \beta = -17.7$ $\beta + \gamma = -3.5$ | $-6.2 = (\alpha \beta)_o$ $+4.5 = (\beta \gamma)_o$ | |
|  | -30.5 -28.9 $+6.1$ | $2\alpha = -43.8$ $\alpha + \gamma = -29.6$ $2\beta = +8.4$ | $+13.3 = (\alpha \alpha)_m$ $+0.7 = (\alpha \gamma)_m$ $-2.3 = (\beta \beta)_m$ | |
|  | -17.4 | $\alpha + \beta = -17.7$ | $+0.3 = (\alpha \beta)_p$ | |
|  | -39.0 | $2\alpha + \gamma = -51.5$ | $+12.5$ | |
|  | -33.4 | $2\alpha + 2\beta = -35.4$ | $+2.0$ | |

^a Relative to external benzene. ^b Estimated reliability is ± 0.6 ppm.

fortuitous, since the six pairwise contributions almost cancel one another.

For 1,2,4-triazine, direct additivity predicts the shifts of carbons 3, 5, and 6 to be -39.6 , -25.4 , and -13.5 ppm, respectively. In marked contrast, the inclusion of the pairwise terms yields -32.2 , -19.9 , and -21.7 ppm, respectively. The ¹³C spectrum of this molecule has not been reported and, consequently, a comparison with experiment cannot be made at this time. These calculations, however, illustrate how the pairwise correlation can be used as a guide for making spectral assignments.

¹H Shifts of Substituted Benzenes

Many attempts have been made to correlate ring proton shifts of substituted benzenes with substituent parameters.¹⁰⁻¹⁸ Anomalies from direct additivity have led research workers to conclude that a variety of ef-

- (9) P. C. Lauterbur, *J. Chem. Phys.*, **43**, 360 (1965).
- (10) P. Diehl, *Helv. Chim. Acta*, **44**, 829 (1961).
- (11) J. S. Martin and B. P. Dailey, *J. Chem. Phys.*, **39**, 1722 (1963).
- (12) T. K. Wu and B. P. Dailey, *ibid.*, **41**, 2796 (1964).
- (13) W. A. Gibbons and V. M. S. Gil, *Mol. Phys.*, **9**, 163, 167 (1965).
- (14) F. Hruska, H. M. Hutton, and T. Schaefer, *Can. J. Chem.*, **43**, 2392 (1965).
- (15) W. B. Smith and J. L. Roark, *J. Amer. Chem. Soc.*, **89**, 5018 (1967).
- (16) J. E. Loemker, J. M. Read, Jr., and J. H. Goldstein, *J. Phys. Chem.*, **72**, 991 (1968).
- (17) Y. Nomura and Y. Takeuchi, *Org. Magn. Resonance*, **1**, 213 (1969).
- (18) J. J. R. Reed, *Anal. Chem.*, **39**, 1586 (1967).

Table II: Direct and Pairwise Contributions to Proton Shifts of Substituted Benzenes

| Molecule | | Direct Contributions | | |
|----------------------------------|------------|--------------------------------------|--------------------------|---|
| | | Obsd proton shifts, ppm ^a | | |
| | | α | β | γ |
| C ₆ H ₅ Cl | | -0.03 ^b | +0.02 ^b | +0.09 ^b |
| C ₆ H ₅ OH | | +0.53 ^c | +0.12 ^c | +0.43 ^c |
| | | Pairwise Corrections | | |
| Substituted benzene | Proton | Direct additivity, ppm | Obsd, ^{a,c} ppm | Diff = pair correction, ppm |
| 1,2-Cl | 3, 6 | -0.01 | -0.16 | -0.15 = (α -Cl β -Cl) _o |
| | 4, 5 | +0.11 | +0.09 | -0.02 = (β -Cl γ -Cl) _o |
| 1,3-Cl | 2 | -0.06 | -0.10 | -0.04 = (α -Cl α -Cl) _m |
| | 4, 6 | +0.06 | +0.06 | 0.00 = (α -Cl γ -Cl) _m |
| | 5 | +0.04 | +0.06 | +0.02 = (β -Cl β -Cl) _m |
| 1,4-Cl | 2, 3, 5, 6 | -0.01 | +0.01 | +0.02 = (α -Cl β -Cl) _p |
| 1-OH, 2-Cl | 3 | +0.09 | 0.00 | -0.09 = (α -Cl β -OH) _o |
| | 4 | +0.45 | 0.46 | +0.01 = (β -Cl γ -OH) _o |
| | 5 | +0.21 | 0.11 | -0.10 = (γ -Cl β -OH) _o |
| | 6 | +0.55 | 0.29 | -0.26 = (β -Cl α -OH) _o |
| 1-OH, 3-Cl | 2 | +0.50 | 0.46 | -0.04 = (α -Cl α -OH) _m |
| | 4 | +0.40 | 0.39 | -0.01 = (α -Cl γ -OH) _m |
| | 5 | +0.14 | 0.14 | 0.00 = (β -Cl β -OH) _m |
| | 6 | +0.62 | 0.60 | -0.02 = (γ -Cl α -OH) _m |
| 1-OH, 4-Cl | 2, 6 | +0.55 | 0.55 | 0.00 = (β -Cl α -OH) _p |
| | 3, 5 | +0.09 | 0.10 | +0.01 = (α -Cl β -OH) _p |

^a Measured at 4.0 wt % in CCl₄ and referenced with respect to external benzene at 4.0 wt % in CCl₄. Downfield shifts are negative.

^b Based on data of K. Hayamizu and O. Yamamoto, *J. Mol. Spectrosc.*, **28**, 89 (1968). ^c Based on data of J. J. R. Reed, *Anal. Chem.*, **39**, 1586 (1967).

fects (such as magnetic anisotropy, electric fields, steric interactions, etc.) are operative. Recently, Reed¹⁸ postulated that the substituent affects the aromatic ring protons in just three distinct ways: (1) directly through space (restricted to ortho protons), (2) indirectly by influencing the ring which then interacts with the proton, and (3) a sandwich effect produced by the mutual interaction between a pair of α substituents which flank the proton. This empirical approach has been the most successful to date. The purpose of the present paper is to draw attention to the fact that the proton shifts of aromatic compounds obey pairwise additivity and that all of the above postulated effects are taken into account by this correlation.

The introduction of substituent groups into the benzene ring system does not alter the spatial geometry of the ring and does not destroy the π -electron system, though it causes alterations in the electronic wave functions of the groups and π electrons. Following the arguments of Vladimiroff and Malinowski,¹ we first choose benzene to represent the core molecule. When a hydrogen is replaced by a substituent, the electronic wave functions, including the π electrons, experience a perturbation. When a second substituent is introduced, all of the electrons, including those belonging to the first substituent, experience an additional perturbation. According to Vladimiroff and Malinow-

ski, a first-order perturbation in the electronic wave functions of one group, upon the introduction of another group, gives rise to a pairwise contribution to the chemical shift.

From the shifts of monosubstituted benzenes, we can determine the direct effects of substituents located α , β , and γ to the proton in question. These values for chlorine and hydroxyl groups are listed in Table II. For some disubstituted benzenes, Table II also shows a comparison between the observed shifts and those calculated by direct additivity. For *o*-dichlorobenzene, this difference is as large as 0.15 ppm, far in excess of experimental error, which is estimated to be approximately ± 0.01 ppm. This difference represents the contribution due to the pair of substituents. In designating this pairwise term, we use the symbol (α -Cl α -Cl)_m to indicate that both chlorines are located α to the proton in question and meta to one another.

Using the direct substituent effects and the pairwise corrections listed in Table II, we calculated the proton shifts of a large variety of highly substituted benzenes containing chlorine and hydroxyl groups. The details of these calculations are presented in Table III. The agreement between the predicted and observed values is excellent. When pairwise terms are not included, the correlation shows severe deviations from the observed shifts.

Table III: Comparison between Calculated and Observed Proton Shifts^a of Highly Substituted Benzenes

| Substituted benzene | Proton | Direct additivity, ppm | Pairwise additivity, ppm | Obsd. ^b ppm |
|---------------------|---------|------------------------|--------------------------|------------------------|
| 1,2,3-Cl | 4, 6 | +0.08 | -0.09 | -0.10 |
| | 5 | +0.13 | +0.11 | +0.15 |
| 1,2,4-Cl | 3 | -0.04 | -0.21 | -0.21 |
| | 5 | +0.08 | +0.08 | +0.10 |
| | 6 | +0.01 | -0.10 | -0.12 |
| 1,3,5-Cl | 2, 4, 6 | +0.03 | -0.01 | 0.00 |
| 1,2,3,4-Cl | 5, 6 | +0.10 | -0.05 | -0.05 |
| 1,2,3,5-Cl | 4, 6 | +0.05 | -0.14 | |
| 1,2,4,5-Cl | 3, 6 | -0.02 | -0.32 | -0.31 |
| 1,2,3,4,5-Cl | 6 | +0.07 | -0.25 | -0.30 |
| 1-OH, 2,3-Cl | 4 | +0.42 | +0.27 | +0.27 |
| | 5 | +0.23 | +0.11 | +0.16 |
| | 6 | +0.64 | +0.34 | +0.36 |
| 1-OH, 2,4-Cl | 3 | +0.06 | -0.06 | -0.06 |
| | 5 | +0.18 | +0.09 | +0.13 |
| | 6 | +0.57 | +0.33 | +0.33 |
| 1-OH, 2,6-Cl | 3, 5 | +0.18 | -0.01 | +0.04 |
| | 4 | +0.47 | +0.51 | +0.49 |
| 1-OH, 3,4-Cl | 2 | +0.52 | +0.33 | +0.34 |
| | 5 | +0.11 | -0.03 | -0.01 |
| | 6 | +0.64 | +0.60 | +0.61 |
| 1-OH, 3,5-Cl | 2, 6 | +0.59 | +0.53 | +0.55 |
| | 4 | +0.37 | +0.31 | +0.31 |
| 1-OH, 2,4,5-Cl | 3 | +0.08 | -0.17 | -0.17 |
| | 6 | +0.49 | +0.08 | +0.11 |
| 1-OH, 2,4,6-Cl | 3, 5 | +0.15 | -0.07 | -0.01 |

^a Measured at 4.0 wt % in CCl₄ and referenced with respect to external benzene at 4.0 wt % in CCl₄. Downfield shifts are negative. ^b Based on data of J. J. R. Reed, *Anal. Chem.*, **39**, 1586 (1967).

¹⁹F Shifts of Chlorine-Substituted Perfluorobenzenes

The arguments presented here are of a general nature and are applicable to ¹⁹F shifts of substituted fluorobenzenes. In this case it is essential that all shifts be referenced with respect to hexafluorobenzene. It is also important that all measurements be conducted in the same solvent at the same temperature and at infinite dilution in order to minimize solvent effects and molecular interactions between the solute molecules. The data of Boden, Emsley, Feeney, and Sutcliffe¹⁹ meet all of these criteria and were utilized in the present study.

Table IV shows the direct effect of chlorine upon the ¹⁹F shifts of substituted perfluorobenzenes. For molecules containing two or more chlorines, deviations from direct additivity are due to pairwise interactions. Values for such contributions are deduced as shown in Table IV. Table V shows a comparison between direct

and pairwise additivity used in the prediction of the shifts of various tri-, quater-, and quaterchloro-substituted perfluorobenzenes. Although the pairwise terms are relatively small in comparison to the direct terms, we see that their inclusion produces noticeable improvement in predictability.

Table IV: Direct Contributions and Pairwise Corrections to Fluorine Shifts^a and Chloro-Substituted Perfluorobenzenes

| Direct Contribution, ^a ppm | | | | |
|---------------------------------------|--------------|------------------------|------------------------|---|
| | α -Cl | β -Cl | γ -Cl | |
| | 21.69 | 1.03 | 6.22 | |
| Pairwise Corrections | | | | |
| Substituted perfluorobenzene | Fluorine | Direct additivity, ppm | Obsd. ^a ppm | Diff = pair correction, ppm |
| 1,2-Cl | 3, 6 | 22.72 | 26.17 | +3.45 = (α -Cl β -Cl) _o |
| | 4, 5 | 7.25 | 6.65 | -0.60 = (β -Cl γ -Cl) _o |
| 1,3-Cl | 2 | 43.38 | 43.88 | +0.50 = (α -Cl α -Cl) _m |
| | 4, 6 | 27.91 | 27.74 | -0.17 = (α -Cl γ -Cl) _m |
| | 5 | 2.06 | 1.64 | -0.32 = (β -Cl β -Cl) _m |
| 1,4-Cl | 2, 3, 5, 6 | 22.72 | 22.28 | -0.56 = (α -Cl β -Cl) _p |

^a Measured at infinite dilution in CCl₄ and referenced with respect to external hexafluorobenzene at infinite dilution in CCl₄; data of N. Boden, J. W. Emsley, J. Feeney, and L. H. Sutcliffe, *Mol. Phys.*, **8**, 133 (1964).

Table V: Fluorine Shifts Calculated by Direct and Pairwise Additivity Compared to Observed Shifts^a

| Substituted perfluorobenzene | Fluorine | Direct additivity, ppm | Pairwise additivity, ppm | Obsd. ^a ppm |
|------------------------------|----------|------------------------|--------------------------|------------------------|
| 1,2,3-Cl | 4, 6 | 28.93 | 31.71 | 31.71 |
| | 5 | 8.27 | 6.76 | 6.51 |
| 1,2,4-Cl | 3 | 44.41 | 47.80 | 47.88 |
| | 5 | 28.93 | 27.61 | 27.69 |
| | 6 | 23.74 | 26.32 | 26.14 |
| 1,3,5-Cl | 2, 4, 6 | 49.60 | 49.76 | 49.59 |
| 1,2,3,4-Cl | 5, 6 | 29.96 | 31.17 | 31.35 |
| | 3, 6 | 45.44 | 51.40 | 51.18 |
| 1,3,4,5-Cl | 2, 6 | 50.63 | 53.08 | 53.27 |
| | 6 | 51.66 | 56.08 | 56.83 |

^a Measured at infinite dilution in CCl₄ and referenced with respect to external hexafluorobenzene at infinite dilution in CCl₄; data of N. Boden, J. W. Emsley, J. Feeney, and L. H. Sutcliffe, *Mol. Phys.*, **8**, 133 (1964).

(19) N. Boden, J. W. Emsley, J. Feeney, and L. H. Sutcliffe, *Mol. Phys.*, **8**, 133 (1964).

Action of Hemoglobin. Cooperative and Bohr Effects

by H. A. Saroff

National Institute of Arthritis and Metabolic Diseases, National Institutes of Health, Public Health Service, U. S. Department of Health, Education and Welfare, Bethesda, Maryland 20014 (Received May 13, 1971)

Publication costs assisted by the National Institutes of Health

Present models for the action of hemoglobin separate the cooperative effect (steepening of the oxygen binding curve) from the Bohr effect (shift in oxygen binding curve with pH). This approach is shown to be inconsistent with the effects of both pH and salt concentration on the action of hemoglobin. A model is proposed in which both the Bohr effect and the cooperative effect derive from the properties of the Bohr sites.

Introduction

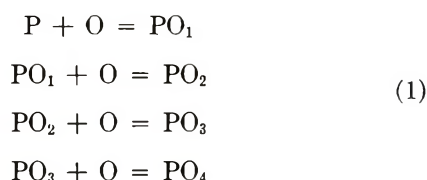
Oxygen binding to hemoglobin is characterized by a perturbed reaction of the simple equilibrium $H_b + O_2 = H_bO_2$, where H_b is a subunit of hemoglobin to which one oxygen molecule binds. The perturbation of the simple equilibrium is one which increases the rate of change of oxygen binding with change in oxygen concentration or pressure. The phenomenon is considered to be a cooperative one, and the factor representing the free energy of stabilization was called the heme-heme interaction factor by Pauling.¹ In this paper, a model is developed for this reaction where the oxygen-linked Bohr² sites generate the cooperative phenomena.

The essential difference between the model of this paper and the Pauling-Wyman models that have been generally used lies in the assumptions made on the nature of the interactions between the hemes (oxygen binding sites) and the acid groups (Bohr sites). In the Pauling-Wyman model, interactions are assumed to occur between (1) a heme and the acid groups of its own subunit and (2) a heme and the heme of a neighboring subunit. No interactions are assumed to occur between a heme and the acid groups of a neighboring subunit.

In the model of this paper the acid groups are assumed to be located between the subunits. The interactions are assumed to occur between a heme and all of the acid groups bordering on the domain of its subunit. No interactions are assumed to occur between a heme and the heme of a neighboring subunit.

The Adair, Hill, and Statistical Equations

Consider the following series of reactions



where P represents the hemoglobin tetramer, O the molecule O_2 , and PO_i the hemoglobin tetramer with i

molecules of bound oxygen. The number of oxygen molecules bound per mole of hemoglobin tetramer, \bar{v}_0 , is then defined as follows.

$$\bar{v}_0 = \frac{\sum_{i=0}^4 i PO_i}{\sum_{i=0}^4 PO_i} \quad (2)$$

An apparent constant, K_i , defines each step of these reactions by the equation

$$\frac{\sum PO_i}{\sum PO_{(i-1)}} = K_i c_0 \quad (3)$$

where c_0 is the concentration of oxygen, or oxygen pressure. Equations 2 and 3 combined give rise to the Adair equation³

$$\frac{\bar{v}_0}{4} = y = \frac{K_1 c_0 + 2K_1 K_2 c_0^2 + 3K_1 K_2 K_3 c_0^3 + 4K_1 K_2 K_3 K_4 c_0^4}{4(1 + K_1 c_0 + K_1 K_2 c_0^2 + K_1 K_2 K_3 c_0^3 + K_1 K_2 K_3 K_4 c_0^4)} \quad (4)$$

When the relative concentration of species P (or the sum of all species containing no oxygen) in eq 1 is taken as unity, then the relative concentrations of the species represented by PO_1 , PO_2 , PO_3 , and PO_4 are $K_1 c_0$, $K_1 K_2 c_0^2$, $K_1 K_2 K_3 c_0^3$, and $K_1 K_2 K_3 K_4 c_0^4$, respectively. Once eq 1 is assumed to obtain, the four apparent constants of Adair may be determined from oxygen binding data and represent values to which all parameters may be related.

If intermediate species are considered to have a concentration of zero, then $[P] + n[O] = [PO_n]$ and

$$\bar{v}_0 = \frac{n[PO_n]}{[P] + [PO_n]} = \frac{nKc_0^n}{1 + Kc_0^n} \quad (5)$$

where $K = [PO_n]/[P]c_0^n$. When the value of \bar{v}_0 is normalized by dividing by four

$$y = \bar{v}_0/4 = Kc_0^n/(1 + Kc_0^n) \quad (6)$$

(1) L. Pauling, *Proc. Nat. Acad. Sci. U. S.*, **21**, 186 (1935).

(2) C. Bohr, K. Hasselbach, and A. Krogh, *Skand. Arch. Physiol.*, **16**, 402 (1904).

(3) G. S. Adair, *J. Biol. Chem.*, **63**, 529 (1925).

Equation 6 is the equation of Hill.⁴ Because of its simplicity, the equation of Hill is used to characterize oxygen binding curves by identifying the value of n required to fit a given set of oxygen binding data. Equations 4 and 6 become identical when $K_1 = 4k_0$, $K_2 = 6/4k_0$, $K_3 = 4/6k_0$, $K_4 = 1/4k_0$, and $n = 1$. Under these conditions

$$\bar{v}_0/4 = k_0 c_0 / (1 + k_0 c_0) \quad (7)$$

The binding curve developed by this equation is illustrated by the dashed curve of Figure 1. Equation 7 will be referred to as the unperturbed or statistical binding equation and k_0 will be called the unperturbed binding constant.

The value of the statistical constant, k_0 , cannot be measured directly; its value can only be estimated by some extrapolation process. The approach taken in this paper is that extrapolation to a value of k_0 may be made when the normal hemoglobin tetramer is subjected to perturbations. Wyman⁵ considered the perturbations resulting from the dissociation of the native tetramer of mammalian hemoglobin under the influence of urea solutions. From the data on changes of both oxygen affinity (negative logarithm of the oxygen pressure at one-half saturation, $-\log(c_0)_{1/2}$) and shape of the binding curve (Hill n) (see Table I), Wyman concluded that the stabilizing interactions involved the unoxxygenated subunits.

Similar shifts to values of higher apparent oxygen affinity also occur with the following perturbations: (1) dilution of the salt in which hemoglobin is dissolved (when the salt solution in which hemoglobin is dissolved is changed from approximately 0.2 M ("normal" conditions) to $1 \times 10^{-5} M$, the apparent oxygen affinity increases and the shape of the oxygen binding curve approaches that of the statistical curve⁶ (Table I)); (2) modification of the SH groups^{7,8} (these modifications change the oxygen affinity to higher values and concomitantly decrease the steepness of the oxygen binding curve; other chemical modifications such as removal of terminal residues,⁹ partial oxidation of the heme iron atom,¹⁰ and complexation with haptoglobin¹¹ bring about similar changes (Table I)); (3) genetic changes, which may be the most subtle modifications in the structure of hemoglobin. Usually (but not always) the apparent oxygen affinity increases with genetic change¹² (see Table I). The assumption is made that the hemoglobin tetramer, when perturbed, ordinarily tends to revert to a molecule more like that of the "isolated" monomer. Thus when the general changes in apparent oxygen binding constants and shape of the oxygen binding curve are considered, it is reasonable to assume that the hemoglobin tetramer is destabilized on oxygenation. (Equation 31¹³ appears more reasonable than eq 29,¹³ which, in turn, appears more reasonable than eq 30.¹³)

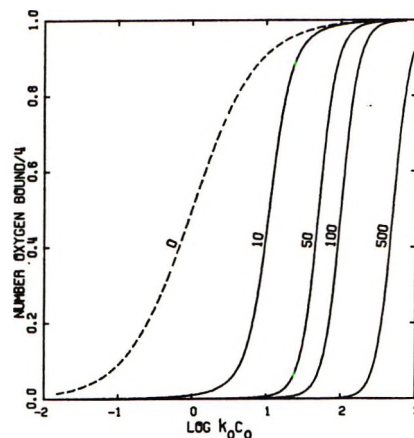
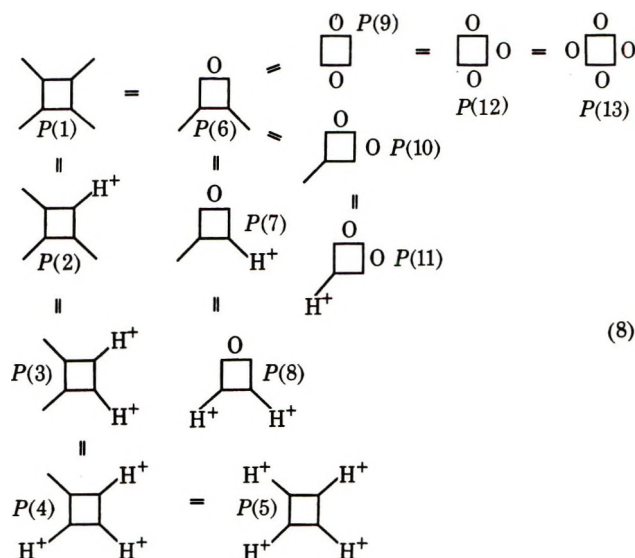


Figure 1. Effect of the value of the product k_{HCB} on the oxygen binding curves calculated with eq 13.

Combined Cooperative and Bohr Effects

(1) *Simple Model—No Interaction Factor.* An alternate method for introducing both the cooperative effect and the Bohr effect¹³ is illustrated in a simplified square model with 13 molecular species, represented schematically in eq 8. In eq 8, the species whose



- (4) A. V. Hill, *J. Physiol.*, **40**, IVP (1910).
 (5) J. Wyman, *Advan. Protein Chem.*, **4**, 407 (1948).
 (6) A. Rossi-Fanelli, E. Antonini, and A. Caputo, *J. Biol. Chem.*, **236**, 397 (1961).
 (7) A. Riggs and R. A. Wolbach, *J. Gen. Physiol.*, **39**, 58 (1956).
 (8) A. Riggs, *J. Biol. Chem.*, **236**, 1948 (1961).
 (9) E. Antonini, J. Wyman, R. Zito, A. Rossi-Fanelli, and A. Caputo, *J. Biol. Chem.*, **236**, PC 60 (1961).
 (10) R. C. Darling and F. J. W. Roughton, *Amer. J. Physiol.*, **137**, 56 (1942).
 (11) R. L. Nagel, J. B. Wittenberg, and H. M. Ranney, *Biochim. Biophys. Acta*, **100**, 286 (1965).
 (12) M. F. Perutz and H. Lehman, *Nature (London)*, **219**, 902 (1968).
 (13) Equations for the cooperative effect, the interaction factor, and the Bohr effect for the Pauling-Wyman model will appear following these pages in the microfilm edition of this volume of the journal. Single copies may be obtained from the Business Operations Office, Books and Journals Division, American Chemical Society, 1155 Sixteenth Street, N.W., Washington, D. C. 20036, by referring to code number JPC-72-1597. Remit check or money order for \$3.00 for photocopy or \$2.00 for microfiche.

Table I: Changes in Apparent Oxygen Affinity and n Value of Hill for Various Perturbations of the Hemoglobin Tetramer

| Hemoglobin species | Conditions of measurement | Perturbation | Apparent oxygen affinity, $-\log (c_0)_{1/2}$ (c_0 in Torr) | Hill n |
|--------------------|---|---|--|---------------------------------------|
| Horse | pH 7.0 0.3 M phosphate 25° | None | -1.30 | $\sim 3^a$ |
| | pH 7.0 0.3 M phosphate 25° 4.6 M urea | Dissociation | 0.65 | 1.9 ^a |
| Human | pH 7.0 0.25 M phosphate 20° | None | -0.98 | 2.9 ^b |
| | pH 7.0 2.5×10^{-4} M phosphate 20° | Dilution of salt | -0.39 | 1.5 ^b |
| | pH 7.0 0.2 M phosphate 25° | None Removal of His(146) β | -0.96 -0.40 | 2.8 ^c 2.5 ^c |
| | pH 7.13 0.1 M phosphate 25° | None Modification of Cys(93) β | -0.85 -0.27 | 3.1 ^d 2.0 ^d |
| | pH 7.4 0.6 M phosphate 37° | None Partial oxidation of heme iron | -1.29 -1.04 | 2.5 ^e 1.5 ^e |
| | pH 7.02 0.1 M phosphate 20° | None Complex formation with haptoglobin | -0.95 0.52 | 2.7 ^f 0.89 ^f |
| | pH 7.2 0.1 M phosphate 10° | None | -0.39 | 2.8 ^g |
| | pH 7.3 0.1 M phosphate 10° | Genetic, Arg(92) α changed to Leu(92) α | 0.42 | 1.3 ^g |

^a Reference 5. ^b Reference 6. ^c J. V. Kilmartin and J. F. Wooton, *Nature (London)*, **228**, 767 (1970). ^d Reference 8. ^e Reference 10. ^f Reference 11. ^g R. L. Nagel, Q. H. Gibson, and S. Charache, *Biochemistry*, **6**, 2395 (1967).

relative concentration is represented by $P(1)$ is the tetramer of hemoglobin with no bound oxygen or protons. The species represented by $P(1)$ – $P(5)$ inclusive may be summarized by eq 9, where $P(1)$ is chosen as

$$\sum_{i=1}^5 P(i) = P(1)(1 + 4k_H c_H + 6k_H^2 c_H^2 + 4k_H^3 c_H^3 + k_H^4 c_H^4 = P(1)(1 + K_{HC_H})^4 \quad (9)$$

the reference species, k_H is the association constant for the binding of protons to a Bohr site, and c_H is the concentration (activity) of hydrogen ions. (In this simplified model, four equivalent Bohr sites are assumed. These four Bohr sites will not, of course, satisfy the requirements for the differential titration data of German and Wyman¹⁴ and Rossi-Bernardi and Roughton.¹⁵) The Bohr protons in this model are considered to lie in regions between the subunits as pro-

posed by Perutz, Muirhead, Cox, and Goaman¹⁶ and Perutz.¹⁷ The molecule is considered to be symmetrical with reference to both the oxygen and proton binding sites. The species whose concentration is represented by $P(6)$ has an oxygen molecule bound to one subunit of the tetramer of hemoglobin. The assumption is made that when an oxygen molecule binds to a subunit, the process by which the binding occurs perturbs the two Bohr proton binding sites bordering on the domain of the subunit. For simplicity, consider that the perturbation lowers the values of k_H such that $k_{HC_H} \rightarrow 0$. Thus the species $P(6)$ may bind only two Bohr protons and

(14) B. German and J. Wyman, *J. Biol. Chem.*, **117**, 533 (1937).

(15) L. Rossi-Bernardi and F. J. W. Roughton, *ibid.*, **242**, 784 (1967).

(16) M. F. Perutz, H. Muirhead, J. M. Cox, and L. C. G. Goaman, *Nature (London)*, **219**, 131 (1968).

(17) M. F. Perutz, *ibid.*, **228**, 726 (1970).

Table II: Apparent Constants and Their Ratios for Various Models

| Adair constants | Statistical eq 7 | Pauling ^a square | Pauling ^{a,b} square with Bohr effect | Eq 13 | Eq 19 |
|-----------------|------------------|--------------------------------|---|----------------------|-----------------------------------|
| K_1 | $4k_0$ | $4k_0$ | $4(H_2^2/H_1^2)k_0$ | $(4/H^2)k_0$ | $4k_0(H_3^3/H_1H_2^2)$ |
| K_2 | $(^8/4)k_0$ | $[(2\alpha + 1)/2]k_0$ | $[(2\alpha + 1)/2] \times (H_2^2/H_1^2)k_0$ | $[(2H + 1)/2H^2]k_0$ | $k_0(2H_1 + 4H_2)H_3^2/4H_1H_2^2$ |
| K_3 | $(^4/6)k_0$ | $[2\alpha^2/(2\alpha + 1)]k_0$ | $[2\alpha^2/(2\alpha + 1)] \times (H_2^2/H_1^2)k_0$ | $[2/(2H + 1)]k_0$ | $4k_0H_3/(2H_1 + 4H_2)$ |
| K_4 | $(^1/4)k_0$ | $(\alpha^2/4)k_0$ | $(\alpha^2/4)(H_2^2/H_1^2)k_0$ | $^1/4k_0$ | $^1/4k_0$ |
| K_2/K_1 | $^3/8$ | $(2\alpha + 1)/8$ | $(2\alpha + 1)/8$ | $(2H + 1)/8$ | $(H_1 + 2H_2)/8H_3$ |
| K_3/K_1 | $^1/6$ | $\alpha^2/2(2\alpha + 1)$ | $\alpha^2/2(2\alpha + 1)$ | $H^2/2(2H + 1)$ | $H_1H_2^2/(2H_1 + 4H_2H_3^2)$ |
| K_4/K_1 | $^1/16$ | $\alpha^2/16$ | $\alpha^2/16$ | $H^2/16$ | $H_1H_2^2/16H_3^3$ |

^a See ref 13. ^b $H_i = (1 + k_{H_i}c_H)$.

$$\sum_{i=6}^8 P(i) = P(1)[4k_0c_0(1 + 2k_{HC_H} + k_{H^2}c_{H^2})] = P(1)[4k_0c_0(1 + k_{HC_H})^2] \quad (10)$$

Continuing this reasoning

$$\sum_{i=9}^{11} P(i) = P(1)[4k_0^2c_0^2(1 + k_{HC_H}) + 2k_0^2c_0^2] \quad (11)$$

and

$$P(12) + P(13) = P(1)[4k_0^3c_0^3 + k_0^4c_0^4] \quad (12)$$

The equation containing no interaction factor and generating the steepened oxygen binding curve for this simplified model follows.

$$\bar{v}_0/4 = \frac{k_0c_0(1 + k_{HC_H})^2 + k_0^2c_0^2(3 + 2k_{HC_H}) + 3k_0^3c_0^3 + k_0^4c_0^4}{(1 + k_{HC_H})^4 + 4k_0c_0(1 + k_{HC_H})^2 + 2k_0^2c_0^2(3 + 2k_{HC_H}) + 4k_0^3c_0^3 + k_0^4c_0^4} \quad (13)$$

As the value of the quantity k_{HC_H} increases, eq 13 will generate steepened oxygen binding curves with the (now apparent) cooperative interaction, Figure 1. The apparent cooperative effect derives from the asymmetrical perturbation of the proton binding sites on the binding of oxygen. The first oxygen perturbs two proton binding sites. The second oxygen perturbs one and one-half proton binding sites. (Four of the microspecies perturb one each and two of the microspecies perturb two each.) The third oxygen perturbs the remaining one-half Bohr site, and the fourth perturbs no Bohr site. This decrease in rate of perturbation on the binding of oxygen makes the value of the apparent oxygen affinity of eq 13 less than rather than greater than that of the unperturbed constant, k_0 .

The steepness of the oxygen binding curves may be defined using the four apparent constants of Adair. Thus the shape of an oxygen binding curve is determined by the three ratios K_2/K_1 , K_3/K_1 , and K_4/K_1 . When these ratios are larger than $3/8$, $1/6$, and $1/16$, respectively, the oxygen binding curve is steepened.

This increase in ratios obtains when the interaction factor $\alpha > 1$ for the interactive models¹³ and when $(1 + k_{HC_H}) > 1$ for eq 13. Table II summarizes the values of K_1 , K_2 , K_3 , and K_4 and their ratios for the statistical model, the interactive models, and the model represented by eq 13.

Variation of Oxygen Equilibria with Salt. An argument in favor of a model similar to that represented by eq 13 is the effect of salt on the binding of oxygen. At constant pH, dilution of salt brings about a shift in the oxygen binding equilibria⁶ similar to that illustrated in Figure 1, where on decreasing the value of the product k_{HC_H} , the apparent cooperative effect is decreased (the oxygen binding curves are less steep) but the value of the apparent oxygen binding constant increases. At constant pH, however, with the interactive models, a decrease in the steepness resulting from a decrease in the interaction factor, α , brings about a corresponding decrease in apparent oxygen binding constant.¹³ If anion binding were assumed to be the primary cause of the salt effect, then dilution would shift the apparent oxygen binding constant to higher values, but no change in the shape of the binding curve should occur. To characterize the shifts in the value of the apparent oxygen binding constant for the Pauling-Wyman model,¹³ the value of the oxygen concentration at which the oxygen saturation is half of the total is found by setting $\bar{v}_0/4 = 1/2$ and solving for c_0 . When this is done

$$\log (c_0)_{1/2} = \log \frac{H_1H_2}{H_3H_4} + \log \frac{1}{\alpha k_0} \quad (14)$$

where $\log (c_0)_{1/2}$ is the log of the concentration of oxygen yielding half saturation. In eq 14, $H_i = (1 + k_{H_i}c_H)$, where the subscripts i refer to the Bohr sites of the Wyman model.⁵ Subscripts 1 and 3 refer to the four acid Bohr sites in the deoxy- and oxyhemoglobin, respectively, and the subscripts 2 and 4 refer to the four alkaline Bohr sites in the deoxy- and oxyhemoglobin, respectively. The shift in the oxygen binding curve in going from a pH_1 to a pH_2 will then be

$$\Delta \log (c_0)_{1/2} = \log \left[\left(\frac{H_1 H_2}{H_3 H_4} \right)_{\text{pH}_1} \left(\frac{H_3 H_4}{H_1 H_2} \right)_{\text{pH}_2} \right] \quad (15)$$

If the pH is now kept constant with the assumption that the anion binding occurs at the protonated Bohr sites, then eq 14 becomes

$$\Delta \log (c_0)_{1/2} = \log \frac{(H_1' H_2') c_{A1}}{(H_1' H_2') c_{A2}} \quad (16)$$

where the additional (simplifying) assumption is made that the anion binding occurs in the deoxygenated form of hemoglobin only and $H_1' = 1 + k_{H_1} c_H (1 + k_A c_A)$ and $H_2' = 1 + k_{H_2} c_H (1 + k_A c_A)$, where k_A symbolizes the association constant for the binding of anions to the protonated Bohr site and c_A represents the concentration of the free anions in solution. The proposed binding of anions to deoxygenated hemoglobin is considered to be similar to the binding of anions to clusters of ionizable groups in ribonuclease.¹⁸ Perutz¹⁷ has proposed similar clusters for some of the Bohr sites of hemoglobin. Thus, with $c_{A1} > c_{A2}$ (in a range of concentration where the binding of anions changes), the value of $\Delta \log (c_0)_{1/2}$ will be positive, indicating a shift to a higher apparent oxygen binding constant. Although the Pauling–Wyman¹³ model will thus allow a shift in the proper direction with anion binding, the shape of the oxygen binding curve would still be determined by the ratios $(2\alpha + 1)/8$, $\alpha^2/2(2\alpha + 1)$, and $\alpha^4/16$ (see Table II). Fitting the data with the Pauling–Wyman model would then require, in addition to the parameter, k_A , the introduction of even another effect—the effect of the salt on the parameter α .

The model of eq 13 allows for changing both the shape of the oxygen binding curve and the value of the apparent oxygen binding constant with the single additional parameter, k_A . The equation analogous to eq 16 becomes

$$\Delta \log (c_0)_{1/2} = \log \frac{(H') c_{A1}}{(H') c_{A2}} \quad (17)$$

(Note that this equation will not generate the differential titration data of German and Wyman.¹⁴ This point is taken up below with eq 27.) Now, however, the shape of the oxygen binding curve is changed because the ratios K_2/K_1 , K_3/K_1 , and K_4/K_1 contain the terms $(H') c_{A1}$ and $(H') c_{A2}$. With the model of eq 13, decreasing salt concentration and decreasing hydrogen ion concentration will therefore bring about similar effects.

Additional data on the action of salt are reported by Enoki and Tyuma¹⁹ who determined the values of K_1 and K_4 of the equation of Adair. In no salt $K_1 = 0.15$ and $K_4 = 3.8$. In 1.0 M salt $K_1 = 0.01$ and $K_4 = 2.5$. While the K_1 values changed by a factor of 15, the values of K_4 changed by a factor of only 1.5. Similar results were reported by Torelli, *et al.*²⁰ The effect of salt on the values of K_1 , K_2 , K_3 , and K_4 of the equa-

tion of Adair should be the same if the Pauling–Wyman model applies (with the assumption of anion binding). For the interactive model salt should have no effect on K_4 and should only affect K_1 , K_2 , and K_3 . Thus, the model of eq 13 is consistent with the available salt data.

While experiments at constant pH with varying salt are available,⁶ analogous experiments at constant salt with varying hydrogen ion concentration have not yet been done because of the custom of using buffers of differing concentration and with different salts for achieving pH control.

The Cooperative Effect and the Value of n of the Hill Equation. The cooperative effect of the oxygenation process is measured by the shape of an oxygen binding curve and is determined by the three ratios K_2/K_1 , K_3/K_1 , and K_4/K_1 of Table II, while the position of the oxygen binding curve on the concentration scale is determined by the value of K_1 . Unfortunately, it has become the custom in hemoglobin studies to characterize data on the cooperative effect of oxygen binding by means of the n value of the Hill equation and to characterize the apparent binding constant by the concentration of oxygen yielding half saturation. Emphasis on these parameters tends to ignore the importance of the variations in shape of the oxygen binding curves (the ratios K_2/K_1 , K_3/K_1 , and K_4/K_1) under the conditions of the experimental observations.

Since Pauling¹ and Wyman⁵ concluded from the data of Ferry and Green²¹ that the shape of the oxygen binding curve was independent of pH, this impression has almost become dogma. While data are not available for a proper evaluation of the effect of pH because of the custom of using buffers, as mentioned above, it is of interest to assay some data as summarized in Table III, where the pH was controlled with the buffers as indicated.

Values of n and K in Table III were determined by minimizing the sum of the squares of the differences between the data and those values calculated using the equation of Hill. There are, at present, no recognized general methods for presenting errors in values of n for a given error for each point in a set of data. A graphical method for evaluating an error for the data of Roughton and Lyster²² at pH 7.0 is presented in Figures 2 and 3. In Figure 2 is presented a composite of the 16 curves generated by the equation of Adair and the following values of K with their errors as reported by Roughton and Lyster: $K_1 = 0.0493 \pm 0.0035$, $K_2 = 0.0427 \pm 0.0286$, $K_3 = 0.2208 \pm 0.1730$, and $K_4 = 0.3204 \pm 0.0662$. Included in Figure 2 are the seven

(18) G. I. Loeb and H. A. Saroff, *Biochemistry*, **3**, 1819 (1964).

(19) Y. Enoki and I. Tyuma, *Jap. J. Physiol.*, **14**, 280 (1964).

(20) G. Torelli, A. Pini, and R. Margaria, *Atti Accad. Nat. Lincei, Cl. Sci. Fis., Mat. Natur., Rend.*, **36** (6), 798 (1964).

(21) R. M. Ferry and A. A. Green, *J. Biol. Chem.*, **81**, 175 (1929).

(22) F. J. W. Roughton and R. L. J. Lyster, *Hvalradets Skrifter*, **48**, 185 (1965).

Table III: Values of n and K of the Equation of Hill for Three Sets of Data

| Horse Hemoglobin $1 \times 10^{-3} M$, Phosphate Buffers $0.167 M^a$ | | |
|--|--------------------------|---------|
| pH | n | Log K |
| 6.40 | 3.01 | -3.81 |
| 6.77 | 3.01 | -3.75 |
| 7.00 | 3.17 | -3.68 |
| 7.38 | 2.44 | -2.29 |
| Human Hemoglobin $1.5 \times 10^{-5} M$, Phosphate Buffers $0.1 M^b$ | | |
| pH | n | Log K |
| 6.97 | 2.57 | -2.89 |
| 7.38 | 2.38 | -2.09 |
| Human Hemoglobin $6.21 \times 10^{-4} M$, pH 7.0, $0.6 M$ Phosphate Buffer; pH 9.1, $0.2 M$ Borate Buffer ^c | | |
| pH | n | Log K |
| 7.0 | 2.74 ± 0.5 -0.1 | -2.63 |
| 9.1 | 2.32 ± 0.3 -0.1 | 0.115 |

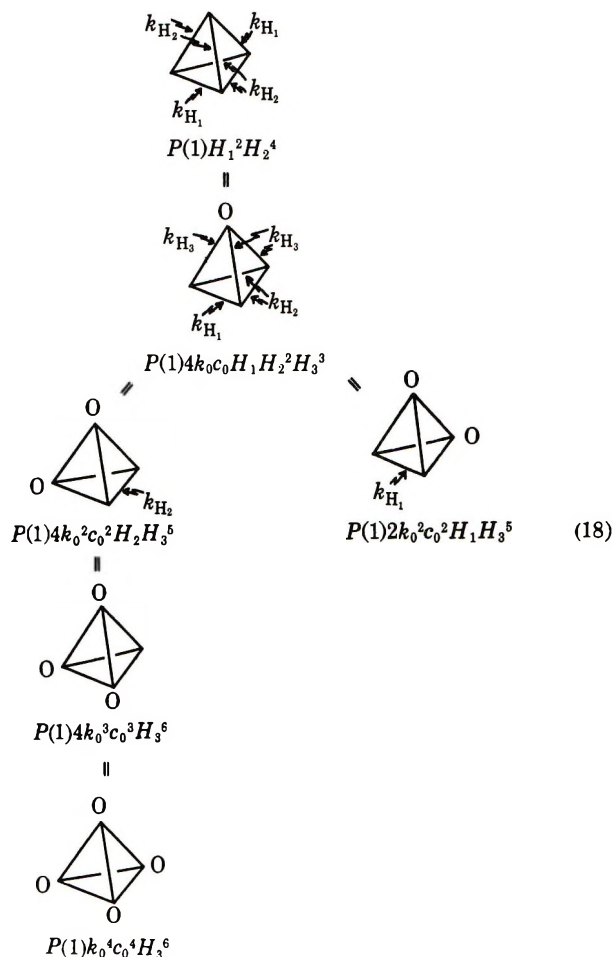
^a Reference 21. ^b R. Benesch and R. E. Benesch, *J. Biol. Chem.*, **236**, 405 (1961). ^c Reference 23.

curves generated by the equation of Hill with the following values of n and $\log K$: $n = 2.6$, $\log K = -2.50$; $n = 2.7$, $\log K = -2.60$; $n = 2.8$, $\log K = -2.70$; $n = 2.9$, $\log K = -2.79$; $n = 3.0$, $\log K = -2.89$; $n = 3.1$, $\log K = -2.99$; and $n = 3.2$, $\log K = -3.08$. Each of these curves constitutes a best fit for the given value of n with the value of K allowed to vary. A best fit is determined by minimizing the sum of the squares of the differences between the actual value of the data and the calculated value using the equation of Hill. In Figure 3 is illustrated the plot of $\log (y/1 - y)$ for these same data ($y = \bar{v}_0/4$). Since $n = 2.7$ constitutes the best fit on varying both n and K , the value of n may be given as $2.7 (+0.5, -0.1)$ based on the errors calculated for the values of K_1 , K_2 , K_3 , and K_4 by Roughton and Lyster.²² The same technique yielded a value of $2.3 (+0.3, -0.1)$ for the data at pH 9.1 of Table III.

Data of unusually high precision are thus required to evaluate the shapes of oxygen binding curves in terms of the n value of Hill when the values of n are above 2.5. In addition, the values of n only characterize the curves in a limited region and the shapes at low and high saturation with oxygen are ignored, thus limiting the assay of the cooperative effect.

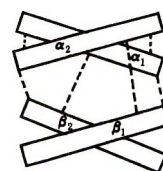
(2) *Intermediate Model—No Interaction Factor.* (a) *Description.* In order to generate the differential titration curve, the simplified eq 13 must be modified to conform with eq 25 of Appendix A. Since six Bohr sites

are sufficient for the differential titration curve, a tetrahedron with its six edges representing the interacting surfaces between subunits may be used to symbolize the hemoglobin tetramer, as shown in eq 18,



where $H_i = (1 + k_{H_i}c_{H_i})$.

A symmetrical tetrahedron is used for simplicity in this representation. Slightly different equations would be generated with the following arrangement of subunits, with the dotted lines representing interacting surfaces



In the tetrahedron the interacting surfaces would be $\alpha_1\beta_1$, $\alpha_2\beta_2$, $\alpha_1\alpha_2$, $\beta_1\beta_2$, $\alpha_1\beta_2$, and $\alpha_2\beta_1$, while in the less symmetrical arrangement shown above the interacting surfaces could be $\alpha_1\beta_1$, $\alpha_2\beta_2$, $\alpha_1\alpha_2$, $\alpha_2\alpha_1$, $\alpha_1\beta_2$, and $\alpha_2\beta_1$. The groups interacting at the surfaces $\alpha_1\alpha_2$, $\alpha_2\alpha_1$, $\alpha_1\beta_2$, and $\alpha_2\beta_1$, have been proposed by Perutz¹⁷ as accounting for the alkaline Bohr effect. With this arrangement the 24 molecular species represented by $4k_0c_0H_1H_2^2H_3^3$ of eq 26 become the 44 species represented by $2k_0c_0(H_1H_2^2H_3^3 + H_1H_2H_3^4)$. The 24 species

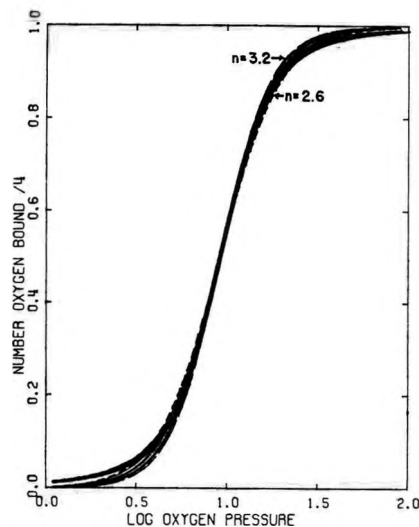


Figure 2. A composite of 16 oxygen binding curves calculated with the equation of Adair, plus a composite of 7 curves with the equation of Hill. Values of parameters in text.

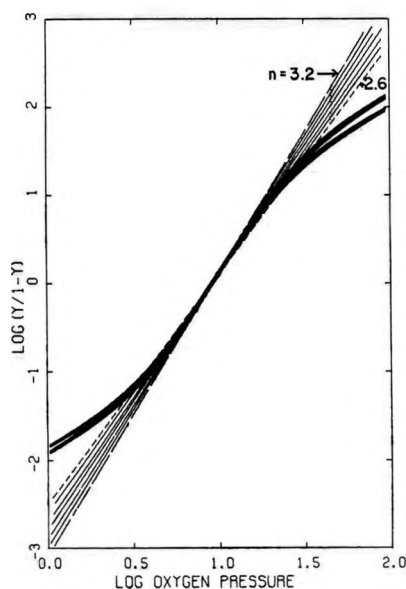


Figure 3. Hill plot. Composite of 16 curves calculated with the equation of Adair and 7 curves (lines) calculated with the equation of Hill; values in text.

represented by $k_0^2 c_0^2 (2H_1 H_3^5 + 4H_2 H_3^5)$ become $k_0^2 c_0^2 \cdot (H_2^2 H_3^4 + H_3 + 2H_1 H_3^5 + 2H_2 H_3^5)$, representing 46 species. The expressions representing species with zero, three, and four oxygen molecules remain the same. Equations 18 represent 77 molecular species, and the expression for the binding of oxygen becomes

$$\bar{v}_0 = \frac{k_0 c_0 H_1 H_2^2 H_3^3 + k_0^2 c_0^2 H_3^5 (H_1 + 2H_2) + 3k_0^3 c_0^3 H_3^6 + k_0^4 c_0^4 H_3^6}{4 \frac{H_1^2 H_2^4 + 4k_0 c_0 H_1 H_2^2 H_3^3 + 2k_0^2 c_0^2 H_3^5 \times (H_1 + 2H_2) + 4k_0^3 c_0^3 H_3^6 + k_0^4 c_0^4 H_3^6}{(H_1 + 2H_2) + 4k_0^3 c_0^3 H_3^6 + k_0^4 c_0^4 H_3^6}} \quad (19)$$

In the model of eq 19 there are two sets of Bohr sites on the deoxygenated hemoglobin, the first with two sites

represented by k_{H_1} and the second with four sites represented by k_{H_2} . The process by which an oxygen molecule binds to the heme perturbs the Bohr proton binding sites bordering on the domain of the subunit to which the oxygen binds. Thus the first oxygen molecule will perturb three Bohr sites, the second will perturb two Bohr sites, and the third will perturb the remaining Bohr site. All of the Bohr sites, when perturbed, are represented by the same association constant, k_{H_i} .

The model of eq 19 is now consistent with the differential titration data and has cooperative properties similar to those of the simpler model of eq 13. Some variations of the cooperative and Bohr effects with pH predicted by eq 19 are given in Appendix B.

(b) *Nature of the Bohr Sites.* Examination of the data available from X-ray analysis of hemoglobin^{16,17} reveals areas between the subunits where there are possible clusters of positive charges, with the effects of these charges modulated by the presence of one or more carboxylate ions in the vicinity. These clusters of positive charges are considered in this paper to interact with carboxylate ions within the molecule or with anions from the solution (eq 16 above). Interactions of this kind have been demonstrated in ribonuclease.¹⁸ In the model of eq 18, the Bohr sites are considered to be six regions between the subunits where clusters of ionizable groups occur. The groups within a single site or cluster are considered to be made of side chains of two neighboring subunits. Thus, oxygenation (and a configurational change) of a single subunit is detected by its neighboring subunits as a shift in the apparent pK value of the shared Bohr sites.

For a given Bohr site, the pK value assigned to it is considered to represent the apparent value applicable to the cluster rather than that of a single group. For the differential titration data on horse^{14,15} and human²³⁻²⁵ hemoglobin, only six sites (or clusters) are required to fit the data (see Appendix A). It appears that six, or less, sites are required to fit the reported data on the various other hemoglobins. The equation required to describe these six, or fewer, pK values may be a simple one even though the process bringing about the changes in pK values may be highly complicated. Some of these changes, particularly those in the positions of the last three amino acids of the β chain in oxygenated and deoxygenated hemoglobin, have been reported by Perutz.¹⁷

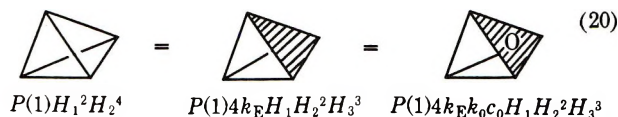
(3) *Allosteric Model—No Interaction Factor.* The allosteric extension of the model of eq 18 expands the number of species to 198 when the following assumptions are made: (a) each subunit is allowed to exist in-

(23) R. L. Nagel, Q. H. Gibson, and S. Charache, *Biochemistry*, **6**, 2395 (1967).

(24) F. J. W. Roughton, *J. Gen. Physiol.*, **49**, 105 (1965).

(25) J. E. Bailey, J. G. Beetlestone, and D. H. Irvine, *J. Chem. Soc. A*, 756 (1970).

independently in two forms, A and B; (b) when all of the subunits are in the form A, then the six Bohr sites exist in two groups, one group of two sites with values k_{H_1} , the other group of four sites with the values k_{H_2} ; (c) when a subunit exists in the form B, the three Bohr sites bordering on its domain have the value k_{H_3} ; (d) only form B may bind an oxygen molecule. These assumptions may be represented partially by the following schematic equilibria



where k_E is the equilibrium constant describing the reaction $A = B$. The following equation describes the relative concentrations of the molecular species

$$\sum_{i=1}^{198} P(i) = P(1)[H_1^2H_2^4 + 4k_E(1 + k_0c_0)H_1H_2^2H_3^3 + k_E^2(1 + k_0c_0)^2(2H_1H_3^5 + 4H_2H_3^5) + 4k_E^3(1 + k_0c_0)^3H_3^6 + k_E^4(1 + k_0c_0)^4H_3^6] \quad (21)$$

The term k_0c_0 of eq 18 is replaced with $k_E(1 + k_0c_0)$ in eq 21. This is not a simple replacement, because in the expression $P(1)[k_E^2(1 + k_0c_0)^2H_1H_3^5]$, for example, there are species with no oxygen bound, $P(1)k_E^2H_1H_3^5$, with one oxygen molecule bound, $P(1)2k_E^2k_0c_0H_1H_3^5$, and species with two oxygen molecules bound, $P(1) \cdot k_E^2k_0^2c_0^2H_1H_3^5$. The allosteric terms of the model of eq 21 are thus different from those of Koshland, Nemethy, and Filmer,²⁶ where k_0 is simply replaced by k_0k_E . The allosteric extension represented by eq 21 is a more reasonable physical model than that of eq 18 if the free energy change for the transition $A = B$ is near zero or $k_E \cong 1$. Under these conditions the concentrations of oxygen, hydrogen ions, and anions will shift the equilibrium readily between the two forms A and B to give the characteristic hemoglobin behavior.

Equation 21 describes a hemoglobin molecule in which there are at least three distinctive species from the standpoint of the properties of the heme group. Thus there are the two forms without oxygen, A and B, and the oxygenated form of B.

Discussion

(a) *pH and the Interaction Energy.* The model proposed in this paper is derived essentially from considerations that stabilizing interactions between deoxygenated subunits are considered to control the oxygenation process. The interaction factor of the Coryell¹³ idea (derived from the Pauling model) is replaced in eq 19 and 21 by a factor containing the ionization constants of the Bohr sites. In replacing the interaction factor with the ionization constants, a simplifying assumption was made that the predominant interactions

between subunits which varied on oxygenation were pH dependent. Biological feedback systems are seldom simple. There is probably a pH-independent component in the interacting forces between subunits which changes on oxygenation, and the terms $1 + k_{H,C_H}$ should be $\alpha(1 + k_{H,C_H})$, with α differing from unity by only a small amount. In the present model α is taken as unity.

(b) *Conclusions.* The mammalian tetramer of hemoglobin has an apparent oxygen binding constant which is smaller in value than that of the related monomeric species. When this fact is considered along with the steep oxygen binding curves and the Bohr effect, inconsistencies develop in arguments based on models which separate the cooperative effect (steep binding curve) from the Bohr effect. These inconsistencies may be summarized as follows.

(I) The shapes of the oxygen binding curves are not independent of pH. This point is somewhat beclouded by the lack of control of the salt concentration, but three sets of facts are worth considering. (A) Values of n of the Hill equation contain large errors and show consistent variations to give smaller values at lower hydrogen ion concentrations. (B) Constants derived from the upper part of the oxygen binding curve are less sensitive to pH changes than those derived from the lower part of the oxygen binding curve. (C) The rate of release of hydrogen ions with the binding oxygen at high degrees of saturation of oxygen is much smaller than that at low degrees of saturation.

(II) Perturbations of the hemoglobin tetramer which are independent of pH and decrease the cooperative effect should also decrease the value of the apparent oxygen binding constant according to equations similar to eq 29.¹³ The reverse effect is found. At constant pH a reduction of salt concentration lowers the cooperative effect and at the same time increases the apparent oxygen binding constant.

(III) Salt concentration, as well as hydrogen ion concentration, perturbs the first constant of Adair much more than the last constant. This fact tends to relate both salt and hydrogen ions to the same effect.

Because of these inconsistencies in the present models for the action of hemoglobin, the separation of the cooperative effect (homotropic interaction) from the Bohr effect (heterotropic interaction) is abandoned and a model is proposed in this paper which links directly the cooperative effect to the Bohr effect.

Appendix A. Ramifications of the Bohr Effect

(a) *The Equation of Adair.* Roughton²⁴ has analyzed the pH dependence of some oxygen binding data using the four apparent constants of the equation of Adair.³ The value of K_4 of the Adair equation was found to be

(26) D. E. Koshland, G. Nemethy, and D. Filmer, *Biochemistry*, **5**, 365 (1966).

relatively insensitive to pH, while the values of K_1 , K_2 , and K_3 were more pH dependent. The model of eq 13 is consistent with the fact that K_4 is insensitive to pH. The model of Pauling and Wyman, however, requires that all four of the apparent constants be affected by pH changes in the same manner (see Table II).

(b) *Rate of Change of Proton Binding with Oxygen Binding.* Some data are available on the displacement of the Bohr protons on the progressive binding of oxygen to hemoglobin. Equations 13, 21, and 32¹³ may be used to generate the values of $\bar{\nu}_H/4$ as a function of $\bar{\nu}_0/4$, where $\bar{\nu}_H = \sum_{i=1}^4 iPH_i / \sum_{i=0}^4 PH_i$ and PH_i represents a species of hemoglobin with i protons bound to the Bohr sites. Figure 4 illustrates the curve of $(\Delta H^+)_f$ as a function of $\bar{\nu}_0/4$, where

$$(\Delta H^+)_f = [(\bar{\nu}_H/4)_{\text{deoxy}} - (\bar{\nu}_H/4)_{\text{O}_2}] / [(\bar{\nu}_H/4)_{\text{deoxy}} - (\bar{\nu}_H/4)_{\text{oxy}}] \quad (22)$$

In eq 22 $(\bar{\nu}_H/4)_{\text{deoxy}}$ and $(\bar{\nu}_H/4)_{\text{oxy}}$ represent the binding of Bohr protons to the completely deoxygenated and completely oxygenated hemoglobin, respectively, and $(\bar{\nu}_H/4)_{\text{O}_2}$ represents the number of Bohr protons bound to hemoglobin in equilibrium with some intermediate concentration of oxygen to give partial saturation. Calculations with eq 13, illustrated in Figure 4, show that while the value of $(\Delta H^+)_f$ as a function of $\bar{\nu}_0/4$ is not linear, it is almost linear between 15 and 85% saturation.

Antonini, *et al.*,²⁷ have presented data on the displacement of the Bohr protons, $(\Delta H^+)_f$, on the binding of carbon monoxide and interpreted their data to support the invariance of the shape of the oxygen binding curve with pH. An implied assumption in their calculations was the invariance in the rate of change of proton binding with oxygen binding as the maximum oxygen (or carbon monoxide) binding was reached. With the Pauling-Wyman model, the change in proton binding should be linear with oxygen binding at all degrees of saturation with oxygen. With the model of eq 13, the change in proton binding becomes very small at high degrees of saturation with oxygen (or carbon monoxide). Glauser²⁸ has presented data indicating that little detectable displacement of H^+ occurs in the region of high saturation with oxygen. In Figure 6 are illustrated the data of Antonini, *et al.*,²⁷ recalculated with the maximum carbon monoxide binding occurring at a larger volume than that deduced from the apparent maximum change in pH. Included in Figure 4 is the calculated curve for the model of eq 13 and the more appropriate eq 21.

Thus the model of eq 13 is consistent with the data of Antonini, *et al.*,²⁷ and in addition is consistent with the data of Roughton²⁴ and Glauser.²⁸

(c) *The Differential Titration.* When no oxygen is bound to hemoglobin, Wyman⁵ gives the expression $k_{H_1C_H} / (1 + k_{H_1C_H}) + k_{H_2C_H} / (1 + k_{H_2C_H})$ for the binding

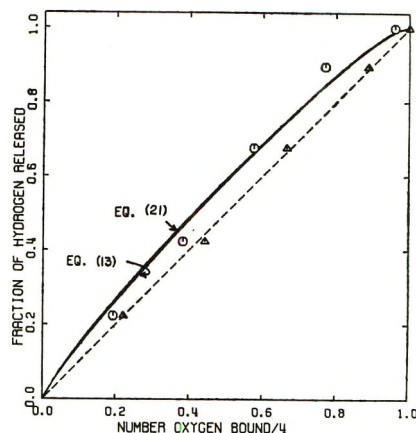


Figure 4. Release of protons on the binding of carbon monoxide. Δ , data of Antonini, *et al.*;²⁷ \circ recalculated data; see text. Curves calculated with eq 13 and 21.

of hydrogen ions to a single subunit. When hemoglobin is saturated with oxygen, this expression becomes $k_{H_1C_H} / (1 + k_{H_1C_H}) + k_{H_2C_H} / (1 + k_{H_2C_H})$. The difference between these two expressions is the differential titration, $\Delta H^+ / 4$

$$\frac{\Delta H^+}{4} = \frac{k_{H_1C_H}}{1 + k_{H_1C_H}} + \frac{k_{H_2C_H}}{1 + k_{H_2C_H}} - \frac{k_{H_1C_H}}{1 + k_{H_1C_H}} - \frac{k_{H_2C_H}}{1 + k_{H_2C_H}} \quad (23)$$

Equation 23 requires eight protons per tetramer of hemoglobin for the Bohr effect. (Note that the k_{H_i} 's are association constants.) Differential titration data on horse^{14,15} and human^{14,21} hemoglobin may be explained with eq 23 and with the following two equations as well²⁹

$$\frac{\Delta H^+}{4} = \frac{k_{H_1C_H}}{1 + k_{H_1C_H}} + \frac{k_{H_2C_H}}{1 + k_{H_2C_H}} - \frac{2k_{H_3C_H}}{1 + k_{H_3C_H}} \quad (24)$$

$$\frac{\Delta H^+}{4} = \left(\frac{1}{2}\right) \frac{k_{H_1C_H}}{1 + k_{H_1C_H}} + \frac{k_{H_2C_H}}{1 + k_{H_2C_H}} - \left(\frac{3}{2}\right) \frac{k_{H_3C_H}}{1 + k_{H_3C_H}} \quad (25)$$

Equation 24 requires, as in eq 23, eight protons per tetramer. Equation 25, however, requires only six protons per tetramer of hemoglobin and may be used to introduce the concept of Bohr sites situated between, shared by, and affected by neighboring subunits.²⁹ Table IV summarizes the values of the constants required to fit the data for horse and human hemoglobin.

(27) E. Antonini, J. Wyman, M. Brunori, E. Bucci, C. Franticelli, and A. Rossi-Fanelli, *J. Biol. Chem.*, **238**, 2950 (1963).

(28) S. Glauser, *Fed. Proc., Fed. Amer. Soc. Exp. Biol.*, **22**, 516 (1963).

(29) H. A. Saroff, *Proc. Nat. Acad. Sci. U. S.*, **67**, 1662 (1970).

Table IV: Values of Association Constants for Bohr Proton Binding Sites for Eq 23, 24, and 25

| Eq | Log k_{H_1} | Log k_{H_2} | Log k_{H_3} | Log k_{H_4} | Ref |
|-------------------------------|---------------|---------------|---------------|---------------|----------|
| Horse Hemoglobin ^a | | | | | |
| 23 | 5.23 | 7.81 | 5.68 | 6.79 | |
| 24 | 5.51 | 7.67 | 7.75 | | |
| 25 | 5.17 | 7.75 | 6.50 | | |
| Human Hemoglobin | | | | | |
| 23 | 5.13 | 7.84 | 5.60 | 6.84 | <i>b</i> |
| | 4.97 | 7.80 | 5.59 | 6.68 | <i>c</i> |
| | 4.38 | 7.62 | 5.27 | 6.41 | <i>d</i> |
| 24 | 5.47 | 7.68 | 6.37 | | <i>b</i> |
| | 5.49 | 7.74 | 6.29 | | <i>c</i> |
| | 4.85 | 7.51 | 5.95 | | <i>d</i> |
| 25 | 5.03 | 7.78 | 6.57 | | <i>b</i> |
| | 4.89 | 7.75 | 6.43 | | <i>c</i> |
| | 4.0 | 7.55 | 6.14 | | <i>d</i> |

^a Reference 14. ^b Reference 15. ^c See footnote *c*, Table I. ^d Reference 25.

Appendix B. The Cooperative Effect (Expressed by the n Value of Hill), the Bohr Effect (Expressed by $(c_0)_{1/2}$), and pH as Developed by Eq 19

The following equation analogous to eq 14 is derived from eq 19.

$$\log (c_0)_{1/2} = (1/2) \log \frac{H_1 H_2^2}{H_3^3} - \log k_0 \quad (26)$$

Given the value of $(c_0)_{1/2}$, the n value of the Hill equation is calculated by

$$n = \frac{d \ln (\bar{v}_0/4/(1 - \bar{v}_0/4))}{d \ln (c_0)} \quad (27)$$

For the interactive model,¹³ the value of $\log (c_0)_{1/2}$, eq 14, varies with pH, whereas the value of n is invariant with pH for a given value of the interaction factor, α (see Figure 5).

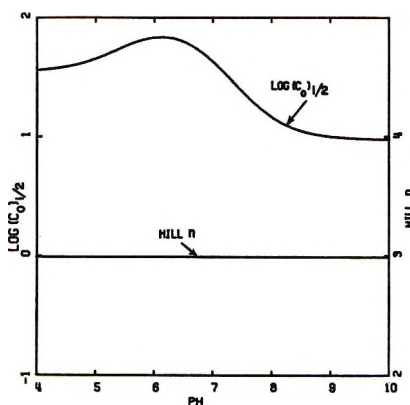


Figure 5. Calculated values of $\log (c_0)_{1/2}$ and n as a function of pH. Interactive model, $\log k_{H_1} = 5.23$, $\log k_{H_2} = 7.81$, $\log k_{H_3} = 5.68$, $\log k_{H_4} = 6.79$, $\log k_0 = -2.12$, and $\alpha = 14$.

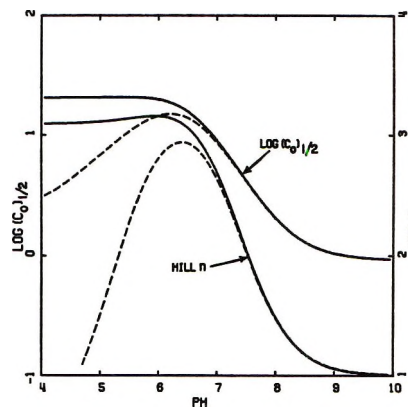


Figure 6. Calculated values of $\log (c_0)_{1/2}$ and n as a function of pH (eq 19): solid curves $\log k_{H_1} = 5.95$, $\log k_{H_2} = 8.12$, $\log k_{H_3} = 6.50$, and $\log k_0 = 0.034$; dashed curves same values except $\log k_{H_1} = 4.0$.

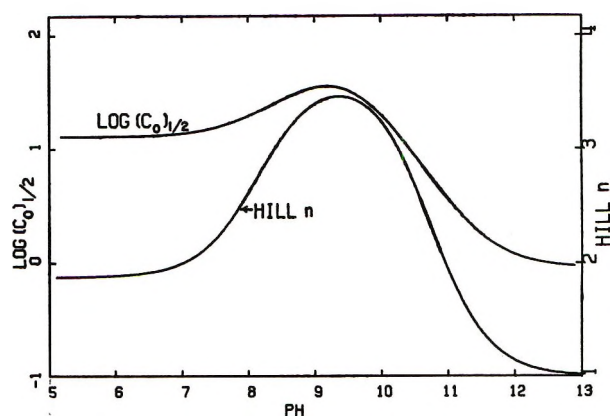


Figure 7. Calculated values of $\log (c_0)_{1/2}$ and n as a function of pH (eq 19): $\log k_{H_1} = 7.8$, $\log k_{H_2} = 11.5$, $\log k_{H_3} = 9.5$, and $\log k_0 = 0.04$.

The characteristics of the values of $\log (c_0)_{1/2}$ and n for eq 19 are illustrated in Figures 6–9. For $\log k_{H_1} = 6.42$, $\log k_{H_2} = 8.39$, and $\log k_{H_3} = 6.50$, eq 19 generates the curves drawn with solid lines in Figure 6. If the value of $\log k_{H_1}$ is lowered to 4.0 from 6.42, then the dashed curves for $\log (c_0)_{1/2}$ and n are generated. When all of the Bohr constants are shifted to higher values, the curves of Figure 7 are generated. These curves of Figure 7 illustrate properties similar to those of component *S* of salmon (*Oncorhynchus keta*) hemoglobin reported by Hashimoto, Yamaguchi, and Matsuura,³⁰ where there is no apparent Bohr effect between the pH values of 5.0 and 8.5, but where the value of n is about 2.4 in this pH range.

Additional properties may be generated by selective elimination of individual Bohr sites. For example, if two adjacent sites of those with values of k_{H_i} are eliminated ($k_{H_i} c_{H^+} \rightarrow 0$ so that $(1 + k_{H_i} c_{H^+}) \rightarrow 1$), the equation equivalent to eq 26 becomes

(30) K. Hashimoto, Y. Yamaguchi, and F. Matsuura, *Bull. Jap. Soc. Sci. Fish.*, **26**, 827 (1960).

$$2H_1^2H_2^2 + k_0c_0(H_1H_2^2H_3 + 2H_1H_2H_3^2 + H_1H_3^3) - 4k_0^3c_0^3H_3^4 - 2k_0^4c_0^4H_3^4 = 0 \quad (28)$$

Equation 28 may be solved by iterative procedures to give the physically significant value of c_0 at half saturation, and the characteristic curves of $\log (c_0)_{1/2}$ and n vs. pH for this model with only four Bohr sites may be calculated and are illustrated in Figure 8. Illustrated by these curves are properties representing an apparent normal Bohr effect with very little apparent heme-heme interactions ($n = 1.6-1.0$).

Other changes in the values of k_{H_1} , k_{H_2} , and k_{H_3} will generate properties in which the cooperative effect is replaced by apparent repulsive effects. Curves calcu-

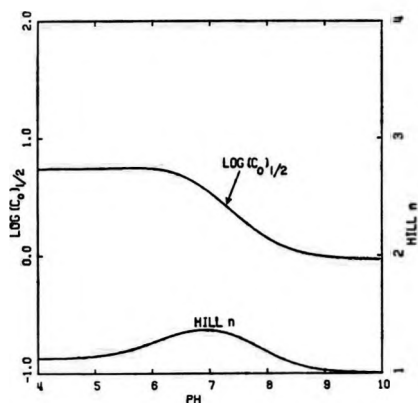


Figure 8. Calculated values of $\log (c_0)_{1/2}$ and n as a function of pH; eq 19 with two of the k_{H_2} groups eliminated: $\log k_{H_1} = 5.94$, $\log k_{H_2} = 8.12$, $\log k_{H_3} = 6.50$, and $\log k_0 = 0.034$.

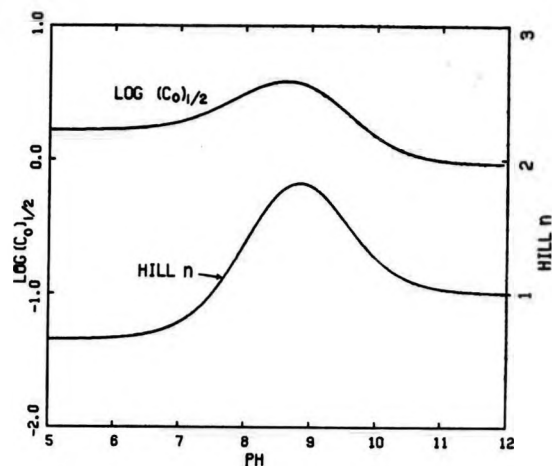


Figure 9. Calculated values of $\log (c_0)_{1/2}$ and n as a function of pH (eq 19): $\log k_{H_1} = 7.4$, $\log k_{H_2} = 9.9$, $\log k_{H_3} = 8.9$, and $\log k_0 = 0.034$.

lated from eq 19, where the values $\log k_{H_1} = 7.4$, $\log k_{H_2} = 9.9$, $\log k_{H_3} = 8.9$, and $\log k_0 = 0.034$, give values of n varying from 0.8 to 0.9 in the pH range from 5 to 7; see Figure 9.

After the collection of sufficiently detailed data on genetically and chemically modified hemoglobin molecules, it may become possible to identify the Bohr sites in terms of this proposed model.

Acknowledgments. Thanks are due Miss Jean M. Dunnington and Miss Michelle A. Kominz for their help in the programming necessary for the preparation of the figures used in this paper.

Relative Partial Molar Enthalpies and Heats of Dilution of Electrolytes in Water

by Lowell W. Bahe

Department of Chemistry, University of Wisconsin—Milwaukee, Milwaukee, Wisconsin 53201
(Received November 29, 1971)

Publication costs assisted by the University of Wisconsin—Milwaukee

The expression for the activity coefficients of electrolytes in solution based on the three-dimensional face-centered-cubic array¹ can be used to find an expression for the relative partial molar enthalpies and the heats of dilution. Analysis of tabulated data shows excellent agreement with predicted results up to concentrations of about 1 *M*. This is further evidence that an analysis of the forces and energies between ions immersed in a dielectric medium must include the dielectric gradient effects as well as the classical coulombic effects.

In a previous paper,¹ 1:1 electrolytes in solution in water were shown to assume a loose face-centered-cubic lattice. An analysis of the forces and energies acting between these structured ions, based on Coulomb's law and the field-dielectric-gradient effect, resulted in an expression for the electrical free energies (activity coefficients) that was a simple function of the concentration. The application of classical thermodynamics to the free energy expression should allow the determination of relative partial molar enthalpies or of heats of dilution. This paper shows the results of such an application.

The free energy of 1:1 electrolytes in solution is given by²

$$\bar{G}_2 = \bar{G}_2^\circ + RT \ln X^2 + RT \ln f_{\pm}^2 \quad (1)$$

where \bar{G}_2 is the partial molar Gibbs free energy, X is the mean ionic mole fraction, and f_{\pm} is the rational or mean mole fraction ionic activity coefficient. Dividing by T and taking the derivative with respect to T at constant P and constant composition gives

$$\frac{\partial \left(\frac{\bar{G}_2 - \bar{G}_2^\circ}{T} \right)}{\partial T} = - \frac{(\bar{H}_2 - \bar{H}_2^\circ)}{T^2} = 2R \left(\frac{\partial \ln f_{\pm}}{\partial T} \right)_{P,n} \quad (2)$$

where \bar{H}_2 and \bar{H}_2° are the partial molar enthalpy and the standard partial molar enthalpy, respectively, of the salt. The previous development¹ has shown that

$$\log f_{\pm} = -Ac^{1/3} + Bc \quad (3)$$

or that

$$\ln f_{\pm} = -2.3026Ac^{1/3} + 2.3026Bc \quad (4)$$

The derivative with respect to T is, therefore

$$\left(\frac{\partial \ln f_{\pm}}{\partial T} \right)_{P,n} = 2.3026 \left[-A \left(\frac{\partial c^{1/3}}{\partial T} \right)_{P,n} - c^{1/3} \left(\frac{\partial A}{\partial T} \right)_{P,n} + B \left(\frac{\partial c}{\partial T} \right)_{P,n} + c \left(\frac{\partial B}{\partial T} \right)_{P,n} \right] \quad (5)$$

The terms in eq 5 which explicitly contain the deriva-

tive of c , which, as will be seen later, are small at low concentrations, and the term linear in c , which will be small compared to the cube root term at low concentrations, will be considered later. We therefore treat

$$2R \left(\frac{\partial \ln f_{\pm}}{\partial T} \right)_{P,n} = 2(2.3026)R \left[- \left(\frac{\partial A}{\partial T} \right)_{P,n} \right] c^{1/3} \quad (6)$$

The previous development¹ has shown that

$$A = \frac{N(\text{Mad})Z^2e^2 \left(\frac{2N}{1000} \right)^{1/3}}{2(2.3026)R} \frac{1}{kT} \quad (7)$$

where (Mad) is the Madelung constant, Z is the number of charges, e is the charge on the electron, R is the gas constant, N is Avogadro's number, k is the dielectric constant of the medium, and T is the absolute temperature. Taking the derivative with respect to T gives

$$\left(\frac{\partial A}{\partial T} \right)_{P,n} = -A \left(\frac{1}{T} + \frac{\partial \ln k}{\partial T} \right)_{P,n} \quad (8)$$

The derivative of the natural logarithm of the dielectric constant of water with respect to temperature has been measured³ and at 25° has the value $-45.88 \times 10^{-4} \text{ deg}^{-1}$. Using this value along with $T = 298.15^\circ$ and $A = 0.28894^1$ allows the evaluation of eq 8 in water to give

$$\left(\frac{\partial A}{\partial T} \right)_{P,n} = 3.56547 \times 10^{-4} \quad (9)$$

Combining eq 2 and 6 gives

$$\bar{H}_2 - \bar{H}_2^\circ = \bar{L}_2 = 2(2.3026)RT^2 \left(\frac{\partial A}{\partial T} \right)_{P,n} c^{1/3} \quad (10)$$

where \bar{L}_2 is the relative partial molar heat content of the salt. Using $R = 1.9872 \text{ cal/mol deg}$ and eq 9 gives at 25°

(1) L. W. Bahe, *J. Phys. Chem.*, **76**, 1062 (1972).

(2) H. S. Harned and B. B. Owen, "Physical Chemistry of Electrolytic Solutions," 3rd ed, Reinhold, Princeton, N. J., 1958, p 11.

(3) B. B. Owen, R. C. Miller, C. E. Milner, and H. L. Cogan, *J. Phys. Chem.*, **65**, 2065 (1961).

$$\bar{H}_2 - \bar{H}_2^\circ = 290.05c^{1/3} \quad (11)$$

Following the development in Harned and Owen,⁴ we see that

$$H_2 - H_2^\circ = \bar{L}_2 = \frac{\partial(m\phi_L)}{\partial m} = d_0^{1/3}(290.05)m^{1/3} \quad (12)$$

which leads to

$$\phi_L = -\Delta H_D = 3/4d_0^{1/3}(290.05)m^{1/3} = 217.5c^{1/3} \quad (13)$$

where ϕ_L is the apparent relative molar heat content and ΔH_D is the heat of dilution.

Equation 13 indicates that at low concentrations a plot of the relative apparent molar heat content against $c^{1/3}$ should give a straight line with slope 217.5. Since the reported values of ϕ_L were arrived at by an extrapolation using the square root of m , the line might not pass through zero but might require a constant term which should be added to eq 13 to correct for the previous extrapolation. We therefore look for, at concentrations approaching zero, a fit to the equation

$$\phi_L = 217.5c^{1/3} + \phi_L^\circ \quad (14)$$

where ϕ_L° is a constant to correct for the previous extrapolation.

Figure 1 shows a plot of ϕ_L for NaCl against $c^{1/3}$ and indeed a very nice straight line is obtained. The data for this plot were taken from Harned and Owen.⁵ Method-of-least-squares treatment of the data gives a slope of 217.0 and an intercept of -9.4 . The agreement between the experimental and predicted results is excellent. This simple test must be applied cautiously, however, since very precise experimental results at very low concentrations are needed; the inclusion of at least the term linear in c is usually required for an adequate interpretation, even at these low concentrations.

At higher concentrations terms in addition to the cube-root term must be taken into account. Combining eq 2 and 5 and rearranging gives

$$\bar{H}_2 - \bar{H}_2^\circ = \bar{L}_2 = 2(2.3026)RT^2 \left[\left(\frac{\partial A}{\partial T} \right) c^{1/3} - \left(\frac{\partial B}{\partial T} \right) c + \left(\frac{A}{3c^{2/3}} - B \right) \left(\frac{\partial c}{\partial T} \right) \right] \quad (15)$$

and

$$\bar{L}_2 - 2(2.3026)RT^2 \left[\left(\frac{\partial A}{\partial T} \right) c^{1/3} + \left(\frac{A}{3c^{2/3}} - B \right) \times \left(\frac{\partial c}{\partial T} \right) \right] = \bar{L}_2^\circ - 2(2.3026)RT^2 \left(\frac{\partial B}{\partial T} \right) c \quad (16)$$

\bar{L}_2° in eq 16 is a constant to allow for the different extrapolation carried out originally to arrive at the literature values of \bar{L}_2 .

As described below, it is possible to evaluate dc/dT in eq 16 so that everything on the left-hand side can be

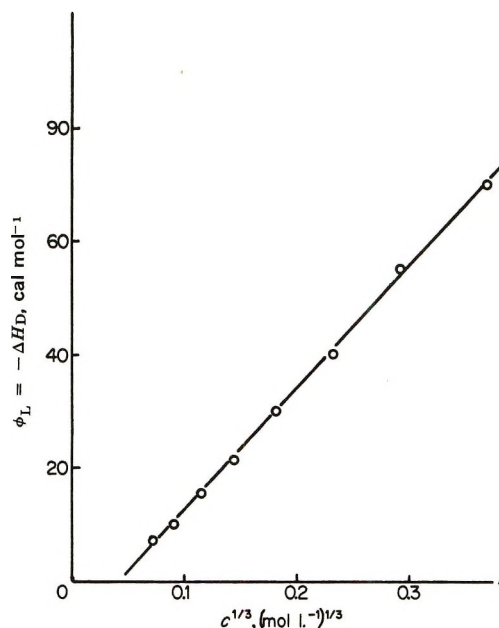


Figure 1. The variation of apparent relative partial molar heat contents (negative heats of dilution) of NaCl with the cube root of the molar concentration at 25° at very low concentrations. Experimental slope, 217.0; predicted slope, 217.5.

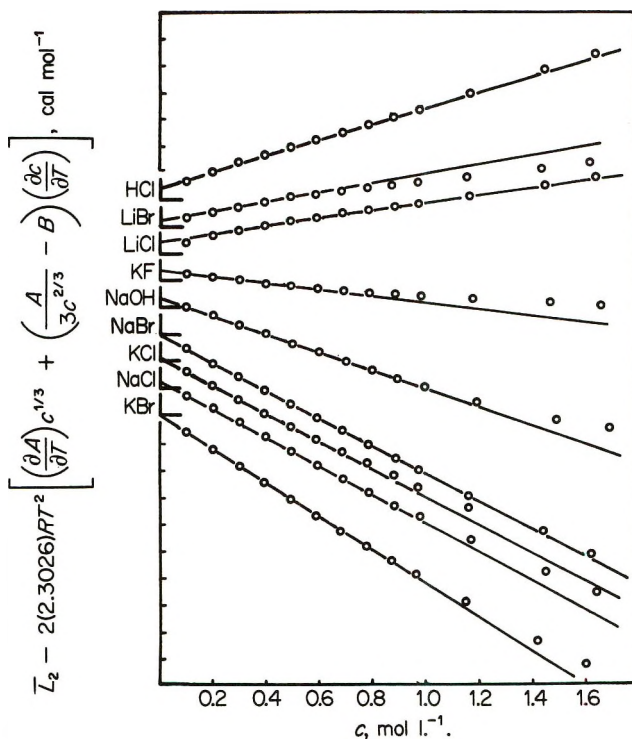


Figure 2. The variation of the left-hand side of eq 16 with molar concentration for nine simple 1:1 electrolytes at 25°. The abscissa is the same for each salt. The data for each salt have been displaced 100 cal mol⁻¹ from each neighbor on the vertical scale. The right angle adjacent to each salt represents the origin (0,0) for that salt. Each segment on the ordinate represents 100 cal mol⁻¹.

(4) H. S. Harned and B. B. Owen, "Physical Chemistry of Electrolytic Solutions," 3rd ed, Reinhold, Princeton, N. J., 1958, p 322 ff.

(5) H. S. Harned and B. B. Owen, ref 4, p 333.

Table I: Data for the Computation of the Left-Hand Side of Eq 16 for HCl at 25°

| \bar{L}_1 | m | c | $c^{1/3}$ | dc/dT | Col. 6 ^a | Col. 7 ^b |
|-------------|--------|--------|-----------|------------|---------------------|---------------------|
| HCl | | | | | | |
| 202.000 | 0.1000 | 0.0995 | 0.4634 | -0.0000251 | 129.116 | 72.883 |
| 273.000 | 0.2000 | 0.1986 | 0.5835 | -0.0000506 | 165.407 | 107.592 |
| 332.000 | 0.3000 | 0.2974 | 0.6675 | -0.0000763 | 191.973 | 140.026 |
| 383.000 | 0.4000 | 0.3958 | 0.7342 | -0.0001024 | 213.890 | 169.109 |
| 430.000 | 0.5000 | 0.4939 | 0.7904 | -0.0001287 | 232.997 | 197.002 |
| 475.000 | 0.6000 | 0.5916 | 0.8395 | -0.0001554 | 250.191 | 224.808 |
| 518.000 | 0.7000 | 0.6889 | 0.8832 | -0.0001823 | 265.990 | 252.009 |
| 560.000 | 0.8000 | 0.7859 | 0.9228 | -0.0002096 | 280.721 | 279.278 |
| 604.000 | 0.9000 | 0.8825 | 0.9592 | -0.0002371 | 294.604 | 309.395 |
| 645.000 | 1.0000 | 0.9788 | 0.9928 | -0.0002650 | 307.799 | 337.200 |
| 728.000 | 1.2000 | 1.1701 | 1.0537 | -0.0003216 | 332.565 | 395.434 |
| 853.000 | 1.5000 | 1.4545 | 1.1330 | -0.0004087 | 366.737 | 486.262 |
| 934.000 | 1.7000 | 1.6423 | 1.1798 | -0.0004683 | 388.087 | 545.912 |
| 1055.000 | 2.0000 | 1.9212 | 1.2431 | -0.0005600 | 418.562 | 636.437 |
| 1269.000 | 2.5000 | 2.3787 | 1.3349 | -0.0007187 | 466.449 | 802.550 |
| 1484.000 | 3.0000 | 2.8272 | 1.4140 | -0.0008850 | 511.958 | 972.041 |

$${}^a 2(2.3026)RT^m \left[\left(\frac{\partial A}{\partial T} \right) c^{1/3} + \left(\frac{A}{3c^{2/3}} - B \right) \left(\frac{\partial c}{\partial T} \right) \right]. \quad {}^b \bar{L}_2 - 2(2.3026)RT^2 \left[\left(\frac{\partial A}{\partial T} \right) c^{1/3} + \left(\frac{A}{3c^{2/3}} - B \right) \left(\frac{\partial c}{\partial T} \right) \right].$$

measured or calculated. A plot of the left-hand side against c should give a straight line if dB/dT is a constant with respect to c .

Harned and Owen⁶ give factors for converting m to c at various temperatures for several 1:1 electrolytes. These data were used to estimate values of dc/dT . In one method, the derivative was estimated by

$$\left(\frac{\partial c}{\partial T} \right)_{25^\circ} = \frac{c_{30} - c_{20}}{30 - 20} \quad (17)$$

In the second method, d_0 ⁶ and A' ⁶ (A' is used here for Harned and Owen's A) were found as functions of t by multiple regression analysis, and dc/dt was found from

$$\left(\frac{\partial c}{\partial T} \right) = \frac{m dd_0}{dt} - m^2 \left(\frac{dA'}{dt} \right) \quad (18)$$

The multiple regression analysis to terms in t^3 gave

$$d_0 = 0.99992 + 0.48312 \times 10^{-4}t - 0.72689 \times 10^{-3}t^2 + 0.30044 \times 10^{-7}t^3 \quad (19)$$

$$\left(\frac{\partial d_0}{\partial t} \right) = 0.48312 \times 10^{-4} - 0.145378 \times 10^{-4}t + 0.90132 \times 10^{-7}t^2 \quad (20)$$

$$\left(\frac{\partial d_0}{\partial t} \right)_{25^\circ} = -0.25880 \times 10^{-3} \quad (21)$$

For HCl it was found that

$$A' = 0.016988 + 0.80757 \times 10^{-4}t - 0.16158 \times 10^{-5}t^2 + 0.92722 \times 10^{-8}t^3 \quad (22)$$

$$\left(\frac{\partial A'}{\partial t} \right) = 0.80757 \times 10^{-4} - 0.32316 \times 10^{-5}t + 0.27817 \times 10^{-7}t^2 \quad (23)$$

$$\left(\frac{\partial A'}{\partial t} \right)_{25^\circ} = 0.17352 \times 10^{-4} \quad (24)$$

Both methods of evaluating dc/dT gave essentially the same results. The $\Delta c/\Delta t$ method was used for the results reported in this paper except for LiCl, LiBr, and KF where eq 18 was used. The left-hand side of eq 16 was determined from literature data^{6,7} and a plot of the left-hand side of eq 16 against c for HCl, NaCl, KCl, NaBr, KF, KBr, NaOH, LiCl, and LiBr is shown in Figure 2. A detailed analysis of the data required for this plot is shown for HCl in Table I.⁸ A linear plot out to approximately 1 M was obtained in each case. The slope and intercept, determined by the method of least squares, for each salt are listed in Table II. Where available, the data needed for Table I were taken from ref 7. The B of eq 3 needed in eq 16 was taken from ref 1 except for NaOH, LiBr, and KF which were calculated as in ref 1 from tabulated data of Robinson and Stokes⁹ and were found to be, respectively, 0.097, 0.0955, and 0.013. The variation of concentration with temperature was taken from Harned and Owen⁶ except for LiCl, LiBr, and KF. Values for these three salts are not given by Harned and Owen,

(6) H. S. Harned and B. B. Owen, ref 4, p 725.

(7) H. S. Harned and B. B. Owen, ref 4, p 710.

(8) The detailed analysis of the data for each of the nine electrolytes, HCl, NaCl, KCl, NaBr, KBr, KF, NaOH, LiCl, and LiBr, is shown in the complete Table I which will appear immediately following this article in the microfilm edition of this volume of the journal. Single copies may be obtained from the Business Operations Office, Books and Journals Division, American Chemical Society, 1155 Sixteenth Street, N.W., Washington, D. C. 20036, by referring to code number JPC-72-1608. Remit check or money order for \$3.00 for photocopy or \$2.00 for microfiche.

(9) R. A. Robinson and R. H. Stokes, "Electrolyte Solutions," 2nd ed revised, Butterworths, London, 1959, pp 491, 492, 494.

Table II: Slopes and Intercepts of the Linear Portions of the Curves for the Nine Simple 1:1 Electrolytes in Figure 2 at 25°

| Salt | Slope | Intercept |
|------|--------|-----------|
| HCl | 296.0 | 48.8 |
| NaCl | -528.5 | 30.3 |
| KCl | -518.8 | 14.8 |
| NaBr | -515.7 | -1.5 |
| LiCl | 141.0 | 50.4 |
| LiBr | 168.5 | 22.9 |
| KBr | -621.0 | -0.4 |
| NaOH | -337.3 | 37.8 |
| KF | -119.1 | 40.0 |

and the data in the "International Critical Tables" were either incomplete or contained inconsistencies and anomalies that could not be accounted for. For these latter three salts, eq 18 was used with $dA'/dt = 0$. Tests on other salts indicated that this approximation did not affect the results significantly at concentrations below about 1 *M*. In addition, the original calorimetric data for LiCl are not as complete as for some of the other salts.¹⁰ Therefore, the results for LiCl, LiBr, and KF are less reliable than the results for the other salts in Figure 2.

Discussion

Figure 2 shows that the left-hand side of eq 16 plotted against *c* does follow a straight line out to concentrations of about 1 *M*. This is a much higher concentration than the 0.04 *M* claimed previously as the upper bound even when arbitrary terms had been added to the Debye-Hückel limiting term.¹¹

However, Figure 2 does indicate that the lines do deviate from a straight line relationship at concentrations above about 1 *M*. A possible explanation rests with the approximations involved in the derivation of eq 3.¹ Equation 3 is mathematically most valid at small concentrations. The deviations from agreement with eq 3 may result from the approximate nature of the equation. Another possible explanation is that dB/dT may not be constant with *c*. This would mean that dB/dc is not equal to zero despite the fact that the free energy (activity coefficient) data¹ indicate that the derivative is zero out to fairly high concentrations.

As pointed out in the earlier paper,¹ finding agreement to concentrations as low as 0.001 *M* is surprising. Solutions of 1:1 electrolytes in water behave as if they retain face-centered-cubic structure to very low concentrations. The agreement shown in Figure 1 and the fit for several other electrolytes in Figure 2 are further evidence that univalent salts in solution exhibit three-dimensional, face-centered-cubic structure. This agreement is further evidence that an analysis of the forces and energies between ions immersed in a dielectric medium must include the dielectric gradient effects as well as the classical coulombic effects.

This approach will require that literature values of ϕ_L and \bar{L}_2 be adjusted to account for the new extrapolation. No attempt to carry out these corrections has been made in this paper since the purpose is illustrative. The task of altering data tables in the literature lies outside the scope of this paper.

(10) H. S. Harned and B. B. Owen, "Physical Chemistry of Electrolytic Solutions," 3rd ed, Reinhold, Princeton, N. J., 1958, p 343.

(11) H. S. Harned and B. B. Owen, ref 10, p 339.

Significant Structure Liquid Theory of the Alkali Metals over the Normal Melting to Boiling Range

by Chen C. Hsu, Allen K. MacKnight, and Henry Eyring*

Department of Chemistry, University of Utah, Salt Lake City, Utah 84112 (Received September 27, 1971)

Publication costs assisted by the National Institutes of Health

Using a significant structure theory partition function for liquid metals, a set of satisfactory thermodynamic properties of the liquid alkali metals from the normal melting point to the boiling point has been obtained. The partition function derived correctly describes the volume and temperature-dependent properties of the solid metals. It should be emphasized that unlike most calculations of this kind, having once written down the Helmholtz free energy A as a function of volume and temperature all thermodynamic properties can be calculated. The energy of sublimation E_s and the Einstein characteristic temperature θ are each considered as a function of the solidlike molar volume V_s and their temperature dependence is taken into account. The results are compared with the observed values in the tables and in the figures. The reasons for this successful application are discussed.

Introduction

Liquid metals are an interesting and important class of liquids that should be amenable to treatment by liquid theories. They are generally considered to be monatomic simple liquids. The significant structure model was first applied to liquid metals by Carlson, Eyring, and Ree.¹ Recently Vilcu and Misdolea² extended these calculations by using Carlson, Eyring, and Ree's partition function for the alkali metals giving results only for the heat capacities, C_p and C_v , and mechanical coefficients of thermal expansion α and isothermal compressibility β . They also did not calculate the volume from their partition function but introduced experimental volumes to calculate the other properties. Their results were generally good in α and C_v , but the calculated values of C_p and β were off by orders of magnitude. The present work was therefore undertaken to find a partition function by which all thermodynamic properties can be calculated completely theoretically from the expression for the Helmholtz free energy as a function of volume and temperature.

The Model

The significant structure model of a liquid has been described previously.³ Briefly, the liquid state is taken to be composed of two significant structures, a solidlike portion and a gaslike portion. Molecules remain at liquid lattice sites until their kinetic energy is great enough to overcome the surrounding potential forces and so preempt a neighboring vacancy. While the molecule is moving to the vacancy it has gaslike degrees of freedom. When it is closely confined by neighbors, it has solidlike degrees of freedom.

A mole of liquid contains $N(V_s/V)$ solidlike degrees of freedom. The number of gaslike degrees of freedom is $N(1 - V_s/V)$, where N is Avogadro's number, V_s is

the molar volume of the solid, and V the molar volume of the liquid.

The partition function of a liquid, f_l , is a product of the solidlike partition function, f_s , and the gaslike partition function, f_g , weighted by the appropriate number of molecules

$$f_l = f_s^{N(V_s/V)} f_g^{N(V-V_s)/V} \quad (1)$$

For simple liquids

$$f_s = \frac{e^{E_s/RT}}{(1 - e^{-\theta/T})^3} \left(1 + n \left(\frac{V - V_s}{V_s} \right) \times \exp \left[\frac{-aE_s V_s}{(V - V_s)RT} \right] \right) \quad (2)$$

$$f_g = \frac{(2\pi mkT)^{3/2} eV}{h^3 N} \quad (3)$$

The symbols are defined as follows: E_s and θ are the energy of sublimation and the Einstein characteristic temperature; n and a are dimensionless parameters that express the degree of positional degeneracy of the solidlike structure; m , k , h , R , and N are the mass of a metal atom, Boltzmann's constant, Planck's constant, the gas constant, and Avogadro's number, respectively. The independent variables are the absolute temperature, T , and the molar volume, V , of the liquid.

Liquid Metals

The alkali metals melt at comparatively low temperatures compared with other metals and with a small change in volume compared with simple liquids like

(1) C. M. Carlson, H. Eyring, and T. Ree, *Proc. Nat. Acad. Sci. U. S. A.*, **46**, 649 (1960).

(2) R. Vilcu and C. Misdolea, *J. Chem. Phys.*, **49**, 3179 (1968).

(3) H. Eyring and M. Jhon, "Significant Liquid Structures," Wiley, New York, N. Y., 1969.

argon. These facts led Carlson, *et al.*,¹ to postulate that only the metal ions have gaslike properties, not the entire metal atoms. Since the ions are roughly one-third the size of the atoms the holes are also proportionately smaller. This means that n in the positional degeneracy term in the solidlike partition function should be increased by roughly a factor of 3 compared to a simple liquid. The parameter n has a value of 10.8 for argon which is a measure of the number of nearest neighbors. For liquid metals n was empirically found to be about 37 indicating the greater positional degeneracy of the metal ions for the same expansion.

Since there is a small volume change on melting (2.5% for sodium compared with 12.2% for argon), the fraction of solidlike degrees of freedom V_s/V is proportionately larger. This means that the solidlike partition function f_s will be more important in determining the thermodynamic properties of the liquid. We therefore expect a liquid metal to resemble a close-packed solid more than simple fluids do.

A study of solid sodium showed that the energy of sublimation and the characteristic temperature are volume dependent. The volume of the solid V_s is in turn a function of temperature. The following relations gave good results for the solid

$$E_s = E_{so} \left[2 \left(\frac{V_{so}}{V_s} \right)^q - \left(\frac{V_{so}}{V_s} \right)^{2q} \right] \quad (4)$$

$$\theta = \theta_o \left(\frac{V_{so}}{V_s} \right)^\gamma \quad (5)$$

$$V_s = V_{so}(1 + \alpha_s T) \quad (6)$$

The exponent q was taken to give the best solid state thermodynamic properties and Gruneisen's constant, γ , was taken from the solid state literature.⁴ The remaining parameters, E_{so} , V_{so} , and θ_o , which are the quantities at the absolute zero of temperature, were adjusted to give the best liquid state parameters of E_s , θ , and V_s at the melting point. Thus, the solidlike partition function has the same functional dependence as the solid state partition function, but the absolute value changes somewhat with melting as expected.

Results for Thermodynamic Properties

The thermodynamic properties of liquid metals were calculated from the liquid partition function formulated in eq 1-6. The Helmholtz free energy, A , is related to the partition function, f_1 , by

$$A = -kT \ln f_1 \quad (7)$$

The other thermodynamic properties can be found by taking volume and temperature derivatives of eq 7. The molar volume and equilibrium vapor pressure are found from the tangent to a plot of the Helmholtz free energy against volume.⁵ The points of tangency are the liquid and vapor molar volumes and the slope of the tangent is the vapor pressure since $p = -(\partial A / \partial V)_T$.

The values of the parameters, a , n , E_s , V_s , and θ were adjusted to give the best agreement with the observed results at the melting point. The parameters used are given in Table I.

Table I: Parameters Used in Calculations

| | Li | Na | K | Rb | Cs |
|--|--------|--------|--------|--------|--------|
| q | 0.667 | 0.875 | 0.95 | 0.95 | 0.95 |
| $\alpha_s \times 10^4, \text{ deg}^{-1}$ | 1.30 | 1.90 | 1.70 | 1.80 | 1.72 |
| γ | 0.86 | 1.10 | 1.30 | 1.37 | 1.20 |
| $V_{so}, \text{ cm}^3 \text{ mol}^{-1}$ | 12.59 | 22.95 | 44.14 | 54.20 | 67.15 |
| $E_{so}, \text{ kcal mol}^{-1}$ | 37.298 | 24.795 | 21.000 | 19.223 | 18.123 |
| $\theta_o, \text{ }^\circ\text{K}$ | 293.9 | 108.37 | 66.82 | 45.05 | 31.73 |
| $a \times 10^6$ | 8.00 | 5.27 | 8.37 | 9.06 | 9.03 |
| n | 46 | 37 | 35 | 36 | 36 |

All the liquid properties considered were calculated at 100° increments from the melting to the boiling point.⁶ The calculated melting point and boiling point results are compared with the observed values for each metal in Table II.⁷⁻²⁰ The standard deviations of the calculated properties are given in Table III. The results for each property are discussed separately below.

Molar Volume. The molar volumes calculated using the tangent method are compared with the experimental observations in Figure 1. Equation 6 expresses the expansion of the solidlike structure. This contribution was found to be necessary in order to account for the temperature-dependent volume change of the liquid alkali metals. The most divergent calculated value of the coefficient of thermal expansion for the

(4) D. Martin, *Phys. Rev.*, **139**, A150 (1965).

(5) H. Eyring, T. Ree, and N. Hirai, *Proc. Nat. Acad. Sci. U. S.*, **44**, 683 (1958).

(6) Complete results are available from the senior author (H. E.).

(7) An. N. Nesmeyanov, "Vapor Pressure of the Elements," Academic Press, New York, N. Y., 1961.

(8) R. R. Miller, "Liquid Metals Handbook," R. N. Lyon, Ed., Atomic Energy Commission and Department of the Navy, Washington, D. C., 1952.

(9) W. H. Evans, J. Jacobson, T. R. Munson, and D. D. Wagman, *J. Res. Nat. Bur. Stand.*, **55**, 83 (1955).

(10) F. Simon and R. C. Swain, *Z. Phys. Chem. (Leipzig)*, **B28**, 189 (1935).

(11) C. Smithells, "Metals Reference Handbook," 4th ed, Plenum Publishing Co., New York, N. Y., 1967.

(12) P. W. Bridgman, *Proc. Phys. Soc.*, **41**, 341 (1929).

(13) G. Melina, "Handbuch der Anorganischen Chemie," Vol. 2, 8th ed, Natrium Verlag Chemie, Weinheim/Bergstr., Germany, 1965, p 560.

(14) E. L. Dunning, Atomic Energy Commission Report, ANL-6246 (1960).

(15) O. Kleppa, *J. Chem. Phys.*, **18**, 1331 (1960).

(16) T. E. Pochopsky, *Phys. Rev.*, **84**, 553 (1951).

(17) E. Rinck, *C. R. Acad. Sci., Paris*, **189**, 39 (1929).

(18) D. R. Stull and G. C. Sinke, *Advan. Chem. Ser.*, **No. 18**, 72 (1956).

(19) J. Jarzynski and T. Litovitz, *J. Chem. Phys.*, **41**, 1290 (1964).

(20) T. Goltsova, *Teplofiz. Vys. Temp.*, **4**, 3 (1966).

Table II: Calculated and Observed Properties of the Alkali Metals at Melting Point and Boiling Point

| T , °K | P , atm ^a | V , cm ³ mol ⁻¹ | S , cal deg ⁻¹ mol ⁻¹ | C_v , cal deg ⁻¹ mol ⁻¹ | C_p , cal deg ⁻¹ mol ⁻¹ | α , deg ⁻¹ × 10 ⁴ | β , atm ⁻¹ × 10 ⁵ |
|------------------------|---------------------------|--|---|---|---|---|--|
| Lithium | | | | | | | |
| 500 ^b calcd | 1.137×10^{-11} | 13.55 | 10.41 | 5.81 | 7.01 | 3.37 | 15.2 |
| obsd | 7.761×10^{-12} | 13.53 ^c | 11.71 ^d | 5.35 ^e | 7.20 ^d | 1.80 ^f | 7.5 ^g |
| 1000 calcd | 8.988×10^{-4} | 14.91 | 16.44 | 5.79 | 7.96 | 3.21 | 17.2 |
| obsd | 9.722×10^{-4} | 14.86 | | | 6.89 | | |
| 1623 calcd | 0.629 | 16.76 | 20.72 | 5.68 | 9.35 | 3.30 | 19.5 |
| obsd | 0.985 | 16.95 | | | | | |
| Sodium | | | | | | | |
| 371 calcd | 3.02×10^{-10} | 24.81 | 14.46 | 5.91 | 7.41 | 3.83 | 21.84 |
| obsd | 1.58×10^{-10} | 24.8 ^h | 15.51 ⁱ | 6.7 ^j | 7.62 ⁱ | 2.80 ^f | 18.88 ^k |
| 800 calcd | 8.712×10^{-3} | 28.03 | 21.37 | 5.81 | 8.54 | 4.06 | 28.23 |
| obsd | 8.713×10^{-3} | 27.82 | 21.06 | | 6.96 | | |
| 1173 calcd | 0.6873 | 31.15 | 24.85 | 5.66 | 10.40 | 4.31 | 34.63 |
| obsd | 1.000 | 31.32 | | | | | |
| Potassium | | | | | | | |
| 337 calcd | 1.172×10^{-9} | 47.24 | 16.84 | 5.93 | 7.63 | 3.73 | 31.6 |
| obsd | 1.186×10^{-9} | 47.27 ^l | | 6.9 ^j | | 2.91 ⁿ | 39.5 ^j |
| 700 calcd | 8.157×10^{-3} | 52.64 | 23.46 | 5.77 | 8.81 | 3.70 | 40.4 |
| obsd | 9.085×10^{-3} | 52.40 | 23.35 ^m | | 7.13 ^m | | |
| 1049 calcd | 0.639 | 58.40 | 27.15 | 5.63 | 10.02 | 3.92 | 52.1 |
| obsd | 1.000 | 58.47 | | | | | |
| Rubidium | | | | | | | |
| 312 calcd | 2.550×10^{-9} | 58.06 | 18.88 | 5.92 | 7.64 | 4.05 | 41.8 |
| obsd | 1.606×10^{-9} | 58.05 ^o | | 6.7 ^j | | 3.40 ^j | 48.4 ^j |
| 600 calcd | 3.272×10^{-3} | 63.77 | 24.85 | 5.78 | 8.88 | 4.16 | 51.9 |
| obsd | 3.128×10^{-3} | | 25.26 ^m | | 7.50 ^m | | |
| 978 calcd | 0.7234 | 72.26 | 29.38 | 5.61 | 10.47 | 4.49 | 71.1 |
| obsd | 1.000 | | | | | | |
| Cesium | | | | | | | |
| 302 calcd | 4.131×10^{-9} | 71.74 | 20.76 | 5.92 | 7.38 | 3.76 | 51.2 |
| obsd | 2.496×10^{-9} | 71.74 ^o | | 6.7 ^j | | 3.70 ^j | 66.1 ^j |
| 600 calcd | 5.718×10^{-3} | 79.15 | 26.95 | 5.77 | 8.56 | 3.99 | 65.6 |
| obsd | 5.722×10^{-3} | 78.54 | 27.17 ^m | | 7.60 ^m | | |
| 959 calcd | 0.7720 | 89.33 | 31.20 | 5.59 | 9.85 | 4.32 | 91.0 |
| obsd | 1.000 | | | | | | |

^a See ref 7. ^b Melting point of lithium is 453°. ^c See ref 8. ^d See ref 9. ^e Value at 300°K for solid; see ref 10. ^f See ref 11.
^g Value at 298° for solid; see ref 12. ^h See ref 13. ⁱ See ref 14. ^j See ref 15. ^k See ref 16. ^l See ref 17. ^m See ref 18. ⁿ See ref 19.
^o See ref 20.

Table III: Standard Deviation^a between Calculated and Observed Results

| | $\log (P/\text{atm})$ | V , cm ³ mol ⁻¹ | S , cal deg ⁻¹ mol ⁻¹ | C_v , cal deg ⁻¹ mol ⁻¹ | C_p , cal deg ⁻¹ mol ⁻¹ | α , deg ⁻¹ × 10 ⁴ | β , atm ⁻¹ × 10 ⁵ |
|----|--------------------------|--|---|---|---|---|--|
| Li | 0.1231 (10) ^b | 0.09 (10) | 0.47 (19) | 0.46 (1) | 1.31 (11) | 1.57 (1) | 7.5 (1) |
| Na | 0.1562 (10) | 0.16 (11) | 0.74 (9) | 0.79 (1) | 2.08 (10) | 1.03 (1) | 3.0 (1) |
| K | 0.1118 (9) | 0.15 (10) | 0.57 (7) | 0.97 (1) | 1.75 (7) | 0.82 (1) | 8.2 (1) |
| Rb | 0.1106 (8) | 0.05 (3) | 0.59 (6) | 0.78 (1) | 1.77 (6) | 0.62 (1) | 7.2 (1) |
| Cs | 0.1114 (8) | 0.44 (6) | 0.43 (6) | 0.78 (1) | 1.32 (6) | 0.06 (1) | 14.8 (1) |

^a Standard deviation is defined as $\sigma = \left\{ \left[\sum_{i=1}^n (x_{\text{calcd}} - x_{\text{obsd}})^2 \right] / n \right\}^{1/2}$. ^b The numbers in parentheses are the numbers of points.

solidlike structure α_s was 50% smaller than the experimental value for the solid state of rubidium at the melting point. For other metals the agreement was within 10%.

Vapor Pressure. The vapor pressures of the liquid alkali metals are also calculated using the tangent method and are compared with the recommended values of Nesmeyanov⁷ in Figure 2. The calculated results fall within the scatter of experimental points that Nesmeyanov used to compute his recommended values. In some cases there is a 100% variance in the experimental results especially at the lower temperatures.

Entropy. A comparison of the calculated and observed entropies for the alkali metals is shown in Figure 3. The calculated temperature dependence is greater than that observed.

Coefficients of Thermal Expansion and Compressibility. The results of the calculation of these properties can be seen in Tables II and III. In most cases only one observed value could be found for comparison. The solidlike lattice contributions to α_s and β_s were added to the compressibility and expansivity arising from the added holes as follows

$$\beta_l = \beta_f + \frac{V_s}{V} \beta_s \quad (8)$$

$$\alpha_l = \alpha_f + \frac{V_s}{V} \alpha_s \quad (9)$$

The fluid coefficients β_f and α_f were calculated by using the complete partition function for the liquid. The solidlike coefficients β_s and α_s were calculated by using the solidlike partition function which is a function of V_s . These results are much better than those obtained by Vilcu and Misdolea.²

Heat Capacity, C_v and C_p . The results of the calculation of these properties are shown in Tables II and III. There is very little experimental data for C_v , so not much of a comparison can be made. One would expect from the temperature dependence of the entropy, Figure 3, that the overall calculated values of C_v would be larger than the experimental results. The heat capacity at constant pressure, C_p , was calculated from C_v using the thermodynamic relation

$$C_p = C_v + \frac{VT\alpha^2}{\beta} \quad (10)$$

Consequently the errors in C_v , α , and β may accumulate or cancel in the calculation of C_p . As a result, C_p is the calculated property that shows the largest deviations from the experimental results.

Discussion

Vilcu and Misdolea left out of account the part of the coefficient of compressibility arising from compression of the solidlike structure. Omitting this solid structure compressibility is not as serious for argon where the

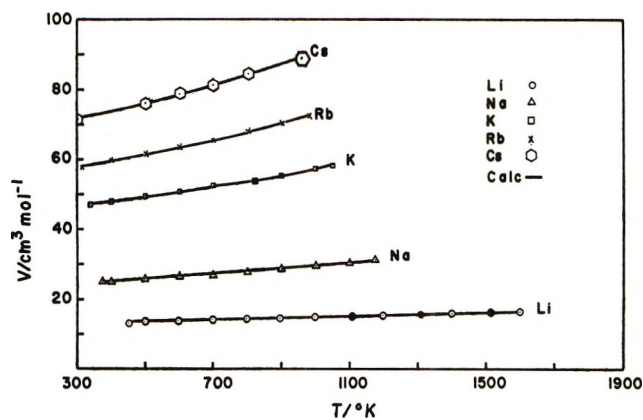


Figure 1. Molar volume of alkali metals.

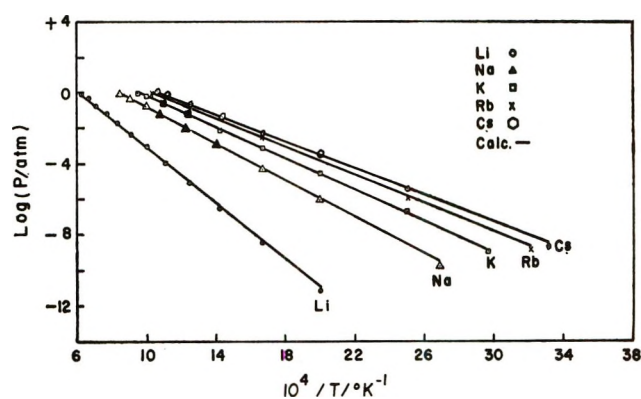


Figure 2. Vapor pressure of alkali metals.

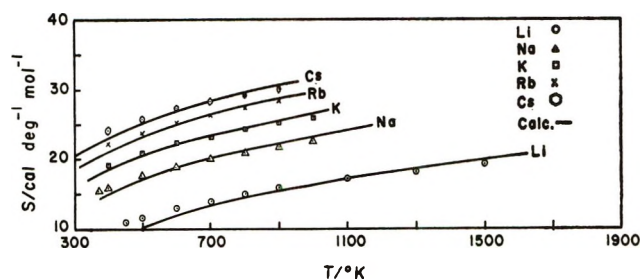


Figure 3. Entropy of alkali metals.

disappearance of vacancies contributes much more to the compressibility of the lattice. For the alkali metals, this omission, however, leads to errors in β and C_p of orders of magnitude as Vilcu and Misdolea found. This difficulty is resolved in this paper by taking into proper account the compressibility of the lattice by using a volume-dependent energy of sublimation and following Gruneisen in giving the frequency of molecular vibration as volume dependent. The improvement reduces the errors in β and C_p from orders of magnitude to the order of 10% and improves the rest of the calculated thermodynamic properties. Furthermore, by considering the solidlike molar volume V_s as a function of temperature which takes account of the variation of the solidlike structure with temperature, the

calculated molar volumes of the liquid alkali metals at various temperatures agree almost exactly with the observed values.

The most difficult part of applying the significant structure theory to calculate the thermodynamic properties of liquids is to find the equilibrium vapor pressure and the molar volume of the liquid. By using the tangent method mentioned earlier, the equilibrium vapor pressure and the molar volume of the liquid are obtained. The calculated molar volume is then used to calculate all thermodynamic properties. Vilcu and Misdolea omitted this important part and used the experimental molar volume of the liquid alkali metals to carry out their calculations. They in all probability would not have obtained the observed volumes which they introduced had they used their theoretical Helmholtz free energy to calculate these volumes.

There are two key steps to take account of in the theory of metals. (1) The volume dependence of the solidlike structure of liquid metals must be taken into account. (2) Because the metal ions move independently of the conduction electrons, they require only about a third as much volume increase as the atoms would to give an alternative position. The model presented goes far beyond anything developed heretofore in giving a proper picture of the important way volume enters into the behavior of solid and liquid metals.

Acknowledgment. The authors wish to thank the National Institutes of Health, Grant GM 12862, National Science Foundation, Grant GP 28631, and the Army Research-Durham, Contract DA-ARO-D-31-124-72-G15, for support of this work.

Thermochemistry of Fused Halide Systems. Enthalpies of Mixing of the Alkaline Earth Halides with the Alkali Halides

by Terje Østvold

Institute of Physical Chemistry, The University of Trondheim, Trondheim, Norway (Received September 9, 1971)

Publication costs borne completely by The Journal of Physical Chemistry

The enthalpies of mixing of the fused alkali halides except the fluorides with the alkaline earth halides (common anion) have been measured. The results are compared with similar data reported by Kleppa and McCarty for the magnesium chloride-alkali chloride melts and discussed with respect to the following points: (1) comparison with the conformal solution theory of Davis; (2) influence of the common anion on the enthalpy of mixing; (3) concentration dependence of the enthalpy of mixing; and (4) temperature dependence of the enthalpy of mixing. It can be concluded from the present investigation that the enthalpies of mixing at constant temperature and *volume*, calculated by the conformal solution theory in its simplest form, do not compare with the enthalpies of mixing measured at constant temperature and *pressure*. A very recent conformal solution theory developed by Davis for charge-unsymmetrical fused salt systems at constant temperature and pressure show that the enthalpy of mixing should be a linear function of the difference in the cation-anion distances for the two salts, $d_1 - d_2$, as long as one salt is kept as a common salt. This is in agreement with the present experimental observations. The variations in slopes and intercepts at $\delta_{12} = (d_1 - d_2)/d_1d_2 = 0$ observed when ΔH^{obsd} is plotted *vs.* δ_{12} is explained in terms of the very simple Førland and Lumsden models where the change in cation-cation Coulomb and cation-anion polarization energies by the process of mixing, respectively, were considered.

Introduction

Since 1960 a great deal of new information relating to thermodynamic properties of binary mixtures of simple fused salts has become available. A significant part of this information has become available by the work of Kleppa and coworkers on the enthalpy of mixing, ΔH^M , of charge-symmetrical and charge-unsymmetrical fused salts.

Among the charge-symmetrical systems studied are the binary mixtures formed by the alkali nitrates,¹ alkali fluorides,² alkali chlorides and alkali bromides,³ alkali iodides,⁴ alkali sulfates,⁵ and the mixtures of

(1) O. J. Kleppa and L. S. Hersh, *J. Chem. Phys.*, **34**, 351 (1961).

(2) J. L. Holm and O. J. Kleppa, *ibid.*, **49**, 2425 (1968).

(3) L. S. Hersh and O. J. Kleppa, *ibid.*, **42**, 1309 (1965).

silver and thallium chlorides and nitrates with the corresponding alkali salts.⁶⁻⁸ Recently the binary mixtures formed among the alkaline earth chlorides⁹ and among the transition metal dichlorides and the binary mixtures of the transition metals with calcium and magnesium chloride were investigated.¹⁰ Most recently the binary anion mixtures formed by the alkali halides¹¹ and the alkali metaphosphates¹² were investigated calorimetrically.

The enthalpy of mixing data were interpreted in light of the conformal solution theories for fused salts developed by Reiss, Katz, and Kleppa (RKK),¹³ Blander,¹⁴ and Davis and Rice (DR).¹⁵ It is, however, interesting to note that the enthalpy of mixing of several of the above mentioned binary mixtures deviates significantly from the theoretical predictions. The difference between theoretical predictions and actual data is most pronounced when the simple theories are applied to calculate the enthalpy of mixing. This is not at all surprising since these theories neglect the contribution to the enthalpy of mixing from the well known polarization interactions. In the DR theory, however, these interactions are included as a perturbation to the Coulomb potential. The basic assumption in the DR theory is that the Coulomb part of the pair potential is of significantly larger magnitude than the contribution from the particular short-range interactions under consideration. For the alkali-common halide mixtures it turns out that polarization and van der Waals interactions amount to a significant part of the total enthalpy of mixing. In their study of the mixtures formed by the alkali sulfates, Østvold and Kleppa⁵ studied the effect on the enthalpy of mixing of the doubly charged sulfate anion. They found that the results could be interpreted in terms of the DR theory suitably modified to take into account the higher charge on the anion. Mixtures formed among the alkaline earth halides containing magnesium or mixtures formed among the transition metal chlorides show a much more endothermic enthalpy of mixing than what should be expected from the above-mentioned theories. Papatheodorou and Kleppa^{9,10} explained these positive contributions to the enthalpy of mixing as a consequence of the covalent character of the magnesium and the transition metal chloride melts.

Several charge-unsymmetrical fused salt systems have also been investigated by Kleppa and coworkers. Among the systems studied are the binary mixtures of the alkaline earth nitrates with the alkali nitrates,^{16,17} lead and magnesium chloride with the alkali chlorides,^{18,19} beryllium fluoride with the alkali fluorides,²⁰ and the transition metal chlorides (CdCl_2 ,²¹ MnCl_2 , FeCl_2 , CoCl_2 ,²² NiCl_2)²³ with the alkali chlorides. The enthalpy of mixing data were for some of the systems interpreted in terms of the conformal solution theory for charge-unsymmetrical fused salts by Davis.²⁴ The Davis theory is based on Coulomb interactions only

between the ions of the salt mixture. As a first approximation the Davis theory predicts a linear relationship between the interaction parameter, $\lambda = \Delta H^M / x_1 x_2$, and the distance parameter, $\delta_{12} = (d_1 - d_2) / d_1 d_2$, at constant temperature, volume, and composition. x_1 and x_2 are the mole fractions of the two components and d_1 and d_2 are the cation-anion distance for the two-component salts. The alkaline earth-alkali nitrate²⁴ mixtures and the magnesium-alkali and lead-alkali chloride^{18,19} mixtures all give approximate straight lines when the interaction parameter, λ , is plotted vs. δ_{12} for systems having a common salt. For the transition metal dichloride-alkali chloride mixtures the limiting interaction parameter, $\lambda(x_{\text{MCl}_2} = 0)$ was changing linearly with δ_{12} while the limiting interaction parameter $\lambda(x_{\text{MCl}_2} = 1)$ deviated somewhat from a straight line relationship for common MCl_2 systems.^{22,23}

The concentration dependence of the interaction parameter, however, shows a much more complex behavior in the magnesium and transition metal dichloride melts than in the simple charge-unsymmetrical nitrate, chloride, and bromide mixtures involving the calcium, strontium, and barium salts. This is due to the additional forces which are present between the ions in the magnesium and transition metal dichloride mixtures. These forces are covalent in nature and sufficiently strong to modify the thermodynamic properties of the salt mixture as well as the local arrangement of the ions to a significant degree. The beryllium-alkali fluoride melts studied by Holm and Kleppa²⁰ also show a much more complex concentration dependence than the simple charge-unsymmetrical fused salt systems.

- (4) M. E. Melnichak and O. J. Kleppa, *J. Chem. Phys.*, **52**, 1790 (1970).
- (5) T. Østvold and O. J. Kleppa, *Acta Chem. Scand.*, **25**, 919 (1971).
- (6) O. J. Kleppa, R. B. Clarke, and L. S. Hersh, *J. Chem. Phys.*, **35**, 175 (1961).
- (7) O. J. Kleppa and L. S. Hersh, *ibid.*, **36**, 544 (1962).
- (8) L. S. Hersh, A. Navrotsky, and O. J. Kleppa, *ibid.*, **42**, 3752 (1965).
- (9) G. N. Papatheodorou and O. J. Kleppa, *ibid.*, **47**, 2014 (1967).
- (10) G. N. Papatheodorou and O. J. Kleppa, *ibid.*, **51**, 4624 (1969).
- (11) M. T. Melnichak, unpublished results.
- (12) H. C. Ko and O. J. Kleppa, *Inorg. Chem.*, **10**, 771 (1971).
- (13) H. Reiss, J. L. Katz, and O. J. Kleppa, *J. Chem. Phys.*, **36**, 144 (1962).
- (14) M. Blander, *ibid.*, **37**, 172 (1962).
- (15) H. T. Davis and S. Rice, *ibid.*, **41**, 14 (1964).
- (16) O. J. Kleppa and L. S. Hersh, *Discuss. Faraday Soc.*, **32**, 99 (1962).
- (17) O. J. Kleppa, *J. Phys. Chem.*, **66**, 1668 (1962).
- (18) F. G. McCarty and O. J. Kleppa, *ibid.*, **68**, 3846 (1964).
- (19) O. J. Kleppa and F. G. McCarty, *ibid.*, **70**, 1249 (1966).
- (20) J. L. Holm and O. J. Kleppa, *Inorg. Chem.*, **8**, 207 (1969).
- (21) G. N. Papatheodorou and O. J. Kleppa, *ibid.*, **10**, 872 (1971).
- (22) G. N. Papatheodorou and O. J. Kleppa, *J. Inorg. Nucl. Chem.*, **33**, 1249 (1971).
- (23) G. N. Papatheodorou and O. J. Kleppa, *ibid.*, **32**, 889 (1970).
- (24) H. T. Davis, *J. Chem. Phys.*, **41**, 2761 (1964).

The purpose of the present work is first of all to present new reliable enthalpy of mixing data for binary mixtures of charge-unsymmetrical fused salts. The second task is to compare these data with the present theories describing charge-unsymmetrical fused salt systems to see if some of the properties of these mixtures can be described within the framework of these theories.

Experimental Section

Apparatus. All calorimetric experiments reported in the present work were performed in a single unit microcalorimeter suitable for work up to 1100°. Apart from its single (rather than twin) construction, this apparatus is similar to the one used by Hersh and Kleppa³ at temperatures up to 800°. In the absence of a twin construction, the furnace surrounding the calorimeter is equipped with a Leeds and Northrup proportional temperature controller giving a stable temperature ($\pm 0.1^\circ$) in the furnace system. The calorimeter assembly is heavily lagged with respect to the furnace so as to avoid as far as possible short-term drifts resulting from slight variations in the controlled temperature.

The temperature-sensing device of this calorimeter consists of a 54 + 54 junction Pt—Pt—13%Rh thermopile, the output of which is amplified by means of a Leeds and Northrup 9835-B DC amplifier and recorded on a Leeds and Northrup Type H-Azar recorder. The emf *vs.* time curves were integrated by means of an Ott precision planimeter. In this way the area between curve and base line, which is proportional to the total heat, could be determined with a precision of about 0.3%.

All experiments were performed in fused silica containers under an excess pressure of 10 mm of pure dry nitrogen to prevent moisture from entering the system. The container was maintained in the calorimeter inside a fused silica envelope of about 24 mm o.d., 32 in. long. The lower 10 in. of this envelope was reduced in diameter to 22 mm o.d. to fit snugly inside the calorimeter proper. At the top of the envelope was a gas inlet and a female standard-taper 29/42 ground joint. The male part of this joint supported a "charging and mixing device." This consisted of an outer fused silica tube of 9 mm o.d. with six blown radiation shields and a central manipulation tube of 6 mm o.d. The latter was used to move the break-off tube up and down. Its bore served as a channel for the platinum-drop calibrations and as a gas inlet. The fused silica break-off tubes, which were connected to the manipulation tube with a thin platinum wire, were ≈ 10 mm o.d. and 5–7 in. long. At the bottom of each there was a fine break-off tip. During the mixing experiments reported here, one of the two fused salts was contained in the breakoff tube and the second salt in a fused silica test tube of about 18 mm

o.d. and 5.5 in. length. The bottom of the break-off tube had an increased diameter (≈ 12 mm o.d.) to prevent the salt in the test tube from creeping up between the walls of the break-off and the test tube.

Chemicals. The sources of, major impurities in, and over-all purity of the salts used in the present work are given in Table I.²⁵ Due to high hydroxide content in the commercial products of the most hygroscopic salts, these salts were prepared by the present author from the carbonate and the hydrogen halide. After neutralization of the carbonate with acid the water solution containing the alkali or alkaline earth halide was heated until most of the excess water had evaporated. The salt was separated from the solution by filtration. By dissolving the salt and repeating the evaporation and filtering processes pure salt ready for drying was obtained. All the salts except the lithium iodide, strontium iodide, and magnesium bromide were dried in the following manner. The drying device consisted of a 6 cm o.d. and 30 cm long Pyrex tube with a Pyrex fritted disk at the bottom. At the top of the tube was a standard-taper 45/50 ground joint; 250–500 g of salt was added to a fused-silica cylinder which fitted into the Pyrex tube. The Pyrex tube was placed in a furnace and slowly heated from room temperature to 450° over a period of 20–60 hr. Pure dry nitrogen or pure dry hydrogen halide was passed through the salt bed. The gases leaving the drying apparatus passed through a mercury trap. The hydrogen halides were absorbed in a second water trap. Hydrogen halide was used only to dry the magnesium, calcium, and strontium salts. Strontium and lithium iodide were dried under vacuum by slowly increasing the temperature of the salts up to 300° over a period of 3 weeks; otherwise rapid hydrolysis occurred. Before the salts were used they were finally fused under vacuum. The strontium iodide was separated from insoluble strontium oxide by means of vacuum filtration. The magnesium bromide, however, was more difficult to dehydrate. The salt made from magnesium carbonate and hydrogen bromide (E. Merck AG.) of analytical reagent grade quality was first heated slowly under vacuum from room temperature to 200° over a period of 3–4 days. The salt was then transferred to the gas flushing apparatus where dry hydrogen bromide was passed through the salt for 1–2 days while the temperature was increased to 400°. The salt was then sublimed under vacuum. All the salts were analyzed for cation impurities by a semiquantitative spectrographic method. All the salts

(25) Listings of source and impurity of salts and enthalpies of mixing at different temperatures and concentrations for the present systems will appear in Tables 1 and 3–9 immediately following this article in the microfilm edition of this volume of the journal. Single copies may be obtained from the Business Operations Office, Books and Journals Division, American Chemical Society, 1155 Sixteenth St., N.W., Washington, D. C. 20336, by referring to code number JPC-72-1616. Remit check or money order for \$4.00 for photocopy or \$2.00 for microfiche.

were also tested for neutrality with phenolphthalein and the hydroxide content was determined if the salts were basic. The overall purity was determined in the following manner. About 4 mmol of the salts were dissolved in distilled deionized water. By passing this solution through a cation-exchange column and titrating the resulting solution with standardized 0.1 *N* sodium hydroxide solution, the total content of alkali or alkaline earth halide in the sample could be determined.

Procedure. In the course of the present investigation only liquid-liquid experiments were carried out. The salts were maintained in an inert atmosphere of pure dry nitrogen gas which was passed through the silica liner at a flow rate sufficient to keep an overpressure of 10 mm in the liner when the outlet was closed.

Prior to each calorimetric experiment the fused silica liner with its content was preheated to a temperature about 50° above that of the calorimeter proper. This served to reduce the thermal disturbance which was associated with the introduction of the loaded liner into the calorimeter. In typical runs the mixing experiment was carried out 1-1.5 hr after the liner had been introduced. By preheating the liner, adjustment of the liquid levels in the break-off and test tube could also be obtained. This is important when measuring small heat effects because of the vertical temperature gradient in the calorimeter. This gradient was for the present work about 0.05°/cm over 18 cm. The actual mixing operation was initiated by breaking the fine tip of the break-off tube. Stirring was achieved by moving the break-off tube up and down in the test tube. Corrections to the enthalpy of mixing from the breaking of the tip and stirring were negligible for the present work. All weighings of the hygroscopic salts were carried out in the drybox. The weighed samples of the two salts to be mixed (one in the test tube and the other in the break-off) were transferred from the drybox to the fused-silica envelope. The total time of exposure of the sample to air was of the order of 30 sec. The calibration of the calorimeter was carried out by dropping, from room temperature into the apparatus at working temperature, small pieces of pure 2 mm o.d. Pt wire weighing a total of about 0.5 g. The evaluation of the resulting endothermic heat effect was based on Kelley's equation for the heat content of platinum. During its fall into the calorimeter, the platinum wire picked up some heat. The magnitude of this effect was determined in separate experiments by carrying out calibrations with platinum wire of different diameters. Extrapolation to zero surface area showed that, for 2 mm o.d. wires, this pick-up of heat represented 0.5% at 690°, 1.5% at 800°, 3% at 900°, 4% at 1000°, and 6% at 1090°. The calorimeter temperature was measured with a Pt-Pt-13%Rh

thermocouple. The thermocouple was standardized against a National Bureau of Standards calibrated Pt-Pt-10%Rh couple.

Results

A total of 32 binary alkali-alkaline earth halide systems were studied by liquid-liquid experiments. Twenty-seven of them were studied in detail; *i.e.*, the dependence of the enthalpy of mixing on composition was explored. For 7 of these systems involving cesium, rubidium, and potassium salts, the temperature dependence of the enthalpy of mixing was also investigated. The remaining 5 systems, the strontium-alkali iodide systems, were studied only near the 50-50 composition.

For one system, CaCl₂-CsCl, a few dilution experiments were carried out in addition to the normal mixing of the pure components. This was necessary for the present system at low temperature (810°) because of the formation of CsCaCl₃ crystals (*T*_i = 910°). When mixing the salts in the break-off tube and in the crucible, CsCaCl₃ crystals can be formed. Due to the stirring some of these crystals might stick to the walls of the tubes and consequently not dissolve in the fused salt mixture. Because of the high negative enthalpy of formation of CsCaCl₃,²⁶ too negative values of the enthalpy of mixing were obtained. Dilution experiments were thus carried out at concentrations close to the composition where the first crystals should form to get correct information on the enthalpy of mixing in this concentration range. The experimental results are recorded in Tables III-IX.²⁵ In these tables the first column gives the binary system investigated and the temperature of the investigation, the second the mole fraction of the final mixture, the third the total number of moles used in each experiment, the fourth the molar enthalpy of mixing, ΔH^M , and the fifth the enthalpy interaction parameter, $\lambda = \Delta H^M/x_1x_2$. The enthalpy changes actually measured ranged from 1.3 cal in SrBr₂-LiBr to 200 cal for certain compositions in the MgBr₂-CsBr binary. In Figures 1-6 the interaction parameter, $\lambda = \Delta H^M/x_1x_2$, is plotted *vs.* mole fraction for the systems investigated. The lines drawn in these figures represent curves obtained by the method of least squares. The standard deviation represents 0.2-10% (0.5% in the SrCl₂-KCl to 10% in the SrBr₂-LiBr system) of the interaction parameter, depending on its absolute magnitude. For each system which was studied in detail except the magnesium bromide systems, the enthalpy of mixing was fitted by an expression of the type

$$\Delta H^M = x_1x_2\{a + bx_2 + cx_2^2 + dx_2^3\} \quad (1)$$

where x_2 is the mole fraction of alkaline earth halide in the mixture. The constants *a*, *b*, *c*, and *d* were de-

(26) G. N. Papatheodorou, private communication.

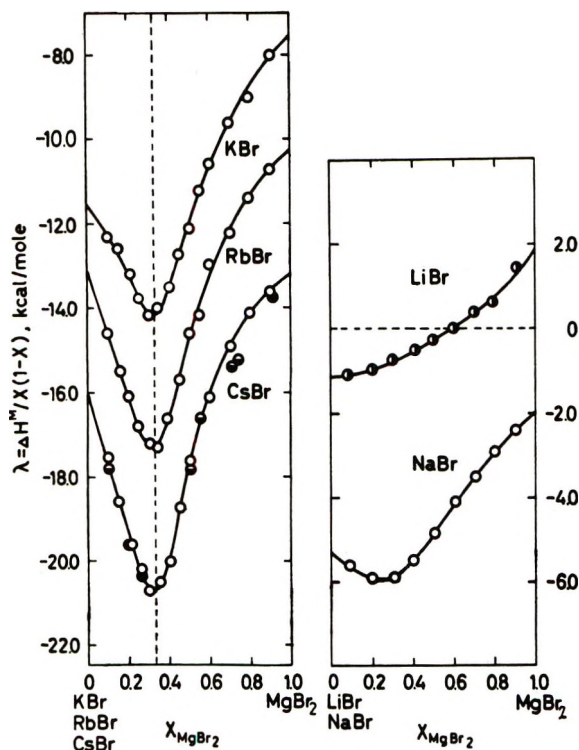


Figure 1. Interaction parameter, $\Delta H^M/x(1-x)$, in liquid mixtures of magnesium bromide with the alkali bromides: \circ , 772°; \odot , 722°; \ominus , 715°.

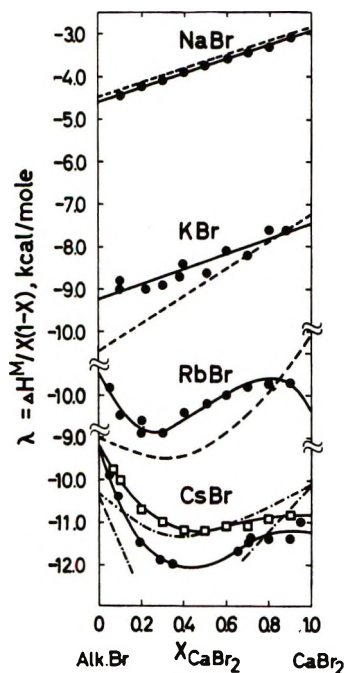


Figure 2. Interaction parameter, $\Delta H^M/x(1-x)$, in liquid mixtures of calcium bromide with the alkali bromides: \bullet , 810°; \square , 894°; $-\cdot-$, $-$, corresponding chlorides.

terminated by the method of least squares. In some cases it was not possible to calculate the constants c and d because of too great scatter in the experimental data or too few data points. A summary of the ex-

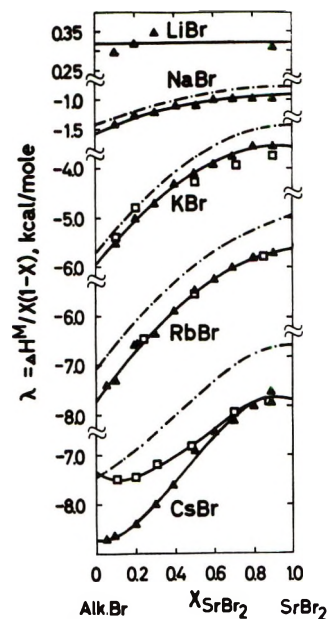


Figure 3. Interaction parameter, $\Delta H^M/x(1-x)$, in liquid mixtures of strontium bromide with the alkali bromides: \blacktriangle , 760°; \square , 894°; $-\cdot-$, corresponding chlorides.

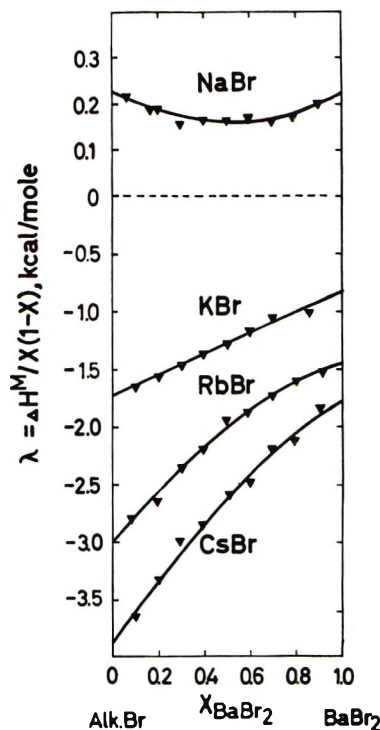


Figure 4. Interaction parameter, $\Delta H^M/x(1-x)$, in liquid mixtures of barium bromide with the alkali bromides: \blacktriangledown , 863°.

perimentally determined coefficients a , b , c , and d for all the systems investigated together with the standard deviation of the enthalpy interaction parameter, λ , is given in Table II. For the iodide systems, where the concentration dependence of the enthalpy of mixing was not determined, only the interaction parameter at the 50–50 point can be given.

Table II: Summary of Enthalpy of Mixing, ΔH^M , Data for the Binary Alkali-Alkaline Earth Halide Systems ($\Delta H^M/x_1x_2 = a + bx_2 + cx_2^2 + dx_2^3$ Where x_2 Is the Mole Fraction of the Alkaline Earth Halide in the Mixture)

| System | T, °C | a, kcal/mol | b, kcal/mol | c, kcal/mol | d, kcal/mol | Std dev, kcal/mol |
|-------------------------|----------|----------------|--------------------------|----------------|----------------|----------------------|
| MgBr ₂ -LiBr | 772 | -0.25 | | | | |
| -NaBr | 772 | -4.8 | | | | |
| -KBr | 772 | -11.9 | = 4 $\Delta H^{M_{0.5}}$ | | | |
| -RbBr | 772 | -14.7 | | | | |
| -CsBr | 772 | -17.6 | | | | |
| -CsBr | 715 | -17.8 | | | | |
| CaCl ₂ -LiCl | 810 | -0.483 | | -0.090 | 0.284 | |
| -NaCl | 810 | -4.482 | 1.602 | | | 0.07 |
| -KCl | 810 | -10.447 | 3.257 | | | 0.159 |
| -RbCl | 810 | -10.945 | -3.524 | 6.012 | | 0.236 |
| -RbCl | 894 | -10.897 | 0.253 | 1.829 | | 0.200 |
| -CsCl | 863 | -10.179 | -10.742 | 20.026 | -9.239 | 0.084 |
| -CsCl | 894 | -10.117 | -7.195 | 12.499 | -5.263 | 0.099 |
| CaBr ₂ -NaBr | 810 | -4.589 | 1.657 | | | 0.034 |
| -KBr | 810 | -9.263 | 1.801 | | | 0.192 |
| -RbBr | 810 | -9.484 | -10.901 | 26.877 | -16.798 | 0.166 |
| -CsBr | 810 | -9.143 | -16.757 | 29.082 | -14.426 | 0.132 |
| -CsBr | 894 | -9.127 | -10.528 | 16.517 | -7.671 | 0.052 |
| SrCl ₂ -NaCl | 894 | -1.505 | 1.554 | -0.792 | | 0.014 |
| -KCl | 894 | -5.716 | 5.066 | -2.499 | | 0.022 |
| -RbCl | 894 | -7.045 | 5.281 | -2.198 | | 0.050 |
| -CsCl | 894 | -7.463 | 1.939 | 4.471 | -3.721 | 0.051 |
| SrBr ₂ -LiBr | 760 | 0.320 | | | | 0.030 |
| -NaBr | 760 | -1.599 | 1.480 | -0.790 | | 0.020 |
| -KBr | 760 | -5.969 | 5.125 | -2.719 | | 0.038 |
| -RbBr | 760 | -7.718 | 5.641 | -2.536 | | 0.086 |
| -CsBr | 760 | -8.730 | 0.115 | 10.389 | -7.701 | 0.095 |
| -CsBr | 894 | -7.387 | 1.919 | 9.694 | -6.408 | 0.041 |
| SrI ₂ -LiI | 695 | 0.27 | | | | |
| -NaI | 695 | -1.45 | | | | |
| -KI | 695 | -4.6 | = 4 $\Delta H^{M_{0.5}}$ | | | |
| -RbI | 695 | -6.4 | | | | |
| -CsI | 695 | -8.2 | | | | |
| BaBr ₂ -NaBr | 863 | 0.228 | | -0.263 | 0.263 | |
| -KBr | 863 | -1.734 | 0.908 | | | 0.036 |
| -RbBr | 863 | -3.049 | 2.581 | -0.983 | | 0.040 |
| -CsBr | 863 | -3.887 | 2.925 | -0.804 | | 0.070 |

Since the concentration dependence of the enthalpy of mixing for the magnesium bromide-alkali bromide melts were much more complex than the concentration dependence for the other alkaline earth-alkali halide mixtures, a least-square treatment was not performed for the enthalpy of mixing for these melts, and the interaction parameter at the 50-50 point only is given in Table II.

Discussion

A Comparison between Conformal Solution Theory and Experimental Data. For simple fused-salt mixtures experiments show that the enthalpy of mixing is frequently negative. When mixing two salts with a common anion, the change in repulsive energy between the cations is an important part of the enthalpy of mixing. The change in cation-cation repulsion on mixing for a linear array of three ions was calculated by Førlund.²⁷ For charge-symmetrical mixtures the

Førlund model suggests an enthalpy of mixing approximately proportional to δ_{12}^2 . For charge-unsymmetrical mixtures of the type MX_2 -MeX, Braunstein, Romberger, and Ezell²⁸ pointed out that the Førlund model should give a change in Coulomb repulsion energy of next nearest neighbor cations for the mixing process

$$(M^{2+}X^{-}M^{2+})(l) + (Me^{+}X^{-}Me^{+})(l) = 2(M^{2+}X^{-}Me^{+})_{\text{mix}}(l)$$

equal to

$$\Delta E_C = e^2 \left\{ \frac{1}{2d_{MeX}} - \frac{2(d_{MeX} - d_{MX})}{d_{MX}(d_{MX} + d_{MeX})} \right\} \quad (2)$$

The principal variation in this equation is in the term

(27) T. Førlund, *Norg. Tek. Vitenskapsakad. Skr.* 2, 4, 4 (1957).

(28) J. Braunstein, K. A. Romberger, and R. Ezell, *J. Phys. Chem.*, 74, 4383 (1970).

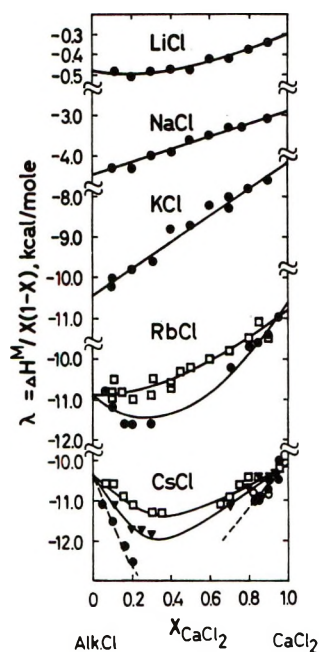


Figure 5. Interaction parameter, $\Delta H^M/x(1-x)$, in liquid mixtures of calcium chloride with the alkali chlorides: ●, 810°; ▼, 863°; □, 894°; ○, 810° dilution experiments.

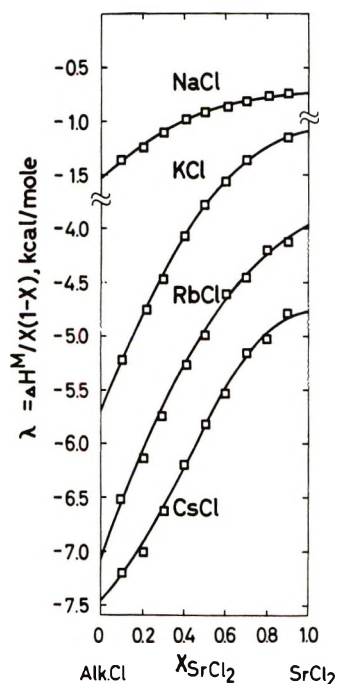


Figure 6. Interaction parameter, $\Delta H^M/x(1-x)$, in liquid mixtures of strontium chloride with the alkali chlorides: □, 894°.

$(d_{MeX} - d_{MX})$. The first term on the right-hand side is constant for a given univalent solvent, while the second term is roughly proportional to δ_{12} . Equation 2 is thus consistent with the equations correlating enthalpies and Gibbs energies of mixing with the δ_{12} parameter developed by Davis.²⁴ According to Davis,

the constant temperature and volume molar excess Gibbs energy or enthalpy interaction parameter developed to the first order in δ_{12} will have the form

$$\frac{\Delta H^M}{x(1-x)} = A + B\delta_{12} \quad (3)$$

Both A and B are universal functions of the reduced temperature, τ , and volume, ν . Since the enthalpy of mixing for most systems is almost temperature independent, the above equation can be used to compare enthalpies of mixing for different systems, $(Me^+ - M^{z+})X^-$, as long as the comparison is made at constant x , z , τ , and ν . It must be mentioned, however, that even if the constant temperature and volume enthalpy of mixing very well might be different from the constant temperature and pressure enthalpy of mixing, the functional dependence on distance parameter, δ_{12} , will be similar²⁹ (compare eq 2.44 in ref 13 with eq 21 in ref 29). Most of the simple binary mixtures of unsymmetrical fused salts investigated by Kleppa and coworkers¹⁶⁻¹⁹ show enthalpies of mixing which roughly followed the theoretical predictions. Significant differences occur, however, between different anion systems and between different common-cation subsystems. In Figure 7 the enthalpy interaction parameter for the alkali halide-alkaline earth halide mixtures is plotted *vs.* the δ_{12} parameter at $x_{MX_2} = 0$. It can be observed from this figure that there is a rather "weak" connection between the theoretical eq 3 given by Davis and the experimental data. There are several obvious reasons why eq 3 might fail to predict the experimental enthalpies: (1) τ and ν are changing from system to system; (2) the second-order term in δ_{12} is not negligible; (3) the approximate pair potential on which eq 3 is based is not sufficient to account qualitatively for the change in ionic interactions on mixing.

Although we do not have values for the dielectric constant, κ , for these mixtures, this quantity should not vary much for common anion systems since the cations are not very polarizable. We have simply set κ equal to unity in comparing the reduced temperatures for the mixtures shown in Figure 7.

The reduced temperatures are changing considerably from one common salt subsystem to another. There is a 28% change from the common $BaBr_2$ systems to the common $MgBr_2$ systems and a 31% change from the common $LiCl$ to the common $CsCl$ systems while τ is constant for a series of binary systems with a common salt. We can therefore not expect a straight line relationship between enthalpy and distance parameter from the present systems. By plotting the enthalpy interaction parameter, λ , *vs.* δ_{12} at constant composition for systems where either an alkali halide or an alkaline earth halide is a common salt, however,

(29) H. T. Davis and J. McDonald, *J. Chem. Phys.*, **48**, 1644 (1968).

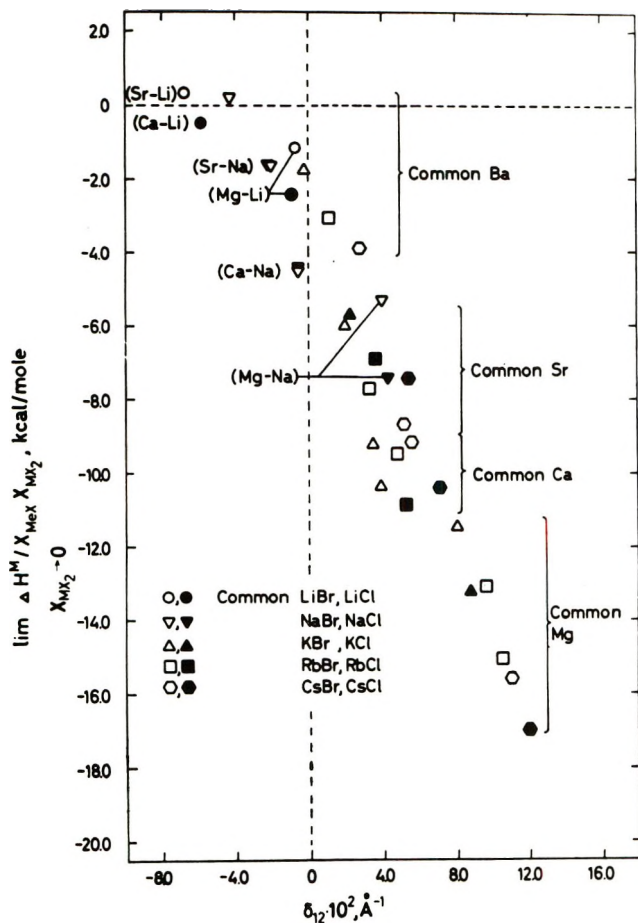


Figure 7. Limiting enthalpy interaction parameter in the alkali-alkaline earth halides vs. the distance parameter, δ_{12} . The data for the magnesium-alkali chloride melts are from a paper by Kleppa and McCarty.

we may expect a better agreement between the theoretical predictions and the experimental results. As can be seen from Figure 7 through Figure 11 this is indeed the case. The interaction parameter, λ , is a linear function of δ_{12} : as long as we have binary systems with a common salt. This is also in agreement with a very recent extension of the earlier conformal solution theory for charge-unsymmetrical fused salt mixtures developed by Davis.³⁰ In the latest version of this theory the enthalpy of mixing at constant temperature and pressure is calculated. The calculated enthalpy of mixing is shown to be a linear function of the difference in the cation-anion distances for the two salts, $d_1 - d_2$, for binary mixtures with a common component. The constants in this equation which is similar to eq 3 are, however, difficult to calculate.

The values of the constants A and B in eq 3 can be estimated when this equation is fitted to the experimental results. A systematic change in A and B is observed going from one series of binary systems with a common component to another. In the following discussion we will therefore try to rationalize the

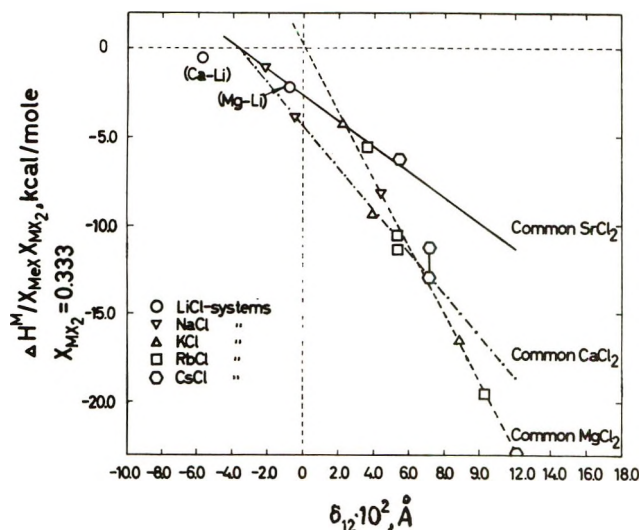


Figure 8. Interaction parameter, $\Delta H^M/x(1-x)$, in the alkali-alkaline earth chloride (bromide) mixtures vs. the distance parameter, δ_{12} , at $x_{Mx_2} = 0.333$. The data for the magnesium-alkali chloride melts are from a paper by Kleppa and McCarty.

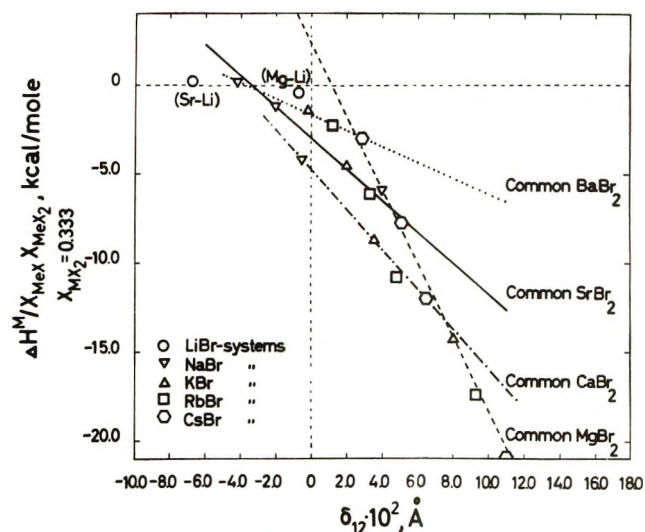


Figure 9. (See caption to Figure 8 for details.)

change in these "Davis plot" constants in terms of the predominant interionic interactions in these melts.

The Variation in the Davis Theory Constants. Let us consider the energy change which follows the substitution of one alkali ion by another in a liquid alkaline earth-alkali halide mixture. When structural changes by this process are minor, so that the number of neighbors in the nearest coordination shells is not changed, the change in cation-cation repulsion energy is an important part of the energy change. When the anion-cation distances can be assumed constant and equal to the sum of the Pauling radii, the change in

(30) H. T. Davis, *J. Phys. Chem.*, **76**, 1629 (1972).

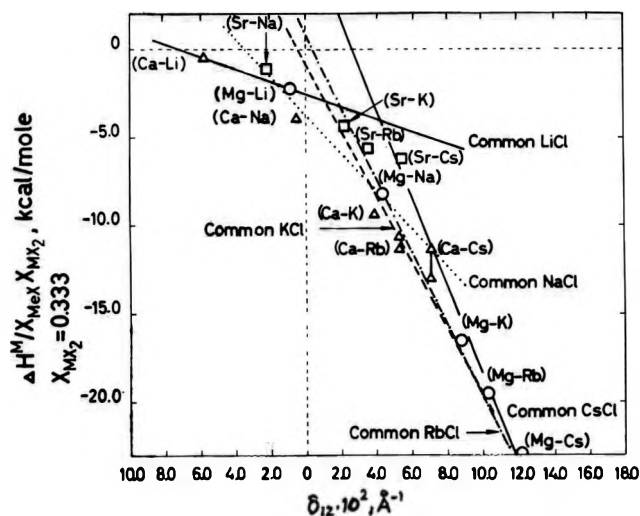


Figure 10. Interaction parameter, $\Delta H^M/x(1-x)$, in the alkali-alkaline earth chloride (bromide) mixtures vs. the distance parameter, δ_{12} , at $x_{MX_2} = 0.333$. The data for the magnesium-alkali chloride melts are from a paper by Kleppa and McCarty.

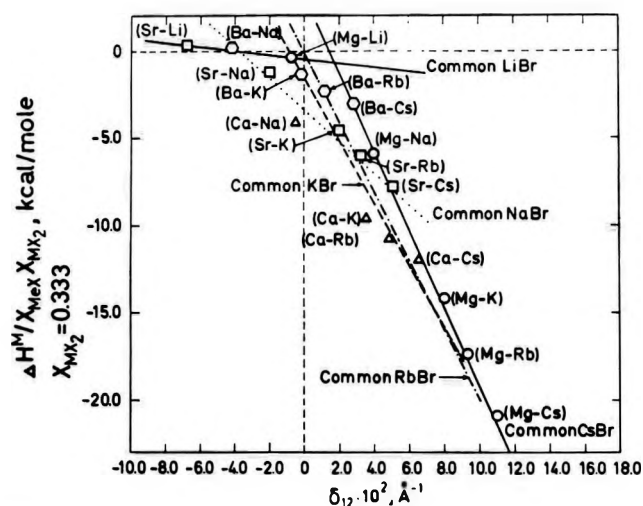
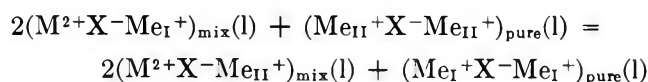


Figure 11. (See caption to Figure 10 for details.)

energy following the substitution due to the change in cation-cation repulsion may be illustrated by a model introduced by Fjørland.²⁷ Let us consider the following substitution reaction



with the change in energy

$$\Delta E_{MX_2} = 2E_{MXMe_{II}} - 2E_{MXMe_I} + E_{Me_I X Me_I} - E_{Me_{II} X Me_{II}}$$

According to the Fjørland model illustrated in Figure 12 the change in Coulombic energy following the above substitution may roughly be described by the equation

$$\Delta E_{MX_2}^C \simeq e^2 \left\{ \frac{4}{d_{MX} + d_{Me_I X}} - \frac{4}{d_{MX} + d_{Me_{II} X}} + \frac{1}{2d_{Me_I X}} - \frac{1}{2d_{Me_{II} X}} \right\} \quad (4)$$

where e is the electronic charge and d 's with suffixes are the interatomic distances. In Table X estimated values of $\Delta E_{MX_2}^C$ and $\Delta E_{MX_2}^C/\Delta\delta_{12}$ are given for different reactions of the above type. It is apparent from these values that the changes in Coulomb interaction when one alkali ion is substituted with another in a binary alkali-alkaline earth halide mixture will tend to give the Davis plot (λ vs. δ_{12}) a negative slope, that is a negative value of the constant B in eq 3. This slope will get more negative when the radius of the common alkaline earth ion is decreasing.

Table X: The Change in Coulombic Energy Occurring in a Binary Alkali-Alkaline Earth Halide Mixture When One Alkali Ion Is Substituted by Another

| Alkaline earth chloride MCl_2 | Alkali chloride $Me_I Cl$ | AlkaliII chloride $Me_{II} Cl$ | $\Delta E_{MCl_2}^C/e^2, \text{Å}^{-1}$ | $\Delta E_{MCl_2}^C/e^2\Delta\delta_{12}$ |
|---------------------------------|---------------------------|--------------------------------|---|---|
| MgCl ₂ | LiCl | NaCl | -0.029 | -0.55 |
| | LiCl | KCl | -0.60 | -0.62 |
| | LiCl | RbCl | -0.071 | -0.64 |
| | LiCl | CsCl | -0.085 | -0.66 |
| CaCl ₂ | LiCl | NaCl | -0.022 | -0.42 |
| | LiCl | KCl | -0.046 | -0.48 |
| | LiCl | RbCl | -0.056 | -0.50 |
| | LiCl | CsCl | -0.068 | -0.53 |
| SrCl ₂ | LiCl | NaCl | -0.019 | -0.36 |
| | LiCl | KCl | -0.041 | -0.44 |
| | LiCl | RbCl | -0.050 | -0.45 |
| | LiCl | CsCl | -0.061 | -0.48 |
| BaCl ₂ | LiCl | NaCl | -0.016 | -0.30 |
| | LiCl | KCl | -0.036 | -0.37 |
| | LiCl | RbCl | -0.042 | -0.38 |
| | LiCl | CsCl | -0.052 | -0.40 |

In addition to the change in Coulomb interaction occurring when an alkali ion is substituted by another according to the above-mentioned reaction, there will also be a change in polarization of the common anion due to the change in the cation environment. Fjørland²⁷ and Lumsden³¹ pointed out that an anion X^- would become polarized by the unsymmetrical electric field due to the different size and charge of the two cations on opposite sides of the anion (Figure 12). In the group $(M^{2+}X^-Me^+)$ the anion X^- is subjected to an electric field

$$F = e(2/d_{MX^2} - 1/d_{MeX^2})$$

If α is the polarizability of the anion, the polarization energy of a $(M^{2+}X^-Me^+)$ group is

(31) J. Lumsden, *Discuss. Faraday Soc.*, **32**, 138 (1961).

$$E^P = -\alpha F^2/2 = -\frac{\alpha e^2}{2} \left(\frac{\sqrt{2d_{MeX}} - d_{MX}}{d_{MeX}d_{MX}} \right)^2 \left(\frac{\sqrt{2d_{MeX}} + d_{MX}}{d_{MeX}d_{MX}} \right)^2$$

The change in polarization energy following the above reaction can thus be approximated by the expression

$$\Delta E_{MX_2}^P \simeq -\alpha e^2 \left\{ 1/d_{MeIX}^4 - 1/d_{MeIX}^4 - 4/d_{MX}^2(1/d_{MeIX}^2 - 1/d_{MeIX}^2) \right\} \quad (5)$$

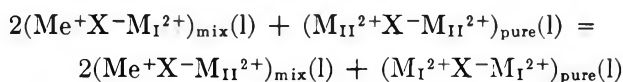
The polarization energy of the pure salts can be neglected. In Table XI estimated values of the change in polarization energy, $\Delta E_{MX_2}^P$, following the substitution are given together with the contribution of this energy change to the Davis plot slope, $\Delta E_{MX}^P/\Delta\delta_{12}$. It is apparent from the data in Table XI that the change in polarization energy following the substitution tend to give a negative Davis plot slope. This slope is increasing with increasing size on the common alkaline earth ion.

Table XI: The Change in Polarization Energy Occurring in a Binary Alkali-Alkaline Earth Halide Mixture When One Alkali Ion Is Substituted by Another

| Alkaline earth chloride MCl_2 | Alkali chloride $MeICl$ | AlkaliII chloride $MeIICl$ | $\Delta E_{MCl_2}^P/\alpha e^2, \text{ \AA}^{-1}$ | $\Delta E_{MCl}^P/\alpha e^2\Delta\delta_{12}$ |
|---------------------------------|-------------------------|----------------------------|---|--|
| MgCl ₂ | LiCl | NaCl | -0.0146 | -0.28 |
| | LiCl | KCl | -0.0274 | -0.28 |
| | LiCl | RbCl | -0.0315 | -0.28 |
| CaCl ₂ | LiCl | CsCl | -0.0367 | -0.28 |
| | LiCl | NaCl | -0.0084 | -0.16 |
| | LiCl | KCl | -0.0166 | -0.18 |
| SrCl ₂ | LiCl | RbCl | -0.0195 | -0.18 |
| | LiCl | CsCl | -0.0231 | -0.18 |
| | LiCl | NaCl | -0.0065 | -0.12 |
| BaCl ₂ | LiCl | KCl | -0.0134 | -0.14 |
| | LiCl | RbCl | -0.0157 | -0.14 |
| | LiCl | CsCl | -0.0188 | -0.14 |
| BaCl ₂ | LiCl | NaCl | -0.0040 | -0.08 |
| | LiCl | KCl | -0.0089 | -0.10 |
| | LiCl | RbCl | -0.0107 | -0.10 |
| | LiCl | CsCl | -0.0132 | -0.10 |

From the above calculations we can conclude that the Davis plot slopes for the common alkaline earth systems should increase in the sequence Mg, Ca, Sr, Ba. This is indeed experimentally observed. Figures 8 and 9 show the interaction parameter, λ , at $x_{MX_2} = 0.333$ as a function of the distance parameter, δ_{12} , for the alkali-alkaline earth chloride and bromide mixtures. Except for the lithium-alkaline earth halide systems, the data are well represented by a Davis plot for each common alkaline earth halide subsystem. As observed from these figures the Davis plot slopes are increasing, that is getting more positive, when the radius of the common alkaline earth ion is increasing.

Let us now consider the reaction



with the change in energy

$$\Delta E_{MeX} = 2E_{MeXM_{II}} - 2E_{MeXM_I} + E_{M_IXM_I} - E_{M_IXM_{II}}$$

According to the Førlund model illustrated in Figure 12 the change in Coulombic energy following the substitution may roughly be described by the equation

$$\Delta E_{MeX}^C \simeq e^2 \left\{ \frac{4}{d_{MeX} + d_{M_{II}X}} - \frac{4}{d_{MeX} + d_{M_IX}} + \frac{4}{2d_{M_IX}} - \frac{4}{2d_{M_{II}X}} \right\} \quad (6)$$

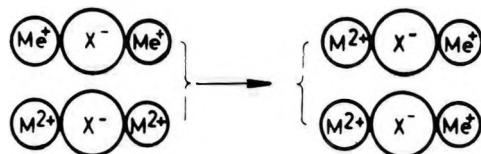
where e is the electronic charge and d 's with suffixes are the interatomic distances. Estimated values of ΔE_{MeX}^C and $\Delta E_{MeX}^C/\Delta\delta_{12}$ for different alkali-alkaline earth chloride mixtures show that the changes in Coulomb interaction when substituting one alkaline earth ion by another in a binary alkali-alkaline earth halide melt will tend to give negative Davis plot slopes which are decreasing when the size of the common alkali ion is increasing.

The change in polarization energy which follows the substitution of one alkaline earth halide by another can be estimated in the same way as outlined previously. The change in polarization energy following the above reaction can be approximated by the expression

$$\Delta E_{MeX}^P \simeq -\alpha e^2 \left\{ 4/d_{M_{II}X}^4 - 4/d_{MeX}^4 - 4/d_{MeX}^2(1/d_{M_{II}X}^2 - 1/d_{MeX}^2) \right\} \quad (7)$$

Estimated values of ΔE_{MeX}^P and $\Delta E_{MeX}^P/\Delta\delta_{12}$ for different substitutions of the above type show that the change in polarization energy following the substitution will tend to give negative Davis plot slopes which are decreasing with increasing size of the common alkali ion.

In Figures 10 and 11 the interaction parameter, λ , is plotted vs. δ_{12} at $x_{MX_2} = 0.333$. As observed from

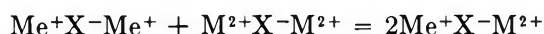


$$\Delta E^C = e^2 \left\{ \frac{4}{d_{MeX} + d_{MX}} - \frac{1}{2d_{MeX}} - \frac{4}{2d_{MX}} \right\}$$

Figure 12. Change in cation-cation repulsion energy, ΔE^C , by the process of mixing.

these figures the Davis plot is a good approximation for each common alkali halide subsystem. For the common alkali salt mixtures the slopes of the lines are decreasing with increasing size on the common cation in agreement with the above calculation.

From Figures 8–11 we can observe that the enthalpy interaction parameter at $\delta_{12} = 0$ for the common-salt subsystems is increasing when the radius of the common-salt cation is increasing. The only exceptions are the common lithium and common magnesium systems. Let us consider the change in energy due to Coulomb repulsion between next nearest neighbors and due to changes in the polarization of the common anion for the mixing process



When $d_{\text{MeX}} = d_{\text{MX}} = d$, the change in Coulomb energy according to the Førland model will be

$$\Delta E^C = -\frac{e^2}{2d} \quad (8)$$

and the change in polarization energy according to Lumsden will be

$$\Delta E^P = -\alpha \frac{e^2}{4d^4} \quad (9)$$

It is apparent from these equations that the energy of formation of the binary reference mixture will become more negative when the common-salt cation radius is decreasing. At small cation radii, however, anion-anion repulsion will become significant and contribute to a positive enthalpy of mixing. This is probably the case for the common lithium and common magnesium systems where an increase in the enthalpy of mixing of the reference mixture ($\delta_{12} = 0$) compared to the enthalpy of mixing of the common sodium and common calcium systems, respectively, is observed.

Influence of the Common Anion on the Enthalpy of Mixing. When we change the anion in a strontium-alkali halide mixture from chloride to bromide and from bromide to iodide, the enthalpy of mixing is decreasing. For all systems the enthalpy interaction parameter, λ , is a linear function of δ_{12} with the usual exceptions for the lithium containing mixtures. In Figure 13 the interaction parameter at the 50–50 composition is plotted vs. δ_{12} for the strontium containing melts. Two important features with this plot should be noted: (1) the enthalpy of mixing is decreasing in the sequence common chloride, common bromide, common iodide; (2) the slope of the λ vs. δ_{12} plot is also decreasing in the above sequence.

The entropies of mixing for mixtures involving strontium and barium do not deviate much from the ideal entropy of mixing.³² The relatively simple nature of these melts therefore indicates that the variation in the enthalpy of mixing with the common anion

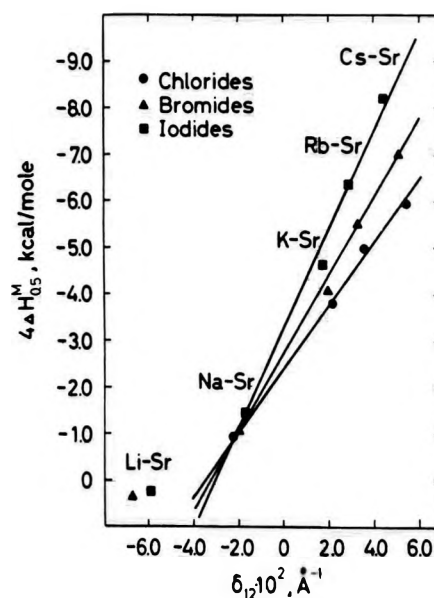


Figure 13. Interaction parameter, $\Delta H^M/x(1-x)$, in liquid mixtures of strontium-alkali halides vs. the distance parameter, δ_{12} , at $x_{\text{SrX}_2} = 0.5$.

ought to be explainable by a model taking into account Coulomb and polarization interactions between the ions in a fairly simple manner.

Let us consider the energy change which follows the substitution of one alkali ion by another in the liquid strontium-alkali halide melts. Following the arguments presented previously, the results given in Table XII are obtained. It is apparent from these results that the slope of the Davis plot lines should decrease with increasing polarizability of the common anion. The change in size of the common anion does not change the value of the constant B to any significant extent. This is true also for the Davis plot intercept, A . According to eq 8 and 9 this intercept should be roughly equal to a constant plus a term proportional to the polarizability of the common anion. The following values of λ at $\delta_{12} = 0$ are taken from Figure 13: $\lambda_{\text{Cl}^-}(\delta_{12} = 0) = -2.4$ kcal/mol, $\lambda_{\text{Br}^-}(\delta_{12} = 0) = -2.7$ kcal/mol, and $\lambda_{\text{I}^-}(\delta_{12} = 0) = -3.3$ kcal/mol. These values show, as predicted, a straight line relationship when plotted vs. the polarizability of the common anion.

The dependence of the enthalpy of mixing on the common anion is more complex for the magnesium and calcium mixtures. This is not surprising since these mixtures contain cations with considerable difference in properties. The anion-cation association in the magnesium halide-alkali halide melts, for example, will undoubtedly be dependent on the size of the common anion. This size effect will contribute to a change in the enthalpy of mixing going from one common anion system to another.

(32) T. Østvold, *J. High Temp. Sci.*, **4**, 51 (1972).

Table XII: The Change in Coulombic and Polarization Energy Occurring in a Binary Strontium-Alkali Halide Mixture When One Alkali Ion Is Substituted by Another

| Common salt, SrX ₂ | Alkali _I halide Me _I X | Alkali _{II} halide Me _{II} X | $\Delta E_{SrX_2}^C / e^2 \Delta \delta_{12}$ | $2\Delta E_{SrX_2}^P / e^2 \Delta \delta_{12}$ (average values) |
|----------------------------------|---|---|---|--|
| SrCl ₂ | LiCl | NaCl, KCl RbCl, CsCl | -0.43 | -0.41 |
| SrBr ₂ | LiBr | NaBr, KBr RbBr, CsBr | -0.45 | -0.56 |
| SrI ₂ | LiI | NaI, KI RbI, CsI | -0.45 | -0.64 |

We will not at the present stage try to put forward any detailed analysis of how the common anion influences the enthalpy of mixing in these systems. With additional structural information, like X-ray and/or Monte Carlo radial distribution functions, however, a possible explanation for the difference between the chlorides and the bromides might be found.

The Concentration Dependence of the Enthalpy Interaction Parameter. In a previous paper,³² we discussed the concentration dependence of the enthalpy and entropy of mixing in the binary magnesium chloride-alkali chloride, a few calcium chloride-alkali chloride, and a few strontium and barium chloride-alkali chloride melts. It was apparent from this discussion that no simple quasi-lattice models could account quantitatively for the concentration dependence of these thermodynamic functions. The interaction parameter, λ , was changing with concentration, and the change was dependent on the properties of the ions constituting the binary mixture. The enthalpy interaction parameter was varying considerably with concentration in systems where "complexing" occurs, but when the ionic potentials of the two cations are comparable the concentration dependence of λ was approaching the regular solution behavior, namely a constant. For most of the binary charge-unsymmetrical systems investigated, however, there seems to be at least some regularity when we compare one system with another. For 28 systems among the 32 charge-unsymmetrical fused alkali halide-alkaline earth halide mixtures investigated, the partial enthalpy of mixing of an alkali halide in the pure alkaline earth halide, $\Delta \bar{H}_{MeX}(x_{MeX} \rightarrow 0)$, is more positive than the partial enthalpy of the alkaline earth halide in the pure alkali halide, $\Delta \bar{H}_{MX_2}(x_{MX_2} \rightarrow 0)$. Note that

$$\Delta \bar{H}_1(x_1 \rightarrow 0) = \lim_{x_1 \rightarrow 0} \Delta H^M / x_1 x_2 \quad (10)$$

The only exceptions are the {Mg-Cs(Rb)}Cl and the {Ca-Cs(Rb)}Br mixtures.

We can also observe from Figures 1-6 that the interaction parameter, λ , is increasing with increasing content of alkaline earth halide in binary mixtures where the cation properties are not too different. These effects may be elucidated by the following argument.

The volumes of most fused salt mixtures are roughly determined by the anions. The density of cations in charge-unsymmetrical salt mixtures will therefore decrease with a decrease in concentration of lower-valent cations. This may be described as a change in the anion-cation nearest neighbor coordination number. From the assumption that the anion-cation coordination number is determined by the number of anions follows that the coordination number of nearest cations in pure MeX is two times the coordination number of nearest cations in pure MX₂. Let us further assume that in a mixture the number of nearest cations, z , varies with mixture composition according to the expression

$$z = z_0 \frac{n_{MeX} + n_{MX_2}}{n_{MeX} + 2n_{MX_2}} \quad (11)$$

where z_0 is the coordination number of nearest cations in pure MeX, and n_i is the number of moles of component i .

The enthalpy of mixing is roughly equal to the difference between the repulsion energies in the mixture and the repulsion energies in the pure components. On the basis of these very questionable assumptions, it can easily be shown that

$$\Delta H^M \simeq (2n_{MX_2} + n_{MeX})x'_{MX}x'_{MeX}b \quad (12)$$

where the primed x denotes equivalent fraction. Since b is negative for almost all the mixtures investigated, we can easily verify that

$$\Delta \bar{H}_{MeX}(x_{MeX} \rightarrow 0) > \Delta \bar{H}_{MX_2}(x_{MX_2} \rightarrow 0) \quad (13)$$

From eq 12 we can further observe that $\Delta H^M / x_1 x_2$ is increasing when x_{MeX} is decreasing.

The Temperature Dependence of the Enthalpy of Mixing. For a few binary charge-unsymmetrical fused-salt systems the temperature dependence of the enthalpy of mixing was investigated. Some variation with temperature was observed in the CaCl₂(Br₂)-CsCl(Br), CaCl₂-RbCl, and SrBr₂-CsBr mixtures (see Figures 2, 3, and 5) while no significant change with temperature was found in the enthalpy of mixing for the MgBr₂-CsBr and SrBr₂-KBr(RbBr) mixtures. Papatheodorou and Kleppa²² discussed the observed temperature dependence in the enthalpy of mixing for the alkali chloride-transition metal chloride melts in terms of the covalent character of the cation-anion bonds. They found a satisfactory agreement between observed and predicted temperature dependences.

The present investigation shows enthalpies which are changing with temperature for the CaCl₂(Br₂)-RbCl(Br) and CaCl₂(Br₂)-CsCl(Br) systems mainly. These systems have an intermediate compound of the type CaMeX₃ with a melting point higher than the melting point of the pure salts. The vapor pressures of the rubidium and cesium salts are increasing fairly rapidly with temperature. The range of temperature variation

was accordingly below the melting point of the intermediate compound. When mixing the pure salts, CaMeX_3 crystals might form. Due to the experimental arrangements these crystals might not dissolve in the fused mixture resulting in an incorrect enthalpy of mixing. Even so we believe that the difference between the enthalpies of mixing measured at the various temperatures reported in the present investigation is significant.

For the calcium-cesium and calcium-rubidium halide melts the tendency for association between the divalent cation and the anion is much "weaker" than in the analogous magnesium mixtures, but definitely stronger than in the corresponding strontium and barium melts. We can observe from Figures 5 and 2 that some of the calcium melts exhibit weak minima in λ around the 50-50 composition. These minima indicate a tendency toward a special stability of the melts at this composition. The association or ordering of the ions around this composition is so "weak," however, that an increase in temperature, resulting in higher thermal energy, will tend to randomize the ions in the mixture and thus increase the enthalpy of mixing. When the tendency for association is even "weaker" than in these calcium mixtures, no temperature dependence of the enthalpy of mixing will be observed. When the tendency for complexing is greater as in the magnesium case, the association equilibrium will not be shifted by a small change in thermal energy since the energy of association or complexing is much greater than RT thus resulting in no variation in the enthalpy of mixing with temperature. These arguments are in

fair agreement with the experimental observations. However, since the present data are encumbered with the above-mentioned experimental uncertainties and since no systematic information is available on the temperature dependence of enthalpies of mixing of simple fused-salt systems, we do not want to carry these arguments any further.

In summary, the enthalpies of mixing of several alkali-alkaline earth halide mixtures have been experimentally determined and compared with conformal solution theory calculations performed by Davis. It can be concluded that the enthalpy of mixing is changing linearly with the distance parameter, δ_{12} , in agreement with theoretical predictions for a series of binary mixtures with one common salt. The variations in slopes and intercepts at $\delta_{12} = 0$ of these linear relationships are elucidated in terms of the very simple Førland and Lumsden models where the change in cation-cation Coulomb and cation-anion polarization energies by the process of mixing, respectively, were considered.

Acknowledgments. This work has been performed in the laboratories of Professor O. J. Kleppa at The James Franck Institute, University of Chicago. I want to thank Professor Kleppa not only for providing the necessary facilities during my one-year stay at the institute, but as much for his interest in my work and his guidance. This work has been supported by the National Science Foundation Grants (GP-7782 and GP-14064) given to Professor Kleppa. The spectrochemical analyses were performed by Miss M. C. Batchelder.

Theory of Heats of Mixing of Certain Charge-Unsymmetrical Molten Salts

by H. Ted Davis

Departments of Chemical Engineering and Chemistry, University of Minnesota, Minneapolis, Minnesota 55465 (Received November 29, 1971)

Publication costs borne completely by The Journal of Physical Chemistry

The conformal solution theory originally developed by the author for mixing of charge unsymmetric solutions at constant temperature and volume is given for mixing at constant temperature and pressure. Ion-induced dipole interactions are included in the potential energy model. The thermodynamic mixing quantities are given as a sum of a reference mixing quantity plus terms that depend explicitly on the ionic diameters and polarizabilities of the mixture components and on the correlation functions of the reference mixtures.

Introduction

Reiss, Katz, and Kleppa¹ developed a conformal solution theory for charge-symmetric molten salts based on a simple model potential energy to account for the ionic interactions. The results of their theory were quite useful in comparing the thermodynamic excess functions for many molten salt solutions.² The author³ extended the RKK model to charge-unsymmetric salt solutions and predicted some of the observed trends for some of these systems.

The theory as originally developed by RKK and the author was for constant temperature, T , and volume, V , mixing experiments while most mixing experiments have been performed at conditions of constant temperature, T , and pressure, P . McDonald and the author⁴ remedied this situation for charge symmetric solutions by developing the original RKK theory constant T and P experiments. In addition to the heats and free energies of mixing, they predicted the volume of mixing for charge-symmetric salts and obtained a fairly good prediction for the magnitude of the mixing volume for alkali halides.

Recently, a great deal of heat of mixing data at constant T and P have been obtained by Ostvold⁵ for charge-unsymmetric systems (in particular for alkaline earth halide-alkali halide systems). Thus, it seems useful to extend the author's original work to the constant T and P case. Such extension is the purpose of this article. The potential model used herein includes also the ion-induced dipole interaction previously neglected by the author. On the basis of a simple model calculation Ostvold has suggested that this interaction contributes significantly to the energy of mixing in the charge-unsymmetric systems. The present theory gives the excess mixing properties in terms of a reference mixing quantity plus terms that depend explicitly on the ionic diameters and polarizabilities of the mixture components and the pair correlation functions of the reference mixtures. It is the lack of knowledge of the correlation function that prevents further quantitative development of the theory. Hopefully, X-

ray and neutron scattering data will someday provide this knowledge, or better yet, theory may provide it.

Theory

In a previous paper,³ the author has considered a conformal solution theory of the *constant volume* Helmholtz free energy of mixing of common anion binary mixtures of charge-unsymmetric molten salts, *e.g.*, binary mixtures between CaCl_2 and the alkali chlorides. It was assumed that like ion pairs interact according to the potential model

$$u(r) = \frac{z_\alpha^2 q^2}{\kappa r} \quad (r \geq 0) \quad (1)$$

while the unlike ion pairs interact according to the model

$$\begin{aligned} u(r) &= +\infty & (r \geq \lambda) \\ &= +\frac{z_\alpha z_\beta q^2}{\kappa r} & (r > \lambda) \end{aligned} \quad (2)$$

In eq 1 and 2, r denotes interionic separation, q is the unit electronic charge, z_α is the valence of the α th ion, κ is a local dielectric constant to account for the polarizability of the ions and the ionic medium, and λ is the cation-ion "hard core" diameter. λ will be approximately equal to the sum of the anion and cation radii determined from crystal studies. The eq 1 and 2 are a special case of the potential model used by Reiss, Katz, and Kleppa¹ in developing a conformal solution theory of charge-symmetric molten salt mixtures.

The quantity κ appearing in eq 2 is not to be viewed as a macroscopic dielectric constant but rather as a microscopic dielectric constant characterized by a small

(1) H. Reiss, J. L. Katz, and O. J. Kleppa, *J. Chem. Phys.*, **36**, 144 (1962).

(2) See, for example, C. S. Horsh and O. J. Kleppa, *ibid.*, **42**, 1309 (1965), and numerous references contained therein.

(3) H. T. Davis, *ibid.*, **41**, 2761 (1964).

(4) H. T. Davis and J. McDonald, *ibid.*, **48**, 1644 (1968).

(5) T. Ostvold, *J. Phys. Chem.*, **76**, 1616 (1972).

sample containing the nearest neighbors or perhaps the next nearest neighbors of an ion pair. A justification for this claim is that relatively small neutral unit cells serve to approximate fairly well the Madelung constants. Moreover, one can argue strongly that $\kappa \equiv 1$ is the best choice for describing the interactions in molten salt by eq 1 and 2, for one obtains from these equations with $\kappa \equiv 1$ good predicted⁶ lattice energies for simple ionic crystals such as the alkali halides and several of the alkaline earth oxides and halides. The lattice energy predicted from eq 1 and 2 is

$$U_L = -\frac{NA|z_+z_-|e^2}{\kappa\lambda} \quad (3)$$

where N is the number of molecules in the system, z_+ and z_- are the cation and anion valences, respectively, and A (about 1.6 for most ionic crystal structures) is the Madelung constant. Since U_L is of the order of -200 kcal/mol and is inversely proportional to κ , any appreciable deviation of κ from unity would result in large disagreement between eq 3 and experiment. Thus, it is the author's opinion that one should set $\kappa \equiv 1$ in using eq 1 and 2 to develop a theory of solutions of molten salts, especially since it is generally felt that most excess thermodynamic solution properties can be explained in terms of nearest and next nearest neighbor interactions so that one expects little dielectric screening and, therefore, $\kappa \simeq 1$. On the other hand, recent experiments of Ostvold indicate that the ionic polarizability contributes substantially to the heats of mixing of the alkaline earth halides with the alkali halides. Consequently, it seems useful to extend the author's previous treatment of the conformal solution theory of charge-unsymmetric salts whose interactions are described by eq 1 and 2 to systems whose interactions are of the form

$$u(r) = \frac{z_\alpha^2 q^2}{r} - \frac{z_\alpha^2 q^2 \alpha_\alpha}{r^4} \quad (4)$$

for like ion pairs and

$$u(r) = +\infty \quad (r \leq \lambda) \\ = \frac{z_\alpha z_\beta q^2}{r} - \frac{z_\alpha^2 q^2 \alpha_\beta}{2r^4} - \frac{z_\beta^2 q^2 \alpha_\alpha}{2r^4} \quad (r > \lambda) \quad (5)$$

for unlike ion pairs. In keeping with the preceding argument, κ has been set to unity. The quantity α_i is the polarizability of the i th ion. In most alkaline earth-alkali halide mixtures the anion polarizability is much larger than that of either of the cations.

Consider a mixture of $x_1 N$ molecules of the salt MX , where M^+ and X^- are univalent ions, and $x_2 N$ molecules of the salt QX_z , where Q^{+z} is a cation of valence z . N is the total number of molecules of salt in the mixture and x_i is the mole fraction of salt i . Instead of a constant volume mixing theory, it is more useful

to develop a constant pressure theory since most of the available experimental data refer to constant-pressure experiments. Conformal solution theory proceeds by relating the properties of a given melt to those of a reference melt at the same thermodynamic conditions (in the present case at the same temperature T and pressure P). The mixture configuration partition function Z_{12} is a function of the molecular parameters z , λ_1 , λ_2 , α_1 , α_2 , and α_A , where α_1 , α_2 , and α_A are the polarizabilities of the univalent cation of salt 1, the polyvalent cation of salt 2, and the common anion, respectively. The reference mixture will be characterized by the parameters z , $\lambda_1 = \lambda_2$, λ_2 , $\alpha_1 = \alpha_1^r$, $\alpha_2 = \alpha_2^r$, and $\alpha_A = \alpha_A^r$.

Using the standard procedure of conformal solution theory and the technique^{4,7} of converting from constant T, V to constant T, P results, one finds the following expression for the Gibbs free energy of mixing

$$\Delta G_m(T, P) = \Delta G_m^r(T, P) - T\Gamma \quad (6)$$

where $\Delta G_m^r(T, P)$ is the free energy of mixing of the reference mixture and

$$\Gamma = k \left(\frac{\lambda_1 - \lambda_2}{\lambda_2} \right) (a_{12}^r - x_1 a_1^r) + \\ k \frac{\alpha_1 - \alpha_1^r}{\alpha_1^r} \left(b_{12}^r - \sum_i x_i b_i^r \right) + \\ k \frac{(\alpha_2 - \alpha_2^r)}{\alpha_2^r} \left(c_{12}^r - \sum_{i=1}^2 x_i c_i^r \right) + \\ k \frac{(\alpha_A - \alpha_A^r)}{\alpha_A^r} \left(d_{12}^r - \sum_{i=1}^2 x_i d_i^r \right) \quad (7)$$

where the quantities a_{12}^r , b_{12}^r , etc., are defined in the Appendix. With the aid of the thermodynamic relation

$$\Delta H_m = -T^2 \left(\frac{\partial \Delta G_m}{\partial T} \right)_{P, N, x_i}$$

equation 6 yields the following expression for the heat of mixing

$$\Delta H_m(T, P) = \Delta H_m^r(T, P) + T^2 \left(\frac{\partial \Gamma}{\partial T} \right)_{P, N, x_i} \quad (8)$$

In the special case of a sequence of mixtures containing a common anion, $\alpha_A = \alpha_A^r$, and a common charge-unsymmetric cation, $\alpha_2 = \alpha_2^r$ and for which the term proportional to $(\alpha_1 - \alpha_1^r)$ is negligible in Γ , the following simple result obtains

(6) See, for example, C. Kittel, "Introduction to Solid State Physics," 3rd ed, Wiley, New York, N. Y., 1967, p 97.

(7) K. D. Luks and H. T. Davis, *Ind. Eng. Chem., Fundam.*, **6**, 194 (1967).

$$T^2 \left(\frac{\partial \Gamma}{\partial T} \right)_{P,N,x_1} = \left(\frac{\lambda_2 - \lambda_1}{\lambda_2} \right) 4\pi R T^2 x_1 \lambda_2^3 \times \left\{ \frac{\partial}{\partial T} [n_{12}^r (1 + x_2(z-1)) g_{AC_1}^r(\lambda_2; x_1, T, V_{12}^r) - n_1^r g_{AC_1}^r(\lambda_2; T, V_1^r)] \right\}_{P,N,x_1} \quad (9)$$

R is the gas constant. Equation 9 is the constant temperature and pressure version of the constant temperature and volume result previously published by the author.³ It is eq 9 (or eq 8 if the polarizability is to be included) that should be compared with Ostovold's experimental results. Unfortunately, the pair correlation functions are not available for molten salts and their mixtures to any degree of accuracy. Thus, the only deduction that one can make from eq 9 is that the heats of mixing of a given charge unsymmetric salt QX_z with the alkali salts $AlkX$ (a given common anion) will be a linear function of $(\lambda_2 - \lambda_1)$ at fixed T , P , and x_1 . This conclusion is in agreement with Ostovold's experimental results.⁵ Comparison among systems having different anions is difficult since the implicit dependence of the pair correlation function on α_A is not known. The quantities λ_1 and λ_2 can be taken to be temperature dependent to allow for the actual "softness" of ions.

Acknowledgment. The author is grateful to the ARO-D for financial support of this research.

Appendix

The evaluation of the quantities appearing in eq 7 is straightforward, so only the results will be given here.

$$a_{12}^r \equiv \lambda_2 \left. \frac{\partial \ln Z_{12}}{\partial \lambda_1} \right|_{\text{ref}} = -4\pi N \lambda_2^3 x_1 n_{12}^r [1 + x_2(z-1)] \bar{g}_{AC_1}^r \quad (r = \lambda_2, x_1, x_2, T, V_{12}^r) \quad (A1)$$

$$b_{12}^r \equiv \alpha_1^r \left. \frac{\partial \ln Z_{12}}{\partial \alpha_1} \right|_{\text{ref}} = \frac{x_1 N^2}{kT} \left\{ [1 + x_2(z-1)] \left\langle \frac{q^2 \alpha_1^r}{2r_{AC_1}^4} \right\rangle_{12}^r + x_1 \left\langle \frac{q^2 \alpha_1^r}{2r_{C_1 C_1}^4} \right\rangle_{12}^r + x_2 \left\langle \frac{z^2 q^2 \alpha_1^r}{2r_{C_1 C_2}^4} \right\rangle_{12}^r \right\} \quad (A2)$$

$$c_{12}^r \equiv \alpha_2^r \left. \frac{\partial \ln Z_{12}}{\partial \alpha_2} \right|_{\text{ref}} = \frac{x_2 N^2}{kT} \left\{ [1 + x_2(z-1)] \left\langle \frac{q^2 \alpha_2^r}{2r_{AC_2}^4} \right\rangle_{12}^r + x_2 \left\langle \frac{z^2 q^2 \alpha_2^r}{2r_{C_2 C_2}^4} \right\rangle_{12}^r + \left\langle \frac{q^2 \alpha_2^r}{2r_{C_1 C_2}^4} \right\rangle_{12}^r \right\} \quad (A3)$$

$$d_{12}^r \equiv \alpha_A^r \left. \frac{\partial \ln Z_{12}}{\partial \alpha_A} \right|_{\text{ref}} = [1 + x_2(z-1)] \frac{N^2}{kT} \left\{ x_1 \left\langle \frac{q^2 \alpha_A^r}{2r_{AC_1}^4} \right\rangle_{12}^r + x_2 \left\langle \frac{z^2 q^2 \alpha_A^r}{2r_{AC_2}^4} \right\rangle_{12}^r + [1 + x_2(z-1)] \left\langle \frac{q^2 \alpha_A^r}{2r_{AA}^4} \right\rangle_{12}^r \right\} \quad (A4)$$

The pointed brackets $\langle L \rangle_{12}^r$ denote the canonical ensemble average of L with respect to the reference ensemble of composition x_1, x_2 at T and P . The quantity $g_{AC_1}^r$ denotes the contact value of the pair correlation function for an anion and a cation of salt 1 in the reference mixture $n_{12}^r \equiv N/V_{12}^r$. The quantities $a_i^r = \lim_{x_i \rightarrow 1} a_{12}^r$, $b_i^r = \lim_{x_i \rightarrow 1} b_{12}^r$, etc.

Vapor-Phase Absorbance and Thermodynamic Properties of Cuprous Chloride and Cuprous Bromide

by David L. Hilden and N. W. Gregory*

Department of Chemistry, University of Washington, Seattle, Washington 98195 (Received December 9, 1971)

Publication costs assisted by the National Science Foundation

The temperature dependence of the near-ultraviolet optical absorbance spectrum of vapors in equilibrium with condensed phases of CuCl and of CuBr has been observed. Results are used to derive enthalpies of vaporization, crystal-phase transition, and melting. Evidence that the absorbing species is the trimer is presented. Significant amounts of tetramer occur in CuCl vapor, but only minor amounts of tetramer occur in CuBr vapor. A value for the enthalpy of dissociation of $\text{Cu}_3\text{Br}_3(\text{g})$ to $\text{CuBr}(\text{g})$ is estimated from absorbance data observed in double-oven experiments.

A significant amount of work has been published concerning the molecular composition of the cuprous halide vapors. In 1950 Brewer and Lofgren, in a study of the reaction of hydrogen chloride with copper in the temperature range 988–1340°K, concluded that in the temperature and pressure range of their work Cu_3Cl_3 is the dominant vapor species.¹ They also derived equilibrium data for the vapor-phase dissociation of the trimer to the monomer. Wong and Schomaker proposed a structure for the trimer based on electron diffraction experiments.² In recent effusion studies of the vapor pressure of CuCl(s) in the vicinity of its melting point, authors have generally assumed the trimer to be the only vapor species of importance.^{3–5} However, mass spectrometric studies of CuCl show the presence of significant amounts of tetramer along with trimer in the saturated vapor below the melting point.^{6,7} Derivation of thermodynamic properties is further complicated by the existence of a phase transition in solid CuCl in the vicinity of its melting point.^{8,9}

We wish to report a study of vaporization characteristics of CuCl and of CuBr by observation of the spectrophotometric absorbances of the saturated vapors as functions of temperature. Relatively sharp peaks, suitable for quantitative measure of concentration changes, are observed in the vicinity of 230 nm. Evidence is presented to show that the trimer species of these substances are responsible for the main absorbance peaks. Heats of vaporization of the trimer from various condensed phases are derived. Double-oven experiments are also reported which provide evidence of change in molecular composition of the vapor when the temperature is increased at constant pressure.

Experimental Part

Absorbance measurements were made with a modified Beckman DU spectrophotometer^{10,11} and with a Cary 14H spectrophotometer.^{12,13} A representative

spectrum of each compound over the wavelength range studied is shown in Figures 1 and 2, respectively. For CuCl, a major peak with a maximum at 223.5 nm, having narrow shoulders at 218 and 238 nm and a broad knee with maximum at approximately 273 nm, is observed. The spectrum displays a minimum at 205 nm below which the absorbance rises rapidly to the wavelength limit of the spectrophotometer (186.5 nm). CuBr shows a major peak with a maximum at 229 nm, a narrow shoulder at 245 nm, and a broad knee with maximum at approximately 280 nm. Again the spectrum displays a minimum (213 nm) below which the absorbance rises steadily; a shoulder on the low-wavelength side of the major peak is not observed in CuBr vapor, however.

Two previous reports of the near-ultraviolet spectrum of vapors developed over the copper halides have been found.^{14,15} In both instances the absorption spec-

- (1) L. Brewer and N. L. Lofgren, *J. Amer. Chem. Soc.*, **72**, 3038 (1950).
- (2) C.-H. Wong and V. Schomaker, *J. Phys. Chem.*, **61**, 358 (1957).
- (3) D. W. Magee, Ohio State University, 1955; University Microfilms Order No. 14,474, Ann Arbor, Mich. 48106.
- (4) R. A. J. Shelton, *Trans. Faraday Soc.*, **57**, 2113 (1961).
- (5) R. R. Hammer and N. W. Gregory, *J. Phys. Chem.*, **68**, 3229 (1964).
- (6) H. M. Rosenstock, J. R. Sites, J. R. Walton, and R. Baldock, *J. Chem. Phys.*, **23**, 2442 (1955).
- (7) M. Guido, G. Balducci, G. Gigli, and M. Spoliti, *ibid.*, **55**, 4566 (1971).
- (8) M. Lorenz and J. S. Prener, *Acta Crystallogr.*, **9**, 538 (1956).
- (9) J. Teltow, *Z. Phys. Chem. (Leipzig)*, **211**, 241 (1959).
- (10) J. D. Christian, University of Washington, 1965; University Microfilms Order No. 66-5850, Ann Arbor, Mich. 48106.
- (11) A. A. Passchier, University of Washington, 1968; University Microfilms Order No. 68-12,709, Ann Arbor, Mich. 48106.
- (12) "Cary 14H Instruction Manual," Serial No. 1811, Cary Instruments, Monrovia, Calif.
- (13) Experimental details may be found in the thesis of D. L. Hilden, University of Washington, Seattle, Wash., 1971.
- (14) S. K. Butkowiak and S. Boizowa, *Phys. Z. Sowjetunion*, **5**, 393 (1934).

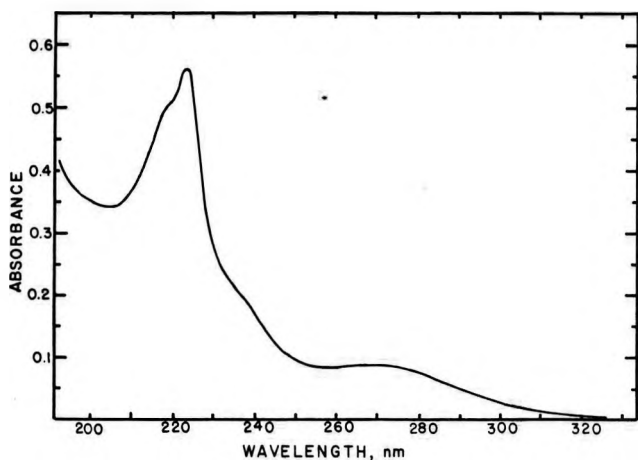


Figure 1. A representative ultraviolet spectrum (Cary 14H) of cuprous chloride vapor: condensed sample at 441°; vapor compartment at 447°; fused silica cell, 5.000-cm path length.

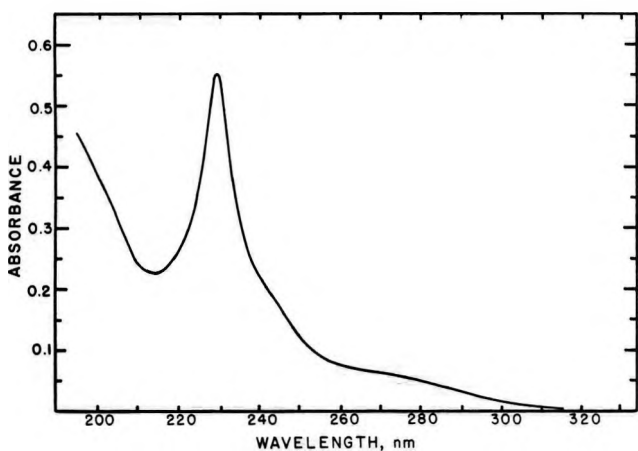


Figure 2. A representative ultraviolet spectrum (Cary 14H) of cuprous bromide vapor: condensed sample at 480°; vapor at 485°; fused silica cell, 5.000-cm path length.

trum was photographed; Terrien¹⁵ locates the principal maxima at 223 nm for CuCl and 230 nm for CuBr, in good agreement with the present findings.

In the present study the half-widths of the major peaks (the half-widths on the long-wavelength side were 64 Å for CuCl and 71 Å for CuBr) were, within experimental error, independent of temperature. From this we conclude that the molar absorptivity at the wavelength of the maximum may be assumed virtually independent of temperature over the range studied.¹⁶⁻¹⁸ Hence the ideal gas partial pressure of the absorbing species may be assumed proportional to the product of the absorbance (A) and the absolute temperature (T), divided by the cell path length (b). Heats of vaporization were derived by a least-squares treatment of the data in the form $\ln(AT/b)_{\lambda_{\max}} = -MT^{-1} + N$, where $M = \Delta H^\circ/R$.

Three independently prepared samples of CuCl were used to study the temperature dependence of the main

absorption peak with the vapor in equilibrium with relatively large amounts of the condensed phase. For sample 1, Merck and Co. CuCl (assay; minimum 90% CuCl) was repeatedly resublimed under high vacuum until the product was white; then 0.054 g was transferred into a Beckman DU quartz cell (path length 4.907 cm; all cells used had diameters of ~ 1.8 cm) and the cell was attached to a vacuum system. The cell was evacuated to 10^{-6} Torr and heated to 250° before it was sealed by collapsing the Pyrex side of a graded seal attached to a side arm. Sample 2 was prepared by reaction of Cu foil (Baker Analyzed reagent, 99.96% Cu) with Cl₂ gas (produced by thermal decomposition of dehydrated Baker Analyzed reagent grade CuCl₂·2H₂O, 100.0%). The CuCl formed was resublimed twice over copper foil. Approximately 0.1 g was placed in a Beckman DU cell (path length 4.816 cm) along with some copper foil. The cell was baked out and degassed as described for the first sample. The third sample was produced in a similar way as the second, and was finally sublimed directly into a Cary 14H cell (path length 5.000 cm) under vacuum. Excess copper was not present in this sample.

Three samples of CuBr were also prepared. The first, studied with the Beckman DU (cell path length 4.916 cm), was formed by reaction of Baker Analyzed reagent bromine, 99.8%, with the copper foil at 200°. The CuBr₂ formed was subsequently decomposed under vacuum to yield CuBr which was then repeatedly resublimed under vacuum to yield a pale green product. The second sample was prepared in the same way, with material finally sublimed into a Cary 14H cell of 2.500-cm path length. The third sample was prepared with bromine, produced by thermal decomposition of Baker Analyzed reagent CuBr₂, reacting with an excess of copper and the CuBr sublimed away from the copper. This sample was introduced into a 5.000-cm Cary 14H cell, which was evacuated to 10^{-6} Torr and degassed at 300° for several hours before it was sealed.

During absorbance measurements, cell temperatures were measured with chromel-alumel thermocouples, calibrated against NBS standards, which were placed in contact with the cell window, the cell center, and the tip of the side arm, respectively. The cell windows and body were held several degrees above the temperature of the tip of the side arm, in which the condensed material collected, to avoid condensation of material on the windows. The temperature of the tip was used to correlate the equilibrium vapor pressure data.

Results and Discussion

Cuprous Chloride. CuCl has been shown to undergo

(15) J. Terrien, *Ann. Phys. (Leipzig)*, **9**, 477 (1938).

(16) C. Sandorfy, "Electronic Spectra and Quantum Chemistry," Prentice-Hall, Englewood Cliffs, N. J., 1964.

(17) R. S. Mulliken, *J. Chem. Phys.*, **7**, 14 (1939).

(18) P. Sulzer and K. Wieland, *Helv. Phys. Acta*, **25**, 653 (1952).

a transition from the zincblende structure (γ phase) to a wurtzite structure (β phase) at 407° ; the β phase persists up to the melting point at 424° .⁸ A number of workers were unaware of the γ to β transition and this has led to questionable values for the heat of fusion.¹⁹ Watanabe, in a study of the hydrogen reduction of cuprous chloride, derived a value for the difference in enthalpy of the γ and liquid phases, by passing the β phase, of 3871 cal per formula weight of CuCl .²⁰ More recently, Carre, Pham, and Rolin²¹ have published results of a differential thermal analysis and drop calorimeter study of the cuprous halides. Their value for the γ to β transition is subject to large uncertainty because of poor definition of the β phase; however, one expects their combined heat of transition ($\gamma \rightarrow$ liquid; 2680 cal) to be more reliable. A comparison of these results with the present findings provides evidence about the degree of polymerization of the species responsible for the vapor phase absorbance.

The dependence of the absorbance on temperature observed for each of the three samples is shown in Figure 3. Data from each sample correlate well independently and show breaks at the expected transition temperatures. Although the latter are less evident when results from all three samples are put together, the three sets are considered to be within absolute experimental error; no distinguishing characteristics related to the mode of preparation can be seen. For each sample the data were separated into three temperature intervals, and a least-squares treatment carried out over each interval in the linear form $\ln AT/b = -MT^{-1} + N$. Results, together with the standard enthalpies of vaporization derived, are shown in Table I. Recommended values for the vaporization enthalpies are based on a weighted average (using weighting factors equal to the number of experimental observations in each set) and, alternatively, on a least-squares treatment using all points from the three independent samples. Results of the two approaches agree well. The combined data least-squares lines are drawn in Figure 3.

The polymerization number for the absorbing vapor species indicated by dividing Watanabe's value for the combined $\gamma \rightarrow \beta$ and melting transition heats into the value evaluated from data in Table I is very close to three. However, if the result of Carre, Pham, and Rolin is used, the polymerization number appears closer to four. Other observations to be discussed support the conclusion based on Watanabe's heat, *i.e.*, that the vapor species responsible for the major peak at 223.5 nm is the trimer. Hence, the enthalpies of vaporization in Table I have been associated with the process $3\text{CuCl}(\text{condensed}) = \text{Cu}_3\text{Cl}_3(\text{g})$. Correspondingly, heats for transitions between the various condensed phases were also derived.

Cuprous Bromide. CuBr undergoes two solid-state transitions in the temperature interval of interest.

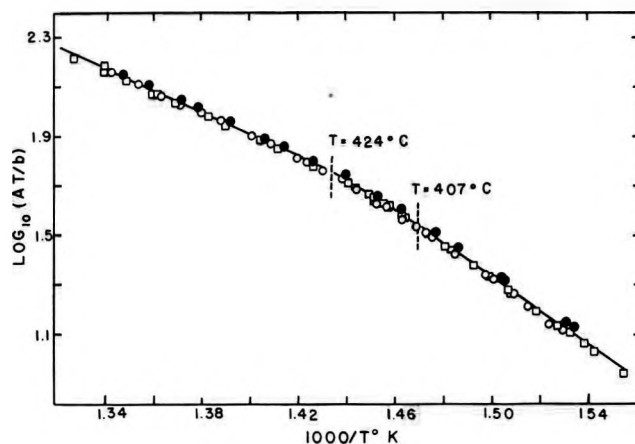


Figure 3. Logarithm at AT/b for cuprous chloride vapor at 223.5 nm vs. reciprocal temperature. The two dashed vertical lines correspond to the $\gamma \rightarrow \beta$ and melting transitions, respectively. The solid lines are linear least-square fits of the combined data in the three regions: (●) sample 1, (□) sample 2, (○) sample 3.

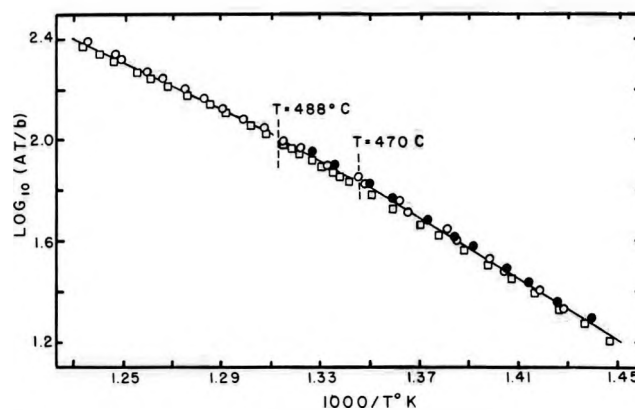


Figure 4. Logarithm of AT/b for cuprous bromide vapor absorbance at 229 nm vs. reciprocal temperature. The two dashed vertical lines correspond to the $\beta \rightarrow \alpha$ and melting transitions, respectively. The solid lines are linear least-square fits of the combined data in the three regions: (●) sample 1, (□) sample 2, (○) sample 3.

Hoshino gives the γ (zincblende) to β (hexagonal, probably wurtzite) transition temperature as 385° and the β to α (body-centered cubic) transition temperature as 470° .²² The commonly accepted melting temperature is $487\text{--}488^\circ$.^{21,23} Absorbance data were not obtained in the stability range of the γ phase. My, Perinet, and Bianco used differential thermal analysis experiments to derive an overall value for the $\beta \rightarrow$ liquid transition of 1.4 kcal per formula weight of CuBr .²⁴ Carre, Pham,

(19) D. R. Stull, Ed., "JANAF Thermochemical Tables," The Dow Chemical Co., Midland, Mich., 1963.

(20) M. Watanabe, *Sci. Rep. Tohoku Univ., Ser. 1*, 22, 423 (1933).

(21) J. Carre, H. Pham, and R. Rolin, *Bull. Soc. Chim. Fr.*, 2322 (1969).

(22) S. Hoshino, *J. Phys. Soc. Jap.*, 7, 560 (1952).

(23) J. Nölting, D. Rein, and J. Troe, *Nachr. Wiss. Goettingen, Math-Phys. Kl.*, 2, 31 (1969).

(24) L. My, G. Perinet, and P. Bianco, *Bull. Soc. Chim. Fr.*, 3651 (1965).

Table I: Enthalpies of Transition

| | $\Delta H^\circ,^a$ kcal mol $^{-1}$ | | | $\Delta H^\circ,^b$ kcal | | Temp. °C Mean or transition c |
|---|--------------------------------------|-----------|-----------|--------------------------|---------------------|--|
| | Sample | | | Wt av | Combined LS b | |
| | 1 | 2 | 3 | | | |
| $\gamma \rightarrow \text{Cu}_3\text{Cl}_3(\text{g})$ | 30.9 (6) | 32.1 (13) | 32.6 (9) | 32.0 | 32.0 | 388 |
| $\beta \rightarrow \text{Cu}_3\text{Cl}_3(\text{g})$ | 28.0 (3) | 26.8 (10) | 27.7 (6) | 27.3 | 27.9 | 415 |
| Liquid $\rightarrow \text{Cu}_3\text{Cl}_3(\text{g})$ | 20.5 (8) | 20.3 (12) | 20.8 (11) | 20.5 | 20.4 | 452 |
| $\gamma \rightarrow \beta$ (CuCl) | 1.0 | 1.8 | 1.6 | 1.6 | 1.4 | 406 |
| $\beta \rightarrow$ liquid (CuCl) | 2.5 | 2.2 | 2.3 | 2.3 | 2.5 | 424 |
| $\beta \rightarrow \text{Cu}_3\text{Br}_3(\text{g})$ | 27.4 (9) | 28.2 (9) | 27.3 (11) | 27.6 | 27.8 | 445 |
| $\alpha \rightarrow \text{Cu}_3\text{Br}_3(\text{g})$ | 25.6 (2) | 23.3 (4) | 26.0 (8) | 25.2 | 24.1 | 479 |
| Liquid $\rightarrow \text{Cu}_3\text{Br}_3(\text{g})$ | | 22.2 (10) | 21.2 (11) | 21.7 | 21.6 | 512 |
| $\beta \rightarrow \alpha$ (CuBr) | 0.6 | 1.6 | 0.4 | 0.8 | 1.2 | 464 |
| $\alpha \rightarrow$ liquid (CuBr) | | 0.4 | 1.6 | 1.2 | 0.8 | 498 |

a Weighting factors used to derive average values. b LS = least squares. c Transition temperature indicated by intersection of combined-data least-squares lines.

and Rolin²¹ report 2.1 kcal, based on drop calorimetry experiments.

Absorbance data for cuprous bromide were treated in the same way described for the chloride. Results are displayed in Figure 4, and the enthalpies of transition derived shown in Table I. The polymerization number for the species absorbing at 229 nm, indicated by comparison of the combined least-squares value for the enthalpy with the results of Carre, Pham, and Rolin, is 3. My, Perinet, and Bianco's result gives 4.3, not compatible with other observations. The condensed-phase transition heats are very small for the bromide, and the values derived from the absorbance data as well as those of the earlier workers are relatively uncertain. The absorbance data are clearly unsuited for a reliable determination of the transition temperatures. We have assumed the species absorbing at 229 nm is Cu_3Br_3 .

Temperature-Gradient Experiments. The Cary 14H furnace was designed so that the absorbance cell and its side-arm temperatures were controlled by separate furnaces. Hence it was possible to observe the temperature dependence of the absorbance of the vapor with the condensed phase held at much lower temperatures. Temperature gradients up to 150° were generated. The pressures within the cell in these experiments were in the hydrodynamic flow range; hence, it was assumed that the pressure remained constant at the value characteristic of the equilibrium vapor pressure at the temperature of the condensed phase. The absorbance A'' of the vapor at the higher temperature T'' was then compared with the vapor absorbance A' under conditions of thermal equilibrium at the temperature T' of the condensates. In the absence of any dissociation phenomenon, one expects A'/A'' to equal T''/T' .

With CuCl, a change in the character of the spectrum was observed. The shoulder (Figure 1) around 218 nm diminished in intensity as the temperature gradient

was increased; the shoulder was not detectable with the vapor at 570° and the condensed phase at 430°, for example. The appearance of the spectrum under these conditions was similar (but with the main peak still at 223.5 nm with the same width) to that of the bromide as displayed in Figure 2. It was also observed that A'/A'' was less than T''/T' , i.e., the concentration of the trimer did not decrease as much as expected. Such behavior can be explained if a higher polymer present at T' dissociates into the trimer to a greater degree as the temperature is raised to T'' without change in the total pressure.

These observations are consistent with the suggestion that the shoulder at 218 nm is due to absorbance by the tetramer. Rosenstock, *et al.*,⁶ report detection of the tetramer parent peak in mass spectral studies of the vapor emitted from CuCl at 150°. In conjunction with the present work, D. W. Schaaf has used a Spectrascan Mass Analyzer in our laboratory to study the vapors in a beam emitted from an effusion cell containing CuCl at temperatures in the range of the spectrophotometric study and observed the tetramer parent peak to have an intensity comparable to that of the trimer parent peak. A more detailed Knudsen mass spectrometric study of cuprous chloride vapor was published after completion of our work. Guido, *et al.*,⁷ also found Cu_4Cl_4 and Cu_3Cl_3 to be the dominant species in the saturated vapor in the temperature range of interest. They derive an enthalpy of vaporization for the trimer of $\Delta H^\circ_{640^\circ\text{K}} = 33.7$ kcal mol $^{-1}$ and for the tetramer of 34.6 kcal mol $^{-1}$. The value for the trimer is slightly larger than the 32.0 kcal derived from absorbance studies (Table I). However the difference is probably not appreciably beyond the combined experimental uncertainties. This evidence is taken as further support for the assumption that the peak at 223.5 nm is due to the trimer and that at 218 nm due to the tetramer. Enhanced dissociation of the tetramer in the temperature gradient experiments then provides

a reasonable explanation for the change in character of the spectrum and the relative intensities of the trimer peak.

Similar experiments with CuBr show different behavior. As noted previously a low-wavelength shoulder is not apparent in Figure 2. Correspondingly, mass analysis of the effusion beams by Mr. Schaaf shows the intensity of the tetramer mass peak in the bromide to be only a few per cent of the trimer peak. Furthermore, with the bromide the absorbance ratio A'/A'' is consistently greater than T''/T' rather than smaller, as observed for the chloride. The bromide behavior suggests that the concentration of the trimer at higher temperatures (in these experiments) is reduced by increased trimer dissociation rather than enhanced by dissociation of a higher polymer. We have assumed the monomer to be the dissociation product and estimated the equilibrium constant for the dissociation by an iterative process. Initially the concentration of the monomer was assumed negligible at T' and its concentration at T'' fixed by the observed difference between A'' observed and A'' predicted if no dissociation occurred. For this purpose a molar absorptivity, ϵ 28,000 mol⁻¹ cm⁻¹ for the trimer, was estimated by comparing Shelton's vapor pressure results⁴ with absorbances measured in this work. The equilibrium constants estimated in this way were least squared in the form $\log K$ vs. $1/T$ and used to predict the actual value K at T' . With this value a new estimate of the monomer concentration was found at T' and again at T'' , and the process repeated by computer; the results quickly converged.

Because of the relatively large uncertainty in the equilibrium constants, the apparent heat of the reaction $\text{Cu}_3\text{Br}_3(\text{g}) = 3 \text{CuBr}(\text{g})$ was derived using an estimated entropy change of 62.5 eu, corresponding to the value reported for the decomposition of Cu_3Cl_3 , ca. 800°K.^{1,19} Values of ΔH° were then derived from each experimental value of the equilibrium constant (see Table II). The corresponding heat of reaction for cuprous chloride is 125 kcal.^{1,19}

Molar Absorptivities. At this time the molar absorptivities of the trimer molecules can only be estimated by comparison of absorbance data with published vapor pressure data for the cuprous halides. This procedure is not very satisfactory. In the case of the chloride, effusion data³⁻⁵ must be corrected for the contribution of the tetramer. Guido, *et al.*,⁷ estimate partial vapor pressures for the tetramer and trimer by use of a sensitivity factor for their mass spectrometer, determined by calibration with silver, and estimated ionization cross sections. They also report a rather large temperature gradient across their Knudsen cell (25°) which adds to the uncertainty of the pressures derived. Although the tetramer does not appear to be at significant concentrations in the bromide system, the heat derived for the β to $\text{Cu}_3\text{Br}_3(\text{g})$ transition from

Table II: Thermodynamic Constants Derived for the Assumed Reaction $(\text{CuBr})_3(\text{g}) = 3\text{CuBr}(\text{g})$

| A' | A'' | T' , °K | T'' , °K | K'' , atm ² | $\Delta H^\circ T''$, kcal |
|------------------------------------|-------|--------------|---------------|-----------------------------|--------------------------------|
| 0.211 | 0.171 | 715.0 | 814.0 | 8.57×10^{-12} | 92.1 |
| 0.222 | 0.179 | 716.9 | 821.9 | 8.86×10^{-12} | 92.9 |
| 0.254 | 0.203 | 722.0 | 830.9 | 1.28×10^{-11} | 93.3 |
| 0.274 | 0.217 | 725.0 | 839.4 | 1.73×10^{-11} | 93.8 |
| 0.310 | 0.243 | 729.8 | 848.3 | 2.56×10^{-11} | 94.1 |
| 0.347 | 0.267 | 734.2 | 857.5 | 4.47×10^{-11} | 94.2 |
| 0.435 | 0.364 | 743.9 | 822.9 | 4.28×10^{-11} | 90.5 |
| 0.467 | 0.386 | 746.9 | 831.5 | 5.85×10^{-11} | 90.9 |
| 0.481 | 0.393 | 748.1 | 835.1 | 7.59×10^{-11} | 90.9 |
| 0.463 | 0.371 | 746.5 | 839.2 | 9.54×10^{-11} | 90.9 |
| 0.473 | 0.381 | 747.4 | 842.5 | 8.29×10^{-11} | 91.5 |
| 0.472 | 0.372 | 747.3 | 846.8 | 1.18×10^{-10} | 91.4 |
| 0.503 | 0.394 | 750.0 | 851.0 | 1.50×10^{-10} | 91.4 |
| 0.505 | 0.389 | 750.2 | 855.5 | 1.92×10^{-10} | 91.5 |
| 0.501 | 0.380 | 749.8 | 859.0 | 2.24×10^{-10} | 91.6 |
| 0.503 | 0.380 | 750.0 | 862.7 | 2.29×10^{-10} | 92.0 |
| 0.516 | 0.387 | 751.1 | 866.8 | 2.57×10^{-10} | 92.2 |
| Av | | | | | 92.1 |
| Estimated uncertainty ± 8 kcal | | | | | |

effusion data,⁴ including an assumed $\gamma \rightarrow \beta$ transition heat of 1.4 kcal,²² is ca. 10% larger than the value based on the absorbance data (Table II).

In view of these uncertainties, an effort was made in the present study to obtain information about the molar absorptivities of the trimers by measurement of the absorbance of a known quantity of vapor.¹³ The attempt was unsuccessful for both CuCl and CuBr because the very small samples required for complete vaporization showed evidence of contamination through interaction with the Pyrex tip on the quartz cells. Melting points of the microgram quantities of sample could be seen (by following the absorbance of the vapor as a function of temperature) to have been significantly lowered, and traces of copper colored stain were observed on the glass. Vapor pressures were also lowered and complete vaporization was not achieved. Hence the amount of copper halide in the vapor was not known, even though the quantity originally placed in the cell could be determined. The impurity introduced (believed to be sodium halide by a surface exchange reaction with the glass²⁵) appeared to be limited to microgram quantities in the earlier experiments as well, since no detectable melting point lowering was seen when samples of the order of 0.1 g of copper halide were used. Nothing was observed to suggest that glass interaction produced any measurable effect on the vapor-phase absorbance studies used to derive the vaporization heats. Spectra showed no time-dependent behavior.

(25) W. A. Weyl and E. C. Marboe, "The Constitution of Glasses—A Dynamic Interpretation," Vol. 2, Part 2, Interscience, New York, N. Y., 1967, p 1082.

Mixture of CuCl and CuBr. The absorbance of vapors generated by a mixture of 0.3180 g of CuBr and 0.0292 g of CuCl, placed in a Cary 14H cell, was observed as a function of temperature. The vapor formed constituted an insignificant fraction of the total sample; hence, the condensed phase was assumed to be a solution⁶ with mole fraction of CuBr of 0.883. The spectrum observed corresponded closely in shape to that of CuBr (Figure 2), but with the main peak maximum shifted to 228 nm. A van't Hoff type plot showed a break at 445°, assumed to be the melting point of the mixture; the apparent heat of vaporization below this temperature was 28.5 kcal and that above was 22.3 kcal mol⁻¹. The melting point indicated is somewhat below that expected for this composition according to the phase diagram of Teltow.⁹

The shape of the absorbance peak and its intensity

were found to correlate well with prediction only if formation of mixed-halide species Cu₃Cl₂Br and Cu₂-ClBr₂ along with Cu₃Cl₃ and Cu₃Br₃ is assumed. The concentration of tetramer is not expected to be significant at the low mole fraction of chloride present. A model assuming averaged intermediate peak locations and molar absorptivities for the mixed halides and concentrations corresponding to random distribution of halogens in trimer molecules, with the vapor in equilibrium with an ideal condensed solution, gave an excellent fit with the observed absorbance curve. A mixture which neglects formation of mixed-halide molecules gives predicted absorbances 30% less than observed.¹³

Acknowledgment. Support of this work by National Science Foundation Grant No. GP 6608X is acknowledged with thanks.

Columns of Liquids Bearing a Constrained Chemical Activity Gradient

by Robert C. Plumb* and Wilbur B. Bridgman

Department of Chemistry, Worcester Polytechnic Institute, Worcester, Massachusetts 01609 (Received December 2, 1971)

Publication costs borne completely by The Journal of Physical Chemistry

Standard analytical procedures for the thermodynamics of solutions involving gravitational potentials, hydrostatic pressure, and chemical activity are applied to columns of solutions. A previously unanalyzed case, that of a column of solution with a constrained chemical activity gradient which exactly cancels the gravitational potential gradient, leads to some interesting results. The hydrostatic pressure in the column is constant, the column is mechanically supported by whatever devices impose the chemical activity gradient, and flow of solvent through the column is hydrodynamic and not controlled by diffusion. Some mechanisms by which such columns may be constructed are suggested. Such columns are probably of importance in biological systems.

We will analyze the chemical thermodynamics of a static vertical column of a two-component system, an aqueous solution, under the special constraint that the solute is not uniformly distributed and is immobilized. As far as we can determine from the literature, this type of column has not been analyzed before. The results are of some practical significance. The thermodynamic procedures are well known; a number of texts discuss thermodynamic effects of gravitational fields.¹ The columns which we will consider will be of standard barometer-type geometry in which the top end of the column is closed and the bottom end is exposed to atmospheric pressure.

The differential of the total chemical potential of a component, *i*, of a system at constant temperature, taking into account the gravitational potential, the

hydrostatic pressure, the chemical effects of interaction with the other components of the system, and the chemical effects of concentration, is

$$d\mu_i = \left(\frac{\partial\mu_i}{\partial z}\right)_{P,a_i} dz + \left(\frac{\partial\mu_i}{\partial P}\right)_{z,a_i} dP + \left(\frac{\partial\mu_i}{\partial a_i}\right)_{z,P} da_i \quad (1)$$

where *z* is the position in the earth's gravitational field, *a_i* is the activity of the *i*th component, and the other symbols have their usual meaning.

For heights with which we will be concerned, the gravitational potential gradient is a constant

$$\left(\frac{\partial\mu_i}{\partial z}\right)_{P,a_i} = M_i g \quad (2)$$

(1) See, for example, J. G. Aston and J. J. Fritz, "Thermodynamics and Statistical Mechanics," Wiley, New York, N. Y., 1959, pp 237-240.

where M_i is the molecular weight of the i th component and g is the gravitational constant.

$$\left(\frac{\partial \mu_i}{\partial P}\right)_{z, a_i} = \bar{V}_i \quad (3)$$

and

$$\left(\frac{\partial \mu_i}{\partial a_i}\right)_{z, P} = \frac{RT}{a_i} \quad (4)$$

If the i th component is the solvent and is incompressible, then \bar{V}_i is a constant, and if the solution is dilute this constant is approximately \bar{V}^0 , the molar volume of the pure solvent.

Thus for water in a dilute aqueous solution

$$d\mu_{\text{H}_2\text{O}(l)} = M_{\text{H}_2\text{O}}g dz + \bar{V}^0_{\text{H}_2\text{O}(l)} dP + \frac{RT}{a_{\text{H}_2\text{O}(l)}} da_{\text{H}_2\text{O}(l)} \quad (5)$$

The activity of H_2O can be expressed in terms of the osmotic pressure, Π , defined as the additional pressure which must be applied to a solution to produce osmotic equilibrium with pure water. Again assuming incompressibility and diluteness

$$\bar{V}^0_{\text{H}_2\text{O}(l)} d\Pi = -\frac{RT}{a_{\text{H}_2\text{O}(l)}} da_{\text{H}_2\text{O}(l)} \quad (6)$$

giving

$$d\mu_{\text{H}_2\text{O}(l)} = M_{\text{H}_2\text{O}}g dz + \bar{V}^0_{\text{H}_2\text{O}}(dP - d\Pi) \quad (7)$$

The general condition for equilibrium for H_2O throughout the column is that $\mu_{\text{H}_2\text{O}}$ be constant, independent of height, *i.e.*

$$\frac{d\mu_{\text{H}_2\text{O}(l)}}{dz} = M_{\text{H}_2\text{O}}g + \bar{V}^0_{\text{H}_2\text{O}(l)} \left(\frac{dP}{dz} - \frac{d\Pi}{dz}\right) = 0 \quad (8)$$

In the usually considered cases, $d\Pi/dz = 0$. This would be true, for example, for a pure solvent or for a solution of uniform composition, therefore of constant osmotic pressure. With columns of moderate height (even hundreds of feet) the effect of sedimentation equilibrium in the earth's gravitational field is so small that the assumption of uniform composition is reasonable.

Any case of uniform composition leads to

$$\frac{dP}{dz} = -\frac{M_{\text{H}_2\text{O}}g}{\bar{V}^0_{\text{H}_2\text{O}(l)}} \quad (9)$$

which is equal to $-0.0965 \text{ atm m}^{-1}$ for H_2O at 25° .

If the pressure is 1.0 atm at the base of the column, the hydrostatic pressure P would fall to zero at 10.3 m and become negative at higher levels. At a level slightly below 10.3 m, P would become less than the vapor pressure of H_2O from the liquid and any liquid above that level is in a metastable state, thermodynamically unstable with respect to decomposition into vapor.

The unique case that we wish to consider is a column of nonuniform composition, the composition varying with height in such a manner that

$$\frac{d\Pi}{dz} = \frac{M_{\text{H}_2\text{O}}g}{\bar{V}^0_{\text{H}_2\text{O}(l)}} \quad (10)$$

This requires a continuous increase in concentration of solute with height corresponding to decreasing activity of the water and increasing osmotic pressure.

For this case the requirement that $d\mu_{\text{H}_2\text{O}}/dz = 0$ is satisfied by $dP/dz = 0$. This implies that the hydrostatic pressure is uniform, independent of height. If the pressure is 1 atm at the base of the column, it remains 1 atm throughout the column. The vapor pressure of water is always exceeded and the liquid column is stable with respect to vaporization at any height. These most unusual properties (in comparison to columns of homogeneous solutions or pure liquids) prompt one to ask what holds up such a column. How is hydrostatic equilibrium achieved? How would one build such a column? These questions and the unusual transport properties of such a column are discussed in the following sections.

Mechanics and Construction of the Proposed Column

In a conventional column of a pure liquid or of a dilute solution of uniform concentration, the mechanical stability arises from the fact that the differential in pressure in an increment of height precisely balances the differential in gravitational potential, *i.e.*, the gravitational force operating on an increment of height of the column. Equation 9 for dilute aqueous solutions of uniform concentration is a specific case of the general equation for hydrostatic equilibrium

$$\frac{dP}{dz} = -g\rho \quad (11)$$

where ρ is the density.

The column which we have proposed does not satisfy this hydrodynamic equation, and yet it satisfies the condition for thermodynamic equilibrium of solvent throughout the column. It is interesting to inquire into the balance of forces which produce mechanical stability in the hypothetical column. If it does not satisfy the general equation for hydrostatic equilibrium, what forces do permit the column to be at mechanical equilibrium? We will see that the mass of the column is supported by whatever structure maintains the chemical activity gradient and these structures in turn are held in place by the walls of the column so that overall the column of solution is held up by the walls of the column.

A simple method of constructing a column with a pressure gradient which is approximately zero is to divide the column into segments with membranes permeable to solvent but impermeable to solute and adjust the solute concentrations to approximate the

correct gradient in osmotic pressure. For example, a column of water could have membranes at each meter of elevation and contain solutes such that $\Pi = 0.0$ up to 1 m, $\Pi = 0.1$ from 1 to 2 m, $\Pi = 0.2$ from 2 to 3 m, etc. If the pressure at the base of the column were 1.0 atm, then the pressure would decrease with height to a value of 0.9 atm just below the first membrane. Osmotic equilibrium requires a pressure increase of 0.1 atm in going from the more dilute lower solution to the more concentrated upper solution. Thus the pressure just above the membrane is 1.0 atm. Continuing up the column the cycle will repeat; the pressure will be 0.9 atm just below each membrane and 1.0 atm just above each. There is a pressure differential across each membrane and the solution exerts a net downward force on the membranes. The walls of the column support the membranes and, hence, indirectly support the column of solution. In a column 10.3 m high the net pressure on a series of closely spaced membranes would be 1.0 atm, which is precisely the pressure required to balance the gravitational force on the mass of water in a column 10.3 m high—hence the mechanical stability.

Rather high columns could be built with relatively dilute solutions. Since a 1 M solution exerts an osmotic pressure of 22 atm, a column could be built which is 226 m high in which the hydrostatic pressure is approximately a constant 1 atm throughout and the solution at the top need be only 1 M in concentration.

It is conceivable that a column having zero pressure gradient could be constructed without using membranes to constrain the osmotic pressure gradient. This might be done by the use of filamentary molecules attached to the walls of the column. These molecules serve the function of solute and the attachments to the wall serve the same functions as the semipermeable membranes in the previous case. Providing the filaments are monomolecular, with internal degrees of freedom, the osmotic pressure produced by them can be quite substantial. For example, if they contain N segments and we assume the limiting ideal case that each segment has complete free rotation, then the segments have $2N$ degrees of freedom, $2/3$ of the translational degrees of freedom of N separate solute molecules. The osmotic pressure gradient could be achieved by having a proper variation of the number density of filamentary molecules over the length of the column. This method of constructing columns would be feasible only in columns of a very small diameter. An estimate of the concentration of filamentary molecules which would have to be present in the xylem conduits of tall trees is given in a related paper.²

Transport Characteristics

The transport characteristics of a column in which there is a fixed concentration distribution of solute are markedly different from those of a column of a

solution without this constraint. It appears that when the concentration of solute as a function of height is fixed, the steady-state flow of solvent is hydrodynamic if the concentration of solute is small and diffusion controlled if the concentration of solute is very large. When the concentration of solute as a function of height is not fixed, the steady-state flow of solvent is always diffusion controlled. This effect of concentration gradient constraints will be shown by considering the behavior of columns of binary gas mixtures where the effect is easily visualized. The proof may be generalized to the case of ideal solutions with a little additional effort.

We may construct a column of a binary mixture of gases in which the total pressure in the column is independent of height using the same principle which we have suggested for columns of liquid solutions. Let component A be the mobile species which will, at equilibrium, be distributed according to

$$RT \, d \ln P_A = -M_A g \, dz \quad (12)$$

Let component B be constrained in its distribution by membranes permeable to A but impermeable to B. To make the total pressure independent of height it is simply necessary to choose the pressures of B such that P_B increases with height at the same rate as P_A decreases with height.

Consider a column of such a binary gas mixture and assume that at the top the component A may escape to the surroundings through a membrane. In the surroundings A is assumed to have a lower chemical potential. Then there will be flow of component A from the bottom to the top of the column. Our analysis will be directed to determining whether the flow is hydrodynamic or controlled by diffusion. The chemical potential of A may be expressed as

$$\mu_A = \mu_A^0 + Mgz + RT \ln P + RT \ln X_A \quad (13)$$

If P and X_A are expressed in terms of n_A and n_B , the numbers of moles of each component present in a small volume, V , the expression for μ_A becomes

$$\mu_A = \mu_A^0 + Mgz + RT \ln [(n_A + n_B)RT/V] + RT \ln [n_A/(n_A + n_B)] \quad (14)$$

Let the volume element V be located at the top of the column and let n_A be changed by an amount dn_A , corresponding to removal of a small amount of A from the column. The resulting change in μ_A upsets the equilibrium condition, causing flow of A from lower volume elements into V . If the change in μ_A depends primarily on the pressure term, we will conclude that a pressure differential results that produces hydrodynamic flow of A from the lower portion of the column. On the other hand, if the effect is related primarily to the concentration term, diffusion would appear to be the

(2) R. C. Plumb and W. B. Bridgman, *Science*, in press.

most probable means of returning the system to equilibrium. We will determine which by differentiating (13) and (14), equating equivalent terms, and comparing the magnitudes of the terms derived from P and from X_A . We obtain

$$RT \left(\frac{\partial \ln P}{\partial n_A} \right)_{V, n_B} = RT / (n_A + n_B) \quad (15)$$

$$RT \left(\frac{\partial \ln X_A}{\partial n_A} \right)_{V, n_B} = RT n_B / n_A (n_A + n_B) \quad (16)$$

and the relative values

$$\left(\frac{\partial \ln P}{\partial n_A} \right)_{V, n_B} = \frac{n_A}{n_B} \left(\frac{\partial \ln X_A}{\partial n_A} \right)_{V, n_B} \quad (17)$$

Thus if $n_A \gg n_B$ a change in n_A will produce primarily a pressure change and hydrodynamic flow of A restoring equilibrium. If A is the minor component, diffusion flow of A will result. A change in n_A produces no net effect on the chemical potential of B. With B constrained by the membranes as we have postulated, n_B remains constant as A flows. (If B were free to move, the hydrodynamic flow would carry B along with it. This would increase the concentration of B at the top of the column, lowering the chemical potential A to the point where it approached the value in the surroundings. A steady state in this case would

correspond to upward transport of A being limited by the downward diffusion of B.)

Just as the transport of one gas in a mixture in which the concentration of the other is constrained is hydrodynamic rather than controlled by diffusion, so is the transport of solvent, A, in a liquid solution in which the concentration of solute, B, is constrained. Assuming that the solution is dilute and ideal, following Raoult's law, the chemical potential of the solvent is

$$\mu_A = \mu_A^0 + \bar{V}_A(P - 1) + M_A g z + RT \ln X_A \quad (18)$$

Following through the same logic as was used for the gas column and using appropriate numerical values, one finds that in dilute aqueous solutions the transport of the water is hydrodynamic if the distribution of solute is constrained.

Possible Applications to Biological Systems

It appears that balancing the gradient in gravitational potential with a gradient in chemical activity is an elementary elegant technique for constructing transport systems in the earth's gravitational field which man has not recognized but which nature may be exploiting. It is probable that nature uses this technique in biological structures in animals and plants. An application in tree physiology is discussed in a related article.²

Adsorption in Mordenite. I. Calculation of Adsorption Potentials of Nonpolar Molecules¹

by Guillermo D. Mayorga and Donald L. Peterson*

California State College, Hayward, Hayward, California 94542 (Received October 16, 1971)

Publication costs assisted by California State College, Hayward

Adsorption potential contour maps are presented for a series of six nonpolar molecules of varying size within the H-mordenite lattice. The interactions were found with the aid of inverse 6-8-10-12 summations within a sufficient volume to assure convergence. The adsorption volume in mordenite consists of parallel channels lined with small side pockets. The potential maps show that double occupancy of the side pockets may occur with atoms as large as argon, that propane is the largest molecule which the side pocket can accommodate, that greater than one-dimensional diffusion may occur with molecules as small as hydrogen, helium, and neon, and that minima along the channels occur outside the side-pocket entrances. It is found that essential features of the maps are produced by Lennard-Jones sums extending only moderately beyond nearest neighbors.

Studies of adsorption in zeolites are timely for at least three major reasons. First, the wide variety of stereospecific environments of known geometry presented by the various zeolites offers a spectrum of cases against which predictions of postulated models may be tested. Second, a knowledge of the specific interactions existing in zeolites may be of practical value, both in surface chemistry research and in commercial applications. Third, the vast deposits of natural zeolites represent an as yet untapped natural resource of appreciable dimensions. While great strides have been made in recent years, it is still not possible to predict with any reasonable certainty, on the basis of atomic and molecular properties and a known crystal structure, adsorption properties of a pure compound, let alone of mixtures. At the base of such predictions is a description of the adsorption potential between an adsorbed molecule and the crystal lattice. Even with a precise description the expectations of a given model are usually subject to uncertainties due to numerous remaining approximations.

Of practicable procedures for evaluating adsorption potentials, the most reliable is that utilizing a summation of interactions between an adsorbed molecule and all the atoms of the host adsorbent. Summations evaluated by computer over enough of the lattice to assure convergence have been reported in few instances. An example is that of CO₂ adsorbed in zeolite A² wherein the summation for each position of the adsorbed molecule was found to require of the order of 10⁴ terms. There are more examples of hand computations in which only nearby atoms are considered³⁻⁵ or in which all but nearest atoms are treated as distributed continuously.^{6,7} This approach may be likened to the more familiar example of adsorption on graphite. In this case it has been shown⁸ that the results of sum-

mations are very closely approximated by treating the carbon atoms as distributed continuously in infinite planar sheets. In zeolites A and X, the distribution of oxygen atoms lining the large cavities approximates a spherical one, providing convenient lower limits for the analytical integration over the presumed continuously distributed matter beyond.⁶ Comparisons with results of summations like that available for graphite would still be needed to justify this significant simplification.

In the case of all other zeolites, however, the replacing of summations by integrations is exacerbated by the lower crystal symmetry. The intracrystalline channel network in mordenite, for example, consists⁹ of parallel right elliptical cylinders girthed by rings of 12 oxygen atoms. These are lined with subsidiary cavities entered through eight-membered rings. A view parallel to one of the main channels is shown in Figure 1. Some earlier calculations⁵ of adsorption potentials in mordenite were confined to molecules sufficiently small as to enter these side pockets and in-

(1) Adapted from a thesis presented in partial fulfillment of the requirements for the degree of Master of Science in Chemistry by G. D. Mayorga, California State College, Hayward, Aug 1971, and presented in part at the 7th Western Regional Meeting of the American Chemical Society, Oct 18-20, 1971, Anaheim, Calif.

(2) R. W. H. Sargent and C. J. Whitford, *Advan. Chem. Ser.*, **No. 102**, 144 (1971).

(3) R. M. Barrer and G. C. Bratt, *J. Phys. Chem. Solids*, **12**, 154 (1959).

(4) R. M. Barrer and R. M. Gibbons, *Trans. Faraday Soc.*, **59**, 2569 (1963).

(5) R. M. Barrer and D. L. Peterson, *Proc. Roy. Soc., Ser. A*, **280**, 466 (1964).

(6) R. M. Barrer and W. I. Stuart, *ibid.*, **249**, 464 (1959).

(7) R. M. Barrer and P. J. Reucroft, *ibid.*, **258**, 449 (1960).

(8) A. D. Crowell, *J. Chem. Phys.*, **22**, 1397 (1954).

(9) W. M. Meier, *Z. Kristallogr.*, **115**, 439 (1961).

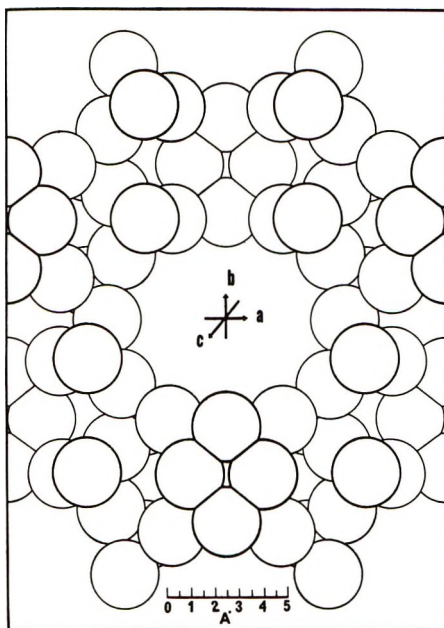


Figure 1. View parallel to the c axis of the oxygen atom network in mordenite.

cluded interactions only with the 37 oxygen atoms forming the wall of the pocket.

As the starting point of a general program aimed at providing accurate adsorption potential surfaces in a variety of zeolites, lattice summations were undertaken for nonpolar molecules in H-mordenite.

The objects of the general program are (1) to provide a body of information with the aid of which reliable predictions of models of adsorption may be made, (2) to provide a sound basis for approximate potential calculations by integration or other simplified methods, and (3) to help decide the most appropriate values for the interaction parameters.

The use of mordenite permits a comparison with earlier measurements and calculations, provides an example for parallel-channel networks, and allows the neglect of interactions with counterions.

Adsorption Potential Calculation

A highly siliceous zeolite, mordenite enjoys a high acid stability¹⁰ and capability of essentially complete counterion exchange with hydronium ion. The dehydrated form contains too little water to account for all the cation positions⁵ and therefore must contain the protons in intimate association with the anionic oxygen network. This makes the close approach of a guest molecule to a cation site unlikely, so that lattice monopole-guest molecule interactions, and particularly the induction terms, will tend to cancel.¹¹ The interaction, at least for the nonpolar molecules considered here, is therefore adequately described by dispersion and repulsion terms. Whereas it is usual to ignore the inverse eighth and tenth terms in the (attractive) dispersion potential, Kiselev and coworkers¹² find this not

always to be advisable. Inclusion of these terms requires only moderate additional computer time. The potential energy gained by molecules i and j on being brought from infinity to internuclear separation s_{ij} is written thus as

$$P_{ij} = -A_{ij}s_{ij}^{-6} - B_{ij}s_{ij}^{-8} - C_{ij}s_{ij}^{-10} + R_{ij}s_{ij}^{-12} \quad (1)$$

The total interaction of a guest molecule i with the crystal lattice is then

$$\varphi_i = \sum_j P_{ij} = -\sum_j A_{ij}s_{ij}^{-6} - \sum_j B_{ij}s_{ij}^{-8} - \sum_j C_{ij}s_{ij}^{-10} + \sum_j R_{ij}s_{ij}^{-12} \quad (2)$$

The summations include the 96 oxygen, 40 silicon, and 8 aluminum atoms in each of the unit cells covered. The Kirkwood-Müller¹³ formula was used for A_{ij}

$$A_{ij} = 6mc^2\alpha_i\alpha_j \frac{1}{\frac{\alpha_i}{\chi_i} + \frac{\alpha_j}{\chi_j}}$$

and related ones¹² for B_{ij} and C_{ij}

$$B_{ij} = \frac{45h^2\alpha_i\alpha_j}{32\pi^2m} \left[\frac{1}{4\left(\frac{\alpha_j/\alpha_i}{\chi_j/\chi_i} + 2\right)} + \frac{1}{4\left(\frac{\alpha_i/\alpha_j}{\chi_i/\chi_j} + 2\right)} \right]$$

$$C_{ij} = \frac{105h^4\alpha_i\alpha_j}{256\pi^4m^3c^2} \left[\frac{\alpha_i/\alpha_j}{3\left(\frac{\alpha_j/\alpha_i}{\chi_j/\chi_i} + 1\right)} + \frac{3}{4\left(\frac{\chi_i}{\alpha_i} + \frac{\chi_j}{\alpha_j}\right)} + \frac{\alpha_j/\alpha_i}{3\left(\frac{\alpha_i/\alpha_j}{\chi_i/\chi_j} + 1\right)} \right]$$

Where r_i and r_j are the van der Waals radii of the guest molecule and of a lattice atom, respectively, the repulsion constant was evaluated by

$$R_{ij} = \frac{A_{ij}(r_i + r_j)^6}{2}$$

Values of r_i , α_i , and χ_i used in the calculations are given in Table I.¹⁴⁻¹⁷ The value of α for oxygen is

(10) L. B. Sand in "Molecular Sieves," Society of Chemical Industry, London, 1968, p 71.

(11) Even when the more numerous cations of type A zeolite are included in calculations of CO₂ interactions, the monopole-induced dipole contribution is observed² in general to be small. The monopole-quadrupole term, however, dominates in regions of potential minima near cations.

(12) N. N. Avgul, A. A. Isirikyan, A. V. Kiselev, I. A. Lygina, and D. P. Poshkus, *Bull. Acad. Sci. USSR, Div. Chem. Sci. (Eng. Transl.)*, **11**, 1334 (1957).

(13) J. G. Kirkwood, *Phys. Z.*, **33**, 57 (1932), and H. R. Müller, *Proc. Roy. Soc., Ser. A*, **154**, 624 (1936).

(14) R. M. Barrer and D. J. Ruzicka, *Trans. Faraday Soc.*, **58**, 2253 (1962).

(15) H. H. Landolt-Bornstein, "Zahlenwerte und Funktionen," Springer-Verlag, Berlin, 1951.

(16) C. K. Hersch, "Molecular Sieves," Reinhold, New York, N. Y., 1961, p 33.

based on the refractivity of the representative aluminosilicate mineral, K-feldspar.⁵ Values of all three parameters for silicon are for the quadruply charged ion. The same values are used for aluminum, whose positions in the structure have not been definitely identified anyway. In any event the effect of this substitution and of the use of parameters for bare Si⁴⁺ ions is unlikely to lead to significant errors, not only because of the preponderance of oxygen atoms in closer proximity with the channel volume, but also because even in chemical combination with oxygen, the polarizability and magnetic susceptibility of Si⁴⁺ are necessarily much smaller than those of bound oxygen. Several nonpolar guest molecules were employed mainly to bring out clearly the effect of molecular size. Thus, light paraffins are used as a convenient homologous series, but all members are necessarily treated as spherical.

Table I: Values of Atomic and Molecular Parameters

| Molecule(i) | Radius r_i , Å | Polarizability α_i , cm ³ /mol | Magnetic susceptibility $-\chi_i$, cm ³ /mol $\times 10^6$ | Ionization potential E_i , eV |
|--------------------------------|------------------------|--|---|---------------------------------------|
| Argon | 1.91 ^a | 0.981 ^a | 19.39 ^a | 15.76 ^b |
| Krypton | 2.01 ^a | 1.493 ^a | 28.00 ^a | 14.00 ^b |
| Methane | 2.19 ^b | 1.565 ^b | 12.2 ^b | 14.40 ^b |
| Ethane | 2.50 ^b | 2.992 ^b | 27.3 ^b | 12.80 ^c |
| Propane | 3.26 ^d | 3.788 ^c | 40.5 ^c | 11.21 ^c |
| <i>n</i> -Butane | 3.89 ^d | 4.890 ^c | 57.4 ^c | 10.80 ^c |
| Oxygen (zeolitic) | 1.40 ^e | 0.994 ^a | 12.58 ^e | 13.55 ^a |
| Silicon (Si ⁴⁺) | 0.42 ^c | 0.01204 ^c | 1.00 ^f | 166.73 ^c |

^a Reference 5. ^b Reference 14. ^c Reference 15. ^d Reference 16. ^e Reference 4. ^f Reference 17.

Values of the parameters in eq 2 are contained in Table II. In a few instances calculations were made using the Lennard-Jones potential (A and R terms only), and in others, the London formula¹⁸

$$A_{Lij} = \frac{3}{2} \alpha_1 \alpha_2 \frac{E_1 E_2}{E_1 + E_2} \quad (3)$$

The ionization potentials used are in Table I.

The potential was evaluated at 0.4 Å increments in a grid whose plane is normal to the main channels (parallel to the c direction), and at a sufficient number of points (up to 200) to span regions of attractive potential within the main channel and the side pocket. Because of the cylindrical shape of the channels, maps were constructed only at two elevations, $z = 0$ and $z = c/4$ (1.88 Å). The (001) planes, as well as the (002), bisect the openings to the side pockets, and therefore contain the adsorption potentials within the pocket, at

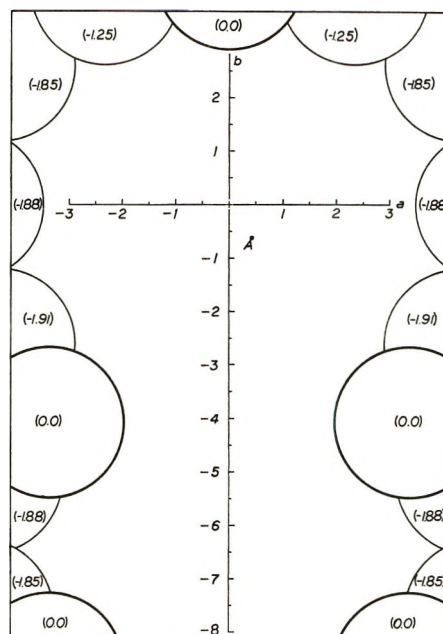


Figure 2. View along the c axis of the oxygen network in the vicinity of $z = 0$. Numbers in parentheses are z coordinates of O atoms.

least in a plane normal to c . The oxygen atoms nearest to these planes are shown in Figure 2 along with their z coordinates; the plane of the paper, $z = 0$, is a reflection plane. Most of the important features within the pocket are shown by maps in these planes, from which a plane bisecting the pocket entrance and at right angles (normal to a) differs only in minor details. So far as adsorption in the main channels is concerned, the picture is expected to vary fairly regularly in the c direction, reaching a modest extremum halfway between opposed eight-membered rings, *viz.*, at the equivalent elevations, $z = c/4$ and $z = 3c/4$.

The sums were evaluated within a rectangular parallelepiped of dimensions $3a$ (51.39 Å), $3b$ (61.47 Å), and $9c$ (67.68 Å). The center of this roughly cubic volume lies simultaneously also on the axes of a main channel and of a side pocket, and is the origin in Figure 2. As an expedient, sums were formed by varying the position of the guest molecule within this volume and including interactions with all lattice atoms within it. The effect of this simplification on results was checked in the instance of methane at the origin by summing within spheres of increasing size. These values are compared with that for the entire 81 cells in Table III. It appears that the major contribution is made by atoms within the nearest 10 Å, although accumulation of 99% of an extrapolated limit necessitates summing within nearly 20 Å. Since the mini-

(17) J. O. Hirschfelder, C. F. Curtiss, and R. B. Bird, "Molecular Theory of Gases and Liquids," Wiley, New York, N. Y., 1954, p 193.

(18) F. London, *Z. Phys. Chem. (Leipzig)*, **B11**, 222 (1930).

Table II: Values of Pairwise Interaction Parameters

| Guest molecule (i) | Equilibrium separation, $r_i + r_j$, Å | A_{ij} , Å ⁶ -kcal/mol $\times 10^3$ | B_{ij} , Å ¹² -kcal/mol $\times 10^3$ | C_{ij} , Å ¹⁰ -kcal/mol $\times 10^3$ | R_{ij} , Å ¹² -kcal/mol $\times 10^6$ | A_{Lij} , Å ⁶ -kcal/mol $\times 10^3$ |
|--------------------|---|---|--|--|--|--|
| | | | Oxygen (j) | | | |
| Argon | 3.31 | 1.467 | 1.328 | 2.728 | 0.964 | 0.681 |
| Krypton | 3.41 | 2.186 | 2.021 | 4.201 | 1.718 | 0.974 |
| Methane | 3.59 | 1.462 | 2.119 | 7.018 | 1.565 | 1.028 |
| Ethane | 3.90 | 2.936 | 3.643 | 9.949 | 5.165 | 1.716 |
| Propane | 4.66 | 4.253 | 5.126 | 13.54 | 21.77 | 2.265 |
| <i>n</i> -Butane | 5.29 | 5.769 | 6.618 | 16.55 | 63.22 | 2.809 |
| | | | Silicon (j) | | | |
| Argon | 2.33 | 0.037 | 0.016 | 0.021 | 0.0029 | 0.016 |
| Krypton | 2.43 | 0.054 | 0.025 | 0.034 | 0.0055 | 0.022 |
| Methane | 2.61 | 0.026 | 0.026 | 0.097 | 0.0041 | 0.024 |
| Ethane | 2.92 | 0.057 | 0.044 | 0.124 | 0.0177 | 0.037 |
| Propane | 3.68 | 0.084 | 0.062 | 0.164 | 0.1045 | 0.047 |
| <i>n</i> -Butane | 4.31 | 0.118 | 0.080 | 0.191 | 0.3783 | 0.057 |

Table III: Convergence of Summations Evaluated at the Origin for Methane

| Volume summed | $-\phi$, kcal/mol | Fraction of summation over 81 cells |
|-----------------------|--------------------|-------------------------------------|
| Sphere of radius 5 Å | 1.699 | 0.553 |
| Sphere of radius 10 Å | 2.926 | 0.951 |
| Sphere of radius 15 Å | 3.033 | 0.985 |
| Sphere of radius 20 Å | 3.063 | 0.995 |
| Sphere of radius 25 Å | 3.074 | 0.9985 |
| 81 cells | 3.078 | 1.0000 |

mum distance to the boundaries of the 81 cells encountered was slightly over 20 Å, the effect of this simplification is considered negligible.

Results and Discussion

Contour maps of eq 2 are shown for four of the molecules studied in Figures 3 through 6 at the more informative elevation, $z = 0$. The outermost contour of $\phi = 0$ encloses in each case the region of net attractive potential in which contours are drawn at 2 kcal/mol increments. The van der Waals molecular diameter is shown near the top of each figure.

From the map for argon, it may be noted that a molecule of this size enjoys considerable translational freedom within the zeolite. There appears to be sufficient space, for example, for two argon atoms to pass each other with ease in the main channel, and perhaps even within the side pocket. The closer quarters of the latter produces a minimum potential of 9.1 kcal/mol, about 25% lower than the minimum near the wall of the main channel. The contour map for krypton¹⁹ is similar to that for argon except that the relative depth in the pocket is now 30% lower than near the channel wall. The regions of slowly varying potential within the steep rises near the oxygen atoms

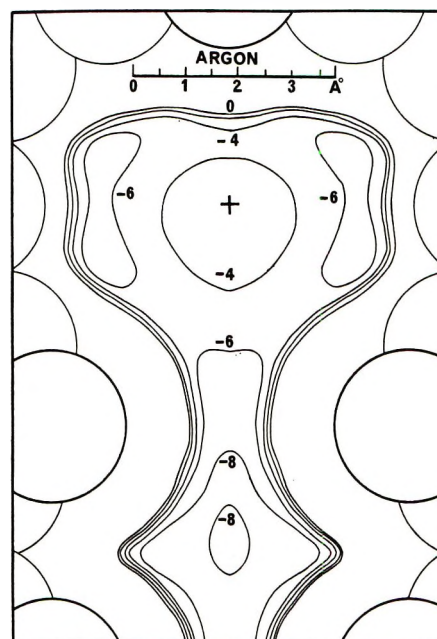


Figure 3. Potential energy contour map for argon at $z = 0$. Contours are drawn at 2 kcal/mol increments starting at $\phi = 0$; numerical values of contours are shown in possibly ambiguous cases. The scale at the top shows the van der Waals radius in angstroms of an argon atom (3.84 Å).

of the channel walls are much smaller in size, and although free passage of atoms still is possible in the main channel, it does not now appear likely within the pocket.

(19) Contour maps for the other two molecules, krypton and *n*-butane, at $z = 0$, and for a representative molecule, ethane, at $z = c/4$, together with a view of the oxygen network along the c axis at $z = c/4$, will appear immediately following this article in the microfilm edition of this volume of the journal. Single copies may be obtained from the Business Operations Office, Books and Journals Division, American Chemical Society, 1155 Sixteenth Street, N.W., Washington, D. C. 20036 by referring to code number JPC-72-1641. Remit check or money order for \$3.00 for photocopy or \$2.00 for microfiche.

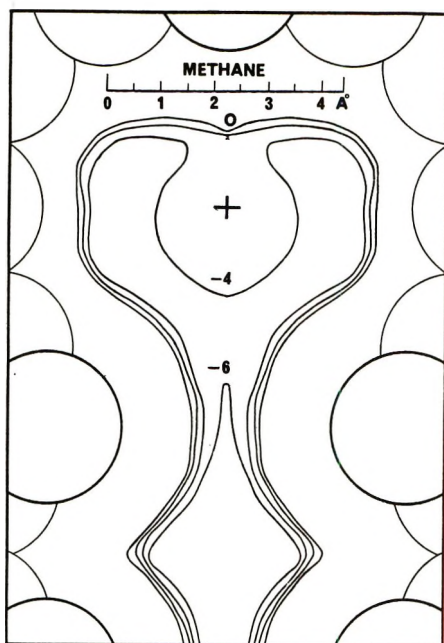


Figure 4. Potential energy contour map of methane at $z = 0$. See caption of Figure 3 for conventions.

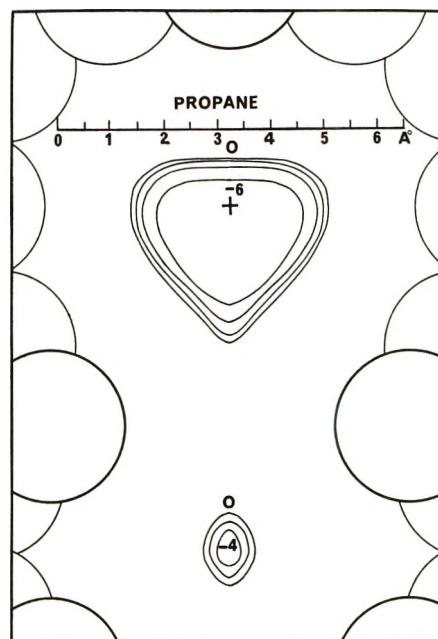


Figure 6. Potential energy contour map of propane at $z = 0$. See caption of Figure 3 for conventions.

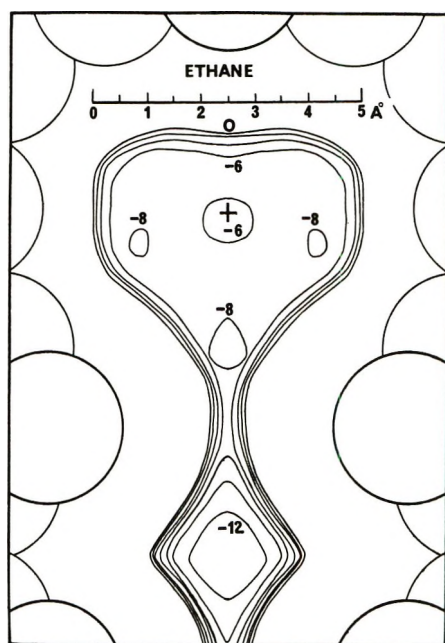


Figure 5. Potential energy contour map of ethane at $z = 0$. See caption of Figure 3 for conventions.

The maps for methane and ethane (Figures 4 and 5) also predict single occupancy of side pockets with increasing relative stabilities in this location. A small activation energy accompanies passage of an ethane molecule through the eight-membered ring. Further, ethane molecules can pass one another in the main channel without experiencing an appreciable repulsion only by making use of entrances to side pockets. To account for self-diffusion of propane (Figure 6) and butane¹⁹ in H-mordenite, relaxation of the spherical

molecule assumption appears necessary. The fact that the saturation capacity of H-mordenite for *n*-butane is very close to the "geometrical" free volume of the main channels⁶ suggests that *n*-butane molecules must at least partially occupy the side pockets or their entrances. From the contours in Figure 6 it may be concluded that the propane molecule closely measures the adsorption capacity of the side pocket.

An idea of the variation of the potential surface in the *c* direction was gained from a comparison of the maps constructed at $z = 0$ and $z = c/4$. In the instance of ethane, the region of appreciable attractive potential shrinks from a breadth of 4 to 4.5 Å to one of only 3 to 3.5 Å, while the minimum rises by 15%. It is believed that these (*xy*) minima at $z = c/4$ are maxima with variation in z (saddle points in $\varphi(x,z)$) and thus that all locations of potential minima lie on (002) planes. Values at the minima are contained in Table IV. Those for argon and methane lie below the lower boundaries of Figures 3 and 4.

It is well known that an adsorbed molecule can approach a lattice atom more closely than it can the same atom outside the influence of the other lattice atoms. Thus one has long accepted the rapid adsorption of normal paraffins (diameter $\cong 5.0$ Å) by zeolites 5A (critical diameter $\cong 4.2$ Å). The present calculations afford some interesting comparisons along these lines. Table IV contains internuclear separations for isolated guest molecule-oxygen atom pairs at the equilibrium position, r_e , for which φ_{\min} is given, and at the position corresponding to $\varphi = 0$, r_0 (according to eq 1). These data are to be compared with the same quantities from the potential contour maps. Guest

Table IV: Comparison of Isolated Pair Interactions to Those Occuring within the Zeolite

| | Guest molecule-O atom interaction | | | Guest molecule-lattice interaction | | | | |
|------------------|-----------------------------------|--------------|---------------------------------|------------------------------------|----------------|---------------------------------|------------------------|----------------------------|
| | r_e , Å | r_0 , Å | $-\varphi_{\min}$, kcal/mol | r_e^a , Å | r_0^a , Å | $-\varphi_{\min}$, kcal/mol | Location of minimum | Overlap, ^b Å |
| Argon | 3.4 | 2.75 | 0.58 | 3.1 | 2.6 | 9.8 | Pocket | 0.15 |
| Krypton | 3.55 | 2.95 | 0.78 | 3.4 | 2.7 | 13.4 | Pocket | 0.25 |
| Methane | 3.45 | 3.05 | 0.45 | 3.5 | 2.75 | 7.9 | Pocket | 0.3 |
| Ethane | 3.9 | 3.35 | 0.47 | 4.1 | 3.0 | 13.0 | Pocket | 0.35 |
| Propane | 4.4 | 4.1 | 0.24 | 4.7 | 3.4 | 7.4 | Channel | 0.7 |
| <i>n</i> -Butane | 5.3 | 4.7 | 0.14 | 4.9 | 4.0 | 7.3 | Channel | 0.7 |

^a Measured from lattice oxygen atom nearest the location of φ_{\min} . ^b Differences of columns 3 and 6.

molecule-lattice internuclear separations are measured from the oxygen atom nearest the position of φ_{\min} . Because of the gradual variation in φ on the inside of the minimum, comparisons based on r_e values can be misleading. According to the r_0 values, an argon atom, for example, can approach an oxygen atom in H-mordenite 0.15 Å more closely than it can an isolated atom without experiencing a net repulsion.

The lattice structure of Na-mordenite is such that halfway between adjoining channels in the *b* direction there are two sodium ions, each in the center of a distorted eight-membered ring. These rings are roughly normal to the *c* axis, face into pockets on neighboring channels, and have a free diameter of only 2.8 Å. If the hydrogen ions replacing the sodium ions are indeed buried in the oxygen framework as suggested earlier, these apertures may be open to the possible passage of sufficiently small molecules between pockets. Calculations carried out with guest molecules at the position of a vacant sodium atom (Table V) show that

Table V: Potential Energy of Molecules Located at the Sodium Ion Lattice Position

| Molecule | Potential at the sodium ion position, kcal/mol |
|----------|--|
| Argon | -3.71 |
| Krypton | +0.29 |
| Methane | +7.1 |
| Ethane | +58.5 |

argon may be the only molecule of those considered here which could literally squeeze through the window (the "overlap" is 0.55 Å). However, even this atom encounters an activation energy of about 6 kcal/mol, which is almost as large as (the negative of) its calculated heat of adsorption. Thus, two-dimensional diffusion, if it occurs in H-mordenite, would be expected to take place freely only with molecules of smaller diameter than that of argon, *i.e.*, with H₂, He, or Ne.

Finally, the results of the potential calculations may be compared with those making use of alternate as-

sumptions. Comparisons are made only for positions along the axis of the side pocket. Three cases are included: (1) Kirkwood-Müller formula, 6-12 potential, 81-cell summation; (2) London formula (eq 3), 6-12 potential, 81-cell summation; and (3) London formula, 6-12 potential, 37 nearest O-atom summation⁵ (Ar and Kr only). Compared to (1) above, the 6-8-10-12 potential surface is qualitatively similar, but displaced by amounts leading in extreme cases to as much as 0.5 Å in positions of minima.

Values at the minima are compared in Table VI for the four procedures. Differences are representative in the range of coordinates covered. Inclusion of the inverse eighth and tenth terms has the effect of increasing the magnitude of the potential by about 10% on the average. As is usually the case, use of the London formula leads to about one-half the interaction potential. The summation over nearest lattice oxygen atoms includes about 80% of the total interaction.

Table VI: Comparison of Adsorption Potential Minima on *y* Axis Computed by Alternate Procedures

| Molecule | Kirkwood-Müller 6-8-10-12 81 cells | Kirkwood-Müller 6-12 81 cells | London 6-12 81 cells | London 6-12 37 O atoms ^a |
|------------------|--|-------------------------------------|----------------------------|--|
| Argon | 9.8 | 8.8 | 4.1 | 3.3 |
| Krypton | 13.4 | 12.2 | 5.3 | 4.5 |
| Methane | 7.9 | 6.8 | 4.8 | |
| Ethane | 13.0 | 11.8 | 6.9 | |
| Propane | 7.4 | 7.0 | 3.7 | |
| <i>n</i> -Butane | 7.3 | 6.8 | 3.3 | |

^a Reference 5.

Conclusion

The reported calculations of adsorption potentials of nonpolar molecules in H-mordenite appear to limit the size of molecules capable of rapid two-dimensional diffusion to that of neon, of multiple occupancy of side pockets to that of argon, and of single occupancy of side pockets to that of propane. It is inferred that these conclusions, as well as other semiquantitative

features of the adsorption potential surfaces within H-mordenite, would be as accurately predicted by use of the simple Lennard-Jones potential, by summations including lattice atoms up to about only 10 Å distance from the adsorbed molecule, and that inclusion of only nearest neighbors in summations may for many purposes be adequate. Although these approaches differ vastly in complexity and required computer time, their predictions are far more coincident, at least in

the present instances, than those of procedures using the alternate formulas for interaction parameters.

It is concluded that the use of the 6-12 potential in summations extending only moderately beyond nearest lattice atom neighbors, with scaling between Kirkwood-Müller and London parameters, and perhaps beyond, left as an empirical degree of freedom, offers the most expedient means of seeking generalities characteristic of adsorption in zeolites.

Adsorption in Mordenite. II. Gas Chromatographic Measurement of Limiting Heats of Adsorption of Nonpolar Molecules

by Guillermo D. Mayorga and Donald L. Peterson*

California State College, Hayward, Hayward, California 94542 (Received October 12, 1971)

Publication costs assisted by California State College, Hayward

A comparison between heats of adsorption derived from chromatographic retention-volume measurements and values predicted on the basis of adsorption potential calculations shows the latter to be quite successful in the case of atomic adsorbates when the interaction parameters are evaluated by the London formula. The poor agreement in the case of nonpolar molecular adsorbates reflects an inadequacy of treating the molecules as spherical, possibly even in the case of methane.

The availability of contour maps of adsorption potentials of a series of nonpolar molecules in H-mordenite¹ makes possible the prediction of their heats, free energies, and entropies of adsorption. For comparisons of the predicted heats, available experimental data² were augmented by a series of chromatographic measurements of adsorbabilities of these compounds at several temperatures, from which heats of adsorption at vanishing coverage were estimated.

A further purpose of the reported measurements is to augment a prior demonstration³ of the utility of mordenite as a gas chromatographic packing material. The unidimensionality of mordenite's pore structure raises some doubts about whether equilibrium will be reached, and the operating assumption of chromatography realized, on the time scale of practicable chromatographic measurements.

Experimental Section

A Varian Aerograph Model 90-P3 chromatograph, which comes equipped with a flow control system that operates under 65 psi pressure of carrier gas, was modified with the aid of a Moore Flow Control and a precision Whitey needle valve to allow use of a lower

pressure (10 psi or less), and precise control of the flow rate.

A modified 0.25-in. Swagelok tee was attached to the injection port with one of the free sides of the tee serving as the new injection port. The free side of the tee was connected through a valve to a mercury manometer. The inlet pressure was read to within 0.005 cm with the aid of a cathetometer.

The carrier gas was helium; this and the argon, methane, ethane, propane, and *n*-butane used in the experiments were instrument grade gases from Matheson Co. The neon and krypton were high-purity grade gases from the General Electric and Air Reduction Co., respectively. The H-mordenite was produced by exchanging Na-mordenite (Zeolon Lot HB-8E, Code SM710) thrice with 1 *M* NH₄NO₃ over a period of 3 days. Between exchanges the sample was washed with deionized water. After the final exchange the

(1) G. D. Mayorga and D. L. Peterson, *J. Phys. Chem.*, **76**, 1641 (1972).

(2) R. M. Barrer and D. L. Peterson, *Proc. Roy. Soc., Ser. A*, **280**, 466 (1964).

(3) K. Torii, M. Asaka, and H. Yamazaki, *Kogyo Kagaku Zasshi*, **72**, 661, 664 (1969).

sample was washed until no sodium could be detected in the effluent. Retention of crystallinity was verified by X-ray powder photography. Flame photometric analysis showed the product to contain 0.02% wt sodium or about one sodium atom in each 35 unit cells.

The column packing was prepared by pelletizing the ammonium mordenite and then grinding and screening the pellets to obtain a 40–60 mesh fraction. This was packed in a column 50.5 cm in length and 0.47 cm in internal diameter. Dehydrated mordenite in the hydrogen form was produced by passing helium through the column at 350° and the nominal flow rate for 24 hr; in this form the packing weighed 4.73 g.

Retention volumes were measured at temperatures between 30 and 350° using a helium flow rate of ca. 30 ml/min, under which conditions the number of theoretical plates was between 80 and 300. The ratio of the column inlet pressure, P_i , to that at the outlet, P_o , varied between 1.2 and 1.4. The flow rate, f_o , was measured at the column exit pressure and at room temperature, T_r , with the aid of a conventional soap-bubble flowmeter in which the vapor pressure of water was P_w . The corrected retention volume, V_R° , referred to dry carrier gas at the column temperature, T_c , is given by

$$V_R^\circ = j(t_R - t_V)f_o \frac{T_c}{T_r} \left(\frac{P_o - P_w}{P_o} \right)$$

in which t_R and t_V are the observed retention times for the compound studied and for a nonadsorbed component, respectively, and

$$j = \frac{3}{2} \frac{(P_i/P_o)^2 - 1}{(P_i/P_o)^3 - 1}$$

is the correction factor of James and Martin⁴ for the variable pressure within the column. Where c is the molar concentration of a solute in the carrier gas, q is the number of moles of solute per unit mass of adsorbent, and m is the mass of the adsorbent in the column, the fundamental relationship of gas chromatography is

$$V_R^\circ = \frac{q}{c} m$$

Adsorption coefficients are more commonly expressed as volume of gas at STP adsorbed per gram adsorbent-atmosphere pressure, v_{sp} , than as q/c . For an ideal gas at standard temperature and pressure,

$$v_{sp} = \frac{273.16}{T_c m} V_R^\circ \left(\frac{\text{cc(STP)}}{\text{g-atm}} \right)$$

Independence of v_{sp} on carrier gas flow rate was shown in the instance of propane at 276°. Successive reductions of flow rate of as much as 40% of the nominal rate produced random variations in v_{sp} not exceeding 3%.

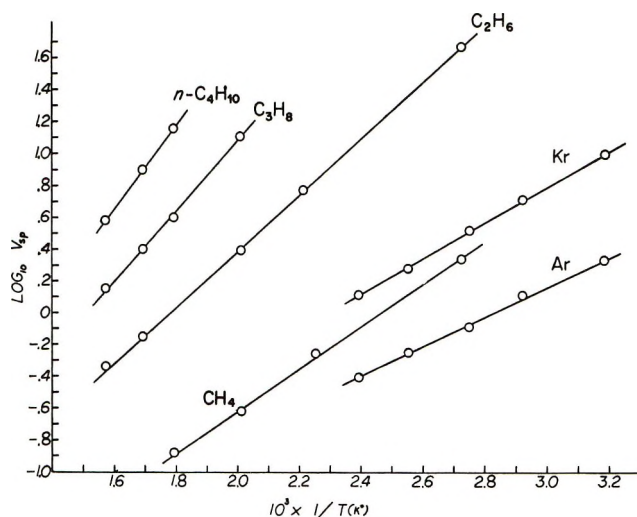


Figure 1. Variation of the specific retention volume with the column temperature for argon, krypton, and n -alkanes.

Results and Discussion

Logarithmic plots of observed values of v_{sp} are shown in Figure 1. Values of the limiting heat of adsorption

$$\Delta H^\circ = -R \frac{d \ln v_{sp}}{d(1/T)}$$

are contained in Table I. In the two instances where a comparison with other measurements is possible, the agreement is viewed as satisfactory, particularly when the lower Na-ion content of the present sample is taken into account. A comparison with predictions based on adsorption potential calculations was made with the aid of statistical considerations which lead,⁵ for the present cases, to

$$\Delta H^\circ = \varphi_{\min} + \frac{RT}{2}$$

Table I also contains predicted values of ΔH° found from the minimum values of adsorption potential surfaces computed with the aid of two alternate formulas, those of Kirkwood and Müller⁶ and of London,⁷ for interaction parameters. The calculations treat the paraffin molecules as spherical. Thus, the inclusion of ethane, and more particularly, of propane and n -butane, serves mainly to illustrate the magnitude of errors introduced by this assumption. The calculated values of ΔH° shown in Table I utilize the Lennard-Jones 6–12 potential. In the case of summations using the Kirkwood–Müller formula, values computed by the 6–8–10–12 potential exceeded those of the 6–12 by about 10%. Inclusion of the 8–10 terms in the London

(4) A. T. James and A. P. Martin, *Biochem. J.*, **50**, 679 (1952).

(5) T. L. Hill, *J. Chem. Phys.*, **17**, 520 (1949).

(6) J. G. Kirkwood, *Phys. Z.*, **33**, 57 (1932), and H. R. Müller, *Proc. Roy. Soc., Ser. A*, **154**, 624 (1936).

(7) F. London, *Z. Phys. Chem. (Leipzig)*, **B11**, 222 (1930).

summation may be expected to produce a similar effect. This would bring the predicted heats using this formula very nearly into quantitative agreement with the observed values for the rare gases. That the value predicted by this method for methane, even allowing for the effect of these terms, is smaller than observed may be an indication that even methane is inadequately treated as spherical for these purposes.

Table I: Comparison of Observed and Predicted Limiting Heats of Adsorption in H-Mordenite

| Molecule | ΔH° , kcal/mol | | | |
|------------------|-----------------------------|-------------|--------------|-------|
| | Calcd | | Obsd | |
| | Kirkwood-Müller 6-12 | London 6-12 | Present work | Ref 2 |
| Argon | 8.4 | 3.7 | 4.2 ± 0.3 | 4.6 |
| Krypton | 11.6 | 4.9 | 5.1 ± 0.2 | 5.5 |
| Methane | 6.4 | 4.4 | 6.1 ± 0.5 | |
| Ethane | 11.3 | 6.4 | 8.0 ± 0.3 | |
| Propane | 6.4 | 3.1 | 10.0 ± 0.7 | |
| <i>n</i> -Butane | 6.2 | 2.7 | 12.0 ± 0.3 | |

Figure 2 shows the observed linear dependence of limiting heat of adsorption for the normal paraffins on their carbon number n

$$-\Delta H^\circ = 4.0 + 2.0n \text{ kcal/mol}$$

An indirect comparison may be made between the extrapolated value for *n*-hexane (16.0 kcal/mol) and a reported⁸ one of 15.7 to 16.2 kcal/mol at relatively low coverage on H-mordenite. These observations may be further compared with those on other zeolites not in the hydrogen form. Limiting heats of light normal paraffins on zeolite Ca-X, for example, follow approximately a very similar linear relation⁹

$$-\Delta H^\circ = 4.5 + 2.2n \text{ kcal/mol}$$

The two cases share the interesting feature of a large (negative) ΔH° intercept, a property not shown, at least in the case of Ca-X,¹⁰ when heats at appreciable coverages are used. Limiting heats for light paraffins on zeolite Ca-A provide another example, for which the reported values¹¹ are approximated by

$$-\Delta H^\circ = 1.7 + 2.3n \text{ kcal/mol}$$

While more examples are needed to make clear the influence of channel structure and cation composition on the parameters of these relations, it would not be too surprising to find that the slope is a relatively invariant quantity. Thus, the predicted values for so different an adsorbent as graphite (with which observed values are in good agreement) are given by a line of quite similar slope, albeit much smaller intercept¹²

$$-\Delta H^\circ = 0.85 + 1.88n \text{ kcal/mol}$$

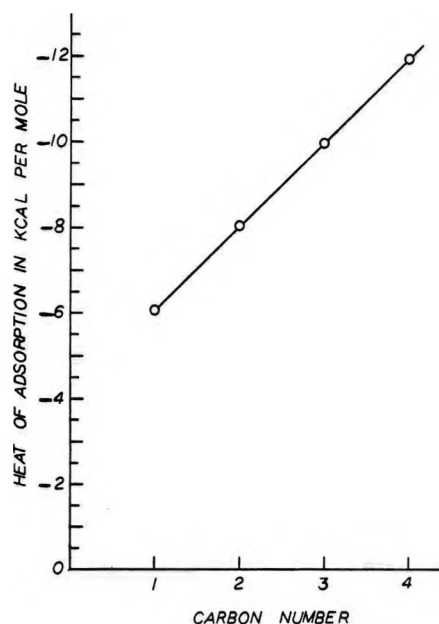


Figure 2. Dependence of the observed limiting heat of adsorption of the *n*-alkanes on the number of carbon atoms in the chain.

Thus, limiting heats of adsorption of at least light *n*-alkanes in mordenite appear not to be unique: the discontinuity predicted by the assumption of spherical shapes is, as expected, wholly artificial. However, it may be expected that heats of adsorption of isobutane or neopentane will be smaller than those of their normal isomers, suggesting a possibly high normal/branched selectivity in this zeolite in spite of competitive adsorption.

Conclusion

It appears that the use of the London formula in extended summations of interactions with lattice atoms, and of a polarizability for the oxygen atoms of the lattice² which reflects their actual state of chemical combination, leads to eminently satisfactory predictions of the heats of adsorption of atomic adsorbates. The agreement in these instances is even improved by the inclusion of the inverse eighth and tenth terms in the dispersion potential. If this success can be taken seriously, then the need of accounting for molecular geometry, even in the case of spherical tops like methane is at once apparent.

The predictions even of limiting adsorption coeffi-

(8) P. E. Eberly, *J. Phys. Chem.*, **67**, 2404 (1963).

(9) H. W. Habgood, *Can. J. Chem.*, **42**, 2340 (1964).

(10) R. M. Barrer and J. W. Sutherland, *Proc. Roy. Soc., Ser. A*, **237**, 439 (1956).

(11) A. V. Kiselev, Y. V. Khrapova, and K. D. Shcherbakova, *Petrol. Chem. USSR*, **2**, 558 (1963).

(12) N. N. Avgul, A. A. Isirikyan, A. V. Kiselev, I. A. Lygina, and D. P. Poshkus, *Bull. Acad. Sci. USSR, Div. Chem. Sci. (Eng. Transl.)*, **11**, 1334 (1957).

cients, since they depend exponentially on the adsorption potentials, seems a futile task indeed until such time as adsorption heats can be predicted with more

confidence. It is hoped that the extension of the sorts of comparisons made here to other zeolites and adsorbates will make this possible.

Correlations between the Electrochemical and Spectroscopic

Behavior of Some Benzophenones and Thiobenzophenones¹

by Rafik O. Loutfy* and Raouf O. Loutfy

University of Western Ontario, Photochemistry Unit, London 72, Ontario, Canada (Received September 27, 1971)

Publication costs assisted by the Photochemistry Unit, University of Western Ontario

The electrochemistry of a number of benzophenones and the corresponding thio ketones have been investigated, using ac polarographic technique. The half-wave potentials ($E_{1/2}$'s) were found to be linearly related to the n, π^* triplet energies. This relation enabled an estimate to be made of the position of the n, π^* triplet energies of those compounds where n, π^* triplet states were not observed spectroscopically. A linear dependence between the half-wave potentials of the carbonyl and the corresponding thiocarbonyl has also been observed. The usual Hammett correlation was obtained for both series of compounds. The heterogeneous rate constants for several of these compounds have been determined by Randel's method of analyzing the ac data. A reversible ($K_{app} > 1 \times 10^{-2}$ cm/sec) one-electron reduction was found for these compounds. The heterogeneous rate constants have been compared with the hyperfine splitting constants and a fair prediction of the variation in the experimental rate constant with structure was found.

Introduction

It has been well established that polarographic half-wave potentials are linearly related to the calculated energy of the lowest vacant molecular orbital, both for the unsaturated² and aromatic^{3,4} hydrocarbons. This linear dependence has also been extended to the energy of the lowest excited state.⁵

The electrochemical reduction of benzophenones, in aqueous media, has been studied by Zuman, *et al.*⁶ The substituent effects on $E_{1/2}$'s were determined using Hammett plots.

Recently the electrolytic reduction of a number of derivatives of benzophenone^{6,7} and thiobenzophenone⁸ has been studied in aprotic solvents. It has been shown that these compounds⁶⁻⁸ undergo a one-electron reduction to form a stable anion radical in dimethylformamide and acetonitrile. However, there have been no kinetic studies reported of the electron transfer for these compounds.

In the present paper, the results of a kinetic study of the electroreduction of benzophenone, 4,4'-dimethoxybenzophenone, and bis(dimethylamino)benzophenone and the corresponding thio ketones are reported. A correlation between the n, π^* triplet energies and the $E_{1/2}$'s are presented and discussed.

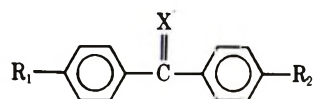
Experimental Section

All experiments were carried out in acetonitrile (AN) containing 0.05 *M* tetraethylammonium perchlorate (TEAP). The solvent purification procedure is described in detail in ref 9. The accessible potential range of the solvent was +2.7 to -2.1 V on Pt and +0.6 to -2.8 V on dropping mercury electrode *vs.* (Ag|AgCl|0.1 *M* TEAP in AN||0.05 *M* TEAP in AN). TEAP was recrystallized from hot water and dried for

- (1) Publication No. 26 from the Photochemistry Unit.
- (2) A. Maccok, *Nature (London)*, **163**, 178 (1949).
- (3) (a) A. Streitwieser, Jr., "Molecular Orbital Theory for Organic Chemists," Wiley, New York, N. Y., 1961, pp 173-185; (b) M. E. Peover in "Electroanalytic Chemistry," Vol. II, A. J. Bard, Ed., Marcel Dekker, New York, N. Y., 1967, Chapter 1.
- (4) H. B. Mark, Jr., *Rec. Chem. Progr.*, **29**, 217 (1968).
- (5) (a) E. S. Pysh and N. C. Yang, *J. Amer. Chem. Soc.*, **85**, 2124 (1963); (b) A. Mazzenga, D. Lomnitz, J. Villegas, and C. J. Palowczyk, *Tetrahedron Lett.*, **21**, 1665 (1969).
- (6) P. Zuman, O. Exner, R. F. Rekber, and W. Nauta, *Collect. Czech. Chem. Commun.*, **33**, 3213 (1968).
- (7) J. M. Saveant and L. Nadjó, *J. Electroanal. Chem.*, **30**, 41 (1971).
- (8) (a) L. Lunazzi, G. Maccagnani, G. Mazzanti, and G. Plaucci, *J. Chem. Soc. B*, 162 (1971); (b) R. M. Eloffson, F. F. Gadallah, and L. A. Gadallah, *Can. J. Chem.*, **47**, 3979 (1969).
- (9) W. R. Fawcett, P. A. Forte, R. O. Loutfy, and J. M. Prokipcak, *ibid.*, **50**, 263 (1972).

48 hr at 60° under vacuum. Benzophenones, commercially available (Aldrich), were purified by recrystallization followed by zone refining. Thiobenzophenones were used as supplied by (K & K Laboratories). Table I shows the structures of the compounds investigated. The numbers on the table will be used to designate the particular compounds throughout this paper.

Table I: Number Assignments of Compounds Studied



| No. | X | R ₁ | R ₂ |
|-----|---|----------------------------------|----------------------------------|
| 1 | O | H | H |
| 2 | O | CH ₃ O | CH ₃ O |
| 3 | O | N(CH ₃) ₂ | N(CH ₃) ₂ |
| 4 | O | Cl | Cl |
| 5 | O | CF ₃ | H |
| 6 | O | CH ₃ | CH ₃ |
| 7 | O | Br | Br |
| 8 | O | OH | OH |
| 9 | S | H | H |
| 10 | S | CH ₃ O | CH ₃ O |
| 11 | S | N(CH ₃) ₂ | N(CH ₃) ₂ |

The electrochemical cell was specially designed for use with a controlled dropping mercury electrode (dme). All experiments were conducted in a drybox containing a nitrogen atmosphere at a temperature of 25.0 ± 0.5°. The counter electrode was a cylinder of platinum (2 cm²), whereby the working electrode was positioned to be in the center to achieve a symmetrical field around the working electrode. The reference electrode (Ag|AgCl|0.1 M TEAP in AN||), placed close to the working electrode, was enclosed in a glass sleeve and joined to the system under investigation by a center glass disk.

Current-voltage curves were obtained using a PAR Model 170 electrochemistry system, in conjunction with PAR Model 171 controlled-drop timer. The latter was fixed to 5-sec drop time. A current-sampled ac polarographic technique was used in which a small amplitude (5 mV) alternating potential was superimposed on the dc potential, which varies linearly with time. The application of operational amplifier circuitry, built into the PAR Model 170, with a three-electrode system, drastically reduced the sources of ohmic resistance, and the use of a phase-selective locking amplifier method for recording the ac currents made this method superior to conventional dc polarography. For more details on ac polarographic techniques, refer to ref 10. Six frequencies (25, 45, 75, 95, 200, and 400 cps) were employed to determine the kinetics of the reaction. Depolarizer concentrations were in the range 1 × 10⁻⁴–5 × 10⁻⁴ M.

Results and Discussion

Polarography. All compounds gave well-characterized ac waves with a width at half-height of 90 ± 1 mV. This corresponds to a one-electron reduction to give radical anions, in agreement with previous work.⁶⁻⁸ The summit potentials were independent of frequency or scan rate (2–20 mV/sec), *i.e.*, as a first approximation the reduction processes proceed reversibly.¹⁰

The half-wave potentials for all the compounds were obtained from cathodic and anodic sweeps of the ac wave in the usual manner. The $E_{1/2}$'s are shown in Table II.

Table II: Electrochemical Data and n , π^* Triplet Energies of Benzophenones and Thiobenzophenones Studied

| No. | $-E_{1/2}$, V | $E_T(n, \pi^*)$, kcal/mol | $E_B(n, \pi^*)$, kcal/mol |
|-----|----------------|----------------------------|----------------------------|
| 1 | 1.84 | 68.6 ^b | 77.2 |
| 2 | 2.01 | 69.4 ^b | 78.33 |
| 3 | 2.16 | (70.1) ^d | (79.5) ^e |
| 4 | 1.68 | 68.0 ^b | |
| 5 | 1.61 | 67.6 ^b | |
| 6 | 1.883 | 68.90 ^a | |
| 7 | 1.695 | 68.07 ^a | |
| 8 | 2.372 | 69.50 ^a | |
| 9 | 1.17 | 40.6 ^a | 45.67 ^c |
| 10 | 1.35 | 42.1 ^a | 47.4 ^c |
| 11 | 1.51 | 43.4 ^a | 49.0 ^c |

^a From emission spectra in EPA at 77°K; see ref 13 for experimental detail. ^b See ref 12 and references therein. ^c From ultraviolet absorption spectra at 77°K. ^d Predicted n, π^* triplet energy. ^e Reference 14.

On substitution of a group with a lone pair of electrons, such as NR₂, OR, or X, into the aromatic rings of benzophenones or thiobenzophenones, resonance interaction or even the inductive effect will cause a pronounced effect on both the π and π^* levels, while the n level will be largely unaffected by such interaction owing to its orthogonality with respect to the π system.¹¹ It is anticipated, therefore, that a substituent would perturb the π^* level in the benzophenone series to the same extent as it would for the thiobenzophenone series. Since the $E_{1/2}$ is a measure of the relative position of the lowest vacant molecular orbital, *i.e.*, π^* level, and, assuming the above hypothesis is valid, a linear correlation, with a slope of 1, between the $E_{1/2}$'s of thiobenzophenones and benzophenones is to be expected. This relation was found (see Figure 1), and a slope close to unity was obtained. The equation giving the best fit for the $E_{1/2}(C=S)$ and $E_{1/2}(C=O)$ is

(10) D. E. Smith in ref 3b, Vol. I, 1966, Chapter 1.

(11) S. Nagakura, *Bull. Chem. Soc. Jap.*, 25, 164 (1952).

$$E_{1/2}(C=S) = 1.06E_{1/2}(C=O) - 0.785 \quad (1)$$

The above results are contradictory to those reported in ref 8a, where a slope of 2 was obtained. This discrepancy could be due to the different techniques for determining the reduction potential.

Correlation between the $E_{1/2}$'s and the n, π^* Singlet and Triplet Energies. It is reasonable to predict that the $E_{1/2}$'s, assuming that the n level of the carbonyl or the thione compounds will be unaffected by the substituents, would correlate with the n, π^* transition.

The lowest triplet state of the benzophenones have been thoroughly studied,¹² and those of thiobenzophenones have recently been investigated.¹³ The n, π^* triplet and singlet energies (E_T) and (E_S), respectively, for the compounds investigated are given in Table II.

It has been noted¹⁴ that the singlet-triplet splitting of benzophenones and thiobenzophenones (shown in Figure 2) are remarkably constant. It has also been found¹⁴ that the differences in singlet or triplet energies between benzophenones and the corresponding thio ketones, for a given substituent, are almost constant and approximately equal to the differences in the bond strength. As an implication one would expect that both E_T and E_S would correlate linearly with $E_{1/2}$'s. These relations are given in Figure 3 for the thiones. The slopes of $E_{1/2}$ vs. E_T and E_S were found to be 0.357 and 0.425, respectively. These slopes are much lower than the theoretical value of 2¹⁵ expected from the plot of the absorption spectra of the $\pi \rightarrow \pi^*$ band against the half-wave potentials.

It is worth mentioning that the slopes obtained here are also lower than 0.6, which was reported previously^{8b} for the $n-\pi^*$ vs. $E_{1/2}$'s of some thiones. However, these authors based the singlet energies of the thiones studied on the shortest wavelength maxima, with absorption spectra measured at room temperature. It has been shown¹³ that in some cases (xanthione and

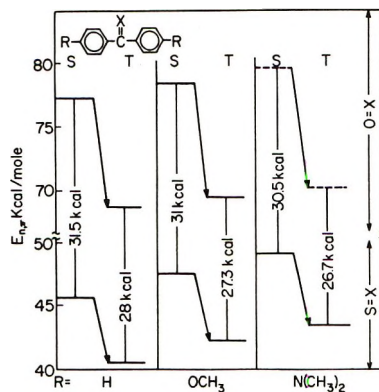


Figure 2. Correlation diagram of n, π^* singlet (E_S) and triplet (E_T) levels of benzophenones and analogous thiobenzophenones.

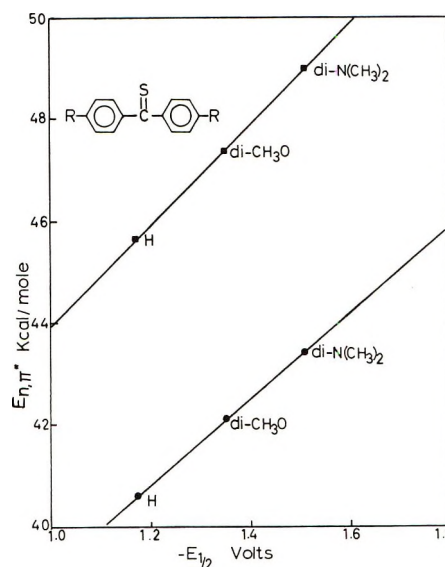


Figure 3. Half-wave potentials of thiobenzophenones vs. n, π^* (■) singlet and (●) triplet energies.

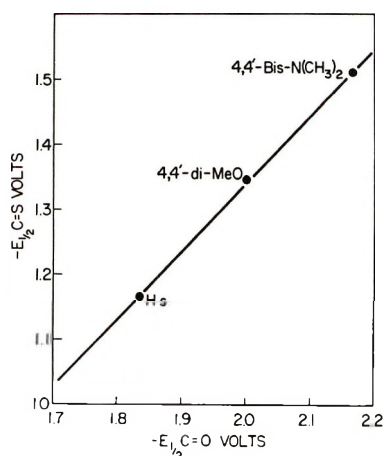


Figure 1. Relationship between $E_{1/2}$'s of thiobenzophenones (E_{cs}) and analogous benzophenones (E_{co}).

thiocamphor) the shortest wavelength maxima under the above conditions, does not represent the $S \rightarrow S_1$ transition, but rather the $S \rightarrow T$ transition, which makes their calculations erroneous.

A linear correlation of $E_{1/2}$'s vs. E_T 's for the benzophenones is given in Figure 4, with a slope of 0.192, which is about half of that obtained for the thiones.

In polar solvents, the lowest triplet state of Michler's ketone, **3**, is believed to be of a charge-transfer (CT) character, $E_T = 61$ kcal/mol.¹⁶ This assumption was

(12) D. R. Arnold, *Advan. Photochem.*, **6**, 306 (1968), and references therein.

(13) D. Blackwell, C. C. Liao, R. O. Loutfy, P. de Mayo, and S. Paszyc, *J. Mol. Photochem.*, in press.

(14) Rafik O. Loutfy, Ph.D. Thesis, University of Western Ontario, London, Ontario, 1972.

(15) A. T. Watson and F. A. Matsen, *J. Chem. Phys.*, **18**, 1305 (1950).

(16) J. Pitts, H. Johnson, and T. Kuwana, *J. Phys. Chem.*, **66**, 245 (1962).

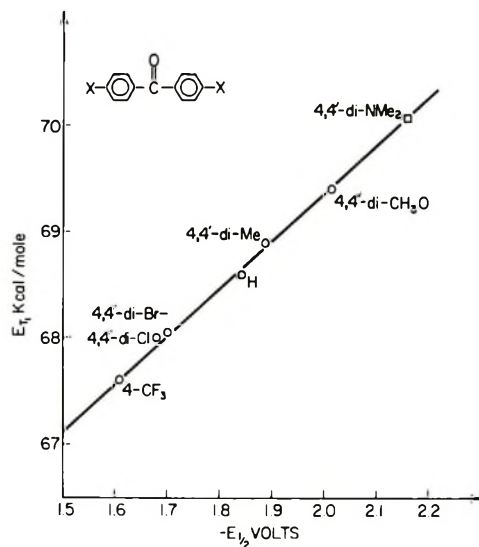


Figure 4. Half-wave potentials of benzophenones vs. the n, π^* triplet energies, E_T .

based on spectroscopic evidence together with the very low reactivity in the polar solvents toward photo-reduction.¹⁷ Suppan, *et al.*,^{17,18} reported a large change in the phosphorescence lifetime of Michler's ketone, in hydrocarbon solvents, and an increase in reactivity. These factors were considered as important evidence that crossing of a n, π^* and a CT state had taken place. As mentioned before, the energy of the lowest triplet state of Michler's ketone in a polar solvent is estimated to be ≈ 62 kcal/mol. From the measured half-wave potential, the energy of the n, π^* triplet state was found to be ≈ 70 kcal/mol (see Figure 4). Even allowing for the known large shift of the charge-transfer state energy level, on changing the solvent from polar to nonpolar, we believe that inversion of states is unlikely. Nevertheless, the CT and n, π^* states may almost be degenerate.

The emission spectra of 4,4'-dibromo- and 4,4'-dihydroxybenzophenone were measured in a 4:1 mixture of MCH and *n*-P at 77°K (for experimental details, see ref 13). Both compounds were found to have low-lying n, π^* triplets, with $E_T = 68.07$ and 68.50 kcal/mol, respectively. The latter compound showed n, π^* triplet emission in EPA at 77°K with an $E_T = 69.6$ kcal/mol, while at pH 8, a long-lived emission was observed ($E_T = 70.6$ kcal/mol) which probably originates from a CT state.

For 4,4'-dibromobenzophenone, two ac waves have been observed, with the second wave located at the same potential as in the unsubstituted benzophenone. This is in agreement with the results obtained by Saveant, *et al.*,⁷ where the first wave corresponds to anion radical formation of the original compounds and the second ac wave is due to the formation of benzophenone anion radical after a reductive cleavage of the carbon-bromine bonds. It can be seen from

Figure 4 that the $E_{1/2}$ obtained from the first ac wave correlates with the other substituted benzophenones, indicating that there is no change in the reduction mechanism.

The half-wave potential obtained for the 4,4'-dihydroxybenzophenone (8) is remarkably high and does not correlate with the n, π^* triplet energy. A possible reason is that under our experimental conditions, the compound was in a deprotonated form, in which case the lowest excited state is CT in character. From Figure 4 the expected n, π^* triplet energy of the deprotonated form of compound 8 was found to be 71 kcal/mol. The $E_{1/2}$ of the protonated compound can be predicted, from Figure 4, using the n, π^* triplet energy obtained spectroscopically in EPA, which was found to be -2.03 V.

From Figure 3 it is obvious that the lowest triplet state of Michler's thione (11) is of n, π^* character rather than a CT triplet, which is in agreement with work done previously.¹³

Therefore, a correlation of the type obtained in this work, Figures 3 and 4, can be used to determine the nature of the lowest triplet state. It could also be utilized to estimate the n, π^* triplet energy of compounds of known electrochemistry.

Knowing the electrochemistry of a compound in a one class, it is possible to obtain the half-wave potential of the corresponding compound in the other series (see Figure 1). From this value one can obtain the n, π^* triplet state using Figure 3 or 4. For example, from the $E_{1/2}$ of 4,4'-dichlorobenzophenone, $E_{1/2}$ of the corresponding thione was found to be -1.02 V; accordingly, the expected E_T is 39.4 kcal/mol. The same argument can be applied to the $E_{1/2} - E_s$ correlation for thiobenzophenones, giving a singlet energy of 42.2 kcal/mol.

The half-wave potentials have been correlated with the Hammett constant for both series. The Hammett reaction constant for both the benzophenones and thiobenzophenones is $\rho = 0.384$, which is in agreement with the value obtained for benzophenone reduction in DMF.⁷ The fact that the slope of the Hammett plot is almost identical for both series indicates a remarkable parallel change of properties due to the substituents.

Measurement of Heterogeneous Electron-Transfer Rates. The effects of substituents on electrochemical kinetics through stabilization of the transition state are much less understood than the substituent effects on electrochemical thermodynamics, which are well documented.^{6,19} Accordingly, the heterogeneous rate constants K_a of the three thiones investigated and the

(17) G. Porter and P. Suppan, *Trans. Faraday Soc.*, **61**, 1664 (1965).

(18) P. Suppan, *Ber. Bunsenges. Phys. Chem.*, **72**, 321 (1968).

(19) O. Ryba, J. Pilar, and J. Petranek, *Collect. Czech. Chem. Commun.*, **33**, 26 (1968).

corresponding carbonyl compounds were measured and correlated to the esr spectra obtained from ref 8, in an attempt to elucidate the dependence of the electrode kinetics on the structure.

Of the many techniques for measuring electrode kinetics, the ac technique, with a phase-sensitive locking amplifier to separate the in-phase and out-of-phase components, was used. This technique involved measuring the Faradaic impedance in the presence of a direct current flow. However, Randles²⁰ showed that the classical theory of the Faradaic impedance, derived from an electrode at equilibrium, remains valid in the presence of a direct current provided that the electrode reaction is sufficiently rapid. The advantage of this technique is, of course, the on-site generation of the reactants; also, problems with adsorption are immediately apparent from the experimental results.

The present work employs the classical approach developed by Randles,²¹ in which the resistive (R_f) and reactive (C_f) components of the Faradaic impedance are plotted against $\omega^{-1/2}$, where ω is the angular frequency of the alternating voltage. The K_a 's were obtained from these measurements through the following relation²¹

$$R_f - 1/\omega C_f = RT/n^2 F^2 A C K_a \quad (2)$$

where A is the area of the electrode, C is the concentration of the depolarizer, and the other terms have their usual meaning. The diffusion coefficient of the depolarizer, D_{ox} , can be obtained from the slope, S , of impedance plots, where S at $E_{1/2}$ is given by²²

$$S = 2.83RT/n^2 F^2 C D_{ox}^{1/2} \quad (3)$$

Figure 5 shows some representative plots of the components of the Faradaic impedance. The rate constants (K_a 's) and the diffusion coefficients are given in Table III.

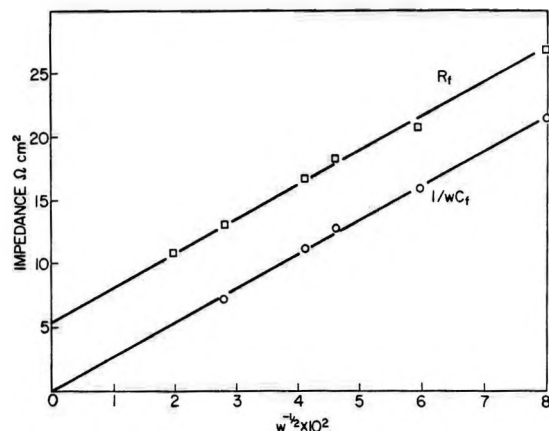


Figure 5. Components of the Faradaic impedance at $E_{1/2}$ of thiobenzophenones. (For w read ω .)

zophenones are also higher than those of the thiobenzophenones; this is probably due to difference in the magnitude of solvation.

Correlation between K_a and Structure. Peover and Powell²³ have published the only known direct correlation between the hyperfine splitting (hfs) constants and the electrode kinetics. The logarithms of the rate constants for one-electron reduction were found to vary linearly with the hfs constants of the reaction site. This behavior is explained in terms of the influence of excess charge at the reaction site on the solvation energy of the radical anion. The more the odd electron is localized on the reaction site, the higher the energy of the transition state and the slower the reaction.

From the esr results obtained for compounds 1, 2, 9, and 10 in ref 8, the hyperfine splitting constants, a_p , at the reactive site (C=S or C=O) were calculated. These values are shown in the last column of Table III. However, it was not possible to obtain the values for compounds 3 and 11 owing to the complex nature of the spectra.²⁴ It can be seen qualitatively that the rate constants, K_a , are inversely related to a_p . This will explain the result that thiobenzophenones have slightly lower K_a 's than the corresponding benzophenones because the C=S group has a higher charge density than the C=O group.

To correlate this relation on a quantitative basis, one has to consider the solvation energy of the anion radical on the basis of a model consisting of three spheres, one representing the functional group of radius approximately $r_p = 2.75 \text{ \AA}$, and two spheres, one repre-

Table III: The K_a 's and D_{ox} 's of Benzophenones and Thiobenzophenones

| No. | K_a , cm/sec | $D_{ox}^{1/2} \times 10^3$, cm/sec ^{1/2} | a_p^a |
|-----|-------------------|---|---------|
| 1 | 0.177 | 6.70 | 5.8 |
| 2 | 0.154 | 6.25 | 15.9 |
| 3 | 0.127 | 6.20 | |
| 9 | 0.173 | 5.35 | 8.15 |
| 10 | 0.143 | 5.45 | 17.0 |
| 11 | 0.114 | 5.50 | |

^a Reference 8.

It can be observed from Table III that K_a 's are in the reversible range ($K_a > 1 \times 10^{-2}$ cm/sec) and that benzophenones have slightly higher values than the corresponding thiobenzophenones. The D_{ox} 's of ben-

(20) J. E. B. Randles in "Transaction of the Symposium on Electrode Processes," E. Yeager, Ed., Wiley, New York, N. Y., 1961, Chapter 11.

(21) J. E. B. Randles, *Discuss. Faraday Soc.*, No. 1, 11 (1947).

(22) T. Biegler and H. A. Laitinen, *Anal. Chem.*, **37**, 572 (1965).

(23) M. E. Peover and J. S. Powell, *J. Electroanal. Chem.*, **20**, 427 (1969).

(24) E. G. Janzen and C. M. Dubose, Jr., *J. Phys. Chem.*, **70**, 3372 (1966).

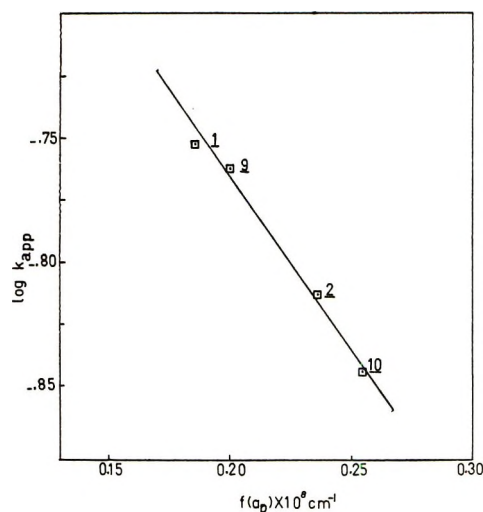


Figure 6. Dependence of experimental rate constant on spin density at the reaction site.

sending each phenyl part of the molecule with an average radius of $r_{ring} = 3.5 \text{ \AA}$ for compounds 1 and 6 and 5.3 \AA for 2 and 7.

Peover and Powell²³ showed that the heterogeneous rate constant can be given as follows

$$\ln K_a \approx \ln Z - Ne^2(1/D_{op} - 1/D_s)f(a_p)/8RT + Ne^2(1/D_{op} - 1/D_s)/16\delta RT \quad (4)$$

where, using our model²⁵

$$f(a_p) = \sum (a_p Q_p)^2 / r_p + (1 - a_p Q_p)^2 / 2r_{ring} + 2a_p Q_p (1 - a_p Q_p) / R$$

Q_p is McConnell's constant, taken as $1/27$;⁸ δ is the distance from the center of the reactant to the electrode surface; D_{op} and D_s are the local optical and static dielectric constants, respectively; R is the distance between the spheres in the above model, assumed to be 5 \AA ; Z is the collision frequency, $\approx 10^4 \text{ cm/sec}$; and other terms have their usual meanings. δ , D_{op} , and D_s are constants; accordingly, eq 4 predicts a straight-line relation between the logarithms of the K_a 's and the $f(a_p)$ term; this relation is shown in Figure 6. The slope is equivalent to the theoretical value of

$$Ne^2(1/D_{op} - 1/D_s)/18.424RT$$

This shows a fair prediction of the variation of the experimental rate constant with the structure, *i.e.*, substituents and functional groups.

Acknowledgment. The authors wish to express their sincerest thanks and appreciation for having this work completed to Professor P. de Mayo, University of Western Ontario, Chemistry Department, London, Ontario, and Department of Chemistry, University of Guelph, Guelph, Ontario.

(25) J. M. Hale, "Reactions of Molecules at Electrodes," N. S. Hush, Ed., Wiley-Interscience, New York, N. Y., 1971, Chapter 4.

Electric Conduction of the Aluminum-Auramine-Stannic Oxide System

by H. Shimoda, M. Sukigara, T. Sakata,* and K. Honda

Institute of Industrial Science, University of Tokyo, Roppongi, Minato-ku, Tokyo, Japan (Received November 1, 1971)

Publication costs borne completely by The Journal of Physical Chemistry

Electric conduction in an n-type SnO₂-auramine hydrochloride-Al sandwich cell was studied. The cell showed a rectification characteristic in the dark conduction, but a larger photocurrent density was obtained when the applied field was in such direction that the dark current was suppressed. These phenomena were interpreted as follows. Electrons are the majority carriers in the dark conduction regardless of the direction of the electric field, but the probability of electron transfer from the conduction band of SnO₂ to the conductive level of auramine is very small. In the photoconduction electrons are still the majority carriers in the bulk of the auramine film, but the recombination of photogenerated holes with electrons accumulated in the SnO₂ electrode at the interface greatly increases the photocurrent.

Introduction

In a photoelectric cell containing an organic photoconductor, carrier transport in the bulk of the organic material has been a main subject for many workers.¹⁻³ Although the mechanism of the bulk conduction of very

slow carriers in a crystal and in an amorphous state is a very interesting problem, a transfer of photogenerated charge carriers through an interface of a semiconductor

* Address correspondence to Department of Electro-Photo-Optics, Tokai University, Kanagawa, Japan.

and a layer of organic material is also a problem of special interest. The transfer of charge carriers through the interface sometimes plays a main role in photoconduction phenomena. In such a junction as that of two electrically same type materials, *e.g.*, an n-type semiconductor and an n-type organic photoconductor, an electron transfer between the two conduction bands need not always occur in photoconduction. Rather, the role of the minority carriers should sometimes be emphasized for a large current under illumination. We prepared an n-type SnO₂-auramine hydrochloride-Al sandwich cell and attempted to investigate the role of the stannic oxide-auramine interface in the dark conduction and photoconduction behavior of the cell.

Experimental Section

The cell with a transparent electrode was prepared by the following procedure. Ni was evaporated on both ends of a glass plate which had been coated with n-type SnO₂ to two-thirds of the surface. The resistance of the SnO₂ film was 2 k Ω . Auramine hydrochloride (Aur-HCl), which was recrystallized several times from an isopropyl alcohol solution, was vacuum sublimated on the transparent electrode with a thickness of 10⁻⁴ cm; then Al was evaporated on it. The structure of the cell is illustrated in Figure 1. Electrical measurements were made under vacuum (10⁻⁸ Torr) under steady-state conditions. Temperature was controlled between -180 and +100° with a copper-constantan thermocouple and a programmed electronic temperature regulator with an accuracy within $\pm 0.1^\circ$. Takeda-Riken vibrating reed electrometers, TR84B and TR84M, were used for the voltage and current measurements. In the photocurrent measurements the sample was irradiated through the transparent electrode with monochromatic light from a 150-W Xe short arc through a Carl Leiss monochromator. The light intensity was varied by using Kodak Wratten Gelatin ND filters. The absorption spectra of the sublimated film and alcoholic solution of AurHCl were measured with a Shimadzu recording spectrophotometer, MPS-50A.

Results

Figure 2 shows the electronic absorption spectra of AurHCl under various conditions. In an ethanol solution absorption peaks were observed at 372 and 432 nm in the visible region with molecular extinction coefficients of 2.19×10^4 and 4.70×10^4 , respectively. In a thin sublimated film on a SnO₂-coated glass a sharp absorption peak appeared at 395 nm in addition to the smaller peaks at 380 and 440 nm (Figure 2b). Increasing the thickness of the sublimated film resulted in the relative decrease of the intensity of the 395-nm absorption band and the increase of the intensities of the 380- and 440-nm bands.

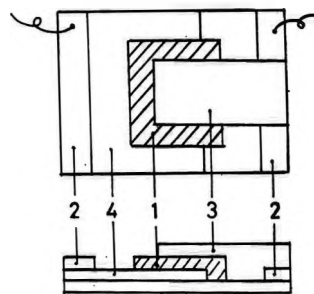


Figure 1. The structure of the cell: 1, AurHCl; 2, nickel; 3, aluminum; 4, SnO₂.

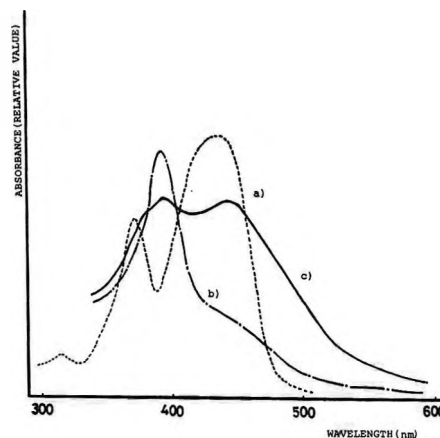


Figure 2. The absorption spectra of auramine hydrochloride: a, alcoholic solution; b, thin sublimated film; c, sublimated film of the thickness, 10⁻⁴ cm.

Figure 3 shows the current-voltage characteristics of the sandwich cell at 20° in the dark. In this figure and hereafter, SnO₂(+) means that the sign of the applied voltage is positive at the SnO₂ electrode and *vice versa*. Dark current (I_d) was nearly proportional to the applied voltage (V), *i.e.*, the dark conduction apparently obeys Ohm's law. Activation energies for the dark conduction at 1-V bias were estimated from the Arrhenius plots, assuming the following temperature dependence

$$I = I_0 \exp(-E/kT)$$

and listed in Table I.

The response spectrum of photocurrent at 1-V bias voltage at 20° is shown in Figure 4, where the ordinate is a magnitude of photocurrent divided by the relative number of incident photons. Irrespective of the directions of bias voltage, broad peaks appeared at 510, 440, 400, and 380 nm. In Figure 5 photocurrent (I_p) was plotted against the applied voltage (V). The activation energies of I_p in both the SnO₂(+) and Sn-

(1) F. Gutmann and L. E. Lyons, "Organic Semiconductors," Wiley, New York, N. Y., 1967.

(2) N. Inokuchi, "Yuki Handotai (Organic Semiconductors)," Maki Shoten Inc., Japan, 1966.

(3) G. C. B. Garrett, "Semiconductors," N. B. Hannay, Ed., Reinhold, New York, N. Y., 1959.

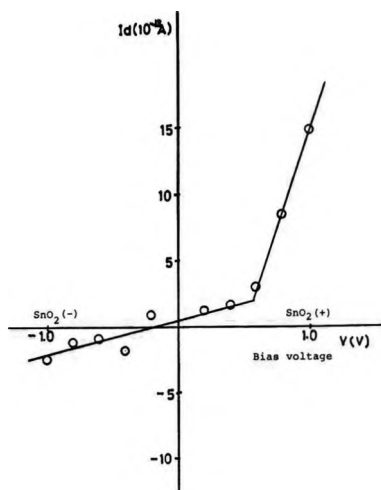


Figure 3. The current-voltage characteristics of dark current at 20°.

Table I: The Activation Energies of Dark Conductions and Photoconductions (eV)

| | Dark conduction | | Photoconduction | | |
|--------------------------------------|-----------------|------|-------------------------|------|------|
| | -1.0 | +1.0 | Voltage, V ^a | | |
| | | | -1.0 | +0.5 | +1.0 |
| Activation energies, ^b eV | 0.78 | 0.69 | 0.49 | 0.40 | 0.35 |
| | | | 0.67 | 0.67 | 0.67 |

^a The sign of the bias voltage was taken so that + means that the SnO₂ electrode was positively biased and *vice versa*.
^b The temperature dependence of dark conductions and photoconductions was assumed to be the type $I = \Sigma I_i \exp(-E_i/kT)$.

O₂(-) cases were estimated from the Arrhenius plots of photocurrents, assuming the same temperature dependence as that of dark conduction, and listed in Table I. Photocurrents at 1-V bias were linearly dependent on the light intensity at 30°.

Discussion

The absorption spectrum of the sublimated AurHCl film on the SnO₂ substrate had a new absorption peak at 395 nm, and the response spectrum of the photoconduction showed two peaks at 510 and 400 nm which did not correspond to the absorption bands of the monomeric dye. These transitions would not be due to impurities or decomposition products in the sublimated film since a previously sublimated film which was dissolved in ethanol gave the same spectrum as the un-sublimated material. The possibility of an electronic interaction between the dye molecule and the semiconductor may be excluded since similar peaks were observed at 400 and 520 nm in a response spectrum of the photocurrent in an Al-AurHCl-Al sandwich cell. The origin of the new peaks, therefore, should be looked for in electronic interactions in the dye film. First, we consider the dipole interaction of the electronic transi-



Figure 4. The response spectrum of the photoconduction of the cell; temp, 20°; applied voltage, 1 V (SnO₂(+)).

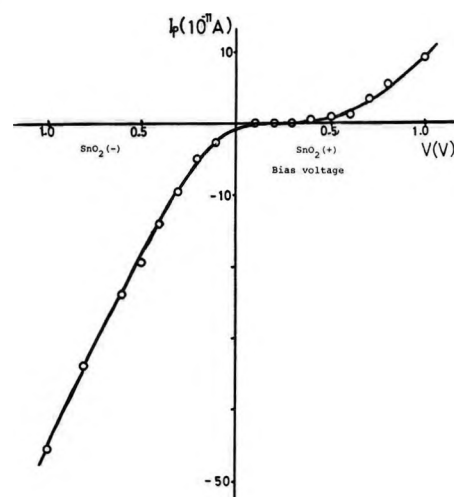


Figure 5. The current-voltage characteristics of the photocurrent; wavelength of the incident light, 500 nm; temp, 20°.

tions.⁴ PPP molecular orbital calculation^{5,6} carried out by the present authors showed that the transition dipole at 440 nm is in the direction of the long axis of the molecule. The oscillator strength of the transition was evaluated from the absorption spectrum to be 0.518. Molecular arrangement in the sublimated film is not known at present, and tentatively it was assumed to be a dimeric structure with distance r (Å) between the centers of the molecules and angle θ between the principal axes of the two molecules. The interaction

(4) A. S. Davydov, "Theory of Molecular Exciton," McGraw-Hill, New York, N. Y., 1962.

(5) R. Pariser and R. G. Parr, *J. Chem. Phys.*, **21**, 466, 767 (1953).

(6) J. A. Pople, *Trans. Faraday Soc.*, **49**, 1375 (1953).

energy was estimated to be $58.2r^{-3} \cos \theta$ eV regarding the two transition dipoles to be point dipoles. To fit the calculated energy shift with the observed energy difference of 0.28 eV between the two absorption peaks at 400 and 440 nm, the distance r was taken to be 5.9 Å when the angle θ was assumed to be zero. The actual molecular arrangement may be different from the assumed dimeric structure, but the above value of r seems to be reasonable since the closest approach of two molecules in organic molecular crystals is usually around 3.5 Å. The electronic transition at 510 nm carries a very small transition dipole but actually contributes in the photoresponse very effectively. We may expect the presence of an absorption band around 490 nm originating from the band at 440 nm by the dipole interaction, even if the transition probability is very small. Nelson and Takeda measured the ionization energy⁷ and electron affinity⁸ of solid AurHCl. Their values were 5.4 and 2.8 eV, respectively. The difference of the two values is 2.6 eV, *i.e.*, 477 nm. The origin of the new band at 510 nm, observed in the response spectrum of the photocurrent, may be sought for in a direct transition to a conductive state or in a mixing of charge transfer and neutral excitons. Optical data for a single crystal of AurHCl will be necessary for further discussion of the origin of the new band.

The most significant feature of the current-voltage characteristics of the cell is the apparent rectifying behavior in the dark conduction and the drastic increase of the photocurrent at SnO₂(-) where the dark current was depressed. Meier⁹ classified AurHCl into an n-type photoconductor. Nelson¹⁰ found out that, in general, cationic dyes tend to be n-type semiconductors. Energy diagram consideration, which will be mentioned in the following discussion, also suggests that electrons are responsible for the conduction through the AurHCl film. However, the current-voltage behavior of the photoconduction does not seem to be interpretable by taking only electrons into consideration. Rather, both electrons and holes should be taken into consideration for the explanation of the photoresponse of the cell.

Figure 6 illustrates the energy diagram for the composition of the cell. The value of the band gap in SnO₂ for the indirect transition was reported by Spence.¹¹ The position of the conduction band of the n-type SnO₂, in which the Fermi level is placed very close to the bottom of the conduction band, was estimated to be 3.5 eV from the work function.¹² However, the SnO₂ electrode was attached to nickel. Then, the position of the conduction band in the SnO₂ electrode would be lowered nearly to the Fermi level of nickel (4.5 eV).¹³ Although the difference of the Fermi levels of the two materials is large, the resistance of this junction could always be neglected in the present experiment. The values of the electron affinity⁸ and the ionization energy⁷ of AurHCl are the experimen-

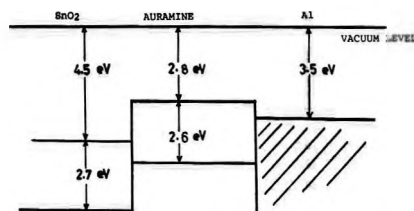


Figure 6. The energy diagram of the cell.

tally measured values. We assumed that the position of the conductive level is the same as the electron-capturing level. The position of the Fermi level of aluminum was measured to be 3.5 eV using the Kelvin method.¹⁴ In the dark conduction, a higher current density was obtained when the aluminum electrode was biased more negatively than 0.5 V. This phenomenon will fit the energetic relation shown in Figure 6. In such a region of applied voltage the Fermi level of the aluminum electrode may be lifted upwards, and electron transfer from aluminum to AurHCl becomes much easier when the energy difference between the Fermi level of aluminum and the conductive level of AurHCl becomes zero. In the SnO₂(-) region electron transfer from SnO₂ to AurHCl will always be difficult in the present experimental condition. When the cell was illuminated with light in the visible region, electron-hole pairs are generated in the AurHCl film near the interface of SnO₂ and AurHCl. The photogenerated electrons will be transferred to the conduction band of SnO₂ leaving positive charge in the AurHCl film when the SnO₂ electrode is positively biased. A part of these positive holes would contribute in the photoconduction, but some of these will make space charge in the AurHCl film (Figure 7a) and will be recombined with electrons injected from aluminum electrode. In Figure 8 log (I_p/V) was plotted against $1/V$. A linear relation between these two quantities has been sometimes obtained experimentally for tunneling conduction.¹⁵ In the case of SnO₂(-), photogenerated electrons can move through the AurHCl film to the aluminum electrode, and holes may accumulate in the AurHCl film (Figure 7b). Electrons would not be injected from the SnO₂ electrode to the conductive level of AurHCl at a lower applied electric field. However, the present experiment showed that higher steady-state photocurrent

(7) S. Takeda, Thesis, The Ohio State University, 1969.

(8) R. C. Nelson, unpublished result; *J. Chem. Phys.*, **20**, 1327 (1952).

(9) H. Meier, *Z. Wiss. Photo. Photophys. Photochem.*, **53**, 1 (1958); *Z. Phys. Chem. (Leipzig)*, **208**, 340 (1958).

(10) R. C. Nelson, *J. Chem. Phys.*, **29**, 388 (1958); **30**, 406 (1959).

(11) W. Spence, *J. Appl. Phys.*, **38**, 3767 (1967).

(12) K. Takahashi, private communication.

(13) K. S. Krishnan and S. C. Jain, *Nature (London)*, **170**, 759 (1952).

(14) J. J. Thomson, *Phil. Mag.*, **46**, 82 (1898).

(15) D. R. Lamb, "Electrical Conduction Mechanisms in Thin Insulating Films," Methuen and Co., Ltd., 1967, p 67.

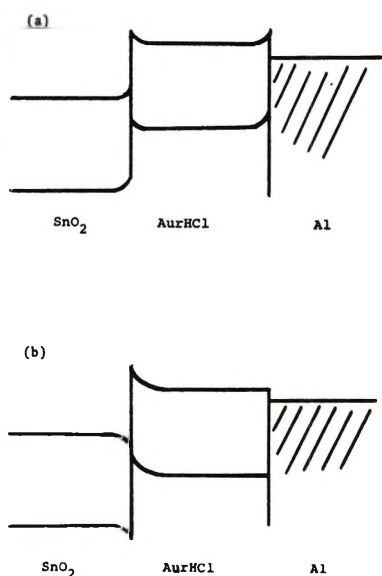


Figure 7. The energy diagram of the cell at the illuminated state: a, SnO₂ (+); b, SnO₂ (-).

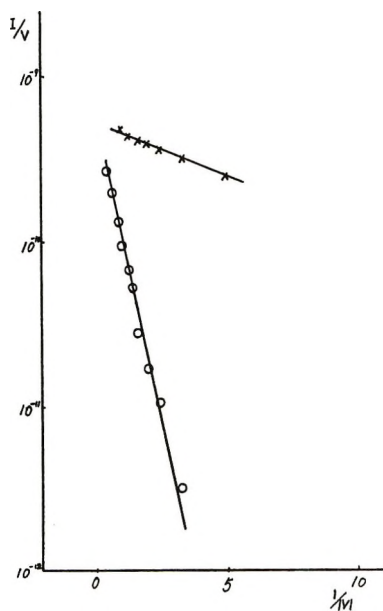


Figure 8. The current-voltage characteristics of the photoconduction: $(\ln(I_p/V) \text{ vs. } 1/V)$: O, SnO₂ (+); X, SnO₂ (-).

density could be obtained when the SnO₂ electrode was negatively biased. Our interpretation of this fact is that the photocurrent flows through the interface between AurHCl and SnO₂ by the recombination of the accumulated holes in AurHCl with the accumulated electrons in SnO₂ at the interface. If the recombination process occurs effectively, a large current can flow through the cell.

Takeda⁷ reported the values of activation energy for

the dark currents and photocurrents of a sublimated AurHCl film to be 0.78 and 0.29 eV, respectively. The activation energies of the dark currents in the present experiment nearly coincide with his value, except the very small value (0.026 eV) which appeared at SnO₂(+). His experiment was carried out in the temperature range from 30 to 60°. We obtained the smaller value of activation energy in the temperature range below -25°. In addition, zero activation energy was obtained for the photoconduction at SnO₂(+) below -50°. The presence of the carrier transport process with such small activation energy suggests that the mobility of the charge carrier is independent of temperature. If hopping of self-trapped electrons is the elementary process of the conduction, mobility should be temperature dependent. If electrons transfer from molecule to molecule by a tunneling mechanism with a larger transition probability than the frequency of molecular vibration, mobility need not necessarily be dependent on temperature. We carried out open-shell molecular orbital calculations of AurH and AurH²⁺ ((CH₃)₂NC₆H₄C(NH₂)C₆H₄N(CH₃)₂) with the method proposed by one of the present authors.¹⁶ The calculation showed that about 70% of an excess electron is localized at the imine group (C=NH₂). On the other hand, a hole is spread over the molecule excluding the imine group where the hole density is zero. If the molecules were arranged in the AurHCl film in such a manner that imine groups can overlap to a particular direction, then an excess electron will have a large tunneling probability because of a large electron transfer interaction.¹⁷ However, quantitative discussions cannot be done without knowledge of the structure of solid AurHCl. Some of the other activation energies may be attributed to traps and/or to some surface states. Thermally stimulated currents were measured to know the energy distribution of traps, but reliable results could not be obtained. Takeda found a tandem two photon ionization energy at 3.14 eV below the vacuum level.⁷ If this level is attributed to a trap level, then the depth of a trap is 0.34 eV below the conductive level. Although the value coincides with some of the activation energies in the photoconduction (0.40 eV at +0.5 V and 0.35 eV at +1.0 V), the origin of the observed activation energies of the dark current and photocurrent is still obscure at present.

Acknowledgment. The authors are grateful to Professor R. C. Nelson for valuable discussions by letters. They also thank Mr. Y. Kurosaki for his help in some of the experiment.

(16) R. G. Selsby and M. Sukigara, *J. Mol. Spectrosc.*, **29**, 461 (1969).

(17) M. Sukigara and R. C. Nelson, *Mol. Phys.*, **17**, 387 (1969).

The Apparent Hydration Numbers of Alcohols in Aqueous Solution

by Charles H. Spink* and John C. Wyckoff

Department of Chemistry, State University College, Cortland, New York 13045 (Received June 16, 1971)

Publication costs borne completely by The Journal of Physical Chemistry

The near-infrared difference spectra of methanol, ethanol, 2-propanol, and *tert*-butyl alcohol in aqueous solution have been obtained from 860 to 1020 nm. Resolution of the components of the difference spectra has yielded the spectra of the hydrated alcohol solutes and has allowed the determination of apparent hydration numbers for the alcohols in dilute aqueous solutions. Values for the hydration numbers at infinite dilution in water are 4.0, 1.5, 1.3, and 1.0 for *tert*-butyl alcohol, 2-propanol, ethanol, and methanol, respectively. The apparent hydration numbers were found to decrease with increasing concentration of alcohol. Results have been interpreted in terms of the structure of the dilute solutions.

Introduction

Experimental evidence on the behavior of binary mixtures of simple aliphatic alcohols and water has indicated that dilute solutions of the higher alcohol homologs cause the structure of water to be enhanced.¹⁻³ An explanation of the structure enhancement, recently reviewed by Franks and Ives,¹ is that the hydrocarbon groups in the alcohols provide sites for the buildup of structure around the alcohol molecule. The exact nature of this "hydration" around the nonpolar portion of the alcohol solutes is not clear. However, the peculiar structural features of aqueous alcohol solutions produce remarkable effects on the kinetics of reactions,⁴ on the mobility of ions in the mixed solvents,⁵ and on the thermodynamic behavior of solutes upon transfer from water to alcohol-water mixtures.^{4,6} Because of the nature and magnitude of the observed effects on solutes and because the structural properties of these solutions are not completely clear, it seemed important to obtain more information on the nature of the hydration of alcohol solutes.

Recently, a number of investigators have used the near-infrared (NIR) bands of water to study association in aqueous solutions.⁷⁻¹⁰ Of particular interest is the work of Bonner⁹ and Fisher¹⁰ on the use of the NIR difference spectra of water to obtain information on the hydration of solutes. In Fisher's method the observed difference spectrum is considered to be made up of contributions from three components: a negative component due to absorption by water in the reference cell, a positive component due to the absorption by the solute in the sample cell, and a positive contribution from the water of hydration of the solute. (It is presumed that the hydration water has a different spectrum from normal water.) The resolution of these contributions allows calculation of the minimum amount of water involved in hydration of the solute.¹⁰

We felt that the above approach could be useful in the study of the hydration of alcohols. In the experiments of Fisher,¹⁰ the difference spectra were recorded

in the vicinity of the 1400-nm band of water. Because of the rather strong absorption by the alcohols in this region, the water band at 980 nm was chosen for this study. Luck⁷ and Bonner⁹ have used the 980-nm band for related studies on electrolyte solutions. Below are reported the results of a study of the NIR difference spectra of aqueous alcohol solutions, and estimates of the apparent hydration numbers for methanol, ethanol, 2-propanol, and *tert*-butyl alcohol in dilute solution in water.

Experimental Section

The methanol, 2-propanol, and *tert*-butyl alcohol used in the experiments were Fisher Certified reagent grade and were used without further purification. The ethanol was 95.6% azeotrope obtained by fractional distillation of 95% ethanol from Commercial Solvents Co. All solutions were made up by weight to known volumes.

Difference spectra were recorded with a Cary 14 spectrophotometer, using 5-cm matched cells, with the alcohol solutions in the sample cell and water in the reference cell. The cell compartments were thermostated at $25.0^\circ \pm 0.3^\circ$ by circulating constant temperature water. All spectra were corrected for a slight cell mismatch, the correction obtained by running water *vs.* water. Spectra were recorded over a period of several

- (1) F. Franks and D. Ives, *Quart. Rev.*, **20**, 1 (1966).
- (2) G. Wada and S. Umeda, *Bull. Chem. Soc. Jap.*, **35**, 646 (1962).
- (3) J. A. V. Butler, *Trans. Faraday Soc.*, **32**, 229 (1936).
- (4) E. M. Arnett, P. M. Dugglesby, and J. J. Burke, *J. Amer. Chem. Soc.*, **85**, 1351 (1963).
- (5) T. L. Broadwater and R. L. Kay, *J. Phys. Chem.*, **74**, 3802 (1970).
- (6) C. H. Spink and M. Aufer, *ibid.*, **74**, 1742 (1970).
- (7) W. Luck, *Ber. Bunsenges. Phys. Chem.*, **67**, 186 (1963); **69**, 69 (1965).
- (8) G. R. Choppin and K. Buijs, *J. Chem. Phys.*, **39**, 2035 (1963); *ibid.*, **39**, 2042 (1963).
- (9) O. D. Bonner and G. B. Woolsey, *J. Phys. Chem.*, **72**, 899 (1968).
- (10) W. C. McCabe and H. F. Fisher, *ibid.*, **74**, 2990 (1970).

hours to ensure that the cells were at temperature equilibrium. The difference spectra were recorded at a slow scan rate to allow adequate time for the slit servo to respond to absorption in the reference beam due to the water blank. The base line was found to be reproducibly constant using these techniques. Spectra of the pure alcohols were run in 1-cm cells against CCl_4 , using a 0–0.1 absorbance slide-wire.

Results

Difference Spectra of Alcohol Solutions. The difference spectra of methanol, ethanol, 2-propanol, and *tert*-butyl alcohol were determined in at least four different concentrations in each case in the range of from 0.3 to 4.0 *M* alcohol. Examples of the spectra for *tert*-butyl alcohol solutions are given in Figure 1. The spectra of the other alcohols are generally similar. The spectra consist of major negative absorption in the vicinity of 970 nm and a small positive peak near 910 nm. As was pointed out by Fisher,¹⁰ the solute occupies a specific volume in the sample cell that is occupied by an equivalent volume of water in the reference cell. Thus, the negative absorption in the vicinity of 970 nm is due to the excess water in the reference. A spectrum of pure water is given in Figure 1 for comparison. This region of water absorption (950–980 nm) has been specified by several workers as either a combination ($2\nu_1 + \nu_3$) band¹¹ or an overtone ($3\nu_1$) band.¹²

The small positive absorption around 910 nm must be from the alcohol solute molecules. To better understand the absorption due to the alcohol solutes, spectra of the pure liquid alcohols were obtained in the region from 850 to 1050 nm and were compared with published data.^{7,13,14} The band at 910 nm appears in the spectra of all the alcohols. LeFevre, Roper, and Williams¹³ have made a systematic study of the NIR spectra of normal alcohols and *n*-alkyl bromides. The 910-nm band appeared at the same frequency for all of the alcohols and bromides studied, and the intensities were in proportion to the number of C–H bonds in the molecules. The band was assigned as the fourth harmonic of the C–H stretching frequency, and we shall assume in what follows that this assignment is correct.

The NIR spectra also show that all of the alcohols have a broad absorption which peaks at about 1015 nm, and all except methanol have a small, sharp band around 965 nm. The band at 965 nm has been assigned by Luck⁷ and by Kempster and Mecke¹⁴ as due to nonbonded OH absorption in the alcohols. The intensity is greatest in *tert*-butyl alcohol, decreases in 2-propanol and in ethanol, and is not seen distinctly at all in methanol. These results are consistent with the idea that there is less intermolecular hydrogen bonding in the sterically hindered *tert*-butyl alcohol, as compared with methanol, and there is thus a proportionately higher concentration of free OH groups. The

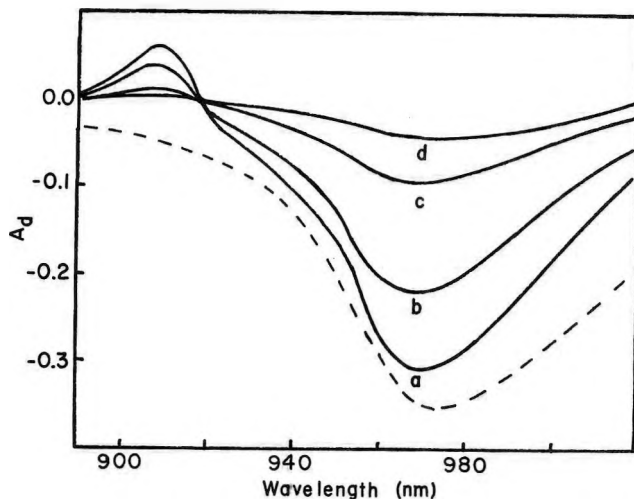


Figure 1. Differential absorption spectra of aqueous *tert*-butyl alcohol solutions: (a) 3.14 *M*, (b) 2.12 *M*, (c) 0.76 *M*, (d) 0.35 *M*. The dashed curve is a scaled-down (factor of 3.1) spectrum of pure water vs. CCl_4 .

broad absorption at around 1015 nm is the hydrogen-bonded region of OH absorption of the alcohols¹⁴ and represents the total absorption due to dimers, trimers, and other higher aggregates that are possible, particularly in methanol.

Resolution of the Difference Spectra. The method of Fisher¹⁰ provides a means for resolving the difference spectra of the alcohol solutions into the component parts. In this approach it is assumed that the normal water present in sample and reference cells cancel each other. The expected contributions to the difference spectrum are from three sources. First, there is a positive contribution resulting from any absorption due to the alcohol solute in the sample cell. The 910-nm C–H band and the OH band near 1015 nm might be expected to appear in the spectrum of the hydrated solute. Second, it is possible that if there is any spectroscopically unique hydration water associated with the alcohol solute, or if the absorption of normal water is altered by the presence of the solute, there will be a net contribution from this “hydration” water that will appear as a positive absorption. (In what follows we will not distinguish between specifically bound water and water that has been perturbed by the solute. Water that has a spectrum different from normal water is spectroscopically important here.) Third, there is a negative component in the difference spectrum due to the excess absorption by water in the reference cell. This contribution results because the solute occupies

(11) H. Yamatera, B. Fitzpatrick, and B. Gordon, *J. Mol. Spectrosc.*, **14**, 268 (1964).

(12) W. Luck, *Fortschr. Chem. Forsch.*, **4**, 653 (1964).

(13) R. J. W. LeFevre, R. Roper, and A. J. Williams, *Aust. J. Chem.*, **12**, 743 (1959).

(14) H. Kempster and R. Mecke, *Z. Phys. Chem. (Frankfurt am Main)*, **46**, 229 (1940).

volume (called the excluded volume) in the sample cell, which is occupied by water in the reference cell. There is thus a net negative water absorption caused by the volume imbalance between the two cells.

The net absorbance in the sample cell, A_s , at a given wavelength, can thus be expressed in terms of the measured difference absorbance, A_d , and the absorbance of pure water, A_w

$$A_s = A_d + f \cdot A_w \quad (1)$$

The values of A_w are obtained from the spectrum of pure water vs. CCl_4 . The factor, f , is the fraction of the total water absorption which is contributed by the excess water in the reference cell. Therefore, the product, $f \cdot A_w$, is the net absorbance of the excluded volume of water in the reference cell, and f can be identified as the fraction of the total volume of solution that is occupied by the hydrated solute.¹⁰ Calculation of A_s at the wavelengths studied generates an absorption spectrum of the hydrated solute molecule, which is composed of the alcohol solute contribution and any net hydration water that has absorption different from normal water. Thus, if f is known, the spectrum can be calculated from the measured values of A_d and A_w . From spectroscopic measurements alone, the value of f for a given solution cannot be determined. However, a minimum value of the fractional volume, f , can be obtained using eq 1. The procedure is to assume values of f and calculate A_s at the various wavelengths studied. It is a necessary consequence of the differential measurements that the A_s values must be either zero or positive, so by varying f it is possible to find a value which will cause at least one value of A_s to be zero. This value of f is the minimum value, since any smaller number would cause A_s to be negative. Once the minimum value of f is found, the spectrum of the hydrated solute can then be generated using eq 1. This method was used for resolving the components of the alcohol difference spectra and is similar to Fisher's treatment.

For the alcohol solutions we have an additional check on the spectra of the hydrated alcohols that was not possible with the electrolyte solutions studied by Fisher.¹⁰ It would be expected that the C-H absorption of the alcohols should appear in the resolved difference spectra. Thus, if we assume that the 910-nm C-H band obeys Beer's law in these solutions, it should be possible to calculate the expected absorbance at 910 nm for each solution from Beer's law. The calculated value can then be compared with the absorbance at 910 nm in the spectrum of the solute obtained above using eq 1 and the appropriate value of f . This comparison provides a check on the validity of the resolved spectrum and on the choice of f used in the calculation of the spectrum of the hydrated alcohol.

Figures 2 and 3 are the resolved spectra of hydrated *tert*-butyl alcohol and methanol, respectively. The

other alcohol spectra are generally similar. The curves were obtained using the procedure described above and using the f values summarized in Table I. Table I also shows a comparison of the absorbance at 910 nm obtained by a Beer's law calculation with the value found in the hydrated alcohol spectrum. (The molar absorptivities used in the Beer's law calculations were 2.15×10^{-3} , 3.16×10^{-3} , 4.46×10^{-3} , and 6.98×10^{-3} l./mol-cm for methanol, ethanol, 2-propanol, and *tert*-butyl alcohol, respectively, and were obtained from the spectra of the pure liquid alcohols vs. CCl_4). The dashed curves in Figures 2 and 3 are the spectra of the pure liquid alcohols, calculated assuming Beer's law holds at all wavelengths in the spectrum, and are presented for comparison with the spectra of the hydrated solutes.

Table I: Hydration Data for Alcohols

| X_{ROH}^a | f^b | A_{910}^c | A_{910}^d | V_e^e | ϕ_v^f | n^g |
|----------------------------|-------|-------------|-------------|---------|------------|-------|
| <i>tert</i> -Butyl Alcohol | | | | | | |
| 0.006 | 0.050 | 0.010 | 0.011 | 145.0 | 83.7 | 3.4 |
| 0.014 | 0.100 | 0.025 | 0.025 | 131.0 | 84.0 | 2.6 |
| 0.042 | 0.230 | 0.067 | 0.069 | 109.0 | 84.3 | 1.4 |
| 0.072 | 0.290 | 0.101 | 0.103 | 92.3 | 84.4 | 0.4 |
| 2-Propanol | | | | | | |
| 0.008 | 0.040 | 0.009 | 0.009 | 94.6 | 71.4 | 1.3 |
| 0.015 | 0.075 | 0.018 | 0.018 | 93.0 | 71.0 | 1.2 |
| 0.026 | 0.120 | 0.028 | 0.030 | 89.8 | 70.5 | 1.1 |
| 0.048 | 0.200 | 0.050 | 0.051 | 86.2 | 69.8 | 0.9 |
| Ethanol | | | | | | |
| 0.010 | 0.040 | 0.011 | 0.008 | 73.5 | 49.3 | 1.3 |
| 0.019 | 0.073 | 0.020 | 0.016 | 70.9 | 51.5 | 1.1 |
| 0.032 | 0.115 | 0.028 | 0.025 | 69.0 | 52.3 | 0.9 |
| 0.045 | 0.150 | 0.039 | 0.036 | 65.8 | 52.5 | 0.7 |
| Methanol | | | | | | |
| 0.014 | 0.040 | 0.009 | 0.008 | 50.9 | 33.9 | 0.9 |
| 0.029 | 0.075 | 0.017 | 0.015 | 48.8 | 35.8 | 0.7 |
| 0.059 | 0.140 | 0.033 | 0.030 | 45.4 | 36.6 | 0.5 |
| 0.083 | 0.190 | 0.046 | 0.041 | 45.2 | 36.8 | 0.5 |

^a Mole fraction of alcohol. ^b Volume fraction, determined from resolution of difference spectra. ^c Absorbance at 910 nm from hydration spectrum. ^d Absorbance at 910 nm calculated from Beer's law. ^e Excluded volume, calculated using eq 3. ^f Apparent molal volume, obtained from density data. ^g Spectroscopic hydration number.

Several features of the spectra are notable. One is that the absorbances predicted from Beer's law at 910 nm agree well with the absorbances in the spectra of the hydrated alcohols. With uncertainties of ± 0.002 in the absorbances in the hydrated alcohol spectra, and similar uncertainties in the Beer's law absorbances, the agreement is within the experimental error. It is reasonable to expect that the C-H bond absorption

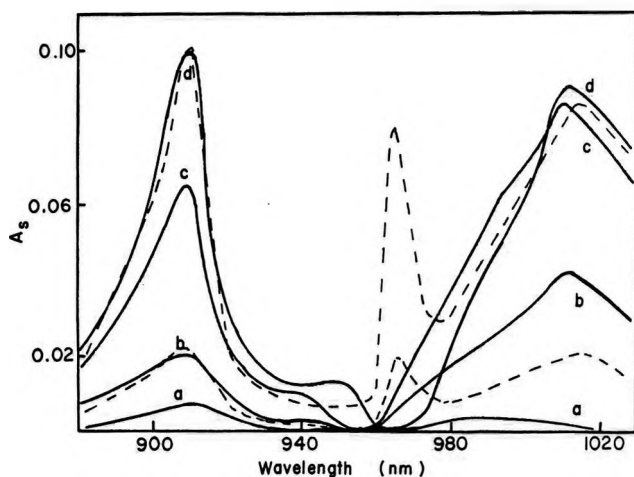


Figure 2. Resolved spectra of hydrated *tert*-butyl alcohol in aqueous solution: (a) 0.35 *M*, (b) 0.76 *M*, (c) 2.12 *M*, (d) 3.14 *M*. The dashed curves are obtained from the spectrum of pure liquid *tert*-butyl alcohol, assuming Beer's law holds at all wavelengths: upper curve for 3.14 *M* and lower curve for 0.76 *M*.

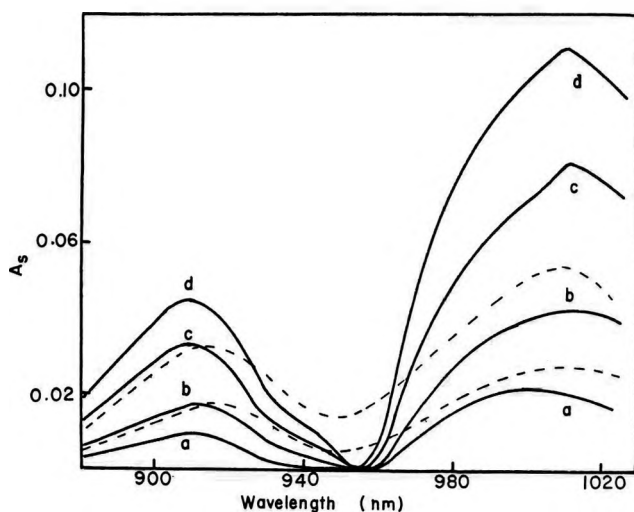


Figure 3. Resolved spectra of hydrated methanol in aqueous solution: (a) 0.79 *M*, (b) 1.54 *M*, (c) 3.08 *M*, (d) 4.21 *M*. The dashed curves are obtained from the spectrum of pure liquid methanol, assuming Beer's law holds at all wavelengths: upper curve for 3.08 *M* and lower curve for 1.54 *M*.

would not be influenced by hydrogen-bonding interactions very strongly, so the rather close agreement between the two absorbances at 910 nm lends support to the choice of f used in the calculations and to the derived absorbances in the resolved spectra of the alcohols.

Another feature of the spectra is the absence of any major absorption in the vicinity of 960–970 nm, the region of nonbonded OH in the spectra of the pure alcohols. For instance, in Figure 2 the large band at 965 nm due to the nonbonded OH in *tert*-butyl alcohol is completely gone in the spectrum of the hydrated alcohol. But the lack of absorbance in this region is

not surprising in the spectra of the hydrated alcohols, since the water molecules are likely to be hydrogen bonded to the OH groups of the alcohols, producing a solution which has very little nonbonded OH.

Thus, the major OH absorption is in the range of 980–1020 nm, where hydrogen-bonded OH is found.¹⁴ Since both alcohol and any spectroscopically unique hydration water could absorb in this region, it is not possible to give unambiguous interpretation to the OH absorption in this region. However, there are several features of the absorption bands in the alcohol series that deserve comment.

In *dilute* solution of *tert*-butyl alcohol there is a general relative increase in absorption compared with the spectrum of the pure alcohol. For the 0.76 *M* solution the absorbance at 1015 nm is almost twice what is expected in the spectrum of the pure alcohol, assuming it obeys Beer's law. Note in Figure 2 that although the C–H bonds at 910 nm almost identically overlap, the OH band around 1015 nm in the spectrum of hydrated *tert*-butyl alcohol is considerably larger than the band for the pure alcohol. Further, as the concentration of alcohol increases, the intensities of the 1015-nm bands for pure alcohol and hydrated alcohol become comparable. (Compare the curves for 3.14 *M* solutions.) For *tert*-butyl alcohol, then, the enhanced intensity is relatively smaller at higher alcohol concentrations.

In the spectra of methanol and ethanol, the enhanced intensity in the region from 980 to 1020 nm remains almost proportionately higher at all concentrations (see Figure 3). The spectra of 2-propanol more closely resemble the *tert*-butyl alcohol spectra in the bonded OH region, but with relatively less dependence of intensity on concentration. It appears that whatever is causing the changes in the OH absorption is more dependent on concentration for *tert*-butyl alcohol and 2-propanol than for ethanol and methanol.

The changes in band intensity in the bonded OH region could arise from two sources. First, changes in the types and relative amounts of alcohol species could effect intensity. The conversion of nonbonded OH to bonded OH in the alcohol solutes, as indicated by loss of the 965-nm bands, would cause an increase in intensity in the region near 980–1020 nm.

On the other hand, changes in intensities could be due to additional OH absorption from hydration water in the 980–1020-nm region. This hydration water would have to be spectroscopically different from normal water, or it would be cancelled when the spectrum of the hydrated alcohol is generated. Hydration water absorption could add to intensity in the bonded OH region producing the overall enhancement of absorption in the more dilute solutions. (Luck⁷ has suggested on the basis of low-temperature spectra of water that bonded OH in water absorbs in the vicinity of 980 nm.) As mentioned above, the bonded OH absorption of the more concentrated *tert*-butyl alcohol solutions more

closely resembles that of the pure alcohol, suggesting that if hydration water is contributing to the spectra, it is becoming less and less important as concentration of alcohol is increased. That is, the loss of absorption in the more concentrated *tert*-butyl alcohol solutions could result from loss of spectroscopically unique hydration water in the vicinity of the alcohol solute.

It is not possible from the spectra alone to determine whether the spectral changes in the OH region are due to hydration water and/or changes in the state of the alcohol solutes themselves. The results of the next section indicate that there are changes in the amount of water involved in hydration, so that at least part of the changes in the spectra could be from that source.

Calculations of Apparent Hydration Numbers. Using the arguments of Fisher,¹⁰ the volume of water in the hydration shell of the alcohols is nV_0 , where n is the hydration number and V_0 is the molar volume of water. This hydration volume can be calculated from the difference between the excluded volume, V_e (the total volume of solute plus hydration shell), and the apparent molal volume of the solute, ϕ_v

$$nV_0 = V_e - \phi_v \quad (2)$$

The excluded volume, V_e , can be obtained from the NIR data by

$$V_e = f \cdot (1000/C) \quad (3)$$

where f is the volume fraction defined in the previous section and C is the molar concentration of alcohol. The apparent molal volume of the alcohol is calculated from density data by the method of Padova.¹⁵ Table I shows values of V_e , ϕ_v , and the hydration numbers, n , for the solutions studied. A value of 18.0 ml/mol was used as the molar volume of water, and density data for the alcohol solutions were obtained from the International Critical Tables.

The data in Table I show that the hydration numbers generally increase with increased dilution, particularly for *tert*-butyl alcohol. The extrapolated values at zero concentration of alcohol are 4.0, 1.5, 1.3, and 1.0 for *tert*-butyl alcohol, 2-propanol, ethanol, and methanol, respectively. The expected uncertainty in the values of the hydration numbers is primarily determined by the uncertainty in V_e , which in turn, relates to the uncertainty of f . Using errors of ± 0.002 in the absorbance values of the components of the difference spectra, the expected relative error in f is about 4% for the higher alcohol concentrations, and increases to about 8% for the most dilute solutions. This error in f , along with relative errors in ϕ_v and C of about 1 and 2%, respectively, produces uncertainties of from 20 to 40% in the spectroscopic hydration numbers. This relatively large error in the value of n results because nV_0 is a small difference between two large numbers. Thus, the values of n at zero alcohol concentration are about 4.0 ± 1.0 , 1.5 ± 0.5 , 1.3 ± 0.4 , and 1.0 ± 0.3

for *tert*-butyl alcohol, 2-propanol, ethanol, and methanol, respectively. It should be emphasized that the values of n are minimum values, determined by the criteria set for obtaining the minimum value of f . However, the absorbance check on the C-H band at 910 nm is relatively sensitive to the choice of f . That is, if f is increased much above the minimum values found, the absorbances at 910 nm no longer agree with the predicted values from Beer's law. For this reason we suggest that the values of n in Table I are reliable estimates of the values for the spectroscopic hydration numbers in these solutions. The values of n obtained from the NIR data are of interest with regard to the nature of the water that is involved in hydration. It is a necessary consequence of the difference method that if the water of hydration is spectroscopically identical with normal water, the values of n must be zero. This condition results because the hydration water absorption would be cancelled by normal water in the reference, making f smaller. The limiting value of f would be that which leads to V_e equal to ϕ_v ; that is, the volume occupied by the solute itself is the only contribution to the difference in absorption by water between the sample and reference cells. Under this condition n is zero. We conclude, then, that the values of n obtained in Table I result from hydration water that is spectroscopically different from normal water. Other water molecules could be involved in hydration, but their spectrum in the region studied would have to be very similar to that of normal water. The actual absorption spectrum of the hydration water is most likely mixed in with the bonded OH absorption from the alcohols, as discussed in the previous section. Thus, although the hydration spectrum can be inferred, it would be difficult to obtain in the alcohol solutions.

Summarizing the trends in the hydration numbers, two factors emerge. One is that the larger alcohols are more highly hydrated. Methanol shows only about 1:1 hydration, while *tert*-butyl alcohol indicates about 4:1 in very dilute solution. The other factor is that the hydration numbers decrease with increasing amount of alcohol in the solutions, all of the alcohols reaching values of n less than 1 before 0.1 mole fraction alcohol.

Discussion

Both the hydration spectra and the spectroscopic hydration numbers indicate the two trends mentioned above. (1) The larger the nonpolar groups in the alcohols, the greater the extent of hydration of the alcohol in dilute solutions. (2) As the concentration of alcohol increases, the extent of hydration decreases. Methanol shows about 1:1 association with water that does not change very much with concentration. It is reasonable to expect that the polar OH group of methanol hydrogen bonds with water, and that this

(15) J. Padova, *J. Chem. Phys.*, **40**, 691 (1964).

type of association would be relatively constant until higher alcohol concentrations, where solute-solute interactions become important. The other alcohols should also indicate at least 1:1 association due to the polar OH. The enhanced values of n for the alcohols with larger nonpolar groups, and especially for *tert*-butyl alcohol, show that other factors than the normal 1:1 intermolecular hydrogen bonding must be in effect.

The larger hydration numbers for the higher homologs could be a result of the slightly increased basicity of the OH groups in the series from methanol to *tert*-butyl alcohol.¹⁶ The more basic OH group in *tert*-butyl alcohol would favor more extensive solvation by water, producing larger aggregates of water molecules extending out from the polar OH dipole of the alcohol. However, this argument does not seem plausible on simple steric grounds. The bulky methyl groups in *tert*-butyl alcohol would interfere with the buildup of very large water cages around the OH group. There is evidence that in the pure liquid alcohols the branched homologs are not as highly associated liquids as either methanol or ethanol due to the steric hindrance of the methyl groups.¹⁷ So, although the OH is more basic in *tert*-butyl alcohol, steric arguments disfavor the buildup of additional hydration around the OH group.

As mentioned in the Introduction, the enhancement of solution structure around alcohols can be explained as occurring within the vicinity of the nonpolar methyl groups. That is, the methyl groups, rather than behaving as steric blocks to the buildup of water structure around the solute are actually providing sites for the enhancement of structure. Frank and Evans have explained the entropies of vaporization of nonpolar molecules from aqueous solutions in terms of solvation of the nonpolar groups by microscopic "icebergs" of water.¹⁸ These hydration shells are thought to be large at low temperature and for molecules with large nonpolar groups. Franks and Ives¹ used similar arguments in their review of the behavior of the heats of mixing, partial molal volumes, and ultrasonic absorption of aqueous alcohol solutions. The extensive thermodynamic data of Knight¹⁹ for dilute aqueous alcohol solutions were interpreted with the view that the alcohols, particularly the larger branched homologs, promote structure in the Frank-Evans sense. Thus, the larger hydration numbers and spectral intensity shifts found in this study for *tert*-butyl alcohol are consistent with a number of other studies of the solution behavior of alcohols and add further support to the concept that nonpolar groups can provide sites for the enhancement of structure.

The concentration dependence of the hydration numbers requires that we consider hydration to be less extensive per mole of solute as the alcohol concentration increases, particularly for *tert*-butyl alcohol. This result suggests that hydration structure is being progressively disrupted as alcohol concentration increases.

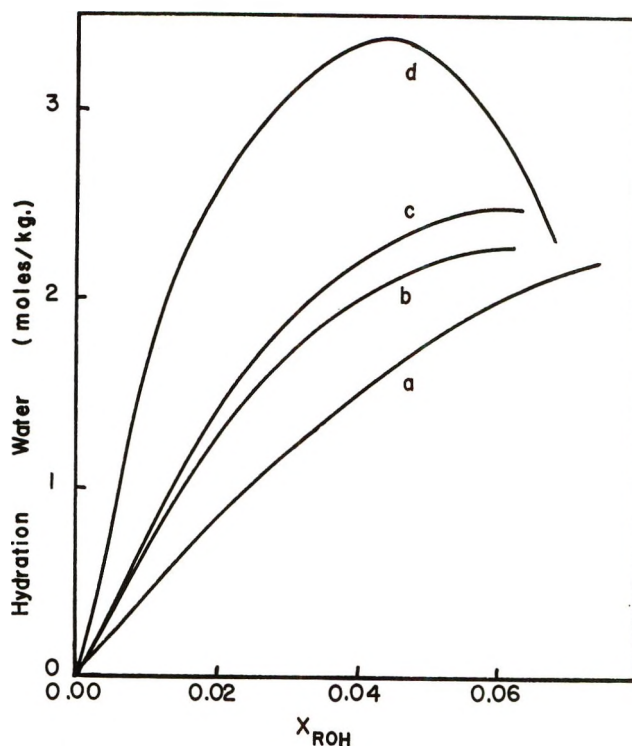


Figure 4. Total molality of spectroscopically unique hydration water vs. mole fraction of alcohol: (a) methanol, (b) ethanol, (c) 2-propanol, (d) *tert*-butyl alcohol

The net effect of the disruption can be seen rather clearly by looking at the total amount of spectroscopically unique hydration water as alcohol mole fraction is increased. The total molality of this hydration water is the product of n , the spectroscopic hydration number, and the number of moles of alcohol solute per 55.5 mol of water at a specified mole fraction of alcohol.²⁰ Figure 4 shows the molality of hydration water vs. mole fraction for the alcohols studied. The curves show that in very dilute solution there is a gradual buildup of total hydration structure, and the effect is greatest for *tert*-butyl alcohol. However, as the concentration increases, hydration increases less rapidly, and eventually begins to decrease, as is clearly shown for *tert*-butyl alcohol. The decrease occurs when the values of n become small enough to compensate for the increased concentration of alcohol in solution. It is interesting to note that the maximum in the curve for *tert*-butyl alcohol occurs at the same mole fraction as the minima in partial molal volumes and the maxima in heats of mixing of the alcohols with water,¹ again showing the

(16) W. Gerrard and E. D. Macklen, *Chem. Rev.*, **59**, 1105 (1959).

(17) R. Mecke, *Discuss. Faraday Soc.*, **No. 9**, 161 (1959).

(18) H. S. Frank and M. W. Evans, *J. Chem. Phys.*, **13**, 507 (1945).

(19) W. S. Knight, Ph.D. Thesis, Princeton University, July 1962.

(20) Since the hydration numbers are calculated from volumes per mole of solute (to account for density differences of the solutions), the total amount of hydration water involved at a given mole fraction of alcohol must be calculated this way.

close correlation of the properties of the alcohol solutions with the hydration phenomena discussed above.

In summary, we believe that the difference spectra method is a good way to study solvation in alcohol-water mixtures and can lead to useful information on the structure of the solutions. It would be of value to give a more thorough interpretation of the spectral bands of the hydration water. We are attempting to get more data for other solutes at a number of temperatures, but the full interpretation requires density data as well. When density and spectral measurements are complete, it will be possible to identify more closely the species responsible for the observed spectral bands, and

possibly to obtain the spectrum of the spectroscopically unique water involved in hydration of the nonpolar groups. It would be of interest to know if the spectrum of the hydration water resembles a modified ice spectrum, or perhaps the spectrum of the gas hydrates of SO_2 reported by Luck.²¹

Acknowledgments. This work was supported by grants from the National Institutes of Health (Grant No. GM-12987), and from the Research Foundation of New York State.

(21) W. A. P. Luck and W. Ditter, *J. Phys. Chem.*, **74**, 3687 (1970).

COMMUNICATIONS TO THE EDITOR

Potential-Dependent Chronoamperometry: the EC Reaction

Publication costs assisted by Texas Tech University

Sir: In the study of chemically complicated electrode processes, the reaction sequence, $A \pm ne \rightleftharpoons B$; $B \xrightarrow{k} C$, occurs quite frequently and in the electrochemical parlance is referred to as an EC reaction.^{1,2} Experimental methods employing polarography,³ stationary electrode voltammetry,⁴ controlled potential coulometry,⁵ chronopotentiometry,⁶ rotating ring-disk voltammetry,^{7,8} and thin layer electrochemistry⁹ have been developed in order to determine the value of the rate constant k for this sequence. Several of these techniques have been applied to a single reaction¹⁰ and Schwarz and Shain¹¹ have divided the various techniques into two categories, single-step and double-step methods. Single-step methods for the most part depend upon potential shifts brought about by the perturbation of the follow-up reaction upon the Nernstian equilibrium. Double-step methods can be thought of as the generation of the reactant in a forward step followed by the monitoring of its disappearance in a reverse step. Double-step chronoamperometry,¹¹ current reversal chronopotentiometry,⁶ and reversal coulometry clearly number among these methods and it requires but little imagination to categorize cyclic voltammetry⁴ and ring-disk voltammetry^{7,8} similarly. It has been pointed out¹¹ that single-step methods suffer from the fact that the observed potential shifts are quite small and that both charge-transfer reversibility and a knowledge of E° are required. This paper will develop the thesis that if single-step chronoamperometry is carried out at potentials insufficient for diffusion control one may measure

the rate constant of an EC reaction without the difficulties normally ascribed to single-step methods. Furthermore it will be shown that this approach possesses certain unique advantages.

The diffusion problem is similar to other chronoamperometric problems with the exception that the surface concentration of species A is not zero, but rather is determined by the applied potential according to the Nernst equation. This treatment presupposes charge-transfer reversibility. Fick's laws including the kinetic complications for this sequence are

$$\frac{\partial C_A}{\partial \tau} = D_A \frac{\partial^2 C_A}{\partial x^2} \quad (1)$$

$$\frac{\partial C_B}{\partial \tau} = D_B \frac{\partial^2 C_B}{\partial x^2} - k C_B \quad (2)$$

The appropriate initial and boundary conditions are

- (1) A. C. Testa and W. Reinmuth, *Anal. Chem.*, **33**, 1320 (1961).
- (2) R. N. Adams, *Accounts Chem. Res.*, **2**, 175 (1969).
- (3) S. G. Mairanovsky, "Catalytic and Kinetic Waves in Polarography," Plenum Press, New York, N. Y., 1968, Chapter VIII and references therein.
- (4) R. S. Nicholson and I. Shain, *Anal. Chem.*, **36**, 706 (1964).
- (5) A. J. Bard and S. V. Tatwawadi, *J. Phys. Chem.*, **68**, 2676 (1964).
- (6) A. C. Testa and W. Reinmuth, *Anal. Chem.*, **32**, 1512 (1960).
- (7) P. A. Malachuk, K. B. Prater, G. Petrie, and R. N. Adams, *J. Electroanal. Chem.*, **16**, 41 (1968).
- (8) W. J. Albery and M. L. Hitchman, "Ring-Disk Electrodes," Oxford University Press, London, 1971.
- (9) A. T. Hubbard and F. C. Anson in "Electroanalytical Chemistry, A Series of Advances," Vol. 4, A. J. Bard, Ed., Marcel Dekker, New York, N. Y., 1970.
- (10) D. M. Oglesby, J. D. Johnson, and C. N. Reilly, *Anal. Chem.*, **38**, 385 (1966).
- (11) W. M. Schwarz and I. Shain, *J. Phys. Chem.*, **69**, 30 (1965).

$$\tau = 0, x \geq 0: C_A = C_A^b, C_B = 0 \quad (3)$$

$$\tau > 0, x \rightarrow \infty: C_A \rightarrow C_A^b, C_B \rightarrow 0 \quad (4)$$

$$\tau > 0, x = 0: C_B = C_A 10^{\pm n(E_{APP} - E^o)/0.059} \quad (5a)$$

$$D_A \frac{\partial C_A}{\partial x} = -D_B \frac{\partial C_B}{\partial x} \quad (5b)$$

and the observed current is

$$i = \pm nFAD_A \left(\frac{\partial C_A}{\partial x} \right)_{x=0} \quad (6a)$$

$$N_{APP} = i\tau^{1/2}/i\tau^{1/2} (\text{Diffusion control}) \quad (6b)$$

where C_A and C_B are the concentrations of the respective species, the superscript b indicates the concentration of the solution bulk, D_A and D_B are the respective diffusion coefficients, and all other notation is standard. For the purposes of this discussion the process will be taken as an oxidation, n will be taken as unity, and the standard assumption $D_A = D_B \equiv D$ will be made.

Denoting the Laplace transform, L , of $C_A(x, \tau)$ and $C_B(x, \tau)$ by $g_A(x, s)$ and $g_B(x, s)$, respectively, eq 1 and 2 are equivalent to

$$\frac{\partial^2 g_A(x, s)}{\partial x^2} = \frac{s}{D} g_A(x, s) - \frac{C_A^b}{D} \quad (7)$$

$$\frac{\partial^2 g_B(x, s)}{\partial x^2} = \left(\frac{s+k}{D} \right) g_B(x, s) \quad (8)$$

These equations have the general solutions

$$g_A(x, s) = \alpha e^{x\sqrt{s/D}} + \beta e^{-x\sqrt{s/D}} + C_A^b/s \quad (9)$$

$$g_B(x, s) = \alpha' e^{x\sqrt{(s+k)/D}} + \beta' e^{-x\sqrt{(s+k)/D}} \quad (10)$$

where α, β, α' , and β' must be determined by the boundary conditions. Since

$$\lim_{x \rightarrow \infty} g(x, s) = L[\lim_{x \rightarrow \infty} C(x, \tau)]$$

for either species, $g_A(x, s) \rightarrow C_A^b/s$ and $g_B(x, s) \rightarrow 0$ as $x \rightarrow \infty$ so $\alpha = \alpha' = 0$. Similarly, because

$$\frac{\partial g(x, s)}{\partial x} \Big|_{x=0} = L \left[\frac{\partial}{\partial x} C(x, \tau) \Big|_{x=0} \right]$$

condition 5b implies $\beta' = -\beta\sqrt{s/(s+k)}$ while 5a determines β

$$\beta = -[\sqrt{s/(s+k)} + 10^\phi]^{-1} 10^\phi C_A^b/s$$

where $\phi = (E_{APP} - E^o)/0.059$. Thus the Laplace transforms of the solutions of eq 1 and 2 which satisfy the boundary conditions 3, 4, and 5 are

$$g_A(x, s) = -10^\phi [\sqrt{s/(s+k)} + 10^\phi]^{-1} \times C_A^b e^{-x\sqrt{s/D}}/s + C_A^b/s \quad (11)$$

$$g_B(x, s) = 10^\phi [\sqrt{s/(s+k)} + 10^\phi]^{-1} \times C_A^b e^{-x\sqrt{(s+k)/D}}/\sqrt{s(s+k)} \quad (12)$$

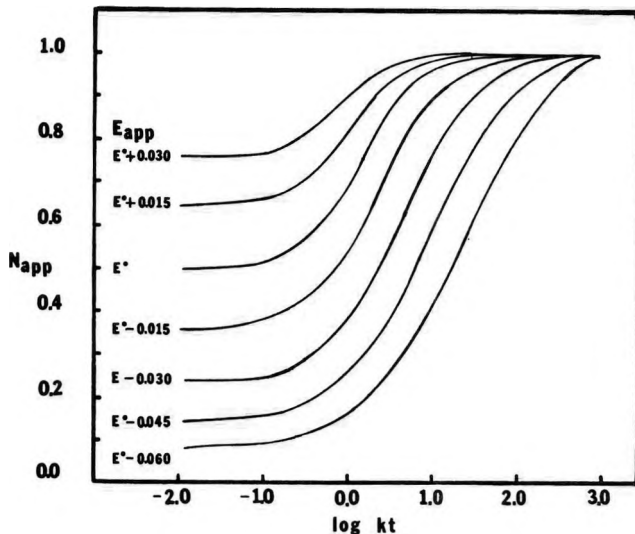


Figure 1.

The inverse Laplace transform, L^{-1} , of these functions cannot be written in closed form. Equation 6, however, only requires

$$\frac{\partial C_A(x, \tau)}{\partial x} \Big|_{x=0} = L^{-1} \left[\frac{\partial g_A(x, s)}{\partial x} \Big|_{x=0} \right] \quad (13)$$

and from eq 11, for $\phi \neq 0$

$$\frac{\partial g_A(x, s)}{\partial x} \Big|_{x=0} = \frac{-C}{\sqrt{D}} \left[\frac{\sqrt{s+k}}{s+b} - 10^\phi \frac{\sqrt{s}}{(s+b)} - 10^\phi \frac{k}{\sqrt{s(s+b)}} \right] \quad (14)$$

where

$$C = \frac{10^\phi C_A^b}{10^{2\phi} - 1}; \quad b = \frac{10^{2\phi} k}{10^{2\phi} - 1} \quad (15)$$

The inverse transform of this simpler function can be written as

$$\frac{\partial C_A}{\partial x} \Big|_{x=0} = \frac{-C}{D} \left\{ \frac{e^{-k\tau}}{\pi^{1/2} \tau^{1/2}} - \frac{10^\phi}{\pi^{1/2} \tau^{1/2}} + \frac{k^{1/2}}{(1 - 10^{2\phi})^{1/2}} e^{-b\tau} \operatorname{erf} \left[\frac{k^{1/2} \tau^{1/2}}{(1 - 10^{2\phi})^{1/2}} \right] - \frac{1}{(1 - 10^{2\phi})^{1/2}} k^{1/2} e^{-b\tau} \operatorname{erf} \left[\frac{10^\phi k^{1/2} \tau^{1/2}}{(1 - 10^{2\phi})^{1/2}} \right] \right\} \quad (16)$$

Using the infinite series representation of the error function

$$\operatorname{erf}(z) = \frac{2}{\sqrt{\pi}} e^{-z^2} \sum_{n=0}^{\infty} \frac{2^n}{(2n+1)!!} z^{2n+1} \quad (17)$$

eq 6b may be put into a form convenient for calculation

$$N_{\text{APP}} = \frac{R}{1 - R^2} \left\{ e^{-k\tau} - R + \frac{2k\tau e^{-k\tau}}{(1 - R^2)} \sum_{n=0}^{\infty} \frac{2^n}{(2n + 1)!!} \left(\frac{k\tau}{1 - R^2} \right)^n - \frac{2Rk\tau}{(1 - R^2)} \sum_{n=0}^{\infty} \frac{2^n}{(2n + 1)!!} \left(\frac{R^2k\tau}{1 - R^2} \right)^n \right\} \quad (18)$$

where $R = 10^\phi$. This result is undefined for the special case $\phi = 0$, but in this case the inverse transform is simpler yielding

$$N_{\text{APP}} = 1 - \frac{1}{2k\tau} (1 - e^{-k\tau}) \quad (19)$$

Careful analysis shows that this is the limit of eq 18.

Results from the numerical evaluation of eq 18 and 19 are shown in Figure 1. The several advantages of this approach over other single-step methods is clear.

This technique requires only charge-transfer reversibility since E° may be experimentally determined from the lower limiting portion of the curve. In this case the measured quantity is current which is more easily and accurately measured than is potential. Furthermore, the variation of the experimental quantity is much greater than in the case of other techniques. The available kinetic range is greater than that of other methods and is to a certain extent tunable. Because the restriction of diffusion control has been lifted, less anodic potentials are required and the study of EC reactions which occur near the background process or near a second electrode process may be carried out.

DEPARTMENT OF CHEMISTRY
TEXAS TECH UNIVERSITY
LUBBOCK, TEXAS 79409

LYNN MARCOUX*
T. J. P. O'BRIEN

RECEIVED FEBRUARY 22, 1972

Here is the ideal way
to obtain the
**most reliable reference data
available today!** All you need
is a subscription to the new
**JOURNAL OF PHYSICAL AND
CHEMICAL REFERENCE DATA**
published by the American Chemical
Society and the American Institute of
Physics for the National Bureau of
Standards.

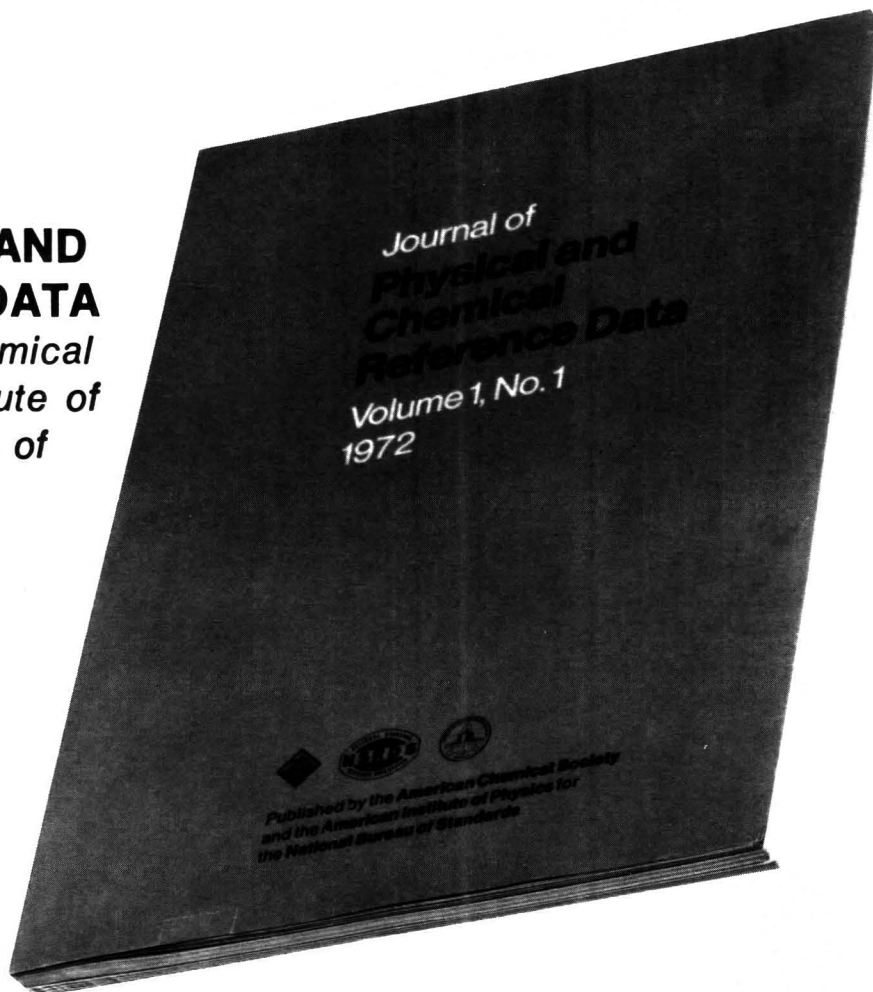
The *Journal of Physical and Chemical Reference Data* fills an important gap in the literature of the physical sciences. Its subject matter is the quantitative numerical data of physics and chemistry. As the new publication vehicle of the National Standard Reference Data System, the *Journal* will contain carefully evaluated data, with recommended values and uncertainty limits chosen by experts in each field. Critical commentary on methods of measurement and sources of error, as well as full references to the original literature, will be an integral part of each compilation.

Examples of some of the critical compilations scheduled for publication in the four issues of Volume 1 (1972) include:

- Tables of Molecular Vibrational Frequencies, Part 5, T. Shimanouchi
- Gaseous Diffusion Coefficients, by T. R. Marrero and E. A. Mason
- The Spectrum of Molecular Oxygen, by P. Krupenie
- Thermal Conductivity of the Elements, by C. Y. Ho, R. W. Powell and P. E. Liley
- Selected Values of Critical Supersaturation for Nucleation of Liquids from the Vapor, by G. M. Pound
- Gas Phase Reaction Kinetics of the Hydroxyl Radical, by W. E. Wilson, Jr.
- Selected Values of Heats of Combustion and Heats of Formation of Organic Compounds Containing the Elements CHNOPS, by E. S. Domalski
- Microwave Spectra of Molecules of Astrophysical Interest: Formaldehyde, Formamide, Thio-Formaldehyde, by D. R. Johnson, F. J. Lovas and W. H. Kirchhoff

Future compilations are expected to cover areas such as the following:

- Band gaps in semiconductors
- Nuclear moments
- Atomic energy levels and transition probabilities
- Diffusion in metals
- Electron swarm data
- Elastic constants of metals
- Surface tension of liquids
- Properties of molten salts
- Activity coefficients of electrolytes
- Equation of state of atmospheric gases
- Ionization and appearance potentials



The *Journal of Physical and Chemical Reference Data* is intended to be a definitive source of reliable data on physical and chemical properties. Just fill in the order form at the bottom of this page to receive this invaluable reference source.

**JOURNAL OF PHYSICAL AND CHEMICAL REFERENCE DATA
AMERICAN CHEMICAL SOCIETY
1155 Sixteenth Street, N.W.
Washington, D.C. 20036**

Yes, I would like to receive the JOURNAL OF PHYSICAL AND CHEMICAL REFERENCE DATA at the one-year rate checked below:

| | U.S. | Canada | PUAS | Other Countries |
|---------------------|---------|---------|---------|-----------------|
| AIP and ACS members | \$20.00 | \$20.00 | \$23.00 | \$23.00 |
| Nonmembers | \$60.00 | \$60.00 | \$63.00 | \$63.00 |

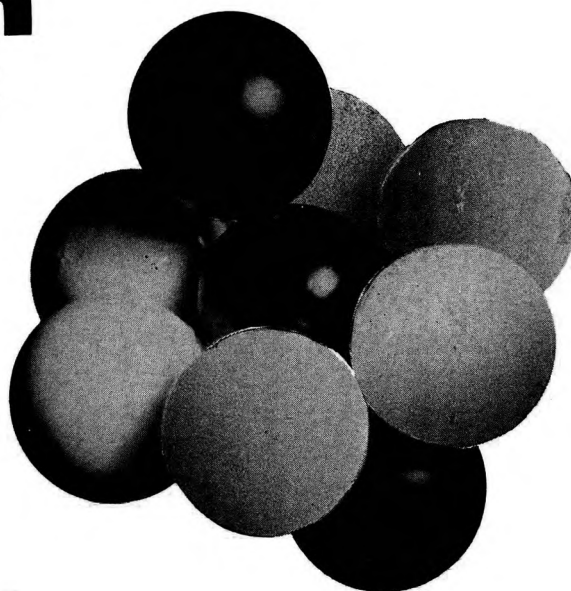
Bill me Bill company Payment enclosed

Name _____

Street _____ Home
Business

City _____ State _____ Zip _____

Molecular Sieve Zeolites



ADVANCES IN CHEMISTRY SERIES No. 101 and 102

Seventy-seven papers from a symposium co-sponsored by the Divisions of Colloid and Surface Chemistry, Petroleum Chemistry, and Physical Chemistry of the American Chemical Society and Worcester Polytechnic Institute, Edith M. Flanigen and Leonard B. Sand, co-chairmen.

Do you need a group of substances that can remove radioactive isotopes from nuclear wastes, remove ammonia from secondary sewage effluents, remove sulfur dioxide from waste gases, foster formation of actinides, or disrupt bacterial cells? These and many other possibilities are available through research on molecular sieve zeolites. For example, they are used for

- separating hydrogen isotopes
- solubilizing enzymes
- carrying active catalysts in curing of plastics
- transporting soil nutrients in fertilizers
- filtering tars from cigarette smoke

"Molecular Sieve Zeolites" reports recent advances in this rapidly developing field. Volume I offers 41 papers devoted to the synthesis, structure, mineralogy, and modification of sieve zeolites. These are followed in Volume II by 36 papers discussing sorption and catalysts.

Volume I: 526 pages with index. Cloth bound (1971)
\$16.00

Volume II: 459 pages with index. Cloth bound (1971)
\$16.00

No. 101 and 102 ordered together \$30.00

Postpaid in U.S. and Canada; plus 35 cents elsewhere.

Set of L.C. cards with library orders upon request.

Other books in the ADVANCES IN CHEMISTRY SERIES of interest to colloid and surface, petroleum, and physical chemists include:

- | | | | | |
|---|-----------|-------------|--------|---------|
| No. 97 Refining Petroleum for Chemicals | 293 pages | Cloth bound | (1970) | \$11.50 |
| No. 89 Isotope Effects in Chemical Processes | 278 pages | Cloth bound | (1969) | \$13.00 |
| No. 87 Interaction of Liquids at Solid Substrates | 212 pages | Cloth bound | (1968) | \$9.50 |
| No. 86 Pesticidal Formulations Research. Physical and Colloidal Chemical Aspects | 212 pages | Cloth bound | (1969) | \$9.50 |
| No. 79 Adsorption from Aqueous Solution | 212 pages | Cloth bound | (1968) | \$10.00 |
| No. 43 Contact Angle, Wettability, and Adhesion | 389 pages | Cloth bound | (1964) | \$10.50 |
| No. 31 Critical Solution Temperatures | 246 pages | Cloth bound | (1961) | \$8.00 |
| No. 29 Physical Properties of Chemical Compounds—III | 489 pages | Cloth bound | (1961) | \$10.00 |
| No. 22 Physical Properties of Chemical Compounds—II | 491 pages | Cloth bound | (1959) | \$10.00 |
| No. 20 Literature of the Combustion of Petroleum | 295 pages | Paper bound | (1958) | \$8.00 |
| No. 15 Physical Properties of Chemical Compounds | 536 pages | Cloth bound | (1955) | \$10.00 |

Order from:

Special Issues Sales
American Chemical Society
1155 16th St., N.W.
Washington, D.C. 20036